SYNTHESIS AND APPLICATION OF LIGHT-ACTIVATED DNA



Denis Hartmann

Department of Chemistry

Wolfson College

A thesis submitted for the degree of Doctor of Philosophy

July 2023

SUMMARY

This thesis describes the synthesis and application of UV- and blue light-activatable oligonucleotides for use in cell-free expression systems. A blue light-activatable photocage was developed for control of linear DNA templates, which has shown excellent caging ability and rapid uncaging with blue light. Due to its orthogonality to UV light, a two wavelength-controlled logic gate was developed, and spatiotemporal control of gene expression using these linear templates was demonstrated with one and two wavelengths in synthetic cells.

The developed photocaging approach could also be employed on antisense oligonucleotides, providing tight caging and photoactivation of gene knockdown in cell-free conditions. Employing this together with the blue light-activatable DNA templates developed previously allowed for two wavelength-controlled transcription and translation. Two orthogonally activatable light-controlled antisense oligonucleotides were also developed, allowing for the orthogonal control of gene knockdown of two different genes in cell-free conditions through choice of appropriate wavelength.

The photocages could also be utilised to form constrained, macrocyclised antisense oligonucleotides by divalent binding of an oligonucleotide to wild-type streptavidin. The resulting handcuff structures showed minimal RNase H activity and were suitable for the control of gene knockdown in cell-free conditions.

Lastly, an alternative caging approach was developed by chemoselectively attaching photocages to phosphorothioate linkages in an antisense oligonucleotide. The resulting oligonucleotides showed drastically reduced duplex formation ability and only minimal RNase H activity and enabled light-controlled gene knockdown in cell-free conditions.

ACKNOWLEDGEMENTS

I would like to thank my supervisor Michael Booth for his excellent supervision and support throughout my DPhil and giving me the freedom to explore the wonders that is nucleic acid chemistry. I would also like to thank my co-supervisor Hagan Bayley for providing me lab space and support throughout.

I would like to thank Michael Fairhead and Mark Howarth for providing the monovalent streptavidin used in this thesis. I also want to thank my industrial mentors Gajan Santhakumar and Robert Hicklin for their scientific input.

I want to thank Jack, Razia, Jeff, Khoa and Assala for being part of this whole journey. I want to thank my two part IIs Rachel and Naoki, as well as our new DPhils Disha and Ellen, for showing me the joys of teaching and passing on skills. I want to thank Sonia for taking over my project and for proofreading my thesis. I want to also thank everyone else in the Booth group I have not named personally, as well as the members of the Bayley group. I would like to highlight a few members of the Bayley group specifically. Yujia, for being both mental and scientific support. Leonie, for being a solid friend in the lab. Xingzao for being the best person to bounce ideas off of.

I want to also thank my friends Catherine, Nameerah, Richard and Elisabeth for supporting me on this journey. I also would like to thank my late friend Becca for her support in the early stages of my DPhil and encouraging me to even apply for the DPhil programme to begin with. Lastly, I would like to thank my housemates over the years, particularly Joe, Darius, Finlay, Katharina and Linda, for being there on a day-to-day basis on this journey.

CONTENTS

1 INTRODUCTION 22

1.1 NUCLEIC ACID STRUCTURE AND FUNCTION 22

1.1.1 STRUCTURE OF COMPONENTS 22

1.1.2 SECONDARY STRUCTURE OF DNA 23

1.2 FUNCTION OF NUCLEIC ACIDS 26

1.3 TRANSCRIPTION AND TRANSLATION 28

1.3.1 THE GENETIC CODE 28

1.3.2 TRANSCRIPTION 29

1.3.3 TRANSLATION 33

1.3.4 MODULATION OF GENE EXPRESSION 34

1.4 CELL-FREE PROTEIN SYNTHESIS 43

1.4.1 LYSATE-BASED CFPS 44

1.4.2 CFPS FROM PURIFIED COMPONENTS 46

1.4.3 APPLICATIONS OF CFPS 48

1.5 PHOTOREMOVABLE PROTECTING GROUPS 51

1.5.1 2-NITROBENZYL PHOTOCAGES 52

1.5.2 COUMARIN-DERIVED PPGS 53

1.6 LIGHT-CONTROLLABLE GENE EXPRESSION 57

1.6.1 CONTROL OF GENE EXPRESSION USING PHOTOCAGED SMALL MOLECULES 58

1.6.2 CONTROL OF GENE EXPRESSION THROUGH PHOTOCAGED TEMPLATES AND MRNA 59

1.6.3 CONTROL OF GENE KNOCKDOWN USING PHOTOCAGED ASOS AND SIRNA 63

1.7 AIMS 65

2 DEVELOPMENT OF A BLUE LIGHT-PHOTOCLEAVABLE CAGING GROUP FOR DNA BASED ON AN EXTENDED COUMARIN SCAFFOLD 66

2.1 INTRODUCTION 66

2.2 SYNTHESIS OF THE BIOTINYLATED COUMARIN PHOTOCAGE 69

2.3 REACTIVITY OF THE BLA-BIOTIN-DERIVATIVES 10A-C WITH DNA 73

2.4 PHOTOCHEMICAL PROPERTIES OF BLA-COUMARINS 76

2.5 PURIFICATION OF FULLY-MODIFIED T7-CONTAINING OLIGONUCLEOTIDE AND OPTIMISATION OF PCR CONDITIONS 79

2.6 Expression of Broccoli Aptamer from Annealed Templates 82
2.7 Control of mVenus Production in a CFPS System..... 84
2.8 Two-Wavelength Control of Gene Expression 89
2.9 Controlled Expression in Giant Unilamellar Vesicles..... 96
2.10 Photopatterning of Emulsion Droplets with one and two Wavelengths of Light 97
2.11 Conclusions..... 103

3 LIGHT-CONTROLLED LA-BIOTIN-MODIFIED ANTISENSE OLIGONUCLEOTIDES 104

3.1 Introduction 104
3.2 Screening for a suitable Oligonucleotide for effective ASO caging..... 106
3.3 Controlled Gene Knockdown in a CFPS System..... 107
3.4 Two-wavelength Control of CFPS..... 108
3.5 Two Wavelength Control of Gene Knockdown 111
3.6 Light-controlled gene knockdown inside emulsion droplets 117
3.7 Conclusions 119

4 CIRCULARISED LA-BIOTIN-CAGED OLIGONUCLEOTIDES 120

4.1 Introduction 120
4.2 Screening for hairpin-forming ASO Sequences..... 122
4.3 Investigation of wtSA Binding to terminal-modified ASOs 123
4.4 Photocleavage Behaviour of handcuffed Oligonucleotides..... 125
4.5 Control of RNase H-mediated Degradation 126
4.6 Use of Sequences with lower Constraints 128
4.7 Control of CFPS using handcuffed Oligonucleotides 130
4.8 Conclusions 132

5 PHOSPHOROTHIOATE-CAGED ANTISENSE OLIGONUCLEOTIDES..... 133

5.1 Introduction 133
5.2 Screening for an Antisense Oligonucleotide against mVenus..... 136
5.3 Optimisation of Reaction Conditions for Phosphorothioate Modification 138
5.4 Characterisation of NV-modified Oligonucleotides 141
5.5 Screening for a truncated ASO for higher caging density 144

5.6 Control of RNase H-mediated degradation with NV-modified Oligonucleotides 145
5.7 Control of Cell-free Protein Synthesis with NV-modified ASOs 148
5.8 Nuclease Stability of NV-modified Oligonucleotides 153
5.9 Conclusions 154

6 CONCLUSIONS AND FUTURE WORK 155

7 MATERIALS AND METHODS 161

7.1 Synthesis 161
7.1.1 General Synthesis 161
*7.1.2 7-(Diethylamino)-4-(hydroxymethyl)-2H-chromen-2-one **1** 162*
*7.1.3 4-(((tert-Butyldimethylsilyl)oxy)methyl)-7-(diethylamino)-2H-chromen-2-one **2** 163*
*7.1.4 3-Bromo-4-(((tert-butyldimethylsilyl)oxy)methyl)-7-(diethylamino)-2H-chromen-2-one **3** 163*
*7.1.5 tert-Butyl-(E)-3-(4-(((tert-butyldimethylsilyl)oxy)methyl)-7-(diethylamino)-2-oxo-2H-chromen-3-yl)acrylate **4** 164*
*7.1.6 tert-Butyl (2-(2-(2-aminoethoxy)ethoxy)ethyl)carbamate **5** 165*
*7.1.7 tert-Butyl-(E)-(2-(2-(2-(3-(4-(((tert-butyldimethylsilyl)oxy)methyl)-7-(diethylamino)-2-oxo-2H-chromen-3-yl)acrylamido)ethoxy)ethoxy)ethyl)carbamate **6A** 165*
*7.1.8 tert-Butyl-(E)-(2-(2-(2-(3-(7-(diethylamino)-4-(hydroxymethyl)-2-oxo-2H-chromen-3-yl)acrylamido)ethoxy)ethoxy)ethyl)carbamate **6B** 166*
*7.1.9 Biotin-N-hydroxysuccinimide ester **7** 167*
*7.1.10 N-(2-(2-(2-((E)-3-(4-(((tert-Butyldimethylsilyl)oxy)methyl)-7-(diethylamino)-2-oxo-2H-chromen-3-yl)acrylamido)ethoxy)ethoxy)ethyl)-5-((3aS,4S,6aR)-2-oxohexahydro-1H-thieno[3,4-d]imidazol-4-yl)pentanamide **8** 168*
*7.1.11 N-(2-(2-(2-((E)-3-(7-(Diethylamino)-4-(hydroxymethyl)-2-oxo-2H-chromen-3-yl)acrylamido)ethoxy)ethoxy)ethyl)-5-((3aS,4S,6aR)-2-oxohexahydro-1H-thieno[3,4-d]imidazol-4-yl)pentanamide **9** 169*
*7.1.12 (7-(Diethylamino)-3-((E)-3,14-dioxo-18-((3aS,4S,6aR)-2-oxohexahydro-1H-thieno[3,4-d]imidazol-4-yl)-7,10-dioxa-4,13-diazaoctadec-1-en-1-yl)-2-oxo-2H-chromen-4-yl)methyl (2,5-dioxopyrrolidin-1-yl) carbonate **10A** ... 170*

*7.1.13 (7-(Diethylamino)-3-((E)-3,14-dioxo-18-((3aS,4S,6aR)-2-oxohexahydro-1H-thieno[3,4-d]imidazol-4-yl)-7,10-dioxa-4,13-diazaoctadec-1-en-1-yl)-2-oxo-2H-chromen-4-yl)methyl (perfluorophenyl) carbonate **10b*** *171*

*7.1.14 (7-(Diethylamino)-3-((E)-3,14-dioxo-18-((3aS,4S,6aR)-2-oxohexahydro-1H-thieno[3,4-d]imidazol-4-yl)-7,10-dioxa-4,13-diazaoctadec-1-en-1-yl)-2-oxo-2H-chromen-4-yl)methyl (4-nitrophenyl) carbonate **10c*** *173*

*7.1.15 N-Boc-N'-biotinyl-3,6-dioxaoctane-1,8-diamine **11*** *174*

*7.1.16 (7-(Diethylamino)-3-((E)-3,14-dioxo-18-((3aS,4S,6aR)-2-oxohexahydro-1H-thieno[3,4-d]imidazol-4-yl)-7,10-dioxa-4,13-diazaoctadec-1-en-1-yl)-2-oxo-2H-chromen-4-yl)methyl prop-2-yn-1-ylcarbamate **12*** *174*

7.2 Oligonucleotide Sequences 176

7.2.1 General *176*

7.2.2 Amine-modified T7-promoter-containing ssDNA Sequences *176*

7.2.3 Broccoli Aptamer DNA Sequences *176*

7.2.4 Antisense Oligonucleotide Sequences *177*

7.2.5 Terminal amine-modified antisense oligonucleotides *179*

7.2.6 PS-containing oligonucleotides *180*

7.2.7 PCR Primers *180*

7.3 Chemical Biology Methods 181

7.3.1 General Chemical Biology Methods *181*

7.3.2 Data Analysis and Plotting *181*

7.3.3 Polyacrylamide Gel Electrophoresis *182*

7.3.4 Agarose Gel Electrophoresis *182*

7.3.5 Preparation of UV light-activatable T7 Primer (uvLA-T7) *182*

7.3.6 Preparation of blue light-activatable-T7 Primer (bLA-T7) *183*

7.3.7 Preparation of uvLA-ASOs from amino-C6-dT Oligonucleotides *183*

7.3.8 Preparation of bLA-ASOs from amino-C6-dT Oligonucleotides *184*

7.3.9 Binding of streptavidin to modified ASOs *184*

7.3.10 Modification of terminal amine-modified Oligonucleotides with uvLA-Biotin *184*

7.3.11 Modification of terminal amine-modified Oligonucleotides with bLA-Biotin *185*

7.3.12 Modification of PS-containing Oligonucleotides with 2NV-Br *185*

7.3.13 Modification of 1PS Oligonucleotides with Ethyl Iodide *185*

7.3.14 Melting Temperature Measurements of NV-modified Oligonucleotides 186
7.3.15 Light-controlled RNase H Assay with NV-modified oligonucleotides 186
7.3.16 Annealing of Broccoli-Construct 187
7.3.17 Plasmid Digestion 187
7.3.18 Preparation of linear Template DNA 187
7.3.19 In vitro Transcription of mRNA 188
7.3.20 Screening for RNase H-active Oligonucleotides against mVenus for Phosphorothioate Caging 188
7.3.21 Screening for Antisense Oligonucleotide Sequences active against mVenus for Circularisation onto wtSA 188
7.3.22 RNase H Assay with handcuffed ASOs 189
7.3.23 Binding of wild-type Streptavidin to terminally-modified Oligonucleotides 189
7.3.24 Control of cell-free Protein Synthesis with handcuffed Oligonucleotides 189
7.3.25 Ethanol Precipitation 190
7.3.26 Screening for PS-modification Conditions 190
7.3.27 Photocleavage of 1PSNV 190
7.3.28 Texas Red-tagged Oligonucleotide Concentration Measurements 191
7.3.29 Preparation of LA-DNA Templates using PCR 191
7.3.30 Streptavidin binding onto T7-modified genes 191
7.3.31 Illumination of DNA for Gels and cell-free Reactions 192
7.3.32 Bulk Molecule Photocleavage 192
7.3.33 Transcription of Broccoli Aptamer 192
7.3.34 Transcription of mVenus, α- and ω-Subunit mRNA 193
7.3.35 Cell-free Protein Synthesis from LA-DNA Templates 193
7.3.36 Light-controlled gene knockdown in cell-free protein synthesis with uvLA-V3 194
7.3.37 Control of Transcription and Gene Knockdown with two Wavelengths in cell-free Protein Synthesis 194
7.3.38 Two-wavelength Control of RNase H-mediated mRNA Degradation 194

7.3.39 Two Wavelength-controlled Gene Knockdown in a cell-free Protein Synthesis System *195*
7.3.40 Cell-free Protein Synthesis with PSNV-oligonucleotides *195*
7.3.41 Nuclease Assay with PSNV Oligonucleotides *195*
7.3.42 Generation of Split β-Galactosidase *196*
7.3.43 Preparation of Synthetic Cells from Giant Unilamellar Vesicles . *198*
7.3.44 Preparation of Synthetic Cells from Emulsion Droplets *199*
7.3.45 Light-controlled Gene Knockdown in Emulsion Droplets *199*
7.3.46 Oligonucleotide Mass Spectrometry *199*
7.4 Python Function for Hairpin Search 202
8 REFERENCES 203
9 APPENDICES 235

List of Tables

Table 5-1: Retention times and observed, deconvoluted, masses of ONs subjected to modification with 2-nitroveratryl bromide in different buffer conditions. 140

Table 5-2: Melting temperatures (T_M) and ΔT_M of the modified oligonucleotides. 144

Table 7-1: ssDNA sequences and the corresponding number of functionalisations. 176

Table 7-2: Broccoli Aptamer DNA sequences. 176

Table 7-3: List of ASOs screened for activity and used in Chapter 3. 177

Table 7-4: Sequences tested for antisense activity against mVenus in Chapter 4. 178

Table 7-5: Antisense oligonucleotides screened for RNase H activity against mVenus in Chapter 5. 178

Table 7-6: Truncated mV antisense oligonucleotides screened for improvement of antisense activity in cell-free conditions. 179

Table 7-7: Scrambled sequences of mV antisense sequence 220. 179

Table 7-8: Oligonucleotides with terminal amine modifiers (AmMOs) used in Chapter 4. 179

Table 7-9: Phosphorothioate (PS)-containing oligonucleotides used in this study. 180

Table 7-10: Primers used in PCR for linear DNA templates and for the generation of split-b-Galactosidase Plasmid DNA 181

Table 7-11: Modified T7-promoter-sequence-containing oligonucleotides and their masses after deconvolution as measured by LCMS. 200

Table 7-12: Amino-C6-dT-modified ASOs and their masses after deconvolution as measured by LCMS. 200

Table 7-13: Terminal amine-modified ASOs and their masses after deconvolution as measured by LCMS. 201

Table 7-14: Nitroveratryl-modified PS-ASOs and their masses after deconvolution as measured by LCMS 201

TABLE 9-1: SEQUENCES OF LINEAR DNA TEMPLATES USED FOR CELL-FREE EXPRESSION, PRODUCED BY PCR. 242

List of Figures

Figure 1-1: Constituent parts of DNA and RNA. 23
Figure 1-2: WCF-base pairing of DNA nucleobases within a duplex. 24
Figure 1-3: A- (left) and B-form (right) helices of nucleic acid duplexes, viewed from the side as well as above. 25
Figure 1-4: C2 vs C3 endo conformations of (2'-deoxy)ribose 26
Figure 1-5: The Central Dogma of Biology 28
Figure 1-6: The standard RNA codon table, organised in a wheel. 29
Figure 1-7: Schematic of the transcription process from a DNA template. 30
Figure 1-8: Simplified diagram showing the individual steps of transcription of mRNA from a DNA template. 31
Figure 1-9: Transcription from eukaryotic DNA and the fate of mRNA. 32
Figure 1-10: Schematic of protein synthesis. 34
Figure 1-11: Mechanisms of gene regulation *via* small nucleic acids 39
Figure 1-12: Comparison of Cellular and Cell-Free Protein Expression. 44
Figure 1-13: The most commonly used cell-free platforms and their applications. 45
Figure 1-14: The PURE Cell-Free Expression System. 47
Figure 1-15: Artificial, light-activated quorum sensing between synthetic cells and bacteria. 50
Figure 1-16: Mechanism of photocleavage of the parent nitrobenzyl-scaffold. 53
Figure 1-17: Summary of coumarin modifications and their effects on the photochemical properties of the coumarin scaffold 54
Figure 1-18: Generalised Mechanism of Photocleavage of Coumarin-PPGs 56
Figure 1-19: Ways of controlling the central dogma of biology with light. 57
Figure 1-20: Modification of the 5' Cap on RNA for control of translation. 60
Figure 1-21 Synthesis of a UV-light activatable T7 promoter for light-controllable gene expression. 62
Figure 1-22: Photocaged antisense oligonucleotides via circularisation. 64
Figure 2-1: Absorption Spectrum of biological tissue. 67

FIGURE 2-2: THE DEVELOPED BLUE LIGHT-ACTIVATABLE DNA TEMPLATES USING A COUMARIN-DERIVED PHOTOCAGE AND THEIR APPLICATIONS IN CELL-FREE EXPRESSION. 69
FIGURE 2-3: SYNTHETIC ROUTE DEVELOPED FOR THE BLUE LIGHT-ACTIVATABLE BIOTIN PHOTOCAGE. 70
FIGURE 2-4: ALTERNATIVE APPROACH TOWARDS BIOTINYLATED COUMARIN 8. 71
FIGURE 2-5: SYNTHESIS OF PROPARGYL-CARBAMATE-APPENDED COUMARIN-BIOTIN. 72
FIGURE 2-6: REACTION OF NHS-COUMARIN 10A WITH DNA CONTAINING TERMINAL HEXYLAMINE AND AMINO-C6-DT NUCLEOTIDES. 73
FIGURE 2-7: TESTING REACTION CONDITIONS WITH PFP-COUMARIN 10B AT DIFFERENT %DMF AND [COUMARIN]. 74
FIGURE 2-8: CONDITION SCREEN FOR MODIFICATION OF 7-AMINO-C6-DT CONTAINING SSDNA. 75
FIGURE 2-9: COMPARISON OF PFP- AND PNP-CARBONATE 10B/C REACTIVITY WITH 7-AMINO-C6-DT-MODIFIED SSDNA. 76
FIGURE 2-10: PHOTOCLEAVAGE OF PFP-COUMARIN 10B (A) AND PNP-COUMARIN 10C (B) 77
FIGURE 2-11: PHOTOCLEAVAGE OF PROPARGYL-COUMARIN 12. 78
FIGURE 2-12: FLUORESCENCE MEASUREMENT OF PROPARGYL-COUMARIN 11 PRE- (A) AND POST-(B) PHOTOCLEAVAGE. 79
FIGURE 2-13: MODIFICATION OF AMINE-CONTAINING T7-SSDNA AND HPLC AND POLYACRYLAMIDE GEL ANALYSIS OF THE MODIFIED ON. 80
FIGURE 2-14: EFFECTS OF DMSO CONCENTRATION ON PCR YIELD WITH THE BLA-T7 PRIMER 81
FIGURE 2-15: FURTHER OPTIMISATION OF PCR YIELD USING THE BLA-T7 BY VARYING REACTION PARAMETERS. 81
FIGURE 2-16: EXPRESSION OF BROCCOLI RNA APTAMER FROM A CAGED BLA-DNA TEMPLATE 83
FIGURE 2-17: PREPARATION OF LA-MV DNA TEMPLATES, ANALYSIS BY AGE AND EXPRESSION OF MV IN A CFPS SYSTEM. 85
FIGURE 2-18: AGE OF BLA-MV DNA WITH DIFFERENT DURATIONS OF BLUE LIGHT ILLUMINATION. 87
FIGURE 2-19: *IN VITRO* TRANSCRIPTION OF MRNA FROM THE BLA-T7 TEMPLATE 88

Figure 2-20: Different amounts of irradiation to express mVenus protein from bLA-mV DNA in CFE. 89
Figure 2-21: Linear PCR products for split b-Gal generation by homologous recombination 90
Figure 2-22: Linear LA-DNA templates encoding for the a- and Ω-subunits of b-Gal with different LA-promoters under different illumination conditions. 91
Figure 2-23: RNA Transcription from the LA-DNA templates uvLA-a and bLA-Ω used in Figure 2-22 under different illumination conditions. 91
Figure 2-24: Schematic of the two-wavelength-controlled AND-gate based on split b-Galactosidase. 92
Figure 2-25: Fluorescence measurements of UCA over 60 minutes after expression of split b-Galactosidase from the LA-DNA parts under different illumination conditions 93
Figure 2-26: DNA gel and transcription reaction gel from the uvLA-a, prepared using the molecule from Ambergen. 94
Figure 2-27: Evolution of fluorescence of UCA over time using the uvLA-a DNA template prepared with the Ambergen molecule together with the bLA-Ω DNA. 95
Figure 2-28: UCA fluorescence at minute 10 (Figure 2-27, orange line) 95
Figure 2-29: Preparation of NH_2- and bLA-mNG DNA 96
Figure 2-30: Controlling synthetic cell activity with bLA-DNA 97
Figure 2-31: One-wavelength spatiotemporal activation of gene expression inside immobilised emulsion droplet-based synthetic cells. 98
Figure 2-32: Immobilised emulsion droplet-based synthetic cells containing NH_2-mNG DNA 99
Figure 2-33: Expression of split b-Galactosidase from NH_2-a and -Ω DNA templates in presence of reporter molecule FDG. 100
Figure 2-34: Two-wavelength-controlled emulsion-based synthetic cells, expressing split b-Galactosidase 101
Figure 2-35: Repeats of the two-wavelength-controlled AND-gate based on split b-Galactosidase inside immobilised emulsion-droplet-based synthetic cells. 102
Figure 3-1: Controllable ASOs based on the LA-biotin technology and their application in cell-free protein synthesis. 105

Figure 3-2: Screening of ASO sequences for RNase H activity against mVenus mRNA. 106
Figure 3-3: Formation of uvLA-ASOs, comparison of different tested ASOs and controllable gene knockdown in a CFPS system. 107
Figure 3-4: Controlled Synthesis of mRNA and subsequent degradation upon activation of the uvLA-V3 ASO. 109
Figure 3-5: Control of transcription with blue light and translation at different timepoints with UV light. 110
Figure 3-6: Control of mRNA degradation with orthogonally light-activatable ASOs 111
Figure 3-7: Screening for ASO sequences active against mCherry. 112
Figure 3-8: Additional mCherry ASO sequences screened and cross-tested against mVenus mRNA 112
Figure 3-9: Testing of cross-reactivity of V2 and C1 against mV and mC mRNA. 113
Figure 3-10: Gel migration and photorelease of the C1 ASO, modified with bLA-Biotin and bound with mSA. 114
Figure 3-11: Controlled RNase H-mediated mRNA degradation using orthogonally light-activated ASOs targeting mV and mC. 115
Figure 3-12: Co-expression and orthogonally activated gene knockdown of mVenus and mCherry in cell-free conditions. 116
Figure 3-13: Light-controlled, patterned gene knockdown inside emulsion-droplet-based synthetic cells. 117
Figure 4-1: Modification of dual-termini amine-modified oligonucleotides with photocleavable biotins for circularisation onto wtSA and release with light. 121
Figure 4-2: Screening for RNase H-active ASO sequences that form a 4-stem hairpin. 122
Figure 4-3: Molecular Model of a DNA Hairpin and wtSA bound together *via* bLA-Biotin. 123
Figure 4-4: PAGE analysis of high dilution conditions for formation of the handcuff ON and the formation of different handcuffed ONs with Sequence 252[4] 124
Figure 4-5: Photolysis of the uvLA- and bLA-252[4] handcuffs 125

FIGURE 4-6: CONTROL OF RNASE H-MEDIATED MRNA DEGRADATION USING THE UVLA- AND BLA-252[4] HANDCUFFS 126
FIGURE 4-7: CONTROL OF RNASE H-MEDIATED MRNA DEGRADATION USING THE UVLA-252[4] PREPARED USING 4 EQ. OF MSA 127
FIGURE 4-8: SCREENING FOR ASO SEQUENCES WITH LOWER CONSTRAINTS 128
FIGURE 4-9: GENERALITY OF CIRCULARISATION CONDITIONS AND EFFECTIVENESS OF CAGING ON NON-HAIRPIN FORMING ON 229[1]. 129
FIGURE 4-10: CONTROL OF CELL-FREE PROTEIN SYNTHESIS USING HANDCUFFED ONS BLA-252[4] AND BLA-229[1]. 131
FIGURE 5-1: CHEMOSELECTIVE CAGING OF ASOS THROUGH ALKYLATION OF THE PS-LINKAGES (A) AND SUBSEQUENT REMOVAL BY UV IRRADIATION (B), ALLOWING FOR LIGHT-CONTROLLABLE ACTIVITY OF RNASE H 136
FIGURE 5-2: OPTIMISATION OF THE RNASE H-MEDIATED DEGRADATION ASSAY THROUGH VARYING CONCENTRATIONS OF RNASE H (A) AND ASO (B). 137
FIGURE 5-3: SCREENING OF ASO SEQUENCES FOR RNASE H-MEDIATED DEGRADATION TO FIND THE BEST ASO AGAINST MVENUS MRNA AND SCRAMBLE CONTROLS FOR THE MV 220 SEQUENCE 138
FIGURE 5-4: SCREENING FOR SUITABLE BUFFER CONDITIONS FOR THE CHEMOSELECTIVE MODIFICATION OF PS-LINKAGES IN A MIXED BACKBONE ON. 139
FIGURE 5-5: PHOTOCLEAVAGE OF THE 1PSNV ON UNDER UV IRRADIATION. 141
FIGURE 5-6: PS-SEQUENCES STUDIED AND THEIR HPLC UV-VIS AND T_M CHARACTERISATION DATA 142
FIGURE 5-7: REPRESENTATIVE MELTING TEMPERATURE CURVES OF THE 1PS, 1PSNV AND 1PSET ONS. 144
FIGURE 5-8: SCREENING FOR A TRUNCATED RNASE H-ACTIVE ANTISENSE OLIGONUCLEOTIDE 145
FIGURE 5-9: DENATURING PAGE OF CRUDE TXRD-ON MODIFICATION REACTIONS WITH 2-NITROVERATRYL BROMIDE (A) AND THEIR UV-VISIBLE ABSORBANCE TRACES AS RECORDED BY HPLC (B). 146
FIGURE 5-10: CONTROL OF RNASE H-MEDIATED DEGRADATION OF TARGET MRNA USING THE PSNV-MODIFIED ONS. 148
FIGURE 5-11: CONTROL OF CFPS USING 20NT-PSNV OLIGONUCLEOTIDES 149
FIGURE 5-12: CONTROL OF CFPS WITH THE 14NT-6PSNV ON 151

FIGURE 5-13: TXRD-FLUORESCENCE MEASUREMENTS OF CFPS REACTIONS (FIGURE 5-11 AND FIGURE 5-12). 152
FIGURE 5-14: STABILITY OF PO, 9PS AND PSNV ONS TOWARDS DNASE I 153

List of Abbreviations and Acronyms

A	Adenine
AA	Acrylamide
Ac	Acetate
AGE	Agarose gel electrophoresis
AGO2	Argonaute 2 protein
AmMO	Amine modifier
AMP	Adenosine monophosphate
APS	Ammonium persulfate
Ar	Aromatic
ASO	Antisense oligonucleotide
ATP	Adenosine triphosphate
BisAA	Bisacrylamide
bLA	Blue light-activatable
Boc	*tert*-Butyloxycarbonyl
BODIPY	Boron dipyrromethene
bp	Base pair
C	Cytosine
CCT	Click-chemistry-tools
CFE	Cell-free expression
CFPS	Cell-free protein synthesis
CHO	Chinese hamster ovary
CM	Coumarin-4-methyl
CUG	Carboxyumbelliferyl-β-D-galactopyranoside
Cy	Cyclohexyl
DCM	Dichloromethane
DEACM	Diethylaminocoumarin
DFHBI	(5*Z*)-5-[(3,5-Difluoro-4-hydroxyphenyl)methylene]-3,5-dihydro-2,3-dimethyl-4H-imidazol-4-one
DIPEA	Diisopropylethylamine
DMAP	Dimethylaminopyridine
DMF	*N,N*-Dimethylformamide
DMSO	Dimethylsulfoxide
DNA	2'-Deoxy-ribonucleic acid
dNTP	2'-Deoxynucleoside triphosphate
DPBS	Dulbecco's phosphate-buffered saline
ds	Double-stranded
E. coli	*Escherichia coli*
EDC	1-Ethyl-3-(3′-dimethylaminopropyl)carbodiimide
EDTA	Ethylenediaminetetraacetic acid
eGFP	Enhanced green fluorescent protein
Em	Emission
ESI	Electrospray ionisation
Et	Ethyl

Ex	Excitation
FDG	Fluorescein-di-β-D-galactopyranoside
FWD	Forward
G	Guanine
GFP	Green fluorescent protein
GTP	Guanosine triphosphate
HAT	Hydrogen atom transfer
HBTU	Hexafluorophosphate benzotriazole tetramethyl uronium
HetAr	Heteroaromatic
HFIP	Hexafluoroisopropanol
His	Histidine
HPLC	High performance liquid chromatography
HRMS	High resolution mass spectrometry
IC	Internal conversion
IP	Ion pairing
IPTG	Isopropylthio-β-D-galactopyranoside
IR	Infrared
ISC	Intersystem crossing
kb	Kilobase
LA	Light-activatable
LCMS	Liquid chromatography mass spectrometry
LG	Leaving group
LNA	Locked nucleic acid
mC	mCherry
Me	Methyl
Met	Methionine
miRNA	microRNA
mNG	mNeonGreen
MP	Membrane protein
mRNA	Messenger RNA
MS	Mass spectrometry
mSA	Monovalent Streptavidin
mV	mVenus
NBS	*N*-Bromosuccinimide
NEB	New England Biolabs
NMR	Nuclear magnetic resonance
NP	2-Nitropiperonyl
nt	Nucleotide
NTP	Nucleoside triphosphate
NV	2-Nitroveratryl
ON	Oligonucleotide
ORF	Open reading frame
PAGE	Polyacrylamide gel electrophoresis
PC	Photocleavable
PC	Phosphatidylcholine
PCR	Polymerase chain reaction

PDB	Protein Databank
PE	Petroleum ether
PFP	Pentafluorophenol
PMO	Phosphorodiamidate morpholino oligomer
PNA	Peptide nucleic acid
pNP	*para*-Nitrophenol
PO	Phosphate
PPG	Photoremovable protecting group
PS	Phosphorothioate
PTM	Posttranslational modification
REV	Reverse
RISC	RNA-induced silencing complex
RNA	Ribonucleic acid
RNAi	RNA interference
RNAP	RNA polymerase
RNase H	Ribonuclease H
rRNA	Ribosomal RNA
SEBS	Styrene-ethylene-butylene-styrene
SEC	Size exclusion chromatography
ss	Single-stranded
T	Thymine
TAE	Tris-acetate-EDTA
TBAF	Tetrabutylammonium fluoride
TBDMS	*tert*-butyldimethylsilyl
TBE	Tris-borate-EDTA
*t*Bu	*tert*-Butyl
TEAB	Triethylammonium bicarbonate
TFA	Trifluoroacetic acid
TIC	Total ion chromatogram
TLC	Thin layer chromatography
TMEDA	N,N'-Tetramethylethylenediamine
tRNA	Transfer RNA
TxRd	Texas Red
U	Uracil
UCA	Umbelliferone-3-carboxylic acid
uORF	Upstream open reading frame
UTP	Uridine triphosphate
UTR	Untranslated region
UV	Ultraviolet
uvLA	UV light-activatable
V. natriegens	*Vibrio natriegens*
WCF	Watson-Crick-Franklin
wtSA	wild-type Streptavidin
β-Gal	β-Galactosidase

List of Appendices

A - DNA Sequences of Genes 236
B - NMR Spectra 243
C - Oligonucleotide Mass Spectra 259
D - Reaction Screening for PS Modification 274
E - Photocleavage Mass Spectrometry Data 280
F - Melting Temperature Data 283
G - HPLC Purifications of modified Oligonucleotides 287

1 INTRODUCTION

1.1 Nucleic Acid Structure and Function

2'-Deoxyribonucleic Acid (DNA) and ribonucleic acid (RNA) are macromolecular biopolymers and the molecular carriers of genetic information. They are comprised of repeating monomeric motifs which encode the genetic information through their specific sequence. They encode and transmit the blueprint for all proteins found in nature, and are thus at the centre of life itself.

1.1.1 Structure of Components

The repeating units of DNA and RNA are called nucleotides (nts). These nucleotides are comprised of a cyclic furanoside sugar, 2'-deoxy-D-ribofuranose (for DNA) or ribofuranose (for RNA) and a heterocylic base attached to the anomeric 1'-position *via* a β-C-N linkage, and phosphate ester at the 5'-hydroxyl group.

An oligonucleotide consists of 2 or more nucleotide units joined *via* the phosphate on the 5'-hydroxyl of one unit to the 3'-hydroxyl of the next unit to form a phosphodiester linkage. At physiological pH (7.4), the phosphates are deprotonated and the resulting polyanions are highly water-soluble. The sequence of such an oligonucleotide is given by the order of the nucleobases, read from the 5'- to the 3'-end of the oligomer, defining its primary structure.[1]

The major heterocyclic bases in DNA are the purine bases Adenine (A) and Guanine (G), and the pyrimidine bases Cytosine (C) and Thymine (T). In RNA, Thymine is replaced by Uracil (U). Their structures and numbering are summarised in **Figure 1-1**. The bases attached to the ribofuranose units are called Adenosine, Guanosine, Cytidine, Thymidine and Uridine, with the prefix ‘deoxy-‘ added for 2’deoxyribofuranose-derived nucleosides and nucleotides. To distinguish them in abbreviations, a lowercase “d” is prefixed to the nucleobases to indicate deoxy-ribonucleosides and -nucleotides.

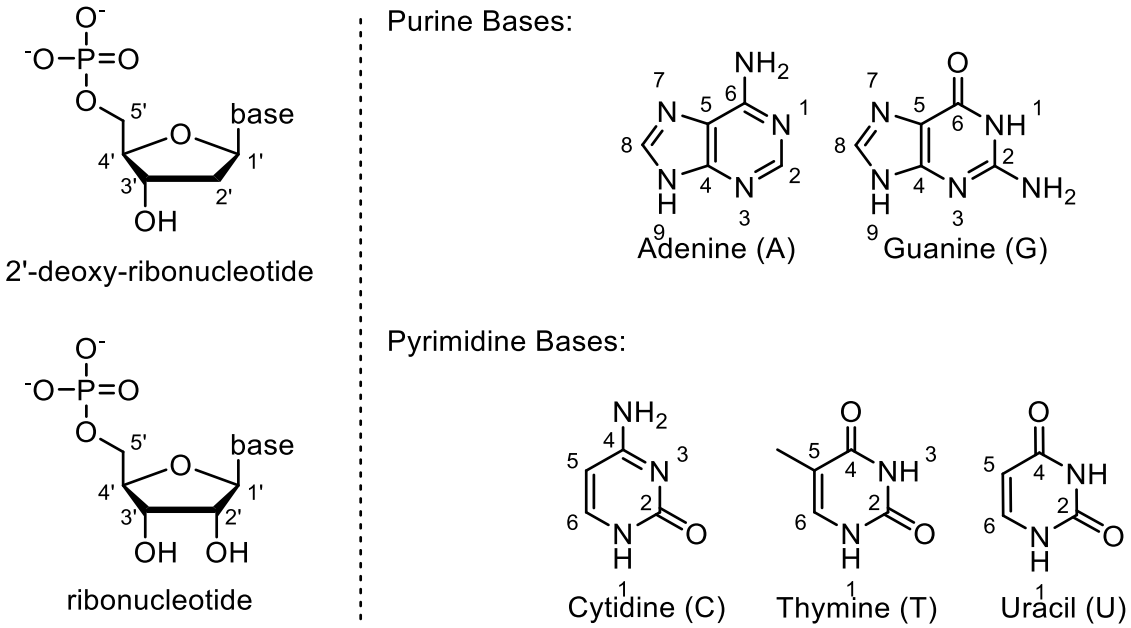


Figure 1-1: Constituent parts of DNA and RNA.

DNA and RNA nucleotides (left) and the major Pyrimidine and Purine Nucleobases of DNA and RNA (right)

1.1.2 Secondary Structure of DNA

One of the most fundamental discoveries in oligonucleotide chemistry was its three-dimensional structure. One crucial step in the elucidation of the structure of DNA was through Chargaff.[2] Chargaff found that in DNA %T ≈ %A and %G ≈ %C. This led to the proposal by Watson and Crick that these pairs of nucleobases are held together by hydrogen bonds. This proposal, together with X-ray crystallographic data from Astbury,[3] Wilkins[4] and Franklin[5] lead to the discovery of the double-helix structure of DNA, held together by hydrogen bonds between complementary nucleobases.[6] This

discovery lead to the nobel prize in chemistry in 1962 and paved the way for future research in biochemistry and genetics.

The double helix consists of 2 single strands of nucleotides running antiparallel to each other. They have a hydrophilic phosphate exterior and a hydrophobic interior composed of the nucleobases, where each nucleobase is linked through hydrogen bonds to its complementary nucleobase on the other strand, holding the strands together.[1]

The so-called canonical or Watson-Crick-Franklin (WCF) base pairs are between C and G, and A and T/U, respectively. C and G form 3, and A and T/U form 2 hydrogen bonds between them and their bonding pattern is shown in **Figure 1-2**.

A number of other pairing motifs are also possible. These include reversed WCF pairs, whereby one of A or T is inverted, as well as Hogsteen and reverse Hogsteen pairing, which differs from the classical WCF pair through the use of alternative hydrogen bonding sites on the purine bases. Lastly, base-mismatches can also occur, leading to so called 'wobble' base pairs.[7] These hydrogen-bonded nucleobases are able to form π-stacks within the double helix, which is another driving force in the formation of the duplex structure.[1]

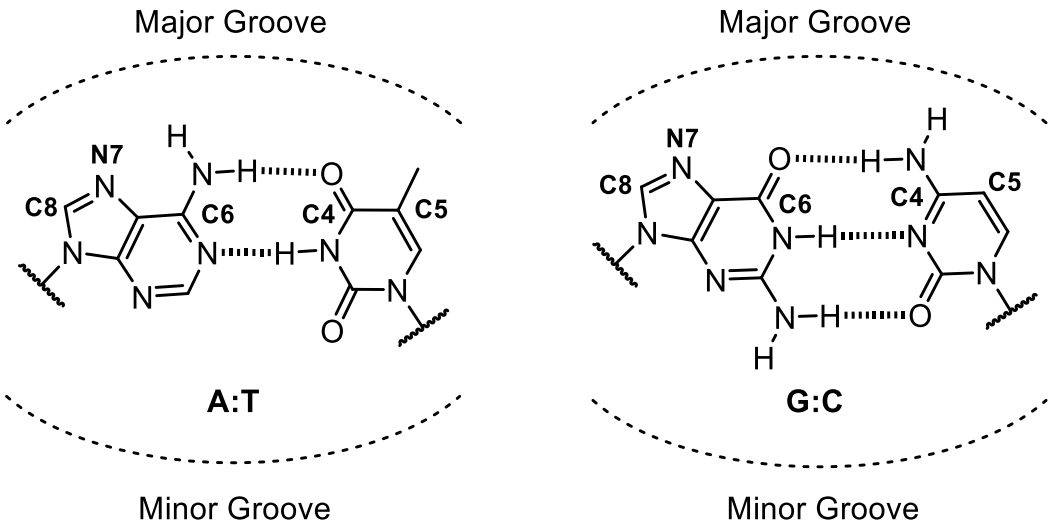


Figure 1-2: WCF-base pairing of DNA nucleobases within a duplex.

A/T form two hydrogen bonds and G/C form 3 hydrogen bonds. The helical duplex structure adopted by oligonucleotides forms a major and minor groove in the helix. The atoms highlighted are the ones accessible from the major groove.

These double helices occur in various forms (**Figure 1-3**). The B form is the most commonly encountered at physiological pH and salt concentrations and is the dominant biologically active form of DNA duplexes.[1] The B-form is a right-handed helix and the distance between successive base pairs in the interior is approximately 3.4 Å.[7] The helix itself is a plectonemic coil,[8] i.e. the two strands coil around the same helical axis while being intertwined with themselves. A full turn of this double helix is repeated every 10.4 base pairs (bp).[9] Another commonly encountered structure is the A form. The A-form is similar in structure to the B-form, as they are both right-handed helices and form plectonemic coils. The helical axis of A-form duplexes is, however, shifted further from the centre of the nucleobase pairs. This form is characterised by an increase of base pairs per turn compared to the B-form and thus a smaller twist-angle. This form also has a decreased rise per turn, meaning that the A-form is shorter, but wider than the B-form. Another physical feature of this form is a deeper, narrower major groove, and a shallower, wider minor groove. This form is most encountered at high salt and low humidity concentrations for DNA and is the structure adopted by RNA- and DNA/RNA hybrid-duplexes.[7,10]

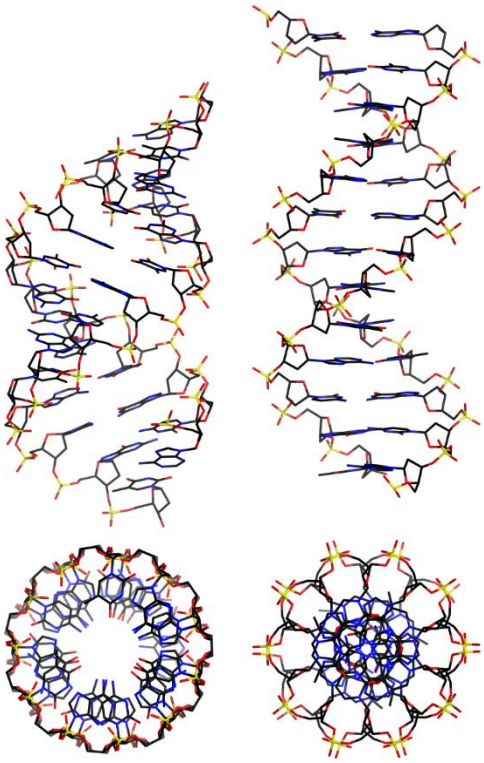


Figure 1-3: A- (left) and B-form (right) helices of nucleic acid duplexes, viewed from the side as well as above.

Figure adapted from Mauroesguerroto *via* Wikimedia Commons under a creative commons licence (CC-BY-SA 4.0, https://creativecommons.org/licenses/by-sa/4.0).

The structural basis of the A-form under physiological conditions arises from the puckering of the ribose unit (**Figure 1-4**). In RNA, the existing 2'-hydroxyl essentially locks the sugar into its C3-endo conformation,[10] whereas in DNA, the lack of a 2'-OH allows for greater flexibility and the adoption of both C2 and C3 endo conformations of the ribose unit.[1,9,11]

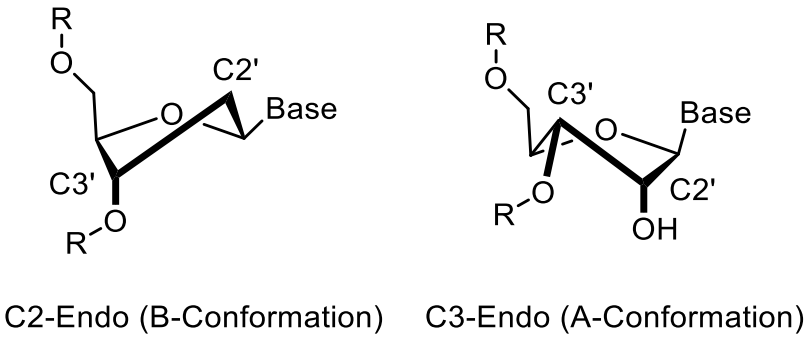


Figure 1-4: C2 vs C3 endo conformations of (2'-deoxy)ribose

Double-helical A and B-form nucleic acids, due to their plectonemic coil structure, have a major and minor groove.[12] The N7 and C6 groups of purines, and the C5 and C4 groups of pyrimidines are accessible from the major groove and can interact with amino acids of proteins, allowing for sequence-specific recognition of DNA.[13–15] Proteins can also bind specifically in the minor groove, as it still enables H-bonding between amino acids and the nucleobases, but this occurs less frequently.[16] The major groove also allows for chemical modification of the nucleobases at the C5 and C8 positions of pyrimidines and purines respectively. This allows any appended modification to protrude from the major groove, allowing chemical accessibility without disturbing the nucleic acid structure.[11]

1.2 Function of Nucleic Acids

The main function of DNA and RNA nucleic acids in nature is as a storage medium for genetic information. This information, encoded in the nucleobase sequence, makes up the genome of an individual. A gene is a stretch of information in the sequence that encodes for a particular function, such as a protein or RNA. Related genes are often found close-by, forming so-called gene-clusters.[17] Genomic DNA can have incredibly large numbers of base pairs found within and thus DNA molecules are normally very long. The diploid human genome consists of 6.4 x 10^9 base pairs for example (divided

into 46 different linear DNA molecules, the chromosomes)[18] with the largest number of reported nucleobases per cell in an organism to date being 1.49 x 10^{11} bases in the flower *Paris japonica*.[19]

Due to its length, DNA has to be highly condensed to fit into cells. In eukaryotic cells, DNA is almost exclusively confined to the nucleus. Eukaryotic genomic DNA is highly organised. To condense the DNA, histone proteins condense the DNA into chromatin. Chromatin consists of a large number of individual histone proteins, which are wrapped by DNA into a nucleosome. In such a nucleosome, the DNA is wrapped around two times across the histone octamer, comprised of two each of the 4 subunits. These nucleosomes are then folded upon themselves to form a 30 nm wide fibre.[12] These fibres are called the chromosomes of a eukaryotic organism.

In prokaryotes, in contrast, DNA is less organised and can be found in the cytosol, due to a lack of a nucleus. It is however organised into a nucleoid, an area of a prokaryotic cell where chromosomal DNA is found, and is also organised by nucleoid-associated proteins.[20] In addition to chromosomal DNA, prokaryotes often also contain extrachromosomal DNA, predominantly in the form of plasmids.[21] These plasmids are circular DNA molecules carrying additional genes that benefit the organism's survival. Plasmids can replicate autonomously and can be transmitted between species, transferring genetic material between organisms as part of a mechanism called horizontal gene transfer.[22]

RNA, in contrast, can have various functions in the cell. The carrier of genetic information in RNA is the messenger (mRNA) as well as its larger precursor molecules termed pre-mRNAs, that are the immediate product of transcription in eukaryotic cells. In addition to carrying the genetic information itself, RNA molecules are also heavily involved in the expression of genes into protein. Ribosomal RNA (rRNA), along with ribosomal proteins, make up the ribosome, which assembles protein. For this, the ribosome recruits transfer RNAs (tRNAs) that carry individual amino acids to assemble polypeptide chains following the genetic code within the mRNA. Lastly, there are other RNA molecules found, such as microRNAs (miRNAs) and small interfering RNAs (siRNAs), which are involved in a process called RNA interference (RNAi), which regulate translation by degradation or inhibition of mRNA.[17]

1.3 Transcription and Translation

Life is dependent on the ability to store and access genetic information from the DNA. The information within the DNA encoding for a protein of interest is accessed through a two-step process. In the first step called Transcription DNA is transcribed into RNA, which in the second step called Translation, gets translated into protein (**Figure 1-5**). This fundamental process of life is also termed 'the central dogma of biology', which states that genetic information can flow between nucleic acids, through DNA replication, transcription or reverse transcription.[23]

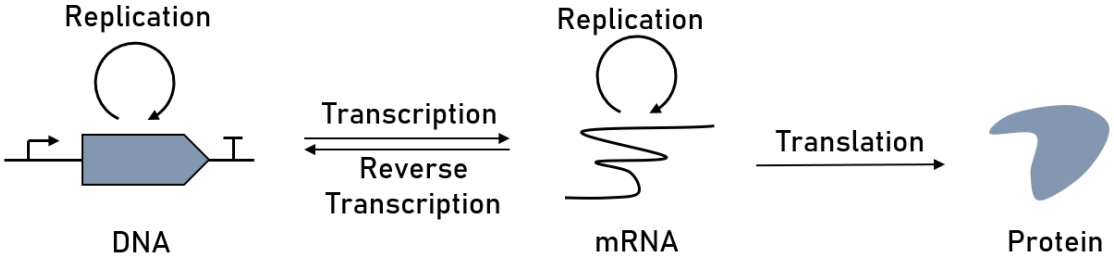


Figure 1-5: The Central Dogma of Biology

Genetic information can be transcribed from DNA into RNA, or reverse transcribed from RNA into DNA. RNA can then be translated into protein.

1.3.1 The Genetic Code

As discussed above, the way genetic information is encoded is through the precise sequence of nucleobases. Proteins are made out of a total of 20 different amino acids. To encode for 20 amino acids, the 4 nucleobases form sets of 3 bases encoding for an amino acid called codons. This triplet code was first demonstrated by Crick, Brenner, Barnett and Watts-Tobin in 1961,[24] with Nirenberg and Matthaei revealing the nature of a codon[25] in the same year. The total number of possible combinations of 4 bases into triplets is 4^3, i.e. 64, and thus has a large number of redundant codons. Because of this, many amino acids are encoded by several codons. The codons and what amino acid they encode is often described in a codon table (**Figure 1-6**). Proteins start with a unique start codon, which in transcribed RNA reads AUG, and encodes for Methionine (Met). This means that the vast majority of proteins when translated start with a Methionine, with alternative start codons possible but rare, and often only differing by one nucleotide.[26] In addition, codons exist that indicate the termination of a protein, the so-called STOP-codons. The frequency of use of codons also varies, providing ways for the organisms to regulate gene expression, a phenomenon termed

codon usage bias.[27,28] The exact list of codons can also vary between source and organisms,[29] with yeast[30] or vertebrate[31] mitochondrial code for example deviating from the standard codons. The stretch of triplets between a start and in-frame stop codon is called the open reading frame (ORF).[32] ORFs occur across the genome, and only a fraction actually get transcribed and translated.

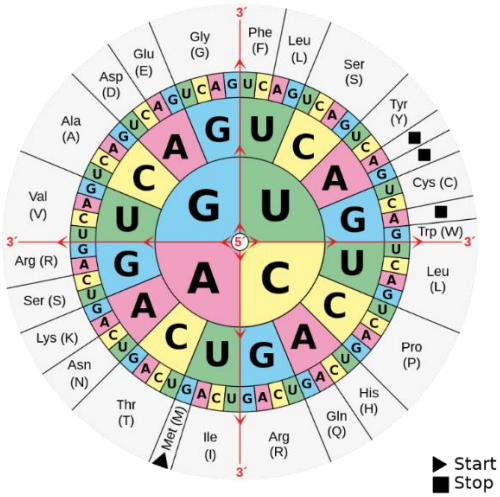


Figure 1-6: The standard RNA codon table, organised in a wheel.

The codon sun shows the code (in mRNA) from the centre outwards in 5'-3' direction. Figure from the public domain.

1.3.2 Transcription

The initial step in accessing genetic information from DNA is Transcription. In this step, DNA gets transcribed into messenger RNA (mRNA). This process converts only one of the two strands in a DNA duplex into the mRNA, as RNA is commonly single stranded. This DNA strand is termed 'antisense' stand and serves as the template, whereas the other strand, which, when read in 5'-3' direction gives the correct gene sequence is thus termed the sense strand (**Figure 1-7**). Transcription therefore happens from the 3'-5' direction on the antisense template strand, yielding RNA in a 5'-3' direction and has a homologous sequence to the sense strand.[33] This process was originally reported in 1970 by Miller, Hamkalo and Thomas, where electron microscopy showed a 'Christmas-Tree-like structure', which were individual mRNA transcripts emerging from the DNA.[34]

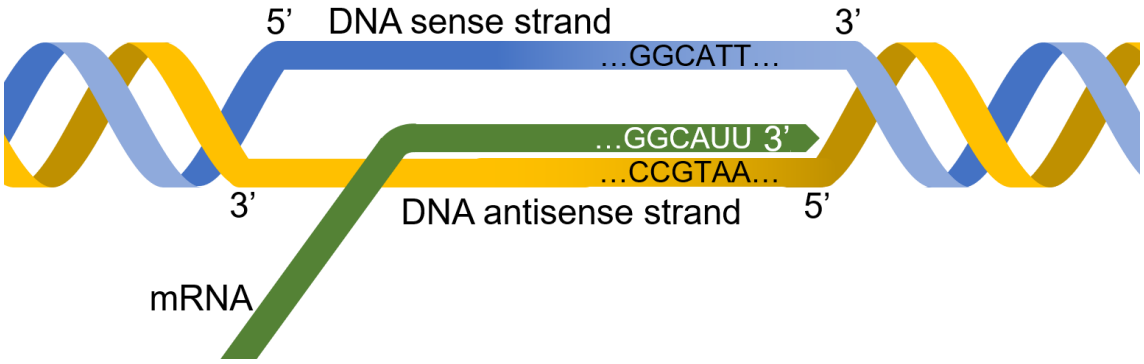


Figure 1-7: Schematic of the transcription process from a DNA template.
RNA gets transcribed by a polymerase from the antisense strand of DNA (read 3’-5’) yielding a 5’-3’ sense mRNA.

The process of transcription entails several steps. (**Figure 1-8**). The first step of transcription to form mRNA is binding of an RNA polymerase (RNAP) to the DNA. In prokaryotes, RNAP holoenzyme (a multimeric protein) binds to a regulatory sequence called a promoter region upstream of the gene to be transcribed. These promoters can vary in size from 20 to 200 bp, but usually are around 40 bp upstream of the transcription start site.[33] This sequence consists of two consensus sequence elements, called the Pribnow box -10 bp from the transcription start site (Sequence TATAAT) and a sequence -35 bp from the sequence start site (sequence TTGACA). In order for transcription to begin, the DNA duplex must be unwound, which is facilitated by the high A:T rich consensus sequences, which lowers the melting temperature (T_m) of the duplex and thus allows more efficient initiation.[10] The RNAP then recruits nucleotide triphosphates (NTPs) to its two binding sites; the initiation and elongation sites. mRNA synthesis usually starts with a purine triphosphate on the initiation site. Following this, an NTP complementary to the template strand binds to the elongation site and a phosphodiester bond is formed between the NTPs, releasing pyrophosphate. RNAP then moves along the template, in a process called chain elongation, where complementary NTPs get incorporated progressively into the growing mRNA. The final step of transcription is termination. This can either be *via* intrinsic termination, or through termination factors. Intrinsic termination is dependent on specific sequences within the DNA called termination sites. These sites contain structural features, such as G:C-rich inverted repeats, which form stem-loop structures, or 6-8 A bases that get transcribed into U. The stem-loop formation causes stalling of the RNAP, whereas the low T_m of the A:U pairs cause spontaneous dissociation of the transcript. In contrast,

the bacterial ρ termination factor is a hexameric protein, and catalyses unwinding of the RNA:DNA hybrid at C-rich regions, releasing the growing mRNA.[33]

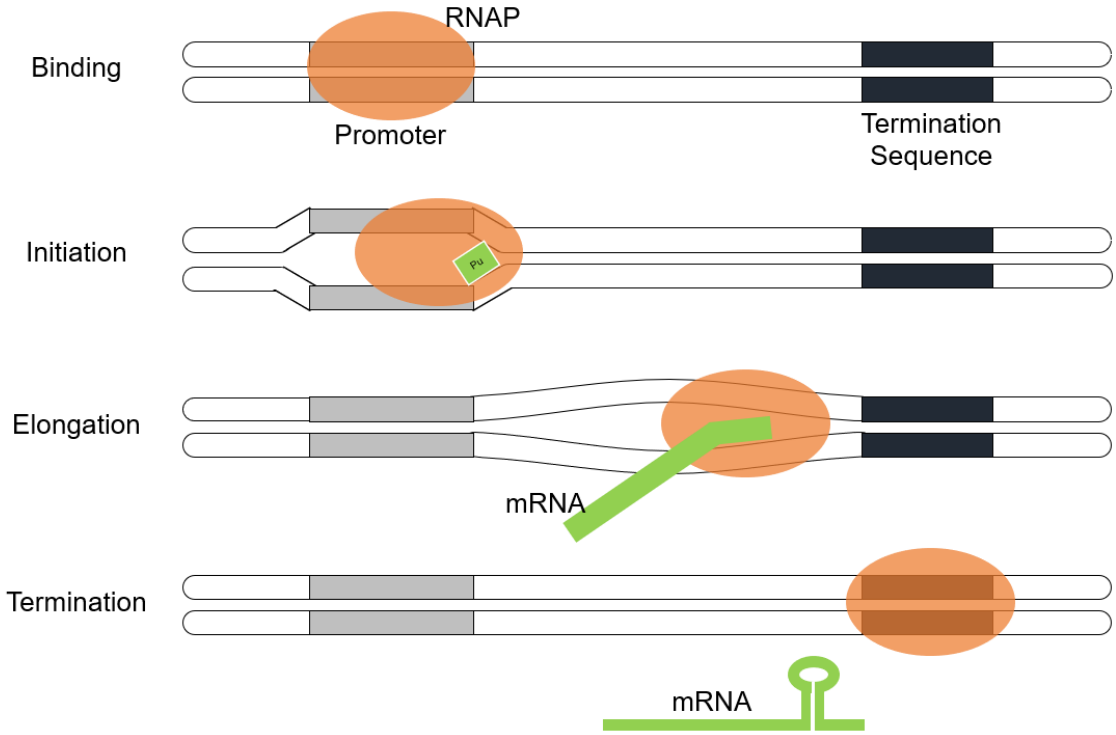


Figure 1-8: Simplified diagram showing the individual steps of transcription of mRNA from a DNA template.

In eukaryotes, the process is fundamentally similar, except that there are three RNA polymerases I, II and III, with RNAP I transcribing ribosomal RNA, RNAP III transcribing tRNA as well as other small RNAs, and RNA polymerase II transcribing all protein-encoding genes. All three RNA polymerases interact with their promoters *via* transcription factors; DNA binding proteins that recognise the promoter sequence, recruit the RNA polymerase and initiate transcription.[35] Eukaryotic promoters are more complicated and consist of a core promoter, and more distantly located regulatory elements. A common feature is the TATA box, which occurs -25 bp from the transcription start site. The regulatory elements can include response elements, which can promote binding or release of transcription factors following external stimuli such as heat or small molecules, or can be general in enhancing or silencing transcription.[33]

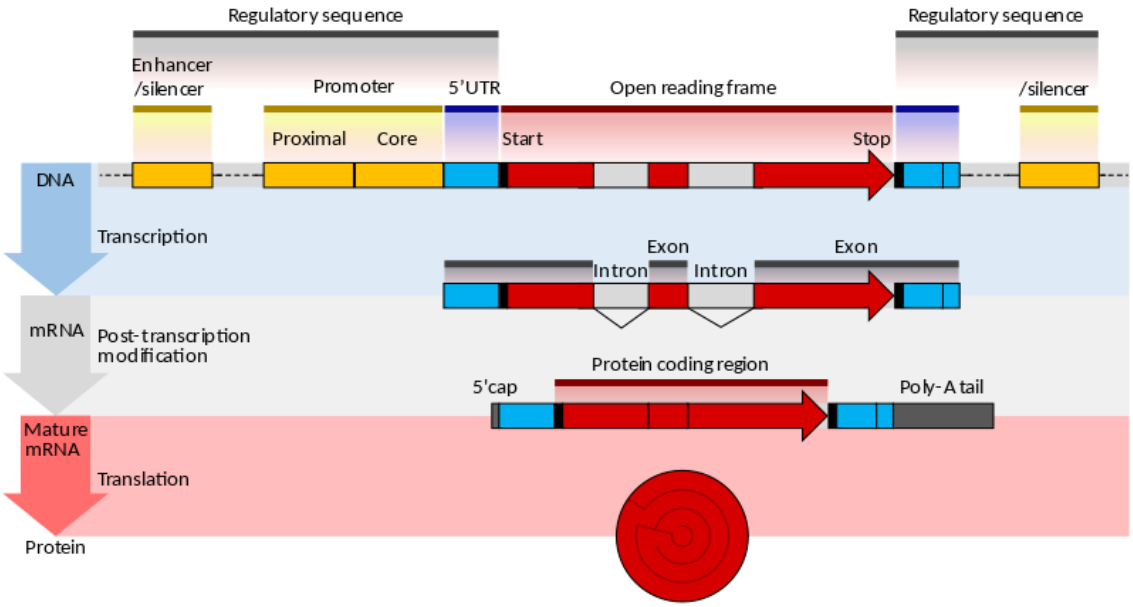


Figure 1-9: Transcription from eukaryotic DNA and the fate of mRNA.
Eukaryotic DNA transcription is controlled by a series of regulatory sequences. The transcribed pre-mRNA then gets processed into mature mRNA through removal of Introns, 5'-capping and the addition of a poly-A tail. Figure reproduced from "eukaryotic and prokaryotic gene structure" by Shafee and Lowe[36] (© 2017) under a creative commons licence (CC-BY 4.0).

The fate of mRNA also differs between prokaryotes and eukaryotes. The mRNA produced in prokaryotes is used directly for translation whereas eukaryotic mRNA undergoes further processing from a pre-mRNA state into mature mRNA (**Figure 1-9**).[37] The eukaryotic pre-mRNA gets capped with a methylated Guanosine *via* an unusual 5'-5' triphosphate linkage, which gets recognised by translation initiation factor eIF-4E.[38] Pre-mRNAs also acquire a poly-A tail at the 3' end, which promotes export from the nucleus, the translation of the mRNA and protects them from degradation.[39] The most complicated processing step of eukaryotic transcripts is splicing. Most genes in eukaryotes consist of coding-regions called exons and non-coding regions called introns. Introns are transcribed into the pre-mRNA and then subsequently excised to form mature mRNA in a process called splicing. This process can produce several mature mRNAs from the pre-mRNA and thus also different protein isoforms depending on splicing patterns, inclusion or exclusion of certain exons, as well as changes in ORF, and thus a whole host of different functionality from one pre-mRNA, including malfunctioning proteins.[40]

One particularly notable example of transcription is the T7 promoter system. Originally derived from bacteriophage T7, this promoter system is especially simple and has thus found widespread use in molecular and synthetic biology.[41] It consists of a single, 18 bp-long promoter sequence (TAATACGACTCACTATAG), which is recognised by T7 RNA polymerase.[42] RNA synthesis commences at the last base of the promoter sequence. RNA synthesis is then terminated at a T7 terminator sequence, or, if linear templates are used, can just 'fall-off' at the end, terminating transcription.[43] The T7 system is also commonly used in conjunction with regulatory mechanisms such as operators (Chapter 1.3.4.1).[44–46]

1.3.3 Translation

To convert mRNA into protein a protein/RNA complex called the ribosome needs to bind to the mRNA. At the 5' end of the mRNA is a stretch of nucleobases upstream of the start codon of the encoded protein called the untranslated region (UTR) or leader sequence. The UTR plays an important part in translation, as it contains regulatory sequences, binding sites for proteins that affect stability of the mRNA and translational regulation and most importantly the ribosome binding site. In bacteria, this ribosome binding site is known as the Shine-Dalgarno sequence (AGGAGG). In vertebrates, a similar sequence exists and is known as the Kozak sequence. At this binding site the small subunit of the ribosome binds, followed by an initiator aminoacyl-tRNA (Met in eukaryotes, formyl-Met in prokaryotes), that recognises the start codon (**Figure 1-10**, A). The large ribosomal subunit then associates, preparing for elongation (**Figure 1-10,** B). mRNAs are translated through a processive mechanism from 5' to 3' of the mRNA in the ORF of the gene. The ribosome has 3 distinct binding sites for tRNAs, the acceptor (A), peptidyl (P) and exit site (E). During elongation, aminoacyl-tRNAs with the corresponding anticodons to the mRNA enter the acceptor site (**Figure 1-10,** C). The large subunit then catalyses peptide bond formation between the growing chain and the new amino acid in the acceptor site; this new reaction transfers the growing peptide chain from the P to the A-site by forming the peptide bond from the amine on the aminoacyl-tRNA and carboxyl-group on the growing chain, which leads to peptides being assembled in an N to C-fashion (**Figure 1-10,** D). Accompanied by this reaction is translocation of the ribosome along the mRNA by one codon (**Figure 1-10**, E) and the movement of the new peptidyl-tRNA to the P slot. The spent tRNA is now in the exit slot and leaves the ribosomal assembly, prior to the cycle continuing.[33]

Termination of protein synthesis occurs once the ribosome encounters a stop codon in the A site. This codon is not recognised by a tRNA, but by release factors (**Figure 1-10**, F). These cause the ester bond of the peptide chain to the peptidyl-tRNA to be cleaved, the synthesised polypeptide then leaves the assembly (**Figure 1-10**, G) and the ribosome disassembles (**Figure 1-10**, H).[12]

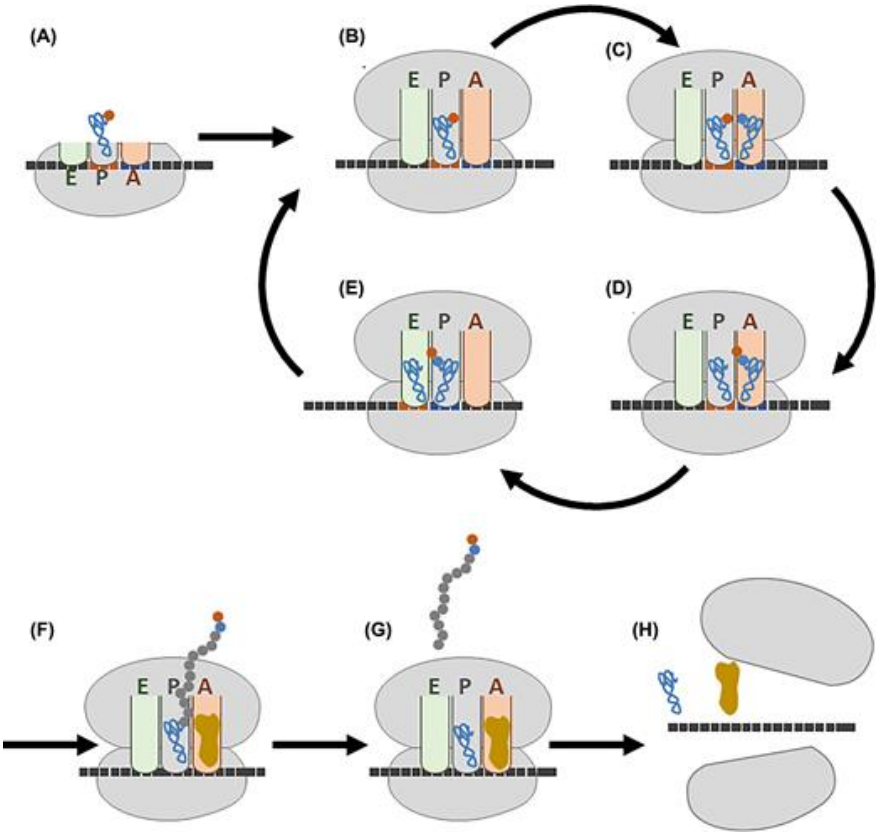


Figure 1-10: Schematic of protein synthesis.

The ribosome assembles on the mRNA and recruits tRNAs corresponding to the codons to assemble a polypeptide chain. Figure reproduced from “Understanding biochemistry: structure and function of nucleic acids” by S. Minchin and J. Lodge (© 2019) under a creative-commons licence (CC-BY 4.0).

1.3.4 Modulation of Gene Expression

Gene expression from the DNA is a tightly regulated process, as lack or overabundance of certain proteins can be detrimental to the organism.[47] The precise regulation of which RNA and protein is expressed at which timepoint is therefore crucial to the existence and survival of the organism. The exact expression levels of RNA (the transcriptome) and protein (the proteome) of a cell also determine the function of that cell, such as a neuron or muscle cell.[48] Control of gene expression can occur at varying stages, either directly at the transcription level, through control of RNA processing, RNA transport and localization, control of translation by the ribosome as

well as through control of mRNA degradation and control of protein activity. Among those, transcriptional control is most paramount for cells, as it is the only control mechanism that does not synthesise superfluous intermediates and is consequently the tightest control mechanism.[48] From a medicinal standpoint, RNA processing and translational control as well as mRNA degradation control are the most important, as these processes can be regulated by therapeutic nucleic acids.[49] For this reason, the focus of this chapter will be on transcriptional control and translational control using nucleic acids.

1.3.4.1 Modulation though DNA-binding proteins

In prokaryotes, the genes encoding for all components of a particular metabolic pathway are often under the control of a single promoter and form a gene cluster, which then are co-transcribed into a single polycistronic (multiple-gene-containing) mRNA, from which all components will be translated and can therefore be regulated simultaneously.[50,51] In eukaryotes, functionally related genes can be often found dispersed across the genome, though with recent acquisition of genomic data, gene organisation has also been found, but the mechanisms underlying are different.[52] In prokaryotes, the most common mechanism for regulation of gene expression is through the use of operators. Operators are regulatory DNA sequences adjacent to the promoter and preceding a gene cluster, with the combination of promoter, operator and polycistronic DNA being called an operon. Interactions of regulatory proteins with their respective operators can then control transcription from this promoter, and many regulatory proteins regulate more than one operon.[51] The operators found within can be classified into activators and repressors. Expression of genes without such regulation is called constitutive expression, and often includes the regulatory proteins.

Repressors are the simplest mechanism of transcriptional control. The repressor protein binds to its DNA target site and sterically blocks access of RNA polymerase to the promoter. These repressors are regulated by chemical or physical signals, for example through binding of small molecules, which causes a conformational change in the protein, that either disables or enables binding to the DNA target site.[51] Increased transcription in response to a particular signal is called induction, whereas decreased transcription is called repression.[33] Examples of such are the *lac* operon

and the *trp* operon, respectively. In the *lac* operon, canonically, the lactose-processing enzyme β-Galactosidase (β-Gal) is encoded. In the absence of lactose this enzyme is basically absent inside the cell, as the lac repressor *lacI*, which is constitutively expressed, is bound to the operator, preventing elongation during transcription. This form of repression is called negative regulation. In the presence of lactose, however, expression is induced, as the small molecule binds to the repressor, causing a conformation change in the protein and thus dissociation from the DNA. As β-Gal processes the lactose present over time, this then causes the inducer to re-bind to the DNA, which is called co-repression. Non-hydrolysable lactose mimics such as isopropyl-β-D-thiogalactopyranoside (IPTG), however, act basically as a non-reversible ON-switch, causing permanent dissociation of the *lac* repressor.[33]
The inverse is true for the *trp* operon. The genes downstream of the *trp* operon synthesise tryptophan. If sufficient tryptophan is produced, the Trp repressor, activated by tryptophan, binds to the operator site, preventing further transcription of tryptophan biosynthesis genes.[51]

Activators, on the other hand, operate differently. The activator serves a role in accelerating the kinetics of transcription, thus stimulating gene expression.[53] Many activators accelerate the rate of RNA polymerase binding, whereas others accelerate DNA unwinding or promoter clearance. Activators often bind to DNA sites upstream near the -35 element of the promoter and make favourable interactions with the RNA polymerase but can sometimes be found far upstream or even downstream. The most well-studied activator is the cyclic adenosine monophosphate (AMP) receptor protein, which binds as a dimer to sites -41 and -61 bp from the transcription initiation site. This protein then interacts with a specific subunit of the RNA polymerase holoenzyme, bringing it into close contact with the DNA, catalysing the formation of the closed promoter complex and thereby accelerating transcription initiation.[54]

Eukaryotic transcriptional regulation, however, is fundamentally more difficult, due to the organisation of the DNA on histones to form nucleosomes, which then form chromatin. These nucleosomes repress gene expression by sterically hindering access of the polymerase to the relevant genes. To regulate transcription and overcome nucleosome repression, two regulation steps are employed: histone-modifying enzymes, that loosen the interaction of the DNA with the histone, as well as

chromatin-remodelling complexes, rearranging the chromatin so that the relevant genes are accessible.[33] Histones can be modified in various ways, by lysine acetylation/deacetylation, by methylation and demethylation of lysine or arginine or phosphorylation. Histone acetylation and phosphorylation reduce the positive charge, disrupting electrostatic interactions with the DNA and thus leading to a less compact structure, facilitating DNA access. In addition, the binding of chromatin-associated factors is modulated, predominantly through methylation/demethylation.[55]

1.3.4.2 Gene Regulatory Nucleic Acids

Antisense oligonucleotides (ASOs) are short, synthetic nucleic acids. In 1978, Zamecnik and Stevenson first showed that such short oligonucleotides can inhibit replication of Rous sarcoma virus *in vitro.*[56] It has been established that ASOs act by directly targeting sequence-complementary RNA. Since then, ASOs have gained a lot of attention as pharmaceuticals, as they target the RNA rather than the protein, which allows for the treatment of diseases involving classically 'undruggable' targets, while also being highly specific to the targeted RNA sequence.[57]

ASOs modulate gene expression through two different mechanisms: target mRNA degradation (**Figure 1-11**, a), or steric block (**Figure 1-11**, b-e). The first mechanism operates through an enzymatic process (**Figure 1-11**, a). The endogenous enzyme Ribonuclease H (RNase H) recognises the DNA:RNA hybrid duplex formed between DNA-based ASOs and the target mRNA, through binding of the duplex *via* the DNA phosphate backbone in an positively charged groove found within the enzyme[58] and catalyses the phosphate hydrolysis of the mRNA backbone *via* a bound divalent cation (Mg^{2+}, Mn^{2+}).[59] Due to the cleavage induced at the ASO binding site within the RNA, the mRNA cannot be effectively translated, as the individual fragments are lacking the 5'-cap[38] or poly-A tail,[39] respectively, and therefore the gene is silenced. Notable is that RNase H is active both in the cytoplasm as well as in the nucleus, enabling the targeting and destruction of pre-mRNA as well as long non-coding RNAs, that are less accessible or targetable by other technologies and mechanisms.[60,61]

In contrast to this, steric blocking ASOs are oligonucleotides that are designed to bind to the target RNA transcripts with high affinity, but without eliciting an RNase H

response, and hence cause no RNA degradation. Uncharged oligonucleotides, such as peptide nucleic acids (PNAs) and phosphorodiamidate morpholino oligomers (PMOs) are thus often employed, as they have a neutral backbone, which does not elicit RNase H binding, but strongly bind to the target, while also providing additional benefits, such as nuclease stability.[62,63]

Alternatively, modifications on DNA such as locked nucleic acids (LNAs) or 2'OH-modifications improve target binding and nuclease stability, but also reduce RNase H activity, and can completely abolish activity if used in high enough amounts in the ASO.[64,65]

Steric blocking ASOs mask specific sequence stretches in the target by strongly binding to it, and therefore blocking interactions with the RNA. The most widely used application of such steric blocking ASOs is in the modulation of splicing of pre-mRNA (**Figure 1-11**, b). Through blocking of the pre-mRNA at splicing signal sequences, and hence making it inaccessible to the spliceosome, exons can be skipped. Such splicing alterations have, for example, been used in the rescue of dystrophin production through restoration of the correct reading frame *via* exon skipping in Duchenne's Muscular Dystrophy, leading to truncated, but functional protein.[66] The same technology can also be used to disrupt translation of a target gene through exon skipping, a process called splice corruption, leading to nonsense-mediated decay of the mRNA.[67] As exon exclusion and inclusion are responsible for proteomic diversity, the exon skipping approach may also be used for isoform switching, reducing expression of harmful and promoting expression of beneficial forms of a protein.[61] Steric blocking ASOs have also been demonstrated to directly inhibit translation initiation by binding to the start codon (**Figure 1-11**, c),[68,69] inhibit upstream ORFs (uORFs)[70] and thus upregulate protein expression (**Figure 1-11**, d),[71] inhibit nonsense-mediated decay by preventing assembly of exon junction complexes[72] or modulate polyadenylation at the 3' end to modulate mRNA stability (**Figure 1-11**, e).[73]

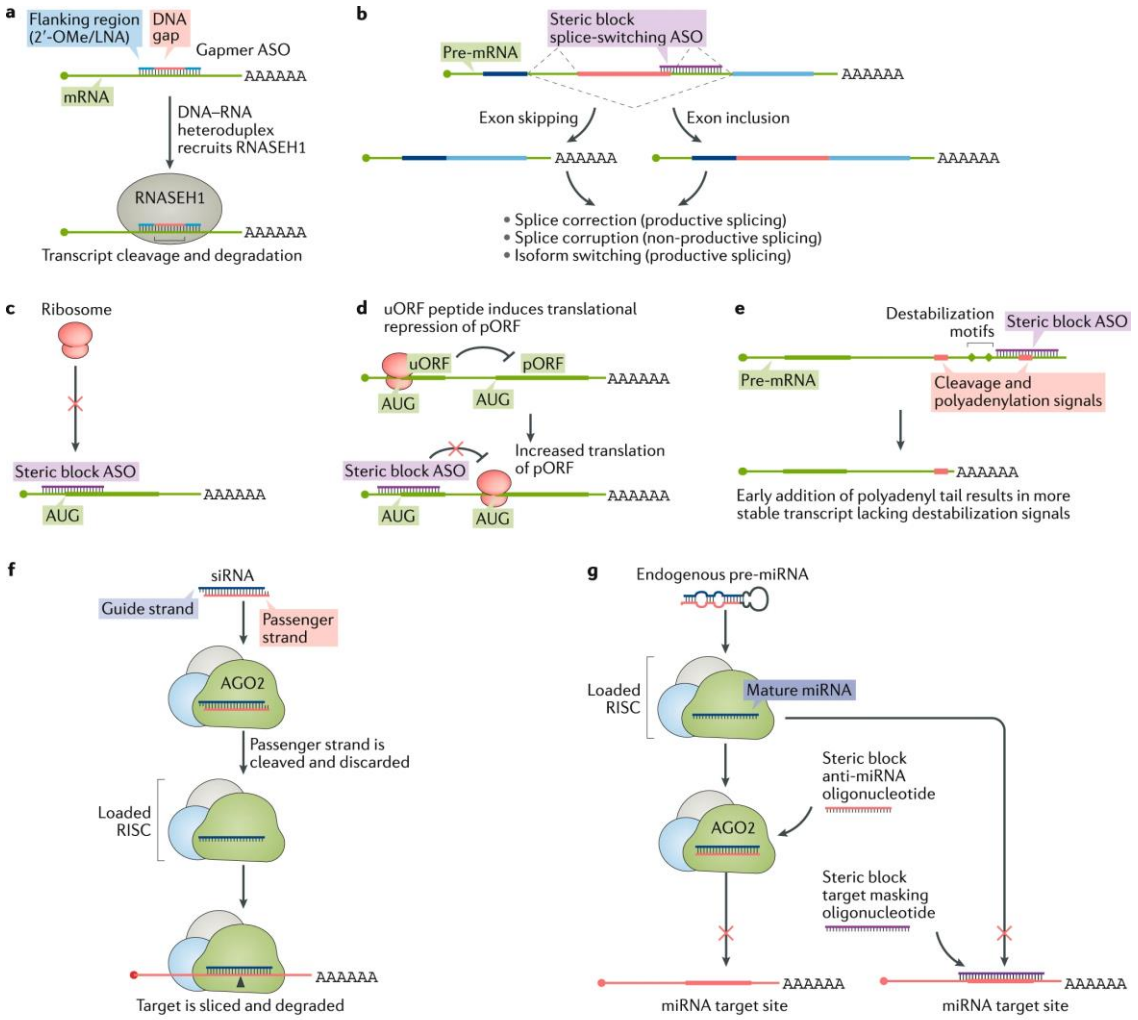


Figure 1-11: Mechanisms of gene regulation *via* small nucleic acids

a) RNase H-mediated degradation of mRNA through recognition of an ASO-mRNA duplex. b) Blocking of Exon regulatory elements by an ASO to mediate splicing. c) Steric blocking of the translation start site by an ASO to prevent ribosome assembly. d) Steric blocking of a uORF by an ASO to increase translation from pORF. e) Steric blocking of a destabilisation signal by an ASO resulting in improved stability of resulting mature mRNA. f) siRNA uptake into AGO2 and RISC-mediated mRNA degradation. g) Blocking of endogenous RNAi through complementary antimir ASO to prevent mRNA degradation. Reproduced and cropped from 'Advances in oligonucleotide drug delivery' by Roberts *et al*.[61] (© 2020) with permission from Springer Nature.

Another gene regulatory mechanism on the translational level is RNA interference (RNAi). In 1998, Fire and Mello identified that short, double-stranded RNA (dsRNA) molecules can interfere with the translation process in *Caenorhabditis elegans*.[74] It was later shown by Elbashir, Caplen *et al*.[75,76] that 21-22 nt dsRNA could induce gene silencing in mammalian cells. Since then, these small, interfering RNA (siRNA)

molecules have become a vital tool in regulation of gene expression and this process has been termed RNAi.

The process of RNAi is more complicated than for ASOs. One of the strands of the double-stranded (ds) siRNA (the antisense strand) is complementary to the target mRNA, and the other strand is called the passenger, or sense strand. The siRNAs get taken up by the argonaute 2 protein (AGO2) as part of the RNA-induced silencing complex (RISC), the passenger strand is discarded, and the antisense strand guides the complex to the complementary target site in the mRNA transcript. At this position, cleavage (or 'slicing') of the mRNA occurs, catalysed by AGO2, which results in silencing of this gene (**Figure 1-11**, f).[77]

The most classical siRNAs consist of a short 19+2mer duplex structure (i.e. a duplex of two 21 nt long RNA strands that have a 19 nt long complementary region and 2 nt overhangs at the 3' termini). However, dicer-substrate RNAs, that have a short hairpin and mimic the endogenous microRNAs (miRNAs) are also often used due to their higher stability and activity, and because they can be expressed from plasmids inside cells.[78] miRNAs themselves are endogenous RNAi triggers and involved in several physiological processes.[79–82] These miRNAs (and their synthetic counterparts) get processed by two RNase enzymes, Dicer and DROSHA, which form the active siRNA.[83–85] These often only bind with partial complementarity to the target and induce silencing *via* a slicer-independent mechanism.[86,87] As miRNAs are also involved in a number of diseases,[88–90] inhibition of miRNAs by binding of a complementary ASO to the RNA in the RISC,[91] and thus sterically blocking them from accessing the mRNA, is also an approach in regulating RNAi, and such ASOs are called anti-miRs or antagomirs (**Figure 1-11**, g).[92]

To improve pharmacological properties such as enhanced target binding, and improved cellular uptake, a cornucopia of modifications are used on ASOs and siRNA. Chemical modifications on the nucleic acid backbone, the ribose sugar and the nucleobase have been extensively employed to enhance delivery, stability and target binding.[93] LNAs, as mentioned above, are for example heavily employed in RNase H-active ASOs. LNAs 'lock' the ribose unit into the C3-endo conformation and this preorganisation causes improved target binding and increases nuclease stability.[94–96]

As this modification also reduces RNase H activity, it is employed in hybrid or chimeric oligonucleotides, where the first and last few nucleotides are replaced by LNA, with DNA in between to keep RNase H activity, forming a gapmer. Similarly, modification of the 2' position with alternative groups such as 2'-OMe or 2'-F improve target binding and nuclease resistance, while again reducing RNase H activity, and are thus often employed in exon skipping ASOs.[97]

Probably the most widely utilised modification in antisense therapeutics is the phosphorothioate (PS) linkage. Replacement of a non-bridging oxygen atom in the phosphate backbone with sulfur yields a PS linkage, which only marginally reduces target binding affinity and increases the size of the backbone, but improves cellular uptake and nuclease stability[98] and is thus commonly used in ASOs,[99] and less so in siRNA as it reduces their activity.[100] As already mentioned above, uncharged PNAs and PMOs are often used for non-RNase H ASOs, as they still provide strong target binding as well as nuclease stability, but do not elicit an RNase H response.[62,63,101,102] Chimeric gapmers have also been prepared that incorporate uncharged amide linkages into the flanking regions of the oligonucleotide, which improve nuclease stability, while keeping a phosphate-linked core to elicit an efficient RNase H response.[103]

Nucleobase modifications have also been investigated to improve their activity and stability. Pyrimidine methylation at the C5 position, yielding 5-methylcytidine and 5-methyluridine/ribothymidine, has been used in ASOs as it increases target binding by ~0.5 °C per substitution[93] and is used in oligonucleotides currently under development.[61] The increase in stability stems from the ability of the methyl-group to stack between the nucleobases in the major groove. The 5-methylcytidine additionally also reduces immunostimulation.[104] These methyl-substituents are, however, not employed on siRNA as they reduce siRNA activity.[93]

Other modified nucleobases for improved antisense therapeutics have also been developed, but so far have not seen widespread use. 5-propyne-modified pyrimidines allow for an even stronger duplex than methylation, likely due to π-stacking interactions between the acetylenes in the major groove.[105] Phenoxazine-based nucleobases have also been developed to replace C that have an appended amine

via a short linker. These improved the planar surface area and thus improved π-stacking within the duplex,[106] while the appended amine allowed for additional hydrogen bonds to G, yielding unparalleled increases in duplex stability.[107,108] Similarly, an aminopropyl-modified Guanosine was prepared, showing enhanced binding properties due to the amine interacting with the phosphate backbone in the major groove.[109]

To enhance the delivery potential of therapeutic nucleic acids, ASOs and siRNA are also often conjugated with various moieties that promote cellular uptake or allow cellular targeting. These modifications include lipids, such as cholesterol,[110–112] peptides,[113–116] aptamers,[117] or sugars, such as *N*-acetylgalactosamine.[118,119]

1.4 Cell-Free Protein Synthesis

Cell-free Protein Synthesis (CFPS) is the production of functional protein from a DNA template or corresponding mRNA *in vitro*, without the use of living cellular organisms. CFPS systems combine cellular lysates or purified components with various substrates to generate and activate cellular processes in a tube, without the constraints of having to sustain life, which allows for the simplified study of fundamental processes in biology and to produce otherwise difficult to obtain protein. The technique of using cellular lysates to unravel biological phenomena was used by Nirenberg and Matthaei in 1961, where they used an *Escherichia (E.) coli*-derived cellular lysate to discover the link between mRNA and protein sequences and the genetic code.[25] Since then, CFPS has seen growing interest as a platform to produce protein for downstream applications as well as a tool in biology and biotechnology, to study fundamental processes, develop synthetic biological systems and engineer bio-based devices.

CFPS provides several benefits compared to the traditional cellular protein synthesis (**Figure 1-12**). In traditional cellular protein expression, a DNA plasmid encoding for the protein of interest needs to be brought into the cellular organism (so-called transformation for bacterial cells, or transfection for mammalian cells). The resulting organisms then need to be grown in a suitable nutrient medium and gene expression often induced at a certain timepoint to ensure high yields. The cells then need to be harvested by centrifugation, lysed and the protein separated from cellular debris and other, native proteins, which can be a long and laborious process. In contrast, for cell-free expression of protein, a cellular extract is prepared by growing up the organism of interest, which is then harvested, lysed and processed to remove endogenous genetic material and cellular membranes to generate a CFPS system. To this, the desired DNA templates can be added and protein expressed and purified. CFPS allows for rapid library creation and prototyping of lots of different genes in parallel, often from linear PCR products, and it eliminates transformation of plasmids, work under sterile conditions and the task of sustaining life.[120] Many cell-free extracts are able to be dried and reconstituted when needed, allowing for easy storage and portability in addition to low temperature storage,[121,122] whereas cellular systems cannot be dried and cellular viability decreases over time even at very low

temperatures.[123] Another benefit of CFPS over *in vivo* protein synthesis is also the ease of expression of difficult proteins, such as membrane proteins (MPs), one of the hardest class of proteins to express and purify *in vivo*. Conventional problems, including translocation of MPs to the membrane, proteolytic degradation and toxicity to the host organism upon membrane insertion are eliminated in CFPS, enabling their preparation.[124] Lastly, the purification of prepared proteins is often facile, as the majority of cellular debris has already been removed, and affinity chromatography can rapidly yield the desired protein in high purity. Considering these benefits, CFPS has thus become the preferred method for high throughput protein study, evolution and preparation and an important tool for synthetic biology.[125]

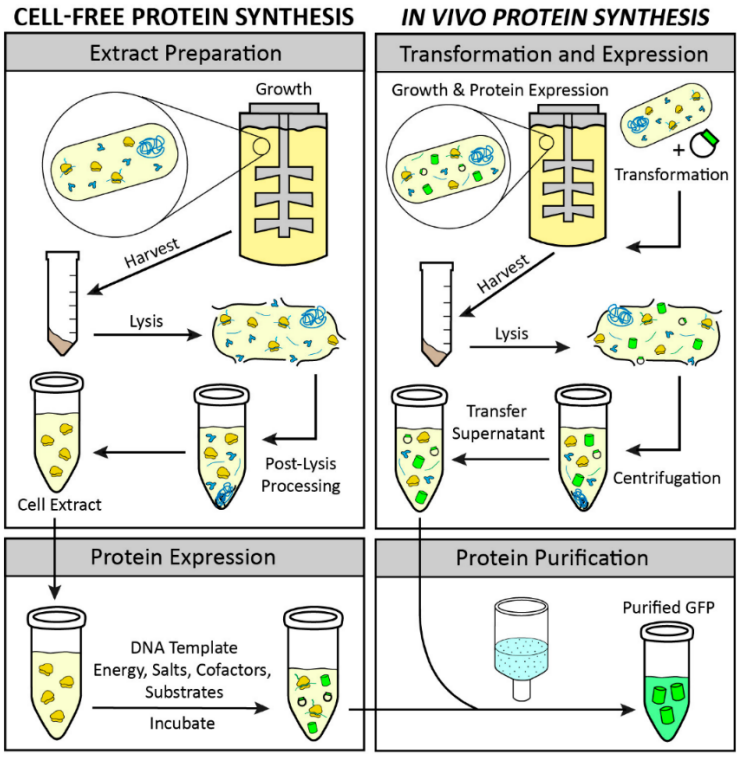


Figure 1-12: Comparison of Cellular and Cell-Free Protein Expression.

Figure reproduced from 'A User's Guide to Cell-Free Protein Synthesis' by Gregorio et. al[126] (© 2019) under a creative commons licence (CC-BY 4.0)

1.4.1 Lysate-based CFPS

The vast majority of CFPS systems are based on cellular lysates. These lysates can be prepared from a large number of organisms and can either be coupled (i.e. are capable of transcription and translation, also sometimes referred to as 'one-pot CFPS') or uncoupled (are only capable of translation), though with many uncoupled systems

having the option of addition of transcriptional machinery (most commonly derived from bacteriophages T7 or SP6).

The most widely used CFPS systems (**Figure 1-13**) are lysates from *E. coli*,[127,128] wheat germ,[129,130] *Saccharomyces cerevisiae (S. cerevisiae)*,[131,132] Insect cells,[133,134] rabbit reticulocyte,[135–137] Chinese Hamster Ovary (CHO),[138] and HeLa cells.[139] These systems are well-optimised and often commercial. Lesser used systems are for example derived from *Vibrio natriegens (V. natriegens)*,[140] *Arabidopsis callus*,[141] Tobacco BY-2[142] or *Bacillus subtilis*,[143] among others.

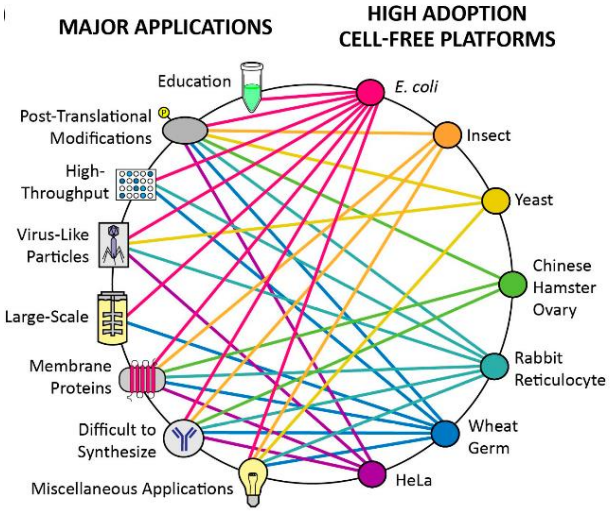


Figure 1-13: The most commonly used cell-free platforms and their applications.
Figure reproduced and cropped from 'A User's Guide to Cell-Free Protein Synthesis' by Gregorio et. al[126] (© 2019) under a creative commons licence (CC-BY 4.0)

The choice of expression platform is based on an individual's needs in terms of yield, scalability, accessibility, and production of the protein of interest. Modern systems offer high yields, fast turnover, ease of use and accessibility, and many are commercially available, enabling the researcher to choose the right system for the required application.[144] For example, large scale production is usually performed in *E. coli*-based and wheat germ-based CFPS and to a lesser degree in *V. natriegens*. These systems have high yields and exist as coupled systems, allowing expression directly from a DNA template. *E. coli*-based systems are also often preferred for their speed in production, due to the fast doubling time of *E. coli* and simple extract preparation, taking usually 1-2 days overall. In contrast, wheat germ and rabbit reticulocyte platforms can take up 9 days for production, particularly if treatment of

animals is needed.[126] For post-translationally modified protein production, *E. coli* systems may not be initially suitable, as eukaryotic cells lack endogenous microsomes and have only a limited set of post-translational modifications (PTMs) possible, and mammalian cell extracts (CHO, HeLa or rabbit reticulocyte), despite being lower yielding, may be a more suitable option.[145,146] A lot of work has gone into developing *E. coli* systems that are capable of various PTMs, however, due to their high yield and ease of production. Supplementation of *E. coli*-based systems with glycosylation machinery allowed for production of glycoproteins,[147–149] and redox conditions could be tuned to make disulfide bonds feasible.[150]

1.4.2 CFPS from Purified Components

A unique approach to CFPS systems is the reconstitution of functional transcription/translation from individually prepared components. More than 100 molecules participate in this process, many of which have been individually prepared for structural and functional studies. The first attempts at reconstituting protein expression was in 1977 by Weissbach.[151] Using purified components, they attempted to express β-Galactosidase, but the results were unsatisfactory, with synthesis rates of only 1% *versus* lysate, which they attributed to missing components as well as the difficulty of obtaining large amounts of purified aminoacyl-tRNA synthetases, which made it necessary to modify the system. Another attempt by Ganoza *et al.*[152] used pre-charged aminoacyl-tRNAs and purified translation factors. The system worked, though with low yields due to no recycling of the tRNAs taking place. Later attempts by Pavlov *et al.*[153,154] supplemented aminoacyl-tRNA synthetases, improving the performance of *in vitro* protein production.

The biggest success was with the introduction of the ‘protein synthesis using recombinant elements’ (PURE) system by Ueda and co-workers (**Figure 1-14**).[155–157] This system consists of purified translation factors recombinantly expressed in *E. coli*, including 20 aminoacyl-tRNA synthetases, initiation, elongation and release factors, ribosome recycling factors, methionyl tRNA formyltransferase and pyrophosphatase, all bearing a 6x Histidine (His)-tag. This is combined with ribosomes, recombinant T7 RNA polymerase, an ATP-generating catalytic module, tRNAs as well as the amino acids and NTPs required.[158] While it requires overexpression and purification of each component, it is highly defined and modular, allowing for the addition and exchange

of individual components, such as chaperones[159] or a disulfide bond enhancer[160] if needed. It is also lacking any protease or nuclease activity often observed in cellular extracts, therefore allowing for the use of linear PCR products as templates without the addition of Gam protein to protect the blunt-ended DNA,[161] or addition of protease inhibitors.[162] Another advantage of the PURE system is also the ease of purification of the desired protein. Due to all synthesised components being His-tagged, ultracentrifugation to remove the ribosome and small molecule components, followed by affinity chromatography rapidly yields the desired protein in high purity.[163] While the PURE system is very time-consuming to prepare, it is also distributed commercially by New England Biolabs (NEB) under the name PURExpress™ as well as by Cosmo Bio under PURESYSTEM, making it highly accessible. However, the kits are expensive compared to extract-based CFPS and also give lower yields.[164]

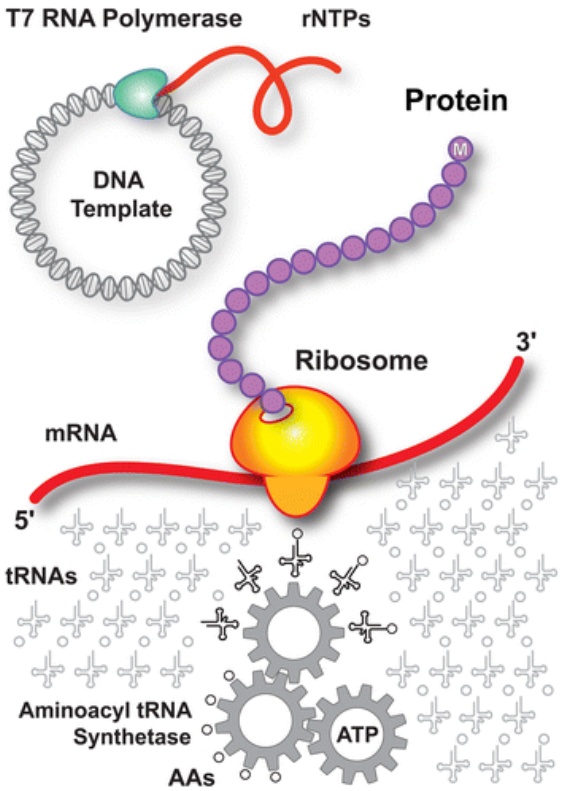


Figure 1-14: The PURE Cell-Free Expression System.

The system includes T7 RNA Polymerase, components for NTP regeneration, aminoacyl tRNA synthetases and tRNAs, and translation machinery comprised of ribosomes, elongation factors, and release factors. Figure reproduced from 'Cell-free protein synthesis: the state of the art' by J. W. Whittaker[158] with permission from Springer Nature.

1.4.3 Applications of CFPS

Besides its use as a tool to express a large variety of proteins, CFPS is widely used in biology, biotechnology and synthetic biology for a variety of applications.[144,165,166] Its use stems from the simplicity, and high-throughput characteristics without the need for sustaining life, allowing for rapid assaying of the system in question. Its modularity also enables fine-tuning of the system for desired applications and allows for exact quantities of reagents to be added and outputs measured quantitatively.

CFPS thus finds widespread use in the prototyping of genetic parts and machinery. Such prototyping studies have included the elucidation of DNA replication in *E. coli* and *Xenopus* lysates,[167,168] the role of mRNA poly-A tails in *S. cerevisiae* lysate and cells[169] as well as siRNA biogenesis in tobacco lysate.[170] More recently, the PURE system was employed to directly probe the dynamics of transcription and translation in bulk as well as in synthetic cells.[171] Other demonstrations of prototyping include the testing of complex regulatory systems such as quorum sensing promoters,[172] riboregulators[173] and synthetic riboswitches.[174,175]

Following on from this, genetic circuits can then be assembled within such systems with high precision. CFPS has found use in the study of interactions of genetic parts, forming genetic control networks or ‘circuits’. As the quantities of each component can be controlled precisely, the relative contributions of all components can be tuned. Using this approach, logic gates,[176,177] cascades[127,178,179] and feedback loops[180,181] have been prototyped in cell-free systems.

CFPS has also found widespread use in biotechnological applications. CFPS-based biosensors have been developed to generate portable detection systems for pathogens, such as zika[182] and norovirus[183] and also for the detection of quorum sensing molecules,[184] and date-rape drugs.[185]

CFPS also has found use in the high-throughput prototyping of protein modifications. As mentioned previously, PTMs can be incorporated within cell-free systems. Studying PTMs in cells directly is difficult, as PTMs often are heterogeneous and specific to a certain locus within the cell.[186] In CFPS, the PTMs to be interrogated can be prepared

selectively and with high sequence specificity. This can either be done through incorporation of isotopically labelled amino acids, allowing for structural or quantitative proteomics using Nuclear Magnetic Resonance (NMR)[187,188] and Mass Spectrometry (MS),[189,190] or through incorporation of PTMs *via* non-canonical amino acids, which are well-tolerated in CFPS and have been used for example with phosphoserine.[191] Impressively, even more complex PTMs such as glycosylation could be probed in CFPS systems.[148,192]

Increasing the complexity of the system, encapsulation of a CFPS system can also be used to form synthetic cells,[193–196] allowing for a bottom-up approach towards studying cellular processes and complex biological phenomena. Through encapsulation in lipid bilayers, liposomes that mimic a cellular membrane can be created.[197,198] For a more rapid screening approach, aqueous water-in-oil droplets can also be formed, encapsulating the CFPS by aqueous droplet stabilisation in an organic phase.[199] These small compartments, while lacking the chemistry of a membrane, still allow for the investigation of biological systems in confinement. Lastly, polymersomes, self-assembled hollow spheres comprised of amphiphilic copolymers (including proteins), are also often used as synthetic cells.[200]

These synthetic cells have successfully been utilised to recreate biological phenomena. Gene expression could be activated using light inside synthetic cells, allowing for the expression of fluorescent proteins as well as membrane pores.[201,202] Cellular communication could also be recreated in synthetic cells.[203] Through diffusion of small molecules through nanopores or direct membrane permeation, gene expression could be activated in sender and receiver cells through the interaction with operators.[204] Gene expression was also activated through a membrane-permeable quorum sensing molecule, which activated the expression of a membrane pore inside synthetic cells, allowing for diffusion of glucose to receiver proteinosome cells, where an enzymatic cascade was activated.[205] Similarly, in our group, quorum sensing could be recreated between synthetic cells and bacteria, through light activation of gene expression in a sender synthetic cell, which then synthesised a membrane-permeable quorum sensing molecule, activating gene expression in the receiver bacteria (**Figure 1-15**).[206]

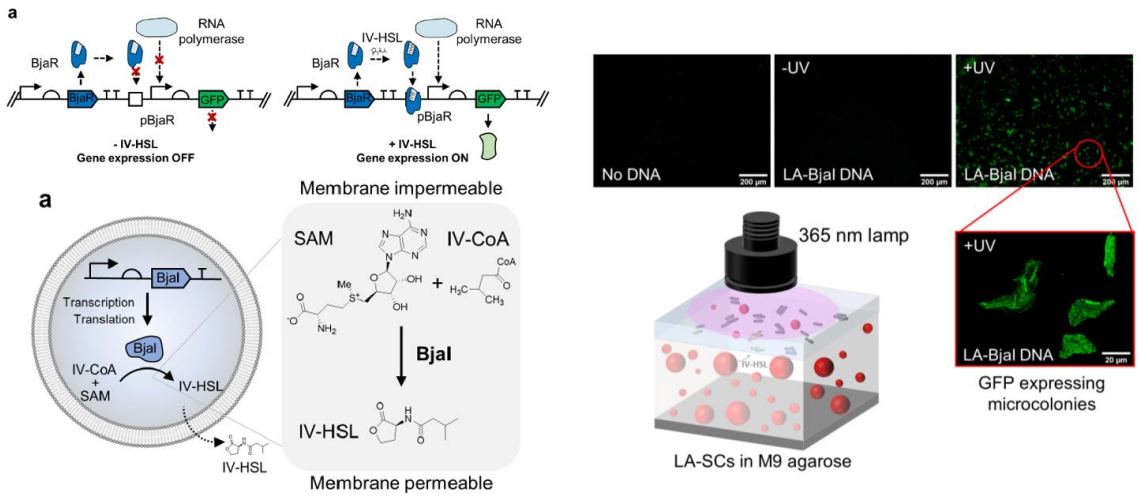


Figure 1-15: Artificial, light-activated quorum sensing between synthetic cells and bacteria. UV irradiation triggers expression of BjaI, and thus production of IV-HSL, which can penetrate the membrane and diffuse to nearby bacteria, inducing gene expression. Figure reproduced and cropped from "Engineering cellular communication between light-activated synthetic cells and bacteria" By J. M. Smith *et al.*[206] (© 2022) under a creative commons licence (CC-BY-NC-ND 4.0)

More complex cellular phenomena are also recreated and investigated in synthetic cells. This includes DNA replication[207,208], cellular division through expression of a minimal divisome,[209] as well as lipid synthesis.[210] Synthetic cells also show promising applications in drug delivery through interactions with living cells as they are fully biocompatible.[211]

1.5 Photoremovable Protecting Groups

To gain control over biological systems, particularly in cells, light is a highly appropriate stimulus, as it can penetrate membranes and allows for remote application and tight control.[212] For this, modification of molecules with a photoremovable protecting group involved in a desired biological pathway is a highly explored avenue, as it renders the molecule inactive until irradiated, enabling the precise study and control of said pathway.[213] Photoremovable protecting groups (also termed photolabile, photoactivatable, photosensitive, or photocleavable protecting groups (PPGs)) are molecular motifs that can be removed by irradiation with light of an appropriate wavelength. First introduced by Barltrop,[214] Barton,[215] Woodward,[216] and Sheehan[217] in organic synthesis in the 1960s and subsequently applied to biological applications by Engels[218] and Kaplan[219] in the 1970s, photoremovable protecting groups have found widespread application in synthetic chemistry and biology.[220]

The reason for their widespread application, particularly in biology, is in the spatiotemporal control of their removal with a stimulus that is largely bioorthogonal (namely electromagnetic radiation), allowing for non-invasive release (or 'uncaging') of a substrate of interest.

Depending on the application, a good PPG in biology fulfils several of the following requirements:[220]

- Strong absorption wavelength well above 300 nm to not cause damage to the biological system, with more red-shifted PPGs being more desireable
- A clean and efficient photoreaction with high quantum yield of release (good on-state)
- A good caging ability, leading to low background levels of activity prior to photorelease (good off-state)
- Breakdown products of the PPG should be compatible to the system of interest (chemically inert, transparent to analysis)

A large number of PPGs have been developed over the years, ranging from photocleavage in the deep UV (phenacyl groups, $\lambda \sim 320$ nm)[221] and near UV/violet (2-nitrobenzyl-derived groups, $\lambda \sim 360$-400 nm)[222] to visible light PPGs spanning from

the violet into the deep Infrared (IR). These visible light PPGs are based on a number of different chromophore scaffolds, the most common of which are coumarins, boron dipyrromethenes (BODIPYs) and cyanines.[223]

1.5.1 2-Nitrobenzyl Photocages

The most commonly employed PPGs are derivatives of the 2-nitrobenzyl-group. Due to their simplicity in chemical structure as well as synthetic accessibility, they are the most widely used PPG and were the first PPG to be utilised in biology through phosphate-caged adenosine triphosphate (ATP) by Kaplan.[219]

The leaving group can directly be attached to the benzylic position, and allows for the rapid release of carboxylic acids,[216] thiols[224] or phosphates.[218,225] Alcohols and amines, however, as they are poor leaving groups (LGs), are usually not attached directly,[226] but instead as carbonates[227–229] and carbamates,[230] which are much better leaving groups, and decarboxylate into the desired compound.

A major limitation of nitrobenzyl-PPGs is that they absorb mostly ultraviolet (UV) light. UV light has limited tissue penetration[231,232] and has been shown to cause damage to biomolecules including DNA,[233–235] thus safer, more red-shifted alternatives are desired.[236] Among the most commonly employed nitrobenzyl-derivatives are 4,5-dimethoxy and 4,5-methylenedioxy 2-nitrobenzyl groups, also called nitroveratryl (NV) and nitropiperonyl (NP), respectively. These substituents on the benzene ring cause a bathochromic shift, allowing for activation at longer wavelengths up to ~400 nm, though they also cause a loss of quantum yield of release.[226]

1.5.1.1 Mechanism of Photocleavage

The mechanism of their photocleavage has been heavily investigated and is summarised in **Figure 1-16**. Irradiation causes the formation of an excited singlet state diradical, centred on the nitro-group, followed by Intersystem crossing (ISC) (Norrish Type II reaction). The photocleavage is then initiated by an intramolecular 1,5-benzylic H-atom transfer (HAT) to a nitro-oxygen. A hydrogen-shift then gives an aci-nitro intermediate. This intermediate can then undergo cyclisation, followed by release of the active species through beta-elimination and the formation of the 2-nitroso-benzyl

carbonyl as a by-product.[237–239] These nitroso-compounds however, are potentially toxic and strongly absorbing, and have been shown to inhibit enzymatic activity.[240]

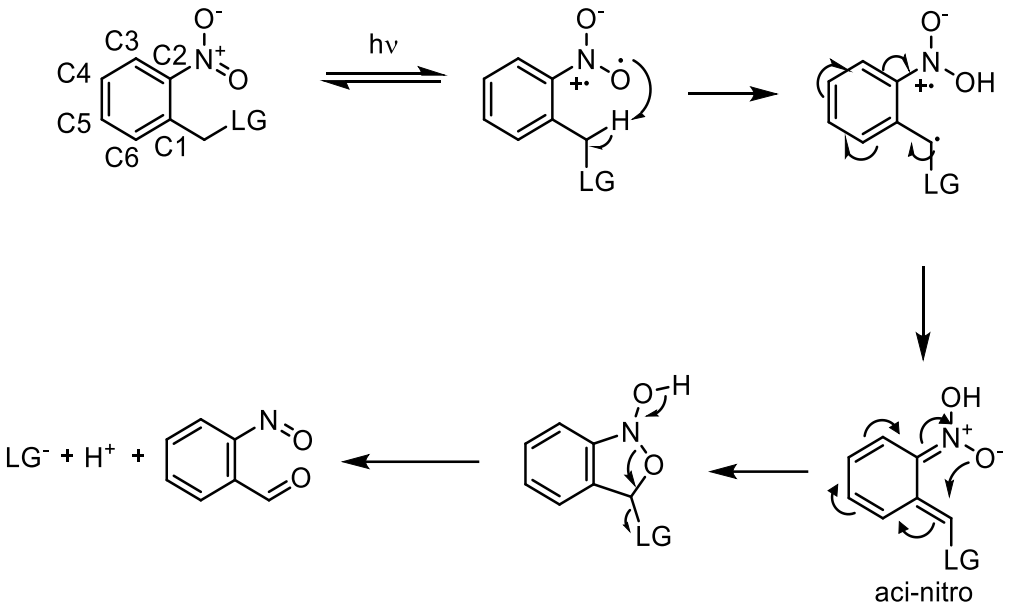


Figure 1-16: Mechanism of photocleavage of the parent nitrobenzyl-scaffold.
The photocleavage of nitrobenzyl-derivatives follows a Norrish Type II reaction. Generation of the diradical species upon excitation and HAT, followed by a cyclisation and fragmentation yields the uncaged product as well as the nitrosoaldehyde biproduct.

1.5.2 Coumarin-derived PPGs

Another commonly encountered PPG are coumarinyl-4-methyl (CM) derivatives and the first demonstration of their photoactivity was by Givens and Matuszewski[241] through photolysis of a 7-methoxycoumarinyl-4-methyl-caged diethyl phosphate. Coumarin-based PPGs are highly attractive, as they have large molar absorption coefficients, fast release rates, high stability and show fluorescence.

1.5.2.1 Improvement of Coumarin-Scaffold

A lot of work has gone into improving the originally used coumarin scaffold, as it already showed very beneficial properties. Modifications on C6 of the 7-alkoxycoumarin derivatives with alkoxy- or bromine substituents, for example, improved the scaffold by red-shifting up to 380 nm and improving aqueous solubility.[220]

Changing C7 from alkoxy- to dialkylamine substituents red-shifted the coumarin to up to 400 nm, while also improving aqueous solubility and large efforts have gone into improving this diethylaminocoumarin (DEACM) scaffold even further (**Figure 1-17**)

and this scaffold is now the most heavily used among the coumarins used as photocages. Changing from the common diethylamine substituent at C7 to azetidine or fused julolidine derivatives further allowed for improvement in photolysis rate through changing the H-bonding characteristics with surrounding solvent.[242]

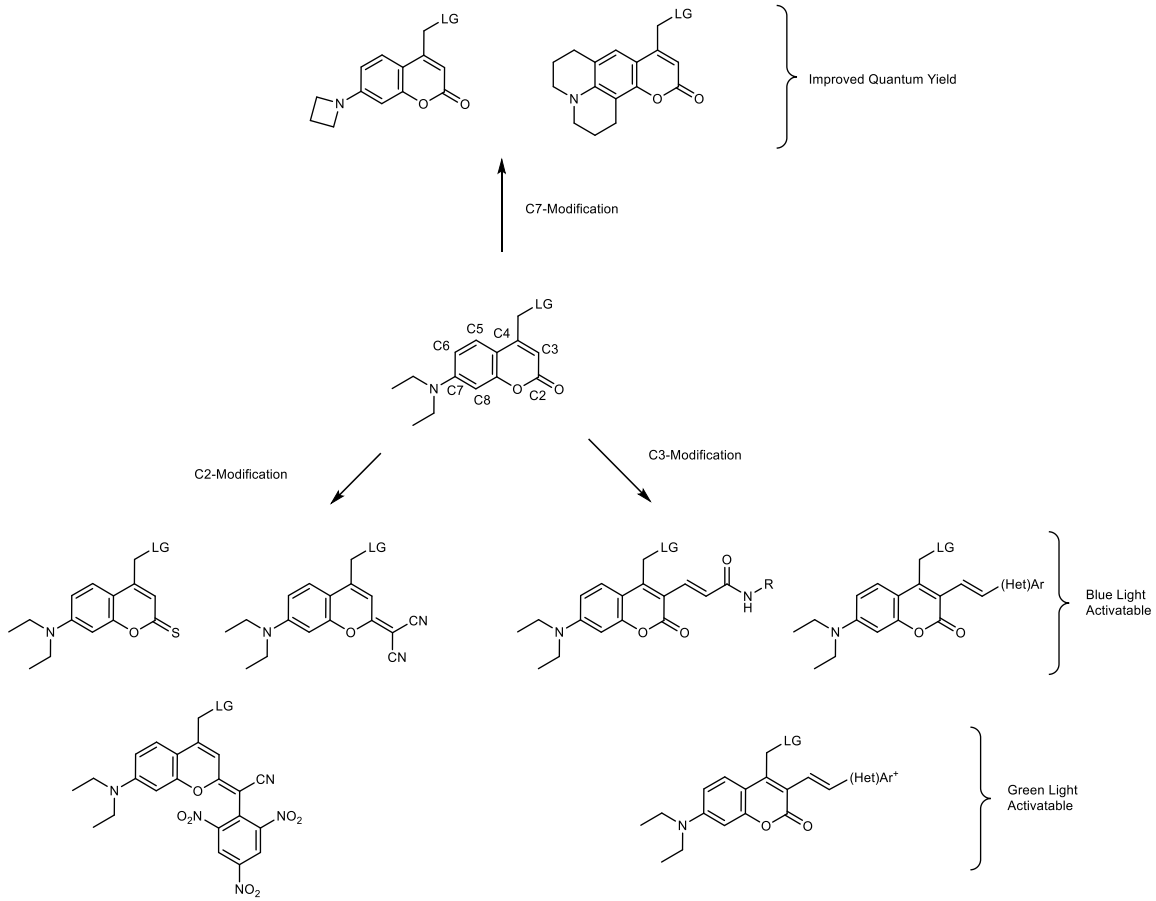


Figure 1-17: Summary of coumarin modifications and their effects on the photochemical properties of the coumarin scaffold

A widely investigated avenue is red-shifting the coumarin absorption for improved use in biological systems. One part of the scaffold that has been investigated for red-shifting and chromophore extension is the C=O bond at C2. Exchange of the oxygen for sulfur on a 7-diethylamino-4-methylcoumarin with a photocaged benzoic acid shifted the absorption maximum (λ_{max}) from 385 nm to 472 nm and with a larger uncaging quantum yield.[243] Exchange of oxygen for the electron-withdrawing dicyanomethylene group shifted the absorption maximum to ~490 nm, allowing for release of a cyclic peptide with green light.[244] The same dicyanomethylene-substituted coumarin system was shown to be able to be fine-tuned for improved quantum yield of uncaging or fluorescence by modifying the methyl group carrying the cargo.[245] This dicyanomethylene-substituted scaffold was also used to circularise and uncage a DNA

oligonucleotide with green light.[246] One cyano-group of this scaffold can also be exchanged for an aromatic ring. Substitution with a nitroaromatic group allowed for a red-shift up to a λ_{max} of 596 nm,[247] and substitution with an alkyl-pyridinium shifted it to a λ_{max} of 557 nm[248] and allowed for the release of the caged benzoic acid with green light in both cases.

Another position heavily investigated for red shifting is the C3 carbon. The C3 carbon allows for easy extension of the π-system through halogenation and Pd-cross-coupling, which has been used to modify the system with a number of vinyl and aryl substituents. This has been used to attach a benzonitrile derivative,[249] which shifted the absorption maximum to ~400 nm. An even larger red-shift was observed with styryl[250] and acrylate[249] moieties, to around 450 nm. These blue-light activatable coumarin derivatives already have found use in biology to release neurotransmitters[249,251] and in luciferase-induced biouncaging[252] and provide the basis for some of the work presented in this thesis.

Heteroaromatic vinyl substituents have also been used for modification at C3. Neutral, electron-withdrawing groups such as vinyl-benzoxazole and -benzothiazole gave a bathochromic shift up to 472 nm.[253] Cationic heteroaromatics, such as vinyl-pyridinium and -benzothiazolium groups provided the largest shift in absorption maximum up to 538 nm, allowing photorelease of appended cargo with green light.[254]

1.5.2.2 Mechanism of Photorelease

The general mechanism of photorelease from the C4-position is as follows (**Figure 1-18**): Following photoexcitation, the molecule relaxes to the lowest (π, π*) excited singlet state [CM-LG]. This is followed by radiationless decay to its ground state, fluorescence or heterolytic C-LG bond cleavage, in line with Kasha's rule. The formed coumarin-4-methyl cation CM^+ can then undergo capture by present nucleophiles or solvent and releases the caged species from the ion pair.[255]

The cargo that can be released from coumarins ranges from carboxylic acids, sulfates and phosphates[246,255,256] and amides[257] to halides,[258] among others and can often

readily be prepared by esterification from the CM-alcohol or through an S_N2 substitution of a CM-bromide. Poor leaving groups such as alcohols and amines do not readily get released by the coumarin photocage, however.[220] In those instances, the cargo can be appended through a carbonate or carbamate linkage,[259] which after loss of CO_2 releases the alcohol or amine, respectively.

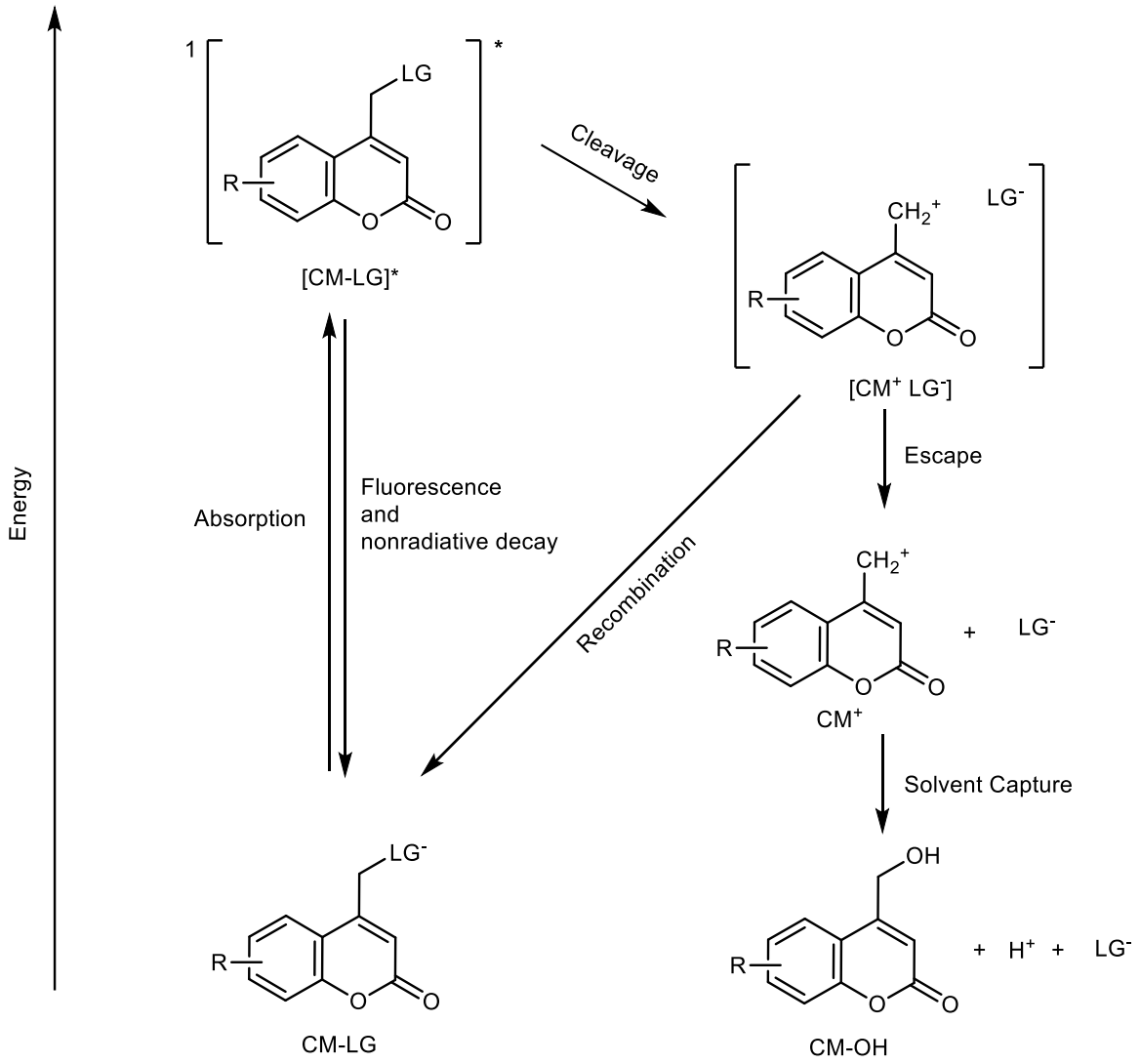


Figure 1-18: Generalised Mechanism of Photocleavage of Coumarin-PPGs

The coumarin with appended leaving group (CM-LG) gets excited by irradiation. The resulting excited state coumarin [CM-LG]* relaxes to its lowest energy singlet excited state S1. From this state, several pathways are possible. Fluorescence or nonradiative decay back to the ground state can occur, which are non-productive pathways for photouncaging. The excited state coumarin can also undergo heterolytic fission, resulting in bond cleavage between the CM and the leaving group (LG).

1.6 Light-controllable Gene Expression

Precise control of expression of genetic information has a wide range of applications, including in biological research, biotechnology, and medicine.[260] Being able to directly control the central dogma of biology by activating/deactivating transcription and/or translation and thus impacting biological function through applied stimuli is highly desirable, with applications ranging from controllable therapeutics and precision medicine to reconstitution of complex biological pathways in CFPS systems.[178,261] To achieve control over these processes, a range of stimuli, including changes in pH,[262] redox potential,[263–265] temperature,[266] and light[212] can be employed. Light as a stimulus is particularly attractive, as it is applied remotely, is largely biorthogonal and has unparalleled spatiotemporal resolution. Several ways have been developed to control the central dogma with light (**Figure 1-19**), either by directly controlling nucleic acids involved (DNA, **Figure 1-19** A, or mRNA, **Figure 1-19** B), or by controlling small molecules, nucleic acids or proteins that can modulate gene expression (**Figure 1-19**, C, D).[212]

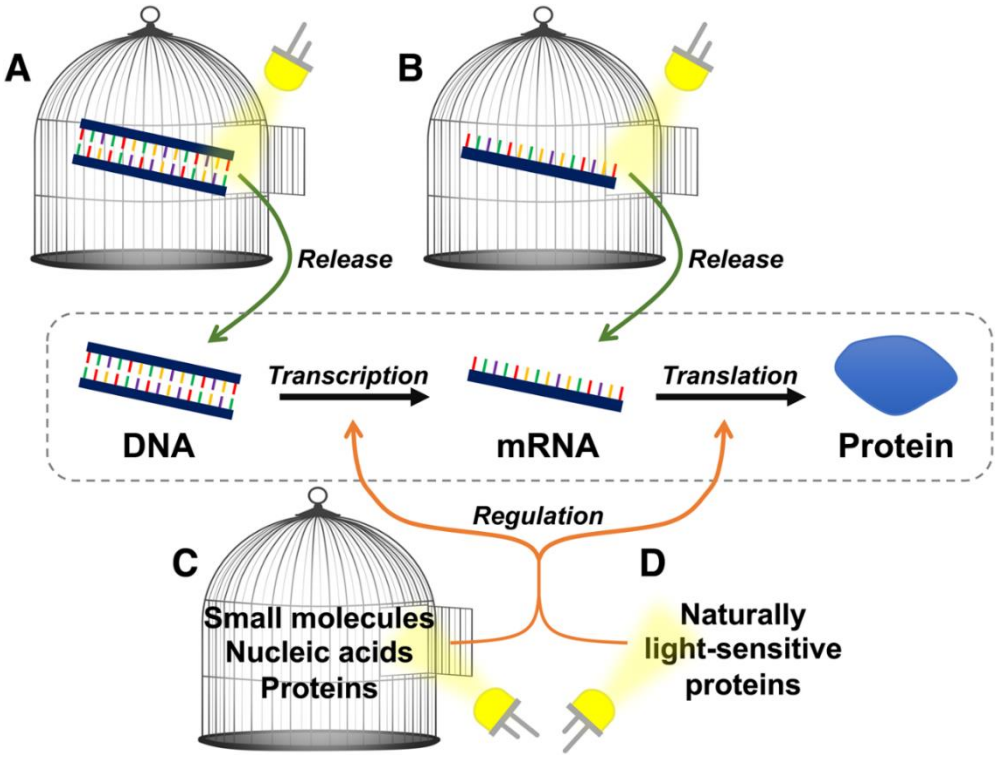


Figure 1-19: Ways of controlling the central dogma of biology with light.

Controlling DNA (A) or mRNA (B) directly, as well as molecules and regulatory nucleic acids and proteins (C) and (D) with light enables control of the central dogma. Figure reproduced from 'Controlling Gene Expression with Light: A Multidisciplinary Endeavour' by Hartmann *et al.*[201] (© 2020) under a creative commons licence (CC BY 4.0)

1.6.1 Control of Gene Expression Using Photocaged Small Molecules

Small molecules can be used to control gene expression, as a large number of small molecules are involved in the regulation of transcription, such as in the control of operators (Chapter 1.3.4.1). One approach taken to control gene expression with small molecules is by directly photocaging nucleotides needed in mRNA synthesis. Photocaged ATP, with either a nitrobenzyl-[267] or coumarin-photocage[268] on the terminal phosphate as well as Uridine Triphosphate (UTP) and Guanosine Triphosphate (GTP)-derivatives with a 2-nitrobenzyl-photocage on the WCF-face of the nucleobase[269] allowed for controlled transcription with T7 RNAP by irradiation with UV-light.

Carbohydrates can also be used to control bacterial gene expression. 2-nitrobenzyl-photocaged arabinose[270] and IPTG,[271,272] which interact with the arabinose and *lac* operator, respectively, could be used to control reporter gene expression and small molecule biosynthesis in bacterial cells.

Molecules that can interact with the oestrogen receptor, a transcription factor in mammalian cells, have also been photocaged with 2-nitrobenzyl-, coumarin- or cyanine derivatives and allowed for controlled gene expression with UV and visible light in mammalian cells and zebrafish.[273–277]

Molecules that can directly interact with the DNA or RNA have also been photocaged to enable light control. Examples of this include 2-nitrobenzyl-photocaged toyocamycin,[278] which controls translation by binding to an mRNA ribozyme, 2-nitrobenzyl-caged theophylline,[279] which controls translation by binding to a riboswitch and also 2-nitrobenzyl-photocaged pyridostatin,[280] which stabilises G-quadruplexes.

Several other small molecules have also been used for control of gene expression. These include 2-nitrobenzyl-caged doxycycline for the commonly used Tetracycline system,[281,282] 2-nitrobenzyl-caged nuclear hormones[283] as well as a coumarin-caged transcription factor inhibitor.[284]

1.6.2 Control of Gene Expression through Photocaged Templates and mRNA

While modifying small molecules involved in gene expression is a highly explored route, directly modifying the nucleic acid templates from which the gene is expressed offers the advantage of not having to add additional components or to clone in regulatory elements into the nucleic acid of interest.

Plasmids are a commonly used tool to introduce genes into an organism.[285] The control of such plasmids with a remote, non-invasive stimulus such as light is thus highly desirable to control the plasmid's function in the genetically modified organism. Such light-activatable plasmids have been created using numerous approaches. Directly caging the WCF face of thymine nucleobases inside the promoter region with a 2-nitropiperonyl-photocage allowed for light-controllable expression of GFP inside mammalian cells as well as zebrafish.[286] A biotinylated coumarin photocage was inserted into a plasmid *via* a 5'-hexylamine linker upstream of the TATA box. Binding streptavidin blocked expression of enhanced Green Fluorescent Protein (eGFP) in HeLa cells with a poor off-state and UV irradiation recovering expression levels almost completely.[287] Nitrobenzyl- and coumarin-based photocages on the backbone have also been employed to cage plasmids.[288–290] This approach uses highly reactive diazo-species, which are not selective. The resulting plasmids show excellent caging, but poor recovery of gene expression upon UV illumination, likely due to the large degree of unselective protection and statistical deprotection. A slightly different approach used photoisomerisable, vinyl-pyrene-modified Guanidine nucleobases inside a G-rich region between promoter and start codon.[291] Through photoisomerization between the trans and cis-states of the vinyl-pyrene, stability of G-quadruplexes and hence stalling of polymerase could be controlled and this allowed for switchable Venus fluorescent protein expression in zebrafish. Switching was also possible through incorporation of azobenzenes into the T7 promoter of a plasmid to control cell-free transcription and translation.[292–294]

mRNA photocaging is also an approach taken to control gene expression. Incorporation of such photocages can be more difficult, as mRNA is inherently less stable. Diazo-nitrobenzyl- and -coumarin groups have been used to modify the mRNA, but suffered similar drawbacks as the similarly caged plasmids.[289,295] A unique

modification position for mRNA is on the 5'-cap. Photocaging of the 7-methyl-G-cap prevents translation initiation by inhibiting eIF4E from binding until illuminated. This has been used to tightly control gene expression using nitrobenzyl-[296] and coumarin-protected[297] caps (**Figure 1-20**). The cap could also be modified with a styryl-based photoswitch, which allowed for controlled Venus expression in HeLa cells.[298] Incorporation of photocages into mRNA has also been achieved enzymatically to cage eGFP mRNA in the 5'UTR.[299]

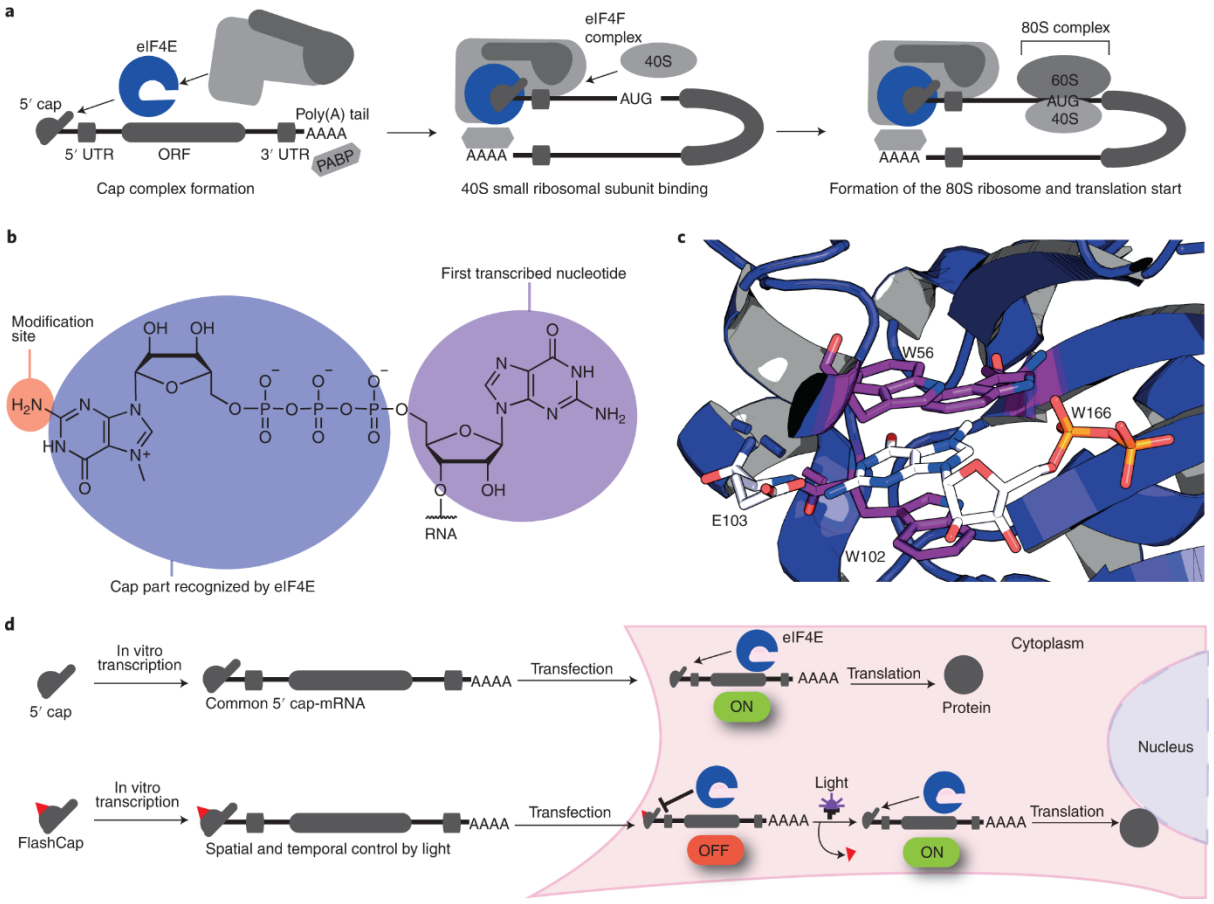


Figure 1-20: Modification of the 5' Cap on RNA for control of translation.

a) eIF4E binds to the 5' cap on mRNA which the recruits the 40S subunit of the ribosome to initiate translation. b) Highlighted modification site on the 5' cap. c) Crystal structure of eIF4E, highlighting important interactions with the 5' cap. d) Controllable translation *via* transfection of 5'-photocaged mRNA followed by removal of the photocage with light to activate translation. Figure reproduced from 'Photocaged 5' cap analogues for optical control of mRNA translation in cells' by A. Rentmeister and co-workers[296] (© 2022) under a creative commons licence (CC BY 4.0)

While many of the aforementioned nucleic acid technologies such as plasmids and mRNA can be used directly in cell-free systems, a unique feature of cell-free systems is the option to use linear templates, which are often easier to prepare. In light of this, various photocontrollable linear DNA templates have been developed. These include WCF-face-caged thymidines[300] or removal of psoralen crosslinks[301] inside a T7 promoter for controllable cell-free transcription. The caging of the WCF-face of adenine could also be achieved using a modified AdoMet enzyme, installing nitrobenzyl-groups into a linearised plasmid.[302] Transcription can also be blocked by incorporation of nitrobenzyl-caged 5-hydroxymethylcytosine and -uracil. Removal with UV light allowed for cell-free transcription at higher yield than in non-hydroxymethylated templates. Hydroxymethyluracil could then be phosphorylated *via* an enzymatic process, turning transcription off again.[303]

One particular example of light-controllable DNA templates is the basis of this work (**Figure 1-21**).[201] A single-stranded DNA (ssDNA) encoding for the T7-promoter was modified through incorporation of 7 amino-C6-dT nucleobases. These bases, which are well-accommodated in double stranded DNA (dsDNA) by protruding from the major groove (as discussed in Chapter 1.1.2), could be modified using a commercial, biotinylated nitrobenzyl-photocage. The ssDNA could then be used as a primer in a polymerase chain reaction (PCR) to generate modified linear DNA templates. By caging of these templates through binding of monovalent Streptavidin (mSA), gene expression was effectively turned off from these templates due to the steric block provided by the protein, preventing access by T7 RNA polymerase. Upon illumination, this steric bulk could be cleaved off, enabling binding of the polymerase and thus cell-free expression. This system has particularly tight control, and has also been used to control synthetic tissues.[202]

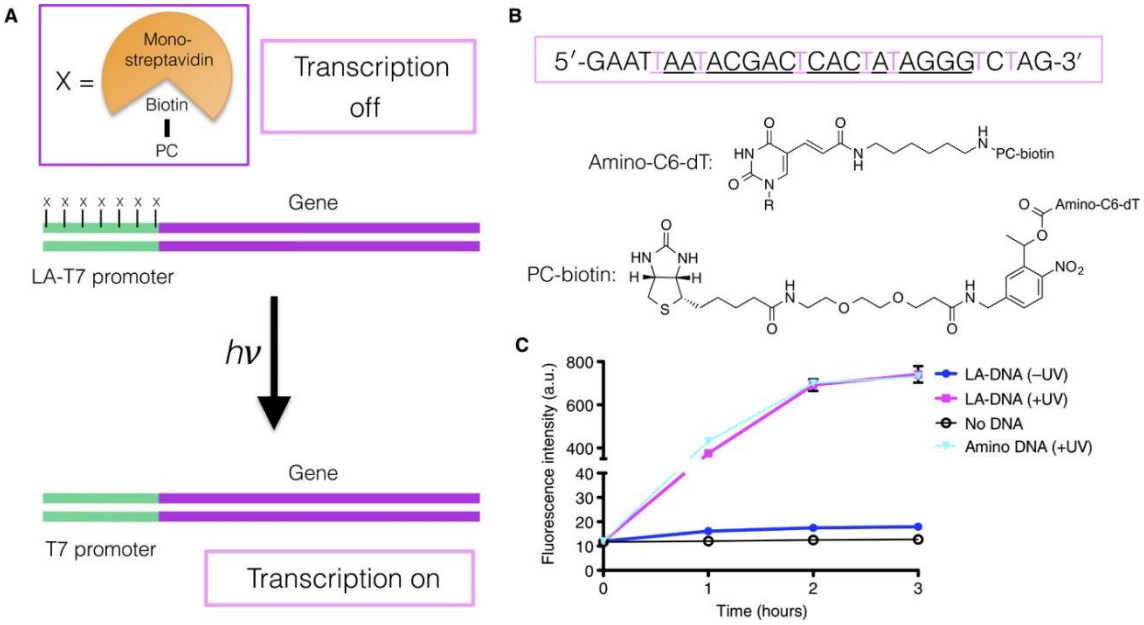


Figure 1-21 Synthesis of a UV-light activatable T7 promoter for light-controllable gene expression.

Modification of amino-C6-dT nucleobases in a T7 promoter sequence with a UV-photocleavable biotin, and binding of monovalent Streptavidin enables UV light-controlled activation of linear templates for cell-free protein synthesis. Figure reproduced from 'Light-activated communication in synthetic tissues' by Booth *et al.*[201] (© 2016) under a creative commons licence (CC BY-NC 4.0)

One striking feature of the aforementioned gene activation technologies is their heavy reliance on UV-based photocages, with very few utilising visible light. While UV photocaging strategies are synthetically easily accessible, their use in biological systems, particularly towards *in vivo* use is heavily disfavoured, as UV-light can cause damage to biological samples[304] and has poor tissue penetration,[231,232] disfavouring their use in more complex biological systems. Thus, a clear need is the development of visible light photocages for activation of gene expression to improve biocompatibility and tissue penetration.

1.6.3 Control of Gene Knockdown using Photocaged ASOs and siRNA

In addition to controlling the expression of a gene through activation of the DNA template encoding for it, there is also the possibility of turning protein expression off through ASOs and siRNA. One benefit of this is that no modified gene needs to be inserted into the organism and thus native genes can be targeted and protein expression levels modulated. Photoactivatable gene knockdown agents such as ASOs and siRNA are particularly valuable, as the gene knockdown can be induced at a defined timepoint as well as spatially controlled, giving unrivalled control over gene expression in the chosen system. Because of this, a large number of such light-controllable agents have been developed using a variety of caging approaches, summarised below.

As already employed previously, 2-nitrobenzyl-caged nucleobases could be incorporated into both ASOs[305,306] and siRNA,[307,308] which prevents target mRNA-binding until irradiated and effectively controlled gene knockdown in mammalian cells. Inhibition of ASO activity *via* a photoremovable complementary strand is also a commonly seen approach. By having the complementary strand attached *via* a photocleavable linker, control of PMO-,[309,310] PNA-[311] and DNA-based[312] ASOs and antagomirs[313] was achieved. Active ASOs could also be deactivated through incorporation of a photocleavable linker inside the sequence, reducing target binding affinity after cleavage.[310]

A very interesting approach that has been employed in caging of ASOs is through conformational restriction. Through circularisation of the otherwise flexible oligonucleotide, effective hybridisation with the target mRNA is hindered until irradiated with light. This avenue has been successful in silencing ASOs with nitrobenzyl-,[314] coumarin-,[315] quinoline-[316] and Ruthenium complex-based[317] photocages (**Figure 1-22**). While the bifunctional linkers can be difficult to synthesise, a large benefit of this method is the very low number of photocages needed for effective silencing.

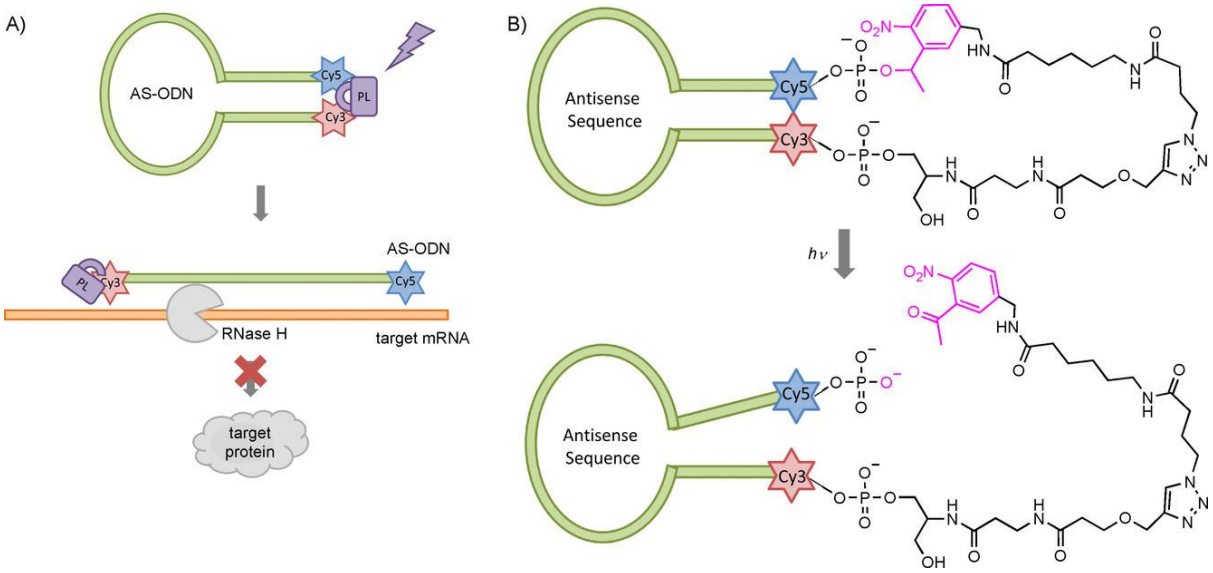


Figure 1-22: Photocaged antisense oligonucleotides via circularisation.

Circularisation of a hairpin-forming antisense oligonucleotide with a nitrobenzyl-derived photocage allows for light-controllable RNase H activity. Figure reproduced from 'Efficient Synthesis of Light-Triggered Circular Antisense Oligonucleotides Targeting Cellular Protein Expression' by I. J. Dmochovski and co-workers[314] (© 2018) with permission from John Wiley and Sons.

Backbone modification of siRNA has also been successfully employed to control its activity. By using the diazo-nitrobenzyl-photocages discussed previously, siRNA could effectively be silenced, either through caging the whole siRNA backbone[318] or through caging of the 4 terminal phosphates of a precursor dsRNA.[319,320] Similarly, one terminus of the siRNA has been caged with a nitrobenzyl-linked folic acid,[321] porphyrin photosensitiser/anthracene pair[322] or aptamer.[323]

There are numerous other ways that ASOs have been photocaged. This includes attachment to nanoparticles,[324–330] which allows for near-infrared light release, or hybridisation-switches through incorporation of azobenzenes into the backbone of siRNA.[331–333]

Interestingly, ASOs and siRNA have not seen much application in cell-free systems, despite their applicability. One recent report showed the development of a transfection method of ASOs for synthetic cells;[334] however, control of cell-free expression with light-controlled ASOs and siRNA is severely underexplored. Incorporation of light-controllable antisense oligonucleotides would allow for their remote control without the need for transfection, as the ASO can be present from the beginning. Hence, in this

work, light-controllable antisense technologies will be explored for use within cell-free expression and also tested in synthetic cells.

1.7 Aims

The work described herein aimed to expand the repertoire of light-controllable nucleic acids for use in cell-free systems. In Chapter 2, a blue light-activatable photocage is developed for the control of linear DNA templates. This photocage is designed to be orthogonal to the UV light-activatable photocage reported[201] and aims to explore the potential of orthogonal, two-wavelength controlled gene expression. The resulting system is then investigated for the remote control of synthetic cells, both in bulk as well as spatially controlled, with one and two wavelengths.

Chapters 3 to 5 aim to explore various methods of controlling antisense oligonucleotides with light in cell-free expression. Chapters 3 and 4 employ the biotinylated photocages previously reported and developed in Chapter 2 to photocage and release ASOs and explore different caging mechanisms, either through steric blocking or conformational constraint, to enable controlled RNase H-mediated mRNA degradation and gene knockdown in cell-free systems.

Chapter 5 aims to explore an alternative photocaging strategy. A method for caging of DNA-based phosphorothioate-containing ASOs is developed. The resulting oligonucleotides are characterised and subsequently tested for their ability to control RNase H-mediated degradation and control of cell-free gene expression.

The work presented in Chapters 2,[335] 3[336] and 5[337] have been preprinted on chemRxiv.

2 DEVELOPMENT OF A BLUE LIGHT-PHOTOCLEAVABLE CAGING GROUP FOR DNA BASED ON AN EXTENDED COUMARIN SCAFFOLD

2.1 Introduction

This chapter describes the development of a blue light-activatable (bLA) photocage for generation of bLA-DNA templates for use in cell-free expression. Our group has previously developed a light-activatable caging system for DNA parts used in CFPS systems.[201] The majority of light-activatable DNAs rely on UV photocages, as has been discussed in Chapter 1.6, including the one developed in our group.

One of the major downsides of UV light to control DNA for gene expression is its damaging nature to biomolecules. This damage occurs predominantly on the DNA, and to a smaller extent other biomolecules.[338] UV-B (280-315 nm) irradiation directly affects the DNA by excitation of the electrons in the nucleobases, leading to DNA lesions through dimerization of pyrimidine nucleobases, and to a lesser extent also with purine bases, and could even lead to DNA strand breaks.[235,339] UV-A (315-400 nm), while not directly damaging to the DNA, as the nucleobases do not absorb in that region, can still cause damage to biological systems indirectly. UV-A radiation can still be absorbed by other chromophores in biological samples, leading to the formation of reactive oxygen species, which can indirectly cause DNA, protein and lipid damage.[340–342] While DNA repair mechanisms have evolved to deal with such lesions in the DNA, and have high fidelity, they cannot repair all. In addition, these

repair mechanisms are absent in CFPS systems. For these reasons UV irradiation should be avoided, if possible, in controlling DNA function.

Another reason to move away from UV irradiation is its poor tissue penetration. Tissue penetration is increased with longer wavelengths (**Figure 2-1**),[231,232] which allows for improved activation past the top layer of a sample. Tissue penetration is poor for UV light, due to a large number of molecules absorbing UV irradiation. Blue light, which penetrates tissues to about 2 mm,[232] is the most efficient in cell culture and the surface of the skin,[231] whereas red/near IR is capable of reaching deeper tissues, due to a lack of absorbing molecules in biological samples. In addition to tissue penetration, light scattering also needs to be taken into account. Biological samples are capable of scattering light, with Rayleigh scattering being inversely proportional to wavelength, leading to less scattering with longer wavelengths.[343,344] Thus, the development of red-shifted photocages, even just in the blue, will pave ways for better activation in downstream applications.

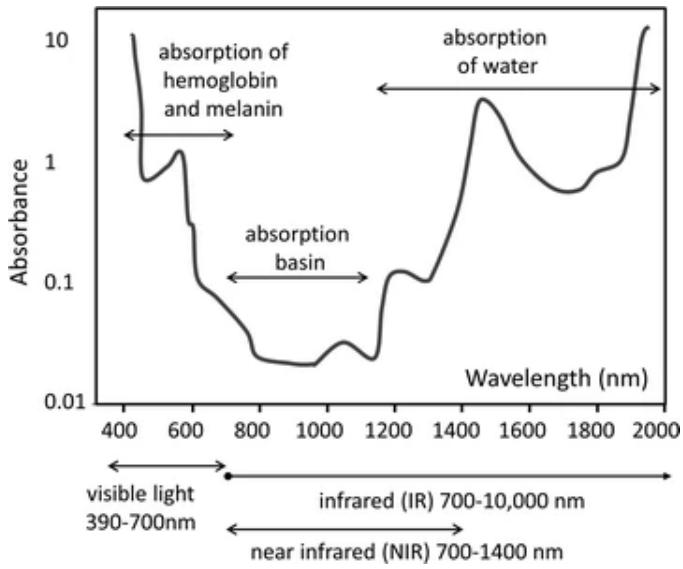


Figure 2-1: Absorption Spectrum of biological tissue.

A clear minimum in absorption of tissue is seen for wavelengths in the red to near-IR due to a lack of absorbing molecules in biological samples. Figure reproduces from 'Optogenetic regulation of transcription'[231] by Polesskaya *et al.* (© 2018) under a creative commons licence (CC-BY 4.0).

An advantage of using light is the possibility to use multiple wavelengths to control different processes. Several published reports have shown sequential activation of two photocages.[240,345,346] However, orthogonal activation of two or more photocages has few reported examples in the literature,[249,347–350] mostly due to overlapping absorbance bands of the used chromophores and thus orthogonal release being difficult.

For the reasons listed above, a new photocage in the visible range was desired to control DNA function. Specifically, a blue light photocage was envisaged, as the chromophores are less complex and thus provide higher synthetic accessibility, and often provide higher aqueous solubility than many red-shifted molecules. Built on the previous light-activated DNA design, blue light-activatable DNA templates through use of an extended coumarin as the photocaging moiety were envisaged (**Figure 2-2**).[249,251] This chromophore was specifically chosen as it has already been shown to work in biological media, and it was also shown to have a minimum at 350-360 nm, meaning that it is likely orthogonal to the UV-photocage employed.

The photocage was designed to be attached to the same amino-C6-dT nucleobases in a ssDNA containing the T7 promoter sequence, as they are commercially available, well tolerated by the DNA by protrusion from the major groove, and use a simple, well-tolerated bioconjugation for modification. In addition, they are the basis of the technology already developed in the group.[201]

This blue light-activated DNA (bLA-DNA) shows a very tight off-state, comparable to the UV-photocage, and very fast photocleavage upon 455 nm illumination. This bLA-DNA was also found to be orthogonal to the previously developed ultraviolet LA-DNA (uvLA-DNA). Through this, both photocages could be used independently to control cell-free systems. With this bLA-DNA, light-control of CFPS systems was achieved. It was possible to control the cell-free expression (CFE) of RNA and protein and spatiotemporally control synthetic cells. In addition, in conjunction with the uvLA-DNA reported previously, an AND-logic gate could be developed with two wavelengths as inputs, which operates both in bulk as well as inside synthetic cells.

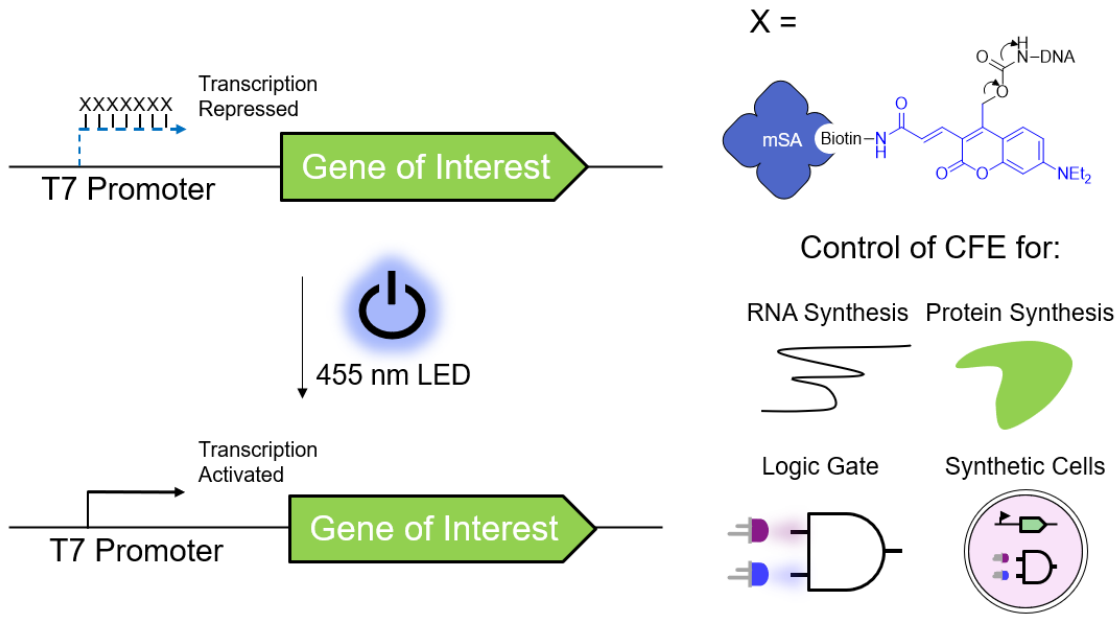


Figure 2-2: The developed blue light-activatable DNA templates using a coumarin-derived photocage and their applications in cell-free expression.
Modification of a T7-promoter region with a coumarin-derived, biotinylated photocage and binding of monovalent Streptavidin (mSA) enables blue light-control of transcription. This has been employed in the control of cell-free RNA and protein synthesis, and was used to control a logic gate and synthetic cells. Figure adapted from "Blue light-activatable DNA for remote controlled logic gates in synthetic cells" by D. Hartmann *et al.*[335] (© 2023) under a creative commons licence (CC-BY 4.0).

2.2 Synthesis of the biotinylated Coumarin Photocage

To synthesise the blue light-activatable photocage, a coumarin derivative was envisaged. Coumarins, as described above in Chapter 1.5.2, are excellent photocages and several modified coumarins that cleave with blue light have been reported. The acrylate-extended coumarin system, originally reported by Ellis-Davies and co-workers,[249,251] was found to be a particularly suitable candidate. It was shown to work in biological systems, is synthetically easily accessible and the acrylate moiety provides a convenient attachment point for the biotinylated linker. Using this scaffold, a blue light-activatable biotin able to react with an amino-C6-dT-modified DNA of interest was prepared and the synthesis is summarised in **Figure 2-3**.

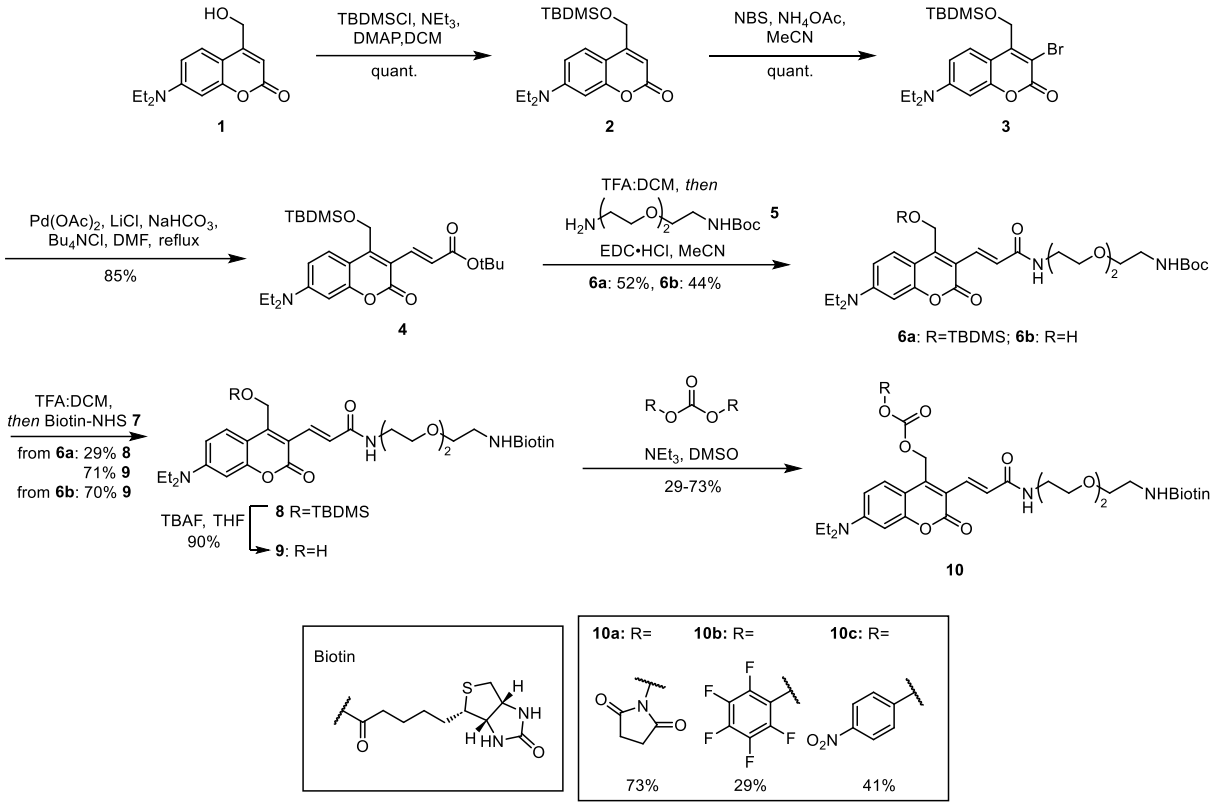


Figure 2-3: Synthetic route developed for the blue light-activatable biotin photocage.
Figure adapted from "Blue light-activatable DNA for remote controlled logic gates in synthetic cells" by D. Hartmann *et al.*[335] (© 2023) under a creative commons licence (CC-BY 4.0).

Synthesis of the parent DEACM-alcohol **1** was performed following a published procedure.[351] Following the procedure by Ellis-Davies and co-workers, the alcohol was protected with a *tert*-butyl dimethylsilyl (TBDMS)-group using the silyl-chloride under basic conditions. Following on from this, the C3 position of the coumarin was brominated using *N*-bromosuccinimide (NBS) and a substoichiometric amount of NH_4OAc, which catalyses the formation of elemental Br_2 from the NBS.[352] This halide now allowed for a Pd-catalysed Heck coupling with *tert*-butyl (*t*Bu) acrylate following the published procedure, giving the fully protected, extended coumarin scaffold **4** in excellent yield.

The acrylate moiety could rapidly be deprotected using a 1:1 mixture of trifluoroacetic acid (TFA) and dichloromethane (DCM). The crude acid prepared from this reaction after removal of TFA:DCM, was subjected to peptide coupling conditions with mono-*tert*-butyloxycarbonyl (Boc)-protected glycol-derived diamine and 1-Ethyl-3-(3-dimethylaminopropyl)carbodiimide (EDC) hydrochloride, giving the acrylamide with an appended, protected linker. This reaction gave two products, the expected TBDMS-

protected coumarin as well as the deprotected alcohol. This could be attributed to the deprotection of the TBDMS group with TFA. The alcohol was protected initially to not interfere in the peptide coupling step; but the free alcohol was not found to interfere in this step, as shown by the high total yield of the glycol-extended coumarin. The Boc group was then able to be taken off under identical conditions to the *t*Bu group with 1:1 TFA:DCM, the solvent removed and the crude amine reacted with Biotin-*N*-hydroxysuccinimide (NHS) Ester in *N,N*-dimethylformamide (DMF) under basic conditions with NEt_3. This yielded the biotinylated, glycol-linked, coumarins **8** and **9** in good yields from both TBDMS-protected coumarin **6a** as well as deprotected coumarin **6b**. In the TBDMS-protected case, deprotection of the TBDMS-group was again observed, but as previous, the free alcohol did not interfere with this reaction step. The TBDMS-group that remained on the coumarin **8** could easily be removed with tetrabutylammonium fluoride (TBAF) in tetrahydrofuran (THF) in great yield to yield **9**.

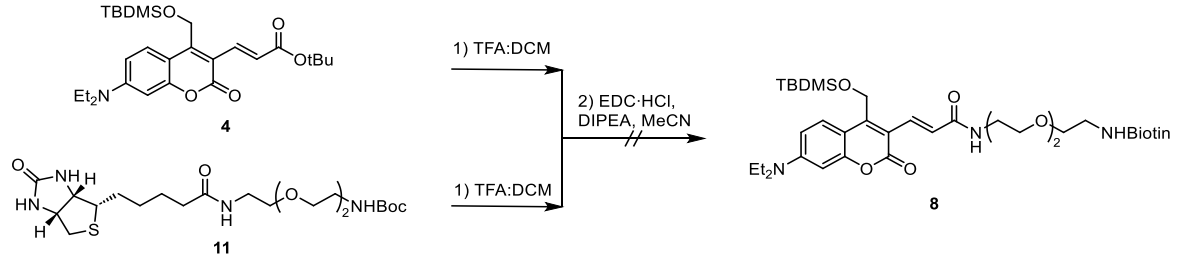


Figure 2-4: Alternative approach towards biotinylated coumarin 8.

Another approach towards this compound was also tested (**Figure 2-4**). Boc-protected, glycol-extended biotin **11** was prepared and deprotection was performed with 1:1 TFA:DCM. The crude, dried amine was used for peptide coupling under conditions as above, with added diisopropylethyamine (DIPEA) with the crude acid from deprotection of **4**; sadly no product was observed after 16 hours.

The free alcohol could now be converted into a reactive carbonate that is able to react with the amino-C6-dTs inside the DNA. For this, the NHS-carbonate was initially synthesised, as this was the group found on the UV-activatable biotin used in the group. The reaction was performed using excess *N*,*N*′-Disuccinimidyl carbonate with triethylamine in a number of solvents. DMF, DCM and MeCN were tested, but did not give the desired reactivity. The reaction in dimethylsulfoxide (DMSO), however, rapidly formed the desired, active NHS carbonate **10a**. Sadly, this group did not provide the desired reactivity with the DNA (**Figure 2-6**). Thus, two further derivatives were

prepared using their corresponding carbonates, namely bis(pentafluorophenyl) carbonate and bis(*para*-nitrophenyl) carbonate, giving the desired pentafluorophenyl (PFP) and *para*-nitrophenyl (pNP) carbonates **10b** and **10c**, respectively.

A surrogate compound **12** was also synthesised for photochemical studies, mimicking the carbamate that is formed between the active carbonate and the amine-modified DNA by reacting the active carbonate **10c** with propargylamine (**Figure 2-5**).

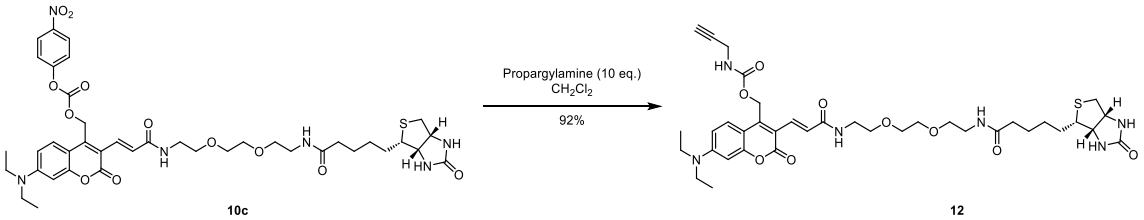


Figure 2-5: Synthesis of propargyl-carbamate-appended coumarin-biotin.

Figure adapted from “Blue light-activatable DNA for remote controlled logic gates in synthetic cells” by D. Hartmann *et al.*[335] (© 2023) under a creative commons licence (CC-BY 4.0).

2.3 Reactivity of the bLA-Biotin-Derivatives 10a-c with DNA

The synthesised NHS-carbonate **10a** was tested for reactivity with amino-functionalised DNA. For this, the NHS carbonate was added to a final concentration of 12.5 mM to the DNA with either 1 5'-terminal C6-amine, 1 5'-terminal C6-amine and 3 amino-C6-dT, or 7 amino-C6-dT in the sequence, with $NaHCO_3$ buffer in 50% DMF. Sadly, in all cases no reaction was observed. This is believed to be due to the rapid hydrolysis of the active NHS carbonate and the lower solubility of the coumarin compared to the nitrobenzyl-biotin photocage.

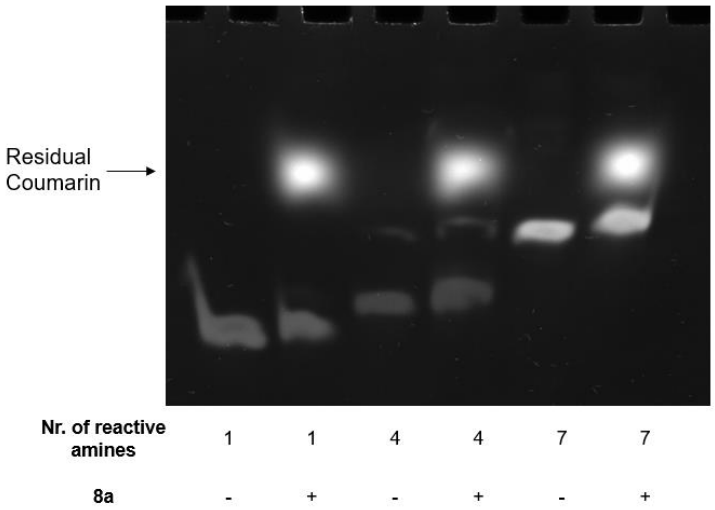


Figure 2-6: Reaction of NHS-Coumarin 10a with DNA containing terminal hexylamine and amino-C6-dT nucleotides.

The molecule showed no reactivity towards amine-modified DNA with $NaHCO_3$. Figure adapted from "Blue light-activatable DNA for remote controlled logic gates in synthetic cells" by D. Hartmann *et al.*[335] (© 2023) under a creative commons licence (CC-BY 4.0).

As the NHS-carbonate was unreactive, the PFP- and pNP-carbonates were prepared, both of which are more hydrolytically stable (**Figure 2-3**). The PFP-carbonate **10b** was then used under identical conditions as the NHS-carbonate and reacted with the 7 amino-C6-dT T7-promoter ssDNA. The reaction was initially performed at 50% and 80% DMF and analysed by PAGE (**Figure 2-7**, a). In both cases, reactivity was observed with the amine-containing ssDNA. In addition, three concentrations were trialled (**Figure 2-7**, b). At 2.5 mM of the coumarin, the reaction was incomplete. Increasing the amount to 5 mM or above shows complete modification on gel.

To better monitor the reaction and find optimal conditions for modification of the DNA, the analysis method was changed from PAGE to Ion-Paring High Performance Liquid Chromatography (IP-HPLC) (**Figure 2-8**), using triethylammonium bicarbonate (TEAB) as the ion pairing buffer, using a gradient of 5-34% MeCN in H_2O over 36 minutes on a polar-embedded C18 column (Agilent Polaris, 50 x 4.6 mm) heated to 50 °C.

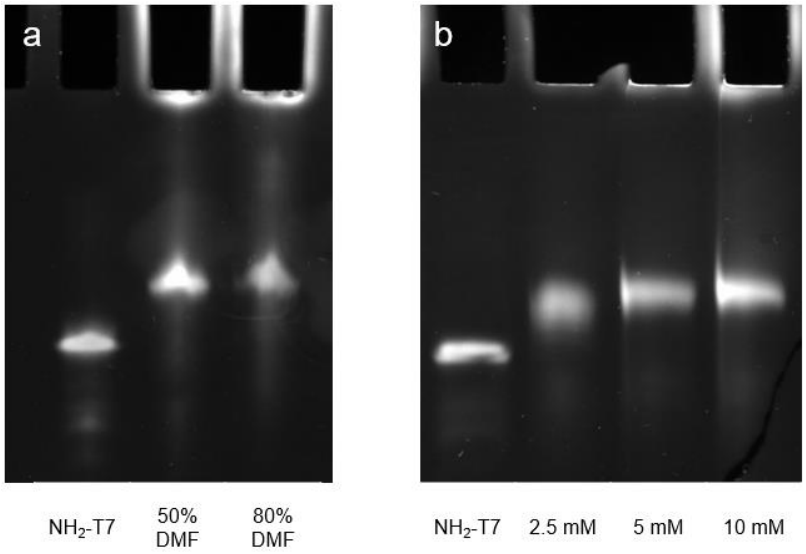


Figure 2-7: Testing reaction conditions with PFP-coumarin 10b at different %DMF and [Coumarin].

Figure adapted from "Blue light-activatable DNA for remote controlled logic gates in synthetic cells" by D. Hartmann *et al.*[335] (© 2023) under a creative commons licence (CC-BY 4.0).

Three conditions were compared, with Conditions A being the previously employed conditions of 100 mM $NaHCO_3$, 25 mM PFP-coumarin **10b** in 50% DMF with the reaction left stirring overnight at room temperature. This reaction was not very clean or had a distinct main product, but the desired oligonucleotide was identified using the UV-Visible spectrum recorded by the HPLC. Conditions B employed the same reaction but exchanged $NaHCO_3$ for MOPS buffer at pH 8.5, which has previously been employed for bioconjugation to amines.[353] This reaction proved to be much cleaner, with the desired product now also being the major product, albeit still in low yield.

To improve this further, the reaction conditions were altered. The amount of buffer was increased to 118 mM, the amount of molecule was halved and the %DMF was increased to 59%, to allow for optimal solubility of the active carbonate. The reaction was then also heated to 37 °C for 3 hours to further improve reactivity. These conditions proved to be very fruitful and yielded the desired, fully modified oligonucleotide in much higher yield than the previous reaction conditions. These reaction conditions were then employed to test both PFP- and pNP-carbonates **10b/c** for bioconjugation (**Figure 2-9**). Both molecules provided the desired, fully modified oligonucleotide as the major product, with yields for the PFP-carbonate being slightly higher.

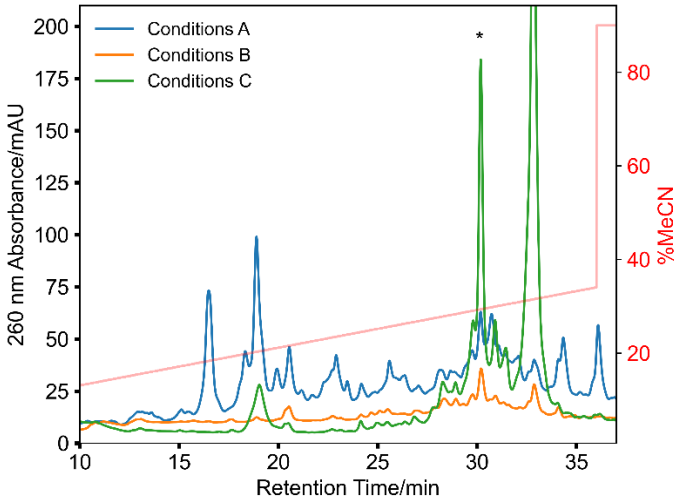


Figure 2-8: Condition Screen for modification of 7-amino-C6-dT containing ssDNA.
Conditions A: 100 mM $NaHCO_3$, 25 mM PFP-coumarin **10b**, 50% DMF in a total volume of 10 µL, reaction left stirring overnight at room temperature. Conditions B: 100 mM MOPS pH 8.56, 25 mM PFP-coumarin **10b**, 50% DMF in a total volume of 10 µL at room temperature overnight. Conditions C: 118 mM MOPS pH 8.56, 12.5 mM PFP-coumarin **10b**, 59% DMF in a total volume of 8.5 µL, heated to 37 °C for 3 hours. The * indicates desired product. Figure adapted from "Blue light-activatable DNA for remote controlled logic gates in synthetic cells" by D. Hartmann *et al.*[335] (© 2023) under a creative commons licence (CC-BY 4.0).

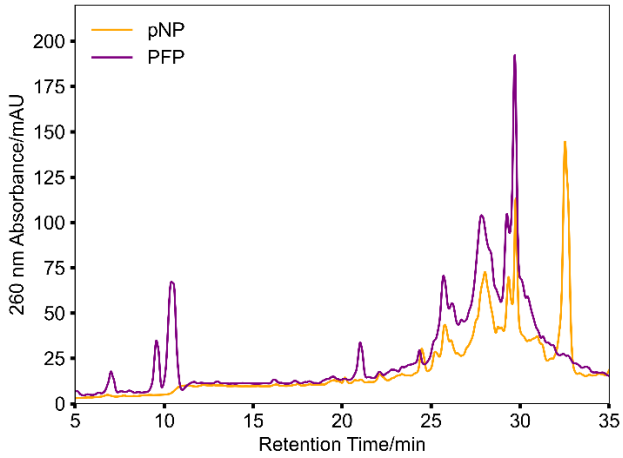


Figure 2-9: Comparison of PFP- and pNP-carbonate 10b/c reactivity with 7-amino-C6-dT-modified ssDNA.

Figure adapted from “Blue light-activatable DNA for remote controlled logic gates in synthetic cells” by D. Hartmann *et al.*[335] (© 2023) under a creative commons licence (CC-BY 4.0).

2.4 Photochemical Properties of bLA-Coumarins

Having determined that both PFP and pNP-Coumarins **10b/c** are suitable for modification of the ssDNA containing amino-C6-dT nucleobases, investigation whether or not these compounds can release cargo under blue light irradiation (**Figure 2-10, a, b**) was undertaken. For this, both compounds were placed in a UV-Visible spectrometer in 0.05% DMF/H_2O at 25 µM concentration and illuminated at 1 minute intervals with a 455 nm LED. In both cases a decrease in absorbance at the λ_{max} of ~450 nm was observed, as well as a small hypsochromic shift.

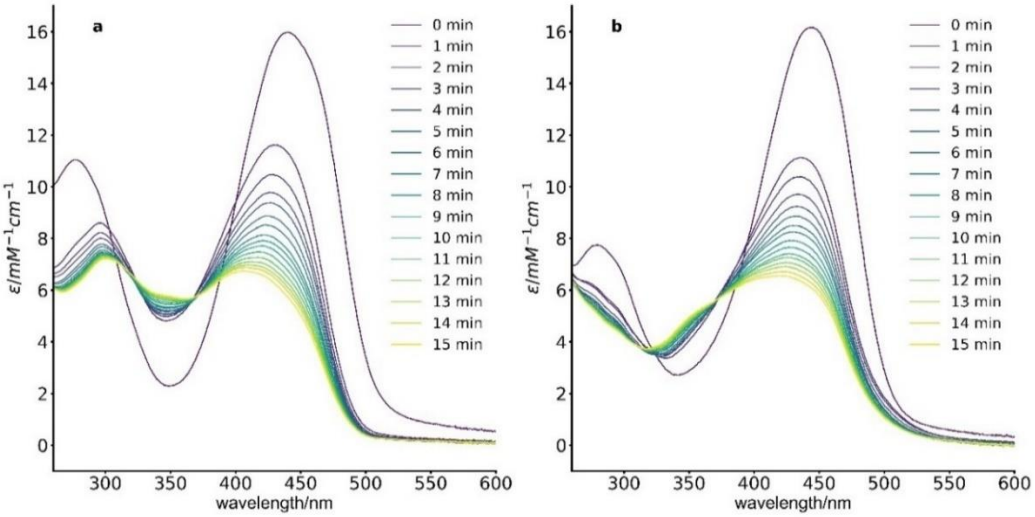


Figure 2-10: Photocleavage of PFP-Coumarin 10b (a) and pNP-Coumarin 10c (b)

Figure adapted from "Blue light-activatable DNA for remote controlled logic gates in synthetic cells" by D. Hartmann *et al.*[335] (© 2023) under a creative commons licence (CC-BY 4.0).

To better understand the cleavage behaviour of appended amines, the surrogate propargyl-modified coumarin **12** was then irradiated with 2 different power settings in 1 minute intervals as a 25 µM solution in 0.05% DMSO/H_2O and monitored by UV/Visible absorbance (**Figure 2-11)**. A rapid decrease in absorbance at λ_{max} of ~450 nm at high light intensity was observed, as well as a small hypsochromic shift, similar to the carbonates measured in **Figure 2-10**. Under low intensity irradiation, photocleavage was drastically slowed, as expected, thus controlled photorelease of the cargo by tuning irradiation conditions should be feasible.

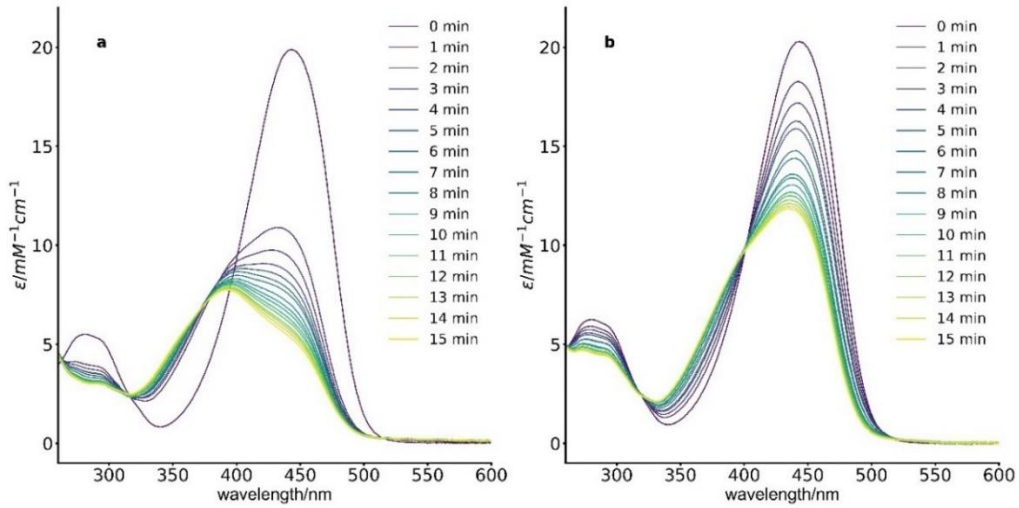


Figure 2-11: Photocleavage of propargyl-coumarin 12.

a) Illumination at 6/6 power (127 mW·cm^{-2}) b) Illumination at 1/6 power (7.34 mW·cm^{-2}). Figure adapted from "Blue light-activatable DNA for remote controlled logic gates in synthetic cells" by D. Hartmann *et al.*[335] (© 2023) under a creative commons licence (CC-BY 4.0).

To check the photochemical product, a solution of the propargyl-modified coumarin **12** in 20% DMSO was irradiated for 5 minutes at the high-power setting (127 mW·cm^{-2}) and the resulting sample analysed by Liquid Chromatography Mass Spectrometry (LCMS). Two major products were observed; product one with a m/z of 674.3 is the expected coumarin-alcohol **9**. The other photolysis product with an m/z of 688.3 and 706.3 could not be identified.

As the coumarin was observed to be highly fluorescent, its 3D-fluorescence pre- and post-photocleavage was recorded **(Figure 2-12**) to account for background observed in downstream applications. It was observed that it has an emission maximum at ~525 nm. Upon photocleavage, a drastic change in the fluorescence profile was observed, with the excitation now being in the near UV and the emission maximum now lying in the blue.

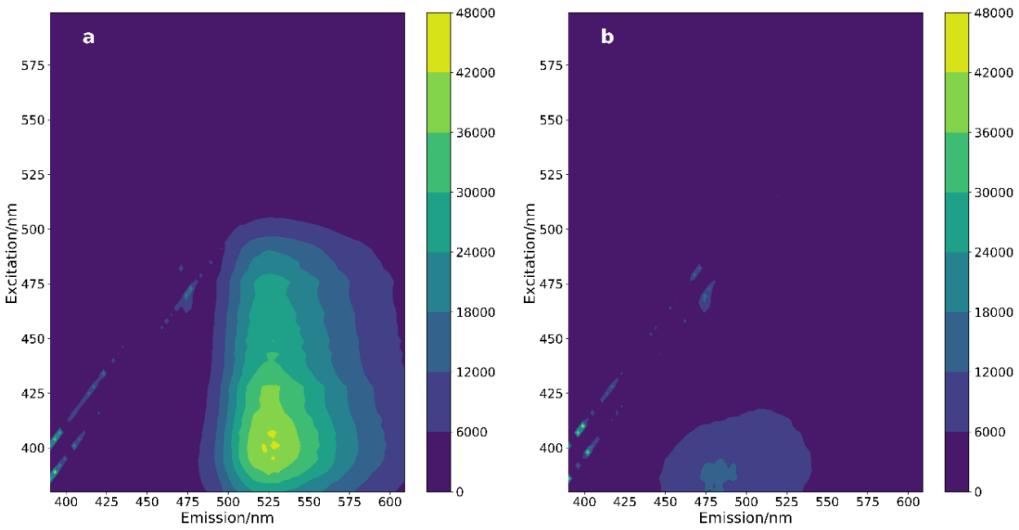


Figure 2-12: Fluorescence Measurement of propargyl-coumarin 11 pre- (a) and post-(b) photocleavage.

Figure adapted from "Blue light-activatable DNA for remote controlled logic gates in synthetic cells" by D. Hartmann *et al.*[335] (© 2023) under a creative commons licence (CC-BY 4.0).

2.5 Purification of fully-modified T7-containing Oligonucleotide and Optimisation of PCR Conditions

After optimisation of the reaction conditions to form the desired bLA-T7 ssDNA, the modified ssDNA was prepared on larger scale using the screened conditions (**Figure 2-13**, a). Washing the resulting solution with chloroform removed the majority of residual coumarin. The aqueous phase, now containing the desired, modified oligonucleotide (ON) as well as any not completely modified DNA could then be purified by IP-HPLC (Conditions detailed in Chapter 7.3.6). The purified ON was analysed by Liquid Chromatography-Mass Spectrometry (LCMS) to validate the desired compound (Appendix C, **Table 7-11**), re-injected into the HPLC to check for purity (**Figure 2-13**, b) and analysed by PAGE (**Figure 2-13**, c). MS showed the expected mass of the oligonucleotide with 7 coumarins appended after deconvolution; HPLC analysis showed high purity of the resulting ssDNA, with only a negligible amount of incompletely modified ssDNA, likely also due to minor exposure to light and the resulting photocleavage. Lastly, PAGE analysis showed a green-fluorescent band prior to gel-staining, as the coumarin photocage is fluorescent, as described above. Post staining with a nucleic acid stain, the band was shown to have lower gel mobility than its parent amino-C6-dT ON, giving further proof that the desired, modified ON had been formed.

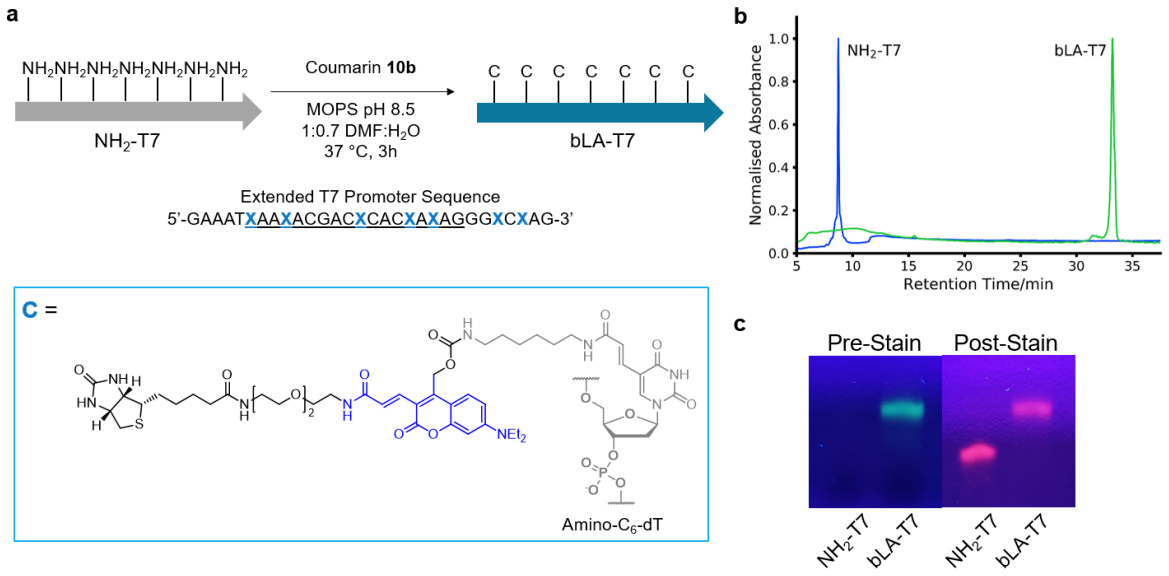


Figure 2-13: Modification of amine-containing T7-ssDNA and HPLC and polyacrylamide gel analysis of the modified ON.

a) Reaction of seven amino-C6-dT containing ssDNA NH_2-T7 with coumarin **10b** to form the bLA-T7 ssDNA. **b**) HPLC analysis of purified bLA-T7 ssDNA compared to NH_2-T7, purified using conditions detailed in Chapter 7.3.6 and Appendix G. **c**) Polyacrylamide gel analysis of purified bLA-T7. Figure adapted from "Blue light-activatable DNA for remote controlled logic gates in synthetic cells" by D. Hartmann *et al.*[335] (© 2023) under a creative commons licence (CC-BY 4.0).

To prepare light-activatable DNA templates from this bLA-T7 ssDNA, polymerase chain reaction is a suitable option. By employing the bLA-T7 ssDNA as a forward primer, it can readily be installed into linear PCR products from a suitable template and reverse primer, as used in the publication by Booth *et al*.[201] Following the previous work in the group, modified, linear DNA templates encoding for the commonly used fluorescent protein mVenus (mV) were prepared. Following the published method using Dreamtaq polymerase, a 2x excess of bLA-T7 to reverse primer and an annealing temperature of 47 °C, gave the desired product as indicated by Agarose Gel Electrophoresis (AGE) at 1 kilobases (kb), but at terrible yields of less than 1/3 of the control using the NH_2-T7 (**Figure 2-14**). Thus, the PCR conditions were optimised on small-scale PCR reactions and analysed by AGE. It was postulated that the modification on the ssDNA caused reduced aqueous solubility, and conditions containing DMSO were trialled. Sadly, DMSO reduced the yields even further, with 5% DMSO abolishing all yield.

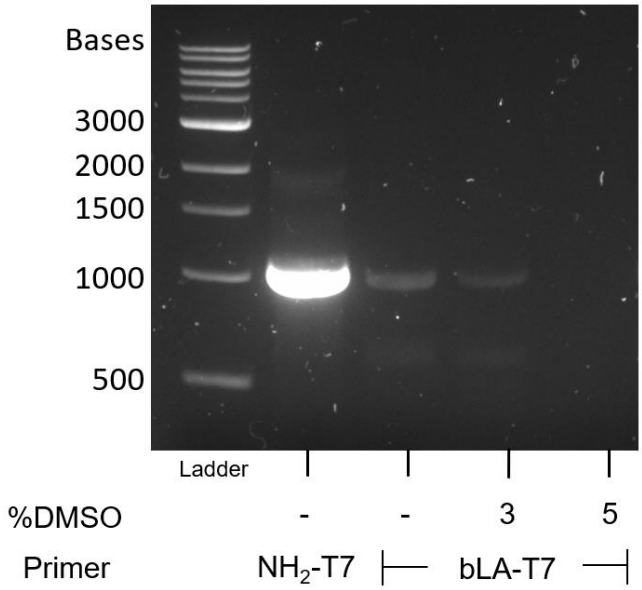


Figure 2-14: Effects of DMSO concentration on PCR Yield with the bLA-T7 primer
Addition of DMSO drastically reduced PCR yield, with 5% DMSO abolishing all yield

The next hypothesis was that the modification reduces the T_m of the ON. Therefore, a longer annealing time (45 seconds vs. 30 seconds previous) and also a lower annealing temperature (45 °C vs. 47 °C previous) (**Figure 2-15**, a) were tested. In both cases, an improvement in yield was observed, with the annealing temperature having the larger effect, and both conditions were taken forward.

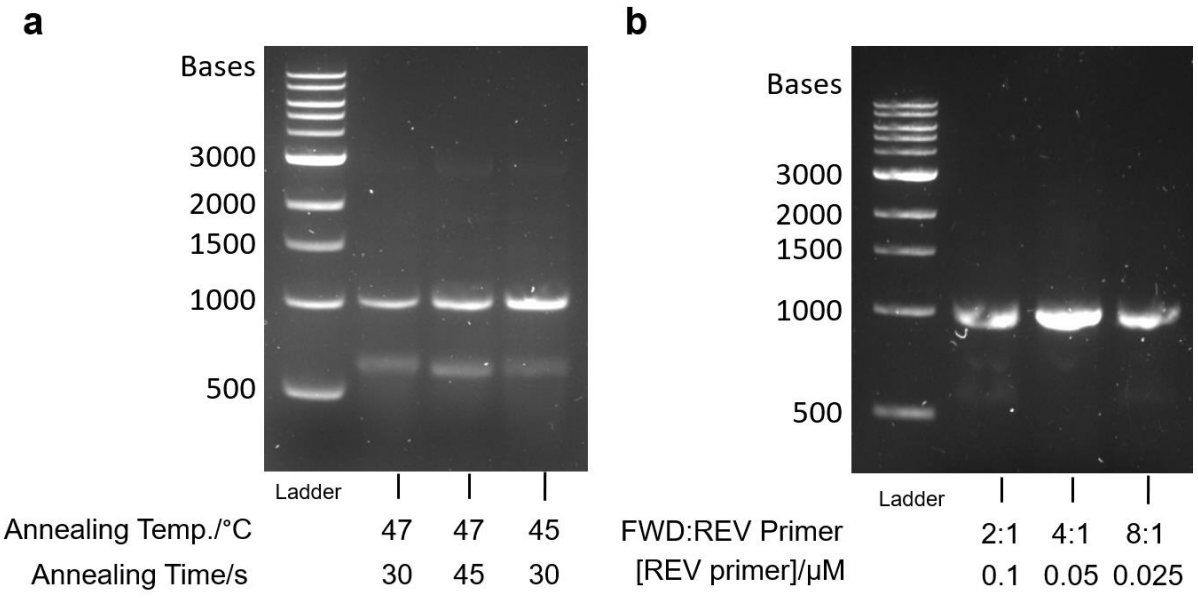


Figure 2-15: Further optimisation of PCR yield using the bLA-T7 by varying reaction parameters.
Reduction of annealing temperature, an increase in annealing time and increasing the amount of forward primer bLA-T7 all increased PCR yield

An off-target band just above the 500 bp marker was observed, however. This was believed to be due to incorrect primer ratios, as the photocage modification alters the absorbance at 260 nm, thus making spectrophotometric quantification inaccurate. Thus, several forward (FWD) to reverse (REV) primer ratios were tried by varying the concentration of the reverse primer in the reaction (**Figure 2-15**, b). It was found that at a 4:1 FWD:REV primer ratio, the off-target band disappeared. The yield and purity of the PCR reaction was now satisfactory and large-scale preparation of the PCR products was undertaken, which worked as expected.

2.6 Expression of Broccoli Aptamer from Annealed Templates

In parallel to PCR optimisation, the bLA-T7 ssDNA could also be annealed to a long ssDNA strand. Annealing the T7-containing ssDNA to a short template strand encoding for a desired gene, as well as the non-template strand, yields a linear DNA template, from which cell-free transcription can occur. To test how effective the caging ability of the coumarin-photocage was on the DNA, an *in vitro* transcription of broccoli aptamer was chosen.[354,355] Broccoli is an RNA aptamer that folds to binds to the small molecule (5*Z*)-5-[(3,5-Difluoro-4-hydroxyphenyl)methylene]-3,5-dihydro-2,3-dimethyl-4*H*-imidazol-4-one (DFHBI). This small molecule is a mimic of the fluorophore of GFP and fluoresces when bound by the aptamer. This makes expression of broccoli aptamer in the presence of DFHBI an excellent reporter for RNA expression levels, as it can be analysed quantitatively by fluorescence in addition to analysis of the transcripts by gel electrophoresis. Broccoli aptamer is also only a very short sequence, and it was thus possible to purchase the complete template strand, without the need for cloning and PCR to prepare the expression template (**Table 7-2**).

The broccoli dsDNA template was prepared from the T7-containing ssDNA (both the unmodified NH_2-T7 and bLA-T7), the template (bottom) strand complementary to the T7-ssDNA and encoding for the broccoli aptamer, and the non-template (top) strand (**Figure 2-16**, a). Due to the high absorbance of the coumarin photocage, an excess of bLA-T7 was employed to balance any inaccuracies in spectrophotometric quantification, as it is believed that any excess of this ssDNA will not partake in the reaction, as T7 RNAP requires dsDNA for recognition. The templates were annealed by heating to 95 °C followed by slowly cooling down to 25 °C. The resulting templates

were then caged by addition of a 50x molar excess of monovalent Streptavidin (mSA, kindly provided by Michael Fairhead) and incubated at 4 °C overnight.

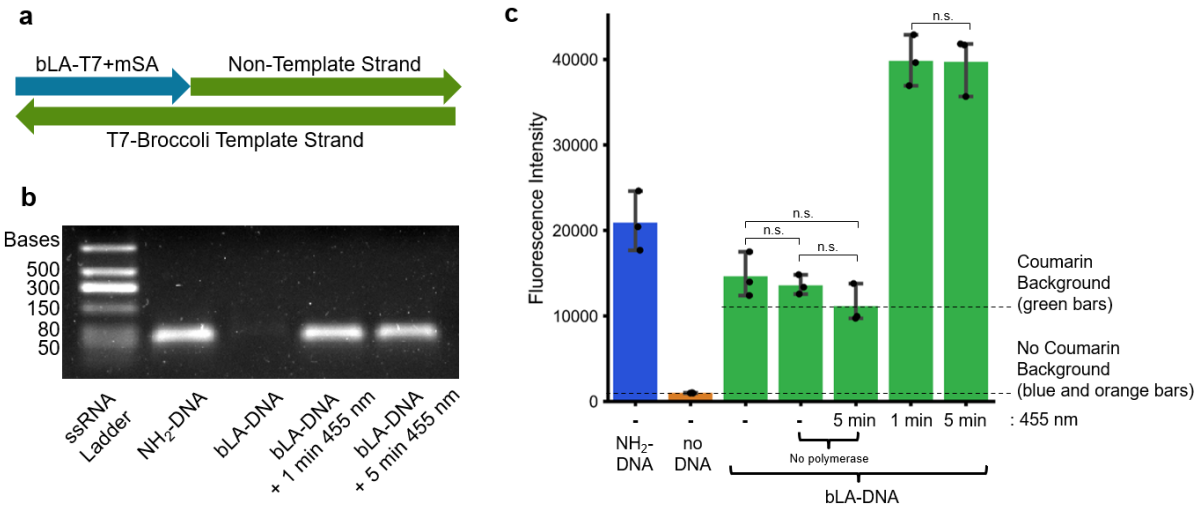


Figure 2-16: Expression of broccoli RNA aptamer from a caged bLA-DNA template

a) Schematic of the broccoli aptamer template DNA from bLA-T7, annealed from bLA-T7, T7-Broccoli Template Strand and Non-template Strand. **b**) Agarose gel electrophoresis of transcribed RNA from NH_2- or bLA-DNA broccoli templates, with or without 455 nm illumination. **c**) Fluorescence measurements of the *in vitro* transcription of broccoli aptamer in presence of DFHBI. A no polymerase control demonstrated the DNA itself showed a strong fluorescence background from the attached coumarin photocage. n.s. – non-significant, i.e. p-value > 0.05. Figure adapted from "Blue light-activatable DNA for remote controlled logic gates in synthetic cells" by D. Hartmann *et al.*[335] (© 2023) under a creative commons licence (CC-BY 4.0).

The fully annealed and caged broccoli templates were then subjected to a transcription reaction under different illumination conditions. As the DFHBI reporter molecule absorbs blue light, this was added after illumination to the reaction. The transcription reactions were run with T7 RNA polymerase with no illumination, or 455 nm illumination for 1 and 5 minutes and then incubated at 37 °C for 4 hours. The reactions were then analysed by AGE (**Figure 2-16**, b) and fluorescence (**Figure 2-16**, c).

Through gel electrophoresis it was found that the bLA-DNA did not show any appreciable amount of RNA (1% band intensity vs. control NH_2-DNA), whereas upon illumination for 1 and 5 minutes, comparable RNA amounts were seen (93% and 90% band intensity for 1- and 5-minutes illumination respectively vs. NH_2-DNA control), showing very tight caging ability of the coumarin-mSA-caged promoter as well as excellent photorelease and recovery upon illumination. The transcription reactions

were also analysed by fluorescence. A very large background was seen for the coumarin-containing samples, due to the coumarin molecule itself having a large overlap in excitation/emission spectra with the broccoli/DFHBI complex, as seen in **Figure 2-12**. To give a more accurate comparison, reactions without polymerase, with or without illumination, were added as control, to demonstrate that the elevated background is due to the presence of the photocage, rather than from expression of RNA. Taking this into account, tight caging of the DNA using the bLA-DNA (non-significant vs. no polymerase controls) and great recovery of transcription upon illumination was seen. In addition, there was no significant difference between 1 and 5 minutes of illumination, showing the non-damaging effect of blue light on the system.

2.7 Control of mVenus Production in a CFPS System

After optimisation of PCR conditions, the efficiency of controlling expression of a protein in a commercial CFPS system (PURExpress) was tested. For this, DNA templates encoding for mV were prepared from the bLA-T7 ssDNA by PCR, using the screened conditions (**Figure 2-17**, a). DNA templates were also prepared with the NH2-T7 ssDNA as a positive control for 100% photocleavage. Lastly, a UV light-activatable (uvLA) DNA template was prepared by preparation of a uvLA-T7 ssDNA from a commercial molecule (obtained from click-chemistry-tools) containing a biotinylated nitrobenzyl photocage, followed by PCR. All three prepared DNA templates were then incubated with mSA overnight to cage them and analysed by AGE under different illumination conditions (**Figure 2-17**, b).

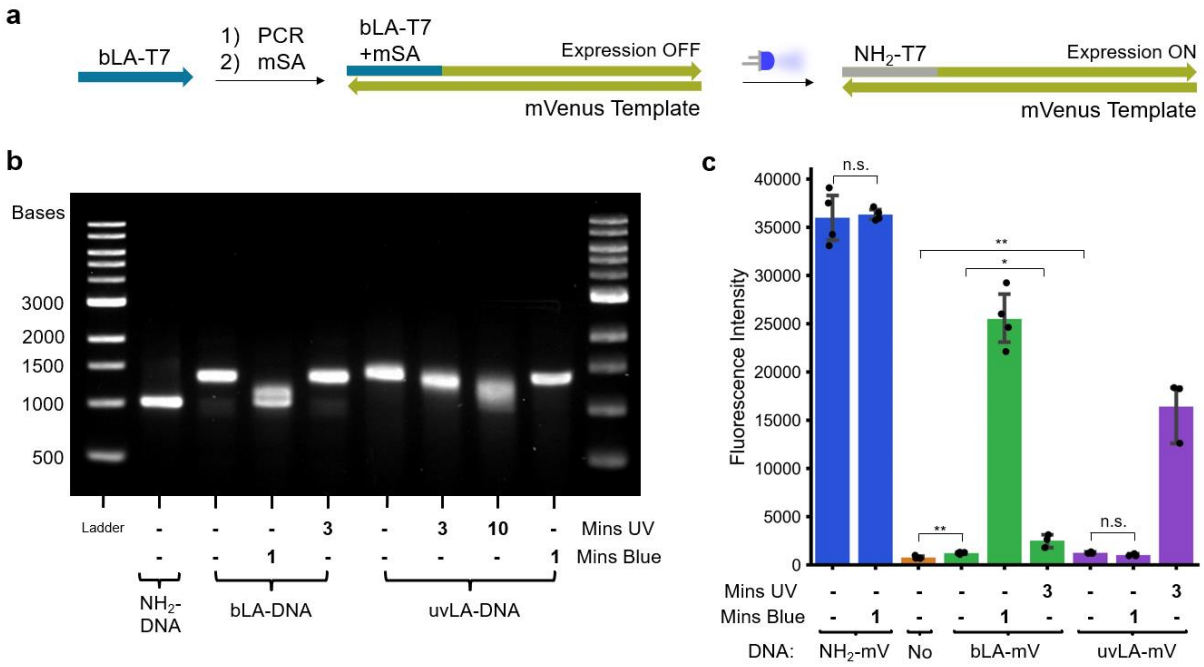


Figure 2-17: Preparation of LA-mV DNA templates, analysis by AGE and Expression of mV in a CFPS system.

a) Preparation of caged, blue light-activatable DNA and uncaging with blue light. bLA-T7 is used as a primer in PCR to generate a modified DNA template, caging with mSA and uncaging with blue light. **b**) Agarose gel electrophoresis of NH_2-, bLA- and uvLA-mV DNA under different illumination conditions. **c**) Cell-free expression of NH_2-, bLA- and uvLA-mV DNA with blue and UV irradiation. n=4 for bLA-DNA (with bLA-DNA +UV being n= 3) and n=3 for uvLA-DNA samples. n.s. - non-significant (p-value > 0.05). * - p-value < 0.05. ** p-value <0.005. Figure adapted from "Blue light-activatable DNA for remote controlled logic gates in synthetic cells" by D. Hartmann *et al.*[335] (© 2023) under a creative commons licence (CC-BY 4.0).

As anticipated, the bLA- and uvLA-mV DNA templates showed decreased electrophoretic mobility on the gel due to the bound mSA, compared to the NH_2-mV DNA, and the absence of a distinct, ladder-like appearance indicated complete modification with mSA, as has been studied by M. Booth previously. Upon irradiation of the bLA-mV DNA with 455 nm for 1 minute, almost full recovery of the NH_2-mV DNA was seen, with small amounts of not fully uncaged DNA. Irradiation of the uvLA-mV DNA with 455 nm for the same amount did not show a discernible shift in gel migration, as expected. Irradiation with 365 nm for 3 minutes, however, did show an increase in electrophoretic mobility, in line with uncaging of the DNA. This effect was even more visible when irradiated for 10 minutes. Most excitingly, however, irradiation of the bLA-mV DNA with UV light for 3 minutes did not show any discernible change in gel

migration, showing minimal uncaging and thus a large degree of orthogonality to UV light.

It was also tested whether the bLA-mV DNA could be uncaged further through longer illumination with 455 nm (**Figure 2-18**). An increase in illumination to 5 and 10 minutes unfortunately did not lead to improved uncaging ability. This is believed to be due to photobleaching of the coumarin, as has been reported for other coumarin-based photocages, where incomplete release was observed.[250,254,356] This is also supported by the bulk molecule photocleavage in **Figure 2-11**, where a drastic reduction in photocleavage is observed after 1 minute of high intensity irradiation.

Following on from analysis of the LA-DNA on gel, their ability to control cell-free protein expression was tested. The DNA templates were used in the PURExpress CFPS system, illuminated as required and the fluorescence of mV measured after 4 hours to quantify relative protein production from the different templates (**Figure 2-17**, c). The damaging effect of blue light irradiation on cell-free expression was tested with the NH_2-mV DNA. Illumination with 455 nm for 1 minute showed no significant difference in expression from the template, indicating no damaging effect of blue light on the CFPS system (p-value = 0.821). The bLA-mV DNA template showed only a minor increase in fluorescence compared to the background observed without template, showing tight caging of the DNA with the coumarin-mSA photocage (p-value = 0.002). Upon illumination with blue light for 1 minute, expression recovered to 70% compared to the control NH_2-mV DNA, giving an on/off ratio for the bLA-mV DNA of 98%. When illuminated with 365 nm light for 3 minutes, however, only a small increase in fluorescence is observed (p-value vs. no illumination = 0.011), showing a large degree of orthogonality of this photocage to UV irradiation. Similarly, a tight off-state was observed for the uvLA-mV DNA without illumination (p-value = 0.005). Expression was recovered to 50% after 365 nm irradiation for 3 minutes, but no increase in expression was observed after illumination with 455 nm for 1 minute (non-significant, p-value = 0.063), showing orthogonality of the uvLA-mV DNA to blue light.

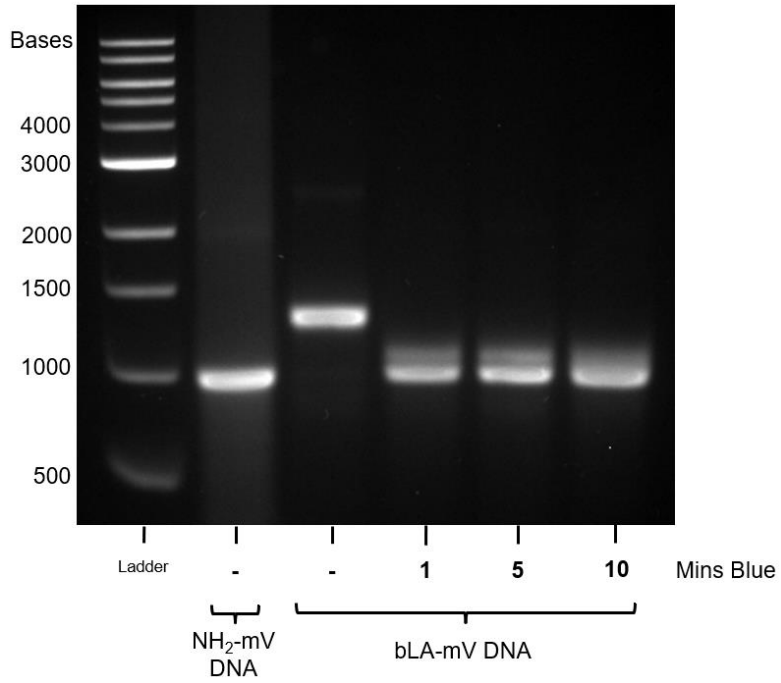


Figure 2-18: AGE of bLA-mV DNA with different durations of blue light illumination.
An increase in illumination time does not show further uncaging of the DNA. Figure adapted from "Blue light-activatable DNA for remote controlled logic gates in synthetic cells" by D. Hartmann *et al.*[335] (© 2023) under a creative commons licence (CC-BY 4.0).

To investigate whether the reduction in protein yield with the bLA-mV template after uncaging is on a transcriptional or translational level, *in vitro* transcription from the template was performed (**Figure 2-19**). As expected, negligible levels of mRNA were produced without illumination. Upon illumination of the bLA-mV DNA template, however, mRNA expression was found to be 70% compared to the NH_2-mV DNA template, as measured by gel band intensity. This mirrors what is observed in the protein expression data, indicating that the reduction in protein yield after illumination is from decreased mRNA expression.

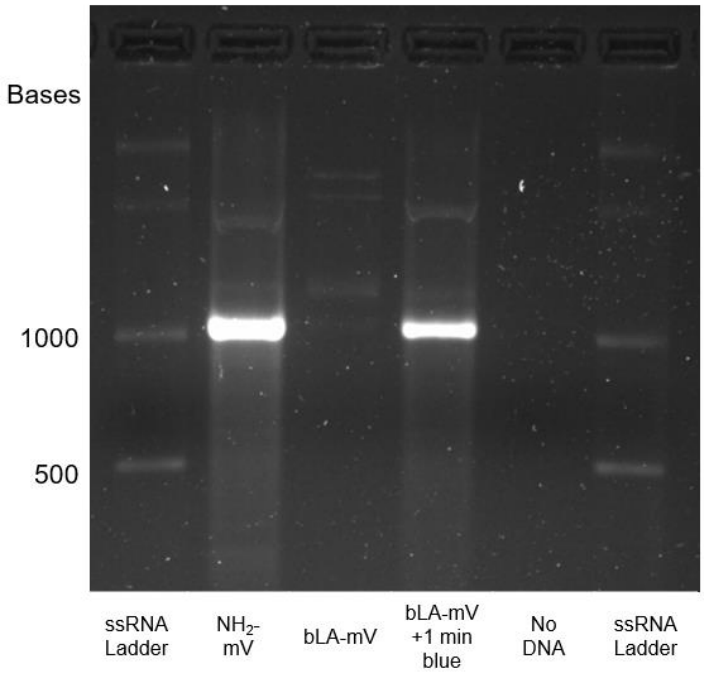


Figure 2-19: *In vitro* transcription of mRNA from the bLA-T7 template

No mRNA is produced from the bLA-mV DNA template in the absence of light, with 70% mRNA yield after illumination with blue light. Figure adapted from "Blue light-activatable DNA for remote controlled logic gates in synthetic cells" by D. Hartmann *et al.*[335] (© 2023) under a creative commons licence (CC-BY 4.0).

Next, it was investigated whether a gradual response can be generated from the bLA-mV DNA template in cell-free expression (Figure 2-20). For this, the samples were irradiated for less time and at lower powers. Even at 10 seconds of illumination at 4/6 LED power, 63% expression was observed vs. the NH_2-mV DNA, with longer illumination only giving marginal increases up to the expected 70% with 1 minute. A decrease in power allowed for a gradual response, giving rise to 3% and 21% activation, respectively.

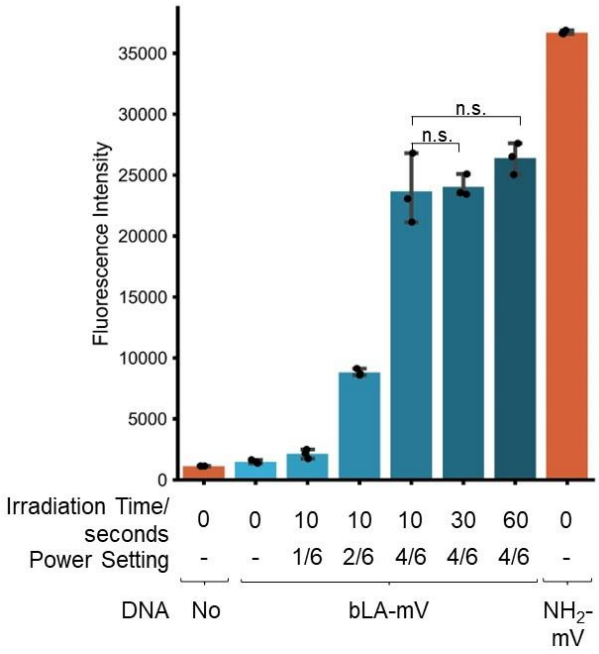


Figure 2-20: Different amounts of irradiation to express mVenus protein from bLA-mV DNA in CFE.

Short illumination at low irradiance allowed for a graduated response. Further illumination past 10 seconds at 4/6 power showed only minimal increases in expression levels, and thus photobleaching of the photocage. 1/6 power corresponds to an irradiance of 7.34 mW·cm^{-2}, 2/6 power corresponds to an irradiance of 17.54 mW·cm^{-2}. Figure adapted from "Blue light-activatable DNA for remote controlled logic gates in synthetic cells" by D. Hartmann *et al.*[335] (© 2023) under a creative commons licence (CC-BY 4.0).

2.8 Two-Wavelength Control of Gene Expression

As the two photocages could be activated orthogonally with their respective wavelengths, the question arose whether this could be used for generation of a light-controlled AND-logic gate. Split proteins are a common way of investigating biological interactions and biomarkers.[357,358] Among the oldest split reporter proteins is the enzyme β-Galactosidase (β-Gal).[359] As several fluorogenic substrates for β-Gal exist as well, it was a prime candidate for the development of a light-controlled AND-gate using the LA-DNA technology. The β-Gal, when split at a loop region, forms two protein parts, labelled α and ω, which individually are inactive, but can spontaneously self-assemble in solution and reconstitute enzymatic activity.[358]

R. Chowdhry in the Booth group had already cloned the *lacZ* gene, encoding for β-Gal, into the PURExpress control template, which is used in the group to prepare linear

templates for cell-free expression. With the help of J. Smith, primers were designed to prepare the split protein parts from the full-length *lacZ* gene inside the control template (splitting the protein at amino acid 738, with a stop codon added to α and a starting Met added to ω), as well as vectors from the plasmid backbone. The designed primers included homologous regions allowing for plasmid preparation by homologous recombination inside bacteria from linear PCR products. These linear DNA products were then prepared by PCR (**Figure 2-21**), prior to transformation into *E. coli* and growth on Ampicillin-containing Luria-Bertani agar plates.

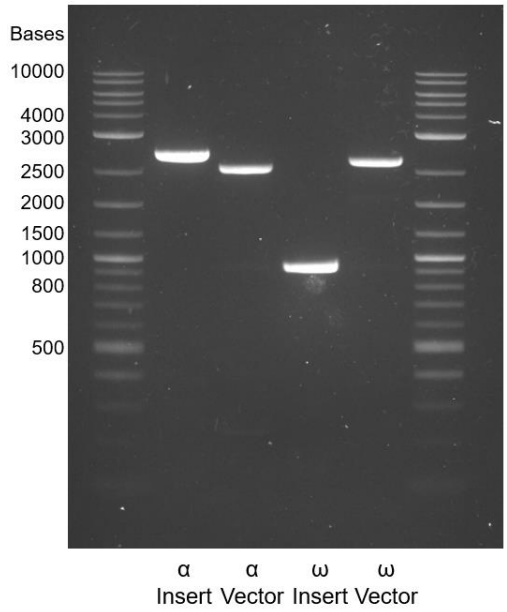


Figure 2-21: Linear PCR products for split β-Gal generation by homologous recombination
Figure adapted from "Blue light-activatable DNA for remote controlled logic gates in synthetic cells" by D. Hartmann *et al.*[335] (© 2023) under a creative commons licence (CC-BY 4.0).

Colonies were tested by PCR using the T7 forward and reverse primers used in the preparation of linear DNA templates for the presence of the desired plasmid. Positive colonies were used for minipreparation of the plasmids, which were sequenced using Sanger sequencing to confirm their identity. Using these plasmids as PCR templates, linear blue light-activatable ω-subunit DNA was prepared using the bLA-T7 ssDNA and linear, UV light-activatable α-subunit DNA was prepared using the uvLA-T7 ssDNA (prepared using the molecule from click-chemistry-tools). In addition, the α and ω linear templates were also prepared using the NH_2-T7 to serve as positive controls for 100% photocleavage, and all linear templates were then incubated with 50x molar excess of mSA. These linear templates were then tested for orthogonality, by looking at their photocleavage (**Figure 2-22**) as well as transcription from them (**Figure 2-23**).

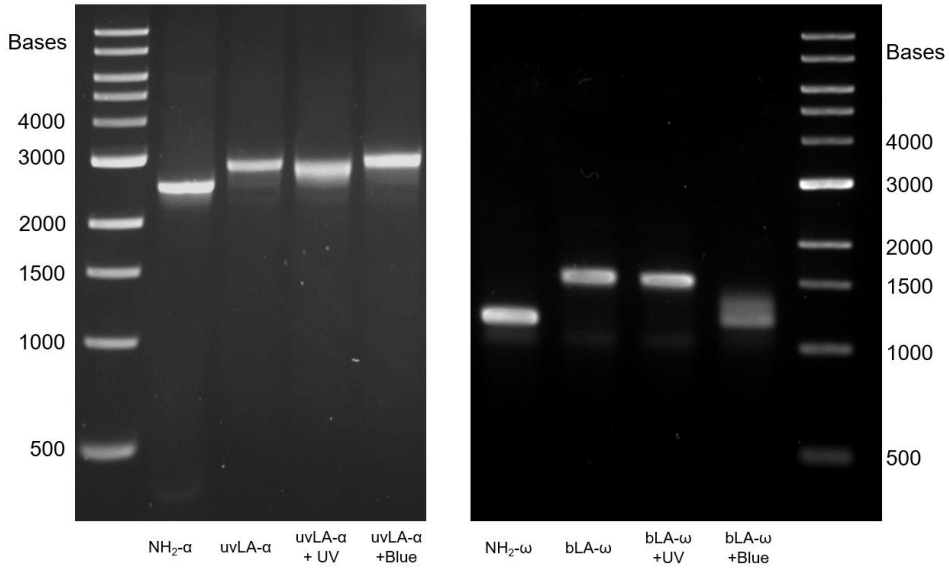


Figure 2-22: Linear LA-DNA templates encoding for the α- and ω-subunits of β-Gal with different LA-promoters under different illumination conditions.

The Linear templates were prepared by PCR. The α-subunit bears the uvLA-T7 promoter (prepared with the click-chemistry-tools molecule) and the ω-subunit the bLA-T7 promoter. The LA-DNAs only show appreciable photocleavage under illumination with their respective wavelength. Figure adapted from "Blue light-activatable DNA for remote controlled logic gates in synthetic cells" by D. Hartmann *et al.*[335] (© 2023) under a creative commons licence (CC-BY 4.0).

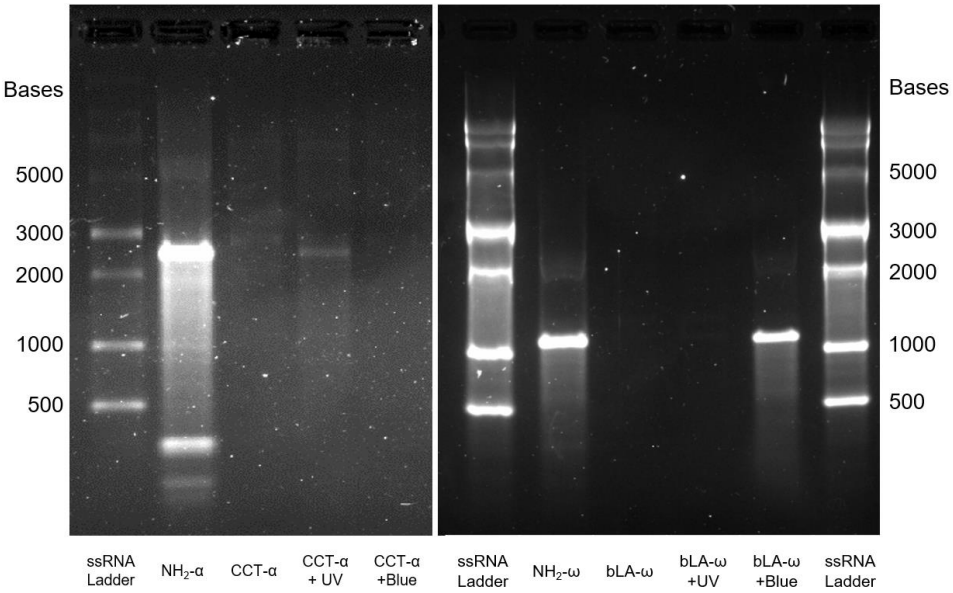


Figure 2-23: RNA Transcription from the LA-DNA templates uvLA-α and bLA-ω used in Figure 2-22 under different illumination conditions.

Transcription of mRNA from the LA-DNAs only occurred after illumination with their respective wavelength. Figure adapted from "Blue light-activatable DNA for remote controlled logic gates in synthetic cells" by D. Hartmann *et al.*[335] (© 2023) under a creative commons licence (CC-BY 4.0).

As expected, the uvLA-α DNA prepared from the click-chemistry-tools molecule showed no cleavage on gel and no expression of mRNA without illumination or with blue light, but did show cleavage and transcription of mRNA with UV light.
Similarly, the bLA-ω DNA showed no discernible change of gel migration and negligible mRNA expression upon UV illumination, but showed cleavage and mRNA production upon irradiation with blue light.

Using these linear DNA parts, a remote-controlled AND-gate could be assembled, using UV and blue light as inputs (**Figure 2-24**). By illuminating with either UV or Blue light alone, only one of the two subunits would be expressed from their respective LA-DNA. When both wavelengths are applied, however, both protein parts should be expressed, which reconstitutes enzymatic activity. To measure the enzymatic activity, non-fluorescent carboxyumbelliferyl-β-D-galactopyranoside (CUG) was chosen as the substrate, which in the presence of the active enzyme gets hydrolysed to the fluorescent umbelliferone-3-carboxylic acid (UCA).

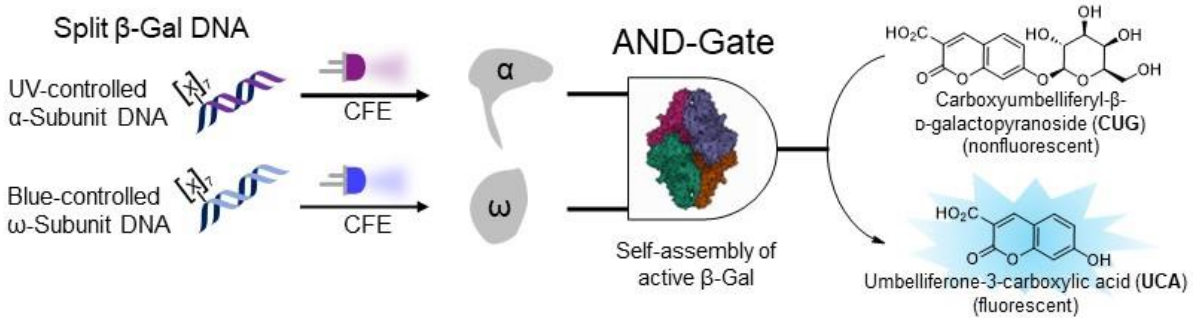


Figure 2-24: Schematic of the two-wavelength-controlled AND-gate based on split β-Galactosidase.

The two inactive β-Gal parts, α and ω, were placed under the uvLA- and bLA-T7 promoters respectively. Activation of both allowed reconstitution of active β-Gal, measured by the enzymatic product UCA. Figure adapted from "Blue light-activatable DNA for remote controlled logic gates in synthetic cells" by D. Hartmann *et al.*[335] (© 2023) under a creative commons licence (CC-BY 4.0).

The two DNA parts were then placed into the CFPS system, illuminated with no, UV-, Blue- or UV and Blue light and incubated for 4 hours at 37 °C. The resulting solutions were then placed into an ice-cold solution of CUG in H_2O and mixed, before transferring them into a chilled 384-well plate. The cooling steps were taken to prevent enzymatic activity prior to the measurement taking place. The 384-well plate was then placed into a plate reader heated to 37 °C and the fluorescence measured at regular

time intervals (**Figure 2-25**). With the NH_2-DNA parts, high activity of β-Gal was observed. With the LA-DNA parts, in the absence of light, no fluorescence increase was measured over 1 hour, showing tight control from both LA-DNA parts. Using irradiation with only UV light, no increase in fluorescence was observed and when irradiated with blue light only, a small increase in fluorescence was observed over 1 hour. Excitingly, with both wavelengths applied, a high amount of activity was observed, showing an AND-gated response. It did not, however, reach activity levels compared to the NH_2-DNA control.

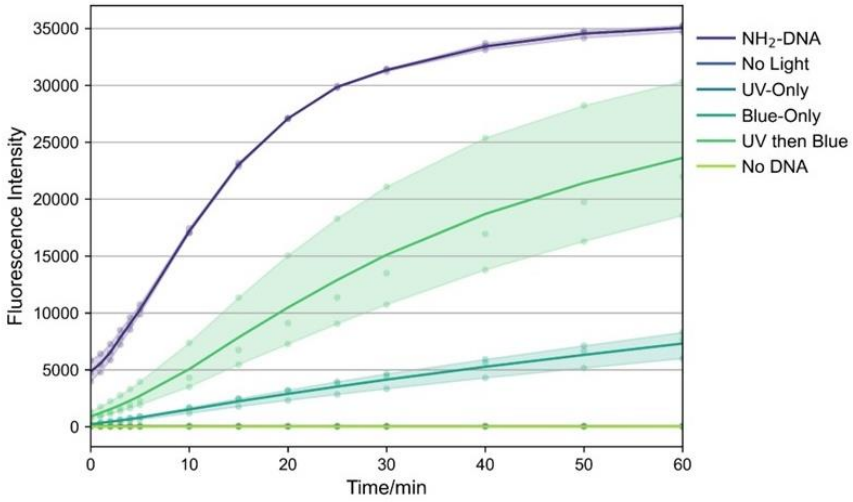


Figure 2-25: Fluorescence measurements of UCA over 60 minutes after expression of split β-Galactosidase from the LA-DNA parts under different illumination conditions.

Figure adapted from "Blue light-activatable DNA for remote controlled logic gates in synthetic cells" by D. Hartmann *et al.*[335] (© 2023) under a creative commons licence (CC-BY 4.0).

As the on-state observed was not reaching high levels, an alternative UV photocage was tested to see if it provided better activity. M. J. Booth and J. Smith in the Booth group have previously been working with an alternative UV-photoactivatable biotin photocage to prepare uvLA-DNA templates, supplied by Ambergen. The reason for not choosing this molecule initially was the high cost and difficulty in acquiring the molecule. It was however used here to prepare an alternative UV light-activatable T7 ssDNA, from which the uvLA-α DNA template could be prepared. This DNA was then again tested by AGE (**Figure 2-26**, a) and in a transcription reaction (**Figure 2-26**, b) under different illumination conditions. The data closely mirrored what was observed for the uvLA-α DNA template prepared using the click-chemistry-tools molecule, with

no cleavage or transcription without light or with blue light, and small amounts of cleavage and transcription observed after irradiation with UV light.

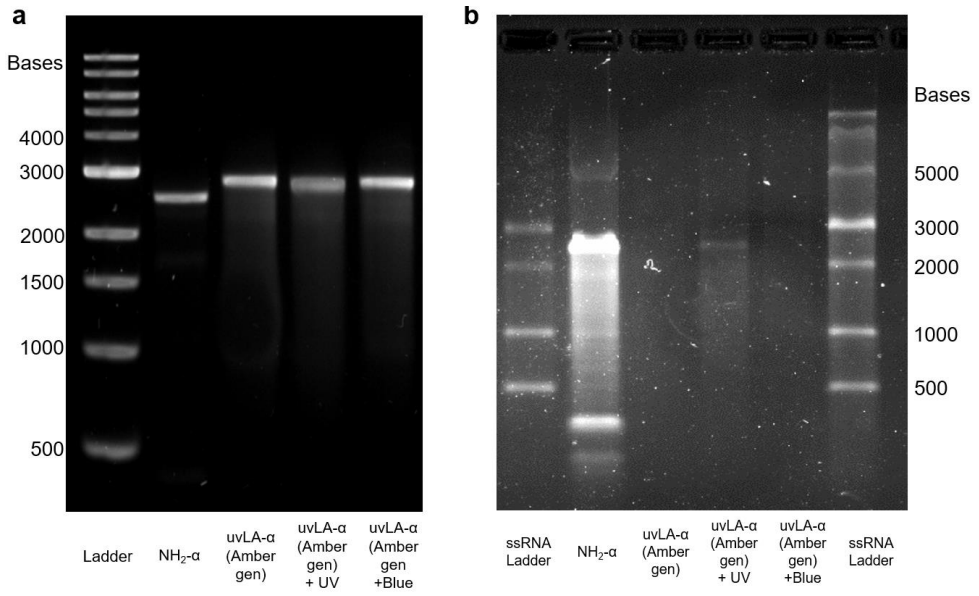


Figure 2-26: DNA gel and transcription reaction gel from the uvLA-α, prepared using the molecule from Ambergen.

Photocleavage and mRNA expression was only observed when illuminated with UV light. Figure adapted from "Blue light-activatable DNA for remote controlled logic gates in synthetic cells" by D. Hartmann *et al.*[335] (© 2023) under a creative commons licence (CC-BY 4.0).

The AND-gate experiment was then repeated with the new uvLA-α DNA template prepared from the Ambergen molecule (**Figure 2-27**). In the absence of light, a very tight off-state was again observed. Upon irradiation with either UV- or blue light, some activation was observed. Excitingly though, with both wavelengths applied, in either order, full activity vs. NH_2-DNA was regained. To quantify this data better, the fluorescence levels were compared where the enzymatic hydrolysis has reached its maximum rate at half the maximum enzymatic output (minute 10, orange line), as product formation was at a steady-state and thus $V_{max} \propto [E]_0$ (**Figure 2-28**). At this timepoint, a very tight off-state of 99.9% was observed in the absence of irradiation. Upon illumination with either UV- or blue light alone, 14% and 17% respectively of the enzyme was produced compared to the positive NH_2-DNA control. With both wavelengths applied, however, in either order, full enzymatic activity was reconstituted, with no significant difference between them or against the NH_2-control, showing the first example of two-wavelength-controlled, cell-free AND gate.

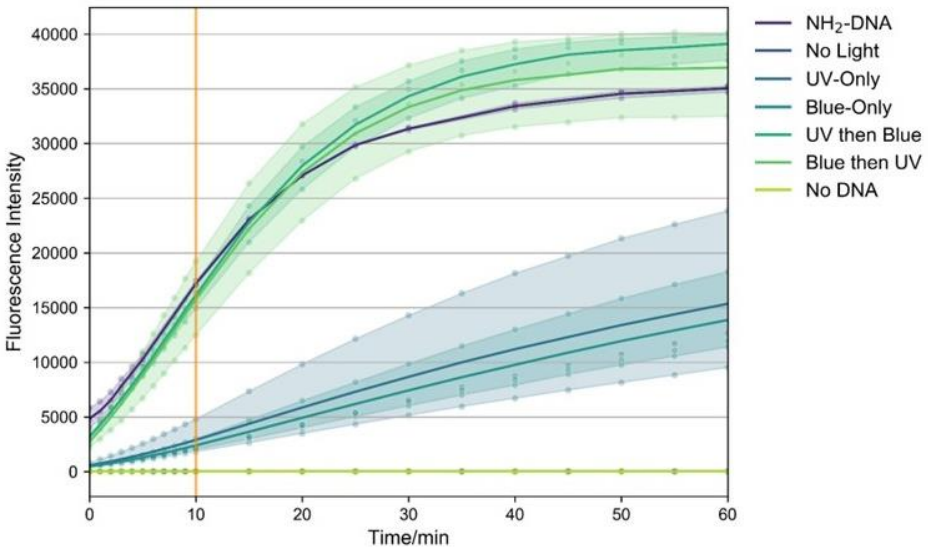


Figure 2-27: Evolution of fluorescence of UCA over time using the uvLA-α DNA template prepared with the Ambergen molecule together with the bLA-ω DNA.

Figure adapted from "Blue light-activatable DNA for remote controlled logic gates in synthetic cells" by D. Hartmann *et al.*[335] (© 2023) under a creative commons licence (CC-BY 4.0).

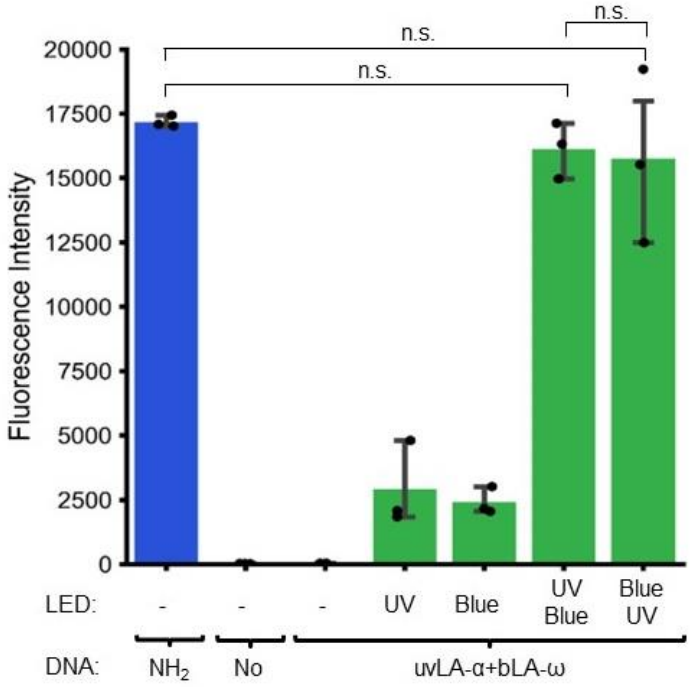


Figure 2-28: UCA fluorescence at minute 10 (Figure 2-27, orange line)

Full split β-Gal activity was only reconstituted when both UV and blue light were applied (in either order), with only minimal activity with only one wavelength. n.s. – non-significant (p-value >0.05). Figure adapted from "Blue light-activatable DNA for remote controlled logic gates in synthetic cells" by D. Hartmann *et al.*[335] (© 2023) under a creative commons licence (CC-BY 4.0).

2.9 Controlled Expression in Giant Unilamellar Vesicles

Synthetic cells are small, bounded compartments that demonstrate minimal cellular function. These synthetic cells show great promise in biology, biotechnology and medicine, as they are fully biocompatible and thus allow for drug delivery,[360] but also allow for the fundamental study of biological processes in a minimal system, as discussed in Chapter 1.4.3.[361]

These synthetic cells, do however, require mechanisms for control of their function, and for this, stimuli that are capable of crossing the compartment boundary need to be employed. Light, as it is completely external, is an ideal candidate. Hence, the bLA-DNA developed was suitable for control of synthetic cells.

bLA-mNeonGreen (mNG) DNA, as well as the NH_2-mNG DNA templates for use in synthetic cells were prepared (**Figure 2-29**). mNG was chosen due to its high brightness, rapid maturation and good overlap with the filter cubes of the epifluorescence microscope.[362]

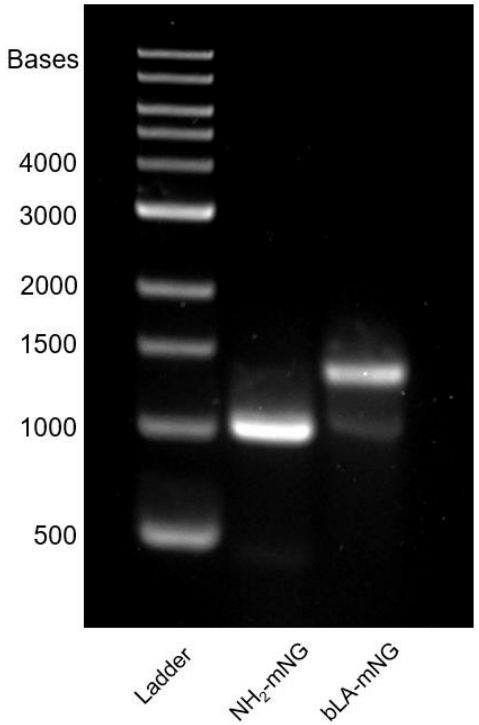


Figure 2-29: Preparation of NH_2- and bLA-mNG DNA

Figure adapted from “Blue light-activatable DNA for remote controlled logic gates in synthetic cells” by D. Hartmann *et al.*[335] (© 2023) under a creative commons licence (CC-BY 4.0).

R. Chowdhry was asked for assistance for this experiment, due to her experience in preparing synthetic cells. R. Chowdhry encapsulated the prepared bLA-mNG DNA, the unmodified NH_2-mNG DNA, or no DNA, with the PURExpress CFPS system and

Texas-Red (TxRd)-Dextran for imaging inside giant unilamellar vesicles (GUVs) made from egg phosphatidyl choline (egg-PC) *via* the inverted emulsion method (**Figure 2-30**, a).[206,363]

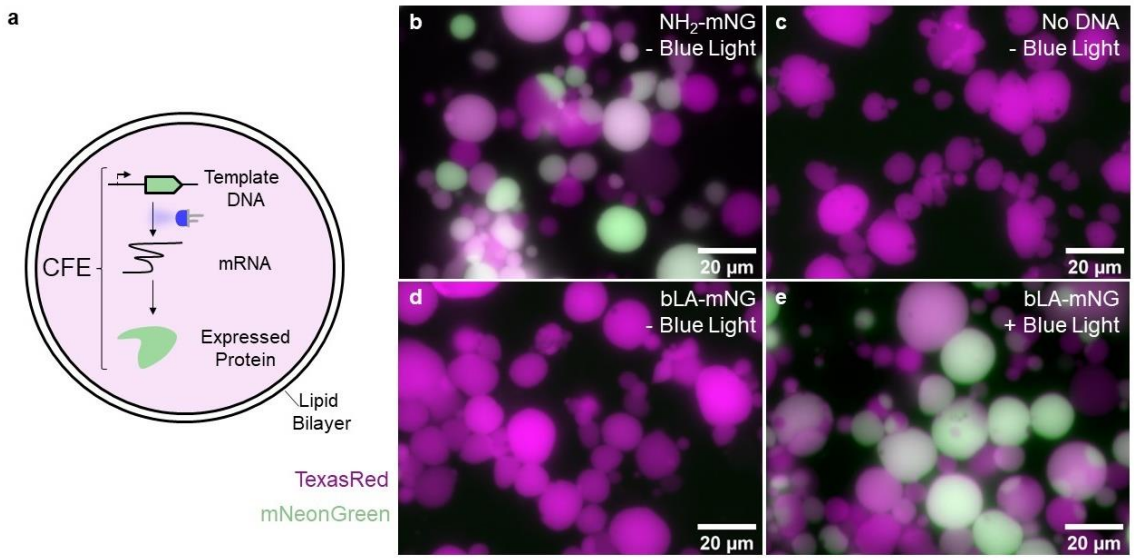


Figure 2-30: Controlling synthetic cell activity with bLA-DNA

Data obtained by R. Chowdhry. In the absence of irradiation, the bLA-mNG containing synthetic cells show no fluorescence of mNG (d) similar to the synthetic cells without DNA (c). Upon irradiation with 455 nm, however, mNG fluorescence is observed (e), similar to cells containing the control NH_2-only DNA (a). Figure adapted from "Blue light-activatable DNA for remote controlled logic gates in synthetic cells" by D. Hartmann *et al.*[335] (© 2023) under a creative commons licence (CC-BY 4.0).

The prepared GUVs were then illuminated as required and incubated at 37 °C for 5 hours, before imaging on the epifluorescence microscope. As anticipated, high fluorescence was observed in GUVs containing unmodified DNA, and no fluorescence was observed in GUVs not containing DNA (**Figure 2-30**, b, c). Pleasingly, without 455 nm irradiation, GUVs containing the bLA-mNG DNA showed no mNG expression. Upon illumination with blue light, however, recovery of expression of mNG was seen (**Figure 2-30**, c, d).

2.10 Photopatterning of Emulsion Droplets with one and two Wavelengths of Light

As controlling synthetic cells worked very well with blue light, it was envisaged they could also be controlled spatiotemporally. For this, water-in-oil emulsion droplets were

chosen, as they are another commonly encountered synthetic cell chassis,[364] can rapidly be prepared through emulsification[199] and immobilised through gelling of the oil phase.[365]

Immobilised, emulsion-based synthetic cells were then prepared using the NH_2- and bLA-mNG DNA and TxRd-Dextran in PURExpress and illuminated through photomasks (**Figure 2-31**, a). The CFPS solution was emulsified with a 50 °C solution of 10 mg/mL styrene-ethylene-butylene-styrene (SEBS) polymer in hexadecane containing 2% Span80 by agitation along a PCR tube rack and placed into black 96-well plates with clear bottoms. The SEBS polymer caused the hexadecane phase to gel at low temperatures immobilising the aqueous droplets suspended within, whereas the Span80 stabilised the aqueous droplets and prevented them from fusing. Photomasks were then applied to the bLA-mNG-containing wells by taping them to the clear bottom of the well followed by illumination with 455 nm light. The wells were illuminated through the bottom of the plate to ensure the light to have the shortest path possible to the droplets, preventing large degrees of scattering and thus untargeted activation of the droplets.

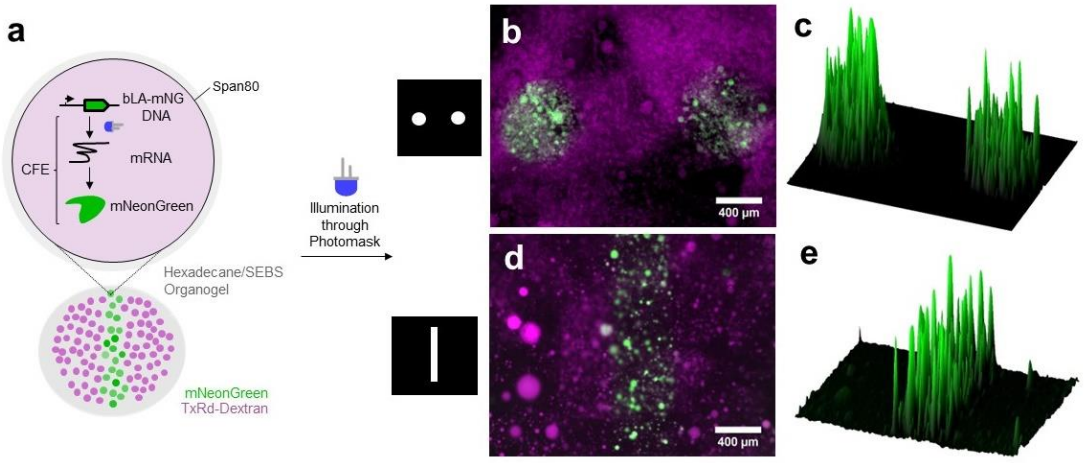


Figure 2-31: One-wavelength spatiotemporal activation of gene expression inside immobilised emulsion droplet-based synthetic cells.

a) Application of photomasks over organogel-immobilised emulsion droplet synthetic cells. Expression patterns of dots (**b-c**) and a line (**d-e**) through controlled activation of mNG expression *via* photomasks. Figure adapted from “Blue light-activatable DNA for remote controlled logic gates in synthetic cells” by D. Hartmann *et al.*[335] (© 2023) under a creative commons licence (CC-BY 4.0).

After illumination with blue light, the 96-well plates were incubated at 37 °C for 4 hours and then imaged on the epifluorescence microscope. The photomasks chosen were

dots and a line. With both the dots (**Figure 2-31**, b, c) as well as the line (**Figure 2-31**, d, e), tight spatiotemporal control of the droplets was observed, as there were clear boundaries to where illumination took place and thus the desired shapes being clearly visible and only a very low background from non-illuminated droplets was seen.

In contrast, droplets containing the unmodified NH_2-mNG DNA all showed fluorescence after incubation (**Figure 2-32**), showing that the developed bLA-DNA technology can spatially and temporally control gene expression.

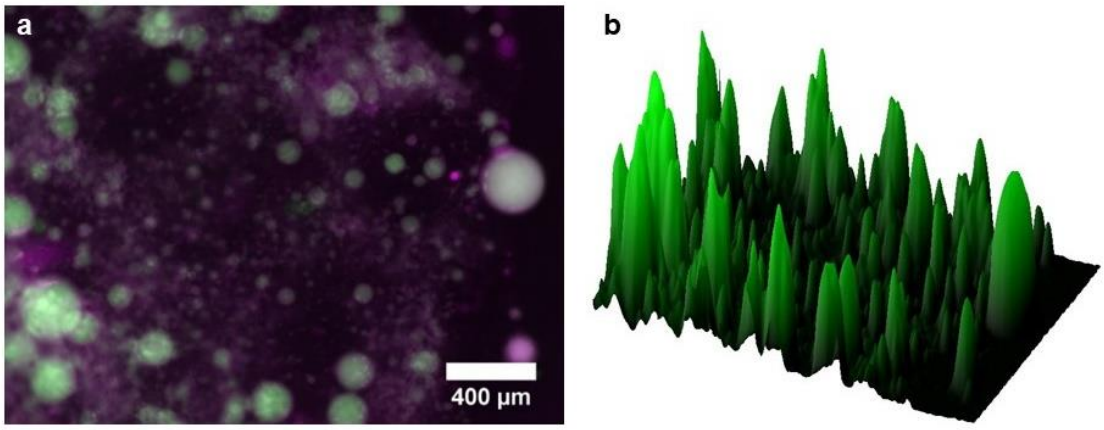


Figure 2-32: Immobilised emulsion droplet-based synthetic cells containing NH_2-mNG DNA
Figure adapted from "Blue light-activatable DNA for remote controlled logic gates in synthetic cells" by D. Hartmann *et al.*[335] (© 2023) under a creative commons licence (CC-BY 4.0).

Next, the question arose if both UV and blue light can be used to spatiotemporally control gene expression by incorporation of the developed split β-Gal-based AND-gate.

Initially, this was performed using the NH_2-α and -ω DNA templates with CUG as substrate, but unfortunately the brightness of the resulting UCA was very low and could not be observed well using the DAPI-channel of the epifluorescence microscope. Due to this, the substrate was changed to fluorescein-di-β-D-galactopyranoside (FDG), another common substrate for β-Gal and its hydrolysis product fluorescein is the brightest of the commercial β-Gal reporter substrates. The produced fluorescein also had excellent overlap with the filter cubes of our microscope. Encapsulation of FDG instead of CUG and incubation for 3 hours at 37 °C showed excellent activity when

used with the NH_2-DNAs in emulsion droplets (**Figure 2-33**) and was taken forward to be employed with the light-controlled AND-gate.

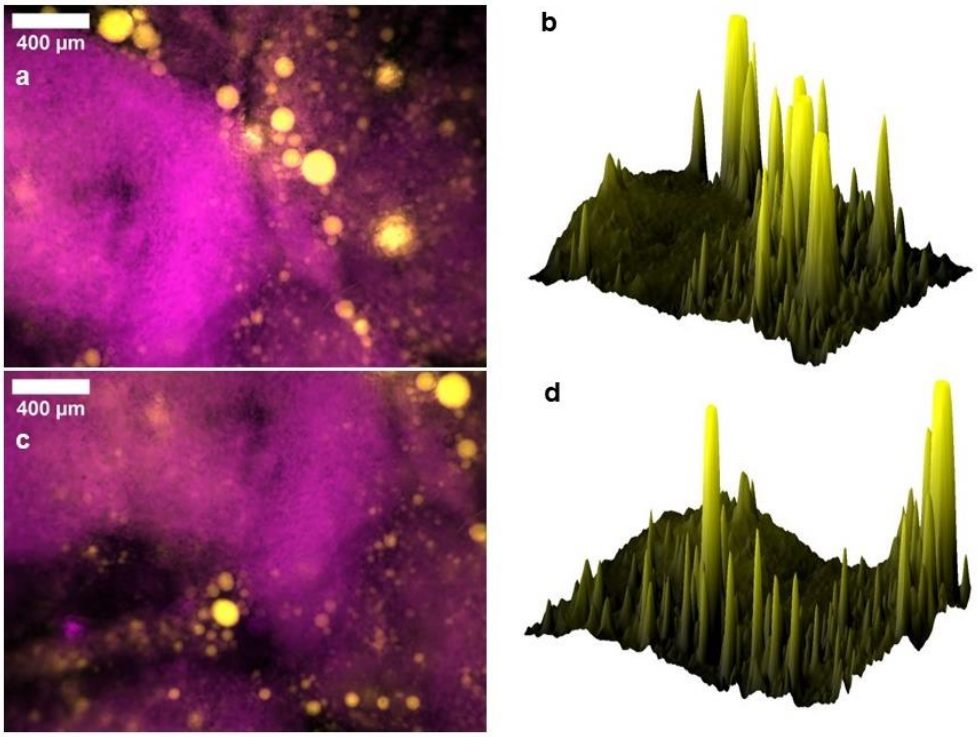


Figure 2-33: Expression of split β-Galactosidase from NH_2-α and -ω DNA templates in presence of reporter molecule FDG.

Images taken from the same well at different positions. Figure adapted from "Blue light-activatable DNA for remote controlled logic gates in synthetic cells" by D. Hartmann *et al.*[335] (© 2023) under a creative commons licence (CC-BY 4.0).

Next, emulsion droplets were prepared using the bLA-ω DNA and the uvLA-α DNA prepared using the click-chemistry-tools molecule, together with FDG and TxRd-Dextran, as described previously. The line photomask was then applied horizontally and the well illuminated with UV light; the photomask was then rotated 90° and the wells illuminated with blue light, before incubation for 3 hours at 37 °C (**Figure 2-34**, a). This resulted in a zone at the intersection of both illumination lines where both wavelengths were applied. Only in this two-wavelength zone, both subunits of the split enzyme should be expressed and only there, fluorescence from fluorescein production should be observed.

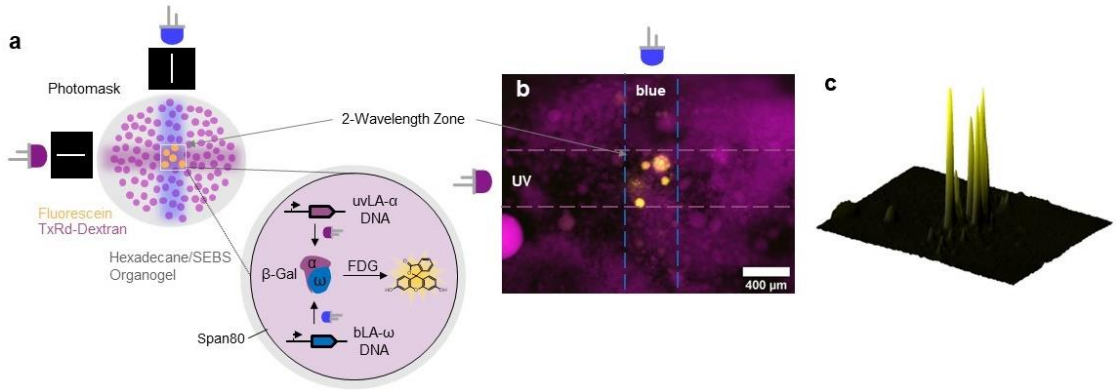


Figure 2-34: Two-wavelength-controlled emulsion-based synthetic cells, expressing split β-Galactosidase.

a) Application of UV and blue light through orthogonal line photomasks onto immobilised emulsion-droplet based synthetic cells, containing the uvLA-α and bLA-ω DNA parts of split β-gal. **b**) Two-wavelength patterning through patterned illumination with both UV and blue light. Fluorescence is only observed in the zone where both wavelengths overlap (**b-c**). Figure adapted from "Blue light-activatable DNA for remote controlled logic gates in synthetic cells" by D. Hartmann *et al.*[335] (© 2023) under a creative commons licence (CC-BY 4.0).

When imaged on the epifluorescence microscope after incubation, this was exactly what was observed (**Figure 2-34**, b, c), with no appreciable fluorescence in the regions that had no or only one wavelength-illumination, but several droplets in the quadrilateral formed by the overlap of the two lines showing strong fluorescence.

To ensure this experiment is robust, this was then repeated a further three times (**Figure 2-35**). In all cases, a clear zone of expression was observed, with few to no off-target droplets showing fluorescence, indicating repeatability of the two-wavelength control of gene expression inside synthetic cells using the developed AND-gate.

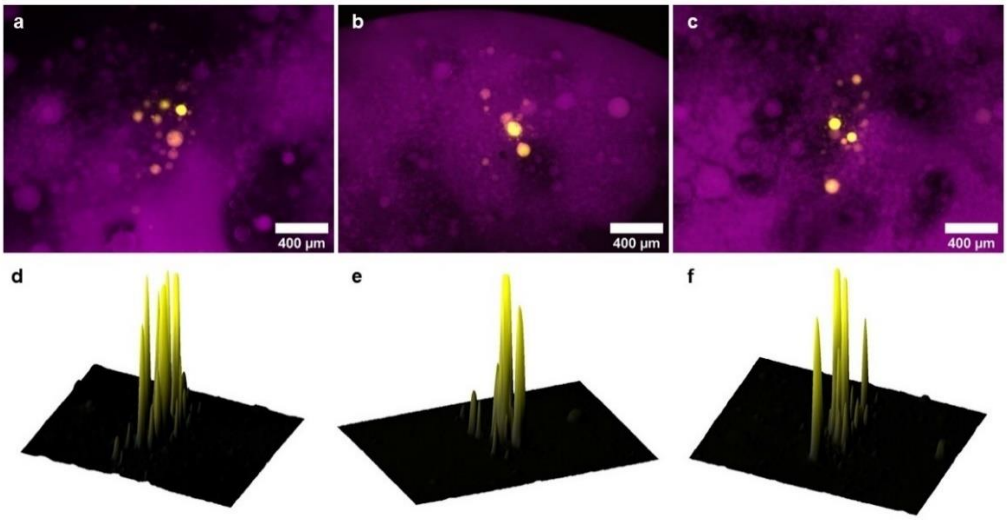


Figure 2-35: Repeats of the two-wavelength-controlled AND-gate based on split β-Galactosidase inside immobilised emulsion-droplet-based synthetic cells.

Figure adapted from “Blue light-activatable DNA for remote controlled logic gates in synthetic cells” by D. Hartmann *et al.*[335] (© 2023) under a creative commons licence (CC-BY 4.0).

2.11 Conclusions

In this chapter, the development of a new, blue-light activatable photocage for light-control of DNA templates was demonstrated. This photocage was synthesised from a previously reported extended coumarin scaffold capable of photocleavage with blue light. The photocage provided a biotin for binding of streptavidin and a reactive warhead for bioconjugation onto amines. Conditions for efficient attachment of the photocage onto amine-modified nucleotides inside a ssDNA containing the T7 promoter sequence were screened. The resulting modified oligonucleotide could be employed in PCR for the generation of light-activatable linear DNA templates. Using this approach, the expression of fluorescent reporter proteins was demonstrated in cell-free conditions as well as inside synthetic cells and showed excellent off-states and high recovery upon illumination. Gene expression inside these synthetic cells could also be performed spatially controlled through the application of photomasks.

The photocage also showed a large degree of orthogonality to UV irradiation and it was thus possible to use it in conjunction with the previously developed UV-activatable photocage. A two-wavelength-controlled AND-gate was developed from split β-galactosidase, by placing the subunits under the UV or blue light-activatable promoter, respectively. The resulting AND-gate uses two wavelengths as inputs and has fluorescent output in the form of an enzymatic hydrolysis through the produced enzyme. This was performed both in bulk, as well as spatially controlled inside synthetic cells, showing very tight off-states, minimal activation with only one wavelength, as well as excellent recovery upon irradiation with both wavelengths.

This technology is believed to be an important addition to the toolkit of synthetic biology, as it allows spatially and temporally defined control of gene expression with two orthogonal wavelengths of light. The approach chosen is also completely independent of the gene used, as demonstrated by the wide range of employed genes in this chapter.

3 LIGHT-CONTROLLED LA-BIOTIN-MODIFIED ANTISENSE OLIGONUCLEOTIDES

3.1 Introduction

It was envisioned that the developed light-activatable biotin technology could also be employed to cage other oligonucleotides. ASOs, as described in Chapter 1.3.4.2, provided an interesting target, as they are heavily investigated for their capabilities of controlling gene expression. ASOs have not extensively been used in CFPS systems to control gene knockdown, but have recently seen a report in being used in synthetic cells.[334] In general, several light-activatable ASOs have been developed as discussed in Chapter 0, but none have been reported for use in cell-free systems. Hence, they provide an important target for the light-control of cell-free systems, as the development of such systems allows for a light-controllable off-switch to gene expression, both in bulk as well as in synthetic cells.

One of the mechanisms of ASO activity is through degradation of mRNA *via* RNase H, as discussed in Chapter 1.3.4.2, which relies on the recognition of an ASO:mRNA hybrid duplex for gene silencing. Through incorporation of amino-C6-dT nucleobases into an ASO, attachment of the UV and blue-light photocleavable biotin photocages would be possible. Binding of streptavidin should then again provide steric block, which, analogous to the LA-DNA templates and T7 RNAP, should disable RNase H from binding to the ASO:mRNA duplex. Irradiation with the appropriate wavelength should then cleave off the photocages, enabling RNase H-mediated degradation and thus provide a way of controlling gene knockdown in cell-free systems with light (**Figure 3-1**, a).

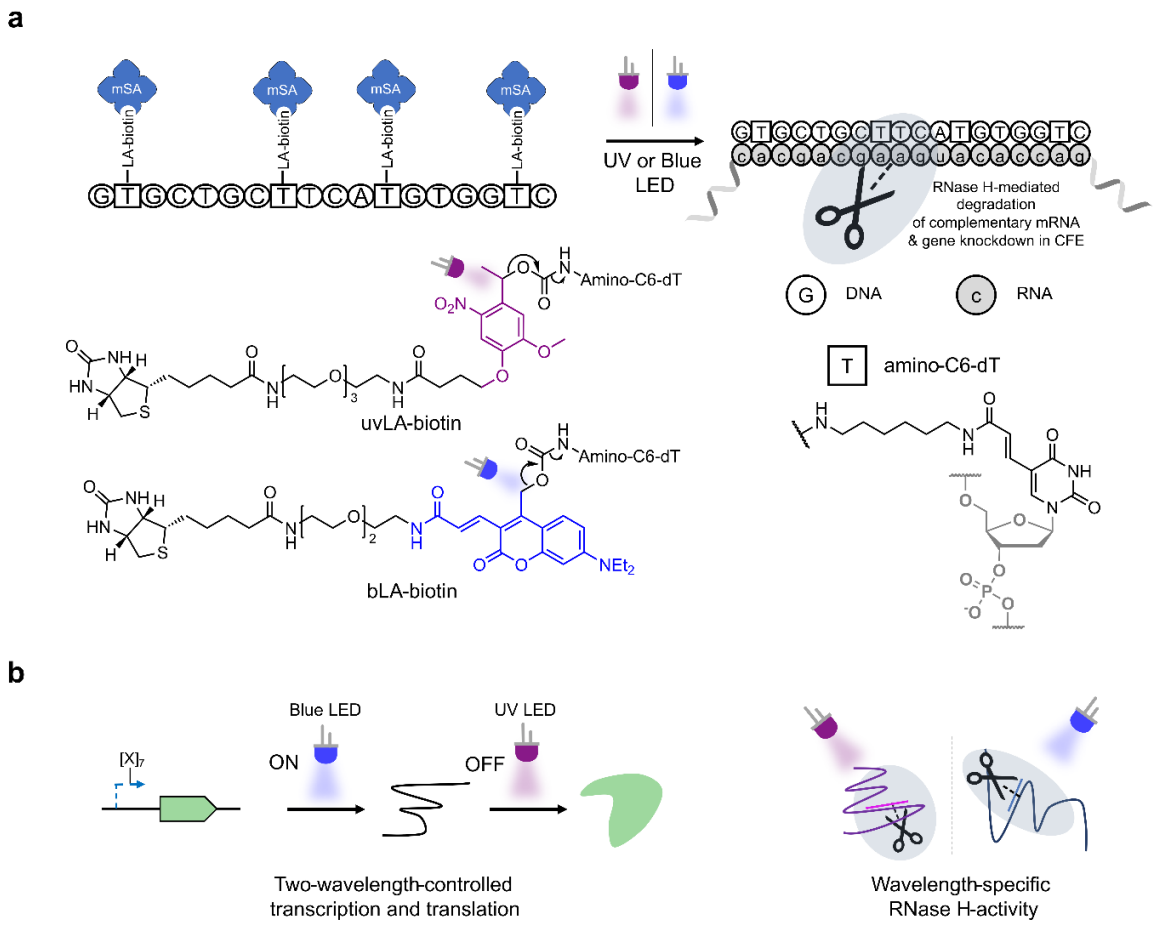


Figure 3-1: Controllable ASOs based on the LA-biotin technology and their application in cell-free protein synthesis.

a) LA-ASOs, modified on amino-C6-dT nucleotides with either uvLA or bLA-biotin, could be uncaged with UV or Blue irradiation, respectively. This allowed for activation of RNase H activity and gene knockdown in cell-free expression. **b**) LA-DNA and LA-ASOs could be employed to control both transcription and translation, as well as wavelength specific RNase H activity, in CFPS systems. Figure adapted from "Precise, orthogonal remote control of cell-free systems using photocaged nucleic acids" by G. Mazzotti *et al.*[336] (© 2023) under a creative commons licence (CC-BY 4.0).

The LA-ASOs of interest were prepared using the chemistry described in Chapter 2. The ASOs were tested for their caging and gene knockdown abilities. A system was further designed using the uvLA-ASO developed herein in conjunction with the bLA-mV DNA templates developed in Chapter 2, to enable two-wavelength, two step control over protein expression in a CFPS system, by activation of gene expression with blue light and activation of gene knockdown with UV light (**Figure 3-1**, b). Lastly, due to the orthogonality of the two photocages, two orthogonally activatable LA-ASOs were prepared targeting different genes, and, using those, orthogonal mRNA

degradation and gene knockdown using the appropriate wavelength was demonstrated (**Figure 3-1**, c).

The data in this Chapter were obtained in collaboration with Giacomo Mazzotti (G. M.), and individual contributions to this project are mentioned with each experiment.

3.2 Screening for a suitable Oligonucleotide for effective ASO caging

An ASO sequence to target mV was screened in Chapter 5.2 (mV220). As the proposed method relies on incorporation of the amino-C6-dT, additional sequences were screened that allowed for a more even distribution of dTs throughout, as well as higher density of dTs over the whole sequence. G M. thus screened additional sequences that bound in the vicinity of the screened mV220 ASO (**Figure 3-2, Table 7-3**). Of those, mV229 proved to be ideal, as it has dTs very evenly spaced over 18 nucleotides; this sequence together with the original mV220 sequence was taken forward. Additional mV220 sequences with different numbers and patterns of amines (**V1, V1b, V1c**), either through terminal modification with a hexylaminophosphate or through incorporation of amino-C6-dT nucleotides, were also tested to see the effect of the amine-modifiers on RNase H activity, and it was found that they do not have a detrimental effect on ASO activity.

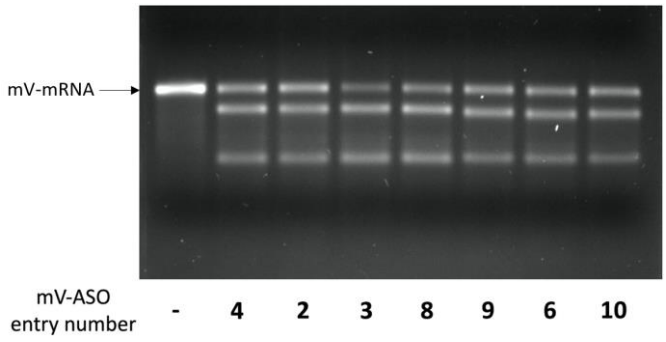


Figure 3-2: Screening of ASO sequences for RNase H activity against mVenus mRNA.
Experiment performed by G.M. Numbers refer to the oligonucleotides found in **Table 7-3**. ASO entry 4 = V1c, ASO entry 2 = V1, ASO entry 3 = V1b. Figure adapted from "Precise, orthogonal remote control of cell-free systems using photocaged nucleic acids" by G. Mazzotti *et al.*[336] (© 2023) under a creative commons licence (CC-BY 4.0).

G.M. then also undertook screening of three amine-modified ONs based on the mV220 and the mV229 sequences, which performed best in the screening. It was believed

that amines internal in the sequence would perform best to prevent RNase H activity. **V1** was taken forward, which has three internal amino-C6-dT and was purchased with an additional amino-C6-dT incorporated, yielding **V2**. Four amino-C6-dT nucleotides were also incorporated into the newly screened mV229, yielding **V3**. These were then modified with the uvLA-biotin groups (using the molecule from click-chemistry-tools), purified by HPLC and mSA bound (**Figure 3-3**, a). The modified ONs were then tested for their ability to control RNase H-mediated degradation of mRNA and compared against their amine-only and unmodified counterparts (**Figure 3-3**, b). All three tested uvLA-ASOs showed a drastic reduction in RNase H activity, with great recovery for all when illuminated with UV light. Of those, uvLA-**V3** was taken forward as it performed best in terms of activity.

3.3 Controlled Gene Knockdown in a CFPS System

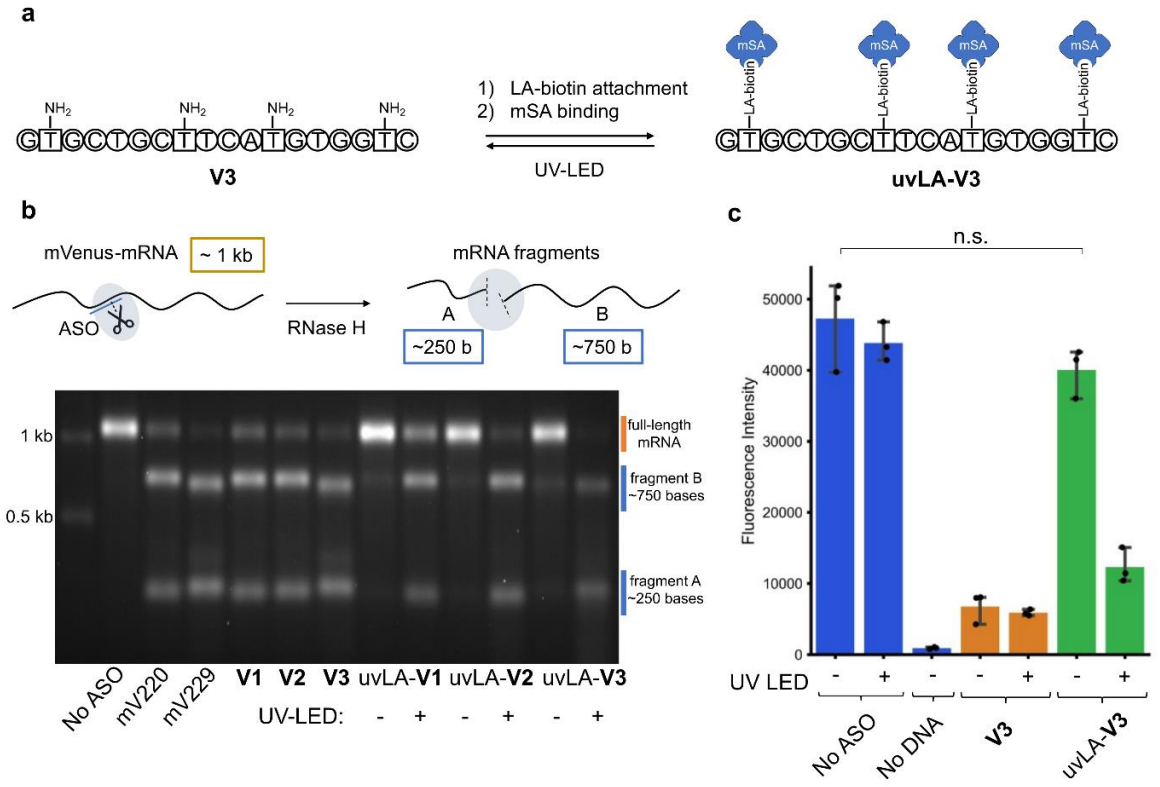


Figure 3-3: Formation of uvLA-ASOs, comparison of different tested ASOs and controllable gene knockdown in a CFPS system.

Experiments performed by both G. M. (**b**) and D. H. (**c**). **a**) preparation and uncaging of the uvLA-**V3** ASO. **b**) RNase H-mediated degradation using **V1**-**V3**. **c**) Control of CFPS using the uvLA-**V3** ASO. Figure adapted from "Precise, orthogonal remote control of cell-free systems using photocaged nucleic acids" by G. Mazzotti *et al.*[336] (© 2023) under a creative commons licence (CC-BY 4.0).

The uvLA-**V3** ASO was then tested by the author in a CFPS system (PURExpress) supplemented with RNase H to control gene knockdown of mV, expressed from a linear template (**Figure 3-3**, c). It was found that the illumination conditions with the UV LED (5 minutes at 2.12 $mW \cdot cm^{-2}$) did not have a damaging effect on the system, in the absence of ASO (non-significant, p-value = 0.23) or presence of the unmodified amino-**V3** ASO (non-significant, p-value = 0.265). The unmodified amino-ASO showed a knockdown efficiency of 89% at the used concentration. With the addition of the uvLA-**V3** ASO to the system, only a minimal decrease in mV fluorescence by ~15% (non-significant, p-value = 0.084) was observed, showing effective caging of the ASO with the LA-Biotin+mSA construct. Upon irradiation with UV light for 5 minutes, activity could be effectively regenerated, giving a knockdown of 75%, corresponding to 84% activation compared to the unmodified amino-**V3** ASO.

3.4 Two-wavelength Control of CFPS

After the screening undertaken by G. M., he also tested whether the ASO could be utilised together with the bLA-DNA template that was developed in Chapter 2.

The bLA-mV DNA template and the uvLA-**V3** ASO were employed in a transcription reaction for 4 hours under different illumination conditions, prior to analysis by AGE (**Figure 3-4**). It was seen that in the absence of any irradiation or under UV irradiation only, no mRNA was produced after 4 hours. Upon illumination with blue light, transcription occurred and could be followed over 4 hours, where minimal RNase H activity was observed. Activation of transcription from the bLA-DNA mV template with blue light and then activation of the uvLA-**V3** ASO after 3 hours initiated almost complete mRNA degradation over the last hour of incubation. This showed that both the template and the ASO could be activated selectively with their respective wavelength, and temporal control of both gene activation and knockdown were possible in the same system through application of orthogonal stimuli.

This system was then implemented by the author in a CFPS system. Combining both the bLA-mV DNA template as well as the uvLA-**V3** ASO allowed for temporal activation of gene expression followed by temporally controlled gene knockdown, providing both an on- and an off-switch for gene expression in a CFPS system (**Figure 3-5**, a). The bLA-mV DNA template, as well as the uvLA-**V3** ASO were placed into the PURExpress CFPS system, which was supplemented with RNase H and incubated for 4 hours at

37 °C, to explore the possibility of controlling transcription and translation with two orthogonal wavelengths.

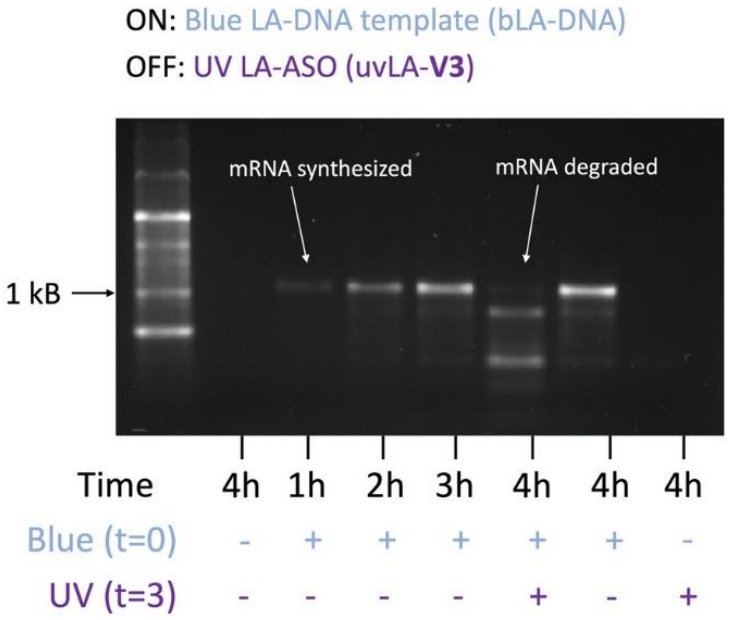


Figure 3-4: Controlled Synthesis of mRNA and subsequent degradation upon activation of the uvLA-V3 ASO.

Experiment performed by G. M. Figure adapted from "Precise, orthogonal remote control of cell-free systems using photocaged nucleic acids" by G. Mazzotti *et al.*[336] (© 2023) under a creative commons licence (CC-BY 4.0).

Addition of the uvLA-**V3** ASO and activation of the bLA-mV DNA template with blue light showed no significant reduction in expression compared to the no ASO control, showing again tight caging of the ASO (**Figure 3-5**). As anticipated, only a minor increase in expression over the no DNA control is seen with UV irradiation, as the bLA-mV DNA template is not activated. The uvLA-**V3** ASO could then, after activation of the bLA-mV DNA template with blue light, be activated at different timepoints with UV light. By activation of the ASO right at the beginning, a large amount of gene knockdown of 74% is observed, in line with what was observed in **Figure 3-3**. Activation after 30 minutes of incubation shows a reduction in gene knockdown down to 49%, as at this point some mRNA and thus also subsequently some protein has already been produced. This effect is particularly seen when activating the ASO after 3 hours of incubation, where protein production is already plateauing,[171] and RNase H-mediated mRNA degradation has no effect on protein yield anymore.

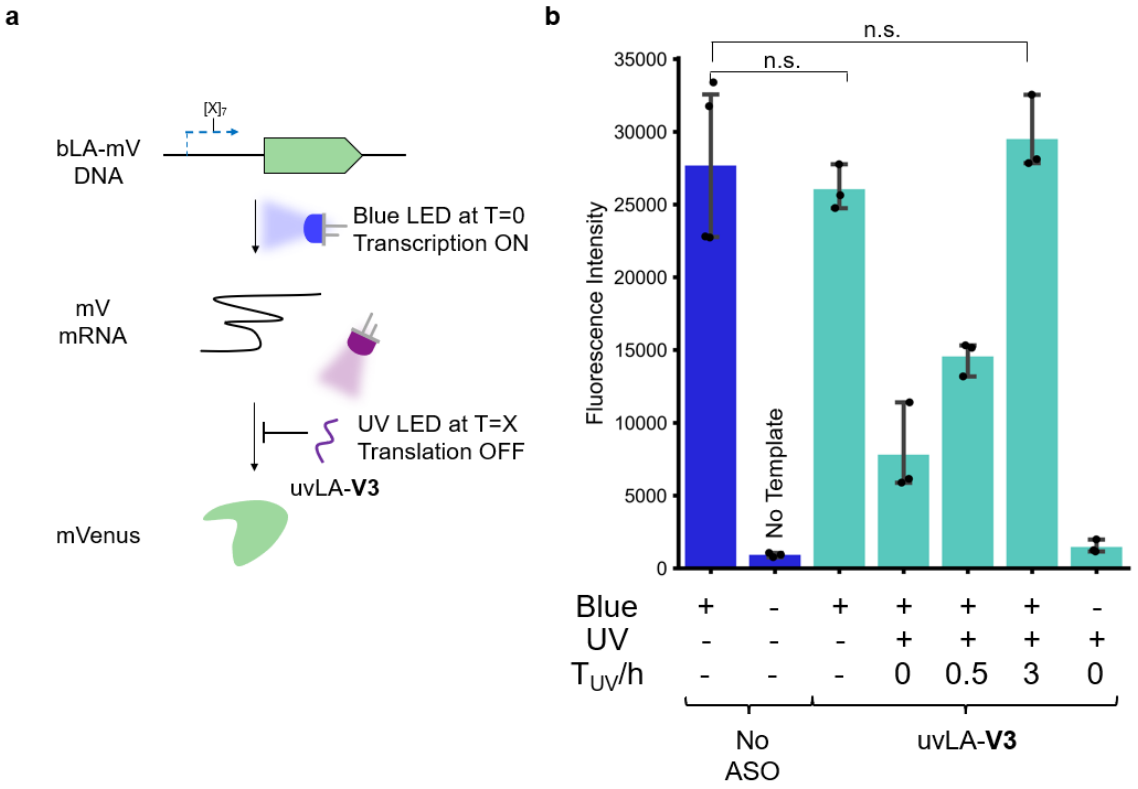


Figure 3-5: Control of transcription with blue light and translation at different timepoints with UV light.

Experiment performed by D. H. **a**) Schematic showing the control transcription with blue light through activation of the bLA-mV DNA template, and the subsequent activation of the uvLA-**V3** ASO to stop translation. **b**) 2-wavelength-controlled CFPS using the bLA-mV DNA template and uvLA-**V3** ASO. Figure adapted from "Precise, orthogonal remote control of cell-free systems using photocaged nucleic acids" by G. Mazzotti *et al.*[336] (© 2023) under a creative commons licence (CC-BY 4.0).

3.5 Two Wavelength Control of Gene Knockdown

As it was observed in both Chapter 2.7 as well as Chapter 3.4, the two employed photocages are orthogonal. As the control of gene knockdown was also very effective with the uvLA-**V3** ASO, it was conceived that by making a blue light-activated ASO targeting another genetic sequence, orthogonal control over knockdown of different genes could be achieved. To allow for a simple output, the fluorescent protein mCherry (mC) was chosen as an additional target. mC has little to no sequence similarity to mV, as they are derived from two fluorescent proteins from two different organisms (mVenus is derived from avGFP isolated from *Aequorea victoria*,[366] mCherry is derived from dsRed isolated from *Discosoma* species[367]), making it an ideal target, in addition to having an orthogonal excitation/emission spectrum to mV.

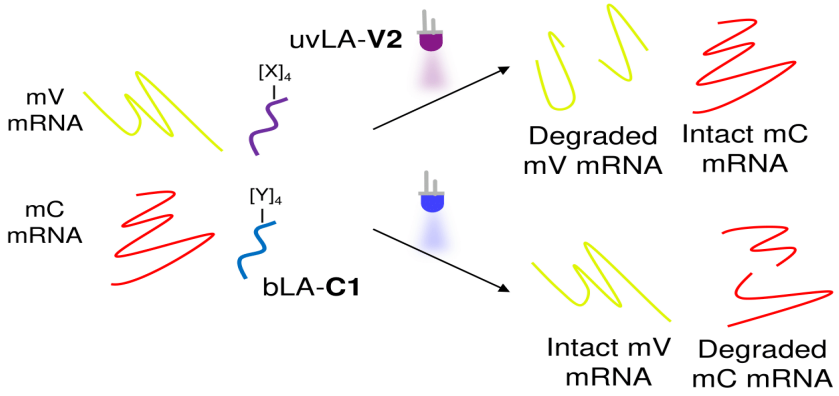


Figure 3-6: Control of mRNA degradation with orthogonally light-activatable ASOs

Figure adapted from "Precise, orthogonal remote control of cell-free systems using photocaged nucleic acids" by G. Mazzotti *et al.*[336] (© 2023) under a creative commons licence (CC-BY 4.0).

G.M. therefore screened for an RNase H-active ASO targeting the red fluorescent protein. Six sequences (**Table 7-3**, Entries 11-16) were originally screened (**Figure 3-7**). Of those, 4 showed activity; however none showed enough activity to be useful in downstream applications. As these sequences screened were not highly active, additional sequences were screened (**Table 7-3**, Entries 17-24, **Figure 3-8**). In addition, to check for orthogonality, these ASO sequences were also cross-screened against mV. Sequence 18 (**Table 7-3**) was most active against mC and showed no cross-reactivity with mV and was thus taken forward, purchased with 4 amino-C6-dT modifications spread throughout the sequence and will further be referred to as **C1**. In

this experiment it was also seen that **V3** showed a small amount of cross-reactivity to mC. Due to this, **V2** was tested to see whether it provides lower cross-reactivity with mC (**Figure 3-9**). It was found that the **V2** ASO provided sufficient selectivity for mV over mC mRNA, with very little cross-reactivity observed for either **C1** or **V2** with their non-targeted mRNA.

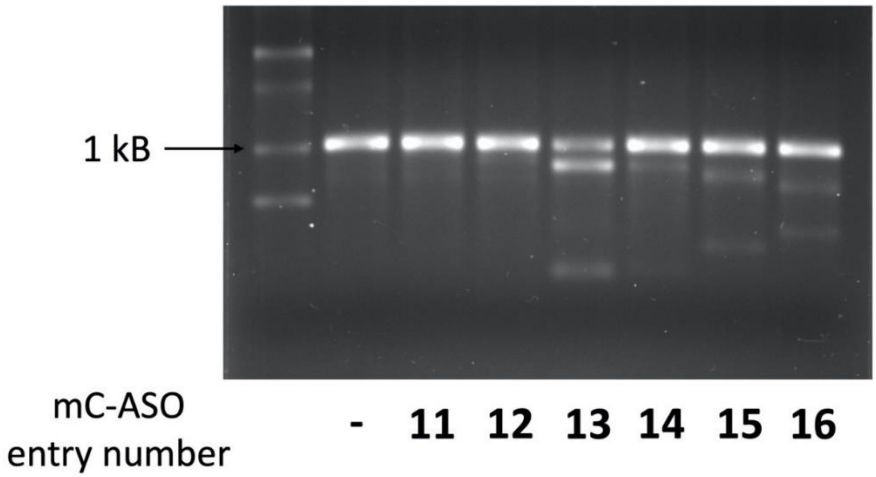


Figure 3-7: Screening for ASO sequences active against mCherry.

Experiment performed by G. M. Numbers refer to the oligonucleotides found in **Table 7-3**. Figure adapted from "Precise, orthogonal remote control of cell-free systems using photocaged nucleic acids" by G. Mazzotti *et al.*[336] (© 2023) under a creative commons licence (CC-BY 4.0).

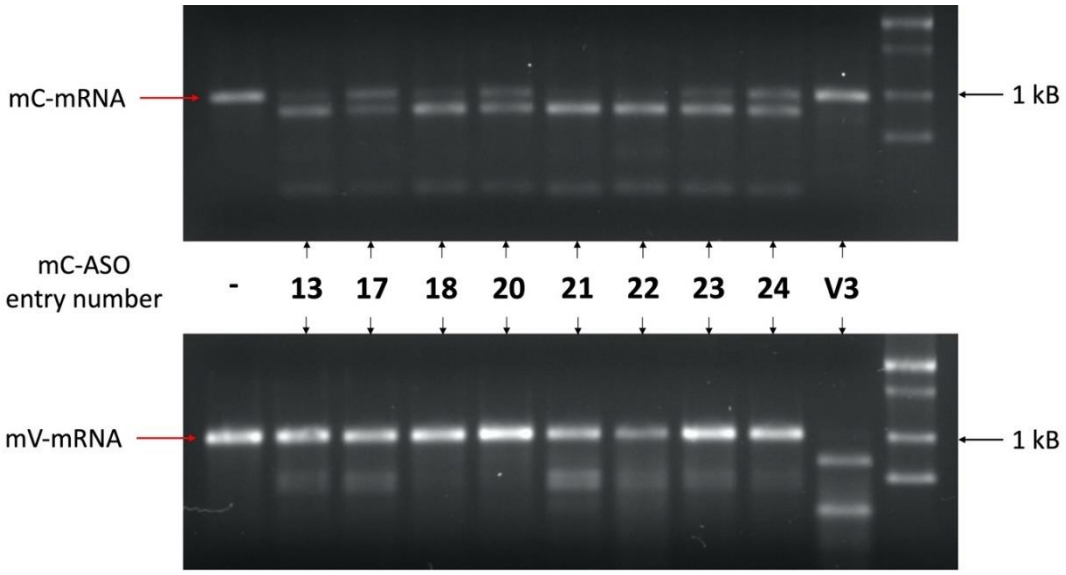


Figure 3-8: Additional mCherry ASO sequences screened and cross-tested against mVenus mRNA

Experiment performed by G. M. Numbers refer to the oligonucleotides found in **Table 7-3**. Figure adapted from "Precise, orthogonal remote control of cell-free systems using photocaged nucleic acids" by G. Mazzotti *et al.*[336] (© 2023) under a creative commons licence (CC-BY 4.0).

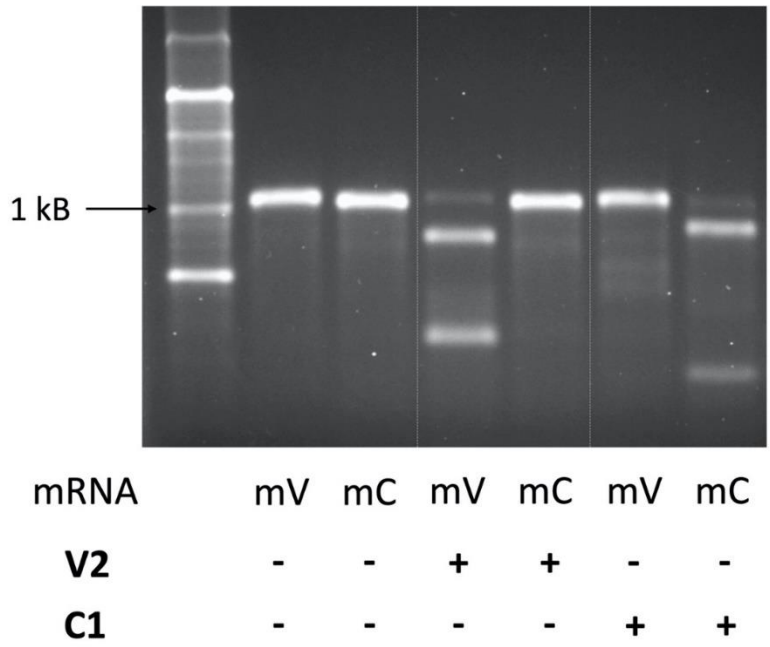


Figure 3-9: Testing of cross-reactivity of V2 and C1 against mV and mC mRNA.
Experiment performed by G. M. Figure adapted from "Precise, orthogonal remote control of cell-free systems using photocaged nucleic acids" by G. Mazzotti *et al.*[336] (© 2023) under a creative commons licence (CC-BY 4.0).

The mC-targeting ASO **C1** was then modified by the author using the PFP-carbonate **10b** prepared in Chapter 2, purified by HPLC and bound with mSA. The electrophoretic mobility prior and after binding of mSA, as well as photorelease of this blue light-activatable ASO (bLA-**C1**) was then analysed by PAGE (**Figure 3-10**). The ASO showed a decrease in gel mobility upon modification with the bLA-Biotin groups. Upon binding of excess mSA, the majority of the ASO was now found in the well of the gel, with a small population, which likely did not have a mSA bound to every biotin, migrating further into the gel. This is supported by the photocleavage, where the intensity of the band in the well decreased, whereas the intensity of the band just below the well increased. In addition, fully uncaged ASO was now also observed.

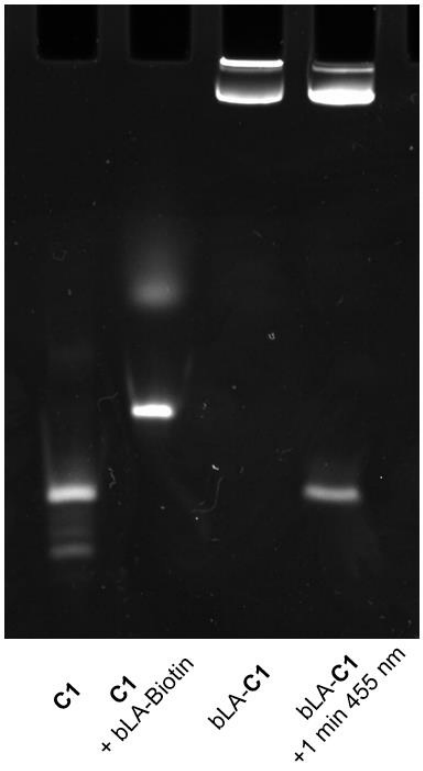


Figure 3-10: Gel migration and photorelease of the C1 ASO, modified with bLA-Biotin and bound with mSA.

Experiment performed by D. H.

This blue light-activated (bLA)-ASO was then used in conjunction with the previously developed uvLA-**V2** ASO to control RNase H-mediated degradation of the two genes, mV and mC, using orthogonal wavelengths (**Figure 3-11)**. When both amine-only-ASOs were added to either the mV and mC mRNA in the presence of RNase H, clear mRNA degradation patterns were observed, that are characteristic of the ASOs used. When the LA-ASOs were added instead, no mRNA degradation was observed in the absence of irradiation. When both the mV and mC mRNA samples with both LA-ASOs are irradiated with UV light, only the mV mRNA showed any degradation, showing that only the uvLA-**V2** ASO activated and the bLA-**C1** stayed silenced. The inverse was true for the samples irradiated with blue light. There, only degradation of mC was observed, in line with only the bLA-**C1** ASO activating under blue irradiation, showing orthogonal activation of ASOs and thus orthogonal control over mRNA degradation by appropriate choice of wavelength.

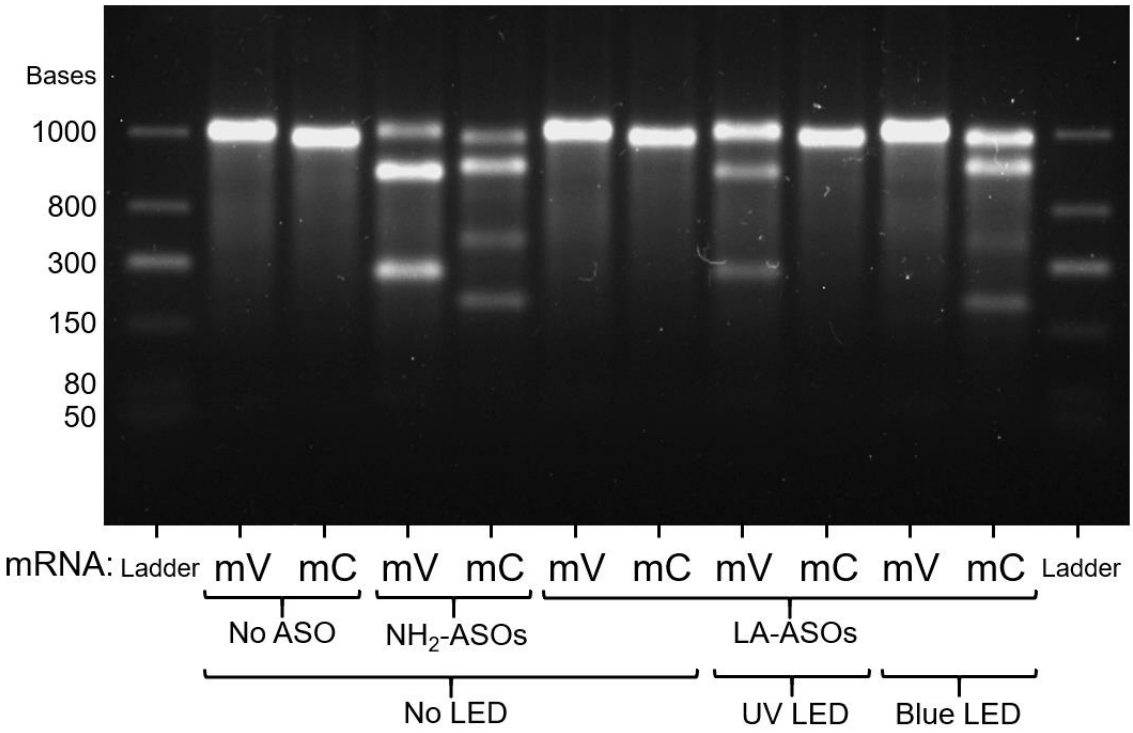


Figure 3-11: Controlled RNase H-mediated mRNA degradation using orthogonally light-activated ASOs targeting mV and mC.

Experiment performed by D. H. The uvLA-**V2** and bLA-**C1** ASOs show no RNase H activity against mV or mC mRNA without illumination. After irradiation with UV light, degradation was only observed for mV, as only **V2** was uncaged. After blue light irradiation, degradation was only observed for mC, as only **C1** was uncaged. Figure adapted from "Precise, orthogonal remote control of cell-free systems using photocaged nucleic acids" by G. Mazzotti *et al.*[336] (© 2023) under a creative commons licence (CC-BY 4.0).

It was then tested whether orthogonally activated gene knockdown is possible in cell-free conditions. For this, both mV and mC were co-expressed from linear templates in a CFPS system (PURExpress) supplemented with RNase H, with addition of the unmodified- or LA-ASOs under different illumination conditions and incubated for 4 hours (**Figure 3-12**). In the presence of the LA-ASOs, but without illumination, both proteins were expressed to similar levels compared to the no ASO control (17% increase for mC, 23% decrease for mV, non-significant). Upon irradiation with UV light, uvLA-**V2** selectively knocked down mV by 56%, whereas only a reduction of 16% was observed in mC (non-significant, p-value = 0.129). Upon blue light irradiation, this trend was reversed, with selective knockdown of mC by 62% through activation of the bLA-**C1** ASO, and only a 30% reduction of mV fluorescence (significant against positive control, p-value = 0.032). This data thus showed orthogonal light control of gene

knockdown of two separate genes in cell-free condition through choice of appropriate wavelength.

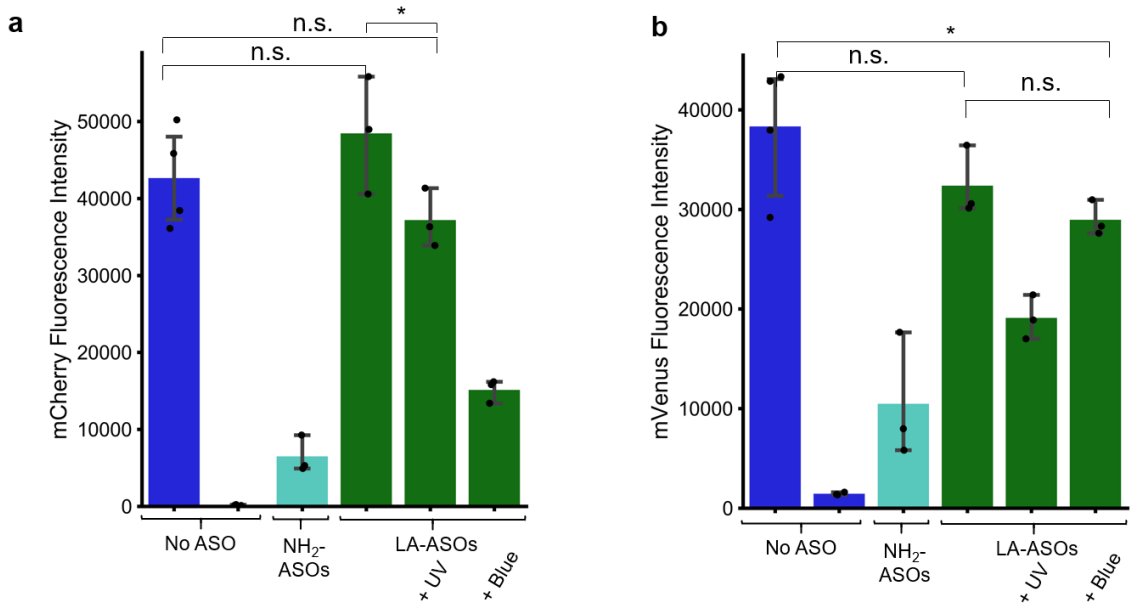


Figure 3-12: Co-expression and orthogonally activated gene knockdown of mVenus and mCherry in cell-free conditions.

Experiment performed by D. H. Without irradiation, expression in presence of the LA-ASOs does not affect mCherry (**a**) or mVenus (**b**) expression. Upon irradiation with UV light, only mVenus knockdown was observed to a substantial degree. Similarly, upon irradiation with blue light, only mCherry knockdown was observed. Figure adapted from "Precise, orthogonal remote control of cell-free systems using photocaged nucleic acids" by G. Mazzotti *et al.*[336] (© 2023) under a creative commons licence (CC-BY 4.0).

3.6 Light-controlled gene knockdown inside emulsion droplets

After having shown tight control of gene knockdown in bulk, it was hypothesised that this can also be performed inside synthetic cells with spatial control. As mV as a reporter protein has poor overlap with the filter cubes of our epifluorescence microscope, this experiment was performed using co-expression of mC and mNG and utilising the bLA-**C1** ASO. The ASO is still orthogonal to mNG, but would allow for spatiotemporal control of gene knockdown of mC selectively upon irradiation. As also previously discussed, blue light is more desirable for such applications due to lower scattering and tissue penetration, and the bLA-photocage employed also shows very rapid uncaging.

Using the method developed in Chapter 2.10, immobilised synthetic cells were prepared by emulsification of the CFPS system, supplemented with RNase H and containing the template DNAs for both mNG and mC as well as the bLA-**C1** ASO, in hexadecane containing 2% Span80 and 10 mg/mL of SEBS. The resulting synthetic cells were then illuminated through a photomask with blue light and incubated at 37 °C for 4 hours before imaging (**Figure 3-13**, a).

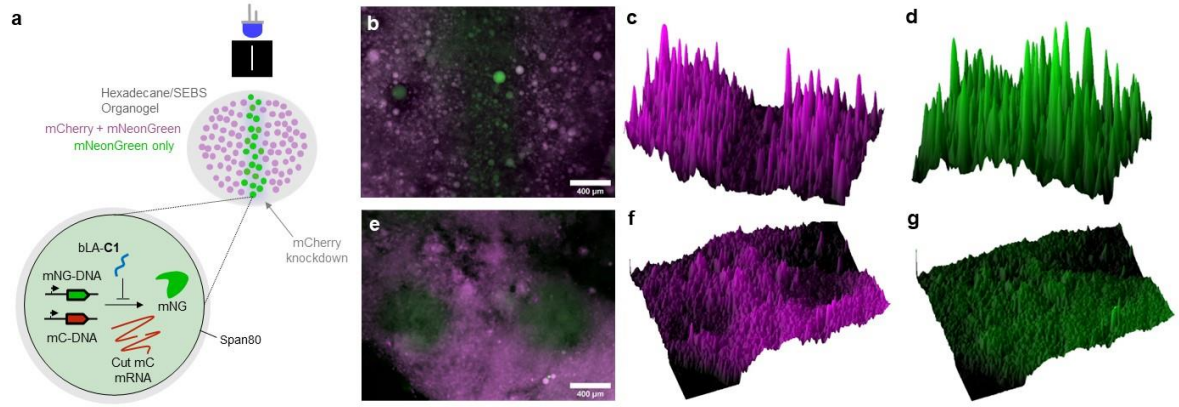


Figure 3-13: Light-controlled, patterned gene knockdown inside emulsion-droplet-based synthetic cells.

Experiment performed by D. H. **a**) Schematic showing patterned and selective mC gene knockdown in emulsion droplet-based synthetic cells containing both mNG- and mC-DNA templates by illumination through a photomask. **b**-**d**) Line patterned gene knockdown of mC. A clear trench was visible in the red channel (**c**) without affecting mNG expression (**d**). **e**-**g**) Dot patterned gene knockdown of mC. Clear circles were observed in the red mC channel (**f**) without affecting mNG expression (**g**).

With the line photomask, a clear area of gene knockdown was observed for mC where the light was applied (**Figure 3-13**, b-d). Looking at the individual channels, in the mC channel a clear trench was observed in the intensity profile, where the photomask was applied (**Figure 3-13**, c), whereas for the same area, no decrease in the mNG signal was observed (**Figure 3-13**, d), indicating both spatially controlled and selective knockdown of mC. Similarly, when a dot photomask was applied, clear demarcations are observed for the dots where the blue light was applied (**Figure 3-13**, e-g). In the mC channel, clear dots were visible with very little gene expression (**Figure 3-13**, f), whereas in the mNG channel, no gene knockdown was observed (**Figure 3-13**, g), again indicating the spatially controlled and selective knockdown of mC inside emulsion droplet-based synthetic cells.

3.7 Conclusions

In this chapter, light-controllable ASOs based on the LA-biotin technology were developed. Through modification of an amino-C6-dT-containing ASO targeting mV with the UV-photocleavable biotin followed by binding of mSA, RNase H activity was effectively silenced but was able to be recovered upon illumination with UV light. This could be employed in a CFPS system to tightly control gene knockdown, where no significant reduction in protein yield was observed with the caged ASO, but excellent recovery was observed upon UV irradiation. Due to the orthogonality of the blue light- and UV light-activatable photocages, these could be employed together in the same system. By using the bLA-mV DNA templates developed in Chapter 2 together with the uvLA-**V3** ASO prepared in this chapter, control over both transcription and translation in the same system could be obtained. The uvLA-ASO could be activated at different timepoints, allowing for temporal control of gene knockdown.

An additional ASO was also screened for, selectively targeting mC, and was modified with the blue light-activatable biotin and caged with mSA. This bLA-**C1** ASO could be used together with the uvLA-**V2** ASO to orthogonally and selectively control mRNA degradation and gene knockdown in cell-free conditions through choice of appropriate wavelength, demonstrating orthogonal, selective and light-controllable gene knockdown in cell-free conditions.

Lastly, spatially controlled and selective gene knockdown could also be achieved inside emulsion droplet-based synthetic cells using the bLA-**C1** ASO. It was possible to pattern both dots and lines through selective gene knockdown of mC without affecting the expression of mNG, showing tight spatial control of ASO activity inside synthetic cells.

4 CIRCULARISED LA-BIOTIN-CAGED OLIGONUCLEOTIDES

4.1 Introduction

The previous method of controlling ASOs relied on sterically blocking access of RNase H to the DNA/mRNA duplex by having monovalent streptavidin bound to the oligonucleotide (ON) *via* the photocleavable biotin linkers (Chapter 3). This method, while effective, does require monovalent streptavidin, which is not easily accessible and needs to be expressed and purified in-house, as it is not commercial. It also required several photocages to provide enough steric block to prevent enzymatic processing, making the uncaging process less efficient and requiring more irradiation for complete uncaging. It also relies on the incorporation of amino-C6-dT oligonucleotides throughout the sequence, which constrains suitable sequences to those that have T spread throughout. The photocage placement also needs to be optimised to provide the highest off-state.

An approach towards silencing short oligonucleotides (ONs) that has already been discussed in Chapter 0 is through circularisation. By forcing the otherwise flexible ssDNA into a circular shape *via* macrocyclization, effective target binding is inhibited as the ssDNA cannot form a rigid duplex structure with the target. This topological constraint has already shown effective caging with various photocages to control morpholino[315–317,368] and DNA[246,314,369,370] ASOs and has even found use in controlling guide RNA for light-control of CRISPR/CAS gene editing.[371]

One important feature of this approach is its potential independence of oligonucleotide sequence, as only the termini of the oligonucleotide need to be modified, though with examples in the literature also having used hairpin-forming sequences.[314,370] In addition, a very small number of photocages are required to effectively silence the oligonucleotide.

The downsides of current circularisation approaches are that to produce the circularised oligonucleotide, it often takes several reaction steps, including the synthesis of the bifunctional photocages used. The circularisation moieties themselves are also hydrophobic and do not provide additional steric block. Rapid derivatisation of the photocage is also not simple, due to the multi-step synthesis involved. Lastly, the circularised ONs often need to be purified from their unwanted side products in the circularisation step, reducing yield.

It was thought that the previously used photocleavable (PC)-biotins could be used together with commercial, wild-type streptavidin (wtSA) to form macrocyclized LA-ASOs through divalent binding of two ASOs per wtSA. wtSA is also a large protein of 53 kDa,[372] providing steric bulk and likely giving additional caging efficiency. It is also highly soluble in aqueous media and allows for further derivatisation through protein fusion with HIV-TAT[373] or antibodies,[374] or bioconjugation of cyclic oligocalchogenides onto its 16 surface lysines[375] for targeting and cellular uptake.

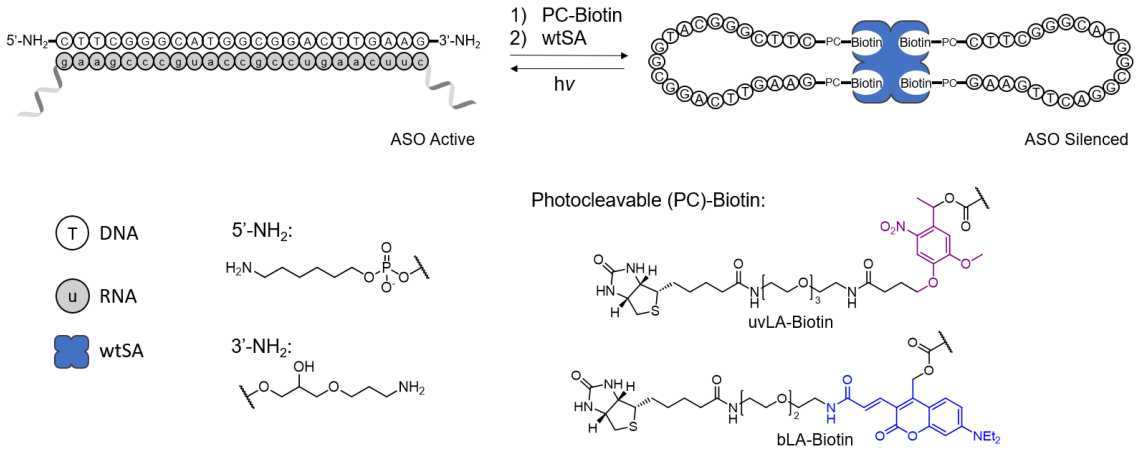


Figure 4-1: Modification of dual-termini amine-modified oligonucleotides with photocleavable biotins for circularisation onto wtSA and release with light.

To prepare these caged ASOs, ONs with commercial terminal amine modifications were modified with the PC-Biotin photocages, before circularisation onto wtSA under high dilution conditions (**Figure 4-1**). These ONs were effectively silenced but could be reactivated through irradiation with UV or blue light, allowing for control of RNase H-mediated mRNA degradation and gene knockdown in cell-free conditions.

4.2 Screening for hairpin-forming ASO Sequences

It was thought that for effective macrocyclization and divalent binding to the same streptavidin through its adjacent binding sites, preorganisation of the ON into a hairpin may be required. Such hairpins were also previously employed to form a similar caged ASO.[314] Because of this, ASOs that form a short hairpin stem were desired. A short python script was employed to scan the sequence of the *mV* gene for stretches that can form hairpins with a stem of 4-6 nts and a total length of 16-24 nts. Five of those were selected that fulfilled ASO criteria, and their corresponding antisense sequences were purchased.

These sequences (**Table 7-4**, Entries 1-5) were then tested in an RNase H assay for their activity in degrading the target mRNA using two different concentrations of ASO (1 and 5 ng) (**Figure 4-2**). Of those, sequence 252[4] (*mV* gene starting nucleotide 252 with a hairpin stem of 4 nts) showed the highest activity and was chosen for further studies.

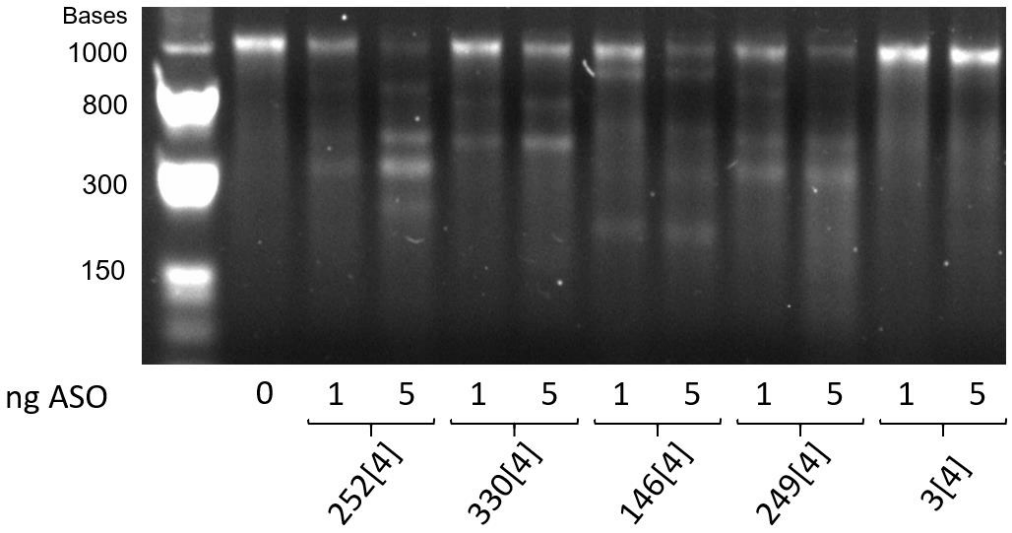


Figure 4-2: Screening for RNase H-active ASO sequences that form a 4-stem hairpin.

Furthermore, to investigate the feasibility of divalent binding (or 'handcuffing') of an ON modified on both termini with photocleavable biotins (attached *via* the commercial 5'-C6-amine and 3'-C3-glyceryl-amine modifications as shown in **Figure 4-1**) to a single streptavidin, a visual model was prepared in Chimera from published crystal structures on Protein Databank (PDB) of wild-type Streptavidin and a DNA hairpin (6J6J[376] and 2VAI[377]) (**Figure 4-3**). From this model, as well as the known distances

of a B-DNA helix and the adjacent binding pockets both being 2.0 nm,[9,378] divalent binding seems feasible and is aided by the added flexibility of the bLA-Biotin linker.

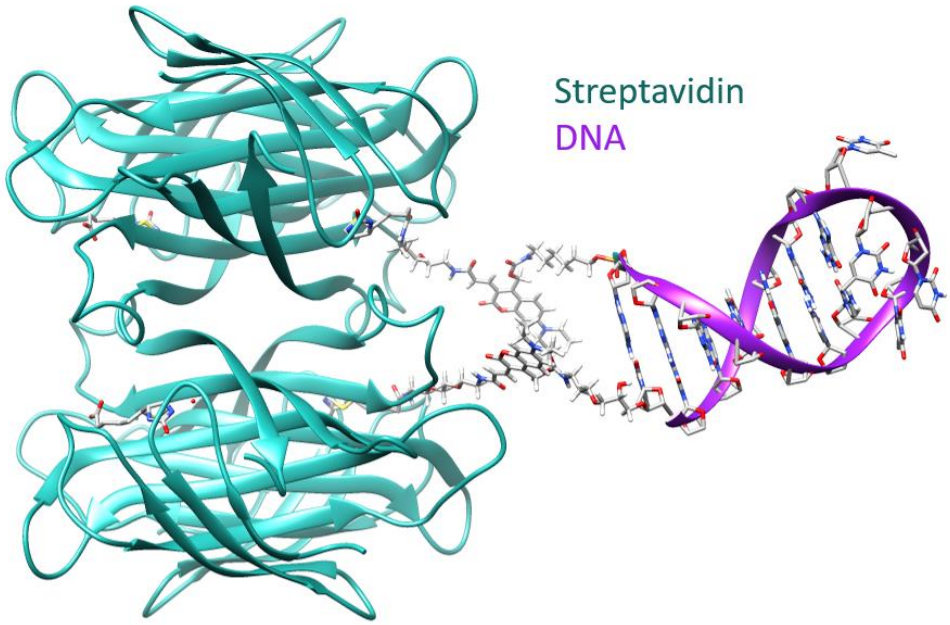


Figure 4-3: Molecular Model of a DNA Hairpin and wtSA bound together *via* bLA-Biotin.
The spacing between the biotin binding sites on wtSA and between the termini of a DNA hairpin is 2.0 nm, allowing for divalent binding of biotinylated hairpin-forming oligonucleotides. Model prepared in Chimera

4.3 Investigation of wtSA Binding to terminal-modified ASOs

With a suitable sequence found (**Table 7-4**, Entry 1), it was then purchased with the 5'-C6-amine and 3'-C3-glyceryl-amine modifications, modified with the bLA-Biotin PFP carbonate **10b** synthesised in Chapter 2.2 and purified by HPLC. To test handcuffing conditions as shown in **Figure 4-1**, a common method for the formation of macrocycles was employed, using high dilution. Three different dilutions were tested with 0.5 eq. of wtSA to investigate the propensity to form the correct handcuff structure and analysed by denaturing PAGE (**Figure 4-4**, a).

At high concentrations (6.6 µM) multiple bands were observed, which at the intermediate concentration (1.3 µM) were reduced but still present. At the lowest concentration tested (0.33 µM), however, only one major band was observed, indicating the formation of the desired oligonucleotide handcuff structure. To confirm that this was indeed DNA bound to protein, the gel was subsequently stained with a protein stain (QuickBlue). The bands that stained previously with the nucleic acid stain

now showed up stained with the protein stain, indicating the formation of the desired DNA/protein conjugate.

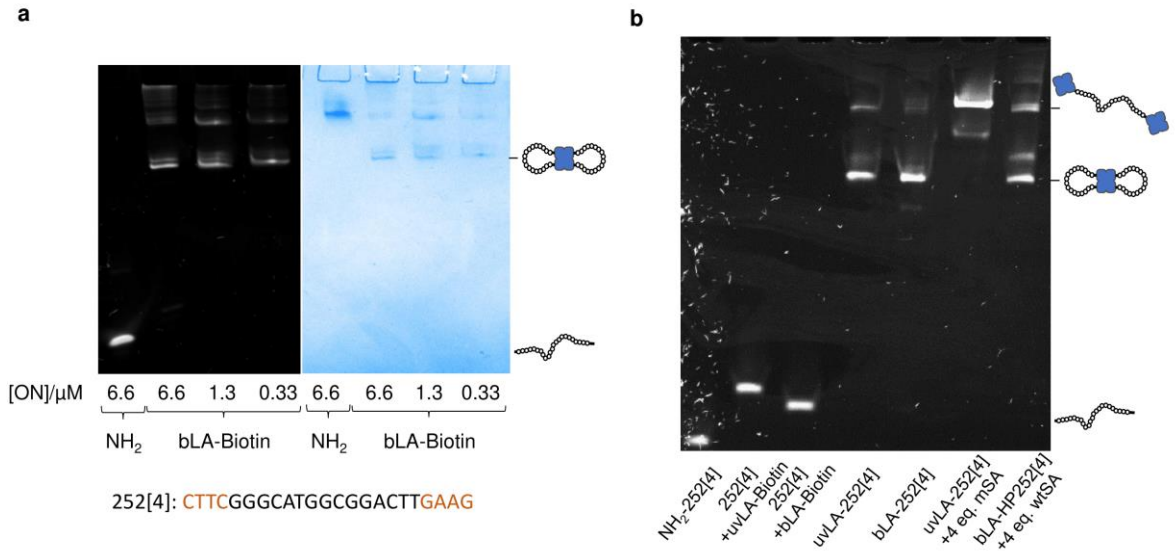


Figure 4-4: PAGE analysis of high dilution conditions for formation of the handcuff ON and the formation of different handcuffed ONs with Sequence 252[4]

At low ON concentrations (**a**), one major band is formed, with electrophoretic mobility being dominated by the protein. uvLA- and bLA-Biotin-modified ONs when incubated with 0.5 equivalents of wtSA show the same gel migration (**b**). DNA incubated with mSA shows much lower electrophoretic mobility. When incubated with an excess of wtSA, the major band formed is still the band with highest electrophoretic mobility.

Following on from this test, the oligonucleotide modified with the UV PC-Biotin groups (click-chemistry-tools) was also prepared and purified by HPLC. Both UV- and Blue-PC Biotin-modified ONs were incubated with 0.5 eq. of wtSA at high dilution to form the oligonucleotide handcuffs uvLA-252[4] and bLA-252[4]. In addition, controls were prepared by incubating the uvLA-Biotin-modified oligonucleotide with 4 eq. of mSA and the bLA-Biotin-modified oligonucleotide with an excess of wtSA.

These ONs were then analysed by denaturing PAGE (**Figure 4-4**, b). A size difference was observed between the ONs modified with UV- and Blue-PC Biotins. This is likely due to the larger hydrodynamic radius of the UV-PC-Biotin as it does have a slightly longer linker unit. Both samples, when bound with 0.5 eq. wtSA, however, showed the same gel migration, which is now dominated by the large protein. It was also seen that for both molecules, the major band was the expected band, with only a very small amount of higher order structures. For the case with mSA, drastically reduced gel

migration was observed, as now two proteins are bound to one ON, yielding a much larger species with reduced charge. When incubated with an excess of wtSA, several bands were observed. The desired, handcuffed ON, comprised of two ONs per wtSA was observed. A band was also observed at the same migration as the ON incubated with mSA, which was likely to be a species of two wtSA bridged with one ON. In between those bands was another, slightly weaker band. This, due to its gel mobility, was believed to be the 1:1 wtSA:ON conjugate.

4.4 Photocleavage Behaviour of handcuffed Oligonucleotides

After verification of the desired product by electrophoretic mobility, the compact structure and photorelease behaviour of the handcuff ONs was investigated. The uvLA-252[4] was irradiated with a 365 nm LED at different time intervals and analysed by denaturing PAGE (**Figure 4-5**). Upon irradiation, bands with a lower electrophoretic mobility than the handcuff ON were initially formed before release of the unmodified amino-252[4] ON. These larger bands were believed to be due to partial release of the ONs from the wtSA, forming species that have the same mass and charge, but a larger hydrodynamic radius, as the partially released ON is now flexible and can extend outwards, causing lower electrophoretic mobility. Full photocleavage is not observed, however, after 10 minutes, with longer irradiation potentially causing damaging effects to the system.

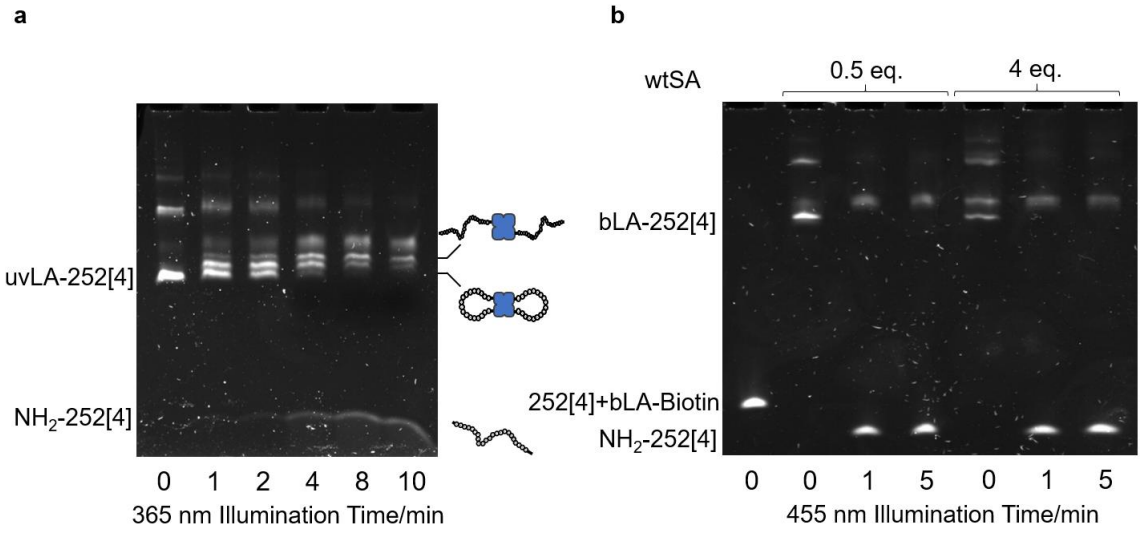


Figure 4-5: Photolysis of the uvLA- and bLA-252[4] handcuffs

UV irradiation of the uvLA-252[4] ON (**a**) showed initially bands with lower electrophoretic mobility, arising from incomplete release of the ON from the handcuff structure, prior to complete release. Irradiation of the bLA-252[4] ON with blue light showed rapid release of the ON.

Following from this, the bLA-252[4] ONs with 0.5 and 4 eq. of wtSA were irradiated with a 455 nm LED. Rapid release was observed, with one minute of irradiation already showing essentially complete release, with a very small amount of partially bound ON unable to be released with additional irradiation, likely due to the photobleaching of the coumarin photocage as observed in Chapter 2.7. Any partial release of ON from the handcuff structure would also likely still be able to bind to the mRNA, as it is no longer conformationally restricted and thus elicit an RNase H response.

4.5 Control of RNase H-mediated Degradation

Having shown both effective formation of the handcuff structure as well as release of the ON from said structure, the ability of the UV and blue-light activatable ONs to control RNase H-mediated degradation of mRNA was tested (**Figure 4-6**). For this, the uvLA- and bLA-252[4] handcuff ONs, along with the bLA-252[4] ON with excess wtSA were incubated with the target mRNA in presence of RNase H, with or without illumination (**Figure 4-6**, b, c).

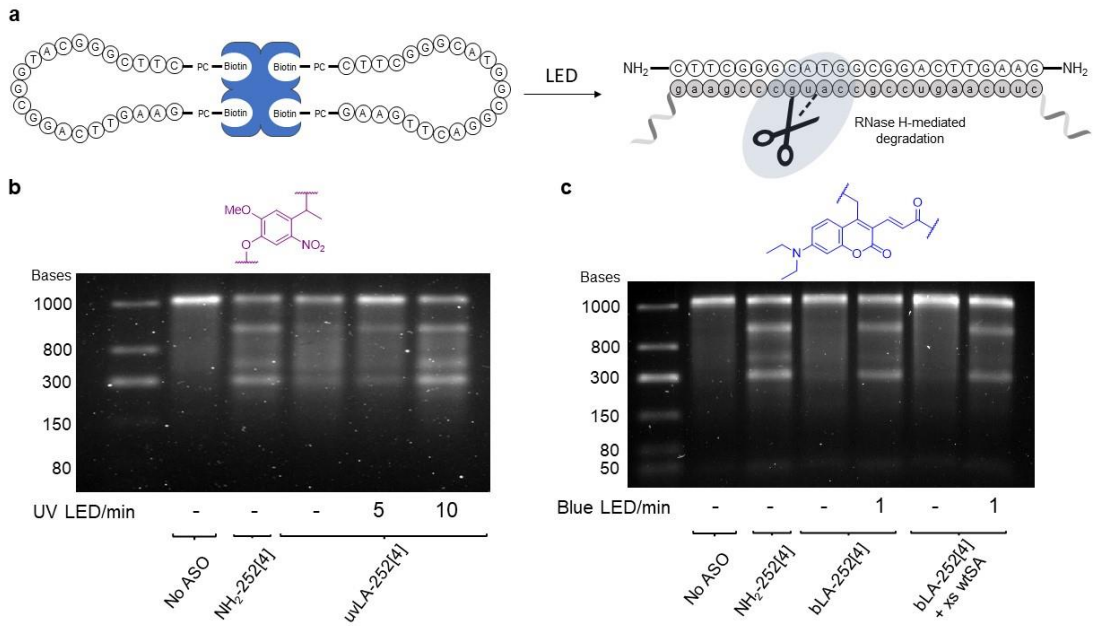


Figure 4-6: Control of RNase H-mediated mRNA degradation using the uvLA- and bLA-252[4] handcuffs

a) Uncaging of the ON from the handcuff structure allows for RNase H-mediated degradation. **b**) Control of RNase H-mediated mRNA degradation with the uvLA-252[4] handcuff. Minimal activity was observed in prior to irradiation, but could be recovered upon illumination with UV light. **c**) the bLA-252[4] handcuff DNA with 0.5 and 4 eq. of wtSA was effectively silenced. Upon illumination with blue light, RNase H activity was effectively restored.

For both uvLA- and bLA-252[4] handcuff ONs, little to no mRNA degradation was observed, which provided further evidence of the correct handcuff structure. In both cases, illumination with the required wavelength restored the activity back to expected levels. The bLA-252[4] handcuff ON overall provided the best performance, with the most effective silencing observed in the caged state and high recovery of activity with very little irradiation. An interesting observation was that when using an excess of wtSA to cage the ON, the ON was still effectively silenced (**Figure 4-6**, c). This showed that the presence of higher order structures had no detrimental effect on activity and the protein also provided a steric component to silencing for these structures.

The dumbbell-shaped ON with mSA was also tested for RNase H-mediated degradation (**Figure 4-7**). For this species, a much smaller difference in mRNA degradation was observed between no irradiation and irradiation of the sample. It showed that not circularising the ON did not cause effective caging, but the reduction in activity with the bound mSA again showed that the protein provided a steric component to the caging.

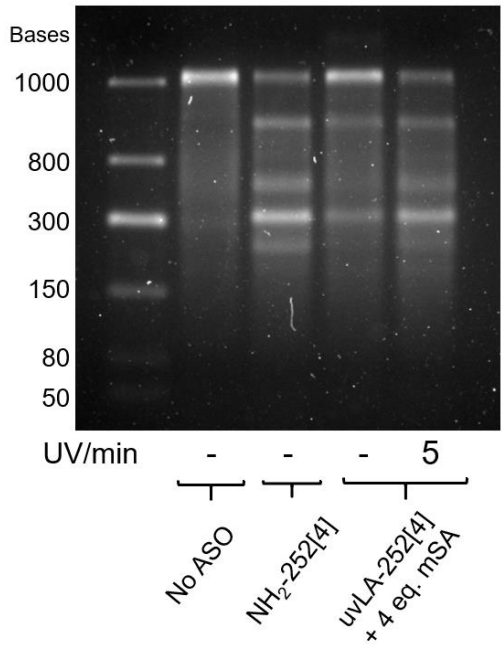


Figure 4-7: Control of RNase H-mediated mRNA degradation using the uvLA-252[4] prepared using 4 eq. of mSA

The dumbbell-shaped uvLA-252[4] ON incubated with mSA showed only minimal reduction in RNase H activity.

4.6 Use of Sequences with lower Constraints

After providing evidence for the formation of the correct structure as well as showing the effectiveness of this silencing approach, the generality of this method towards ONs with lower constraints was investigated. In particular, it was questioned whether the hairpin motif employed is necessary for effective circularisation. Lower constraints on the sequence, particularly a reduction in hairpin stem, would be desirable as this would allow this approach to be more general and it would alleviate the detrimental effect of ON secondary structure, as was observed in the RNase H-assay, where the overall ON activity was poor.

Therefore, the prepared python script was used to screen for sequences with lower constraints, forming between 1 and 4 nts of hairpin (**Table 7-4**, Entries 7-13). Of those, seven were tested against the 252[4] ON employed previously (**Figure 4-8**). From this data, it was clear that ONs with lower constraints performed better as ASOs in mRNA-mediated degradation, as was observed particularly with the ONs 221[2] and 229[1], which performed best and are unlikely to form an actual hairpin motif with only 1 or 2 bases of overlap. The on 229[1] was also the same sequence as mV229 screened in Chapter 3.

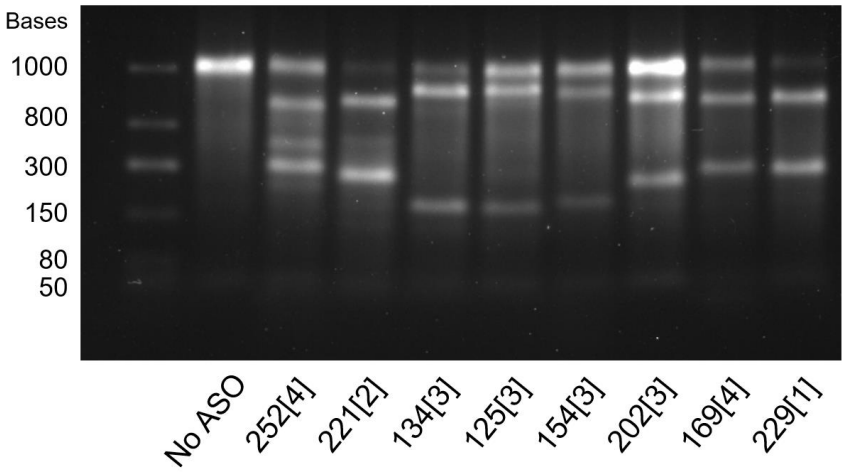


Figure 4-8: Screening for ASO sequences with lower constraints

Sequences that do not form effective hairpin structures performed better in RNase H-mediated mRNA degradation.

To test the circularisation approach, three of the screened sequences were tested and compared to the 252[4] ON. An additional sequence with a 4 nt stem, 169[4], and both 221[2] and 229[1] were purchased with terminal amine modifications and then

modified with the PC biotin PFP-carbonate **10b**, as the bLA-252[4] handcuff ON had performed better in earlier experiments. These sequences were then subjected to the previously screened conditions, using 0.5 eq. of wtSA at an ON concentration of 0.25 µM in Dulbecco's phosphate-buffered saline (DPBS) (**Figure 4-9**, a), incubated overnight and then analysed by denaturing PAGE (**Figure 4-9**, b).

It was observed that that in all cases, the major product was the handcuffed ON, as the electrophoretic mobility of the bands formed in the newly tested ONs very closely matched the bands observed for the bLA-252[4] handcuff ON, with a very similar distribution of higher order structures for all the tested ONs. This showed the generality of this caging approach, providing evidence that circularisation onto wtSA using PC-biotins is not dependent on preorganisation of the ON into a hairpin motif.

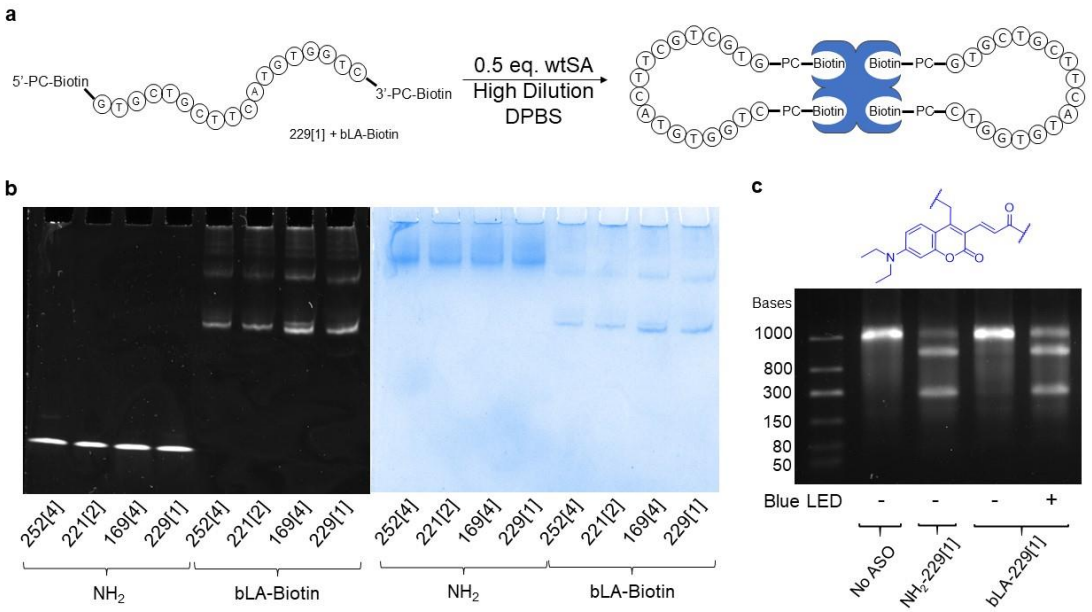


Figure 4-9: Generality of circularisation conditions and effectiveness of caging on non-hairpin forming ON 229[1].

a) Conditions employed for the formation of handcuff ONs. **b**) Comparison of handcuff formation of different ONs. Reactions were performed at 25 µM ON concentration. Hairpin formation was not necessary for effective handcuffing. **c**) Control of RNase H activity using the bLA-229[1] handcuff ON. Minimal RNase H activity was observed from the handcuff ON, which could be effectively restored upon illumination with blue light.

Of those sequences tested, the highest performing bLA-229[1] handcuff ON was then taken forward to explore the effectiveness of caging. The handcuff ON was incubated

again with the mRNA in presence of RNase H, with or without illumination (**Figure 4-9**, c). The caging of the 229[1] ON was again very effective, showing no RNase H-mediated mRNA degradation prior to illumination. Upon irradiation with blue light, the activity recovered to very high levels, showing effective release of the ON from the handcuff structure.

4.7 Control of CFPS using handcuffed Oligonucleotides

To test their utility, their efficacy as OFF-switches in CFPS were investigated. The bLA-252[4] and -229[1] handcuffs were added to a CFPS system (PURExpress) that was supplemented with RNase H and contained a linear DNA template for mVenus (**Figure 4-10**, a). As the 229[1] ON had much higher activity in the RNase H assays performed, a lower concentration of ON was used compared to the 252[4] ON (85 nM vs. 571 nM, respectively).

For the 252[4] ON (**Figure 4-10**, b) we saw knockdown of protein expression with the unmodified amino-252[4] of 77% at the used concentration. The bLA-252[4] handcuff ON showed a good reduction in knockdown, with only 32% reduction in protein yield. The activity was fully recovered upon illumination with blue light, giving 83% knockdown (not significant vs. amine-ASO control, p-value = 0.051).

For the 229[1] ON (**Figure 4-10**, c) even at the much lower concentration used, knockdown with the unmodified amino-229[1] ON was high, giving a reduction of 90%. Upon handcuffing into the bLA-229[1] ON, a drastic reduction in gene knockdown was observed down to only 22% (Significant vs no ASO control, p-value = 0.049). Upon illumination, full recovery was observed, with a knockdown of 86% (not significant vs. amine-ASO control, p-value = 0.951).

The difference in caging ability was believed to be due to the difference in length of the used ONs. the 252[4] ON has 23 nts, whereas the 229[1] ON only has 18 nts, which provided the 252[4] ON with greater flexibility and thus a higher chance to have small amounts of hybridisation with the target mRNA, eliciting a weak RNase H response (as a hybrid duplex of only 4 nts is needed for it to trigger[58]) as well as some steric blocking of the mRNA, which could occur at higher degree also due to the increased amount of ON used.

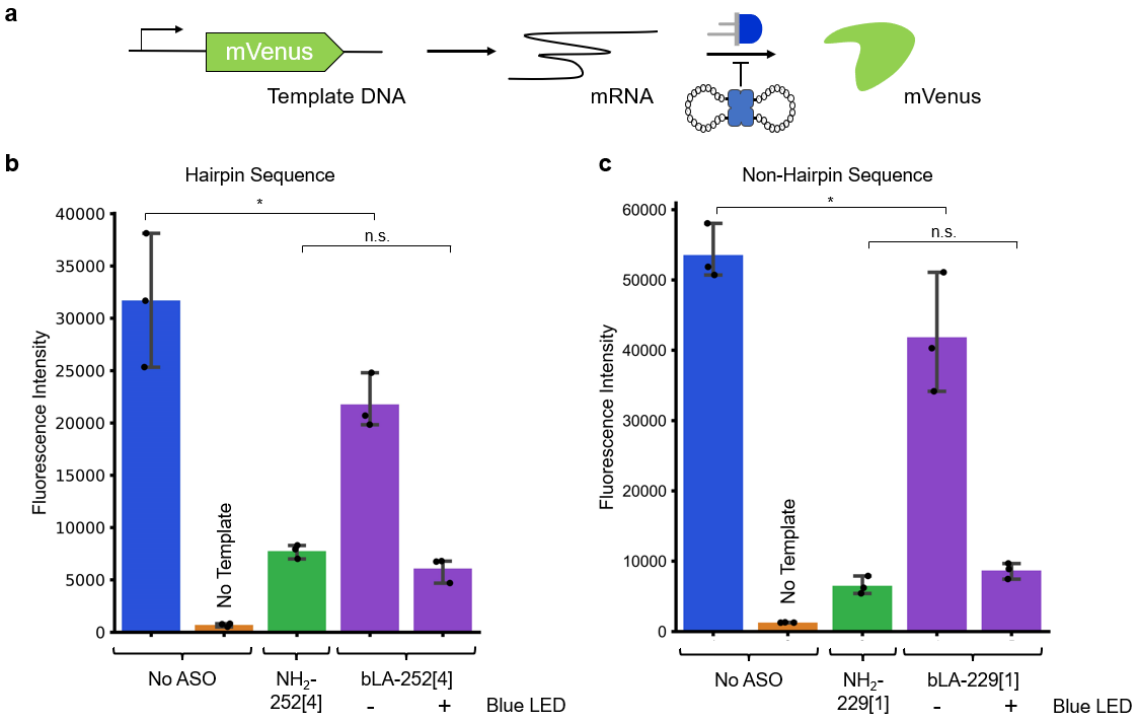


Figure 4-10: Control of cell-free protein synthesis using handcuffed ONs bLA-252[4] and bLA-229[1].

a) Schematic of cell-free protein synthesis from template DNA in the presence of a bLA-ON handcuff. Upon illumination with blue light, translation is interrupted, causing gene knockdown. **b, c**) Control of CFPS using the bLA-252[4] (**b**) and bLA-229[1] (**c**) handcuff ONs. A reduction in gene knockdown is observed with the handcuff ONs, with full knockdown activity restored upon illumination with blue light.

4.8 Conclusions

In this chapter, a circularisation approach was employed to silence ASOs through divalent binding of terminally PC-biotinylated oligonucleotides onto wild-type streptavidin. The approach originally used hairpin-forming oligonucleotides, as the provided secondary structure was believed to aid circularisation onto the same streptavidin. High dilution conditions showed effective circularisation onto the protein, with very few higher order bands observed. These 'handcuffed' oligonucleotides showed interesting photocleavage properties, with intermediate bands of incomplete release of oligonucleotides from the structure showing lower gel migration due to an increase in hydrodynamic radius. The handcuff oligonucleotides were also tested for their ability to control RNase H-mediated mRNA degradation, and it was seen that the circularisation allowed for effective silencing of activity, which could be recovered with light. The circularisation conditions were then trialled on oligonucleotides with lower constraints, i.e. oligonucleotides that form shorter or no hairpins. The conditions employed showed effective circularisation for all oligonucleotides tested, and a high-activity ASO was shown to still be effectively silenced through handcuffing. Lastly, a hairpin-forming and non-hairpin forming ASO were then handcuffed using the blue light photocage and used to control cell-free expression of the target fluorescent protein mVenus. It was found that the circularisation allowed for effective silencing of the oligonucleotide, and full activity could be regained following illumination with blue light.

This approach allowed for rapid generation of caged oligonucleotides with a lower number of employed photocages, allowing for more effective release, by topologically constraining the oligonucleotide, rather than sterically blocking access to it. It could be generated from readily available materials (wild-type streptavidin, terminally amine modified oligonucleotides, commercial UV PC-Biotin) and did not require purification of the final DNA/protein conjugate, as unwanted side products were minimal, and have been shown to not elicit RNase H activity.

5 PHOSPHOROTHIOATE-CAGED ANTISENSE OLIGONUCLEOTIDES

5.1 Introduction

The previous photocaging methods all relied on the use of the light-activatable biotin motif. This motif then allowed for the binding of monovalent streptavidin, providing the steric bulk that prevents enzymes from accessing the DNA until illuminated. While this is a very effective caging strategy, showing excellent off- and on-states, it does have a rather large footprint and requires a large number of non-straightforward components: the biotinylated photocage, which, in case of the blue light-activatable photocage, had to be synthesised; the monovalent streptavidin, which is non-commercial and has to be expressed (or received as a gift from another group, as was the case for us); and lastly the ssDNA with amino-C6-dT oligonucleotides, which were incorporated during solid-phase synthesis.

While the approach of modifying the T7 promoter with the photocages provides a divergent approach for caging multiple genes through the incorporation during PCR, this is also not the case for ASOs modified with the photocleavable biotins, where the amino-C6-dTs need to be incorporated into each sequence that needs to be photocaged, leading to increased cost and a less optimised workflow. It also puts constraints onto the sequences possible. Alternatively, photocaging through circularisation *via* modification of the termini showed to be sequence-independent, but still required the amine modifiers on the termini, where oftentimes other moieties like cellular delivery agents or dyes are attached.

Insertion of photocages onto DNA is often directly performed by incorporating modified phosphoramidites during solid phase synthesis. However, unlike the canonical

phosphoramidites used (including the modified but commercial phosphoramidites such as amino-C6-dT), photocaged phosphoramidite analogues are costly, as they have to be synthesised and may require optimisation of solid-phase conditions due to functional group incompatibilities. The positioning of the photocages will also need to be optimised for each oligonucleotide investigated to ensure efficient caging.

For these reasons, approaches that are independent of oligonucleotide sequence and that use chemistry that does not require extensive modification of the DNA structure are desired. Post-synthesis modification of DNA with photocleavable groups is a very attractive avenue.[201,314,317] One approach of postsynthetically modifying oligonucleotides for photocontrol of DNA function that is independent of the sequence used, and thus does not rely on modified nucleobases, is through the attachment of photoremovable protecting groups directly to the phosphate backbone. Using diazo-activated nitrobenzyl groups and coumarins, it is possible to cage the phosphates of DNA and RNA. As discussed in Chapter 1.6, this approach has been used to modify plasmids encoding for fluorescent proteins[288,289] and mRNA,[289,295] which were activated using UV-irradiation. Gene knockdown using similarly backbone-caged siRNA was also demonstrated.[318,379,380] In all cases though, control of the ON of interest was poor, with leaky off-states and not full reestablishment of the on-state following illumination. This was due to the harsh reagent used for conjugation and the statistical mixture of protection and deprotection. It did, however, utilise native DNA and RNA, not requiring any incorporation of unnatural modifications for the attachment of the photocages.

Among the most commonly used modifications found for oligonucleotides are phosphorothioates, as discussed in Chapter 1.3.4.2.[99] Exchange of a non-bridging oxygen atom for a sulfur atom conserves the charge of the backbone and as sulfur is only slightly larger than oxygen does not increase the backbone size drastically. Synthetically, PS are easily implemented during solid phase synthesis, allowing for oligonucleotides with both fully and partially phosphorothioated backbones.[381]

Such phosphorothioates are commonly used in oligonucleotide-based drugs, as they confer nuclease resistance and thus stability *in vivo*,[382] bind to proteins in plasma due to their more hydrophobic nature, allowing for better tissue distribution and reduced

clearance,[383,384] and greatly improve cellular uptake,[385,386] with recent reports showing thiol-mediated uptake as a potential pathway.[387] Notably, PS-linkages are not exclusively a synthetic modification of DNA and were recently found to occur naturally in bacteria and are believed to be used as an epigenetic regulation mechanism.[388]

As these PS-ONs are already commonly used in therapeutics as they provide several benefits, are cheap and commercially available and fully biocompatible, chemoselective caging of these PS-containing ONs with photoremovable protecting groups is a highly desirable avenue. These PS-ONs provide by themselves an orthogonal, reactive handle with the sulfur on the backbone, which is nucleophilic. This nucleophilicity has already been utilised for modification of the PS linkage with several chemical groups, such as nitroxide spin labels[389] and fluorescent labels,[390,389,391] alkyl-groups[392,393] and even chemotherapeutic drugs.[394] These PS-linkages have also been photocaged previously in a DNAzyme with a phenacyl-group.[395] Due to a rearrangement reaction in the photocaging, however, the resulting product after photocleavage was a phosphate. While the work in this chapter was underway, a new report was released showing the photocaging of a DNAzyme with nitrobenzyl- and coumarin-photocages on PS linkages and their effective removal with light, similar to what is reported in this chapter.[396]

ASOs, as described in Chapter 1.3.4.2, are a promising candidate in the clinic, due to their ability to target several diseases through targeting the mRNA directly. One such pathway, RNase H-mediated mRNA degradation, is particularly promising in reducing levels of harmful protein. One of the downsides of ASO therapeutics at the moment is their wide tissue distribution,[397] potentially causing off-target effects in untargeted tissues. Photocaged ASOs would alleviate this problem through the silencing of systemic activity and the targeted activation in the desired tissue. As these ASOs already are commonly used with PS-linkages throughout,[61] the photocaging of the PS with a photoremovable protecting group is a convenient approach. This approach is also hypothesised to work through a two-fold effect. RNase H has a positively charged, arginine-rich groove that binds to the DNA backbone in a DNA:RNA hybrid duplex.[58] By alkylation of the PS linkage, steric bulk is introduced, in addition to the removal of the negative charge, and the combination of those two factors should prevent RNase H from binding.

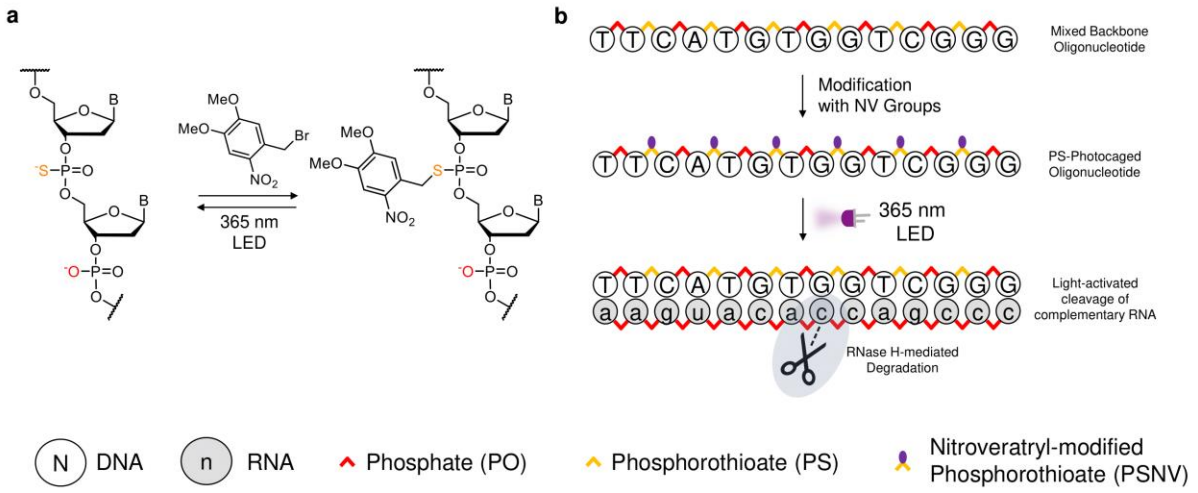


Figure 5-1: Chemoselective caging of ASOs through alkylation of the PS-linkages (a) and subsequent removal by UV irradiation (b), allowing for light-controllable activity of RNase H
Figure adapted from 'Light-controlled cell-free protein synthesis using phosphorothioate-caged antisense oligonucleotides' by D. Hartmann and M. J. Booth[337] (© 2022) under a creative commons licence (CC-BY 4.0).

Hence, in this chapter, a simple, chemoselective caging strategy for PS linkages in a mixed backbone ASO is presented (**Figure 5-1**). The resulting ONs are well-defined, show effective silencing of RNase H activity and allow for controlled uncaging with UV irradiation, enabling RNase H-mediated degradation and gene knockdown in a cell-free system.

5.2 Screening for an Antisense Oligonucleotide against mVenus

As a starting point for this project, a suitable ASO was needed. As mV is already commonly used as a reporter protein, it was desirable to find an ASO sequence against mV. To do so, RNase H-mediated degradation was an effective way of screening for efficient ASOs. The ASOs were generated through the online tool sFold[398] (Software for Statistical Folding of Nucleic Acids and Studies of Regulatory RNAs), which predicts effective ASOs on a given mRNA. Of those, eleven were chosen across the whole gene for testing.

Initially, optimal conditions for the assay had to be screened for. For this, sequence mV 240 (starting oligonucleotide 240 in mVenus ORF DNA sequence) was chosen. 300 ng of target mRNA, prepared by *in vitro* transcription, was used, together with 2.5 ng of ASO (a 2:1 molar ratio of RNA to ASO) at different amounts of RNase H (**Figure**

5-2, a). At 0.6 U/µL RNase H, small amounts of RNA were still undegraded, as was desirable to be able to differentiate efficiency between the tested ASOs.

Following on, the amount of ASO was varied, to see which concentration would be most suitable (**Figure 5-2**, b). 1 ng total ASO was chosen to continue, as this still elicited an RNase H response, but allowed room for improvement to find potentially better-performing ASOs.

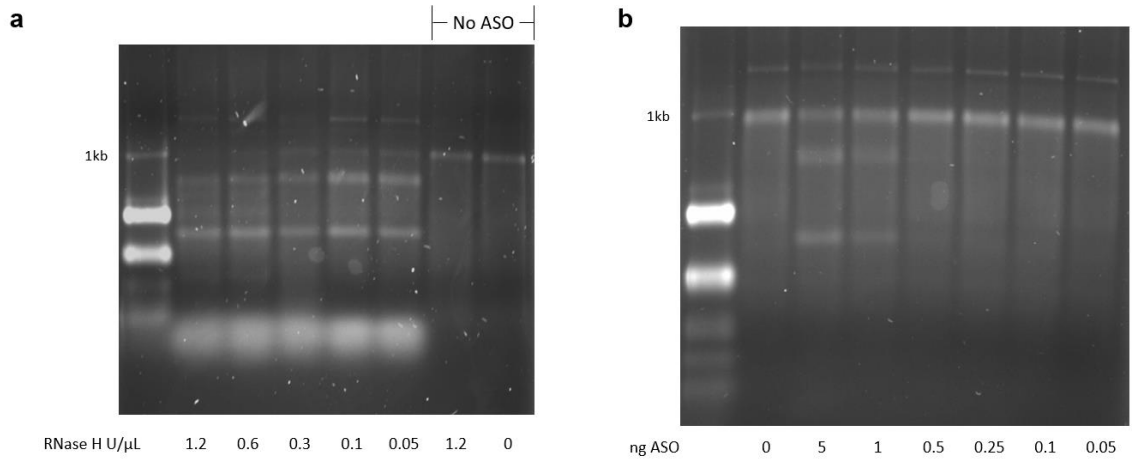


Figure 5-2: Optimisation of the RNase H-mediated degradation assay through varying concentrations of RNase H (a) and ASO (b).

After optimisation of these conditions, all eleven ASOs (**Table 7-5**) were tested in the RNase H assay to find the optimal ASO for further studies (**Figure 5-3**, a). By comparing intensity data of the gel, it was found that sequence mV 220 was particularly active (i.e. the intensity of the intact mRNA band was lowest) and was taken forward for this study. It was also chosen due to it being relatively early in the sequence, hereby preventing truncated, but potentially functional protein being produced. To ensure that the sequence is specific, four scramble controls were designed as well (**Table 7-7**) and tested against mV mRNA with RNase H (**Figure 5-3**, b). All the scrambles were found to be inactive, indicating sequence specificity of the ASO.

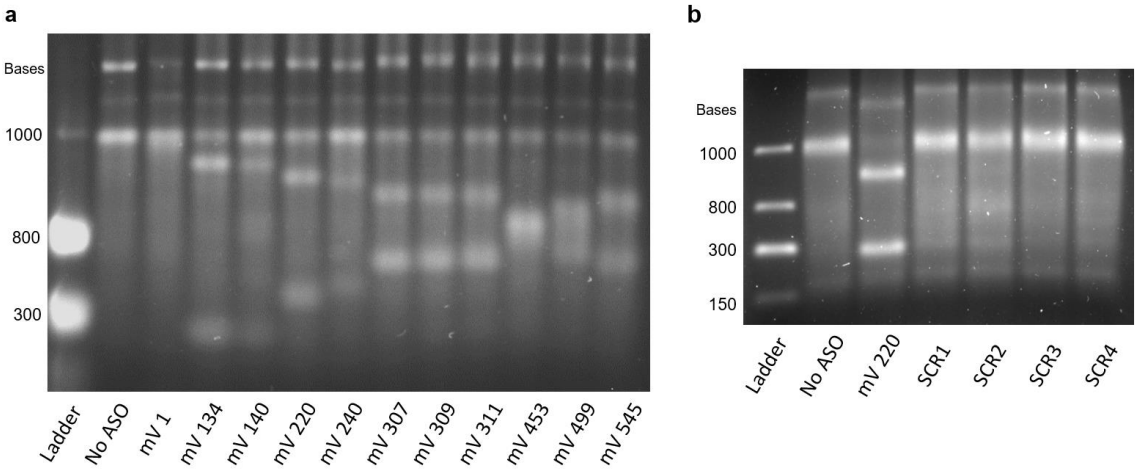


Figure 5-3: Screening of ASO sequences for RNase H-mediated degradation to find the best ASO against mVenus mRNA and scramble controls for the mV 220 sequence

a) Screening of eleven sequences for antisense activity against mV mRNA. mV 220 showed the highest activity and was chosen for further studies. **b**) Scramble controls for the mV 220 sequence. Figure adapted from 'Light-controlled cell-free protein synthesis using phosphorothioate-caged antisense oligonucleotides' by D. Hartmann and M. J. Booth[337] (© 2022) under a creative commons licence (CC-BY 4.0).

5.3 Optimisation of Reaction Conditions for Phosphorothioate Modification

The ON mV 220 was then purchased with a single PS linkage (1PS ON) at the midpoint of the sequence. This was used for screening of suitable chemoselective reaction conditions with 2-nitroveratryl bromide (NV-Br). The ON was incubated with the NV-Br in 50% DMF in different buffers overnight at 37 °C. The mixture was then purified by ethanol precipitation followed by analysis by HPLC (**Figure 5-4**). With $NaHCO_3$, which is a common buffer of choice for bioconjugations with *N*-hydroxysuccinimide esters, a large distribution of products was observed, due to poor chemoselectivity. With tris buffer at pH 8, a cleaner reaction profile was observed, but several products were still seen. With HEPES pH 7, however, very clean and efficient conversion was observed to a product with higher retention time. As the PS-linkage is highly acidic and thus deprotonated even at neutral pH, this was not surprising. Lower pH than 7 was avoided to avoid depurination, but also was believed to reduce effectiveness of the alkylation due to partial protonation of the PS-linkages.

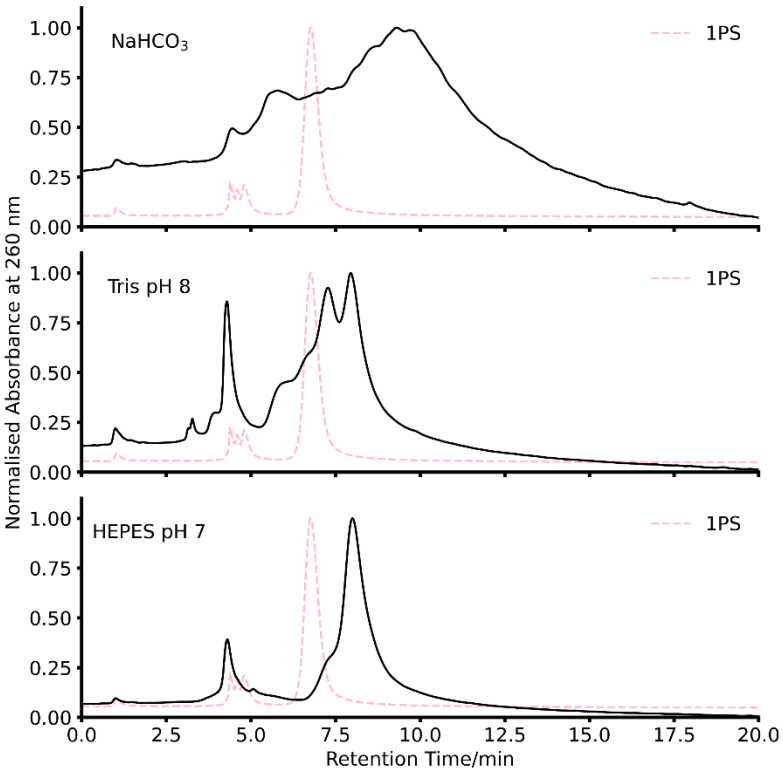


Figure 5-4: Screening for suitable buffer conditions for the chemoselective modification of PS-linkages in a mixed backbone ON.

Figure adapted from 'Light-controlled cell-free protein synthesis using phosphorothioate-caged antisense oligonucleotides' by D. Hartmann and M. J. Booth[337] (© 2022) under a creative commons licence (CC-BY 4.0).

The reaction mixtures were then also analysed by LCMS (**Table 5-1**, Appendix D). With $NaHCO_3$, the desired 1x NV-modified oligonucleotide was observed; however, the additional peaks correspond to uncontrolled alkylation of the ON, as well as desulfurisation of the alkylated PS to a PO linkage, which is known to occur at pH-values above 8.[391] Similarly, for the case with Tris buffer, small amounts of overalkylation, as well as desulfurisation was observed. This feature of the alkylated PS-linkages was taken into account for HPLC analysis and purification, with the buffer employed (NH_4OAc) being at pH 7.5. With HEPES buffer at neutral pH, however, almost exclusively the 1PSNV-modified ON was observed, showing a highly chemoselective conversion to the desired ON under these conditions. To test this chemoselectivity further, the PO-only ON was subjected to identical conditions and also analysed by LCMS after precipitation. The mass of the product corresponded to the starting PO-only ON, providing proof for the chemoselectivity of PS alkylation using these conditions.

Entry	ON	Buffer	Retention Time/minutes	Masses after Deconvolution (Expected Mass) – Modification
1	1PS	$NaHCO_3$	5.18	6220 (6220) – desulfurisation
2	1PS	$NaHCO_3$	5.40	6431 (6431) – 1x 2-NV
3	1PS	$NaHCO_3$	5.5-6.5	6416 (6415) – Desulfurisation and 1x 2-NV 6611 (6610) – Desulfurisation and 2x 2-NV 6625 (6626) – 2x 2-NV 6806 (6806) - Desulfurisation and 3x 2-NV 6823 (6821) – 3x 2-NV 6999 (7001) - Desulfurisation and 4x 2-NV 7016 (7016) – 4x 2-NV 7210 (7211) – 5x 2-NV 7408 (7406) – 6x 2-NV
4	1PS	Tris pH 8	5.20	6219 (6220) – desulfurisation
5	1PS	Tris pH 8	5.40	6431 (6431) – 1x 2-NV
6	1PS	Tris pH 8	5.56	6626 (6626) – 2x 2-NV
7	1PS	HEPES pH 7	5.40	6431 (6431) – 1x 2-NV
8	PO-only	HEPES pH 7	5.18	6219 (6220) – native oligonucleotide

Table 5-1: Retention times and observed, deconvoluted, masses of ONs subjected to modification with 2-nitroveratryl bromide in different buffer conditions.

Next, the 1PSNV was prepared on scale and purified by HPLC. To test its photocleavage, the ON was illuminated with a 365 nm LED and analysed by HPLC (**Figure 5-5**). Photocleavage proceeded as expected, with a decrease in the 1PSNV peak, and appearance of a split peak at lower retention time. This split peak is indicative of the PS-linkage, as there are 2 diastereomers possible, which can be separated. Due to the equal intensity of the split peak apexes, it is also seen that the caging approach works for both possible diastereomers equally and not favouring one particular diastereomer. This peak was also collected, and the reformation of the PS-linkage confirmed by LCMS.

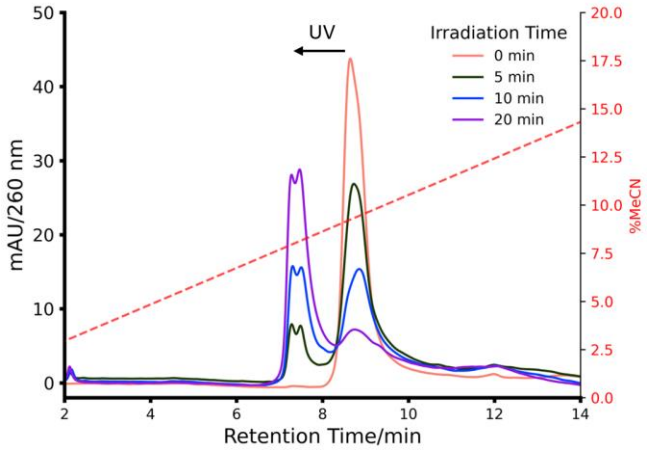


Figure 5-5: Photocleavage of the 1PSNV ON under UV irradiation.
Upon irradiation with UV light, the NV photocage was effectively removed, reforming the PS ON, indicated by the split peak (arising from the diastereomers) with lower retention time. Figure adapted from 'Light-controlled cell-free protein synthesis using phosphorothioate-caged antisense oligonucleotides' by D. Hartmann and M. J. Booth[337] (© 2022) under a creative commons licence (CC-BY 4.0).

5.4 Characterisation of NV-modified Oligonucleotides

To control RNase H activity and therefore gene knockdown, it was anticipated that more than one alkylated PS-linkage is required. The interacting motif of RNase H is through 2 phosphates,[399] so by interspersing the modification and having it evenly modified, any individual part of the ON should be silenced. In addition, this pattern should cause less aggregation than having the modifications focussed on one part of the ON, resulting in an amphiphilic copolymer. For these reasons, ONs were purchased with every 3rd and 2nd PO-linkage replaced by a PS-linkage, resulting in ONs with 6PS and 9PS, respectively, at which alkylation can occur (**Figure 5-6**, a).

These PS-containing ONs were then subjected to the screened modification conditions to produce the PSNV-caged ONs through incubation with NV-Br overnight. It was still possible to modify the PS-linkages chemoselectively on these ONs and it was possible to purify them by HPLC (**Figure 5-6**, b). With increasing number of PSNV-linkages, there was also a large increase in retention time, as is anticipated for the addition of an increasing number of hydrophobic moieties. Their solubility in purely aqueous media was also found to be poor, and hence had to be resuspended in 25% DMSO.

Their UV-visible absorbance was also recorded by the HPLC for characterisation (**Figure 5-6**, c). With increasing numbers of NV-modifications on the ON, there was also an increase in absorbance at ~360 nm, in line with the density of modification of the ON. In addition, a very weak hypsochromic shift of the λ_{max} at ~260 nm was observed with increasing number of NV-modifications, as well as the emergence of a shoulder at ~275 nm.

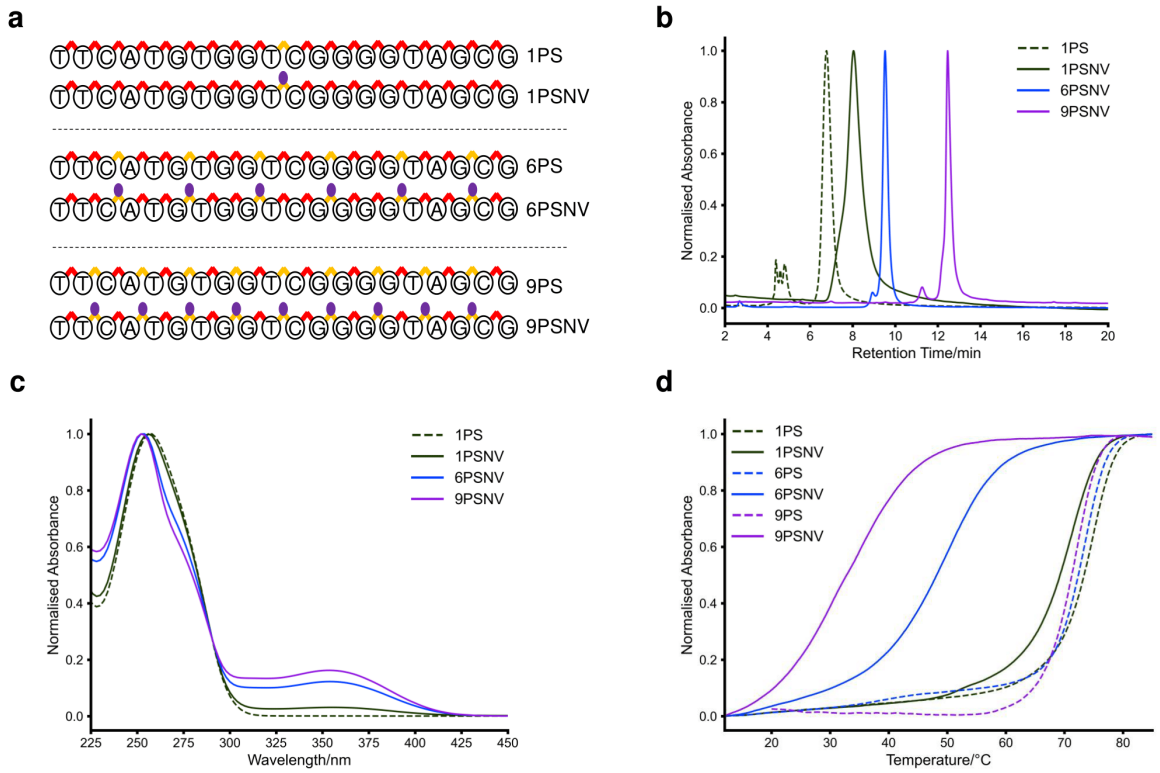


Figure 5-6: PS-sequences studied and their HPLC UV-Vis and T_m characterisation data

a) ONs investigated with 1, 6 and 9 PS linkages. **b**) HPLC retention times of purified PSNV ONs. Retention times increased with increasing NV modification **c**) UV-visible absorbance spectra of PSNV ONs as recorded by HPLC. A clear peak at ~352 nm was visible. **d**) Representative melting temperature curves of PS and PSNV ONs. A clear decrease in melting temperature was observed with increasing NV modification. Figure adapted from 'Light-controlled cell-free protein synthesis using phosphorothioate-caged antisense oligonucleotides' by D. Hartmann and M. J. Booth[337] (© 2022) under a creative commons licence (CC-BY 4.0).

To characterise these ONs even further, and investigate the effect of the NV-modifcation on ON duplex stability and thus hybridisation efficiency with its target mRNA, which is essential for ASO activity, melting temperatures (T_m) were recorded. DNA duplex stability, and consequently their melting temperature is influenced by a

number of factors, including the shielding of the repulsive backbone charges by surrounding ions as well as the π-stacking of the bases.[400] In addition, uncharged nucleic acids such as peptide nucleic acids are still known to effectively hybridise with their target reverse complementary strand.[401] PS-linkages themselves also slightly lower the T_m of an ON, due to a slightly weaker interaction with the surrounding ions.[61]

The T_m of the PS and PSNV ONs were therefore measured in high salt (0.92 M NaCl, 0.92 mM potassium phosphate pH 7.4) buffer containing 1.67% DMSO by incubation with the complementary strand overnight prior to thermal denaturation (**Table 5-2**, **Figure 5-6**, d). As expected, with an increase in PS-linkages there was a small decrease in T_m. Upon modification of the PS-linkages, a drastic decrease in T_m was observed, with a larger decrease with increasing amounts of PSNV-modifications. A ΔT_m of -3.71 °C for the 1PS/1PSNV pair was observed. When dividing the ΔT_m of the 6PS/PSNV and 9PS/9PSNV pairs by the number of modifications, an average ΔT_m of -3.74 °C was obtained, closely matching the decrease observed for the ON with 1 PS linkage, showing that the modification has a predictable effect on T_m. In the T_m data, reduced hysteresis between the heating and cooling cycles was also observed (Appendix F). This indicated a reduction in non-equilibrium secondary structures and likely arose from the same destabilisation observed for the duplex.

To test whether the screened reaction was specific to the NV-Br and to compare the effect on T_m, the previously reported ethylation of PS-linkages[392] was also attempted using our screened conditions for the 1PS ON, forming an ethylated 1PS linkage (1PSEt), and the T_m recorded (**Table 5-2, Figure 5-7**). The T_m was also reduced for the 1PSEt (ΔT_m of -2.12 °C). The magnitude of reduction, however, was larger for the NV-modification than for the Et-modification, likely due to the increased hydrophobic surface of NV compared to Et.

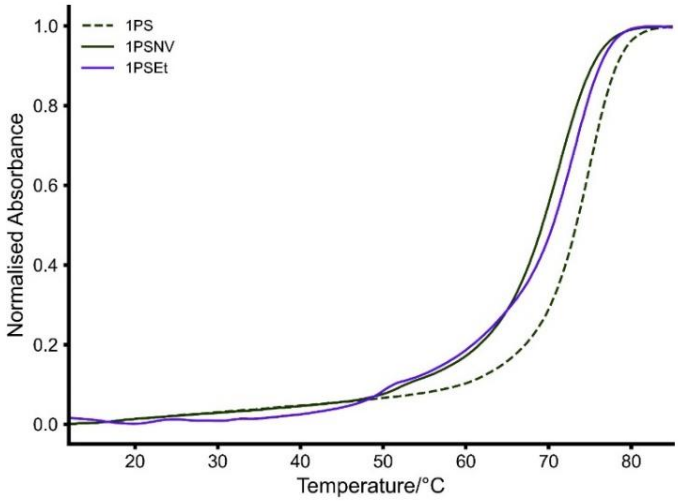


Figure 5-7: Representative melting temperature curves of the 1PS, 1PSNV and 1PSEt ONs. The ethyl-modification showed a smaller reduction in melting temperature than the NV modification. Figure adapted from 'Light-controlled cell-free protein synthesis using phosphorothioate-caged antisense oligonucleotides' by D. Hartmann and M. J. Booth[337] (© 2022) under a creative commons licence (CC-BY 4.0).

Entry	Oligo	T_m /°C	ΔT_m /°C
1	1PS	72.15	
2	1PSNV	68.44	-3.71
3	6PS	71.79	
4	6PSNV	48.76	-23.03
5	9PS	66.91	
6	9PSNV	33.78	-33.13
7	1PSEt	70.03	-2.12

Table 5-2: Melting temperatures (T_m) and ΔT_m of the modified oligonucleotides.

5.5 Screening for a truncated ASO for higher caging density

After the investigation of the 20nt ONs, an additional, truncated sequence was screened for that retained RNase H activity. This shorter sequence would allow for a lower number of PS-linkages over the ON, reducing the number of NV-groups needed and thus potentially better photorelease, but still allowing for a high caging density over the sequence. 16 nt- and 14 nt- long ONs were screened in an RNase H assay

(**Figure 5-8**, a) and in a CFPS system (**Figure 5-8**, b) that were either truncated at the 5', 3' or both ends compared to the 20 nt ON, and an additional 14 nt ON early in the sequence was tested for comparison. From this data, the 3'-truncated 14 nt ON was chosen due to good performance in the assays, showing some improvement over the original 20 nt ON mV 220. This sequence was then chosen to have alternating PO and PS linkages, giving the same pattern as the 20nt-9PS ON, but only having a total of 6 PS-linkages.

5.6 Control of RNase H-mediated degradation with NV-modified Oligonucleotides

It was then investigated if the NV-modified ONs allow for control of RNase H-mediated degradation. It was hypothesised that due to the reduction in duplex stability and hence its affinity for the target mRNA, a reduction in RNase H activity would be expected. In addition, RNase H has a shallow, positively charged groove, which binds the charged PO/PS backbone of the DNA in a DNA/RNA hybrid duplex.[58] Therefore, by alkylating the PS-linkage RNase H would be prevented from recognising any PSNV ONs bound to the mRNA as its substrate as the charge was removed from the PS, thus interrupting ionic interactions with the arginine residues from ionic interactions with the ON, and the steric bulk introduced with the NV group would also disable effective binding.

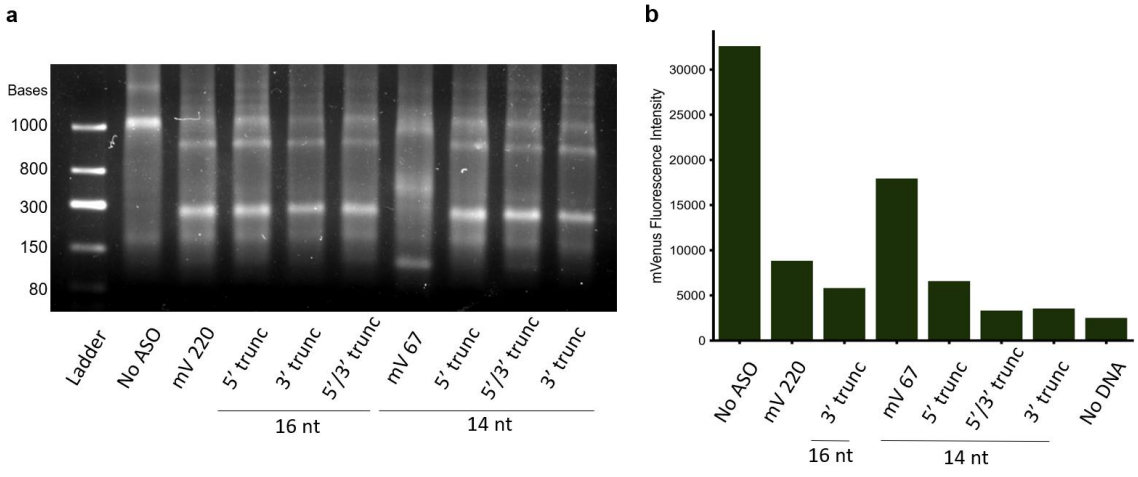


Figure 5-8: Screening for a truncated RNase H-active antisense oligonucleotide

a) RNase H assay to screen for truncated ASO sequences based on mV 220. **b**) Gene knockdown in cell-free protein synthesis using the truncated ASOs from (**a**). Figure adapted from 'Light-controlled cell-free protein synthesis using phosphorothioate-caged antisense oligonucleotides' by D. Hartmann and M. J. Booth[337] (© 2022) under a creative commons licence (CC-BY 4.0).

Due to the nature of attaching photoactive moieties to the DNA, the 260 nm absorbance is likely changed and consequently measurement of ON concentration by spectrophotometric techniques is likely inaccurate. Furthermore, the ONs were dissolved in 25% DMSO, which is incompatible with measurement at 260 nm. For this reason, the PS-modified ONs 20nt-6PS and -9PS, as well as the 14nt-6PS were purchased with a TxRd fluorophore attached to the 5' end for measurement *via* fluorescence. TxRd was chosen as it has no overlap with excitation/emission of mV, the reporter protein utilised here.

To modify these more hydrophobic ONs, the concentration of DMF in the modification reaction was increased to 75% from 50%. These conditions allowed for the largely complete modification of the ONs, as was investigated by denaturing PAGE (**Figure 5-9**). The modified ONs could again be purified by HPLC and were verified using the UV-visible absorbance traces recorded by the machine (**Figure 5-9**) as well as by LCMS.

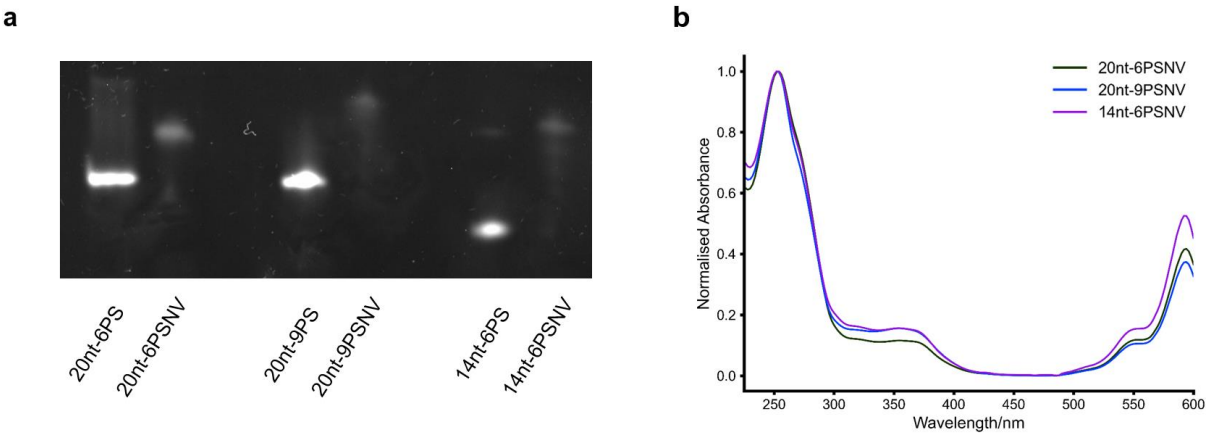


Figure 5-9: Denaturing PAGE of crude TxRd-ON modification reactions with 2-nitroveratryl bromide (a) and their UV-Visible absorbance traces as recorded by HPLC (b).

Figure adapted from 'Light-controlled cell-free protein synthesis using phosphorothioate-caged antisense oligonucleotides' by D. Hartmann and M. J. Booth[337] (© 2022) under a creative commons licence (CC-BY 4.0).

The ability of the PSNV-ONs to control RNase H-mediated degradation with light was then tested (**Figure 5-10**, a). The unmodified PS and PSNV ONs were incubated with the target mRNA in presence of RNase H for one hour at 37 °C, with or without illumination, and the reactions then analysed by AGE.

For the 20nt-6PSNV ON, almost complete abolition of RNase H activity was observed (**Figure 5-10**, b), despite the use of a 0.9:1 molar ratio of ASO to mRNA, showing very tight control of RNase H activity through NV-modification of the backbone PS-linkages. Upon illumination with UV light for 5 minutes, great recovery of activity was observed. This trend was also observed for the 20nt-9PS ON (**Figure 5-10**, c). In the absence of light, the 20nt-9PSNV did not elicit an RNase H-response, again showing effective caging of the ON. Upon illumination with UV light, recovery of RNase H activity was again observed. Due to the increase in the number of photocages, two irradiation times were tried, and it was seen that progressive release and thus an increase in recovery of RNase H activity can be achieved with longer irradiation. Lastly, the 14nt-6PSNV ON was tested (**Figure 5-10**, d). This ON also showed a very tight off-state in the absence of irradiation, and good recovery upon illumination with UV light for 5 minutes, mirroring the data observed for the 20nt-ONs tested.

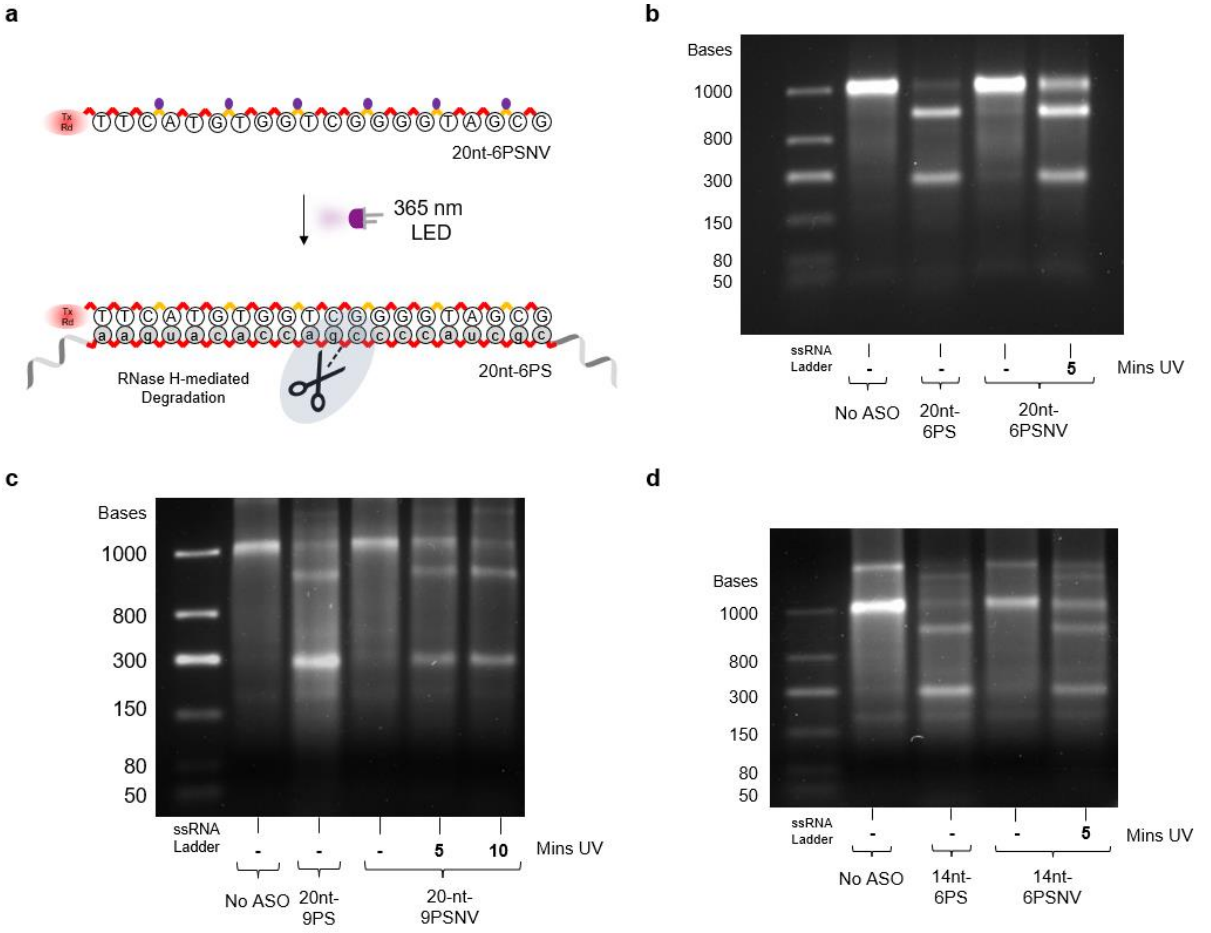


Figure 5-10: Control of RNase H-mediated degradation of target mRNA using the PSNV-modified ONs.

a) Schematic of the uncaging process from the 20nt-6PSNV ON and subsequent RNase H-mediated degradation of complementary mRNA. **b**) UV-light controlled RNase H-mediated mRNA degradation using the 20nt-6PSNV ON. **c**) UV-light controlled RNase H-mediated mRNA degradation using the 20nt-9PSNV ON. **d**) UV-light controlled RNase H-mediated mRNA degradation using the 14nt-6PSNV ON. Figure adapted from 'Light-controlled cell-free protein synthesis using phosphorothioate-caged antisense oligonucleotides' by D. Hartmann and M. J. Booth[337] (© 2022) under a creative commons licence (CC-BY 4.0).

5.7 Control of Cell-free Protein Synthesis with NV-modified ASOs

Encouraged by the results seen on AGE using RNase H-mediated degradation, the NV-modified ONs were then tested for their ability to control CFPS. For this, the light-activatable PSNV-oligonucleotides were placed into a CFPS system (PURExpress), supplemented with RNase H and intact protein output of mV measured by fluorescence after 4 hours of incubation.

Using the unmodified 20nt-6PS ASO (**Figure 5-11**, a), a decrease in protein yield of mV of 70% was observed compared to the system without ASO. Illumination of the system with UV light for 5 minutes showed an even larger decrease in protein yield by 84%, indicating UV-damage to the CFPS system. Using the photocaged 20nt-6PSNV ASO, only a minimal decrease in protein yield of 7.6% was observed. Upon irradiation with UV light of 365 nm, however, the ASO was effectively uncaged and a decrease in protein yield by 70% was measured, showing effective control of CFPS using the NV-caged ASO. Next, the 20nt-9PS ASO was tested to control CFPS (**Figure 5-11**, b). The increase in PS-linkages in the backbone showed no difference in gene knockdown compared to the previous 20nt-6PS ASO. As previous, illumination with UV light for 10 minutes (increased due to the larger number of photocages on the ASO) showed an additional decrease in protein yield, again indicating UV damage to the system. Using the photocaged 20nt-9PSNV ASO, a large decrease in gene knockdown was again observed (17% residual knockdown activity), similar to the 6PSNV ASO. Upon illumination for 10 minutes, gene knockdown recovered to 66%, to very similar levels as the unmodified 20nt-9PS ASO (83% activation compared to the non-modified, illuminated sample), again showing effective control of protein synthesis in cell-free conditions.

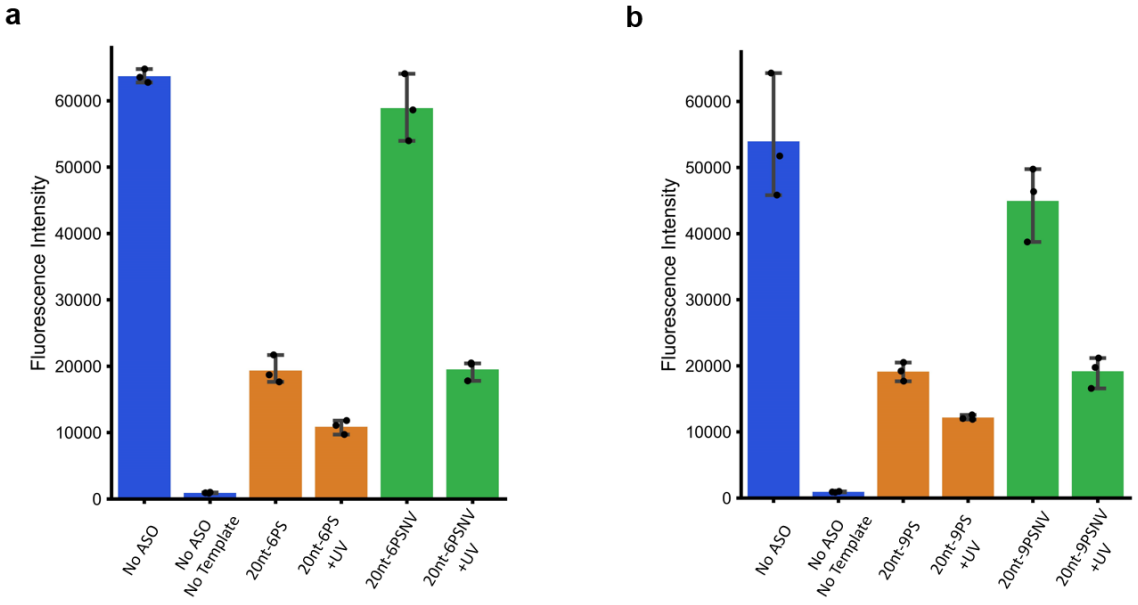


Figure 5-11: Control of CFPS using 20nt-PSNV Oligonucleotides

a) Light-controlled gene knockdown of mV in a CFPS system using the 20nt-6PSNV ON. **b**) Light-controlled gene knockdown of mV in a CFPS system using the 20nt-9PSNV ON. Figure adapted from 'Light-controlled cell-free protein synthesis using phosphorothioate-caged antisense oligonucleotides' by D. Hartmann and M. J. Booth[337] (© 2022) under a creative commons licence (CC-BY 4.0).

Lastly, the 14nt-6PS ASO was tested (**Figure 5-12**). Illumination of the CFPS without any ASO showed a reduction in protein yield with increasing amount of irradiation, as was anticipated from previous data. Gene knockdown with the unmodified 14nt-6PS ASO worked as previous, giving a 77% reduction in protein yield, which, after illumination with UV, increased to 84%, again showing the damaging effect of UV irradiation. The photocaged 14nt-6PSNV ASO showed residual activity, resulting in a 30% reduction in protein expression. Uncaging of the ASO through increasing amounts of UV irradiation allowed for a gradual response of gene knockdown, with 10 minutes of UV irradiation yielding essentially full activation (81% gene knockdown, corresponding to a 97% activation of the ASO compared to the unmodified ASO + 10 minutes of UV).

To decipher whether any residual knockdown is due to mRNA target binding, key experiments were performed without RNase H. It was seen that there is no difference in expression levels between samples without ASO in the presence of absence of RNase H. Addition of the 14nt-6PSNV ASO showed only minor reduction of gene expression in the absence of RNase H, however, showing that the residual activity observed is due to RNase H activity. In addition, Illumination with UV light for 10 minutes showed a reduction in expression to levels observed in the no ASO case with RNase H, showing that the uncaged ASO also has no detrimental effect to expression levels beyond UV damage.

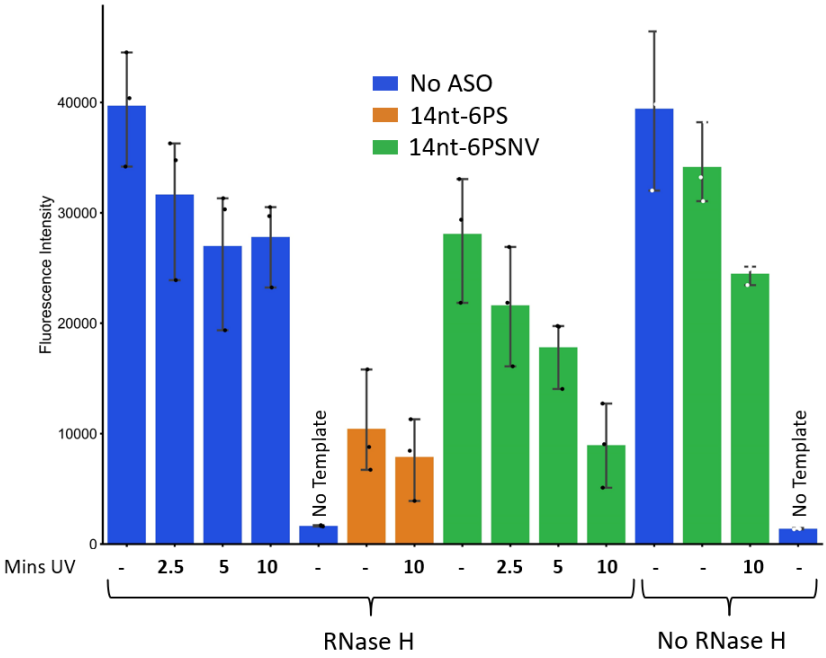


Figure 5-12: Control of CFPS with the 14nt-6PSNV ON

Control of gene knockdown in a CFPS system with the 14nt-6PSNV ON in the presence and absence of RNase H under different illumination conditions. Figure adapted from 'Light-controlled cell-free protein synthesis using phosphorothioate-caged antisense oligonucleotides' by D. Hartmann and M. J. Booth[337] (© 2022) under a creative commons licence (CC-BY 4.0).

In all CFPS experiments using PSNV-ASOs, the TxRd-fluorescence of the ASO was also measured (**Figure 5-13**). In all cases, fluorescence increased after photocleavage of the NV-groups, indicating that the NV-groups caused some degree of fluorescence quenching.

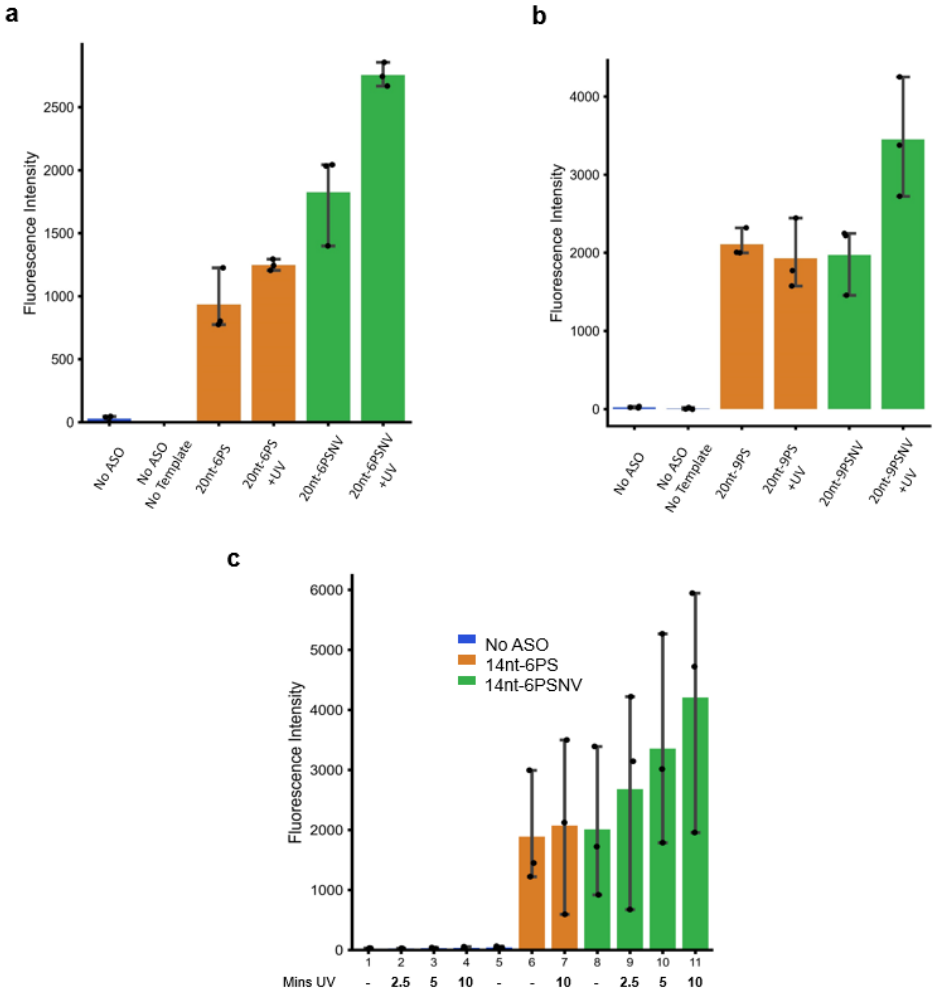


Figure 5-13: TxRd-fluorescence measurements of CFPS reactions (Figure 5-11 and Figure 5-12). **a**) TxRd-fluorescence measurements of CFPS reactions using the 20nt-6PSNV ON. **b**) TxRd-fluorescence measurements of CFPS reactions using the 20nt-9PSNV ON. **c**) TxRd-fluorescence measurements of RNase H-containing CFPS reactions using the 14nt-6PSNV ON. In all cases, uncaging of the NV-modified ON caused an increase in fluorescence. NV-modification was quenching fluorescence of the appended TxRd. Figure adapted from 'Light-controlled cell-free protein synthesis using phosphorothioate-caged antisense oligonucleotides' by D. Hartmann and M. J. Booth[337] (© 2022) under a creative commons licence (CC-BY 4.0).

5.8 Nuclease Stability of NV-modified Oligonucleotides

Lastly, it was tested whether the NV-modification on the PS-linkages could offer additional stability against nucleases, beyond what the PS-linkages provided by themselves, by preventing access to the PO-linkages between modification sites. For this, DNase I was chosen, as it is a highly active nuclease, commonly found in nature and accounts for the majority of nucleolytic activity in serum.[402] As was anticipated, the PO-only ON showed rapid degradation after just one hour (**Figure 5-14**, a). The 20nt-9PS ON, in comparison, showed a drastic increase in stability over twelve hours (**Figure 5-14**, b). To test the impact of the NV-modification, the TxRd-tagged ONs had to be chosen, as it was found that the NV-modification caused a drastic decrease in gel staining. In addition, the pH of the running buffer (TBE) had to be adjusted to 7.5 to ensure stability of the NV-groups, as the alkylated PS-linkages are known to hydrolyse at pH >8.

A reduction in total degradation over the measured 6 hours with the PSNV-modification, compared to the unmodified PS-ON (**Figure 5-14**, c, d) was observed, indicating that NV-modifications hinder access of the DNase I to the PO-linkages.

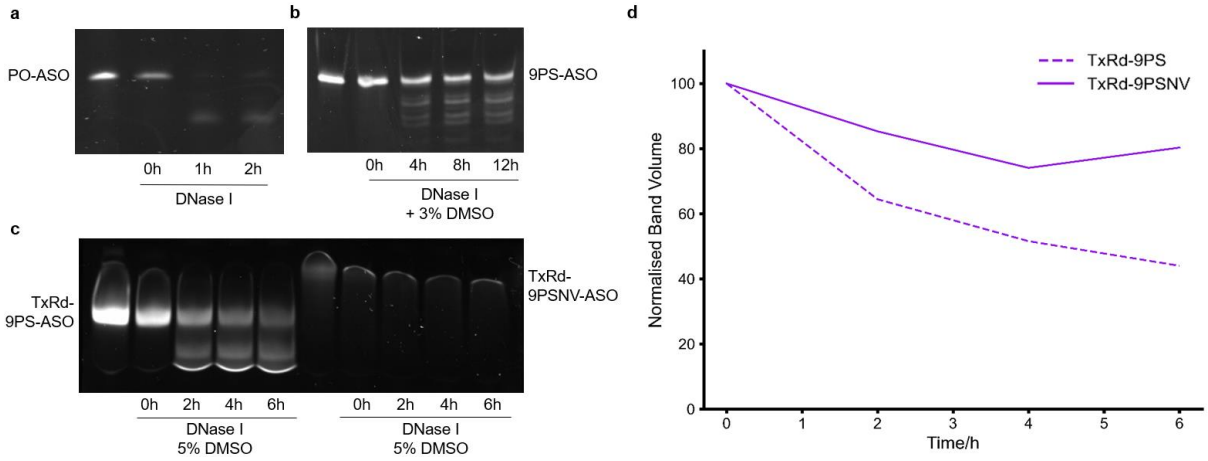


Figure 5-14: Stability of PO, 9PS and PSNV ONs towards DNase I

a) DNase I degradation of PO-only ASO mV 220. **b**) DNase I degradation of the 9PS-containing 20nt mV 220 ASO. PS linkages hindered degradation *via* DNase I. **c**) TxRd-tagged 9PS and 9PSNV ASO degradation *via* DNase I. **d**) Line profile of DNase I mediated degradation of TxRd-tagged ASOs from (**c**). The NV-modification hindered degradation of the ASO compared to the unmodified control. Figure adapted from 'Light-controlled cell-free protein synthesis using phosphorothioate-caged antisense oligonucleotides' by D. Hartmann and M. J. Booth[337] (© 2022) under a creative commons licence (CC-BY 4.0).

5.9 Conclusions

In this chapter, an alternative approach to photocaging, not reliant on photocleavable biotins, was demonstrated. Through utilisation of the commonly used, and mildly reactive phosphorothioate modification of oligonucleotide backbones *via* a chemoselective procedure, UV-photocleavable PPGs could be installed. The resulting oligonucleotides showed the ability to regenerate the original PS-containing oligonucleotide upon irradiation with UV light. The modification also drastically altered the behaviour of the oligonucleotide, with a reduction in aqueous solubility and a drastic reduction in melting temperature being observed. As hypothesised, these backbone-caged oligonucleotides were also effectively silenced and did not elicit RNase H activity, but activity could be effectively regained through irradiation with UV light and the subsequent removal of the photocages. This translated well into control of cell-free expression using these modified oligonucleotides, where only minimal knockdown was observed with the caged oligonucleotide, but great activity and thus gene knockdown could be regenerated through illumination with UV light.

The approach here demonstrated the effective caging through an already commonly used, cheap and commercial oligonucleotide modification. The photocaging procedure also employed a commercial and readily available molecule and a simple reaction setup to generate caged oligonucleotides, making this approach highly accessible. The employed method also was independent of oligonucleotide sequence and should therefore be useable with many oligonucleotides in the future.

The drawbacks of this approach, however, are the reduction in aqueous solubility, the difficulty in analysis and quantification due to fluorescence quenching and the instability of the modification at high pH. The photocages also required UV irradiation, which, as discussed prior, is not ideal for biological systems. Future development in the area can address these issues, however, for example through synthesis of more water-soluble and red-shifted photocages as well as the synthesis of surrogate molecules, allowing for quantification directly by absorbance measurements at the λ_{max} of the photocage.

6 Conclusions and Future Work

In this work, new avenues for the photocontrol of DNA function have been explored. The work in Chapter 2 focussed on the development of a new, blue light-activatable photocage for the silencing and activation of linear DNA templates for use in cell-free expression systems and within synthetic cells. The work presented in Chapters 3 and 4 explored the applicability of the photocleavable biotin technology developed in the group to a different class of DNA, antisense oligonucleotides, and two different modes of caging were tested. The work described in Chapter 5 then investigated a different approach of antisense caging, which was not reliant on the photocleavable biotin technology.

This work demonstrated the high applicability of the photocaging strategy towards multiple oligonucleotides and their control with light to gene expression in cell-free conditions. Due to orthogonality achieved between the blue and UV photocages, the orthogonal remote control of both linear templates as well as antisense oligonucleotides was possible and allowed for the precise control of expression of reporter proteins. The approaches used are highly general. The linear templates are only restricted in that they utilise a T7 promoter, but the gene downstream can be chosen at will. The ASO caging method in Chapter 3 is highly general, but does require the presence of amino-modified bases. The work described in Chapter 4 and 5 provide the most general strategy, in that they are completely independent of sequence or incorporation of modified bases. Chapter 5 in particular is also highly accessible, as all components are readily commercially available and thus allow for rapid access to light-activatable oligonucleotides.

The caging/uncaging behaviour of the developed light-activatable oligonucleotides was also excellent. Compared to many examples in the literature of light-controlled gene expression, which suffer either from high activity in the off-state or poor recovery

upon uncaging, the approaches presented herein enable very tight caging and thus minimal activity in the off-state, and excellent recovery of activity upon uncaging with light, with the amount of light used having had only a small damaging effect on the system. Specifically, the bLA-DNA templates had minimal activity prior to illumination, and rapid recovery to 70% activity upon irradiation with blue light, while also being orthogonal to UV light, under which uncaging was slow. The ASO caging approach in Chapter 3 provided a very tight off-state as well with almost complete recovery of gene knockdown upon illumination. The circularisation approach in Chapter 4 suffered from a leakier off-state than the approach in Chapter 3, but did have superior uncaging to full activity upon irradiation, and is additionally sequence-independent. The caging approach in Chapter 5 was particularly easy to access, and was also independent of sequence, while still providing a very tight off-state and excellent recovery upon illumination, though with the drawback of drastically reducing the oligonucleotide solubility and requiring more UV irradiation.

Future work in this area would include the preparation of more red-shifted analogues for use in such systems, as they provide additional benefits, such as improved tissue penetration, reduced scattering and higher biocompatibility, with the potential of having additional, orthogonal, remote handles to control biological systems with light. Photoactive scaffolds that show release with longer wavelengths include for example BODIPY[403–405] and cyanine dyes,[275,406–408] both of which have shown to be biocompatible and allow for the release of cargo with green or red light. These photocages could either be functionalised with a biotin motif to expand on the LA-Biotin technology or developed and used to functionalise phosphorothioates for photocaging and release of nucleic acids. As the coumarin photocage employed in this work can also be activated through two-photon absorption at 900 nm,[251] release with near-IR light of the already produced DNA reported herein would be possible and could be investigated, allowing for photoactivation in the near-IR.

As an alternative, a different bulk-providing group could be employed that carries alternative functionality. Upconverting nanoparticles,[409] nanoscale particles capable of absorbing two or more low energy photons, followed by emission of a higher energy photon, could be used to provide steric bulk and additional functionality. Through development of photocaging groups that consist of a reactive site for the DNA, a UV

or blue photocage as well as a ligand for the upconversion nanoparticle, it should be possible to effectively cage the DNA through the bulk provided by the nanoparticle, but can be released with higher wavelength light than is usually used for the photocage employed.[410]

Another area for future investigation is the attachment chemistry of the LA-Biotin photocages. Through development of orthogonal attachment chemistry of the photocages, the option to employ multiple photocages on one oligonucleotide through orthogonal chemical approaches would allow for multifunctional DNA architectures. Chemistry in this area that could be developed are 'click'-chemistry methods, such as the copper-catalysed alkyne-azide cycloaddition or the strain-promoted alkyne-azide cycloaddition, which are already commonly used with DNA.[411] These can easily be implemented onto DNA through commercial DBCO-, alkyne-, and azide-functionalised phosphoramidites available. Furthermore, they can also be incorporated enzymatically, as triphosphates with these modifications on the nucleobases are commercially available.

Applying the LA-Biotin technology to other nucleic acids is also an important future avenue. It was demonstrated here that linear DNA templates and ASOs can be controlled using the biotinylated photocages. It would be highly desirable to incorporate these technologies on other nucleic acids, with work being underway in the group implementing this in plasmids as well as siRNA. Plasmids are highly desirable, as they provide *in vivo* stability, whereas siRNA will allow for light-controlled RNAi. One future nucleic acid to be explored would be mRNA, through caging at various positions, such as the poly-A tail, 5'-cap or 2'-OH, or through enzymatic incorporation of modified nucleobases, such as commercial aminoallyl-UTP, and seeing the effect on caging and release efficiencies of these systems.

Similarly, the phosphorothioate caging approach should be applicable to other nucleic acids. Phophorothioates could also be incorporated during solid-phase synthesis into a DNA promoter sequence, similar to the incorporation of amino-C6-dT, allowing for the preparation of photocaged linear DNA templates. Phosphorothioates can also be incorporated enzymatically into longer DNA and RNA using nucleoside 5'-α-thiotriphosphates,[98] and then modified, and the caging density could be modulated

through varying the ratio of the triphosphates and thiotriphosphates during synthesis. In particular for RNA, it has been demonstrated that the enzymatic implementation of phosphorothioates into mRNA enhances expression through the increase in mRNA stability.[412]

It would also be highly advantageous to expand the light-activatable biotin system beyond T7 promoters. Commonly used promoters in chemical and molecular biology, such as the phage promoter SP6,[413] or the bacterial lac,[414] trp[415] and the synthetic tac[416] promoters would be starting points for further control, enabling different polymerases to be utilised for expression. Eukaryotic promoters would be also be useful as they would allow controllable gene expression inside cultured cells, with promoters such as CMV[286] or EF-1α,[417] for example, being desirable targets. Due to the increase in complexity (and length) of eukaryotic promoters, however, they likely require a larger screening effort to find suitable modification sites that allow for tight caging and effective release, without disturbing the transcriptional machinery too much and reducing yield.

As has already been alluded to in Chapter 4, the streptavidin employed could also be modified to provide additional functionality. The modification with cellular delivery agents, either through fusion protein expression[373,374] or bioconjugation approaches,[375] would allow for the preparation of cell-deliverable, light-activatable oligonucleotides, reducing the need for transfection agents in cell culture, but also paving the way for their use in a more clinical setting.

Developing DNA controllable by alternative stimuli such as pH,[262] redox potential,[263–265] temperature,[266] and magnetism[418–422] would also allow for an expanded repertoire of applications. One highly interesting stimulus/trigger is hypoxia. Hypoxia, insufficient oxygen, is a key factor in many diseases such as arthritis, cancer or cardiovascular disease.[423] The biological response to hypoxia is the increased production of reducing enzymes. These strongly reducing cellular conditions can be used to trigger chemical reactions and have been used to develop hypoxia-sensitive prodrugs and sensing systems.[424] Following on from this, the activation of DNA under strongly hypoxic conditions using hypoxia-sensitive caging groups would allow for the self-activation of

DNA in disease-affected tissues, such as in cancerous tumours. This would severely reduce side effects arising from off-target activity and they would also not require remote activation. A chemical system suitable for this would be quinone-based hypoxia-cages, which are highly redox-active and have been shown to release various cargo, such as DNA crosslinkers,[425] 5-fluorodeoxyuridine[426] or fluorescent dyes[424] under hypoxic conditions.

One future application of the phosphorothioate photocaging procedure is the modification of stereopure phosphorothioate drugs. One of the downsides of current PS oligonucleotides is that their synthetic incorporation during solid-phase synthesis generates both enantiomeric forms of the PS linkage, resulting in a large number of possible diastereomeric oligonucleotides. Whereas in small-molecule pharmaceuticals stereopure compounds are the norm, phosphorothioated oligonucleotide therapeutics still contain 2^n diastereomers (with n being the number of PS linkages), as it is not yet feasible to separate the diastereomers or synthesise stereodefined PS-oligonucleotides on scale. This leads to currently FDA-approved oligonucleotide therapeutics like Mipomersen to be administered as a mixture of over 500000 diastereomers.[427] There has been increasing evidence that certain diastereomers perform better in clinical settings[428,429] and thus efforts have been made to generate enantioenriched and -pure phosphorothioates synthetically. Recent approaches[428] showed high coupling yields and stereoselectivity. Notable is an method by Baran and coworkers,[430] who recently generated a limonene-derived chiral auxillary building block based on P(V), which is economic in terms of starting materials for both enantiomers, scalable and redox-economic, and allowed for the stereospecific generation of mixed backbone oligonucleotides.[431] As the devised photocaging approach herein did not discriminate between the diastereomers, as observed in the photocleavage experiment, this method of photocaging should still be valid for a time when stereopure synthesis of PS ONs on scale will become widely accessible.

Lastly, these phosphorothioate-caged oligonucleotides would be highly applicable to cellular work. Due to the reduced charge and higher hydrophobicity, cellular uptake of these oligonucleotides should be enhanced compared to native oligonucleotides. Due to time constraints, this could unfortunately not be tested as part of this work presented here. Their use in cell culture would add to the portfolio of *in vitro* gene control

techniques, allowing for controllable gene knockdown in cell culture and future developments of light-controllable oligonucleotide therapeutics.

In all cases, the developed oligonucleotides will benefit from application in future cell-free biology applications, where tight control of gene expression, particularly using a remote stimulus such as light, is required to control their specific function, without the need for the implementation of more complex gene regulatory mechanisms. The implementation of multiple light-switches in such applications will allow for the precise study of biological phenomena, particularly in synthetic cells. In developing synthetic cellular communication, for example, one can envisage the orthogonal activation of two different enzymatic pathways through use of the developed LA-DNA templates in a sender cell, releasing orthogonal signals to surrounding receiver cells.

In summary, the technologies here present a proof-of-concept study to show multiple wavelength control of different oligonucleotides using several caging methods. The potential for further development in the area and the applicability of the developed systems to cell-free and potentially cellular biology is high and paves the way for futures studies of biological function and pathways and potential controllable therapeutics.

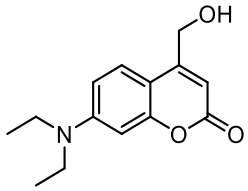
7 MATERIALS AND METHODS

7.1 Synthesis

7.1.1 General Synthesis

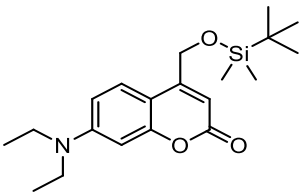
Reagents were purchased from commercial sources (Merck, Acros Organics, Fluorochem and Alfa Aesar) and used without further purification. Solvents were used as supplied (analytical/HPLC-grade from Fisher or Merck) or if dry solvents were required, taken from a solvent drying system (MBraun MB-SPS-5-Bench Top) under nitrogen atmosphere (H_2O content < 20 ppm as determined by Karl Fischer titration). Petroleum ether (PE) over a boiling point range of 40–60 °C was used. Eluent mixtures are reported in volume:volume or %vol. Column chromatography was carried out using Merck Geduran Silica Gel 60 or VWR Silica Gel 40-63 µm under N_2 pressure. Small molecule size exclusion chromatography (SEC) was carried out using Bio-Beads S-X3, 200–400 mesh (BioRad). TLC was carried out on Merck silica gel 60 F254 Al plates. NMR spectroscopy measurements were recorded using a Bruker AVII400, AVII500 or AVIII600 instrument and peaks were referenced to the residual solvent peak. Mass Spectrometry (MS) measurements were carried out on Agilent single quadrupole or Waters LTC (TOF) Mass Spectrometers**.** Liquid Chromatography Mass Spectrometry (LCMS) was performed on a Waters LTC (TOF) MS equipped with a Waters Acquity UPLC. High Performance Liquid Chromatography (HPLC) was carried out on an Agilent Technologies 1260 Infinity Machine equipped with an Agilent Polaris Amide-C18 column or a Supelco Discovery® BIO Wide Pore C18 column. Infrared spectra were recorded on a Bruker Tensor 27 FT-IR and classified as strong (s), medium (m), weak (w) and broad (b). UV/Visible light absorption measurements were performed on a Carys UVBio 50 Spectrometer in 1.4 mL quartz cuvettes (ThorLabs).

7.1.2 7-(Diethylamino)-4-(hydroxymethyl)-2H-chromen-2-one **1**



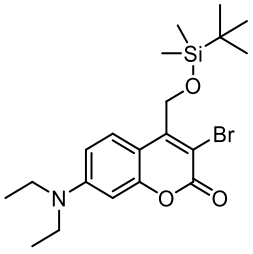
Following a literature procedure:[351] To a solution of 7-(diethylamino)-4-methyl-2H-chromen-2-one (5 g, 21.62 mmol) in DMF (25 mL), *N,N*-dimethylformamide dimethyl acetal (5.74 mL, 43.24 mmol, 2 eq.) was added and the reaction mixture was heated to reflux for 14 hours. Subsequently, conc. $NaHCO_3$ (25 mL) and CH_2Cl_2 (50 mL) are added. The organic layer was separated and the aqueous layer extracted with CH_2Cl_2 (2x 50 mL). The combined organic layers were dried ($MgSO_4$), filtered and the solvent removed *in vacuo*. The resulting residue was dissolved in 1:1 THF/H_2O (65 mL), and $NaIO_4$ (13.86 g, 64.85 mmol, 3 eq.) was added. After stirring for 2 hours at ambient temperature the precipitate was filtered off and washed with EtOAc. The solvent volume was reduced *in vacuo* and saturated $NaHCO_3$ solution (50 mL) was added. The organic layer was separated and the aqueous layer was extracted with CH_2Cl_2 (2x 50 mL). The combined organic layers were dried ($MgSO_4$), filtered and the solvent was removed in vacuo. Subsequently, the residue was dissolved in THF (30 mL), cooled to 0 °C and $NaBH_4$ (1.64 g, 43 mmol, 2 equiv. based on starting coumarin) was added. After stirring for 2 hours at ambient temperature, MeOH was added (5 mL), stirred for 30 minutes and then saturated $NaHCO_3$ solution was added slowly. The organic layer was separated and the aqueous layer was extracted with CH_2Cl_2 (2x 50 mL). The combined organic layers were dried ($MgSO_4$), filtered and the solvent was removed under reduced pressure. Purification by flash column chromatography (SiO_2, EtOAc/$PE_{40\text{-}60}$, 1:1) gave the desired compound as a yellow solid (2.48 g, 10 mmol, 48% over 3 steps). **^{1}H-NMR (400 MHz, $CDCl_3$)** δ/ppm 7.32 (d, J = 9.0 Hz, 1H, C-H_{Ar}), 6.56 (dd, J = 9.0, 2.6 Hz, 1H, C-H_{Ar}), 6.51 (d, J = 2.6 Hz, 1H, C-H_{Ar}), 6.25 (t, J = 1.4 Hz, 1H, C-H), 4.83 (dd, J = 6.2, 1.4 Hz, 2H, CH_2), 3.41 (q, J = 7.1 Hz, 4H, CH_2), 1.97 (t, J = 6.2 Hz, 1H, O-H), 1.20 (t, J = 7.1 Hz, 6H CH_3). **MS (ESI^+)** found 270.0 $[M+H]^+$. Data were in accordance with literature values.[351]

7.1.3 4-(((*tert*-Butyldimethylsilyl)oxy)methyl)-7-(diethylamino)-2H-chromen-2-one **2**



Following a literature procedure:[251] To a 250 mL round-bottom flask equipped with a stirrer bar, coumarin-alcohol **1** (2 g, 8.0 mmol) and *tert*-butyl-dimethylsilyl chloride (1.46 g, 9.6 mmol) were added and dissolved in CH_2Cl_2 (100 mL). To this, 4-dimethylaminopyridine (328 mg, 2.44 mmol) and NEt_3 (0.84 mL, 12 mmol) were added and the reaction stirred for 3 hours. The reaction was quenched by addition of sat. $NaHCO_3$ (50 mL). The aqueous layer was extracted with EtOAc (2x 25 mL), the organic layers combined, dried ($MgSO_4$), filtered and reduced *in vacuo*. The crude residue was then purified by flash column chromatography (SiO_2, 9:1-3:1 Hexane:EtOAc) to yield a pale yellow solid as the desired compound (2.635 g, 7.43 mmol, 98%). **^{1}H-NMR (400 MHz, $CDCl_3$)** δ/ppm 7.24 (s, 1H, C-H_{Ar}), 6.54 (dd, *J* = 8.9, 2.6 Hz, 1H, C-H_{Ar}), 6.51 (d, *J* = 2.6 Hz, 1H, C-H_{Ar}), 6.28 (t, *J* = 1.5 Hz, 1H, C-H), 4.81 (d, *J* = 1.5 Hz, 2H, CH_2), 3.41 (q, *J* = 7.1 Hz, 4H, CH_2), 1.20 (t, *J* = 7.1 Hz, 6H, CH_3), 0.96 (s, 9H, CH_3), 0.14 (s, 6H, CH_3). **MS (ESI^+)** found 362.2 $[M+H]^+$. Data were in accordance with literature values.[251]

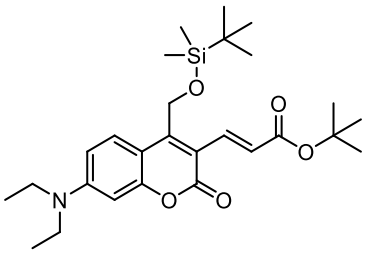
7.1.4 3-Bromo-4-(((*tert*-butyldimethylsilyl)oxy)methyl)-7-(diethylamino)-2H-chromen-2-one **3**



Following a literature procedure:[251] TBDMS-Coumarin **2** (1 g, 2.77 mmol) and *N*-bromosuccinimide (0.55 g, 3.04 mmol) were added to a 50 mL round-bottom flask equipped with a stirrer bar and dissolved in MeCN (9 mL). To this, NH_4OAc (21 mg, 0.27 mmol) was added and the reaction stirred for 1 hour, during which time the reaction turned from yellow to orange. The reaction was then quenched with water (20

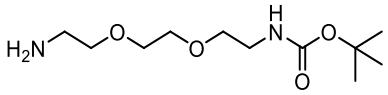
mL), the aqueous layer extracted with EtOAc (2x 20 mL), the organic layers combined, dried ($MgSO_4$), filtered and reduced *in vacuo*. The resulting residue was then subjected to flash column chromatography (SiO_2, 8:1 Hexane:EtOAc) to yield a bright yellow solid as the desired product (1.22 g, 2.77 mmol, 100%). **^{1}H-NMR (400 MHz, $CDCl_3$)** δ/ppm 7.76 (d, *J* = 9.2 Hz, 1H, C-H_{Ar}), 6.61 (dd, *J* = 9.2, 2.6 Hz, 1H, C-H_{Ar}), 6.48 (d, *J* = 2.6 Hz, 1H, C-H_{Ar}), 5.00 (s, 2H, CH_2), 3.42 (q, *J* = 7.1 Hz, 4H, CH_2), 1.21 (t, *J* = 7.1 Hz, 6H, CH_3), 0.90 (s, 9H CH_3), 0.14 (s, 6H, CH_3). **MS (ESI$^+$)** found 440.2 $[M+H]^+$. Data were in accordance with literature values.[251]

7.1.5 *tert*-Butyl-(*E*)-3-(4-(((tert-butyldimethylsilyl)oxy)methyl)-7-(diethylamino)-2-oxo-2H-chromen-3-yl)acrylate **4**



Following a literature procedure:[251] To a solution of bromo-TBDMS-coumarin **3** (2 g, 4.56 mmol) in DMF (44 mL) in a Schlenk flask was added *tert*-butyl acrylate (2.2 mL, 14.96 mmol). To this, LiCl (328 mg, 7.72 mmol), $NaHCO_3$ (1.14 g, 13.6 mmol) and tetrabutylammonium chloride (1.39 g, 5 mmol) were added and the solution degassed through purging with nitrogen for 30 minutes. Then $Pd(OAc)_2$ (52 mg, 0.2 mmol) was added under a gentle stream of nitrogen and the flask sealed under positive pressure. The reaction was then heated to 110 °C for 60 minutes, during which the reaction turned dark orange first, and then blackish green. The reaction was then cooled to room temperature, quenched with water (40 mL), the aqueous layer extracted with EtOAc (3x 30 mL), the organic layers combined, washed with brine (30 mL), dried ($MgSO_4$), filtered and reduced *in vacuo*. The crude mixture was then purified by flash column chromatography (SiO_2, 9:1 PE:EtOAc) to yield the desired compound as an orange-yellow solid (1.9 g, 3.9 mmol, 85%). **^{1}H-NMR (400 MHz, $CDCl_3$)** δ/ppm 7.75 (d, *J* = 15.7 Hz, 1H, C-H), 7.66 (d, *J* = 9.2 Hz, 1H, C-H_{Ar}), 6.99 (d, *J* = 15.6 Hz, 1H, C-H), 6.62 (dd, *J* = 9.2, 2.7 Hz, 1H, C-H_{Ar}), 6.48 (d, *J* = 2.6 Hz, 1H, C-H_{Ar}), 4.91 (s, 2H, CH_2), 3.43 (q, *J* = 7.1 Hz, 4H, CH_2), 1.52 (s, 9H, CH_3), 1.22 (t, *J* = 7.1 Hz, 6H, CH_3), 0.90 (s, 9H, CH_3), 0.15 (s, 6H, CH_3). **MS (ESI$^+$)** found 510.0 $[M+Na]^+$. Data were in accordance with literature values.[251]

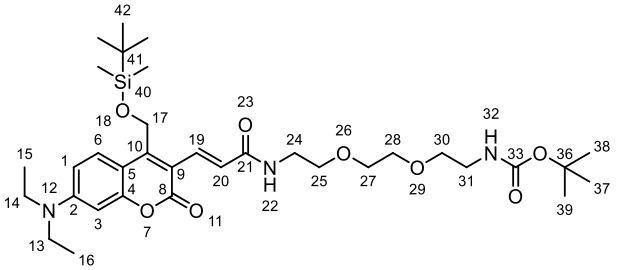
7.1.6 *tert*-Butyl (2-(2-(2-aminoethoxy)ethoxy)ethyl)carbamate **5**



To a solution of 2,2′-(ethylenedioxy)diethylamine (2.7 mL, 10 eq.) in CH_2Cl_2 (174 mL) at 0 °C was added di-*tert*-butyl dicarbonate (567 mg, 2.60 mmol, 0.15 eq.) and the reaction stirred for 3 hours, then allowed to warm to room temperature and left stirring overnight, during which time the reaction became turbid. The organic layer was washed with a dilute solution of NaCl (5x 100 mL), dried ($MgSO_4$), filtered and the solvent reduced in vacuo to yield a clear, colourless oil as the desired compound (484 mg, 1.95 mmol, 75%). **^{1}H-NMR (400 MHz, $CDCl_3$)** δ/ppm 5.11 (bs, 2H, amine N-H), 5.02 (bs, 1H, amide N-H), 3.61 (s, 4H, CH_2), 3.53 (dt, J = 12.6, 5.2 Hz, 4H, CH_2), 3.31 (q, J = 5.3 Hz, 2H, CH_2), 2.88 (t, J = 5.2 Hz, 2H, CH_2), 1.44 (s, 9H, CH_3). **MS (ESI$^+$)** 371.2 $[M+Na]^+$. Data were in accordance with literature values.[432]

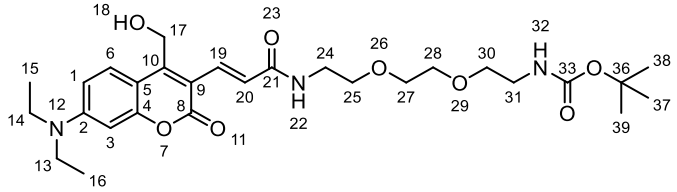
7.1.7 *tert*-Butyl-(*E*)-(2-(2-(2-(3-(4-(((*tert*-butyldimethylsilyl)oxy)methyl)-7-(diethylamino)-2-oxo-2H-chromen-3-yl)acrylamido)ethoxy)ethoxy)ethyl)carbamate **6a**

Coumarin **4** (146.8 mg, 0.301 mmol) was dissolved in 6 mL 1:1 CH_2Cl_2:TFA and left stirring for 30 minutes, until TLC showed full consumption of starting material. The solvent was then removed *in vacuo*, the resulting residue resuspended in CH_2Cl_2 and the solvent removed *in vacuo* again to remove residual TFA. This process was repeated two times. The resulting orange solid was then resuspended in dry MeCN (10 mL). To this was added *N*-Boc-diamine **5** (187 mg, 0.753 mmol, 2.5 eq.) and EDC·HCl (144 mg, 0.753 mmol, 2.5 eq.) and the reaction left stirring overnight. The solvent was then removed *in vacuo* and the crude reaction mixture was purified using flash column chromatography (3:1 EtOAc:PE – 1:0 EtOAc:PE – 1:0 CH_2Cl_2 – 5% MeOH in CH_2Cl_2) to yield TBDMS-protected compound **5a** (104.3 mg, 158 mmol, 52%) as well as deprotected compound **5b** (72.9 mg, 0.133 mmol, 44%) as yellow solids with a combined total yield of 96%.



R_f (SiO_2, 3:1 EtOAc:PE) 0.30. **MS (ESI$^+$)** found 662.3 $[M+H]^+$. **^{1}H-NMR (600 MHz, $CDCl_3$)** δ/ppm 7.84 (d, *J* = 15.1 Hz, 1H, 19, C-H), 7.70 (d, *J* = 9.2 Hz, 1H, 6, CH_{Ar}), 7.24 (d, *J* = 15.1 Hz, 1H, 20, C-H), 6.62 (dd, *J* = 9.2, 2.6 Hz, 1H, 1, CH_{Ar}), 6.47 (d, *J* = 2.6 Hz, 1H, 3, CH_{Ar}), 6.23 (s, 1H, 22, N-H), 5.08 (s, 1H, 32, N-H), 4.96 (s, 2H, 17, CH_2), 3.63 (s, 4H, 27, 28, CH_2), 3.63 – 3.52 (m, 2H, 25, CH_2), 3.43 (q, *J* = 7.1 Hz, 4H, 13, 14, CH_2), 3.35 (s, 2H, 31, CH_2), 1.43 (s, 9H, 44, 45, 46, CH_3), 1.22 (t, *J* = 7.1 Hz, 6H, 15, 16, CH_3), 0.90 (s, 9H, 40, 41, 42, CH_3), 0.17 (s, CH_3, 38, 39, 6H). **^{13}C-NMR (151 MHz, $CDCl_3$)** δ/ppm 166.78 (21), 161.03 (8), 156.22 (33), 155.87 (4), 151.75 (10), 151.11 (2), 132.10 (19), 127.82 (6), 124.97 (20), 113.29 (9), 109.32 (1), 108.62 (5), 97.16 (3), 79.35 (43), 70.54 and 70.43 and 70.30 and 70.16 (4C, 25, 27, 28, 30), 57.73 (17), 44.98 (13, 14), 40.44 (31), 39.62 (24), 28.57 (3C, 44, 45, 46), 25.97 (3C, 40, 41, 42), 18.39 (37), 12.67 (2C, 15, 16), -4.97 (2C, 38, 39). **HRMS (ESI$^+$)** found 662.3831 (theoretical m/z = 662.3831 $[C_{34}H_{56}O_8N_3Si]^+$). **IR** (film, $CDCl_3$/cm^{-1}) 3328 (wb, N-H), 2927 (m), 1711 (s, C=O), 1602 (s, C=O), 1510 (s), 1359 (m), 1091 (m).

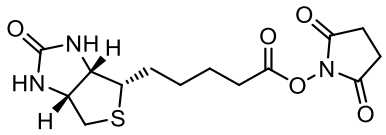
7.1.8 *tert*-Butyl-(*E*)-(2-(2-(2-(3-(7-(diethylamino)-4-(hydroxymethyl)-2-oxo-2H-chromen-3-yl)acrylamido)ethoxy)ethoxy)ethyl)carbamate **6b**



R_f (SiO_2, 5% MeOH/CH_2Cl_2) 0.36. **^{1}H-NMR (500 MHz, $CDCl_3$)** δ/ppm 7.82 (d, *J* = 15.2 Hz, 1H, 19, C-H), 7.73 (d, *J* = 9.2 Hz, 1H, 6, C-H_{Ar}), 7.20 (d, *J* = 15.2 Hz, 1H, 20, C-H), 6.61 (dd, *J* = 9.2, 2.7 Hz, 1H, 1, C-H_{Ar}), 6.52 (s, 1H, 32, N-H), 6.44 (d, *J* = 2.6 Hz, 1H, 3, C-H_{Ar}), 5.16 (s, 1H, 22, N-H), 4.94 (s, 1H, 17, CH_2), 4.21 (s, 1H, 18, O-H), 3.61 (s, 4H, 27, 28, CH_2), 3.61 – 3.49 (m, 4H, 25, 30, CH_2), 3.52 (q, *J* = 5.2 Hz, 2H, 31, CH_2), 3.41 (q, *J* = 7.1 Hz, 4H, 13, 14, CH_2), 3.32 (q, *J* = 6.1, 5.5 Hz, 2H, 24, CH_2), 1.41 (s, 9H, 37, 38, 39, CH_3), 1.20 (t, *J* = 7.1 Hz, 6H, 15, 16, CH_3). **^{13}C-NMR (126 MHz, $CDCl_3$)** δ/ppm 167.35 (21), 161.01 (8), 156.27 (33), 155.91 (4), 152.01 (10), 151.17

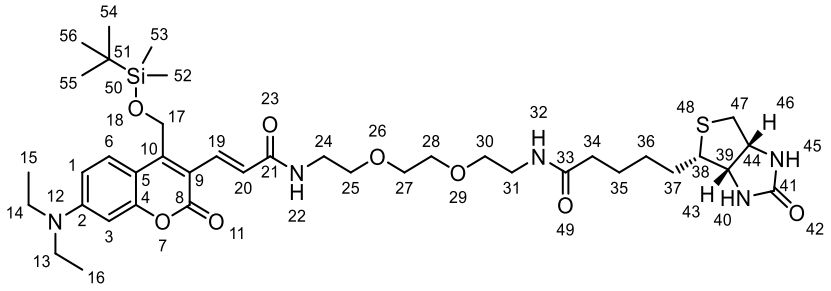
(2), 132.35 (19), 127.64 (6), 124.61 (20), 113.31 (9), 109.54 (1), 108.50 (5), 97.15 (3), 79.38 (36), 70.44 and 70.35 and 70.23 and 69.92 (4C, 25, 27, 28, 30), 56.53 (17), 44.98 (13, 14), 40.40 (24), 39.68 (31), 28.53 (3C, 37, 38, 39), 12.63 (2C, 15, 16). **MS (ESI$^+$)** found 570.2 $[M+Na]^+$. **HRMS (ESI$^+$)** found 570.2786 (theoretical m/z = 570.2786 $[C_{21}H_{41}O_8N_3{}^{23}Na]^+$). **IR** (film, $CDCl_3$/cm^{-1}) 3305 (wb, O-H), 2972 (w C-H_{Ar}), 2928 (w, C-H_{Ar}), 1704 (s, C=O), 1618 (s, C=O), 1596 (s), 1566 (s) 1514 (m).

7.1.9 Biotin-*N*-hydroxysuccinimide ester **7**



Biotin (500 mg, 2.05 mmol) and *N*-hydroxysuccinimide (240 mg, 2.08 mmol) were placed into a 100 mL round bottom flask and dissolved in hot, dry DMF. To this was added dicyclohexylcarbodiimide (550 mg, 2.67 mmol) and the reaction left stirring overnight. The reaction was quenched by pouring into 100 mL of Et_2O, and a white precipitate formed. The precipitate was then filtered off and washed with Et_2O and dried to yield a white powder as the desired compound (710 mg, 2.08 mmol, >100%) with minor impurities of dicyclohexylurea. The compound was used without further purification. **^{1}H-NMR (400 MHz, DMSO-d6)** δ/ppm 6.42 (t, *J* = 1.8 Hz, 1H), 6.36 (s, 1H), 4.38 – 4.24 (m, 1H), 4.15 (ddd, *J* = 7.7, 4.4, 1.8 Hz, 1H), 3.10 (ddd, *J* = 8.1, 6.4, 4.4 Hz, 1H), 2.85 (dd, *J* = 19.3, 14.2 Hz, 1H, SCH_2), 2.81 (s, 4H, NHS-CH_2), 2.71 – 2.63 (m, 2H), 2.58 (d, *J* = 12.4 Hz, 1H), 1.78 – 1.33 (m, 6H). **MS (ESI$^+$)** found 705.2 $[2M+Na]^+$. Data were in accordance with literature values.[433]

7.1.10 *N*-(2-(2-(2-((*E*)-3-(4-(((*tert*-Butyldimethylsilyl)oxy)methyl)-7-(diethylamino)-2-oxo-2H-chromen-3-yl)acrylamido)ethoxy)ethoxy)ethyl)-5-((3aS,4S,6aR)-2-oxohexahydro-1H-thieno[3,4-d]imidazol-4-yl)pentanamide **8**

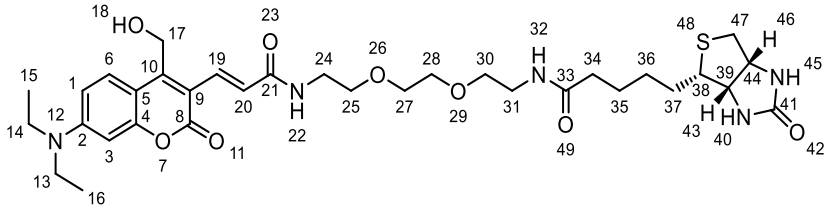


To a solution of TBDMS-protected coumarin **6a** (104 mg, 0.157 mmol) in 2 mL CH_2Cl_2 was added 2 mL of TFA and the reaction mixture stirred for 1 hour at room temperature. The solvent was removed *in vacuo* and the residue redissolved in CH_2Cl_2 and the solvent removed again two times to remove residual TFA. The resulting residue was then dissolved in 2 mL of dry DMF, to which was added dry triethylamine (65 µL, 0.471 mmol, 3 eq.) and then Biotin-NHS **7** was added (75 mg, 1.5 eq.) and the reaction left stirring for 4 hours. The solvent was removed *in vacuo* and the compound was purified using flash chromatography (SiO_2, 10% MeOH/$CHCl_3$) to give compound **8** as a yellow solid (35.3 mg, 0.045 mmol, 29%) as well as compound **9** as a yellow solid (75 mg, 0.111 mmol, 71%).

R_f (SiO_2, 10% MeOH/CH_2Cl_2) 0.48. **^{1}H-NMR (500 MHz, $CDCl_3$)** δ/ppm 7.81 (d, *J* = 15.1 Hz, 1H, 19, C-H), 7.69 (d, *J* = 9.2 Hz, 1H, 6, CH_{Ar}), 7.25 (d, *J* = 14.6 Hz, 2H, 20, C-H, partially covered by $CDCl_3$), 6.91 (t, *J* = 5.4 Hz, 2H, 22, 32, N-H), 6.62 (dd, *J* = 9.2, 2.6 Hz, 1H, 1, CH_{Ar}), 6.45 (d, *J* = 2.7 Hz, 2H, 3, 40, CH_{Ar} and N-H), 5.59 (s, 1H, 45, N-H), 4.94 (s, 2H, 17, CH_2), 4.49 (ddd, *J* = 12.6, 7.7, 4.8 Hz, 1H, 46, C-H), 4.31 (td, *J* = 7.9, 4.3 Hz, 1H, 43, C-H), 3.65 – 3.38 (m, 10H, 24, 25, 27, 28, 30, 31, CH_2), 3.42 (q, *J* = 6.9 Hz, 6H, 13, 14, CH_2), 3.12 (qd, *J* = 7.0, 3.5 Hz, 1H, 38, C-H), 2.87 (dd, *J* = 12.5, 5.0 Hz, 1H, 47, CH_2), 2.72 (d, *J* = 12.4 Hz, 1H, 47, CH_2), 2.22 (t, *J* = 7.4 Hz, 2H, 34, CH_2), 1.87 – 1.56 (m, 4H, 35, 37, CH_2), 1.46 – 1.36 (m, 2H, 36, CH_2), 1.21 (t, *J* = 7.1 Hz, 6H, 15, 16, CH_3), 0.88 (s, 9H, 54, 55, 56, CH_3), 0.15 (s, 6H, 52, 53, CH_3). **^{13}C-NMR (126 MHz, $CDCl_3$)** δ/ppm 173.71 (33), 166.95 (21), 164.11 (41), 161.12 (8), 155.78 (4), 151.88 (10), 151.11 (2), 131.80 (19), 127.82 (6), 125.13 (20), 113.11 (9), 109.39 (1), 108.54 (5), 97.01 (3), 70.29 and 70.17 and 70.10 and 70.05 (4C, 25, 27, 28, 30), 61.89 (39), 60.34 (44), 57.69 (17), 55.68 (38), 44.95 (2C, 13, 14), 40.60 (47), 39.60 (24 or 31) 39.18 (24 or 31) 35.97 (34), 28.15 (36), 25.94 (3C, 54, 55, 56), 25.71 (2C,

35, 37), 18.36 (51), 12.64 (2C, 15, 16), -5.01 (2C, 52, 53). **MS (ESI$^+$)** found 788.3 $[M+H]^+$. **HRMS (ESI$^+$)** found 788.4077 (theoretical m/z = 788.4083 $[C_{39}H_{62}N_5O_8SSi]^+$). **IR** (film, $CDCl_3$) 3291 (wb, N-H), 2926 (m, C-H), 1700 (s, C=O), 1601 (s), 1510 (m), 1083 (m)

7.1.11 *N*-(2-(2-(2-((*E*)-3-(7-(Diethylamino)-4-(hydroxymethyl)-2-oxo-2H-chromen-3-yl)acrylamido)ethoxy)ethoxy)ethyl)-5-((3aS,4S,6aR)-2-oxohexahydro-1H-thieno[3,4-d]imidazol-4-yl)pentanamide **9**



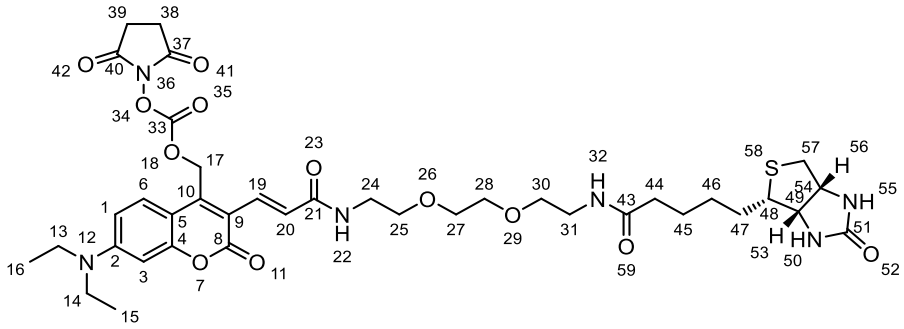
To a solution of OH-coumarin **6b** (40 mg, 0.073 mmol) in CH_2Cl_2 (2 mL) was added TFA (2 mL) and the reaction left stirring for 30 minutes, until TLC indicated full deprotection. The solvent was subsequently removed *in vacuo*, the residue resuspended in CH_2Cl_2 and the solvent removed *in vacuo* again. The residue was then dissolved in DMF (3 mL). To this was added Biotin-NHS Ester **7** (37.5 mg, 0.110 mmol) and NEt_3 (60 µL). The reaction was left stirring for 3 hours. The solvent was removed *in vacuo* and the resulting crude mixture purified using flash column chromatography (SiO_2, 5-10% MeOH/CH_2Cl_2) and further purified using flash chromatography (SiO_2, 10% MeOH/$CHCl_3$) to yield a bright yellow solid as the desired compound (46.3 mg, 0.069 mmol, 69% over 2 steps).

Alternatively, to a solution of Coumarin **8** (219 mg, 0.278 mmol) in THF (3 mL) was added a solution of TBAF in THF (1M, 1.6 mL, 6 eq.) and left stirring for 45 minutes. The solvent was subsequently removed, and the resulting residue purified using flash column chromatography (10% MeOH/$CHCl_3$) to yield **9** as a bright yellow solid (169 mg, 250 mmol, 90%).

R_f (SiO_2, 10% MeOH/CH_2Cl_2) 0.29. **^{1}H-NMR (500 MHz, DMSO-d6)** δ/ppm 8.27 (t, *J* = 5.7 Hz, 1H, 22, N-H), 7.83 (t, *J* = 5.7 Hz, 1H, 32, N-H), 7.76 (d, *J* = 9.3 Hz, 1H, 6, CH_{Ar}), 7.65 (d, *J* = 15.4 Hz, 1H, 19, C-H), 7.13 (d, *J* = 15.4 Hz, 1H, 20, C-H), 6.77 (dd, *J* = 9.3, 2.6 Hz, 1H, 1, CH_{Ar}), 6.53 (d, *J* = 2.5 Hz, 1H, 3, CH_{Ar}), 6.41 (bt, *J* = 1.9 Hz, 1H, 40, N-H), 6.35 (bs, 1H, 45, N-H), 5.57 (t, *J* = 5.5 Hz, 1H, 18, O-H), 4.72 (d, *J* = 4.6 Hz, 2H, 17, CH_2), 4.29 (dd, *J* = 7.7, 5.1 Hz, 1H, 46, C-H), 4.14 – 4.08 (m, 1H, 43, C-

H), 3.55 – 3.49 (m, 4H, 27, 28, CH_2), 3.46 (skewed q, *J* = 6.8 Hz, 6H, 13, 14, 25, CH_2), 3.40 (t, *J* = 5.9 Hz, 2H, 30, CH_2), 3.33 – 3.28 (m, 2H, 24, CH_2 partially hidden in H_2O peak), 3.18 (q, *J* = 5.8 Hz, 2H, 31, CH_2), 3.08 (ddd, *J* = 8.6, 6.2, 4.4 fHz, 1H, 38, C-H), 2.80 (dd, *J* = 12.5, 5.1 Hz, 1H, 47', CH_2), 2.57 (d, *J* = 12.4 Hz, 1H, 47'', CH_2), 2.06 (t, *J* = 7.4 Hz, 2H, 34, CH_2), 1.66 – 1.24 (m, 6H, 35, 36, 37, CH_2 Biotin), 1.13 (t, *J* = 7.0 Hz, 6H, 15, 16, CH_3). **^{13}C-NMR (126 MHz, DMSO-d6)** δ/ppm 172.14 (33), 165.88 (21), 162.70 (41), 159.89 (8), 155.23 (4), 152.41 (10), 150.74 (2), 131.09 (19), 127.96 (6), 125.15 (20), 112.37 (9), 109.38 (1), 107.60 (5), 96.24 (3), 69.56 and 69.53 (2C, 27, 28), 69.18 (25), 69.09 (30), 61.03 (39), 59.18 (44), 55.43 (17), 55.24 (38), 44.10 (13, 14), 39.69 (47), 38.82 (24), 38.44 (31), 35.10 (34), 28.19 (36), 28.04 (37), 25.27 (35), 12.40 (2C, 15, 16). **MS (ESI$^+$)** found 696.2 $[M+Na]^+$. **HRMS (ESI$^+$)** found 696.3036 (theoretical m/z = 696.3038 $[C_{33}H_{47}O_8N_5{}^{23}NaS]^+$). **IR** (neat/$cm^{-1}$) 3284 (sb, O-H), 2924 (w, C-H_{Ar}), 1704 (s, C=O), 1645 (C=O Biotin) 1620 (s, C=O), 1597 (s), 1551 (m), 1515 (m)

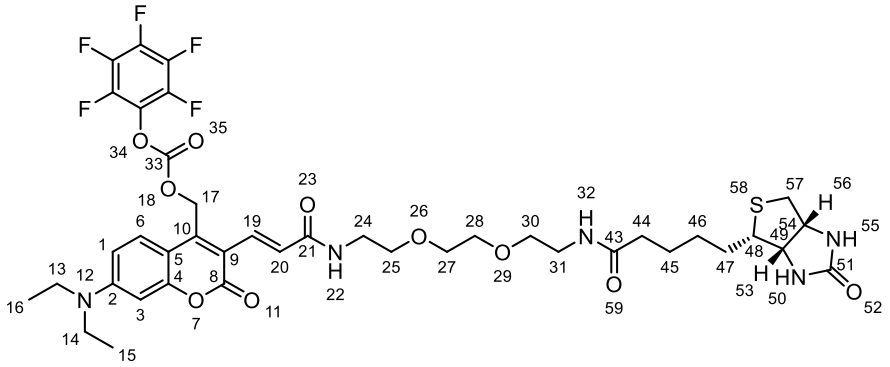
7.1.12 (7-(Diethylamino)-3-((*E*)-3,14-dioxo-18-((3aS,4S,6aR)-2-oxohexahydro-1H-thieno[3,4-d]imidazol-4-yl)-7,10-dioxa-4,13-diazaoctadec-1-en-1-yl)-2-oxo-2H-chromen-4-yl)methyl (2,5-dioxopyrrolidin-1-yl) carbonate **10a**



To a solution of coumarin **9** (24 mg, 0.036 mmol) in dry DMSO (0.7 mL) was added *N,N*-disuccinimidyl carbonate (28 mg, 0.108 mmol) and NEt_3 (15 µL, 0.108 mmol) and the reaction left stirring for 2 hours, during which the reaction turned dark orange. The crude solution in DMSO was lyophilised to remove the solvent and the residue was purified by flash column chromatography (SiO_2, 6:1 $CHCl_3$:MeOH), the fractions containing the molecule combined, dried, resuspended in CH_2Cl_2 and further purified using size exclusion chromatography (BioBeads SX-3, CH_2Cl_2) to yield the desired compound as a dark orange solid (20 mg, 0.026 mmol, 72%). **R_f** (SiO_2, 6:1 $CHCl_3$:MeOH) 0.41. **R_f** (SiO_2, 10%MeOH/CH_2Cl_2) 0.56. **^{1}H-NMR (500 MHz, $CDCl_3$)**

δ/ppm 8.01 (d, *J* = 9.2 Hz, 1H, 6, C-H_{Ar}), 7.76 (d, *J* = 15.6 Hz, 1H, 19, C-H), 7.21 (d, *J* = 15.6 Hz, 1H, 20, C-H), 7.01 (t, *J* = 5.6 Hz, 1H, 22, N-H), 6.82 (t, *J* = 5.7 Hz, 1H, 32, N-H), 6.70 (dd, *J* = 9.2, 2.6 Hz, 1H, 1, C-H_{Ar}), 6.45 (d, *J* = 2.6 Hz, 1H, 3, C-H_{Ar}), 6.35 (s, 1H, 55, N-H), 5.50 (s, 1H, 50, N-H), 5.30 (s, 2H, 17', CH_2), 4.47 (dd, *J* = 7.8, 4.9 Hz, 1H, 56, C-H), 4.33 – 4.26 (m, 1H, 53, C-H), 3.69 – 3.61 (m, 6H, 25, 27, 28, CH_2), 3.61 – 3.53 (m, 4H, 24, 30, CH_2), 3.49 (d, *J* = 5.1 Hz, 0H), 3.49 – 3.36 (m, 2H, 31, CH_2), 3.42 (q, *J* = 7.0 Hz, 4H, 13, 14, CH_2), 3.10 (td, *J* = 7.4, 4.6 Hz, 1H, 48, C-H), 2.87 (dd, *J* = 12.8, 5.0 Hz, 1H, 57', CH_2), 2.79 (s, 4H, 38'', 39'', CH_2), 2.70 (d, *J* = 12.8 Hz, 1H, 57'', CH_2), 2.20 (t, *J* = 7.5 Hz, 2H, 44, CH_2), 1.75 – 1.50 (m, 4H, 45, 47, CH_2), 1.40 (h, *J* = 7.5, 6.8 Hz, 2H, 46, CH_2), 1.21 (t, *J* = 7.1 Hz, 6H, 15, 16, CH_3). **^{13}C-NMR (126 MHz, $CDCl_3$)** δ/ppm 173.60 (43), 171.50 (2C, 37, 40), 166.33 (21), 164.06 (51), 160.93 (8), 155.62 (4), 151.29 (2), 142.46 (10), 131.78 (19), 127.59 (6), 127.32 (20), 117.61 (9), 110.00 (1), 108.70 (5), 97.19 (3), 70.58 (17), 70.32 and 70.30 and 70.03 and 69.97 (4C, 25, 27, 28, 30), 61.92 (49), 60.30 (54), 55.69 (48), 45.04 (2C, 13, 14), 40.65 (57), 39.67 (24), 39.22 (31), 36.04 (44), 28.28 (46), 28.16 (47), 25.81 (2C, 38, 39), 25.70 (45), 12.65 (2C, 15, 16). **IR** (film $CDCl_3$/cm^{-1}) 3293.8 (bw), 2951 (w), 2925 (w), 1698 (m), 1655 (m), 1615 (m) 1601 (m), 1569 (m), 1514 (m), 729 (s). **HRMS (ESI$^+$)** found 815.3279 (theoretical m/z = 815.3280 $[C_{38}H_{51}O_{12}N_6S]^+$).

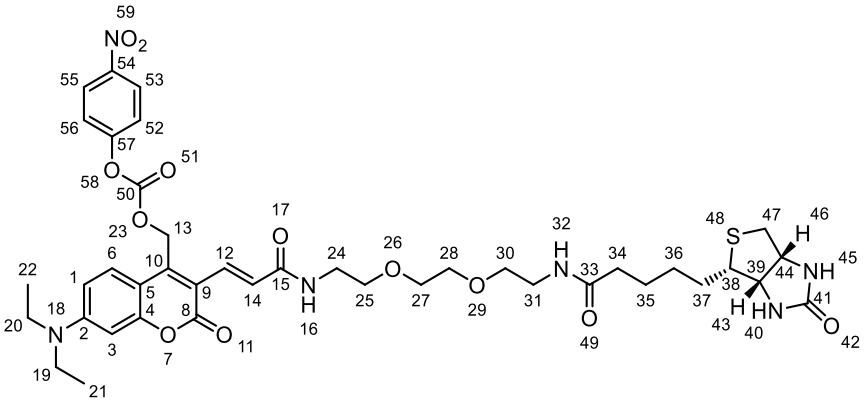
7.1.13 (7-(Diethylamino)-3-((*E*)-3,14-dioxo-18-((3aS,4S,6aR)-2-oxohexahydro-1H-thieno[3,4-d]imidazol-4-yl)-7,10-dioxa-4,13-diazaoctadec-1-en-1-yl)-2-oxo-2H-chromen-4-yl)methyl (perfluorophenyl) carbonate **10b**



To a solution of coumarin **9** (74 mg, 0.111 mmol) in dry DMSO (2 mL) was added Bis(pentafluorophenyl)carbonate (110 mg, 0.278 mmol) and NEt_3 (39 µL, 0.278 mmol) and left stirring for 2 hours protected from light, during which the reaction turned a dark reddish-orange. The crude solution in DMSO was dried under convection to remove

the majority of the solvent and the residue was purified by flash column chromatography (SiO_2, 9:1 CH_2Cl_2:MeOH), the fractions containing the molecule combined, dried, resuspended in CH_2Cl_2 and further purified using size exclusion chromatography (BioBeads SX-3, CH_2Cl_2) to yield the desired compound as a dark orange solid (27 mg, 0.030 mmol, 29%). **R_f** (SiO_2, 10%MeOH/$CHCl_3$) 0.27. **^{1}H-NMR (500 MHz, $CDCl_3$)** δ/ppm 7.80 (d, *J* = 15.1 Hz, 1H, 19), 7.55 (d, *J* = 9.3 Hz, 1H, 6), 7.31 (d, *J* = 15.0 Hz, 1H, 20), 6.91 (t, *J* = 5.4 Hz, 1H, 22), 6.67 (dd, *J* = 9.3, 2.0 Hz, 1H, 3), 6.60 (d, *J* = 5.9 Hz, 1H, 32), 6.50 (d, *J* = 2.5 Hz, 1H, 1), 6.12 (s, 1H, 40), 5.68 (s, 1H, 17), 5.25 (s, 1H, 45), 4.50 (t, *J* = 6.5 Hz, 1H, 46), 4.39 – 4.28 (m, 1H, 43), 3.71 – 3.54 (m, 10H, 24, 25, 27, 28, 30, 31), 3.45 (q, *J* = 7.1 Hz, 6H, 13, 14, 31), 3.13 (td, *J* = 7.4, 4.6 Hz, 1H, 38), 2.89 (dd, *J* = 12.8, 4.9 Hz, 1H, 47'), 2.73 (d, *J* = 12.8 Hz, 1H, 47''), 2.22 (t, *J* = 7.4 Hz, 2H, 34), 1.79 – 1.32 (m, 6H, 35, 36, 37), 1.23 (t, *J* = 7.0 Hz, 6H, 15, 16). **^{13}C-NMR (126 MHz, $CDCl_3$)** δ/ppm 173.49 (33), 166.61 (21), 163.79 (41), 160.42 (8), 155.75 (4), 151.53 (2), 151.15 (50), 144.15 (10), 130.92 (19), 126.64 (6), 126.59 (20), 115.48 (9), 110.01 (3), 107.73 (5), 97.39 (1), 70.33 and 70.21 and 69.99 and 69.95 (4C, 25, 27, 28, 30), 63.14 (17), 61.96 (39), 60.31 (44), 55.55 (38), 45.10 (2C, 13, 14), 40.61 (47), 39.73 (24), 39.18 (31), 36.00 (34), 28.19 (2C, 36, 37), 25.62 (35), 12.64 (2C, 15, 16). Pentafluorophenyl-carbons were not observed due to ^{13}C-^{19}F coupling. **^{19}F-NMR (471 MHz, $CDCl_3$)** δ/ppm -152.26 – -152.95 (m, 2F), -156.96 (t, *J* = 21.8 Hz, 1F), -161.66 (td, *J* = 22.7, 5.0 Hz, 2F). **IR** (film $CDCl_3$/cm^{-1}) 3302 (w), 2927 (w), 1701 (s, C=O), 1620 (s), 1600 (s), 1519 (s). **MS (ESI$^+$)** found 906.3 $[M+Na]^+$. **HRMS (ESI$^+$)** found 884.2949 (theoretical m/z = 884.2958 $[C_{40}H_{47}O_{10}N_5F_5S_1]^+$). **UV/Vis** (0.05% DMF in H_2O) λ_{max}/nm (ε/mM^{-1} cm^{-1}) 280 (7.7), 443 (16.1)

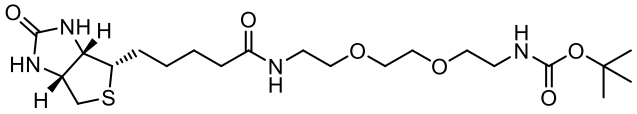
7.1.14 (7-(Diethylamino)-3-((*E*)-3,14-dioxo-18-((3aS,4S,6aR)-2-oxohexahydro-1H-thieno[3,4-d]imidazol-4-yl)-7,10-dioxa-4,13-diazaoctadec-1-en-1-yl)-2-oxo-2H-chromen-4-yl)methyl (4-nitrophenyl) carbonate **10c**



In a 10 mL round-bottom flask covered in foil, coumarin **9** (96.6 mg, 0.143 mmol) and Bis(4-nitrophenyl)carbonate (130 mg, 0.429 mmol) were dissolved in dry DMSO (2.8 mL). To this, NEt_3 (60 µL, 0.429 mmol) was added and left stirring for 2 hours, during which the reaction turned a dark orange. The DMSO was then removed with a strong flow of nitrogen overnight. The resulting residue was purified by flash column chromatography (SiO_2, 5-10% MeOH in $CHCl_3$) to yield a dark yellow solid as the desired product (49.2 mg, 0.059 mmol, 41%). **R_f** (SiO_2, 10%MeOH/$CHCl_3$) 0.37. **^{1}H-NMR (600 MHz, $CDCl_3$)** δ/ppm 8.28 – 8.25 (d, 2H, 55, 57, CH_{Ar}), 7.84 (d, *J* = 15.1 Hz, 1H, 12, C-H), 7.61 (d, *J* = 9.2 Hz, 1H, 6, CH_{Ar}), 7.43 – 7.40 (d, 2H, 54, 58, CH_{Ar}), 7.34 (d, *J* = 15.1 Hz, 1H, 14, C-H), 6.87 (t, *J* = 5.6 Hz, 1H, 16, N-H), 6.67 (dd, *J* = 9.2, 2.6 Hz, 1H, 1, CH_{Ar}), 6.51 (d, *J* = 2.8 Hz, 2H, 3, 32, CH_{Ar} and N-H), 6.02 (s, 1H, 40, N-H), 5.64 (s, 2H, 13, CH_2), 5.06 (s, 1H, 45, N-H), 4.49 (dd, *J* = 7.8, 5.0 Hz, 1H, 46, C-H), 4.32 (dd, *J* = 8.2, 4.8 Hz, 1H, 43, C-H), 3.77 – 3.53 (m, 8H, 25, 27, 28, 30, CH_2), 3.60 (q, *J* = 5.6 Hz, 2H, 24, CH_2), 3.54 – 3.41 (m, 6H, 19, 20, 31, CH_2), 3.14 (td, *J* = 7.3, 4.6 Hz, 1H, 38, C-H), 2.90 (dd, *J* = 12.7, 5.0 Hz, 1H, 47'), 2.72 (d, *J* = 13.2 Hz, 1H, 47'', CH_2), 2.22 (t, *J* = 7.3 Hz, 2H, 34, CH_2), 1.76 – 1.39 (m, 6H, 35, 36, 37, CH_2), 1.23 (t, *J* = 7.1 Hz, 6H, 21, 22, CH_2). **^{13}C-NMR (151 MHz, $CDCl_3$)** 173.39 (33), 166.71 (15), 163.62 (41), 160.48 (8), 155.82 (4), 155.51 (56), 152.30 (50), 151.56 (2), 145.70 (53), 144.81 (10), 131.20 (12), 126.77 (6), 126.45 (14), 125.48 (55, 57), 121.99 (54, 58), 115.42 (9), 109.99 (1), 107.92 (5), 97.43 (3), 70.36 and 70.24 and 69.98 and 96.93 (4C, 25, 27, 28, 30), 62.01 and 61.98 (2C, 13, 39), 60.26 (44), 55.53 (38), 45.12 (19, 20), 40.65 (47), 39.77 (24), 39.18 (31), 36.04 (34), 28.24 (37), 28.21 (36), 25.62 (35), 12.66 (2C, 21, 22). **MS (ESI$^+$)** found 839.3 $[M+H]^+$. **HRMS (ESI$^+$)** found 839.3276

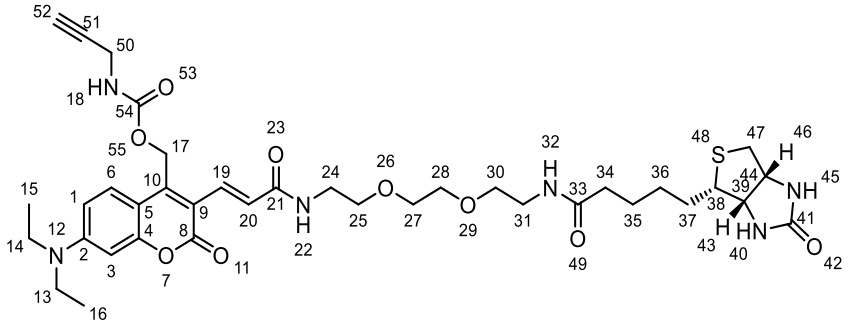
(theoretical m/z = 839.3280 $[C_{40}H_{51}O_{12}N_6S_1]^+$). **IR** (film $CDCl_3$/cm^{-1}) 3293 (wb), 2980 (m, C-H), 2926, 1699 (s, C=O), 1616 (s), 1599 (s), 1523 (m, NO_2), 1350 (m, NO_2), 1313 (m), 1212 (s, C-O), 731 (m, C-H_{Ar}). **UV/Vis** (0.05% DMF in H_2O) λ_{max}/nm (ε/mM^{-1} cm^{-1}) 277 (11.0), 441 (16.0)

7.1.15 *N*-Boc-*N*'-biotinyl-3,6-dioxaoctane-1,8-diamine **11**



Following a literature procedure:[434] To a solution of biotin (440 mg, 1.8 mmol) in dry DMF (33 mL) was added HBTU (600 mg, 1.58 mmol), followed by DIPEA (350 µL, 2.0 mmol). The reaction was stirred for ten minutes until it became clear. Then, the solution was transferred *via* cannula to a round-bottom flask containing 300 mg of Boc-PEG2-amine **5** (300 mg, 1.2 mmol). The reaction was left stirring for 2 hours. The solvent was then removed *in vacuo*, and the resulting residue purified by flash column chromatography (SiO2, 10% MeOH/CH_2Cl_2) to yield a white solid as the desired compound (570 mg, 1.2 mmol, quant.). **^{1}H-NMR (400 MHz, CD_3OD)** δ/ppm 8.03 (t, *J* = 5.5 Hz, 1H), 4.50 (dd, *J* = 7.9, 4.8 Hz, 1H), 4.31 (dd, *J* = 7.9, 4.4 Hz, 1H), 3.61 (s, 4H), 3.53 (dt, *J* = 13.2, 5.6 Hz, 4H), 3.41 – 3.33 (m, 2H), 3.27 – 3.17 (m, 3H), 2.93 (dd, *J* = 12.8, 4.9 Hz, 1H), 2.71 (d, *J* = 12.7 Hz, 1H), 2.23 (t, *J* = 7.3 Hz, 2H), 1.83 – 1.52 (m, 4H), 1.44 (s, 9H). **MS** (ESI^+) found 475.2 $[M+H]^+$. Data were in accordance with literature values.[434]

7.1.16 (7-(Diethylamino)-3-((*E*)-3,14-dioxo-18-((3aS,4S,6aR)-2-oxohexahydro-1H-thieno[3,4-d]imidazol-4-yl)-7,10-dioxa-4,13-diazaoctadec-1-en-1-yl)-2-oxo-2H-chromen-4-yl)methyl prop-2-yn-1-ylcarbamate **12**



To a scintillation vial under argon equipped with a stirrer bar, 49 mg (0.058 mmol) of p-nitrophenyl-carbonate coumarin **10c** was dissolved in dry CH_2Cl_2. To this was added

94 µL (1.47 mmol, 25 eq.) of freshly distilled propargylamine and the reaction vial capped. After 40 minutes, TLC indicated complete conversion. The solvent was removed *in vacuo* and the compound was purified by flash column chromatography (SiO_2, 5-10% MeOH/$CHCl_3$) to yield a bright yellow solid as the desired compound (40.2 mg, 0.052 mmol, 92%). **R_f** (SiO_2, 10% MeOH/CH_2Cl_2) 0.29. **^{1}H-NMR** (600 MHz, $CDCl_3$) δ/ppm 7.76 (d, *J* = 15.2 Hz, 1H, 19, C-H), 7.68 (d, *J* = 9.2 Hz, 1H, 6, CH_{Ar}), 7.24 (d, *J* = 15.2 Hz, 1H, 20, C-H), 7.10 (t, *J* = 5.6 Hz, 1H, 22, N-H), 6.82 (t, *J* = 5.7 Hz, 1H, 32, N-H), 6.62 (dd, *J* = 9.3, 2.6 Hz, 1H, 1, CH_{Ar}), 6.55 (s, 1H, 45, N-H), 6.43 (d, *J* = 2.5 Hz, 1H, 3, CH_{Ar}), 6.12 (t, *J* = 5.7 Hz, 1H, 18, N-H), 5.65 (s, 1H, 40, N-H), 5.47 – 5.31 (m, 2H, 17, CH_2), 4.47 (dd, *J* = 7.8, 4.9 Hz, 1H, 46, C-H), 4.34 – 4.18 (m, 1H, 43, C-H), 3.95 (dd, *J* = 5.7, 2.6 Hz, 2H, 50, CH_2), 3.68 – 3.33 (m, 12H, 24, 25, 27, 28, 30, 31, CH_2), 3.41 (q, *J* = 7.2 Hz, 4H, 13, 14, CH_2), 3.10 (td, *J* = 7.4, 4.6 Hz, 1H, 38, C-H), 2.86 (dd, *J* = 12.8, 4.9 Hz, 1H, 47', CH_2), 2.73 (d, *J* = 12.7 Hz, 1H, 47'', CH_2), 2.23 (t, *J* = 2.5 Hz, 1H, 52, C-H), 2.18 (t, *J* = 7.7 Hz, 2H, 34, CH_2), 1.78 – 1.30 (m, 6H, 35'', 36', 37'', CH_2), 1.20 (t, *J* = 7.1 Hz, 6H, 15, 16, CH_3). **^{13}C-NMR** (151 MHz, $CDCl_3$) δ/ppm 173.79 (33), 167.03 (21), 164.25 (41), 160.75 (8), 155.69 (2C, 4, 54), 151.36 (2), 147.34 (10), 131.86 (19), 127.29 (6), 125.91 (20), 115.14 (9), 109.82 (1), 108.16 (5), 97.16 (3), 79.88 (51), 71.67 (52), 70.23 and 70.15 and 69.94 and 69.91 (4C, 25, 27, 28, 30), 61.97 (39), 60.38 (44), 58.11 (17), 55.73 (38), 45.02 (2C, 13, 14), 40.56 (47), 39.74 (24), 39.19 (31), 36.08 (34), 31.01 (50), 28.33 (35, 36 or 37), 28.23 (35, 36 or 37), 25.73 (35, 36 or 37), 12.65 (2C, 15, 16). **MS (ESI$^+$)** found 755.3 $[M+H]^+$. **HRMS (ESI$^+$)** found 755.3427 (theoretical m/z = 755.3433 $[C_{37}H_{51}O_9N_6S_1]^+$). **IR** (film $CDCl_3$/cm^{-1}) 3306 (w, propargyl-CH), 2929 (w), 1699 (s, C=O), 1652 (m), 1617 (s, C=O), 1601 (s), 1456 (s), 909 (s).

7.2 Oligonucleotide Sequences

7.2.1 General

Amine-modified ssDNA was purchased from atdBio and made up to 100 µM in 10 mM potassium phosphate buffer, pH 8. The modified oligonucleotide sequences employed are referenced by the number of amine modifications throughout the text. Phosphate-only (PO) oligonucleotides were purchased from Merck in desalted and lyophilised form and resuspended in 10 mM Tris pH 8. Phosphorothioate (PS) oligonucleotides were purchased from Merck, HPLC-purified in lyophilised form and dissolved in 10 mM potassium phosphate buffer, pH 7.4. PS-containing sequences are referenced throughout the text by their number of PS linkages in the backbone. Positions of PS linkages are indicated by a * in the sequence.

7.2.2 Amine-modified T7-promoter-containing ssDNA Sequences

Index	Nr of Amines	Length/nt	Sequence (5' - 3')
1	7	29	GAAATXAAXACGACXCACXAXAGGGXCXAG
2	4	20	2TAATXCGACTCXCTATXGGG
3	1	20	2TAATACGACTCACTATAGGG

Table 7-1: ssDNA sequences and the corresponding number of functionalisations.
X = internal C_6-hexylamino-dT modification, 2 = 5'-C6-hexylamino-phosphate modification.

7.2.3 Broccoli Aptamer DNA Sequences

Index	Name	Sequence
1	Template Strand	GGGTCTAGGAGCCCACACTCTACTCGACAGATACGAATATCTG GACCCGACCGTCTCCTAGACCCTATAGTGAGTCGTATTAATTC
2	Comple-mentary Strand	GAGACGGTCGGGTCCAGATATTCGTATCTGTCGAGTAGAGTGT GGGCTCCTAGACCC

Table 7-2: Broccoli Aptamer DNA sequences.

7.2.4 Antisense Oligonucleotide Sequences

Entry	Target	Starting Nucleotide in mRNA	Length/nt	Number of Amines	Name	Sequence (5' → 3')
1	mV	220	20	0		TTCATGTGGTCGGGGTAGCG
2	mV	220	20	3	V1	TXCATGTGGXCGGGGXAGCG
3	mV	220	20	3	V1b	2XCAXGTGGTCGGGGTAGCG
4	mV	220	20	3	V1c	2XCAXGTGGXCGGGGTAGCG
5	mV	220	20	4	V2	TXCATGXGGXCGGGGXAGCG
6	mV	229	18	0		GTGCTGCTTCATGTGGTC
7	mV	229	18	4	V3	GXGCTGCXTCAXGTGGXC
8	mV	224	16	0		TTCATGTGGTCGGGGT
9	mV	229	17	0		TGCTGCTTCATGTGGTC
10	mV	230	16	0		TGCTGCTTCATGTGGT
11	mC	27	19	0		CTCCTTGATGATGGCCATG
12	mC	81	19	0		CTCGAACTCGTGGCCGTTC
13	mC	139	18	0		CTTCAGCTTGGCGGTCTG
14	mC	147	19	0		CTTGGTCACCTTCAGCTTG
15	mC	222	16	0		CTTCACGTAGGCCTTG
16	mC	303	16	0		GTCCTCGAAGTTCATC
17	mC	141	16	0		CTTCAGCTTGGCGGTC
18	mC	139	16	0		TCAGCTTGGCGGTCTG
19	mC	139	16	4	C1	XCAGCTXGGCGGXCXG
20	mC	140	15	0		TCAGCTTGGCGGTCT
21	mC	135	22	0		CTTCAGCTTGGCGGTCTGGGTG
22	mC	139	23	0		GTCACCTTCAGCTTGGCGGTCTG
23	mC	141	21	0		GTCACCTTCAGCTTGGCGGTC
24	mC	142	20	0		GTCACCTTCAGCTTGGCGGT

Table 7-3: List of ASOs screened for activity and used in Chapter 3.

Name indicated the trivial name given to the sequence and is used throughout the text for reference. X = internal C6-hexylamino-dT modification, 2 = 5'-C6-hexylamino-phosphate-dT modification.

Index	Name	Sequence (5'-3')
1	252[4]	CTTCGGGCATGGCGGACTTGAAG
2	330[4]	CGCCCTCGAACTTCACCTCGGCG
3	146[4]	GCACGGGCAGCTTGCCGGTGGTGC
4	249[4]	CTTCGGGCATGGCGGACTTGAAGAAG
5	3[4]	GGTGAACAGCTCCTCGCCCTTGCTCACC
7	221[2]	GCTTCATGTGGTCGGGGTAGC
8	134[2]	TGGTGCAGATGAGCTTCA
9	125[3]	AGCTTCAGGGTCAGCT
10	154[3]	GGCACGGGCAGCTTGCC
11	202[3]	GGCGAAGCACTGCAGGCC
12	169[4]	GAAGAAGTCGTGCTGCTTC
13	229[1]	GTGCTGCTTCATGTGGTC

Table 7-4: Sequences tested for antisense activity against mVenus in Chapter 4.
Numbers in brackets indicate stem-length of the hairpin.

Index	Starting Nucleotide mV mRNA	Sequence (5'-3')
1	1	TCCTCGCCCTTGCTCACCAT
2	134	GGTGGTGCAGATGAGCTTCA
3	140	CTTGCCGGTGGTGCAGATGA
4	220	TTCATGTGGTCGGGGTAGCG
5	240	ACTTGAAGAAGTCGTGCTGC
6	307	GTCTTGTAGTTGCCGTCGTC
7	309	GGGTCTTGTAGTTGCCGTCG
8	311	GCGGGTCTTGTAGTTGCCGT
9	453	GCTTGTCGGCGGTGATATAG
10	499	TCGATGTTGTGGCGGATCTT
11	545	GGGGGTGTTCTGCTGGTAGT

Table 7-5: Antisense oligonucleotides screened for RNase H activity against mVenus in Chapter 5.

Entry	mV Position	Truncation from original ASO	Length/nt	Sequence (5'-3')
1	224	3' truncated	16	TTCATGTGGTCGGGGT
2	220	5' Truncated	16	TGTGGTCGGGGTAGCG
3	222	5'/3' truncated	16	CATGTGGTCGGGGTAG
4	67	N/A	14	TTGTGGCCGTTTAC
5	220	5' truncated	14	TGGTCGGGGTAGCG
6	223	5'/3' truncated	14	ATGTGGTCGGGGTA
7	226	3' truncated	14	TTCATGTGGTCGGG

Table 7-6: Truncated mV antisense oligonucleotides screened for improvement of antisense activity in cell-free conditions.

Entry	Name	Sequence (5'-3')
1	SCR1	AGGTGTGTCGTGCATGGTGC
2	SCR2	GGAGCGGTCGGTATCGTTGT
3	SCR3	TGGTGGCAGCCGTGTTGAGT
4	SCR4	GGATGTGCGGGCTTTCGGAT

Table 7-7: Scrambled sequences of mV antisense sequence 220.

7.2.5 Terminal amine-modified antisense oligonucleotides

Index	Name	Sequence (5'-3')
1	252[4]	/5AmMC6/CTTCGGGCATGGCGGACTTGAAG/3AmMO/
2	221[2]	/5AmMC6/GCTTCATGTGGTCGGGGTAGC/3AmMO/
3	169[4]	/5AmMC6/GAAGAAGTCGTGCTGCTTC/3AmMO/
4	229[1]	/5AmMC6/GTGCTGCTTCATGTGGTC/3AmMO/

Table 7-8: Oligonucleotides with terminal amine modifiers (AmMOs) used in Chapter 4.
5AmMC6 refers to 5'-C6-hexylamino-phosphate modification, 3AmMO refers to 3'-propylamino-glyceryl modification.

7.2.6 PS-containing oligonucleotides

Entry	Number of PS Linkages	Length /nt	Name	Sequence (5'-3')
1	1	20	1PS	TTCATGTGGT*CGGGGTAGCG
2	6	20	6PS	TTC*ATG*TGG*TCG*GGG*TAG*CG
3	9	20	9PS	TT*CA*TG*TG*GT*CG*GG*GT*AG*CG
4	6	20	20nt-6PS	[TxRd]TTC*ATG*TGG*TCG*GGG*TAG*CG
5	9	20	20nt-9PS	[TxRd]TT*CA*TG*TG*GT*CG*GG*GT*AG*CG
6	6	14	14nt-TxRd-6PS	[TxRd]TT*CA*TG*TG*GT*CG*GG
7	0	20	Reverse Complement	CGCTACCCCGACCACATGAA

Table 7-9: Phosphorothioate (PS)-containing oligonucleotides used in this study.

[TxRd] indicates Texas Red dye.

7.2.7 PCR Primers

Index	Primer	Sequence (5'-3')
1	LA-T7 Reverse Primer	GATATAGTTCCTCCTTTCAG
2	T7 Forward Primer	GAAATTAATACGACTCACTATAGGGTCTAG
3	α_ for_I	GCATTTATCAGGGTTATTGTCTCATGAGCGGATAC
4	α_rev_I	CTTACTCGAGAATTCCCGGGATCCTCATTATTAGGCGTGGGACGCGGC
5	α_rev_V	CCGCTCATGAGACAATAACCCTG
6	α_ for_V	AATGAGGATCCCGGGAATTCTCGAGTAAG
7	ω_for_I	GTTTAACTTTAAGAAGGAGGTATACATATGATCCCGCATCTGACCACCAG
8	ω_rev_I	GCCTCCTGCAGGTTAACCTTAC

9	ω_rev_V	CATATGTATACCTCCTTCTTAAAGTTAAACAAAATTATTTCTAG AC
10	ω_for_V	CTCGAGTAAGGTTAACCTGCAGGAG

Table 7-10: Primers used in PCR for linear DNA templates and for the generation of split-β-Galactosidase Plasmid DNA.

7.3 Chemical Biology Methods

7.3.1 General Chemical Biology Methods

All experiments involving bLA-DNA were performed under reduced ambient lighting (direct overhead lights turned off). acrylamide/bisacrylamide (AA/BisAA) (19:1), Urea, Ammonium Persulfate (APS) and Tris-Borate-EDTA (TBE) buffer were purchased from Merck. Agarose (SeaKem®, low electroendosmosis) was purchased from Lonza Bioscience. UltraPure™ Tris-Acetate-EDTA (TAE) buffer (10X) was purchased from ThermoFisher. *N,N'*-tetramethyl ethylene diamine (TMEDA) was purchased from Bio-Rad. Egg-PC was purchased from Avanti Polar Lipids. Water used was purified using a Milli-Q® (Merck Millipore) water purification system. Gels were visualised on a BioRad Gel Doc XR+ gel imager. PCRs and Incubations were performed in an Applied Bioscience 2720, Applied Bioscience ProFlex™ or Peqlabs peqSTAR thermocycler. High Performance Liquid Chromatography (HPLC) purifications were performed on an Agilent 1260 Infinity system. No unexpected or unusually high safety hazards were encountered.

7.3.2 Data Analysis and Plotting

Data were plotted using python's matplotlib and seaborn libraries. Error bars were computed using python's seaborn library and show a 95% confidence interval. T-tests were performed using python's scipy library, using the stats.ttest_ind() method and a two-tailed t-test was applied for Chapter 2, and a one-tailed t-test was applied for Chapters 3 and 4. Activation percentages were computed using the following equation: $\frac{\mu_S - \mu_N}{\mu_R - \mu_N} \times 100$, where μ = mean, N = background sample, S = sample of interest, R = reference sample. Gel electrophoresis data were analysed using ImageLab software. Microscopy images were processed in imageJ.

7.3.3 Polyacrylamide Gel Electrophoresis

Gels were cast by hand with the BioRad Mini-PROTEAN® handcasting equipment at a thickness of 0.75 mm. Denaturing gels were run with 16% (8% for handcuff oligonucleotides) AA/BisAA (19:1), 7M Urea, 1x TBE Buffer (polymerised using 0.8% APS and 0.05% TMEDA) at 250 V in 1X TBE buffer (adjusted to pH 7.5 for PSNV oligonucleotides) and polymerised using 0.8% APS and 0.05% TMEDA at 250 V in 1X TBE buffer. Samples were loaded with 95% formamide, 5 mM EDTA, 0.025% bromophenol blue and 0.025% xylene cyanol. Gels were stained with Gel-Red® nucleic acid stain (Biotium) or TxRd-dye measured without staining.

7.3.4 Agarose Gel Electrophoresis

DNA Gels were prepared at 1% agarose (for DNA with bound streptavidin) in 1X TAE buffer and run at 100 V in 1x TAE buffer. Samples were prepared with purple loading dye (NEB, B7024S) and run against a 1kb DNA ladder (NEB, N3232S). Gels were stained with Gel-Red® nucleic acid stain (Biotium). RNA Gels were prepared at 1.5-2% agarose in 1x TBE buffer, prestained with Sybr® Green II and run at 100 V in 1x TBE buffer. Samples were prepared using RNA loading dye (NEB B0363S) and heated to 70 °C for 10 minutes and cooled on ice before loading to denature the RNA. Samples were run against a low-range ssRNA ladder (NEB, N0364S) or ssRNA ladder (NEB, N0362S).

7.3.5 Preparation of UV light-activatable T7 Primer (uvLA-T7)

Method adapted from Booth *et al.*[201] In a 0.5 mL Eppendorf DNA LoBind Tube, 7 amino-T7 DNA (**Table 7-1**, Entry 1, 10 µM), $NaHCO_3$ (100 mM) and PC Biotin-NHS ester (5 mM, click-chemistry-tools (CCT), Catalogue Nr: 1225) were added in 50% DMF in a total reaction volume of 100 µL. The reaction mixture was vortexed, spun down using a table-top centrifuge and placed in a Thermomixer (Eppendorf) and shaken at 700 rpm, at room temperature, overnight. The reaction mixture was then washed 3 times with chloroform (200 µL) to remove the majority of organic contaminants, diluted to 100 µL with H_2O, spun for 1 minute at 14k RCF to pellet any insoluble impurities and the supernatant transferred to an HPLC injection vial. The oligonucleotide was then purified by HPLC on an Agilent Polaris C18 column (150 x 4.6 mm), heated to 50 °C using a gradient of 5-30% MeCN over 27 minutes, with 10 mM triethylammonium bicarbonate (TEAB) pH 8.5 as an ion-pairing buffer throughout.

The DNA was analysed by LCMS and LC-UV for purity and used in downstream applications.

Analogous to the above, the preparation of the UV-Activatable primer using the PC-Biotin-NHS molecule from Ambergen (PCB-N-001) was performed as previously described[201] on a 50 µL scale and purity was confirmed using oligonucleotide LCMS.

7.3.6 Preparation of blue light-activatable-T7 Primer (bLA-T7)

In a 0.5 mL Eppendorf DNA LoBind Tube, 7-amino-T7 DNA (**Table 7-1,** Entry 1, 11.1 µM), MOPS Buffer pH 8.5 (111 mM) and PFP-Coumarin **10b** (13.89 mM) were added in 70% DMF in a total reaction volume of 34 µL. The reaction mixture was vortexed, centrifuged using a table-top centrifuge and placed in a Thermomixer (Eppendorf), heated to 37 °C and shaken at 800 rpm for 3 hours and then at room temperature overnight. The reaction mixture was then washed three times with chloroform to remove the majority of organic contaminants, diluted to 100 µL with 1:1 MeCN:H_2O, spun for 1 minute at 14k RCF to pellet any insoluble impurities and the supernatant transferred to an HPLC injection vial. The oligonucleotide was then purified by HPLC on an Agilent Polaris C18 column (150 x 4.6 mm) heated to 50 °C using a gradient of 5-34% MeCN over 36 minutes, with 10 mM triethylammonium bicarbonate (TEAB) pH 8.5 as an ion-pairing buffer throughout. The DNA was then analysed by LCMS and LC-UV for purity and used in downstream applications.

7.3.7 Preparation of uvLA-ASOs from amino-C6-dT Oligonucleotides

Amino-modified oligonucleotides (**Table 7-3,** 20 µM) were added to a 0.5 mL DNA LoBind tube (Eppendorf) and reacted with PC Biotin-NHS ester (5 mM, click-chemistry-tools) with 100 mM $NaHCO_3$, in a total volume of 50 µL (50% water 50% DMF). Reactions were incubated in the dark at room temperature for 1 hour, with frequent mixing and centrifugation, then left at 4 °C overnight. Reactions were quenched with 350 µL of 20 mM tris pH 8. The mixtures were then partially purified by centrifugation with Amicon Ultra-0.5 mL centrifugal filters (Merck) according to the manufacturer's protocol, then purified further by HPLC on an Agilent Polaris C-18 column (150 x 4.5 mm), heated to 50 °C, using a gradient of 5-28% MeCN over 36 minutes with 10 mM TEAB pH 8.5 throughout. The resulting oligonucleotides were lyophilised, resuspended in H_2O and analysed by LCMS for purity.

7.3.8 Preparation of bLA-ASOs from amino-C6-dT Oligonucleotides

The amine-modified oligonucleotide (**Table 7-3**, Entry 19, 11.1 µM) was added to a 1.5 mL DNA LoBind Tube (Eppendorf) and reacted with PFP coumarin **10b** (17.5 mM) with MOPS pH 8.5 (119 mM) in 59% DMF in a total reaction volume of 34 µL. The reaction was incubated in a Thermomixer (Eppendorf) at 37 °C and 800 RPM overnight. The solution was diluted to 50 µL with H_2O, washed with $CHCl_3$ (3 x 200 µL), 50 µL DMSO added and transferred to an HPLC injection vial. The modified oligonucleotide was then purified by HPLC on an Agilent Polaris C-18 column (150 x 4.5 mm), heated to 50 °C, using a gradient of 5-35% MeCN over 20 minutes with 10 mM TEAB pH 8.5 throughout. The resulting oligonucleotide was lyophilised, resuspended in H_2O and analysed by LCMS for purity.

7.3.9 Binding of streptavidin to modified ASOs

The amino-C6-dT-biotinylated ASOs were incubated with monovalent streptavidin (kindly provided by Howarth's laboratory, Department of Biochemistry, University of Oxford) or tetravalent streptavidin (NEB) in a 4-fold excess to the number of photocleavable biotin groups. The reactions were incubated in the dark for 2-3 hours at room temperature, then left at 4 °C overnight.

7.3.10 Modification of terminal amine-modified Oligonucleotides with uvLA-Biotin

To a 1.5 mL microcentrifuge tube was added the desired, amine-modified ASO (**Table 7-8**, 10 µM), $NaHCO_3$ (100 mM) and PC-Biotin NHS Ester (click-chemistry-tools, 5 mM) in a total volume of 50 µL and the reaction incubated at room temperature overnight. The solution was diluted to 50 µL with H_2O, washed with $CHCl_3$ (3 x 200 µL), 50 µL DMSO added and transferred to an HPLC injection vial. The oligonucleotide was then purified by HPLC on an Agilent Polaris C18 column (150x4.5 mm), heated to 50 °C, using a gradient of 5-30% MeCN over 20 minutes with 10 mM TEAB pH 8.5 throughout. The resulting oligonucleotide was lyophilised, resuspended in H_2O and analysed by LCMS for purity.

7.3.11 Modification of terminal amine-modified Oligonucleotides with bLA-Biotin

To a 1.5 mL microcentrifuge tube was added the desired, amine-modified ASO (**Table 7-8**, 23.5 µM), MOPS pH 8.5 (119 mM) and PFP-Coumarin **10b** (17.5 mM) in 59% DMF in a final reaction volume of 34 µL. The reaction was incubated in a Thermomixer (Eppendorf) at 37 °C and 800 RPM overnight. The solution was diluted to 50 µL with H_2O, washed with $CHCl_3$ (3x 200 µL), 50 µL DMSO added and transferred to an HPLC injection vial. The oligonucleotide was then purified by HPLC on an Agilent Polaris C18 column (150x4.5 mm), heated to 50 °C, using a gradient of 5-30% MeCN over 20 minutes with 10 mM TEAB pH 8.5 throughout. The resulting oligonucleotide was lyophilised, resuspended in H_2O and analysed by LCMS for purity.

7.3.12 Modification of PS-containing Oligonucleotides with 2NV-Br

To a 1.5 mL centrifuge tube, PS-DNA (**Table 7-9**, 10 µM), HEPES pH 7.0 (100 mM) and 2-nitroveratryl bromide (25 mM) were added in 1:1 H_2O:DMF for untagged- or 1:3 H_2O:DMF for TxRd-tagged ONs in a total reaction volume of 50 µL. The reaction mixture was then vortexed, centrifuged and incubated at 37 °C for 3 days. The reaction mixture was then washed three times with chloroform (200 µL each, vortexed vigorously and centrifuged in a tabletop centrifuge at 14k RCF for 1 minute) to remove the majority of organic contaminants, diluted to 100 µL with DMSO and transferred to an HPLC injection vial. The oligonucleotides were then purified by HPLC on an Agilent Polaris C18 column (150 x 4.6 mm) heated to 50 °C using a gradient of 5-37% MeCN in H_2O over 20 minutes with 10 mM NH_4OAc pH 7-7.5 as an ion-pairing buffer throughout. The DNA was resuspended in 75% DMSO, analysed by LC for purity and used in downstream applications.

7.3.13 Modification of 1PS Oligonucleotides with Ethyl Iodide

To a 1.5 mL centrifuge tube, 1 PS-DNA (**Table 7-9,** Entry 1, 10 µM), HEPES pH 7.0 (100 mM) and 2-nitroveratryl bromide (25 mM) were added in 1:1 H_2O:DMF in a total reaction volume of 50 µL. The reaction mixture was then vortexed, centrifuged and incubated at 37 °C overnight. The solution was diluted to 100 µL with H_2O and the oligonucleotide by HPLC on an Agilent Polaris C18 column (150 x 4.6 mm) heated to 50 °C using a gradient of 5-37% MeCN in H_2O over 20 minutes with 10 mM NH_4OAc

pH 7-7.5 as an ion-pairing buffer throughout. The DNA was resuspended in 75% DMSO analysed by LC for purity and used in downstream applications.

7.3.14 Melting Temperature Measurements of NV-modified Oligonucleotides

To a micro-volume Quartz Suprasil cuvette with 10 mm path length and blackened sides (Hellma 105.201) was added 100 µL of buffer (1 M NaCl, 10 mM potassium phosphate 10 mM, pH 7.4). To this was added 1 µL (1 µg) of Reverse Complement DNA (**Table 7-9**, Entry 7, 100 µM) and either 1 µL of unmodified DNA (**Table 7-9,** 100 µM) or 1.6x excess of the nitroveratryl-modified DNA (to accommodate for any change in 260 nm absorbance caused by the modification) as a solution in 25% DMSO. For all samples, the volume was adjusted to 120 µL total with potassium phosphate 10 mM pH 7.4 and DMSO to a final 1.6% DMSO. The oligonucleotides were then measured on a Jasco V-770 UV-Visible/NIR Spectrophotometer equipped with a Peltier temperature controller at 260 nm from 12 to 85 °C with a ramping rate of 2 °C/minute, and a waiting period of 2 minutes at 85 °C before reversal. Melting temperatures were calculated as an average of 3 forward/reverse runs with individual melting temperatures calculated using in-built software by calculating the median of the two linear regions. Spectra were plotted using python and smoothed using a Savitzky-Golay filter.

7.3.15 Light-controlled RNase H Assay with NV-modified oligonucleotides

To a 200 µL PCR Tube were added 300 ng of mVenus mRNA, 6 U of RNase H (recombinant *E. coli*, Takara), 30 mM HEPES pH 7, 100 mM KCl, 20 mM $MgCl_2$, 2 mM DTT and 5 ng of ASO (if required (0.9 eq. vs. mRNA for the 20nt-ONs or 1.6 eq. vs mRNA for the 14nt-ON) in a total of 10 µL. The resulting solutions were kept at room temperature in the dark and illuminated as required, before placing them in a thermocycler and incubated at 37 °C for 1 hour. To the reactions was then added 10 µL of RNA Loading Dye (2x, NEB) and the samples heated to 70 °C for 10 minutes, cooled to 8 °C and analysed by AGE (2%).

7.3.16 Annealing of Broccoli-Construct

Amine-only-T7 Broccoli DNA was assembled by mixing the template and non-template strands in an equimolar ratio (**Table 7-2**, 1 µL each of a solution of 10 µM in 10 mM Tris pH 8). To this was then added the 7-amine-containing T7 promoter sequence (**Table 7-1,** 1 µL of a 10 µM solution in 10 mM Tris pH 8) and the volume adjusted to 10 µL with H_2O. Similarly, blue light-activatable Broccoli was assembled by mixing template and non-template strands in an equimolar ratio (**Table 7-2,** 0.5 µL each of a solution of 10 µM in 10 mM Tris pH 8) and the blue-light activatable T7 promoter sequence in 4-fold excess (5.41 µL of a 3.7 µM solution in H_2O) and the volume was adjusted to 7 µL with H_2O. The samples were then heated to 95 °C and slowly cooled to 25 °C over 40 minutes in a thermocycler. To this was then added a 50x molar excess of monovalent streptavidin and incubated overnight at 4 °C.

7.3.17 Plasmid Digestion

Plasmids employed include *mVenus*,[201] *mNeonGreen*,[206] *mCherry* and *lacZ*, including α and ω, (described below) inside the PURExpress Control Template.

Full-Length plasmid (5 ng/µL) was digested using HindIII-High Fidelity (0.8 U/µL, NEB R3104S) in 1x CutSmart Buffer (NEB B7204S) in a total volume of 25 µL. The solution was incubated for 30 minutes at 37 °C and then heated to 80 °C for 20 minutes. The resulting digested plasmid was used without further purification in PCR.

7.3.18 Preparation of linear Template DNA

PCR reactions to prepare linear templates were carried out using DreamTaq DNA polymerase MasterMix (2x, ThermoFisher), Forward and Reverse Primers (**Table 7-10**, Entry 1 and 2) at 0.25 µM concentration and 0.04 ng/µL of the HindIII-digested plasmid as template in a total reaction volume of 50 µL. The PCR was carried out according to the manufacturer's protocol for 35 cycles with an annealing temperature of 47 °C for 30 seconds, an extension time of 72 °C for 1 minute (15s/kbp) and a final extension at 72 °C for 10 minutes. The resulting DNA was then purified using the GeneJet PCR purification columns (ThermoFisher) following the manufacturer's protocol and eluted in 50 µL H_2O.

7.3.19 *In vitro* Transcription of mRNA

In vitro transcription was performed using 10 ng/µL of linear template DNA (as prepared above) with the HiScribe™ T7 High Yield RNA Synthesis Kit (NEB), following the manufacturer's protocol in a total volume of 20 µL. Samples were incubated at 37 °C for 4 hours prior to addition of DNase I (1 µL) and further incubation for 30 minutes. Samples were then heated to 80 °C for 20 minutes and the mRNA purified using the GeneJet RNA Cleanup and Concentration Micro Kit (ThermoFisher) following the manufacturer's protocol and eluted in H_2O.

7.3.20 Screening for RNase H-active Oligonucleotides against mVenus for Phosphorothioate Caging

The computational folding algorithm sFold[398] was used to identify potential antisense target sequences through input of the target mRNA. For the work described in Chapter 3, 13 sequences against mCherry with a length of 15-23 nt were chosen and for the work in Chapter 5, 11 sequences of 20 nt were chosen across the whole gene and ordered as phosphate oligonucleotides, ordered by starting nucleotide in the gene sequence (**Table 7-5, Table 7-6**). The sequences were screened against 300 ng of mVenus mRNA, 6 U of RNase H (recombinant *E. coli*, Takara) and 1 ng of ASO in a buffer system containing 30 mM HEPES pH 7, 100 mM KCl, 20 mM $MgCl_2$ and 2 mM DTT in a total of 10 µL. The samples were incubated at 37 °C for 1h, RNA loading dye (NEB, B0363S) added, samples heated to 70 °C for 10 minutes and then analysed by agarose gel electrophoresis (2% agarose, 1x Tris-Borate-EDTA, 1x GelRed, 100 V). Band intensities were analysed using ImageJ by comparing band intensities for starting mRNA and the degradation products.

7.3.21 Screening for Antisense Oligonucleotide Sequences active against mVenus for Circularisation onto wtSA

A python script (Chapter 7.4) was used to identify potential antisense oligonucleotides which form a hairpin structure *via* complementary stem length of 4 nucleotides. Similarly, the constraints were reduced, and oligonucleotides found with a step length of 1, 2 and 3 nucleotides. These oligonucleotides were then ordered and labelled by the starting nucleotide in the mVenus gene sequence, followed by the length of stem in brackets (**Table 7-4**).

The 4-stem oligonucleotides were then screened against its target mVenus mRNA. 30 ng/µL (94 nM) of mVenus mRNA (prepared as above), 0.6 U/µL RNase H (recombinant *E. coli*, Takara), and either 0.1 ng/µL (14.34 nM) or 0.5 ng/µL (71.7 nM) of the ASO in a buffer system containing 30 mM HEPES pH 7, 100 mM KCl, 20 mM $MgCl_2$ and 2 mM DTT in a total of 10 µL were incubated for 1 hour at 37 °C. Similarly, for the lower constraint oligonucleotides, 30 ng/µL (94 nM) of mVenus mRNA, 0.3 U/µL RNase H (recombinant *E. coli*, Takara), and the ASO of interest at a concentration of 71.7 nM were incubated in the buffer mentioned above for 1 hour at 37 °C. RNA loading dye (NEB, B0363S) was then added, samples heated to 70 °C for 10 minutes and then analysed by agarose gel electrophoresis.

7.3.22 RNase H Assay with handcuffed ASOs

30 ng/µL (94 nM) of mVenus mRNA, 0.6 U/µL RNase H (recombinant *E. coli*, Takara), and a concentration of 71.7 nM of the bLA- or uvLA-ASO in a buffer system containing 30 mM HEPES pH 7, 100 mM KCl, 20 mM $MgCl_2$ and 2 mM DTT in a total of 10 µL were incubated for 1 hour at 37 °C. RNA loading dye (NEB, B0363S) was then added, samples heated to 70 °C for 10 minutes and then analysed by agarose gel electrophoresis.

7.3.23 Binding of wild-type Streptavidin to terminally-modified Oligonucleotides

In a 0.5 mL DNA LoBind Tube, LA-Biotin-modified DNA was diluted to a final concentration of 0.2-0.3 µM with Dulbecco Phosphate Buffered Saline (Merck). To this was then added 0.5 molar equivalents of wild-type Streptavidin (NEB, N7021S), unless otherwise indicated, the solution vortexed, covered in foil and incubated at 4 °C overnight.

7.3.24 Control of cell-free Protein Synthesis with handcuffed Oligonucleotides

In a 200 µL PCR tube, 5 ng/µl of linear template DNA for mVenus were added to PURExpress (NEB, E6800) with 0.6 U/µL RNase H (recombinant *E. coli*, Takara) and to this bLA-252[4] (4.34 ng/µL, 571 nM) or bLA-229[1] (0.5 ng/µL, 85 nM) were added. The resulting solutions were kept at room temperature in the dark and illuminated as required, before placing them in a thermocycler and incubated at 37 °C for 4 hours.

2 µL of each solution was then placed into 39 µL of H_2O and mixed by pipetting. 40 µL of the resulting solutions were then transferred into a 384 well plate and placed into a plate reader (Tecan Infinity M1000) and fluorescence measurements were taken for mVenus ($\lambda_{Ex/Em}$: 515/527 nm, gain 173).

7.3.25 Ethanol Precipitation

To a 1.5 mL Eppendorf tube containing DNA in solution was added 10%vol. 3 M NaOAc pH 5.0. The tube was vortexed and centrifuged prior to addition of 2.5 volume equivalents of ice-cold ethanol. The tube was vortexed and incubated at -80 °C for a minimum of 1 hour. The tube was then centrifuged at 16k RCF for 30 minutes at 4 °C, the supernatant removed, and the resulting pellet washed with cold 70% EtOH, prior to centrifugation for another 15 minutes. The supernatant was then removed, the pellet dried and then resuspended.

7.3.26 Screening for PS-modification Conditions

To a 1.5 mL centrifuge tube, 1PS-DNA (**Table 7-9,** Entry 1, 10 µM), the corresponding buffer (100 mM) and 2-nitroveratryl bromide (25 mM) were added in 1:1 H_2O:DMF in a total reaction volume of 50 µL. The reaction mixture was then vortexed, centrifuged and incubated at 37 °C overnight. The reaction mixture was then washed three times with chloroform to remove the majority of organic contaminants, diluted to 100 µL H_2O and ethanol precipitated. The oligonucleotides were then analysed and purified by HPLC on an Agilent Polaris C18 column (150 x 4.6 mm) heated to 50 °C using a gradient of 5-37% MeCN in H2O over 20 minutes with 10 mM NH_4OAc pH 7-7.5 as an ion-pairing buffer throughout, prior to analysis by LCMS.

7.3.27 Photocleavage of 1PSNV

For each sample, 450 ng of 1PSNV DNA were added to a 200 µL PCR Tube in a total volume of 10 µL. The samples were then irradiated with the 365 nm LED as described above for the required time. The samples were then transferred to an HPLC injection vial and analysed on an Agilent Polaris C18 column (150 x 4.6 mm) heated to 50 °C using a gradient of gradient of 2% MeCN for 1 minute, then 2-20% MeCN over 19 minutes with 10 mM NH_4OAc pH 7-7.5 as an ion-pairing buffer throughout. The photocleavage product was collected and analysed by LCMS to confirm the intact PS-linkage.

7.3.28 Texas Red-tagged Oligonucleotide Concentration Measurements

Concentration of Texas Red-tagged, nitroveratryl-modified oligonucleotides was determined by fluorescence. Serial dilutions of unmodified TxRd-tagged oligonucleotides were prepared at concentrations of 10, 5 and 1 µM. The concentration in ng/µL was then determined by nanodrop, corrected for 260 nm absorbance of TxRd. 1 µL of each solution was then added to 39 µL of H_2O in a Corning black 384-well plate and fluorescence measurements taken on a plate reader (Tecan Infinity M1000) with $\lambda_{Ex/Em}$ 596/615 nm at a gain of 170 (for the 20nt-6PSNV) or gain 180 (for 20nt-9PSNV and 14nt-6PSNV) and a calibration curve generated. Concentrations of prepared samples of nitroveratryl-modified oligonucleotides were then measured by placing 1 µL of the oligonucleotide solution into 39 µL of H_2O in a 384-well plate and calculating the concentration from the calibration curve.

7.3.29 Preparation of LA-DNA Templates using PCR

PCR reactions were carried out using DreamTaq DNA polymerase MasterMix (2x, ThermoFisher), reverse primer (**Table 7-10**, Entry 1) at 0.25 µM concentration, uvLA-T7 primer at 0.325 µM effective concentration or bLA-T7 primer at an 0.8 µM effective concentration (determined by A_{260} absorbance) and 0.04 ng/µL of the desired, digested plasmid as template in a total reaction volume of 25 µL. The PCR was carried out according to the manufacturer's protocol for 35 cycles with an annealing temperature of 47 °C for 30 seconds (for uvLA-DNA) or 45 °C for 45 seconds (for bLA-DNA), an extension time of 72 °C for 1 minute 15s/kbp and a final extension at 72 °C for 10 minutes. The resulting DNA was then purified using the GeneJet PCR purification columns (ThermoFisher) following the manufacturer's protocol and eluted in 25 µL H_2O.

Amine-only control DNA was prepared using the same method as for uvLA-DNA, with 0.2 µM forward and reverse primer (**Table 7-1**, Entry 1**,** and **Table 7-10,** Entry 1).

7.3.30 Streptavidin binding onto T7-modified genes

To cage DNA, monovalent streptavidin (provided by Howarth's laboratory, Department of Biochemistry, University of Oxford) was bound to the DNA templates containing the modified T7–promoter. The PCR product was incubated with a 50× molar excess of monovalent streptavidin (1 mg/mL in phosphate buffered saline, pH 7.4)) in protein

LoBind tubes (Eppendorf) overnight at 4 °C. Amine-only DNA was also incubated with monovalent streptavidin in the same manner.

7.3.31 Illumination of DNA for Gels and cell-free Reactions

Samples were held in a PCR tube rack (StarLabs) over aluminium foil with open lids. Irradiation was then performed top-down with a ThorLabs 455 nm LED (M455L4) equipped with a collimator (COP4-A) from a distance of 30 cm at power setting 4/6 (Irradiance of 64 $mW \cdot cm^{-2}$) (unless otherwise indicated, 1/6 power corresponds to an irradiance of 7.34 $mW \cdot cm^{-2}$, 2/6 power corresponds to an irradiance of 17.54 $mW \cdot cm^{-2}$) or a ThorLabs 365 nm LED (M365L3) equipped with a collimator (COP5-A) from a distance of 34 cm at an irradiance of 1.06 $mW \cdot cm^{-2}$ for Chapter 2 and 4, an irradiance of 2.12 $mW \cdot cm^{-2}$ for Chapter 3 and 5.65 $mW \cdot cm^{-2}$ (2/6 power) for Chapter 5. Both LEDs were controlled by a ThorLabs driver (LEDD1B) set at 1 A maximum drive current.

7.3.32 Bulk Molecule Photocleavage

0.5 µL of a 50 mM solution of pNP-coumarin **10c** or PFP-coumarin **10b** in DMF or a solution of propargyl coumarin **11** in DMSO was added to 1000 µL H_2O in a Thorlabs 1 mL cuvette with blackened sides. UV-Visible recordings were performed from 260 to 600 nm on a Varian Cary 50 Bio UV-Visible Spectrophotometer. The sample was then illuminated with a ThorLabs 455 nm LED (M455L4) equipped with a collimator (COP4-A) from a distance of 20 cm in 1-minute intervals at 6/6 power (127 $mW \cdot cm^{-2}$) or 1/6 power (7.34 $mW \cdot cm^{-2}$), controlled by a ThorLabs Driver (LEDD1B) set at 1 A maximum drive current.

7.3.33 Transcription of Broccoli Aptamer

In vitro transcription of broccoli aptamer was performed using 3 ng/µL of template DNA and 2 U/µL T7 RNA polymerase (ThermoFisher) in 40 mM Tris-HCl pH 8.0, 2 mM spermidine, 10 mM DTT, 48 mM $MgCl_2$, 10 mM each of UTP, CTP, ATP and GTP. Samples were illuminated for 1 minute using a 455 nm LED (if required) before the addition of DFHBI to a concentration of 60 µM. The total reaction volume is 6 µL. Samples were then incubated at 37 °C for 4 hours. 5 µL aliquots were then taken and diluted to 41 µL with water. 40 µL of the resulting solutions were then placed into a black polystyrene 384 well plate (OptiPlate, PerkinElmer) and fluorescence

measurements were taken on a plate reader (Tecan infinite M1000Pro) using $\lambda_{ex/em}$:455/506 nm with a bandwidth of 10 nm.

7.3.34 Transcription of mVenus, α- and ω-Subunit mRNA

In vitro transcription was performed using 10 ng/µL (mVenus) or 3 ng/µL (α- and ω-subunit) of template DNA and 2 U/µL T7 RNA polymerase (ThermoFisher) in 40 mM Tris-HCl pH 8.0, 2 mM spermidine, 10 mM DTT, 48 mM $MgCl_2$, 10 mM each of UTP, CTP, ATP and GTP. Samples were then illuminated for 1 minute using a 455 nm LED or 3 minutes using a 365 nm LED, as described. Samples were incubated at 37 °C for 4 hours and 1.5 µL of the resulting solution was then diluted into 10 µL of water. Samples were denatured using 2x RNA loading dye (NEB) and analysed by AGE.

7.3.35 Cell-free Protein Synthesis from LA-DNA Templates

In a 200 µL PCR tube, 10 ng/µL of linear template DNA (amine only or modified, both with 50x molar xs. mSA) were added to PURExpress (NEB, E6800) with 2.67 U/µL RNase Inhibitor (murine, NEB, M0314), as prepared by the manufacturer's protocol, in a total volume of 3 µL. The resulting solutions were kept at room temperature in the dark and illuminated as required, before placing them in a thermocycler and incubated at 37 °C for 4 hours. 2 µL of each solution was then placed into 39 µL of H_2O and mixed by pipetting. 40 µL of the resulting solutions were then transferred into a 384 well plate and placed into a plate reader (Tecan Infinity M1000) and fluorescence measurements were taken ($\lambda_{Ex/Em}$: 515/527 nm for mVenus, Gain: 173).

For the light titration (**Figure 2-20**), reactions were prepared as above on a 2 µL scale, and after incubation, 1.6 µL of the solutions were added to 39.4 µL H_2O, mixed pipetting and 40 µL transferred into the 384 well plate for measurement as above.

Similarly, split β-Gal was expressed by the addition of 3 ng/µL of each α- and ω-template (amine only, or modified, both with 50x molar xs. mSA) as above. After incubation at 37 °C for 4 hours, 2 µL of each solution was then placed into 39 µL of a cold solution of carboxyumbelliferyl-β-D-galactopyranoside (CUG, Abcam, ab275047) in H_2O (100 µM) on ice and mixed by pipetting. 40 µL of the resulting solutions were then transferred into a pre-chilled 384 well plate, placed into a plate reader (Tecan Infinity M1000) heated to 37 °C and fluorescence measurements were taken at regular intervals ($\lambda_{Ex/Em}$: 388/455 nm, Gain: 100).

7.3.36 Light-controlled gene knockdown in cell-free protein synthesis with uvLA-V3

In a 200 µL PCR tube, 5 ng/µl linear mV template DNA was added to PURExpress (NEB, E6800) with 0.67 U/µL RNase H (Takara) and 0.2 ng/µL NH_2-**V3** or uvLA-**V3** ASO. The resulting solutions were kept at room temperature in the dark and illuminated with UV as required (5 minutes), before placing them in a thermocycler and incubated at 37 °C for 4 hours. 2 µL of each solution was then placed into 39 µL of H_2O and mixed by pipetting. 40 µL of the resulting solutions were then transferred into a 384 well plate and placed into a plate reader (Tecan Infinity M1000) and fluorescence measurements were taken ($\lambda_{Ex/Em}$: 515/527 nm, Gain 173).

7.3.37 Control of Transcription and Gene Knockdown with two Wavelengths in cell-free Protein Synthesis

In a 200 µL PCR tube, 5 ng/µL of blue light-activatable mV template DNA were added to PURExpress (NEB, E6800) with 0.67 U/µL RNase H (Takara) and 0.33 ng/µL uvLA-**V3** and 0.2 ng/µL NH_2-**V3** or uvLA-**V3** ASO. The resulting solutions were kept at room temperature in the dark and illuminated as required (1 minute with blue and 3 minutes with UV), before placing them in a thermocycler and incubated at 37 °C. To illuminate at different timepoints, tubes were cooled to room temperature in the dark and illuminated as required, before placing them back into the thermocycler for a total of 4 hours incubation time. 2 µL of each solution were then placed into 39 µL of H_2O and mixed by pipetting. 40 µL of the resulting solutions were then transferred into a 384 well plate and placed into a plate reader (Tecan Infinity M1000) and fluorescence measurements were taken ($\lambda_{Ex/Em}$: 515/527 nm, Gain 173).

7.3.38 Two-wavelength Control of RNase H-mediated mRNA Degradation

1 pmol of either mV or mC mRNA was incubated with 6 U of RNase H (recombinant *E. coli*, Takara) and 1.2 ng of each bLA-**C1** and uvLA-**V3** in a buffer system containing 30 mM HEPES pH 7, 100 mM KCl, 20 mM $MgCl_2$ and 2 mM DTT. The samples were illuminated as required (5 minutes for UV irradiation or 1 minute for blue irradiation), incubated at 37 °C for 1 hour. After incubation, RNA loading dye (NEB, B0363S) was added, the samples heated to 70 °C for 10 minutes and analysed by agarose gel electrophoresis.

7.3.39 Two Wavelength-controlled Gene Knockdown in a cell-free Protein Synthesis System

In a 200 µL PCR tube, 5 ng/µL each of linear mV and mC DNA (as prepared were added to PURExpress (NEB, E6800) with 0.67 U/µL RNase H (Takara), 0.5 ng/µL bLA-**C1** ASO and 0.33 ng/µL uvLA-**V2** ASO. The resulting solutions were kept at room temperature in the dark and illuminated as required (3 minutes for UV irradiation or 1 minute for blue irradiation), before placing them in a thermocycler at 37 °C for 4 hours. 2 µL of each solution were then placed into 39 µL of H_2O and mixed by pipetting. 40 µL of the resulting solutions were then transferred into a 384 well plate and placed into a plate reader (Tecan Infinity M1000) and fluorescence measurements were taken ($\lambda_{Ex/Em}$: 515/527 nm for mV, gain 183, and $\lambda_{Ex/Em}$: 587/610 nm for mC, gain 234).

7.3.40 Cell-free Protein Synthesis with PSNV-oligonucleotides

In a 200 µL PCR tube, 10 ng/µL of linear template DNA for mV were added to PURExpress (NEB, E6800) with 0.6 U/µL RNase H (recombinant *E. coli*, Takara) and then TxRd-tagged oligonucleotides (PS or PSNV) were added to a concentration of 500 pg/µL. The % DMSO in the reactions were 1.01% for both 20nt-6PSNV and 20nt-9PSNV and 2.42% DMSO for the 14nt-6PSNV. The resulting solutions were kept at room temperature in the dark and illuminated as required, before placing them in a thermocycler and incubated at 37 °C for 4h. 2 µL of each solution was then placed into 39 µL of H2O and mixed by pipetting. 40 µL of the resulting solutions were then transferred into a 384 well plate and placed into a plate reader (Tecan Infinity M1000) and fluorescence measurements were taken for mVenus ($\lambda_{Ex}/_{Em}$: 515/527 nm, gain 173 for 20nt-6PSNV and -9PSNV, and gain 181 for 14nt-6PSNV), as well as for TxRd ($\lambda_{Ex}/_{Em}$: 596/615 nm at a gain of 200).

7.3.41 Nuclease Assay with PSNV Oligonucleotides

In a 200 µL PCR tube, 10 ng/µL of PO, PS or PSNV DNA was incubated at 37 °C with DNase I (NEB, M0303, 0.15 U/µL), DNase I Buffer (1x, NEB M0303), and up to 5% DMSO in a total volume of 40 µL. At each timepoint, a 9.5 µL aliquot was taken and diluted into 9.5 µL of 95% formamide with 10 mM HEPES pH 7 and 1% bromophenol blue and stored at 4 °C. The samples were then analysed on denaturing PAGE (7 M

urea, 16%), made with TBE (ThermoFisher, pH-adjusted to 7.5 for TxRd-tagged ONs). Non-TxRd-tagged DNA was then stained using GelRed.

7.3.42 Generation of Split β-Galactosidase

Adapted from a procedure reported by J. P. Basilion.[358] Full Length β-Galactosidase inside the PURExpress control template was used as the starting genetic template (prepared by R. Chowdhry) and split at amino-acid residue 738. The final constructs contained amino acids 1-737 (subunit α) and 738-1024 (subunit ω, with a starting methionine added).

Linear DNA inserts containing the relevant split protein parts as well as vectors to generate full-length plasmid, with homologous regions for recombination to full-length plasmid, were generated *via* PCR (**Table 7-10**).

PCR cycle conditions can be found below. PCR reactions were carried out using Phusion DNA polymerase MasterMix (2x, NEB), primers (forward and reverse) at 0.5 µM concentration, 3% DMSO and 0.04 ng/µL full-length β-Galactosidase plasmid as template in a total reaction volume of 25 µL. 2 µL of the PCR reactions were then analysed by AGE and the to the remainder was added 0.5 µL of Dpn1 (NEB, R0176S, 10 U) and incubated at 37 °C for 1 hour to digest the plasmid template, and then the enzyme heat deactivated at 80 °C for 20 minutes. The DNA was purified using the GeneJet PCR purification kit.

For the α-insert, using Primers 3 and 4 (**Table 7-10**), the following cycle conditions were used:

Temp	Time	
98 °C	30 seconds	
98 °C	30x	10 seconds
69 °C		20 seconds
72 °C		1 minute 30 seconds
72 °C	5 minutes	
4 °C	HOLD	

For the α-vector, using primers 5 and 6 (**Table 7-10**), the following cycle conditions were used:

Temp	Time	
98 °C	30 seconds	
98 °C	30x	10 seconds
66 °C		20 seconds
72 °C		1 minutes 30 seconds
72 °C	5 minutes	
4 °C	HOLD	

For the ω-insert, using Primers 7 and 8 (**Table 7-10**), the following cycle conditions were used

Temp	Time	
98 °C	30 seconds	
98 °C	30x	10 seconds
66 °C		20 seconds
72 °C		30 seconds
72 °C	5 minutes	
4 °C	HOLD	

For the ω-vector, using Primers 9 and 10 (**Table 7-10**), the following cycle conditions were used:

Temp	Time	
98 °C	30 seconds	
98 °C	30x	10 seconds
67 °C		20 seconds
72 °C		1 minute 30 seconds
72 °C	5 minutes	
4 °C	HOLD	

2 µL of the PCR reactions were then analysed using AGE to confirm the correct product.

The linear templates were combined using homologous recombination. For this, the insert and vector were mixed in a 1:1 ratio (for the α-4 subunit) or a 3:1 ratio (for the ω subunit) and 100 ng total was added to 15 µL of XL-10 gold *E. coli* cells (Agilent) in a 14 mL round-bottom centrifuge tube (Falcon). The tube was flicked gently to mix and incubated on ice for 30 minutes. The tubes were placed in a 42 °C water bath for 45 seconds and then immediately placed on ice for around 2 minutes. 300 µL of SOC outgrowth medium (NEB, B9020S) was then added and the tubes incubated in a shaking incubator at 250 rpm for 1 hour. 100 µL of the resulting solution was spread on ampicillin-containing agar plates and grown at 37 °C overnight. Colonies positive for the desired gene were then used to inoculate 5 mL of Lysogeny Broth containing ampicillin in 50 mL centrifuge tubes and grown overnight at 37 °C in a shaking incubator at 200 rpm. Minipreparations were then carried out using the Promega Miniprep Kit, following the manufacturer's protocol and the sequences confirmed by Sanger sequencing (Source Bioscience).

7.3.43 Preparation of Synthetic Cells from Giant Unilamellar Vesicles

This experiment was performed by R. Chowdhry and included for completion.

Lipid films were prepared in 1.5 mL glass vials from solutions of egg-PC in chloroform by drying under N_2 flow and then desiccated for at least 1 hour. Mineral oil was added to a final lipid concentration of 5 mg/mL The lipid/oil mix was vortexed for 1 minute, heated to 80 °C for 10 minutes, vortexed further for 1 minute, sonicated for 1 hour at 50 °C, stored at room temperature overnight and used the next day. PURExpress components with RNase inhibitor, 200 mM Sucrose, 6 ng/µL bLA-DNA and 25 µM Texas-Red Dextran were added to 200 µL of mineral oil and agitated mechanically along a tube rack to produce a water-in-oil emulsion. The emulsion was pipetted on top of an inverted emulsion column in a 1.5 mL Eppendorf tube consisting of 200 µL outer solution buffer (50 mM HEPES, 400 mM Potassium Glutamate, 200 mM Glucose, pH 7.6) and 100 µL of the same lipid/oil mix on top forming a lipid monolayer interface. The tubes were centrifuged at 16,000 x g for 30 minutes, the oil removed, and the GUVs were transferred to a new Eppendorf tube for a wash step with centrifugation at 10,000 x g for 10 minutes. Excess oil and buffer were carefully removed and 30 µL of the GUVs were transferred to a fresh tube and incubated for 5 hours at 37 °C. 25 µL of the GUVs were imaged in Gene Frames on a Leica DMi8 inverted epi-fluorescence microscope.

7.3.44 Preparation of Synthetic Cells from Emulsion Droplets

Cell-free protein synthesis was performed as above using PURExpress containing 25 µM Texas-Red Dextran in a total volume of 3 µL. 5 ng/µL bLA-mNG template or 3 ng/µL each of the uvLA-α (Click-Chemistry-Tools) and bLA-ω templates were used. To the mNG expression was added 2.67 U/µL RNase Inhibitor whereas for split β-Gal, fluorescein-di-β-D-galactopyranoside (FDG, abcam, ab273643) was added to a concentration of 50 µM. In parallel, a solution of 10 mg/mL of Polystyrene-*block*-poly(ethylene-*ran*-butylene)-*block*-polystyrene (SEBS, average M_w ~118000) in hexadecane,[365] containing 2wt% Span80 was melted at 50 °C. 30 µL of this solution was added to a 96 well plate with blackened sides and clear bottom (Corning 3603) and left to solidify to coat the bottom of the well. Then, 40 µL of the polymer solution was added to the prepared PURExpress solution, the solutions were quickly emulsified by agitation along a PCR rack and the resulting emulsion transferred to the pre-coated well and left to set for 5 minutes. The plate was then tilted and any ungelled liquid removed. The plate was illuminated from the bottom (through photomasks if required) and incubated at 37 °C for 3 hours (for split β-Galactosidase) or 4 hours (for mNG) prior to imaging on a Leica DMi8 inverted epi-fluorescence microscope.

7.3.45 Light-controlled Gene Knockdown in Emulsion Droplets

Cell-free protein synthesis was performed as above using PURExpress with 5 ng/µL each of linear mNG and mC DNA templates, 0.6 U/µL of RNase H (recombinant *E. coli*, Takara) and 1.16 ng/µL bLA-**C1** ASO in a total volume of 3 µL. The solution was then emulsified with hexadecane,[365] containing 2wt% Span80 and 10 mg/mL SEBS at 50 °C, as previous. Ungelled liquid was then removed, and the plate illuminated from the bottom through photomasks and incubated for 4 hours prior to imaging on a Leica DMi8 inverted epi-fluorescence microscope.

7.3.46 Oligonucleotide Mass Spectrometry

Oligonucleotide Mass Spectra were recorded on a Waters Xevo G2 QTOF ESI- UPLC-MS system equipped with a Waters ACQUITY UPLC BEH C18 column (130 Å, 1.7 µm, 2.1 mm X 50 mm). A gradient of MeOH in Et_3N and hexafluoroisopropanol (HFIP) was used (buffer A, 8.6 mM Et_3N, 200 mM HFIP in 5% MeOH/H_2O (v/v); buffer B, 20% buffer A in MeOH).[103] Samples were analysed using a gradient of 0-70% buffer B over 8 minutes. For coumarin-modified T7-containing DNA, as well as samples with more

than 1 PSNV linkage, samples were analysed using a gradient of 50-100% Buffer B over 8 minutes. Data were then deconvoluted using MassLynx v4.1.

Entry	Oligonucleotide	Mass after Deconvolution	Expected Mass
1	uvLA-T7 (Click-Chemistry-Tools)	15399	15400
2	uvLA-T7 (AmberGen)	15066	15064
3	bLA-T7	15217	15218

Table 7-11: Modified T7-promoter-sequence-containing oligonucleotides and their masses after deconvolution as measured by LCMS.

Entry	Oligonucleotide	Number of PC-biotin groups	Purified product	Expected mass	Mass after deconvolution
1	**V1**	3	uvLA-**V1** biotin	9149	9148
2	**V2**	4	uvLA-**V2** biotin	9740	9740
3	**V3**	4	uvLA-**V3** biotin	9032	9032
4	**C1**	4	bLA-**C1** biotin	8320	8320

Table 7-12: Amino-C6-dT-modified ASOs and their masses after deconvolution as measured by LCMS.

Entry	Oligonucleotide	Modification	Mass after Deconvolution	Expected Mass	Retention Time/minutes
1	252[4]	uvLA-Biotin	8963	8963	6.65
2	252[4]	bLA-Biotin	8911	8911	7.47
3	221[2]	bLA-Biotin	8299	8300	7.42
4	169[4]	bLA-Biotin	7634	7634	7.52
5	229[1]	bLA-Biotin	7302	7303	7.54

Table 7-13: Terminal amine-modified ASOs and their masses after deconvolution as measured by LCMS.

Entry	Oligonucleotide	Mass after Deconvolution	Expected Mass
1	1PSEt	6265	6265
2	1PSNV	6431	6431
3	6PSNV	7487	7486
4	9PSNV	8121	8120
5	20nt-TxRd-6PSNV	8368	8368
6	20nt-TxRd-9PSNV	9002	9001
7	14nt-TxRd-6PSNV	6473	6473

Table 7-14: Nitroveratryl-modified PS-ASOs and their masses after deconvolution as measured by LCMS.

7.4 Python Function for Hairpin Search

```
def hairpin(input_DNA, filename):

    ''' Reverse Complement'''
    tab = str.maketrans("ACTG", "TGAC") #Makes Complement
    def reverse_complement_table(seq): #Reverses Sequence
        return seq.translate(tab)[::-1]

    arr = np.empty((0,7))

    ''' ASO parameters'''
    len_overlap = (a, b)
    len_aso = (c, d)

    ''' Iteration'''
    for j in range(len_overlap[0], len_overlap[-1]+1):
        for k in range(len_aso[0], len_aso[-1]+1):
            for i in range(0, len(input_DNA)-j):
                q=(input_DNA[i:i+j])
                RC = reverse_complement_table(q)
                if input_DNA[i+k+j:i+k+2*j] == RC:
                    x = np.array([j, i+1, q, k, input_DNA[i+j:i+k+j], i+1+k, RC])
                    arr = np.vstack([arr, x])

    ''' Save File'''
    df = pd.DataFrame(data=arr, columns=["Overlap Length", "Start Site", "Start Sequence", "Spacer Length", "Spacer Sequence", "Complementary Site", "Reverse Complement"])
    df.to_csv(filename + '.csv')
```

8 REFERENCES

(1) *Nucleic Acids in Chemistry and Biology*; Royal Society of Chemistry, 2007. https://doi.org/10.1039/9781847555380.

(2) Elson, D.; Chargaff, E. On the Desoxyribonucleic Acid Content of Sea Urchin Gametes. *Experientia* **1952**, *8* (4), 143–145. https://doi.org/10.1007/BF02170221.

(3) Astbury, W. T.; Bell, F. O. X-Ray Study of Thymonucleic Acid [3]. *Nature* **1938**, *141* (3573), 747–748. https://doi.org/10.1038/141747b0.

(4) Wilkins, M. H. F.; Stokes, A. R.; Wilson, H. R. Molecular Structure of Nucleic Acids: Molecular Structure of Deoxypentose Nucleic Acids. *Nature* **1953**, *171* (4356), 738–740. https://doi.org/10.1038/171738a0.

(5) Franklin, R. E.; Gosling, R. G. Molecular Configuration in Sodium Thymonucleate. *Nature* **1953**, *171* (4356), 740–741. https://doi.org/10.1038/171740a0.

(6) Watson, J. D.; Crick, F. H. C. Molecular Structure of Nucleic Acids: A Structure for Deoxyribose Nucleic Acid. *Nature* **1953**, *171* (4356), 737–738. https://doi.org/10.1038/171737a0.

(7) Hartmann, B.; Lavery, R. DNA Structural Forms. *Q. Rev. Biophys.* **1996**, *29* (4), 309–368. https://doi.org/10.1017/s0033583500005874.

(8) Plectonemic Coils. In *Encyclopedia of Genetics, Genomics, Proteomics and Informatics*; Rédei, G. P., Ed.; Springer Netherlands: Dordrecht, 2008; pp 1512–1512. https://doi.org/10.1007/978-1-4020-6754-9_13032.

(9) Sinden, R. R. CHAPTER 1 - Introduction to the Structure, Properties, and Reactions of DNA. In *DNA Structure and Function*; Sinden, R. R., Ed.; Academic Press: San Diego, 1994; pp 1–57. https://doi.org/10.1016/B978-0-08-057173-7.50006-7.

(10) Dickerson, R. E.; Drew, H. R.; Conner, B. N.; Wing, R. M.; Fratini, A. V.; Kopka, M. L. The Anatomy of A-, B-, and Z-DNA. *Science* **1982**, *216* (4545), 475–485. https://doi.org/10.1126/science.7071593.

(11) Chan, K. Y.; Kinghorn, A. B.; Hollenstein, M.; Tanner, J. A. Chemical Modifications for a Next Generation of Nucleic Acid Aptamers. *ChemBioChem* **2022**, *23* (15), e202200006. https://doi.org/10.1002/cbic.202200006.

(12) Minchin, S.; Lodge, J. Understanding Biochemistry: Structure and Function of Nucleic Acids. *Essays Biochem.* **2019**, *63* (4), 433–456. https://doi.org/10.1042/EBC20180038.

(13) Garvie, C. W.; Wolberger, C. Recognition of Specific DNA Sequences. *Mol. Cell* **2001**, *8* (5), 937–946. https://doi.org/10.1016/S1097-2765(01)00392-6.

(14) Jakubec, D.; Laskowski, R. A.; Vondrasek, J. Sequence-Specific Recognition of DNA by Proteins: Binding Motifs Discovered Using a Novel Statistical/Computational Analysis. *PLOS ONE* **2016**, *11* (7), e0158704. https://doi.org/10.1371/journal.pone.0158704.

(15) Rohs, R.; Jin, X.; West, S. M.; Joshi, R.; Honig, B.; Mann, R. S. Origins of Specificity in Protein-DNA Recognition. *Annu. Rev. Biochem.* **2010**, *79* (1), 233–269. https://doi.org/10.1146/annurev-biochem-060408-091030.

(16) Bewley, C. A.; Gronenborn, A. M.; Clore, G. M. MINOR GROOVE-BINDING ARCHITECTURAL PROTEINS: Structure, Function, and DNA Recognition. *Annu. Rev. Biophys. Biomol. Struct.* **1998**, *27* (1), 105–131. https://doi.org/10.1146/annurev.biophys.27.1.105.
(17) Pierce, B. A. *Genetics: A Conceptual Approach*, 2nd Edition.; W. H. Freeman: New York, NY, 2012.
(18) Brown, T. A. *Genomes*, 2nd ed.; Wiley-Liss: Oxford, 2002.
(19) Pellicer, J.; Fay, M. F.; Leitch, I. J. The Largest Eukaryotic Genome of Them All? *Bot. J. Linn. Soc.* **2010**, *164* (1), 10–15. https://doi.org/10.1111/j.1095-8339.2010.01072.x.
(20) Wang, W.; Li, G.-W.; Chen, C.; Xie, X. S.; Zhuang, X. Chromosome Organization by a Nucleoid-Associated Protein in Live Bacteria. *Science* **2011**, *333* (6048), 1445–1449. https://doi.org/10.1126/science.1204697.
(21) Esser, K.; Kück, U.; Lang-Hinrichs, C.; Lemke, P.; Osiewacz, H. D.; Stahl, U.; Tudzynski, P. *Plasmids of Eukaryotes*; Heidelberg Science Library; Springer: Berlin, Heidelberg, 1986. https://doi.org/10.1007/978-3-642-82585-9.
(22) Rodríguez-Beltrán, J.; DelaFuente, J.; León-Sampedro, R.; MacLean, R. C.; San Millán, Á. Beyond Horizontal Gene Transfer: The Role of Plasmids in Bacterial Evolution. *Nat. Rev. Microbiol.* **2021**, *19* (6), 347–359. https://doi.org/10.1038/s41579-020-00497-1.
(23) Cobb, M. 60 Years Ago, Francis Crick Changed the Logic of Biology. *PLOS Biol.* **2017**, *15* (9), e2003243. https://doi.org/10.1371/journal.pbio.2003243.
(24) Crick, F. H. C.; Barnett, L.; Brenner, S.; Watts-Tobin, R. J. General Nature of the Genetic Code for Proteins. *Nature* **1961**, *192* (4809), 1227–1232. https://doi.org/10.1038/1921227a0.
(25) Nirenberg, M. W.; Matthaei, J. H. The Dependence of Cell-Free Protein Synthesis in E. Coli upon Naturally Occurring or Synthetic Polyribonucleotides. *Proc. Natl. Acad. Sci. U. S. A.* **1961**, *47*, 1588–1602. https://doi.org/10.1073/pnas.47.10.1588.
(26) Kearse, M. G.; Wilusz, J. E. Non-AUG Translation: A New Start for Protein Synthesis in Eukaryotes. *Genes Dev.* **2017**, *31* (17), 1717–1731. https://doi.org/10.1101/gad.305250.117.
(27) Plotkin, J. B.; Kudla, G. Synonymous but Not the Same: The Causes and Consequences of Codon Bias. *Nat. Rev. Genet.* **2011**, *12* (1), 32–42. https://doi.org/10.1038/nrg2899.
(28) Botzman, M.; Margalit, H. Variation in Global Codon Usage Bias among Prokaryotic Organisms Is Associated with Their Lifestyles. *Genome Biol.* **2011**, *12* (10), R109. https://doi.org/10.1186/gb-2011-12-10-r109.
(29) Jukes, T. H.; Osawa, S. Evolutionary Changes in the Genetic Code. *Comp. Biochem. Physiol. Part B Comp. Biochem.* **1993**, *106* (3), 489–494. https://doi.org/10.1016/0305-0491(93)90122-L.
(30) Clark-Walker, G. D.; Weiller, G. F. The Structure of the Small Mitochondrial DNA of Kluyveromyces Thermotolerans Is Likely to Reflect the Ancestral Gene Order in Fungi. *J. Mol. Evol.* **1994**, *38* (6), 593–601. https://doi.org/10.1007/BF00175879.
(31) Temperley, R.; Richter, R.; Dennerlein, S.; Lightowlers, R. N.; Chrzanowska-Lightowlers, Z. M. Hungry Codons Promote Frameshifting in Human Mitochondrial Ribosomes. *Science* **2010**, *327* (5963), 301–301. https://doi.org/10.1126/science.1180674.

(32) Kute, P. M.; Soukarieh, O.; Tjeldnes, H.; Trégouët, D.-A.; Valen, E. Small Open Reading Frames, How to Find Them and Determine Their Function. *Front. Genet.* **2022**, *12*.
(33) Garrett, R. H.; Grisham, C. M. *Biochemistry*, 6th ed.; Brooks Cole, 2016.
(34) Miller, O. L.; Hamkalo, B. A.; Thomas, C. A. Visualization of Bacterial Genes in Action. *Science* **1970**, *169* (3943), 392–395. https://doi.org/10.1126/science.169.3943.392.
(35) Cooper, G. M. Eukaryotic RNA Polymerases and General Transcription Factors. *Cell Mol. Approach 2nd Ed.* **2000**.
(36) Thomas Shafee; Shafee, T.; Lowe, R. Eukaryotic and Prokaryotic Gene Structure. *WikiJournal Med.* **2017**, *4* (1). https://doi.org/10.15347/WJM/2017.002.
(37) Jurado, A. R.; Tan, D.; Jiao, X.; Kiledjian, M.; Tong, L. Structure and Function of Pre-MRNA 5′-End Capping Quality Control and 3′-End Processing. *Biochemistry* **2014**, *53* (12), 1882–1898. https://doi.org/10.1021/bi401715v.
(38) Shatkin, A. J. Capping of Eucaryotic MRNAs. *Cell* **1976**, *9* (4, Part 2), 645–653. https://doi.org/10.1016/0092-8674(76)90128-8.
(39) Proudfoot, N. J. Ending the Message: Poly(A) Signals Then and Now. *Genes Dev.* **2011**, *25* (17), 1770–1782. https://doi.org/10.1101/gad.17268411.
(40) Yang, X.; Coulombe-Huntington, J.; Kang, S.; Sheynkman, G. M.; Hao, T.; Richardson, A.; Sun, S.; Yang, F.; Shen, Y. A.; Murray, R. R.; Spirohn, K.; Begg, B. E.; Duran-Frigola, M.; MacWilliams, A.; Pevzner, S. J.; Zhong, Q.; Trigg, S. A.; Tam, S.; Ghamsari, L.; Sahni, N.; Yi, S.; Rodriguez, M. D.; Balcha, D.; Tan, G.; Costanzo, M.; Andrews, B.; Boone, C.; Zhou, X. J.; Salehi-Ashtiani, K.; Charloteaux, B.; Chen, A. A.; Calderwood, M. A.; Aloy, P.; Roth, F. P.; Hill, D. E.; Iakoucheva, L. M.; Xia, Y.; Vidal, M. Widespread Expansion of Protein Interaction Capabilities by Alternative Splicing. *Cell* **2016**, *164* (4), 805–817. https://doi.org/10.1016/j.cell.2016.01.029.
(41) Wang, W.; Li, Y.; Wang, Y.; Shi, C.; Li, C.; Li, Q.; Linhardt, R. J. Bacteriophage T7 Transcription System: An Enabling Tool in Synthetic Biology. *Biotechnol. Adv.* **2018**, *36* (8), 2129–2137. https://doi.org/10.1016/j.biotechadv.2018.10.001.
(42) Rong, M.; He, B.; McAllister, W. T.; Durbin, R. K. Promoter Specificity Determinants of T7 RNA Polymerase. *Proc. Natl. Acad. Sci.* **1998**, *95* (2), 515–519. https://doi.org/10.1073/pnas.95.2.515.
(43) Calvopina-Chavez, D. G.; Gardner, M. A.; Griffitts, J. S. Engineering Efficient Termination of Bacteriophage T7 RNA Polymerase Transcription. *G3 GenesGenomesGenetics* **2022**, *12* (6), jkac070. https://doi.org/10.1093/g3journal/jkac070.
(44) Chao, Y.-P.; Chiang, C.-J.; Hung, W.-B. Stringent Regulation and High-Level Expression of Heterologous Genes in Escherichiacoli Using T7 System Controllable by the AraBAD Promoter. *Biotechnol. Prog.* **2002**, *18* (2), 394–400. https://doi.org/10.1021/bp0101785.
(45) Chao, Y.-P.; Law, W.-S.; Chen, P.; Hung, W.-B. High Production of Heterologous Proteins in Escherichia Coli Using the Thermo-Regulated T7 Expression System. *Appl. Microbiol. Biotechnol.* **2002**, *58* (4), 446–453. https://doi.org/10.1007/s00253-001-0891-6.
(46) Dubendorf, J. W.; Studier, F. W. Controlling Basal Expression in an Inducible T7 Expression System by Blocking the Target T7 Promoter with Lac Repressor. *J. Mol. Biol.* **1991**, *219* (1), 45–59. https://doi.org/10.1016/0022-2836(91)90856-2.

(47) Le Quesne, J. P.; Spriggs, K. A.; Bushell, M.; Willis, A. E. Dysregulation of Protein Synthesis and Disease. *J. Pathol.* **2010**, *220* (2), 140–151. https://doi.org/10.1002/path.2627.
(48) Alberts, B. *Molecular Biology of the Cell*, Sixth edition.; Garland Science, Taylor and Francis Group: New York, NY, 2015.
(49) Kulkarni, J. A.; Witzigmann, D.; Thomson, S. B.; Chen, S.; Leavitt, B. R.; Cullis, P. R.; van der Meel, R. The Current Landscape of Nucleic Acid Therapeutics. *Nat. Nanotechnol.* **2021**, *16* (6), 630–643. https://doi.org/10.1038/s41565-021-00898-0.
(50) Jacob, F.; Monod, J. On the Regulation of Gene Activity. *Cold Spring Harb. Symp. Quant. Biol.* **1961**, *26*, 193–211. https://doi.org/10.1101/SQB.1961.026.01.024.
(51) Helmann, J. D. Gene Expression and Its Regulation. In *Modern Microbial Genetics*; John Wiley & Sons, Ltd, 2002; pp 47–84. https://doi.org/10.1002/047122197X.ch3.
(52) Lawrence, J. G. Shared Strategies in Gene Organization among Prokaryotes and Eukaryotes. *Cell* **2002**, *110* (4), 407–413. https://doi.org/10.1016/S0092-8674(02)00900-5.
(53) Roy, S.; Garges, S.; Adhya, S. Activation and Repression of Transcription by Differential Contact: Two Sides of a Coin*. *J. Biol. Chem.* **1998**, *273* (23), 14059–14062. https://doi.org/10.1074/jbc.273.23.14059.
(54) Busby, S.; Ebright, R. H. Transcription Activation by Catabolite Activator Protein (CAP). *J. Mol. Biol.* **1999**, *293* (2), 199–213. https://doi.org/10.1006/jmbi.1999.3161.
(55) Bannister, A. J.; Kouzarides, T. Regulation of Chromatin by Histone Modifications. *Cell Res.* **2011**, *21* (3), 381–395. https://doi.org/10.1038/cr.2011.22.
(56) Zamecnik, P. C.; Stephenson, M. L. Inhibition of Rous Sarcoma Virus Replication and Cell Transformation by a Specific Oligodeoxynucleotide. *Proc. Natl. Acad. Sci.* **1978**, *75* (1), 280–284. https://doi.org/10.1073/pnas.75.1.280.
(57) Rinaldi, C.; Wood, M. J. A. Antisense Oligonucleotides: The next Frontier for Treatment of Neurological Disorders. *Nat. Rev. Neurol.* **2018**, *14* (1), 9–21. https://doi.org/10.1038/nrneurol.2017.148.
(58) Cerritelli, S. M.; Crouch, R. J. Ribonuclease H: The Enzymes in Eukaryotes. *FEBS J.* **2009**, *276* (6), 1494–1505. https://doi.org/10.1111/j.1742-4658.2009.06908.x.
(59) Wu, H.; Lima, W. F.; Zhang, H.; Fan, A.; Sun, H.; Crooke, S. T. Determination of the Role of the Human RNase H1 in the Pharmacology of DNA-like Antisense Drugs*. *J. Biol. Chem.* **2004**, *279* (17), 17181–17189. https://doi.org/10.1074/jbc.M311683200.
(60) Liang, X.-H.; Sun, H.; Nichols, J. G.; Crooke, S. T. RNase H1-Dependent Antisense Oligonucleotides Are Robustly Active in Directing RNA Cleavage in Both the Cytoplasm and the Nucleus. *Mol. Ther.* **2017**, *25* (9), 2075–2092. https://doi.org/10.1016/j.ymthe.2017.06.002.
(61) Roberts, T. C.; Langer, R.; Wood, M. J. A. Advances in Oligonucleotide Drug Delivery. *Nat. Rev. Drug Discov.* **2020**, *19* (10), 673–694. https://doi.org/10.1038/s41573-020-0075-7.
(62) Nan, Y.; Zhang, Y.-J. Antisense Phosphorodiamidate Morpholino Oligomers as Novel Antiviral Compounds. *Front. Microbiol.* **2018**, *9*.
(63) Lee, H. T.; Kim, S. K.; Yoon, J. W. Antisense Peptide Nucleic Acids as a Potential Anti-Infective Agent. *J. Microbiol.* **2019**, *57* (6), 423–430. https://doi.org/10.1007/s12275-019-8635-4.

(64) Braasch, D. A.; Corey, D. R. Locked Nucleic Acid (LNA): Fine-Tuning the Recognition of DNA and RNA. *Chem. Biol.* **2001**, *8* (1), 1–7. https://doi.org/10.1016/S1074-5521(00)00058-2.
(65) Yoo, B. H.; Bochkareva, E.; Bochkarev, A.; Mou, T.; Gray, D. M. 2′-O-methyl-modified Phosphorothioate Antisense Oligonucleotides Have Reduced Non-specific Effects in Vitro. *Nucleic Acids Res.* **2004**, *32* (6), 2008–2016. https://doi.org/10.1093/nar/gkh516.
(66) Aartsma-Rus, A.; Straub, V.; Hemmings, R.; Haas, M.; Schlosser-Weber, G.; Stoyanova-Beninska, V.; Mercuri, E.; Muntoni, F.; Sepodes, B.; Vroom, E.; Balabanov, P. Development of Exon Skipping Therapies for Duchenne Muscular Dystrophy: A Critical Review and a Perspective on the Outstanding Issues. *Nucleic Acid Ther.* **2017**, *27* (5), 251–259. https://doi.org/10.1089/nat.2017.0682.
(67) Ward, A. J.; Norrbom, M.; Chun, S.; Bennett, C. F.; Rigo, F. Nonsense-Mediated Decay as a Terminating Mechanism for Antisense Oligonucleotides. *Nucleic Acids Res.* **2014**, *42* (9), 5871–5879. https://doi.org/10.1093/nar/gku184.
(68) Boiziau, C.; Kurfurst, R.; Cazenave, C.; Roig, V.; Thuong, N. T.; Toulmé, J.-J. Inhibition of Translation Initiation by Antisense Oligonucleotides via an RNase-H Independent Mechanism. *Nucleic Acids Res.* **1991**, *19* (5), 1113–1119. https://doi.org/10.1093/nar/19.5.1113.
(69) Baker, B. F.; Lot, S. S.; Condon, T. P.; Cheng-Flournoy, S.; Lesnik, E. A.; Sasmor, H. M.; Bennett, C. F. 2′-O-(2-Methoxy)Ethyl-Modified Anti-Intercellular Adhesion Molecule 1 (ICAM-1) Oligonucleotides Selectively Increase the ICAM-1 MRNA Level and Inhibit Formation of the ICAM-1 Translation Initiation Complex in Human Umbilical Vein Endothelial Cells*. *J. Biol. Chem.* **1997**, *272* (18), 11994–12000. https://doi.org/10.1074/jbc.272.18.11994.
(70) Calvo, S. E.; Pagliarini, D. J.; Mootha, V. K. Upstream Open Reading Frames Cause Widespread Reduction of Protein Expression and Are Polymorphic among Humans. *Proc. Natl. Acad. Sci.* **2009**, *106* (18), 7507–7512. https://doi.org/10.1073/pnas.0810916106.
(71) Liang, X.; Shen, W.; Sun, H.; Migawa, M. T.; Vickers, T. A.; Crooke, S. T. Translation Efficiency of MRNAs Is Increased by Antisense Oligonucleotides Targeting Upstream Open Reading Frames. *Nat. Biotechnol.* **2016**, *34* (8), 875–880. https://doi.org/10.1038/nbt.3589.
(72) Nomakuchi, T. T.; Rigo, F.; Aznarez, I.; Krainer, A. R. Antisense Oligonucleotide–Directed Inhibition of Nonsense-Mediated MRNA Decay. *Nat. Biotechnol.* **2016**, *34* (2), 164–166. https://doi.org/10.1038/nbt.3427.
(73) Vickers, T. A.; Wyatt, J. R.; Burckin, T.; Bennett, C. F.; Freier, S. M. Fully Modified 2′ MOE Oligonucleotides Redirect Polyadenylation. *Nucleic Acids Res.* **2001**, *29* (6), 1293–1299.
(74) Fire, A.; Xu, S.; Montgomery, M. K.; Kostas, S. A.; Driver, S. E.; Mello, C. C. Potent and Specific Genetic Interference by Double-Stranded RNA in Caenorhabditis Elegans. *Nature* **1998**, *391* (6669), 806–811. https://doi.org/10.1038/35888.
(75) Elbashir, S. M.; Harborth, J.; Lendeckel, W.; Yalcin, A.; Weber, K.; Tuschl, T. Duplexes of 21-Nucleotide RNAs Mediate RNA Interference in Cultured Mammalian Cells. *Nature* **2001**, *411* (6836), 494–498. https://doi.org/10.1038/35078107.
(76) Caplen, N. J.; Parrish, S.; Imani, F.; Fire, A.; Morgan, R. A. Specific Inhibition of Gene Expression by Small Double-Stranded RNAs in Invertebrate and Vertebrate

Systems. *Proc. Natl. Acad. Sci.* **2001**, *98* (17), 9742–9747. https://doi.org/10.1073/pnas.171251798.
(77) Liu, J.; Carmell, M. A.; Rivas, F. V.; Marsden, C. G.; Thomson, J. M.; Song, J.-J.; Hammond, S. M.; Joshua-Tor, L.; Hannon, G. J. Argonaute2 Is the Catalytic Engine of Mammalian RNAi. *Science* **2004**, *305* (5689), 1437–1441. https://doi.org/10.1126/science.1102513.
(78) Kim, D.-H.; Behlke, M. A.; Rose, S. D.; Chang, M.-S.; Choi, S.; Rossi, J. J. Synthetic DsRNA Dicer Substrates Enhance RNAi Potency and Efficacy. *Nat. Biotechnol.* **2005**, *23* (2), 222–226. https://doi.org/10.1038/nbt1051.
(79) Svoronos, A. A.; Engelman, D. M.; Slack, F. J. OncomiR or Tumor Suppressor? The Duplicity of MicroRNAs in Cancer. *Cancer Res.* **2016**, *76* (13), 3666–3670. https://doi.org/10.1158/0008-5472.CAN-16-0359.
(80) Bueno, M. J.; Malumbres, M. MicroRNAs and the Cell Cycle. *Biochim. Biophys. Acta BBA - Mol. Basis Dis.* **2011**, *1812* (5), 592–601. https://doi.org/10.1016/j.bbadis.2011.02.002.
(81) Cacchiarelli, D.; Martone, J.; Girardi, E.; Cesana, M.; Incitti, T.; Morlando, M.; Nicoletti, C.; Santini, T.; Sthandier, O.; Barberi, L.; Auricchio, A.; Musarò, A.; Bozzoni, I. MicroRNAs Involved in Molecular Circuitries Relevant for the Duchenne Muscular Dystrophy Pathogenesis Are Controlled by the Dystrophin/NNOS Pathway. *Cell Metab.* **2010**, *12* (4), 341–351. https://doi.org/10.1016/j.cmet.2010.07.008.
(82) Pordzik, J.; Jakubik, D.; Jarosz-Popek, J.; Wicik, Z.; Eyileten, C.; De Rosa, S.; Indolfi, C.; Siller-Matula, J. M.; Czajka, P.; Postula, M. Significance of Circulating MicroRNAs in Diabetes Mellitus Type 2 and Platelet Reactivity: Bioinformatic Analysis and Review. *Cardiovasc. Diabetol.* **2019**, *18* (1), 113. https://doi.org/10.1186/s12933-019-0918-x.
(83) Roberts, T. C. The MicroRNA Machinery. In *microRNA: Basic Science: From Molecular Biology to Clinical Practice*; Santulli, G., Ed.; Advances in Experimental Medicine and Biology; Springer International Publishing: Cham, 2015; pp 15–30. https://doi.org/10.1007/978-3-319-22380-3_2.
(84) Provost, P.; Dishart, D.; Doucet, J.; Frendewey, D.; Samuelsson, B.; Rådmark, O. Ribonuclease Activity and RNA Binding of Recombinant Human Dicer. *EMBO J.* **2002**, *21* (21), 5864–5874. https://doi.org/10.1093/emboj/cdf578.
(85) Lee, Y.; Ahn, C.; Han, J.; Choi, H.; Kim, J.; Yim, J.; Lee, J.; Provost, P.; Rådmark, O.; Kim, S.; Kim, V. N. The Nuclear RNase III Drosha Initiates MicroRNA Processing. *Nature* **2003**, *425* (6956), 415–419. https://doi.org/10.1038/nature01957.
(86) Guo, H.; Ingolia, N. T.; Weissman, J. S.; Bartel, D. P. Mammalian MicroRNAs Predominantly Act to Decrease Target MRNA Levels. *Nature* **2010**, *466* (7308), 835–840. https://doi.org/10.1038/nature09267.
(87) Filipowicz, W.; Bhattacharyya, S. N.; Sonenberg, N. Mechanisms of Post-Transcriptional Regulation by MicroRNAs: Are the Answers in Sight? *Nat. Rev. Genet.* **2008**, *9* (2), 102–114. https://doi.org/10.1038/nrg2290.
(88) Peng, Y.; Croce, C. M. The Role of MicroRNAs in Human Cancer. *Signal Transduct. Target. Ther.* **2016**, *1* (1), 1–9. https://doi.org/10.1038/sigtrans.2015.4.
(89) Rupani, H.; Sanchez-Elsner, T.; Howarth, P. MicroRNAs and Respiratory Diseases. *Eur. Respir. J.* **2013**, *41* (3), 695–705. https://doi.org/10.1183/09031936.00212011.
(90) Intartaglia, D.; Giamundo, G.; Conte, I. The Impact of MiRNAs in Health and Disease of Retinal Pigment Epithelium. *Front. Cell Dev. Biol.* **2021**, *8*.

(91) Roberts, T. C.; Wood, M. J. A. Therapeutic Targeting of Non-Coding RNAs. *Essays Biochem.* **2013**, *54*, 127–145. https://doi.org/10.1042/bse0540127.
(92) Krützfeldt, J.; Rajewsky, N.; Braich, R.; Rajeev, K. G.; Tuschl, T.; Manoharan, M.; Stoffel, M. Silencing of MicroRNAs in Vivo with 'Antagomirs.' *Nature* **2005**, *438* (7068), 685–689. https://doi.org/10.1038/nature04303.
(93) Wan, W. B.; Seth, P. P. The Medicinal Chemistry of Therapeutic Oligonucleotides. *J. Med. Chem.* **2016**, *59* (21), 9645–9667. https://doi.org/10.1021/acs.jmedchem.6b00551.
(94) Kurreck, J.; Wyszko, E.; Gillen, C.; Erdmann, V. A. Design of Antisense Oligonucleotides Stabilized by Locked Nucleic Acids. *Nucleic Acids Res.* **2002**, *30* (9), 1911–1918. https://doi.org/10.1093/nar/30.9.1911.
(95) Frieden, M.; Christensen, S. M.; Mikkelsen, N. D.; Rosenbohm, C.; Thrue, C. A.; Westergaard, M.; Hansen, H. F.; Ørum, H.; Koch, T. Expanding the Design Horizon of Antisense Oligonucleotides with Alpha-l-LNA. *Nucleic Acids Res.* **2003**, *31* (21), 6365–6372. https://doi.org/10.1093/nar/gkg820.
(96) Frieden, M.; Hansen, H. F.; Koch, T. Nuclease Stability of LNA Oligonucleotides and LNA-DNA Chimeras. *Nucleosides Nucleotides Nucleic Acids* **2003**, *22* (5–8), 1041–1043. https://doi.org/10.1081/NCN-120022731.
(97) Chen, S.; Le, B. T.; Chakravarthy, M.; Kosbar, T. R.; Veedu, R. N. Systematic Evaluation of 2′-Fluoro Modified Chimeric Antisense Oligonucleotide-Mediated Exon Skipping in Vitro. *Sci. Rep.* **2019**, *9* (1), 6078. https://doi.org/10.1038/s41598-019-42523-0.
(98) Verma, S.; Eckstein, F. MODIFIED OLIGONUCLEOTIDES: Synthesis and Strategy for Users. *Annu. Rev. Biochem.* **1998**, *67* (1), 99–134. https://doi.org/10.1146/annurev.biochem.67.1.99.
(99) Eckstein, F. Phosphorothioates, Essential Components of Therapeutic Oligonucleotides. *Nucleic Acid Ther.* **2014**, *24* (6), 374–387. https://doi.org/10.1089/nat.2014.0506.
(100) Braasch, D. A.; Jensen, S.; Liu, Y.; Kaur, K.; Arar, K.; White, M. A.; Corey, D. R. RNA Interference in Mammalian Cells by Chemically-Modified RNA. *Biochemistry* **2003**, *42* (26), 7967–7975. https://doi.org/10.1021/bi0343774.
(101) Swenson, C. S.; Lackey, H. H.; Reece, E. J.; Harris, J. M.; Heemstra, J. M.; Peterson, E. M. Evaluating the Effect of Ionic Strength on PNA:DNA Duplex Formation Kinetics. *RSC Chem. Biol.* **2021**, *2* (4), 1249–1256. https://doi.org/10.1039/D1CB00025J.
(102) Stein, D.; Foster, E.; Huang, S.-B.; Weller, D.; Summerton, J. A Specificity Comparison of Four Antisense Types: Morpholino, 2′-O-Methyl RNA, DNA, and Phosphorothioate DNA. *Antisense Nucleic Acid Drug Dev.* **1997**, *7* (3), 151–157. https://doi.org/10.1089/oli.1.1997.7.151.
(103) Epple, S.; Thorpe, C.; Baker, Y. R.; El-Sagheer, A. H.; Brown, T. Consecutive 5′- And 3′-Amide Linkages Stabilise Antisense Oligonucleotides and Elicit an Efficient RNase H Response. *Chem. Commun.* **2020**, *56* (41), 5496–5499. https://doi.org/10.1039/d0cc00444h.
(104) Henry, S.; Stecker, K.; Brooks, D.; Monteith, D.; Conklin, B.; Bennett, C. F. Chemically Modified Oligonucleotides Exhibit Decreased Immune Stimulation in Mice. *J. Pharmacol. Exp. Ther.* **2000**, *292* (2), 468–479.
(105) Wagner, R. W.; Matteucci, M. D.; Lewis, J. G.; Gutierrez, A. J.; Moulds, C.; Froehler, B. C. Antisense Gene Inhibition by Oligonucleotides Containing C-5 Propyne Pyrimidines. *Science* **1993**, *260* (5113), 1510–1513. https://doi.org/10.1126/science.7684856.

(106) Lin, K.-Y.; Jones, R. J.; Matteucci, M. Tricyclic 2'-Deoxycytidine Analogs: Syntheses and Incorporation into Oligodeoxynucleotides Which Have Enhanced Binding to Complementary RNA. *J. Am. Chem. Soc.* **1995**, *117* (13), 3873–3874. https://doi.org/10.1021/ja00118a026.

(107) Flanagan, W. M.; Wolf, J. J.; Olson, P.; Grant, D.; Lin, K.-Y.; Wagner, R. W.; Matteucci, M. D. A Cytosine Analog That Confers Enhanced Potency to Antisense Oligonucleotides. *Proc. Natl. Acad. Sci.* **1999**, *96* (7), 3513–3518. https://doi.org/10.1073/pnas.96.7.3513.

(108) Wilds, C. J.; Maier, M. A.; Tereshko, V.; Manoharan, M.; Egli, M. Direct Observation of a Cytosine Analogue That Forms Five Hydrogen Bonds to Guanosine: Guanidino G-Clamp. *Angew. Chem. Int. Ed.* **2002**, *41* (1), 115–117. https://doi.org/10.1002/1521-3773(20020104)41:1<115::AID-ANIE115>3.0.CO;2-R.

(109) Manoharan, M.; Ramasamy, K. S.; Mohan, V.; Cook, P. D. Oligonucleotides Bearing Cationic Groups: N2-(3-Aminopropyl)Deoxyguanosine. Synthesis, Enhanced Binding Properties and Conjugation Chemistry. *Tetrahedron Lett.* **1996**, *37* (43), 7675–7678. https://doi.org/10.1016/0040-4039(96)01755-8.

(110) Wolfrum, C.; Shi, S.; Jayaprakash, K. N.; Jayaraman, M.; Wang, G.; Pandey, R. K.; Rajeev, K. G.; Nakayama, T.; Charrise, K.; Ndungo, E. M.; Zimmermann, T.; Koteliansky, V.; Manoharan, M.; Stoffel, M. Mechanisms and Optimization of in Vivo Delivery of Lipophilic SiRNAs. *Nat. Biotechnol.* **2007**, *25* (10), 1149–1157. https://doi.org/10.1038/nbt1339.

(111) Soutschek, J.; Akinc, A.; Bramlage, B.; Charisse, K.; Constien, R.; Donoghue, M.; Elbashir, S.; Geick, A.; Hadwiger, P.; Harborth, J.; John, M.; Kesavan, V.; Lavine, G.; Pandey, R. K.; Racie, T.; Rajeev, K. G.; Röhl, I.; Toudjarska, I.; Wang, G.; Wuschko, S.; Bumcrot, D.; Koteliansky, V.; Limmer, S.; Manoharan, M.; Vornlocher, H.-P. Therapeutic Silencing of an Endogenous Gene by Systemic Administration of Modified SiRNAs. *Nature* **2004**, *432* (7014), 173–178. https://doi.org/10.1038/nature03121.

(112) Lorenz, C.; Hadwiger, P.; John, M.; Vornlocher, H.-P.; Unverzagt, C. Steroid and Lipid Conjugates of SiRNAs to Enhance Cellular Uptake and Gene Silencing in Liver Cells. *Bioorg. Med. Chem. Lett.* **2004**, *14* (19), 4975–4977. https://doi.org/10.1016/j.bmcl.2004.07.018.

(113) Eguchi, A.; Meade, B. R.; Chang, Y.-C.; Fredrickson, C. T.; Willert, K.; Puri, N.; Dowdy, S. F. Efficient SiRNA Delivery into Primary Cells by a Peptide Transduction Domain–DsRNA Binding Domain Fusion Protein. *Nat. Biotechnol.* **2009**, *27* (6), 567–571. https://doi.org/10.1038/nbt.1541.

(114) Betts, C.; Saleh, A. F.; Arzumanov, A. A.; Hammond, S. M.; Godfrey, C.; Coursindel, T.; Gait, M. J.; Wood, M. J. Pip6-PMO, A New Generation of Peptide-Oligonucleotide Conjugates With Improved Cardiac Exon Skipping Activity for DMD Treatment. *Mol. Ther. - Nucleic Acids* **2012**, *1*, e38. https://doi.org/10.1038/mtna.2012.30.

(115) Alam, Md. R.; Ming, X.; Fisher, M.; Lackey, J. G.; Rajeev, K. G.; Manoharan, M.; Juliano, R. L. Multivalent Cyclic RGD Conjugates for Targeted Delivery of Small Interfering RNA. *Bioconjug. Chem.* **2011**, *22* (8), 1673–1681. https://doi.org/10.1021/bc200235q.

(116) Ämmälä, C.; Drury, W. J.; Knerr, L.; Ahlstedt, I.; Stillemark-Billton, P.; Wennberg-Huldt, C.; Andersson, E.-M.; Valeur, E.; Jansson-Löfmark, R.; Janzén, D.; Sundström, L.; Meuller, J.; Claesson, J.; Andersson, P.; Johansson, C.; Lee, R. G.; Prakash, T. P.; Seth, P. P.; Monia, B. P.; Andersson, S. Targeted Delivery

of Antisense Oligonucleotides to Pancreatic β-Cells. *Sci. Adv.* **2018**, *4* (10), eaat3386. https://doi.org/10.1126/sciadv.aat3386.

(117) McNamara, J. O.; Andrechek, E. R.; Wang, Y.; Viles, K. D.; Rempel, R. E.; Gilboa, E.; Sullenger, B. A.; Giangrande, P. H. Cell Type–Specific Delivery of SiRNAs with Aptamer-SiRNA Chimeras. *Nat. Biotechnol.* **2006**, *24* (8), 1005–1015. https://doi.org/10.1038/nbt1223.

(118) Matsuda, S.; Keiser, K.; Nair, J. K.; Charisse, K.; Manoharan, R. M.; Kretschmer, P.; Peng, C. G.; V. Kel'in, A.; Kandasamy, P.; Willoughby, J. L. S.; Liebow, A.; Querbes, W.; Yucius, K.; Nguyen, T.; Milstein, S.; Maier, M. A.; Rajeev, K. G.; Manoharan, M. SiRNA Conjugates Carrying Sequentially Assembled Trivalent N-Acetylgalactosamine Linked Through Nucleosides Elicit Robust Gene Silencing In Vivo in Hepatocytes. *ACS Chem. Biol.* **2015**, *10* (5), 1181–1187. https://doi.org/10.1021/cb501028c.

(119) Nair, J. K.; Willoughby, J. L. S.; Chan, A.; Charisse, K.; Alam, Md. R.; Wang, Q.; Hoekstra, M.; Kandasamy, P.; Kel'in, A. V.; Milstein, S.; Taneja, N.; O'Shea, J.; Shaikh, S.; Zhang, L.; van der Sluis, R. J.; Jung, M. E.; Akinc, A.; Hutabarat, R.; Kuchimanchi, S.; Fitzgerald, K.; Zimmermann, T.; van Berkel, T. J. C.; Maier, M. A.; Rajeev, K. G.; Manoharan, M. Multivalent N-Acetylgalactosamine-Conjugated SiRNA Localizes in Hepatocytes and Elicits Robust RNAi-Mediated Gene Silencing. *J. Am. Chem. Soc.* **2014**, *136* (49), 16958–16961. https://doi.org/10.1021/ja505986a.

(120) Jiang, L.; Zhao, J.; Lian, J.; Xu, Z. Cell-Free Protein Synthesis Enabled Rapid Prototyping for Metabolic Engineering and Synthetic Biology. *Synth. Syst. Biotechnol.* **2018**, *3* (2), 90–96. https://doi.org/10.1016/j.synbio.2018.02.003.

(121) Guzman-Chavez, F.; Arce, A.; Adhikari, A.; Vadhin, S.; Pedroza-Garcia, J. A.; Gandini, C.; Ajioka, J. W.; Molloy, J.; Sanchez-Nieto, S.; Varner, J. D.; Federici, F.; Haseloff, J. Constructing Cell-Free Expression Systems for Low-Cost Access. *ACS Synth. Biol.* **2022**, *11* (3), 1114–1128. https://doi.org/10.1021/acssynbio.1c00342.

(122) Pardee, K. Perspective: Solidifying the Impact of Cell-Free Synthetic Biology through Lyophilization. *Biochem. Eng. J.* **2018**, *138*, 91–97. https://doi.org/10.1016/j.bej.2018.07.008.

(123) Sarnaik, A.; Mhatre, A.; Faisal, M.; Smith, D.; Davis, R.; Varman, A. M. Novel Perspective on a Conventional Technique: Impact of Ultra-Low Temperature on Bacterial Viability and Protein Extraction. *PLOS ONE* **2021**, *16* (5), e0251640. https://doi.org/10.1371/journal.pone.0251640.

(124) Schwarz, D.; Junge, F.; Durst, F.; Frölich, N.; Schneider, B.; Reckel, S.; Sobhanifar, S.; Dötsch, V.; Bernhard, F. Preparative Scale Expression of Membrane Proteins in Escherichia Coli-Based Continuous Exchange Cell-Free Systems. *Nat. Protoc.* **2007**, *2* (11), 2945–2957. https://doi.org/10.1038/nprot.2007.426.

(125) Garenne, D.; Haines, M. C.; Romantseva, E. F.; Freemont, P.; Strychalski, E. A.; Noireaux, V. Cell-Free Gene Expression. *Nat. Rev. Methods Primer* **2021**, *1* (1), 1–18. https://doi.org/10.1038/s43586-021-00046-x.

(126) Gregorio, N. E.; Levine, M. Z.; Oza, J. P. A User's Guide to Cell-Free Protein Synthesis. *Methods Protoc.* **2019**, *2* (1), 24. https://doi.org/10.3390/mps2010024.

(127) Garamella, J.; Marshall, R.; Rustad, M.; Noireaux, V. The All E. Coli TX-TL Toolbox 2.0: A Platform for Cell-Free Synthetic Biology. *ACS Synth. Biol.* **2016**, *5* (4), 344–355. https://doi.org/10.1021/acssynbio.5b00296.

(128) Smolskaya, S.; Logashina, Y. A.; Andreev, Y. A. Escherichia Coli Extract-Based Cell-Free Expression System as an Alternative for Difficult-to-Obtain Protein Biosynthesis. *Int. J. Mol. Sci.* **2020**, *21* (3), 928. https://doi.org/10.3390/ijms21030928.
(129) Harbers, M. Wheat Germ Systems for Cell-Free Protein Expression. *FEBS Lett.* **2014**, *588* (17), 2762–2773. https://doi.org/10.1016/j.febslet.2014.05.061.
(130) Tsuboi, T.; Takeo, S.; Arumugam, T. U.; Otsuki, H.; Torii, M. The Wheat Germ Cell-Free Protein Synthesis System: A Key Tool for Novel Malaria Vaccine Candidate Discovery. *Acta Trop.* **2010**, *114* (3), 171–176. https://doi.org/10.1016/j.actatropica.2009.10.024.
(131) Gan, R.; Jewett, M. C. A Combined Cell-Free Transcription-Translation System from Saccharomyces Cerevisiae for Rapid and Robust Protein Synthe. *Biotechnol. J.* **2014**, *9* (5), 641–651. https://doi.org/10.1002/biot.201300545.
(132) Wang, X.; Zhao, L.; Zhao, K.-N. An Optimized Yeast Cell-Free Lysate System for In Vitro Translation of Human Virus MRNA. In *Cell-Free Protein Synthesis: Methods and Protocols*; Alexandrov, K., Johnston, W. A., Eds.; Methods in Molecular Biology; Humana Press: Totowa, NJ, 2014; pp 219–230. https://doi.org/10.1007/978-1-62703-782-2_14.
(133) Ezure, T.; Suzuki, T.; Shikata, M.; Ito, M.; Ando, E. A Cell-Free Protein Synthesis System from Insect Cells. In *Cell-Free Protein Production: Methods and Protocols*; Endo, Y., Takai, K., Ueda, T., Eds.; Methods in Molecular Biology; Humana Press: Totowa, NJ, 2010; pp 31–42. https://doi.org/10.1007/978-1-60327-331-2_4.
(134) Korn, J.; Schäckermann, D.; Kirmann, T.; Bertoglio, F.; Steinke, S.; Heisig, J.; Ruschig, M.; Rojas, G.; Langreder, N.; Wenzel, E. V.; Roth, K. D. R.; Becker, M.; Meier, D.; van den Heuvel, J.; Hust, M.; Dübel, S.; Schubert, M. Baculovirus-Free Insect Cell Expression System for High Yield Antibody and Antigen Production. *Sci. Rep.* **2020**, *10* (1), 21393. https://doi.org/10.1038/s41598-020-78425-9.
(135) Oliver, C. L.; Boyd, C. D. In Vitro Translation of Messenger RNA in a Rabbit Reticulocyte Lysate Cell-Free System. In *Nucleic Acids*; Walker, J. M., Ed.; Methods in Molecular Biology; Humana Press: Totowa, NJ, 1984; pp 145–155. https://doi.org/10.1385/0-89603-064-4:145.
(136) Beckler, G. S.; Thompson, D.; Van Oosbree, T. In Vitro Translation Using Rabbit Reticulocyte Lysate. In *In Vitro Transcription and Translation Protocols*; Tymms, M. J., Ed.; Methods in Molecular Biology; Humana Press: Totowa, NJ, 1995; pp 215–232. https://doi.org/10.1385/0-89603-288-4:215.
(137) Craig, D.; Howell, M. T.; Gibbs, C. L.; Hunt, T.; Jackson, R. J. Plasmid CDNA-Directed Protein Synthesis in a Coupled Eukaryotic in Vitro Transcription-Translation System. *Nucleic Acids Res.* **1992**, *20* (19), 4987–4995. https://doi.org/10.1093/nar/20.19.4987.
(138) Brödel, A. K.; Sonnabend, A.; Kubick, S. Cell-Free Protein Expression Based on Extracts from CHO Cells. *Biotechnol. Bioeng.* **2014**, *111* (1), 25–36. https://doi.org/10.1002/bit.25013.
(139) Ho, K. K. Y.; Murray, V. L.; Liu, A. P. Chapter 16 - Engineering Artificial Cells by Combining HeLa-Based Cell-Free Expression and Ultrathin Double Emulsion Template. In *Methods in Cell Biology*; Ross, J., Marshall, W. F., Eds.; Building a Cell from its Component Parts; Academic Press, 2015; Vol. 128, pp 303–318. https://doi.org/10.1016/bs.mcb.2015.01.014.
(140) Des Soye, B. J.; Davidson, S. R.; Weinstock, M. T.; Gibson, D. G.; Jewett, M. C. Establishing a High-Yielding Cell-Free Protein Synthesis Platform Derived

from Vibrio Natriegens. *ACS Synth. Biol.* **2018**, *7* (9), 2245–2255. https://doi.org/10.1021/acssynbio.8b00252.

(141) Murota, K.; Hagiwara-Komoda, Y.; Komoda, K.; Onouchi, H.; Ishikawa, M.; Naito, S. Arabidopsis Cell-Free Extract, ACE, a New In Vitro Translation System Derived from Arabidopsis Callus Cultures. *Plant Cell Physiol.* **2011**, *52* (8), 1443–1453. https://doi.org/10.1093/pcp/pcr080.

(142) Buntru, M.; Vogel, S.; Spiegel, H.; Schillberg, S. Tobacco BY-2 Cell-Free Lysate: An Alternative and Highly-Productive Plant-Based in Vitro Translation System. *BMC Biotechnol.* **2014**, *14* (1), 37. https://doi.org/10.1186/1472-6750-14-37.

(143) Kelwick, R.; Webb, A. J.; MacDonald, J. T.; Freemont, P. S. Development of a Bacillus Subtilis Cell-Free Transcription-Translation System for Prototyping Regulatory Elements. *Metab. Eng.* **2016**, *38*, 370–381. https://doi.org/10.1016/j.ymben.2016.09.008.

(144) Silverman, A. D.; Karim, A. S.; Jewett, M. C. Cell-Free Gene Expression: An Expanded Repertoire of Applications. *Nat. Rev. Genet.* **2020**, *21* (3), 151–170. https://doi.org/10.1038/s41576-019-0186-3.

(145) Zemella, A.; Thoring, L.; Hoffmeister, C.; Kubick, S. Cell-Free Protein Synthesis: Pros and Cons of Prokaryotic and Eukaryotic Systems. *ChemBioChem* **2015**, *16* (17), 2420–2431. https://doi.org/10.1002/cbic.201500340.

(146) Dondapati, S. K.; Stech, M.; Zemella, A.; Kubick, S. Cell-Free Protein Synthesis: A Promising Option for Future Drug Development. *BioDrugs* **2020**, *34* (3), 327–348. https://doi.org/10.1007/s40259-020-00417-y.

(147) Guarino, C.; DeLisa, M. P. A Prokaryote-Based Cell-Free Translation System That Efficiently Synthesizes Glycoproteins. *Glycobiology* **2012**, *22* (5), 596–601. https://doi.org/10.1093/glycob/cwr151.

(148) Schoborg, J. A.; Hershewe, J. M.; Stark, J. C.; Kightlinger, W.; Kath, J. E.; Jaroentomeechai, T.; Natarajan, A.; DeLisa, M. P.; Jewett, M. C. A Cell-Free Platform for Rapid Synthesis and Testing of Active Oligosaccharyltransferases. *Biotechnol. Bioeng.* **2018**, *115* (3), 739–750. https://doi.org/10.1002/bit.26502.

(149) Jaroentomeechai, T.; Stark, J. C.; Natarajan, A.; Glasscock, C. J.; Yates, L. E.; Hsu, K. J.; Mrksich, M.; Jewett, M. C.; DeLisa, M. P. Single-Pot Glycoprotein Biosynthesis Using a Cell-Free Transcription-Translation System Enriched with Glycosylation Machinery. *Nat. Commun.* **2018**, *9* (1), 2686. https://doi.org/10.1038/s41467-018-05110-x.

(150) Michel, E.; Wüthrich, K. Cell-Free Expression of Disulfide-Containing Eukaryotic Proteins for Structural Biology. *FEBS J.* **2012**, *279* (17), 3176–3184. https://doi.org/10.1111/j.1742-4658.2012.08697.x.

(151) Kung, H. F.; Redfield, B.; Treadwell, B. V.; Eskin, B.; Spears, C.; Weissbach, H. DNA-Directed in Vitro Synthesis of Beta-Galactosidase. Studies with Purified Factors. *J. Biol. Chem.* **1977**, *252* (19), 6889–6894. https://doi.org/10.1016/S0021-9258(17)39933-7.

(152) Ganoza, M. C.; Cunningham, C.; Green, R. M. Isolation and Point of Action of a Factor from Escherichia Coli Required to Reconstruct Translation. *Proc. Natl. Acad. Sci.* **1985**, *82* (6), 1648–1652. https://doi.org/10.1073/pnas.82.6.1648.

(153) Pavlov, M. Yu.; Ehrenberg, M. Rate of Translation of Natural MRNAs in an Optimizedin VitroSystem. *Arch. Biochem. Biophys.* **1996**, *328* (1), 9–16. https://doi.org/10.1006/abbi.1996.0136.

(154) Pavlov, M. Y.; Freistroffer, D. V.; Heurgué-Hamard, V.; Buckingham, R. H.; Ehrenberg, M. Release Factor RF3 Abolishes Competition between Release Factor RF1 and Ribosome Recycling Factor (RRF) for a Ribosome Binding Site11Edited by D. E. Draper. *J. Mol. Biol.* **1997**, *273* (2), 389–401. https://doi.org/10.1006/jmbi.1997.1324.
(155) Shimizu, Y.; Inoue, A.; Tomari, Y.; Suzuki, T.; Yokogawa, T.; Nishikawa, K.; Ueda, T. Cell-Free Translation Reconstituted with Purified Components. *Nat. Biotechnol.* **2001**, *19* (8), 751–755. https://doi.org/10.1038/90802.
(156) Kuruma, Y.; Ueda, T. The PURE System for the Cell-Free Synthesis of Membrane Proteins. *Nat. Protoc.* **2015**, *10* (9), 1328–1344. https://doi.org/10.1038/nprot.2015.082.
(157) Lavickova, B.; Maerkl, S. J. A Simple, Robust, and Low-Cost Method to Produce the PURE Cell-Free System. *ACS Synth. Biol.* **2019**, *8* (2), 455–462. https://doi.org/10.1021/acssynbio.8b00427.
(158) Whittaker, J. W. Cell-Free Protein Synthesis: The State of the Art. *Biotechnol. Lett.* **2013**, *35* (2), 143–152. https://doi.org/10.1007/s10529-012-1075-4.
(159) Niwa, T.; Kanamori, T.; Ueda, T.; Taguchi, H. Global Analysis of Chaperone Effects Using a Reconstituted Cell-Free Translation System. *Proc. Natl. Acad. Sci.* **2012**, *109* (23), 8937–8942. https://doi.org/10.1073/pnas.1201380109.
(160) Tuckey, C.; Asahara, H.; Zhou, Y.; Chong, S. Protein Synthesis Using a Reconstituted Cell-Free System. *Curr. Protoc. Mol. Biol.* **2014**, *108* (1), 16.31.1-16.31.22. https://doi.org/10.1002/0471142727.mb1631s108.
(161) Sun, Z. Z.; Yeung, E.; Hayes, C. A.; Noireaux, V.; Murray, R. M. Linear DNA for Rapid Prototyping of Synthetic Biological Circuits in an Escherichia Coli Based TX-TL Cell-Free System. *ACS Synth. Biol.* **2014**, *3* (6), 387–397. https://doi.org/10.1021/sb400131a.
(162) Ali, M.; Suzuki, H.; Fukuba, T.; Jiang, X.; Nakano, H.; Yamane, T. Improvements in the Cell-Free Production of Functional Antibodies Using Cell Extract from Protease-Deficient Escherichia Coli Mutant. *J. Biosci. Bioeng.* **2005**, *99* (2), 181–186. https://doi.org/10.1263/jbb.99.181.
(163) Shimizu, Y.; Kanamori, T.; Ueda, T. Protein Synthesis by Pure Translation Systems. *Methods* **2005**, *36* (3), 299–304. https://doi.org/10.1016/j.ymeth.2005.04.006.
(164) Hillebrecht, J. R.; Chong, S. A Comparative Study of Protein Synthesis in in Vitro Systems: From the Prokaryotic Reconstituted to the Eukaryotic Extract-Based. *BMC Biotechnol.* **2008**, *8* (1), 58. https://doi.org/10.1186/1472-6750-8-58.
(165) Elowitz, M.; Lim, W. A. Build Life to Understand It. *Nature* **2010**, *468* (7326), 889–890. https://doi.org/10.1038/468889a.
(166) Garenne, D.; Noireaux, V. Cell-Free Transcription–Translation: Engineering Biology from the Nanometer to the Millimeter Scale. *Curr. Opin. Biotechnol.* **2019**, *58*, 19–27. https://doi.org/10.1016/j.copbio.2018.10.007.
(167) Fuller, R. S.; Kaguni, J. M.; Kornberg, A. Enzymatic Replication of the Origin of the Escherichia Coli Chromosome. *Proc. Natl. Acad. Sci. U. S. A.* **1981**, *78* (12 II), 7370–7374. https://doi.org/10.1073/pnas.78.12.7370.
(168) Blow, J. J.; Laskey, R. A. Initiation of DNA Replication in Nuclei and Purified DNA by a Cell-Free Extract of Xenopus Eggs. *Cell* **1986**, *47* (4), 577–587. https://doi.org/10.1016/0092-8674(86)90622-7.
(169) Preiss, T.; Hentze, M. W. Dual Function of the Messenger RNA Cap Structure in Poly(A)-Tail- Promoted Translation in Yeast. *Nature* **1998**, *392* (6675), 516–520. https://doi.org/10.1038/33192.

(170) Sakurai, Y.; Baeg, K.; Lam, A. Y. W.; Shoji, K.; Tomari, Y.; Iwakawa, H. Cell-Free Reconstitution Reveals the Molecular Mechanisms for the Initiation of Secondary SiRNA Biogenesis in Plants. *Proc. Natl. Acad. Sci.* **2021**, *118* (31), e2102889118. https://doi.org/10.1073/pnas.2102889118.

(171) Gonzales, D. T.; Yandrapalli, N.; Robinson, T.; Zechner, C.; Tang, T.-Y. D. Cell-Free Gene Expression Dynamics in Synthetic Cell Populations. *ACS Synth. Biol.* **2022**, *11* (1), 205–215. https://doi.org/10.1021/acssynbio.1c00376.

(172) Halleran, A. D.; Murray, R. M. Cell-Free and In Vivo Characterization of Lux, Las, and Rpa Quorum Activation Systems in E. Coli. *ACS Synth. Biol.* **2018**, *7* (2), 752–755. https://doi.org/10.1021/acssynbio.7b00376.

(173) Senoussi, A.; Lee Tin Wah, J.; Shimizu, Y.; Robert, J.; Jaramillo, A.; Findeiss, S.; Axmann, I. M.; Estevez-Torres, A. Quantitative Characterization of Translational Riboregulators Using an in Vitro Transcription–Translation System. *ACS Synth. Biol.* **2018**, *7* (5), 1269–1278. https://doi.org/10.1021/acssynbio.7b00387.

(174) Saito, H.; Kobayashi, T.; Hara, T.; Fujita, Y.; Hayashi, K.; Furushima, R.; Inoue, T. Synthetic Translational Regulation by an L7Ae–Kink-Turn RNP Switch. *Nat. Chem. Biol.* **2010**, *6* (1), 71–78. https://doi.org/10.1038/nchembio.273.

(175) Espah Borujeni, A.; Mishler, D. M.; Wang, J.; Huso, W.; Salis, H. M. Automated Physics-Based Design of Synthetic Riboswitches from Diverse RNA Aptamers. *Nucleic Acids Res.* **2016**, *44* (1), 1–13. https://doi.org/10.1093/nar/gkv1289.

(176) Lehr, F.-X.; Hanst, M.; Vogel, M.; Kremer, J.; Göringer, H. U.; Suess, B.; Koeppl, H. Cell-Free Prototyping of AND-Logic Gates Based on Heterogeneous RNA Activators. *ACS Synth. Biol.* **2019**, *8* (9), 2163–2173. https://doi.org/10.1021/acssynbio.9b00238.

(177) Takahashi, M. K.; Chappell, J.; Hayes, C. A.; Sun, Z. Z.; Kim, J.; Singhal, V.; Spring, K. J.; Al-Khabouri, S.; Fall, C. P.; Noireaux, V.; Murray, R. M.; Lucks, J. B. Rapidly Characterizing the Fast Dynamics of RNA Genetic Circuitry with Cell-Free Transcription–Translation (TX-TL) Systems. *ACS Synth. Biol.* **2015**, *4* (5), 503–515. https://doi.org/10.1021/sb400206c.

(178) Noireaux, V.; Bar-Ziv, R.; Libchaber, A. Principles of Cell-Free Genetic Circuit Assembly. *Proc. Natl. Acad. Sci.* **2003**, *100* (22), 12672–12677. https://doi.org/10.1073/pnas.2135496100.

(179) Shin, J.; Noireaux, V. An E. Coli Cell-Free Expression Toolbox: Application to Synthetic Gene Circuits and Artificial Cells. *ACS Synth. Biol.* **2012**, *1* (1), 29–41. https://doi.org/10.1021/sb200016s.

(180) Guo, S.; Murray, R. M. Construction of Incoherent Feedforward Loop Circuits in a Cell-Free System and in Cells. *ACS Synth. Biol.* **2019**, *8* (3), 606–610. https://doi.org/10.1021/acssynbio.8b00493.

(181) Hu, C. Y.; Takahashi, M. K.; Zhang, Y.; Lucks, J. B. Engineering a Functional Small RNA Negative Autoregulation Network with Model-Guided Design. *ACS Synth. Biol.* **2018**, *7* (6), 1507–1518. https://doi.org/10.1021/acssynbio.7b00440.

(182) Pardee, K.; Green, A. A.; Takahashi, M. K.; Braff, D.; Lambert, G.; Lee, J. W.; Ferrante, T.; Ma, D.; Donghia, N.; Fan, M.; Daringer, N. M.; Bosch, I.; Dudley, D. M.; O'Connor, D. H.; Gehrke, L.; Collins, J. J. Rapid, Low-Cost Detection of Zika Virus Using Programmable Biomolecular Components. *Cell* **2016**, *165* (5), 1255–1266. https://doi.org/10.1016/j.cell.2016.04.059.

(183) Ma, D.; Shen, L.; Wu, K.; Diehnelt, C. W.; Green, A. A. Low-Cost Detection of Norovirus Using Paper-Based Cell-Free Systems and Synbody-Based Viral

Enrichment. *Synth. Biol.* **2018**, *3* (1), ysy018. https://doi.org/10.1093/synbio/ysy018.

(184) Wen, K. Y.; Cameron, L.; Chappell, J.; Jensen, K.; Bell, D. J.; Kelwick, R.; Kopniczky, M.; Davies, J. C.; Filloux, A.; Freemont, P. S. A Cell-Free Biosensor for Detecting Quorum Sensing Molecules in P. Aeruginosa-Infected Respiratory Samples. *ACS Synth. Biol.* **2017**, *6* (12), 2293–2301. https://doi.org/10.1021/acssynbio.7b00219.

(185) Gräwe, A.; Dreyer, A.; Vornholt, T.; Barteczko, U.; Buchholz, L.; Drews, G.; Ho, U. L.; Jackowski, M. E.; Kracht, M.; Lüders, J.; Bleckwehl, T.; Rositzka, L.; Ruwe, M.; Wittchen, M.; Lutter, P.; Müller, K.; Kalinowski, J. A Paper-Based, Cell-Free Biosensor System for the Detection of Heavy Metals and Date Rape Drugs. *PLOS ONE* **2019**, *14* (3), e0210940. https://doi.org/10.1371/journal.pone.0210940.

(186) Baumann, M.; Meri, S. Techniques for Studying Protein Heterogeneity and Post-Translational Modifications. *Expert Rev. Proteomics* **2004**, *1* (2), 207–217. https://doi.org/10.1586/14789450.1.2.207.

(187) Kigawa, T.; Muto, Y.; Yokoyama, S. Cell-Free Synthesis and Amino Acid-Selective Stable Isotope Labeling of Proteins for NMR Analysis. *J. Biomol. NMR* **1995**, *6* (2), 129–134. https://doi.org/10.1007/BF00211776.

(188) Torizawa, T.; Shimizu, M.; Taoka, M.; Miyano, H.; Kainosho, M. Efficient Production of Isotopically Labeled Proteins by Cell-Free Synthesis: A Practical Protocol. *J. Biomol. NMR* **2004**, *30* (3), 311–325. https://doi.org/10.1007/s10858-004-3534-2.

(189) Narumi, R.; Masuda, K.; Tomonaga, T.; Adachi, J.; Ueda, H. R.; Shimizu, Y. Cell-Free Synthesis of Stable Isotope-Labeled Internal Standards for Targeted Quantitative Proteomics. *Synth. Syst. Biotechnol.* **2018**, *3* (2), 97–104. https://doi.org/10.1016/j.synbio.2018.02.004.

(190) Narumi, R.; Shimizu, Y.; Ukai-Tadenuma, M.; Ode, K. L.; Kanda, G. N.; Shinohara, Y.; Sato, A.; Matsumoto, K.; Ueda, H. R. Mass Spectrometry-Based Absolute Quantification Reveals Rhythmic Variation of Mouse Circadian Clock Proteins. *Proc. Natl. Acad. Sci.* **2016**, *113* (24), E3461–E3467. https://doi.org/10.1073/pnas.1603799113.

(191) Oza, J. P.; Aerni, H. R.; Pirman, N. L.; Barber, K. W.; ter Haar, C. M.; Rogulina, S.; Amrofell, M. B.; Isaacs, F. J.; Rinehart, J.; Jewett, M. C. Robust Production of Recombinant Phosphoproteins Using Cell-Free Protein Synthesis. *Nat. Commun.* **2015**, *6* (1), 8168. https://doi.org/10.1038/ncomms9168.

(192) Kightlinger, W.; Duncker, K. E.; Ramesh, A.; Thames, A. H.; Natarajan, A.; Stark, J. C.; Yang, A.; Lin, L.; Mrksich, M.; DeLisa, M. P.; Jewett, M. C. A Cell-Free Biosynthesis Platform for Modular Construction of Protein Glycosylation Pathways. *Nat. Commun.* **2019**, *10* (1), 5404. https://doi.org/10.1038/s41467-019-12024-9.

(193) Tawfik, D. S.; Griffiths, A. D. Man-Made Cell-like Compartments for Molecular Evolution. *Nat. Biotechnol.* **1998**, *16* (7), 652–656. https://doi.org/10.1038/nbt0798-652.

(194) Noireaux, V.; Libchaber, A. A Vesicle Bioreactor as a Step toward an Artificial Cell Assembly. *Proc. Natl. Acad. Sci. U. S. A.* **2004**, *101* (51), 17669–17674. https://doi.org/10.1073/pnas.0408236101.

(195) Murtas, G.; Kuruma, Y.; Bianchini, P.; Diaspro, A.; Luisi, P. L. Protein Synthesis in Liposomes with a Minimal Set of Enzymes. *Biochem. Biophys. Res. Commun.* **2007**, *363* (1), 12–17. https://doi.org/10.1016/j.bbrc.2007.07.201.

(196) Schwille, P.; Spatz, J.; Landfester, K.; Bodenschatz, E.; Herminghaus, S.; Sourjik, V.; Erb, T. J.; Bastiaens, P.; Lipowsky, R.; Hyman, A.; Dabrock, P.; Baret, J.-C.; Vidakovic-Koch, T.; Bieling, P.; Dimova, R.; Mutschler, H.; Robinson, T.; Tang, T.-Y. D.; Wegner, S.; Sundmacher, K. MaxSynBio: Avenues Towards Creating Cells from the Bottom Up. *Angew. Chem. Int. Ed.* **2018**, *57* (41), 13382–13392. https://doi.org/10.1002/anie.201802288.

(197) Akbarzadeh, A.; Rezaei-Sadabady, R.; Davaran, S.; Joo, S. W.; Zarghami, N.; Hanifehpour, Y.; Samiei, M.; Kouhi, M.; Nejati-Koshki, K. Liposome: Classification, Preparation, and Applications. *Nanoscale Res. Lett.* **2013**, *8* (1), 102. https://doi.org/10.1186/1556-276X-8-102.

(198) Sunami, T.; Sato, K.; Matsuura, T.; Tsukada, K.; Urabe, I.; Yomo, T. Femtoliter Compartment in Liposomes for in Vitro Selection of Proteins. *Anal. Biochem.* **2006**, *357* (1), 128–136. https://doi.org/10.1016/j.ab.2006.06.040.

(199) Torre, P.; Keating, C. D.; Mansy, S. S. Multiphase Water-in-Oil Emulsion Droplets for Cell-Free Transcription–Translation. *Langmuir* **2014**, *30* (20), 5695–5699. https://doi.org/10.1021/la404146g.

(200) Martino, C.; Kim, S.-H.; Horsfall, L.; Abbaspourrad, A.; Rosser, S. J.; Cooper, J.; Weitz, D. A. Protein Expression, Aggregation, and Triggered Release from Polymersomes as Artificial Cell-like Structures. *Angew. Chem. Int. Ed.* **2012**, *51* (26), 6416–6420. https://doi.org/10.1002/anie.201201443.

(201) Booth, M. J.; Restrepo Schild, V.; Graham, A. D.; Olof, S. N.; Bayley, H. Light-Activated Communication in Synthetic Tissues. *Sci. Adv.* **2016**, *2* (4), e1600056. https://doi.org/10.1126/sciadv.1600056.

(202) Booth, M. J.; Restrepo Schild, V.; Box, S. J.; Bayley, H. Light-Patterning of Synthetic Tissues with Single Droplet Resolution. *Sci. Rep.* **2017**, *7* (1), 9315. https://doi.org/10.1038/s41598-017-09394-9.

(203) Smith, J. M.; Chowdhry, R.; Booth, M. J. Controlling Synthetic Cell-Cell Communication. *Front. Mol. Biosci.* **2022**, *8*, 809945. https://doi.org/10.3389/fmolb.2021.809945.

(204) Adamala, K. P.; Martin-Alarcon, D. A.; Guthrie-Honea, K. R.; Boyden, E. S. Engineering Genetic Circuit Interactions within and between Synthetic Minimal Cells. *Nat. Chem.* **2017**, *9* (5), 431–439. https://doi.org/10.1038/nchem.2644.

(205) Tang, T.-Y. D.; Cecchi, D.; Fracasso, G.; Accardi, D.; Coutable-Pennarun, A.; Mansy, S. S.; Perriman, A. W.; Anderson, J. L. R.; Mann, S. Gene-Mediated Chemical Communication in Synthetic Protocell Communities. *ACS Synth. Biol.* **2018**, *7* (2), 339–346. https://doi.org/10.1021/acssynbio.7b00306.

(206) Smith, J. M.; Hartmann, D.; Booth, M. J. Engineering Cellular Communication between Light-Activated Synthetic Cells and Bacteria. *bioRxiv* **2022**, 2022.07.22.500923. https://doi.org/10.1101/2022.07.22.500923.

(207) Fujiwara, K.; Katayama, T.; Nomura, S. M. Cooperative Working of Bacterial Chromosome Replication Proteins Generated by a Reconstituted Protein Expression System. *Nucleic Acids Res.* **2013**, *41* (14), 7176–7183. https://doi.org/10.1093/nar/gkt489.

(208) Su'etsugu, M.; Takada, H.; Katayama, T.; Tsujimoto, H. Exponential Propagation of Large Circular DNA by Reconstitution of a Chromosome-Replication Cycle. *Nucleic Acids Res.* **2017**, *45* (20), 11525–11534. https://doi.org/10.1093/nar/gkx822.

(209) Kretschmer, S.; Ganzinger, K. A.; Franquelim, H. G.; Schwille, P. Synthetic Cell Division via Membrane-Transforming Molecular Assemblies. *BMC Biol.* **2019**, *17* (1), 43. https://doi.org/10.1186/s12915-019-0665-1.

(210) Kuruma, Y.; Stano, P.; Ueda, T.; Luisi, P. L. A Synthetic Biology Approach to the Construction of Membrane Proteins in Semi-Synthetic Minimal Cells. *Biochim. Biophys. Acta BBA - Biomembr.* **2009**, *1788* (2), 567–574. https://doi.org/10.1016/j.bbamem.2008.10.017.
(211) Krinsky, N.; Kaduri, M.; Zinger, A.; Shainsky-Roitman, J.; Goldfeder, M.; Benhar, I.; Hershkovitz, D.; Schroeder, A. Synthetic Cells Synthesize Therapeutic Proteins inside Tumors. *Adv. Healthc. Mater.* **2018**, *7* (9), 1701163. https://doi.org/10.1002/adhm.201701163.
(212) Hartmann, D.; Smith, J. M.; Mazzotti, G.; Chowdhry, R.; Booth, M. J. Controlling Gene Expression with Light: A Multidisciplinary Endeavour. *Biochem. Soc. Trans.* **2020**, *48* (4), 1645–1659. https://doi.org/10.1042/BST20200014.
(213) Deiters, A. Light Activation as a Method of Regulating and Studying Gene Expression. *Curr. Opin. Chem. Biol.* **2009**, *13* (5–6), 678–686. https://doi.org/10.1016/j.cbpa.2009.09.026.
(214) Barltrop, J. A.; Schofield, P. Photosensitive Protecting Groups. *Tetrahedron Lett.* **1962**, *3* (16), 697–699. https://doi.org/10.1016/S0040-4039(00)70935-X.
(215) Barton, D. H. R.; Chow, Y. L.; Cox, A.; Kirby, G. W. Photosensitive Protection of Functional Groups. *Tetrahedron Lett.* **1962**, *3* (23), 1055–1057. https://doi.org/10.1016/S0040-4039(00)70957-9.
(216) Patchornik, A.; Amit, B.; Woodward, R. B. Photosensitive Protecting Groups. *J. Am. Chem. Soc.* **1970**, *92* (21), 6333–6335. https://doi.org/10.1021/ja00724a041.
(217) Sheehan, J. C.; Wilson, R. Marshall. Photolysis of Desyl Compounds. A New Photolytic Cyclization. *J. Am. Chem. Soc.* **1964**, *86* (23), 5277–5281. https://doi.org/10.1021/ja01077a046.
(218) Engels, J.; Schlaeger, E. J. Synthesis, Structure, and Reactivity of Adenosine Cyclic 3',5'-Phosphate-Benzyltriesters. *J. Med. Chem.* **1977**, *20* (7), 907–911. https://doi.org/10.1021/jm00217a008.
(219) Kaplan, J. H.; Forbush, B.; Hoffman, J. F. Rapid Photolytic Release of Adenosine 5'-Triphosphate from a Protected Analogue: Utilization by the Na:K Pump of Human Red Blood Cell Ghosts. *Biochemistry* **1978**, *17* (10), 1929–1935. https://doi.org/10.1021/bi00603a020.
(220) Klán, P.; Šolomek, T.; Bochet, C. G.; Blanc, A.; Givens, R.; Rubina, M.; Popik, V.; Kostikov, A.; Wirz, J. Photoremovable Protecting Groups in Chemistry and Biology: Reaction Mechanisms and Efficacy. *Chem. Rev.* **2013**, *113* (1), 119–191. https://doi.org/10.1021/cr300177k.
(221) Sheehan, J. C.; Umezawa, K. Phenacyl Photosensitive Blocking Groups. *J. Org. Chem.* **1973**, *38* (21), 3771–3774. https://doi.org/10.1021/jo00961a027.
(222) Pelliccioli, A. P.; Wirz, J. Photoremovable Protecting Groups: Reaction Mechanisms and Applications. *Photochem. Photobiol. Sci.* **2002**, *1* (7), 441–458. https://doi.org/10.1039/B200777K.
(223) Josa-Culleré, L.; Llebaria, A. In the Search for Photocages Cleavable with Visible Light: An Overview of Recent Advances and Chemical Strategies. *ChemPhotoChem* **2021**, *5* (4), 296–314. https://doi.org/10.1002/cptc.202000253.
(224) Bayley, H.; Chang, C.-Y.; Todd Miller, W.; Niblack, B.; Pan, P. [7] Caged Peptides and Proteins by Targeted Chemical Modification. In *Methods in Enzymology*; Caged Compounds; Academic Press, 1998; Vol. 291, pp 117–135. https://doi.org/10.1016/S0076-6879(98)91010-2.
(225) Givens, R. S.; Kueper, L. William. Photochemistry of Phosphate Esters. *Chem. Rev.* **1993**, *93* (1), 55–66. https://doi.org/10.1021/cr00017a004.

(226) Weinstain, R.; Slanina, T.; Kand, D.; Klán, P. Visible-to-NIR-Light Activated Release: From Small Molecules to Nanomaterials. *Chem. Rev.* **2020**, *120* (24), 13135–13272. https://doi.org/10.1021/acs.chemrev.0c00663.
(227) Dyer, R. G.; Turnbull, K. D. Hydrolytic Stabilization of Protected P-Hydroxybenzyl Halides Designed as Latent Quinone Methide Precursors. *J. Org. Chem.* **1999**, *64* (21), 7988–7995. https://doi.org/10.1021/jo991085t.
(228) McGall, G. H.; Barone, A. D.; Diggelmann, M.; Fodor, S. P. A.; Gentalen, E.; Ngo, N. The Efficiency of Light-Directed Synthesis of DNA Arrays on Glass Substrates. *J. Am. Chem. Soc.* **1997**, *119* (22), 5081–5090. https://doi.org/10.1021/ja964427a.
(229) Venkatesan, H.; Greenberg, M. M. Improved Utility of Photolabile Solid Phase Synthesis Supports for the Synthesis of Oligonucleotides Containing 3'-Hydroxyl Termini. *J. Org. Chem.* **1996**, *61* (2), 525–529. https://doi.org/10.1021/jo951550w.
(230) Piloto, A. M.; Costa, S. P. G.; Gonçalves, M. S. T. Wavelength-Selective Cleavage of o-Nitrobenzyl and Polyheteroaromatic Benzyl Protecting Groups. *Tetrahedron* **2014**, *70* (3), 650–657. https://doi.org/10.1016/j.tet.2013.11.100.
(231) Polesskaya, O.; Baranova, A.; Bui, S.; Kondratev, N.; Kananykhina, E.; Nazarenko, O.; Shapiro, T.; Nardia, F. B.; Kornienko, V.; Chandhoke, V.; Stadler, I.; Lanzafame, R.; Myakishev-Rempel, M. Optogenetic Regulation of Transcription. *BMC Neurosci.* **2018**, *19* (S1), 12. https://doi.org/10.1186/s12868-018-0411-6.
(232) Ruggiero, E.; Castro, S. A.; Habtemariam, A.; Salassa, L. Upconverting Nanoparticles for the near Infrared Photoactivation of Transition Metal Complexes: New Opportunities and Challenges in Medicinal Inorganic Photochemistry. *Dalton Trans.* **2016**, *45* (33), 13012–13020. https://doi.org/10.1039/C6DT01428C.
(233) Brown, T. M.; Fakih, H. H.; Saliba, D.; Asohan, J.; Sleiman, H. F. Stabilization of Functional DNA Structures with Mild Photochemical Methods. *J. Am. Chem. Soc.* **2023**. https://doi.org/10.1021/jacs.2c08808.
(234) Sinha, R. P.; Häder, D.-P. UV-Induced DNA Damage and Repair: A Review. *Photochem. Photobiol. Sci.* **2002**, *1* (4), 225–236. https://doi.org/10.1039/b201230h.
(235) Rastogi, R. P.; Richa, U.; Kumar, A.; Tyagi, M. B.; Sinha, R. P. Molecular Mechanisms of Ultraviolet Radiation-Induced DNA Damage and Repair. *J. Nucleic Acids* **2010**, *2010*, e592980. https://doi.org/10.4061/2010/592980.
(236) Aujard, I.; Benbrahim, C.; Gouget, M.; Ruel, O.; Baudin, J.-B.; Neveu, P.; Jullien, L. O-Nitrobenzyl Photolabile Protecting Groups with Red-Shifted Absorption: Syntheses and Uncaging Cross-Sections for One- and Two-Photon Excitation. *Chem. – Eur. J.* **2006**, *12* (26), 6865–6879. https://doi.org/10.1002/chem.200501393.
(237) Il'ichev, Y. V.; Schwörer, M. A.; Wirz, J. Photochemical Reaction Mechanisms of 2-Nitrobenzyl Compounds: Methyl Ethers and Caged ATP. *J. Am. Chem. Soc.* **2004**, *126* (14), 4581–4595. https://doi.org/10.1021/ja039071z.
(238) Dunkin, I. R.; Gębicki, J.; Kiszka, M.; Sanín-Leira, D. The Matrix-Isolation IR Spectrum of the o-Quinonoid Intermediate in the Photolysis of 2-Nitrobenzyl Methyl Ether. *Spectrochim. Acta. A. Mol. Biomol. Spectrosc.* **1997**, *53* (14), 2553–2557. https://doi.org/10.1016/S1386-1425(97)00186-8.
(239) Corrie, J. E. T.; Barth, A.; Munasinghe, V. R. N.; Trentham, D. R.; Hutter, M. C. Photolytic Cleavage of 1-(2-Nitrophenyl)Ethyl Ethers Involves Two Parallel Pathways and Product Release Is Rate-Limited by Decomposition of a Common

Hemiacetal Intermediate. *J. Am. Chem. Soc.* **2003**, *125* (28), 8546–8554. https://doi.org/10.1021/ja034354c.
(240) Deng, J.; Bezold, D.; Jessen, H. J.; Walther, A. Multiple Light Control Mechanisms in ATP-Fueled Non-equilibrium DNA Systems. *Angew. Chem. Int. Ed.* **2020**, *59* (29), 12084–12092. https://doi.org/10.1002/anie.202003102.
(241) Givens, R. S.; Matuszewski, B. Photochemistry of Phosphate Esters: An Efficient Method for the Generation of Electrophiles. *J. Am. Chem. Soc.* **1984**, *106* (22), 6860–6861. https://doi.org/10.1021/ja00334a075.
(242) Bassolino, G.; Nançoz, C.; Thiel, Z.; Bois, E.; Vauthey, E.; Rivera-Fuentes, P. Photolabile Coumarins with Improved Efficiency through Azetidinyl Substitution. *Chem. Sci.* **2018**, *9* (2), 387–391. https://doi.org/10.1039/C7SC03627B.
(243) Fournier, L.; Aujard, I.; Le Saux, T.; Maurin, S.; Beaupierre, S.; Baudin, J.-B.; Jullien, L. Coumarinylmethyl Caging Groups with Redshifted Absorption. *Chem. – Eur. J.* **2013**, *19* (51), 17494–17507. https://doi.org/10.1002/chem.201302630.
(244) Gandioso, A.; Cano, M.; Massaguer, A.; Marchán, V. A Green Light-Triggerable RGD Peptide for Photocontrolled Targeted Drug Delivery: Synthesis and Photolysis Studies. *J. Org. Chem.* **2016**, *81* (23), 11556–11564. https://doi.org/10.1021/acs.joc.6b02415.
(245) Gandioso, A.; Palau, M.; Nin-Hill, A.; Melnyk, I.; Rovira, C.; Nonell, S.; Velasco, D.; García-Amorós, J.; Marchán, V. Sequential Uncaging with Green Light Can Be Achieved by Fine-Tuning the Structure of a Dicyanocoumarin Chromophore. *ChemistryOpen* **2017**, *6* (3), 375–384. https://doi.org/10.1002/open.201700067.
(246) Kaufmann, J.; Müller, P.; Andreadou, E.; Heckel, A. Green-Light Activatable BODIPY and Coumarin 5'-Caps for Oligonucleotide Photocaging. *Chem. – Eur. J.* **2022**, *28* (36), e202200477. https://doi.org/10.1002/chem.202200477.
(247) Gandioso, A.; Contreras, S.; Melnyk, I.; Oliva, J.; Nonell, S.; Velasco, D.; García-Amorós, J.; Marchán, V. Development of Green/Red-Absorbing Chromophores Based on a Coumarin Scaffold That Are Useful as Caging Groups. *J. Org. Chem.* **2017**, *82* (10), 5398–5408. https://doi.org/10.1021/acs.joc.7b00788.
(248) López-Corrales, M.; Rovira, A.; Gandioso, A.; Bosch, M.; Nonell, S.; Marchán, V. Transformation of COUPY Fluorophores into a Novel Class of Visible-Light-Cleavable Photolabile Protecting Groups. *Chem. – Eur. J.* **2020**, *26* (69), 16222–16227. https://doi.org/10.1002/chem.202002314.
(249) Olson, J. P.; Banghart, M. R.; Sabatini, B. L.; Ellis-Davies, G. C. R. Spectral Evolution of a Photochemical Protecting Group for Orthogonal Two-Color Uncaging with Visible Light. *J. Am. Chem. Soc.* **2013**, *135* (42), 15948–15954. https://doi.org/10.1021/ja408225k.
(250) Lin, Q.; Yang, L.; Wang, Z.; Hua, Y.; Zhang, D.; Bao, B.; Bao, C.; Gong, X.; Zhu, L. Coumarin Photocaging Groups Modified with an Electron-Rich Styryl Moiety at the 3-Position: Long-Wavelength Excitation, Rapid Photolysis, and Photobleaching. *Angew. Chem. Int. Ed.* **2018**, *57* (14), 3722–3726. https://doi.org/10.1002/anie.201800713.
(251) Olson, J. P.; Kwon, H. B.; Takasaki, K. T.; Chiu, C. Q.; Higley, M. J.; Sabatini, B. L.; Ellis-Davies, G. C. R. Optically Selective Two-Photon Uncaging of Glutamate at 900 Nm. *J. Am. Chem. Soc.* **2013**, *135* (16), 5954–5957. https://doi.org/10.1021/ja4019379.
(252) Chang, D.; Lindberg, E.; Feng, S.; Angerani, S.; Riezman, H.; Winssinger, N. Luciferase-Induced Photouncaging: Bioluminolysis. *Angew. Chem. Int. Ed.* **2019**, *58* (45), 16033–16037.

(253) Klausen, M.; Dubois, V.; Clermont, G.; Tonnelé, C.; Castet, F.; Blanchard-Desce, M. Dual-Wavelength Efficient Two-Photon Photorelease of Glycine by π-Extended Dipolar Coumarins. *Chem. Sci.* **2019**, *10* (15), 4209–4219. https://doi.org/10.1039/C9SC00148D.
(254) Bojtár, M.; Kormos, A.; Kis-Petik, K.; Kellermayer, M.; Kele, P. Green-Light Activatable, Water-Soluble Red-Shifted Coumarin Photocages. *Org. Lett.* **2019**, *21* (23), 9410–9414. https://doi.org/10.1021/acs.orglett.9b03624.
(255) Schmidt, R.; Geissler, D.; Hagen, V.; Bendig, J. Mechanism of Photocleavage of (Coumarin-4-Yl)Methyl Esters. *J. Phys. Chem. A* **2007**, *111* (26), 5768–5774. https://doi.org/10.1021/jp071521c.
(256) Schmidt, R.; Geissler, D.; Hagen, V.; Bendig, J. Kinetics Study of the Photocleavage of (Coumarin-4-Yl)Methyl Esters. *J. Phys. Chem. A* **2005**, *109* (23), 5000–5004. https://doi.org/10.1021/jp050581k.
(257) Bourbon, P.; Peng, Q.; Ferraudi, G.; Stauffacher, C.; Wiest, O.; Helquist, P. Synthesis, Photophysical, Photochemical, and Computational Studies of Coumarin-Labeled Nicotinamide Derivatives. *J. Org. Chem.* **2012**, *77* (6), 2756–2762. https://doi.org/10.1021/jo2025527.
(258) Takano, M.; Abe, M. Photoreaction of 4-(Bromomethyl)-7-(Diethylamino)Coumarin: Generation of a Radical and Cation Triplet Diradical during the C–Br Bond Cleavage. *Org. Lett.* **2022**, *24* (15), 2804–2808. https://doi.org/10.1021/acs.orglett.2c00694.
(259) Suzuki, A. Z.; Watanabe, T.; Kawamoto, M.; Nishiyama, K.; Yamashita, H.; Ishii, M.; Iwamura, M.; Furuta, T. Coumarin-4-Ylmethoxycarbonyls as Phototriggers for Alcohols and Phenols. *Org. Lett.* **2003**, *5* (25), 4867–4870. https://doi.org/10.1021/ol0359362.
(260) Debart, F.; Dupouy, C.; Vasseur, J. J. Stimuli-Responsive Oligonucleotides in Prodrug-Based Approaches for Gene Silencing. *Beilstein J. Org. Chem.* **2018**, *14* (1), 436–469. https://doi.org/10.3762/bjoc.14.32.
(261) Siegal-Gaskins, D.; Tuza, Z. A.; Kim, J.; Noireaux, V.; Murray, R. M. Gene Circuit Performance Characterization and Resource Usage in a Cell-Free "Breadboard." *ACS Synth. Biol.* **2014**, *3* (6), 416–425. https://doi.org/10.1021/sb400203p.
(262) Li, L.; Jiang, Y.; Cui, C.; Yang, Y.; Zhang, P.; Stewart, K.; Pan, X.; Li, X.; Yang, L.; Qiu, L.; Tan, W. Modulating Aptamer Specificity with PH-Responsive DNA Bonds. *J. Am. Chem. Soc.* **2018**, *140* (41), 13335–13339. https://doi.org/10.1021/jacs.8b08047.
(263) Zhang, L.; Li, Y.; Yu, J. C.; Chan, K. M. Redox-Responsive Controlled DNA Transfection and Gene Silencing Based on Polymer-Conjugated Magnetic Nanoparticles. *RSC Adv.* **2016**, *6* (76), 72155–72164. https://doi.org/10.1039/c6ra16578h.
(264) Sahoo, S.; Kayal, S.; Poddar, P.; Dhara, D. Redox-Responsive Efficient DNA and Drug Co-Release from Micelleplexes Formed from a Fluorescent Cationic Amphiphilic Polymer. *Langmuir* **2019**, *35* (45), 14616–14627. https://doi.org/10.1021/acs.langmuir.9b02921.
(265) Wang, Y.; Ma, B.; Abdeen, A. A.; Chen, G.; Xie, R.; Saha, K.; Gong, S. Versatile Redox-Responsive Polyplexes for the Delivery of Plasmid DNA, Messenger RNA, and CRISPR-Cas9 Genome-Editing Machinery. *ACS Appl. Mater. Interfaces* **2018**, *10* (38), 31915–31927. https://doi.org/10.1021/acsami.8b09642.
(266) Knutson, S. D.; Sanford, A. A.; Swenson, C. S.; Korn, M. M.; Manuel, B. A.; Heemstra, J. M. Thermoreversible Control of Nucleic Acid Structure and Function

with Glyoxal Caging. *J. Am. Chem. Soc.* **2020**, *142* (41), 17766–17781. https://doi.org/10.1021/jacs.0c08996.

(267) Chan, V.; Novakowski, S. K.; Law, S.; Klein-Bosgoed, C.; Kastrup, C. J. Controlled Transcription of Exogenous MRNA in Platelets Using Protocells. *Angew. Chem. Int. Ed.* **2015**, *54* (46), 13590–13593. https://doi.org/10.1002/anie.201506500.

(268) Pinheiro, A. V.; Baptistap, P.; Lima, J. C.; Baptista, P.; Lima, J. C. Light Activation of Transcription: Photocaging of Nucleotides for Control over RNA Polymerization | Nucleic Acids Research | Oxford Academic. *Nucleic Acids Res.* **2008**, *36* (14), e90–e90. https://doi.org/10.1093/nar/gkn415.

(269) Ohno, K.; Sugiyama, D.; Takeshita, L.; Kanamori, T.; Masaki, Y.; Sekine, M.; Seio, K. Synthesis of Photocaged 6-O-(2-Nitrobenzyl)Guanosine and 4-O-(2-Nitrobenzyl) Uridine Triphosphates for Photocontrol of the RNA Transcription Reaction. *Bioorg. Med. Chem.* **2017**, *25* (21), 6007–6015. https://doi.org/10.1016/j.bmc.2017.09.032.

(270) Binder, D.; Bier, C.; Grünberger, A.; Drobietz, D.; Hage-Hülsmann, J.; Wandrey, G.; Büchs, J.; Kohlheyer, D.; Loeschcke, A.; Wiechert, W.; Jaeger, K. E.; Pietruszka, J.; Drepper, T. Photocaged Arabinose: A Novel Optogenetic Switch for Rapid and Gradual Control of Microbial Gene Expression. *ChemBioChem* **2016**, *17* (4), 296–299. https://doi.org/10.1002/cbic.201500609.

(271) Young, D. D.; Deiters, A. Photochemical Activation of Protein Expression in Bacterial Cells. *Angew. Chem.* **2007**, *119* (23), 4368–4370. https://doi.org/10.1002/ange.200700057.

(272) Binder, D.; Frohwitter, J.; Mahr, R.; Bier, C.; Grünberger, A.; Loeschcke, A.; Peters-Wendisch, P.; Kohlheyer, D.; Pietruszka, J.; Frunzke, J.; Jaeger, K. E.; Wendisch, V. F.; Drepper, T. Light-Controlled Cell Factories: Employing Photocaged Isopropyl- β-D-Thiogalactopyranoside for Light-Mediated Optimization of Lac-Based Gene Expression and (+)-Valencene Biosynthesis in Corynebacterium Glutamicum. *Appl. Environ. Microbiol.* **2016**, *82* (20), 6141–6149. https://doi.org/10.1128/AEM.01457-16.

(273) Faal, T.; Wong, P. T.; Tang, S.; Coulter, A.; Chen, Y.; Tu, C. H.; Baker, J. R.; Choi, S. K.; Inlay, M. A. 4-Hydroxytamoxifen Probes for Light-Dependent Spatiotemporal Control of Cre-ER Mediated Reporter Gene Expression. *Mol. Biosyst.* **2015**, *11* (3), 783–790. https://doi.org/10.1039/c4mb00581c.

(274) Wong, P. T.; Roberts, E. W.; Tang, S.; Mukherjee, J.; Cannon, J.; Nip, A. J.; Corbin, K.; Krummel, M. F.; Choi, S. K. Control of an Unusual Photo-Claisen Rearrangement in Coumarin Caged Tamoxifen through an Extended Spacer. *ACS Chem. Biol.* **2017**, *12* (4), 1001–1010. https://doi.org/10.1021/acschembio.6b00999.

(275) Gorka, A. P.; Yamamoto, T.; Zhu, J.; Schnermann, M. J. Cyanine Photocages Enable Spatial Control of Inducible Cre-Mediated Recombination. *ChemBioChem* **2018**, *19* (12), 1239–1243. https://doi.org/10.1002/cbic.201800061.

(276) Hamouri, F.; Zhang, W.; Aujard, I.; Le Saux, T.; Ducos, B.; Vriz, S.; Jullien, L.; Bensimon, D. Optical Control of Protein Activity and Gene Expression by Photoactivation of Caged Cyclofen. In *Methods in Enzymology*; Academic Press Inc., 2019; Vol. 624, pp 1–23. https://doi.org/10.1016/bs.mie.2019.04.009.

(277) Fournier, L.; Gauron, C.; Xu, L.; Aujard, I.; Le Saux, T.; Gagey-Eilstein, N.; Maurin, S.; Dubruille, S.; Baudin, J. B.; Bensimon, D.; Volovitch, M.; Vriz, S.; Jullien, L. A Blue-Absorbing Photolabile Protecting Group for in Vivo

Chromatically Orthogonal Photoactivation. *ACS Chem. Biol.* **2013**, *8* (7), 1528–1536. https://doi.org/10.1021/cb400178m.

(278) Young, D. D.; Garner, R. A.; Yoder, J. A.; Deiters, A. Light-Activation of Gene Function in Mammalian Cells via Ribozymes. *Chem. Commun.* **2009**, No. 5, 568–570. https://doi.org/10.1039/b819375d.

(279) Walsh, S.; Gardner, L.; Deiters, A.; Williams, G. J. Intracellular Light-Activation of Riboswitch Activity. *ChemBioChem* **2014**, *15* (9), 1346–1351. https://doi.org/10.1002/cbic.201400024.

(280) Murat, P.; Gormally, M. V.; Sanders, D.; Antonio, M. D.; Balasubramanian, S. Light-Mediated in Cell Downregulation of G-Quadruplex-Containing Genes Using a Photo-Caged Ligand. *Chem. Commun.* **2013**, *49* (76), 8453–8455. https://doi.org/10.1039/c3cc44737e.

(281) Cambridge, S. B.; Geissler, D.; Keller, S.; Cürten, B. A Caged Doxycycline Analogue for Photoactivated Gene Expression. *Angew. Chem. Int. Ed.* **2006**, *45* (14), 2229–2231. https://doi.org/10.1002/anie.200503339.

(282) Cambridge, S. B.; Geissler, D.; Calegari, F.; Anastassiadis, K.; Hasan, M. T.; Stewart, A. F.; Huttner, W. B.; Hagen, V.; Bonhoeffer, T. Doxycycline-Dependent Photoactivated Gene Expression in Eukaryotic Systems. *Nat. Methods* **2009**, *6* (7), 527–531. https://doi.org/10.1038/nmeth.1340.

(283) Link, K. H.; Cruz, F. G.; Ye, H. F.; O'Reilly, K. E.; Dowdell, S.; Koh, J. T. Photo-Caged Agonists of the Nuclear Receptors RARγ and TRβ Provide Unique Time-Dependent Gene Expression Profiles for Light-Activated Gene Patterning. *Bioorg. Med. Chem.* **2004**, *12* (22), 5949–5959. https://doi.org/10.1016/j.bmc.2004.08.022.

(284) Imoto, T.; Kawase, A.; Minoshima, M.; Yokoyama, T.; Bito, H.; Kikuchi, K. Photolytic Release of a Caged Inhibitor of an Endogenous Transcription Factor Enables Optochemical Control of CREB-Mediated Gene Expression. *Org. Lett.* **2020**, *22* (1), 22–25. https://doi.org/10.1021/acs.orglett.9b03568.

(285) Nora, L. C.; Westmann, C. A.; Martins-Santana, L.; Alves, L. de F.; Monteiro, L. M. O.; Guazzaroni, M.-E.; Silva-Rocha, R. The Art of Vector Engineering: Towards the Construction of next-Generation Genetic Tools. *Microb. Biotechnol.* **2019**, *12* (1), 125–147. https://doi.org/10.1111/1751-7915.13318.

(286) Hemphill, J.; Govan, J.; Uprety, R.; Tsang, M.; Deiters, A. Site-Specific Promoter Caging Enables Optochemical Gene Activation in Cells and Animals. *J. Am. Chem. Soc.* **2014**, *136* (19), 7152–7158. https://doi.org/10.1021/ja500327g.

(287) Yamaguchi, S.; Chen, Y.; Nakajima, S.; Furuta, T.; Nagamune, T. Light-Activated Gene Expression from Site-Specific Caged DNA with a Biotinylated Photolabile Protection Group. *Chem. Commun.* **2010**, *46* (13), 2244–2246. https://doi.org/10.1039/b922502a.

(288) Monroe, W. T.; McQuain, M. M.; Chang, M. S.; Alexander, J. S.; Haselton, F. R. Targeting Expression with Light Using Caged DNA. *J. Biol. Chem.* **1999**, *274* (30), 20895–20900. https://doi.org/10.1074/jbc.274.30.20895.

(289) Ando, H.; Furuta, T.; Tsien, R. Y.; Okamoto, H. Photo-Mediated Gene Activation Using Caged RNA/DNA in Zebrafish Embryos. *Nat. Genet.* **2001**, *28* (4), 317–325. https://doi.org/10.1038/ng583.

(290) Schroeder, A.; Goldberg, M. S.; Kastrup, C.; Wang, Y.; Jiang, S.; Joseph, B. J.; Levins, C. G.; Kannan, S. T.; Langer, R.; Anderson, D. G. Remotely Activated Protein-Producing Nanoparticles. *Nano Lett.* **2012**, *12* (6), 2685–2689. https://doi.org/10.1021/nl2036047.

(291) Ogasawara, S. Transcription Driven by Reversible Photocontrol of Hyperstable G-Quadruplexes. *ACS Synth. Biol.* **2018**, *7* (11), 2507–2513. https://doi.org/10.1021/acssynbio.8b00216.
(292) Liang, X.; Wakuda, R.; Fujioka, K.; Asanuma, H. Photoregulation of DNA Transcription by Using Photoresponsive T7 Promoters and Clarification of Its Mechanism. *FEBS J.* **2010**, *277* (6), 1551–1561. https://doi.org/10.1111/j.1742-4658.2010.07583.x.
(293) Kamiya, Y.; Takagi, T.; Ooi, H.; Ito, H.; Liang, X.; Asanuma, H. Synthetic Gene Involving Azobenzene-Tethered T7 Promoter for the Photocontrol of Gene Expression by Visible Light. *ACS Synth. Biol.* **2015**, *4* (4), 365–370. https://doi.org/10.1021/sb5001092.
(294) Asanuma, H.; Tamaru, D.; Yamazawa, A.; Liu, M.; Komiyama, M. Photoregulation of the Transcription Reaction of T7 RNA Polymerase by Tethering an Azobenzene to the Promoter. *ChemBioChem* **2002**, *3* (8), 786–789. https://doi.org/10.1002/1439-7633(20020802)3:8<786::AID-CBIC786>3.0.CO;2-P.
(295) Ando, H.; Kobayashi, M.; Tsubokawa, T.; Uyemura, K.; Furuta, T.; Okamoto, H. Lhx2 Mediates the Activity of Six3 in Zebrafish Forebrain Growth. *Dev. Biol.* **2005**, *287* (2), 456–468. https://doi.org/10.1016/j.ydbio.2005.09.023.
(296) Klöcker, N.; Weissenboeck, F. P.; van Dülmen, M.; Špaček, P.; Hüwel, S.; Rentmeister, A. Photocaged 5′ Cap Analogues for Optical Control of MRNA Translation in Cells. *Nat. Chem.* **2022**, *14* (8), 905–913. https://doi.org/10.1038/s41557-022-00972-7.
(297) Bollu, A.; Klöcker, N.; Špaček, P.; P. Weissenboeck, F.; Hüwel, S.; Rentmeister, A. Light-Activated Translation of Different MRNAs in Cells via Wavelength-Dependent Photouncaging. *Angew. Chem. Int. Ed.* **2023**, *62* (5), e202209975. https://doi.org/10.1002/anie.202209975.
(298) Ogasawara, S. Control of Cellular Function by Reversible Photoregulation of Translation. *ChemBioChem* **2014**, *15* (18), 2652–2655. https://doi.org/10.1002/cbic.201402495.
(299) Zhang, D.; Zhou, C. Y.; Busby, K. N.; Alexander, S. C.; Devaraj, N. K. Light-Activated Control of Translation by Enzymatic Covalent MRNA Labeling. *Angew. Chem. Int. Ed.* **2018**, *57* (11), 2822–2826. https://doi.org/10.1002/anie.201710917.
(300) Kröck, L.; Hechel, A. Photoinduced Transcription by Using Temporarily Mismatched Caged Oligonucleotides. *Angew. Chem. Int. Ed.* **2005**, *44* (3), 471–473. https://doi.org/10.1002/anie.200461779.
(301) Stafforst, T.; Stadler, J. M. Photoactivation of a Psoralen-Blocked Luciferase Gene by Blue Light. *Angew. Chem. Int. Ed.* **2013**, *52* (47), 12448–12451. https://doi.org/10.1002/anie.201306150.
(302) Heimes, M.; Kolmar, L.; Brieke, C. Efficient Cosubstrate Enzyme Pairs for Sequence-Specific Methyltransferase-Directed Photolabile Caging of DNA. *Chem. Commun.* **2018**, *54* (90), 12718–12721. https://doi.org/10.1039/c8cc05913f.
(303) Vaníková, Z.; Janoušková, M.; Kambová, M.; Krásný, L.; Hocek, M. Switching Transcription with Bacterial RNA Polymerase through Photocaging, Photorelease and Phosphorylation Reactions in the Major Groove of DNA. *Chem. Sci.* **2019**, *10* (14), 3937–3942. https://doi.org/10.1039/c9sc00205g.

(304) Cadet, J.; Douki, T. Formation of UV-Induced DNA Damage Contributing to Skin Cancer Development. *Photochem. Photobiol. Sci.* **2018**, *17* (12), 1816–1841. https://doi.org/10.1039/c7pp00395a.

(305) Deiters, A.; Garner, R. A.; Lusic, H.; Govan, J. M.; Dush, M.; Nascone-Yoder, N. M.; Yoder, J. A. Photocaged Morpholino Oligomers for the Light-Regulation of Gene Function in Zebrafish and Xenopus Embryos. *J. Am. Chem. Soc.* **2010**, *132* (44), 15644–15650. https://doi.org/10.1021/ja1053863.

(306) Govan, J. M.; Uprety, R.; Thomas, M.; Lusic, H.; Lively, M. O.; Deiters, A. Cellular Delivery and Photochemical Activation of Antisense Agents through a Nucleobase Caging Strategy. *ACS Chem. Biol.* **2013**, *8* (10), 2272–2282. https://doi.org/10.1021/cb400293e.

(307) Mikat, V.; Heckel, A. Light-Dependent RNA Interference with Nucleobase-Caged SiRNAs. *RNA* **2007**, *13* (12), 2341–2347. https://doi.org/10.1261/rna.753407.

(308) Govan, J. M.; Young, D. D.; Lusic, H.; Liu, Q.; Lively, M. O.; Deiters, A. Optochemical Control of RNA Interference in Mammalian Cells. *Nucleic Acids Res.* **2013**, *41* (22), 10518–10528. https://doi.org/10.1093/nar/gkt806.

(309) Ouyang, X.; Shestopalov, I. A.; Sinha, S.; Zheng, G.; Pitt, C. L. W.; Li, W. H.; Olson, A. J.; Chen, J. K. Versatile Synthesis and Rational Design of Caged Morpholinos. *J. Am. Chem. Soc.* **2009**, *131* (37), 13255–13269. https://doi.org/10.1021/ja809933h.

(310) Tallafuss, A.; Gibson, D.; Morcos, P.; Li, Y.; Seredick, S.; Eisen, J.; Washbourne, P. Turning Gene Function ON and OFF Using Sense and Antisense Photo-Morpholinos in Zebrafish. *Development* **2012**, *139* (9), 1691–1699. https://doi.org/10.1242/dev.072702.

(311) Tang, X. J.; Maegawa, S.; Weinberg, E. S.; Dmochowski, I. J. Regulating Gene Expression in Zebrafish Embryos Using Light-Activated, Negatively Charged Peptide Nucleic Acids. *J. Am. Chem. Soc.* **2007**, *129* (36), 11000–11001. https://doi.org/10.1021/ja073723s.

(312) Tang, X.; Swaminathan, J.; Gewirtz, A. M.; Dmochowski, I. J. Regulating Gene Expression in Human Leukemia Cells Using Light-Activated Oligodeoxynucleotides. *Nucleic Acids Res.* **2007**, *36* (2), 559–569. https://doi.org/10.1093/nar/gkm1029.

(313) Zheng, G.; Cochella, L.; Liu, J.; Hobert, O.; Li, W. H. Temporal and Spatial Regulation of Microrna Activity with Photoactivatable Cantimirs. *ACS Chem. Biol.* **2011**, *6* (12), 1332–1338. https://doi.org/10.1021/cb200290e.

(314) Yang, L.; Kim, H. B.; Sul, J.-Y.; Yeldell, S. B.; Eberwine, J. H.; Dmochowski, I. J. Efficient Synthesis of Light-Triggered Circular Antisense Oligonucleotides Targeting Cellular Protein Expression. *ChemBioChem* **2018**, *19* (12), 1250–1254. https://doi.org/10.1002/cbic.201800012.

(315) Yamazoe, S.; Liu, Q.; McQuade, L. E.; Deiters, A.; Chen, J. K. Sequential Gene Silencing Using Wavelength-Selective Caged Morpholino Oligonucleotides. *Angew. Chem. Int. Ed.* **2014**, *53* (38), 10114–10118. https://doi.org/10.1002/anie.201405355.

(316) O'Connor, M. J.; Beebe, L. L.; Deodato, D.; Ball, R. E.; Page, A. T.; Vanleuven, A. J.; Harris, K. T.; Park, S.; Hariharan, V.; Lauderdale, J. D.; Dore, T. M. Bypassing Glutamic Acid Decarboxylase 1 (Gad1) Induced Craniofacial Defects with a Photoactivatable Translation Blocker Morpholino. *ACS Chem. Neurosci.* **2019**, *10* (1), 266–278. https://doi.org/10.1021/acschemneuro.8b00231.

(317) Griepenburg, J. C.; Rapp, T. L.; Carroll, P. J.; Eberwine, J.; Dmochowski, I. J. Ruthenium-Caged Antisense Morpholinos for Regulating Gene Expression in Zebrafish Embryos. *Chem. Sci.* **2015**, *6* (4), 2342–2346. https://doi.org/10.1039/c4sc03990d.

(318) Blidner, R. A.; Svoboda, K. R.; Hammer, R. P.; Monroe, W. T. Photoinduced RNA Interference Using DMNPE-Caged 2′-Deoxy-2′- Fluoro Substituted Nucleic Acids in Vitro and in Vivo. *Mol. Biosyst.* **2008**, *4* (5), 431–440. https://doi.org/10.1039/b801532e.

(319) Jain, P. K.; Shah, S.; Friedman, S. H. Patterning of Gene Expression Using New Photolabile Groups Applied to Light Activated RNAi. *J. Am. Chem. Soc.* **2011**, *133* (3), 440–446. https://doi.org/10.1021/ja107226e.

(320) Kala, A.; Jain, P. K.; Karunakaran, D.; Shah, S.; Friedman, S. H. The Synthesis of Tetra-Modified RNA for the Multidimensional Control of Gene Expression via Light-Activated RNA Interference. *Nat. Protoc.* **2014**, *9* (1), 11–20. https://doi.org/10.1038/nprot.2013.165.

(321) Yu, L.; Jing, N.; Yang, Z.; Zhang, L.; Tang, X. Caged SiRNAs with Single Folic Acid Modification of Antisense RNA for Photomodulation of Exogenous and Endogenous Gene Expression in Cells. *Org. Biomol. Chem.* **2018**, *16* (38), 7029–7035. https://doi.org/10.1039/c8ob01952e.

(322) Meyer, A.; Mokhir, A. RNA Interference Controlled by Light of Variable Wavelength. *Angew. Chem. Int. Ed.* **2014**, *53* (47), 12840–12843. https://doi.org/10.1002/anie.201405885.

(323) Zhang, L.; Chen, C.; Fan, X.; Tang, X. Photomodulating Gene Expression by Using Caged SiRNAs with Single-Aptamer Modification. *ChemBioChem* **2018**, *19* (12), 1259–1263. https://doi.org/10.1002/cbic.201700623.

(324) Braun, G. B.; Pallaoro, A.; Wu, G.; Missirlis, D.; Zasadzinski, J. A.; Tirrell, M.; Reich, N. O. Laser-Activated Gene Silencing via Gold Nanoshell-SiRNA Conjugates. *ACS Nano* **2009**, *3* (7), 2007–2015. https://doi.org/10.1021/nn900469q.

(325) Huang, X.; Hu, Q.; Braun, G. B.; Pallaoro, A.; Morales, D. P.; Zasadzinski, J.; Clegg, D. O.; Reich, N. O. Light-Activated RNA Interference in Human Embryonic Stem Cells. *Biomaterials* **2015**, *63*, 70–79. https://doi.org/10.1016/j.biomaterials.2015.06.006.

(326) Riley, R. S.; Dang, M. N.; Billingsley, M. M.; Abraham, B.; Gundlach, L.; Day, E. S. Evaluating the Mechanisms of Light-Triggered SiRNA Release from Nanoshells for Temporal Control over Gene Regulation. *Nano Lett.* **2018**, *18* (6), 3565–3570. https://doi.org/10.1021/acs.nanolett.8b00681.

(327) Zhang, P.; Wang, C.; Zhao, J.; Xiao, A.; Shen, Q.; Li, L.; Li, J.; Zhang, J.; Min, Q.; Chen, J.; Chen, H.-Y.; Zhu, J.-J. Near Infrared-Guided Smart Nanocarriers for MicroRNA-Controlled Release of Doxorubicin/SiRNA with Intracellular ATP as Fuel. *ACS Nano* **2016**, *10* (3), 3637–3647. https://doi.org/10.1021/acsnano.5b08145.

(328) Wang, F.; Huang, Q.; Wang, Y.; Shi, L.; Shen, Y.; Guo, S. NIR-Light and GSH Activated Cytosolic P65-ShRNA Delivery for Precise Treatment of Metastatic Cancer. *J. Controlled Release* **2018**, *288*, 126–135. https://doi.org/10.1016/j.jconrel.2018.09.002.

(329) Yang, Y.; Liu, F.; Liu, X.; Xing, B. NIR Light Controlled Photorelease of SiRNA and Its Targeted Intracellular Delivery Based on Upconversion Nanoparticles. *Nanoscale* **2013**, *5* (1), 231–238. https://doi.org/10.1039/c2nr32835f.

(330) Huo, S.; Gong, N.; Jiang, Y.; Chen, F.; Guo, H.; Gan, Y.; Wang, Z.; Herrmann, A.; Liang, X. J. Gold-DNA Nanosunflowers for Efficient Gene Silencing with Controllable Transformation. *Sci. Adv.* **2019**, *5* (10), eaaw6264. https://doi.org/10.1126/sciadv.aaw6264.

(331) Hammill, M. L.; Isaacs-Trépanier, C.; Desaulniers, J.-P. SiRNAzos: A New Class of Azobenzene-Containing SiRNAs That Can Photochemically Regulate Gene Expression. *ChemistrySelect* **2017**, *2* (30), 9810–9814. https://doi.org/10.1002/slct.201702322.

(332) Hammill, M. L.; Islam, G.; Desaulniers, J. P. Reversible Control of RNA Interference by SiRNAzos. *Org. Biomol. Chem.* **2019**, *18* (1), 41–46. https://doi.org/10.1039/c9ob02509j.

(333) Hammill, M. L.; Islam, G.; Desaulniers, J. Synthesis, Derivatization and Photochemical Control of *Ortho* -Functionalized Tetrachlorinated Azobenzene-Modified SiRNAs. *ChemBioChem* **2020**, cbic.202000188. https://doi.org/10.1002/cbic.202000188.

(334) Sato, W.; Rasmussen, M.; Gaut, N.; Devarajan, M.; Stokes, K.; Deich, C.; Engelhart, A. E.; Adamala, K. P. A Gene Expression Control Technology for Cell-Free Systems and Synthetic Cells via Targeted Gene Silencing and Transfection. bioRxiv July 28, 2022, p 2022.07.28.501919. https://doi.org/10.1101/2022.07.28.501919.

(335) Hartmann, D.; Chowdhry, R.; Smith, J.; Booth, M. Blue Light-Activatable DNA for Remote Controlled Logic Gates in Synthetic Cells. ChemRxiv January 4, 2023. https://doi.org/10.26434/chemrxiv-2022-p8xgb-v2.

(336) Mazzotti, G.; Hartmann, D.; Booth, M. Precise, Orthogonal Remote-Control of Cell-Free Systems Using Photocaged Nucleic Acids. ChemRxiv February 2, 2023. https://doi.org/10.26434/chemrxiv-2023-ssv30.

(337) Hartmann, D.; Booth, M. Light-Controlled Cell-Free Protein Synthesis Using Phosphorothioate-Caged Antisense Oligonucleotides. ChemRxiv December 5, 2022. https://doi.org/10.26434/chemrxiv-2022-1lqc8.

(338) Horneck, G. UV Radiation (Biological Effects). In *Encyclopedia of Astrobiology*; Gargaud, M., Amils, R., Quintanilla, J. C., Cleaves, H. J. (Jim), Irvine, W. M., Pinti, D. L., Viso, M., Eds.; Springer: Berlin, Heidelberg, 2011; pp 1724–1726. https://doi.org/10.1007/978-3-642-11274-4_1640.

(339) Rauer, C.; Nogueira, J. J.; Marquetand, P.; González, L. Cyclobutane Thymine Photodimerization Mechanism Revealed by Nonadiabatic Molecular Dynamics. *J. Am. Chem. Soc.* **2016**, *138* (49), 15911–15916. https://doi.org/10.1021/jacs.6b06701.

(340) Alscher, R. G.; Donahue, J. L.; Cramer, C. L. Reactive Oxygen Species and Antioxidants: Relationships in Green Cells. *Physiol. Plant.* **1997**, *100* (2), 224–233. https://doi.org/10.1111/j.1399-3054.1997.tb04778.x.

(341) de Jager, T. L.; Cockrell, A. E.; Du Plessis, S. S. Ultraviolet Light Induced Generation of Reactive Oxygen Species. In *Ultraviolet Light in Human Health, Diseases and Environment*; Ahmad, S. I., Ed.; Advances in Experimental Medicine and Biology; Springer International Publishing: Cham, 2017; pp 15–23. https://doi.org/10.1007/978-3-319-56017-5_2.

(342) Schuch, A. P.; Moreno, N. C.; Schuch, N. J.; Menck, C. F. M.; Garcia, C. C. M. Sunlight Damage to Cellular DNA: Focus on Oxidatively Generated Lesions. *Free Radic. Biol. Med.* **2017**, *107*, 110–124. https://doi.org/10.1016/j.freeradbiomed.2017.01.029.

(343) Mourant, J. R.; Freyer, J. P.; Hielscher, A. H.; Eick, A. A.; Shen, D.; Johnson, T. M. Mechanisms of Light Scattering from Biological Cells Relevant to Noninvasive Optical-Tissue Diagnostics. *Appl. Opt.* **1998**, *37* (16), 3586–3593. https://doi.org/10.1364/AO.37.003586.
(344) Brahma, A.; De, D.; Bhattacharyya, D. Rayleigh Scattering Technique as a Method to Study Protein–Protein Interaction Using Spectrofluorimeters. *Curr. Sci.* **2009**, *96* (7), 940–946.
(345) Zhang, D.; Jin, S.; Piao, X.; Devaraj, N. K. Multiplexed Photoactivation of MRNA with Single-Cell Resolution. *ACS Chem. Biol.* **2020**, *15* (7), 1773–1779. https://doi.org/10.1021/acschembio.0c00205.
(346) Blümler, A.; Schwalbe, H.; Heckel, A. Solid-Phase-Supported Chemoenzymatic Synthesis of a Light-Activatable TRNA Derivative. *Angew. Chem. Int. Ed.* **2022**, *61* (1), e202111613. https://doi.org/10.1002/anie.202111613.
(347) Peterson, J. A.; Yuan, D.; Winter, A. H. Multiwavelength Control of Mixtures Using Visible Light-Absorbing Photocages. *J. Org. Chem.* **2021**, *86* (14), 9781–9787. https://doi.org/10.1021/acs.joc.1c00658.
(348) Bochet, C. G. Wavelength-Selective Cleavage of Photolabile Protecting Groups. *Tetrahedron Lett.* **2000**, *41* (33), 6341–6346. https://doi.org/10.1016/S0040-4039(00)01050-9.
(349) San Miguel, V.; Bochet, C. G.; Del Campo, A. Wavelength-Selective Caged Surfaces: How Many Functional Levels Are Possible? *J. Am. Chem. Soc.* **2011**, *133* (14), 5380–5388. https://doi.org/10.1021/ja110572j.
(350) Hansen, M. J.; Velema, W. A.; Lerch, M. M.; Szymanski, W.; Feringa, B. L. Wavelength-Selective Cleavage of Photoprotecting Groups: Strategies and Applications in Dynamic Systems. *Chem. Soc. Rev.* **2015**, *44* (11), 3358–3377. https://doi.org/10.1039/C5CS00118H.
(351) Weinrich, T.; Gränz, M.; Grünewald, C.; Prisner, T. F.; Göbel, M. W. Synthesis of a Cytidine Phosphoramidite with Protected Nitroxide Spin Label for EPR Experiments with RNA. *Eur. J. Org. Chem.* **2017**, *2017* (3), 491–496. https://doi.org/10.1002/ejoc.201601174.
(352) Tanemura, K.; Suzuki, T.; Nishida, Y.; Satsumabayashi, K.; Horaguchi, T. A Mild and Efficient Procedure for α-Bromination of Ketones Using N-Bromosuccinimide Catalysed by Ammonium Acetate. *Chem. Commun.* **2004**, No. 4, 470–471. https://doi.org/10.1039/B315340A.
(353) Luyai, A.; Lasanajak, Y.; Smith, D. F.; Cummings, R. D.; Song, X. Facile Preparation of Fluorescent Neoglycoproteins Using P-Nitrophenyl Anthranilate as a Heterobifunctional Linker. *Bioconjug. Chem.* **2009**, *20* (8), 1618–1624. https://doi.org/10.1021/bc900189h.
(354) Filonov, G. S.; Moon, J. D.; Svensen, N.; Jaffrey, S. R. Broccoli: Rapid Selection of an RNA Mimic of Green Fluorescent Protein by Fluorescence-Based Selection and Directed Evolution. *J. Am. Chem. Soc.* **2014**, *136* (46), 16299–16308. https://doi.org/10.1021/ja508478x.
(355) Leathers, A.; Walczak, M.; Brady, R. A.; Al Samad, A.; Kotar, J.; Booth, M. J.; Cicuta, P.; Di Michele, L. Reaction–Diffusion Patterning of DNA-Based Artificial Cells. *J. Am. Chem. Soc.* **2022**, *144* (38), 17468–17476. https://doi.org/10.1021/jacs.2c06140.
(356) Kumagai, R.; Ono, R.; Sakimoto, S.; Suzuki, C.; Kanno, K.; Aoyama, H.; Usukura, J.; Kobayashi, M.; Akiyama, H.; Itabashi, H.; Hiyama, M. Photo-Cleaving and Photo-Bleaching Quantum Yields of Coumarin-Caged Luciferin. *J.*

Photochem. Photobiol. Chem. **2023**, *434*, 114230. https://doi.org/10.1016/j.jphotochem.2022.114230.

(357) Shekhawat, S. S.; Ghosh, I. Split-Protein Systems: Beyond Binary Protein–Protein Interactions. *Curr. Opin. Chem. Biol.* **2011**, *15* (6), 789–797. https://doi.org/10.1016/j.cbpa.2011.10.014.

(358) Broome, A. M.; Bhavsar, N.; Ramamurthy, G.; Newton, G.; Basilion, J. P. Expanding the Utility of β-Galactosidase Complementation: Piece by Piece. *Mol. Pharm.* **2010**, *7* (1), 60–74. https://doi.org/10.1021/mp900188e.

(359) Ullmann, A.; Jacob, F.; Monod, J. Characterization by in Vitro Complementation of a Peptide Corresponding to an Operator-Proximal Segment of the β-Galactosidase Structural Gene of Escherichia Coli. *J. Mol. Biol.* **1967**, *24* (2), 339–343. https://doi.org/10.1016/0022-2836(67)90341-5.

(360) Lussier, F.; Staufer, O.; Platzman, I.; Spatz, J. P. Can Bottom-Up Synthetic Biology Generate Advanced Drug-Delivery Systems? *Trends Biotechnol.* **2021**, *39* (5), 445–459. https://doi.org/10.1016/j.tibtech.2020.08.002.

(361) Guindani, C.; da Silva, L. C.; Cao, S.; Ivanov, T.; Landfester, K. Synthetic Cells: From Simple Bio-Inspired Modules to Sophisticated Integrated Systems. *Angew. Chem. Int. Ed.* **2022**, *61* (16), e202110855. https://doi.org/10.1002/anie.202110855.

(362) Shaner, N. C.; Lambert, G. G.; Chammas, A.; Ni, Y.; Cranfill, P. J.; Baird, M. A.; Sell, B. R.; Allen, J. R.; Day, R. N.; Israelsson, M.; Davidson, M. W.; Wang, J. A Bright Monomeric Green Fluorescent Protein Derived from Branchiostoma Lanceolatum. *Nat. Methods* **2013**, *10* (5), 407–409. https://doi.org/10.1038/nmeth.2413.

(363) Pautot, S.; Frisken, B. J.; Weitz, D. A. Production of Unilamellar Vesicles Using an Inverted Emulsion. *Langmuir* **2003**, *19* (7), 2870–2879. https://doi.org/10.1021/la026100v.

(364) Spoelstra, W. K.; Deshpande, S.; Dekker, C. Tailoring the Appearance: What Will Synthetic Cells Look Like? *Curr. Opin. Biotechnol.* **2018**, *51*, 47–56. https://doi.org/10.1016/j.copbio.2017.11.005.

(365) Venkatesan, G. A.; Sarles, S. A. Droplet Immobilization within a Polymeric Organogel Improves Lipid Bilayer Durability and Portability. *Lab. Chip* **2016**, *16* (11), 2116–2125. https://doi.org/10.1039/C6LC00391E.

(366) Kremers, G.-J.; Goedhart, J.; van Munster, E. B.; Gadella, T. W. J. Cyan and Yellow Super Fluorescent Proteins with Improved Brightness, Protein Folding, and FRET Förster Radius,. *Biochemistry* **2006**, *45* (21), 6570–6580. https://doi.org/10.1021/bi0516273.

(367) Shaner, N. C.; Campbell, R. E.; Steinbach, P. A.; Giepmans, B. N. G.; Palmer, A. E.; Tsien, R. Y. Improved Monomeric Red, Orange and Yellow Fluorescent Proteins Derived from Discosoma Sp. Red Fluorescent Protein. *Nat. Biotechnol.* **2004**, *22* (12), 1567–1572. https://doi.org/10.1038/nbt1037.

(368) Pattanayak, S.; Sarode, B. R.; Deiters, A.; Chen, J. K. Bicyclic Caged Morpholino Oligonucleotides for Optical Gene Silencing**. *ChemBioChem* **2022**, *23* (21), e202200374. https://doi.org/10.1002/cbic.202200374.

(369) Wu, L.; Wang, Y.; Wu, J.; Lv, C.; Wang, J.; Tang, X. Caged Circular Antisense Oligonucleotides for Photomodulation of RNA Digestion and Gene Expression in Cells. *Nucleic Acids Res.* **2013**, *41* (1), 677–686. https://doi.org/10.1093/nar/gks996.

(370) Tang, X.; Su, M.; Yu, L.; Lv, C.; Wang, J.; Li, Z. Photomodulating RNA Cleavage Using Photolabile Circular Antisense Oligodeoxynucleotides. *Nucleic Acids Res.* **2010**, *38* (11), 3848–3855. https://doi.org/10.1093/nar/gkq079.

(371) Sun, Y.-J.; Chen, W.-D.; Liu, J.; Li, J.-J.; Zhang, Y.; Cai, W.-Q.; Liu, L.; Tang, X.-J.; Hou, J.; Wang, M.; Cheng, L. A Conformational Restriction Strategy for the Control of CRISPR/Cas Gene Editing with Photoactivatable Guide RNAs. *Angew. Chem. Int. Ed.* **2023**, *62* (5), e202212413. https://doi.org/10.1002/anie.202212413.

(372) Luong, J. H. T.; Vashist, S. K. Chemistry of Biotin–Streptavidin and the Growing Concern of an Emerging Biotin Interference in Clinical Immunoassays. *ACS Omega* **2020**, *5* (1), 10–18. https://doi.org/10.1021/acsomega.9b03013.

(373) Albarran, B.; To, R.; Stayton, P. S. A TAT–Streptavidin Fusion Protein Directs Uptake of Biotinylated Cargo into Mammalian Cells. *Protein Eng. Des. Sel.* **2005**, *18* (3), 147–152. https://doi.org/10.1093/protein/gzi014.

(374) Schultz, J.; Lin, Y.; Sanderson, J.; Zuo, Y.; Stone, D.; Mallett, R.; Wilbert, S.; Axworthy, D. A Tetravalent Single-Chain Antibody-Streptavidin Fusion Protein for Pretargeted Lymphoma Therapy1. *Cancer Res.* **2000**, *60* (23), 6663–6669.

(375) López-Andarias, J.; Saarbach, J.; Moreau, D.; Cheng, Y.; Derivery, E.; Laurent, Q.; González-Gaitán, M.; Winssinger, N.; Sakai, N.; Matile, S. Cell-Penetrating Streptavidin: A General Tool for Bifunctional Delivery with Spatiotemporal Control, Mediated by Transport Systems Such as Adaptive Benzopolysulfane Networks. *J. Am. Chem. Soc.* **2020**, jacs.9b13621. https://doi.org/10.1021/jacs.9b13621.

(376) RCSB Protein Data. *RCSB PDB - 6J6J: Biotin-bound streptavidin*. http://doi.org/10.2210/pdb6J6J/pdb (accessed 2023-01-19).

(377) RCSB Protein Data. *RCSB PDB - 2VAI: Solution structure of a B-DNA hairpin at high pressure*. http://doi.org/10.2210/pdb2VAI/pdb (accessed 2023-01-19).

(378) Hendrickson, W. A.; Pähler, A.; Smith, J. L.; Satow, Y.; Merritt, E. A.; Phizackerley, R. P. Crystal Structure of Core Streptavidin Determined from Multiwavelength Anomalous Diffraction of Synchrotron Radiation. *Proc. Natl. Acad. Sci.* **1989**, *86* (7), 2190–2194. https://doi.org/10.1073/pnas.86.7.2190.

(379) Shah, S.; Rangarajan, S.; Friedman, S. H. Light-Activated RNA Interference. *Angew. Chem. Int. Ed.* **2005**, *44* (9), 1328–1332. https://doi.org/10.1002/anie.200461458.

(380) Shah, S.; Jain, P. K.; Kala, A.; Karunakaran, D.; Friedman, S. H. Light-Activated RNA Interference Using Double-Stranded SiRNA Precursors Modified Using a Remarkable Regiospecificity of Diazo-Based Photolabile Groups. *Nucleic Acids Res.* **2009**, *37* (13), 4508–4517. https://doi.org/10.1093/nar/gkp415.

(381) Iyer, R. P.; Phillips, L. R.; Egan, W.; Regan, J. B.; Beaucage, S. L. The Automated Synthesis of Sulfur-Containing Oligodeoxyribonucleotides Using 3H-1,2-Benzodithiol-3-One 1,1-Dioxide as a Sulfur-Transfer Reagent. *J. Org. Chem.* **1990**, *55* (15), 4693–4699. https://doi.org/10.1021/jo00302a039.

(382) Spitzer, S.; Eckstein, F. Inhibition of Deoxyribonucleases by Phosphorothioate Groups in Oligodeoxyribonucleotides. *Nucleic Acids Res.* **1988**, *16* (24), 11691–11704. https://doi.org/10.1093/nar/16.24.11691.

(383) Gaus, H. J.; Gupta, R.; Chappell, A. E.; Østergaard, M. E.; Swayze, E. E.; Seth, P. P. Characterization of the Interactions of Chemically-Modified Therapeutic Nucleic Acids with Plasma Proteins Using a Fluorescence Polarization Assay. *Nucleic Acids Res.* **2019**, *47* (3), 1110–1122. https://doi.org/10.1093/nar/gky1260.

(384) Watanabe, T. A.; Geary, R. S.; Levin, A. A. Plasma Protein Binding of an Antisense Oligonucleotide Targeting Human ICAM-1 (ISIS 2302). *Oligonucleotides* **2006**, *16* (2), 169–180. https://doi.org/10.1089/oli.2006.16.169.
(385) Crooke, S. T.; Wang, S.; Vickers, T. A.; Shen, W.; Liang, X. Cellular Uptake and Trafficking of Antisense Oligonucleotides. *Nat. Biotechnol.* **2017**, *35* (3), 230–237. https://doi.org/10.1038/nbt.3779.
(386) Gagliardi, M.; Ashizawa, A. T. The Challenges and Strategies of Antisense Oligonucleotide Drug Delivery. *Biomedicines* **2021**, *9* (4), 433. https://doi.org/10.3390/biomedicines9040433.
(387) Laurent, Q.; Martinent, R.; Moreau, D.; Winssinger, N.; Sakai, N.; Matile, S. Oligonucleotide Phosphorothioates Enter Cells by Thiol-Mediated Uptake. *Angew. Chem. Int. Ed.* **2021**, anie.202107327. https://doi.org/10.1002/anie.202107327.
(388) Wang, L.; Jiang, S.; Deng, Z.; Dedon, P. C.; Chen, S. DNA Phosphorothioate Modification—a New Multi-Functional Epigenetic System in Bacteria. *FEMS Microbiol. Rev.* **2019**, *43* (2), 109–122. https://doi.org/10.1093/femsre/fuy036.
(389) Fidanza, J. A.; McLaughlin, L. W. Introduction of Reporter Groups at Specific Sites in DNA Containing Phosphorothioate Diesters. *J. Am. Chem. Soc.* **1989**, *111* (25), 9117–9119. https://doi.org/10.1021/ja00207a028.
(390) Conway, N. E.; McLaughlin, L. W. The Covalent Attachment of Multiple Fluorophores to DNA Containing Phosphorothioate Diesters Results in Highly Sensitive Detection of Single-Stranded DNA. *Bioconjug. Chem.* **1991**, *2* (6), 452–457. https://doi.org/10.1021/bc00012a013.
(391) Chen, M.; Gothelf, K. V. Labeling of DNA via Rearrangement of S-2-Aminoethyl Phosphorothioates to N-(2-Mercaptoethyl)Phosphoramidates. *Org. Biomol. Chem.* **2008**, *6* (5), 908. https://doi.org/10.1039/b717664c.
(392) Burns, J. R.; Stulz, E.; Howorka, S. Self-Assembled DNA Nanopores That Span Lipid Bilayers. *Nano Lett.* **2013**, *13* (6), 2351–2356. https://doi.org/10.1021/nl304147f.
(393) Gut, I. G.; Beck, S. A Procedure for Selective DNA Alkylation and Detection by Mass Spectrometry. *Nucleic Acids Res.* **1995**, *23* (8), 1367–1373. https://doi.org/10.1093/nar/23.8.1367.
(394) Guo, Y.; Zhang, J.; Ding, F.; Pan, G.; Li, J.; Feng, J.; Zhu, X.; Zhang, C. Stressing the Role of DNA as a Drug Carrier: Synthesis of DNA–Drug Conjugates through Grafting Chemotherapeutics onto Phosphorothioate Oligonucleotides. *Adv. Mater.* **2019**, *31* (16), 1807533. https://doi.org/10.1002/adma.201807533.
(395) Wang, X.; Feng, M.; Xiao, L.; Tong, A.; Xiang, Y. Postsynthetic Modification of DNA Phosphodiester Backbone for Photocaged DNAzyme. *ACS Chem. Biol.* **2016**, *11* (2), 444–451. https://doi.org/10.1021/acschembio.5b00867.
(396) Xu, X.; Xiao, L.; Gu, C.; Shang, J.; Xiang, Y. Wavelength-Selective Activation of Photocaged DNAzymes for Metal Ion Sensing in Live Cells. *ACS Omega* **2021**, *6* (20), 13153–13160. https://doi.org/10.1021/acsomega.1c00976.
(397) Geary, R. S.; Norris, D.; Yu, R.; Bennett, C. F. Pharmacokinetics, Biodistribution and Cell Uptake of Antisense Oligonucleotides. *Adv. Drug Deliv. Rev.* **2015**, *87*, 46–51. https://doi.org/10.1016/j.addr.2015.01.008.
(398) Ding, Y.; Chan, C. Y.; Lawrence, C. E. Sfold Web Server for Statistical Folding and Rational Design of Nucleic Acids. *Nucleic Acids Res.* **2004**, *32* (suppl_2), W135–W141. https://doi.org/10.1093/nar/gkh449.
(399) Lee, H.; Cho, H.; Kim, J.; Lee, S.; Yoo, J.; Park, D.; Lee, G. RNase H Is an Exo- and Endoribonuclease with Asymmetric Directionality, Depending on the Binding

Mode to the Structural Variants of RNA:DNA Hybrids. *Nucleic Acids Res.* **2022**, *50* (4), 1801–1814. https://doi.org/10.1093/nar/gkab1064.
(400) Khandelwal, G.; Bhyravabhotla, J. A Phenomenological Model for Predicting Melting Temperatures of DNA Sequences. *PLOS ONE* **2010**, *5* (8), e12433. https://doi.org/10.1371/journal.pone.0012433.
(401) Arangundy-Franklin, S.; Taylor, A. I.; Porebski, B. T.; Genna, V.; Peak-Chew, S.; Vaisman, A.; Woodgate, R.; Orozco, M.; Holliger, P. A Synthetic Genetic Polymer with an Uncharged Backbone Chemistry Based on Alkyl Phosphonate Nucleic Acids. *Nat. Chem.* **2019**, *11* (6), 533–542. https://doi.org/10.1038/s41557-019-0255-4.
(402) Hartmann, G. Chapter Four - Nucleic Acid Immunity. In *Advances in Immunology*; Alt, F. W., Ed.; Academic Press, 2017; Vol. 133, pp 121–169. https://doi.org/10.1016/bs.ai.2016.11.001.
(403) Peterson, J. A.; Wijesooriya, C.; Gehrmann, E. J.; Mahoney, K. M.; Goswami, P. P.; Albright, T. R.; Syed, A.; Dutton, A. S.; Smith, E. A.; Winter, A. H. Family of BODIPY Photocages Cleaved by Single Photons of Visible/Near-Infrared Light. *J. Am. Chem. Soc.* **2018**, *140* (23), 7343–7346. https://doi.org/10.1021/jacs.8b04040.
(404) Kand, D.; Liu, P.; Navarro, M. X.; Fischer, L. J.; Rousso-Noori, L.; Friedmann-Morvinski, D.; Winter, A. H.; Miller, E. W.; Weinstain, R. Water-Soluble BODIPY Photocages with Tunable Cellular Localization. *J. Am. Chem. Soc.* **2020**, *142* (11), 4970–4974. https://doi.org/10.1021/jacs.9b13219.
(405) Poryvai, A.; Galkin, M.; Shvadchak, V.; Slanina, T. Red-Shifted Water-Soluble BODIPY Photocages for Visualisation and Controllable Cellular Delivery of Signaling Lipids. *Angew. Chem. Int. Ed.* **2022**, *61* (34), e202205855. https://doi.org/10.1002/anie.202205855.
(406) Black, C. E.; Zhou, E.; DeAngelo, C. M.; Asante, I.; Louie, S. G.; Petasis, N. A.; Humayun, M. S. Cyanine Nanocages Activated by Near-Infrared Light for the Targeted Treatment of Traumatic Brain Injury. *Front. Chem.* **2020**, *8*, 769. https://doi.org/doi.org/10.3389/fchem.2020.00769.
(407) Zhang, Y.; Yan, C.; Zheng, Q.; Jia, Q.; Wang, Z.; Shi, P.; Guo, Z. Harnessing Hypoxia-Dependent Cyanine Photocages for In Vivo Precision Drug Release. *Angew. Chem. Int. Ed.* **2021**, *60* (17), 9553–9561. https://doi.org/10.1002/anie.202017349.
(408) Janeková, H.; Russo, M.; Ziegler, U.; Štacko, P. Photouncaging of Carboxylic Acids from Cyanine Dyes with Near-Infrared Light**. *Angew. Chem. Int. Ed.* **2022**, *61* (33), e202204391. https://doi.org/10.1002/anie.202204391.
(409) Chen, G.; Qiu, H.; Prasad, P. N.; Chen, X. Upconversion Nanoparticles: Design, Nanochemistry, and Applications in Theranostics. *Chem. Rev.* **2014**, *114* (10), 5161–5214. https://doi.org/10.1021/cr400425h.
(410) Zhang, D.; Peng, R.; Liu, W.; Donovan, M. J.; Wang, L.; Ismail, I.; Li, J.; Li, J.; Qu, F.; Tan, W. Engineering DNA on the Surface of Upconversion Nanoparticles for Bioanalysis and Therapeutics. *ACS Nano* **2021**, *15* (11), 17257–17274. https://doi.org/10.1021/acsnano.1c08036.
(411) Fantoni, N. Z.; El-Sagheer, A. H.; Brown, T. A Hitchhiker's Guide to Click-Chemistry with Nucleic Acids. *Chem. Rev.* **2021**, *121* (12), 7122–7154. https://doi.org/10.1021/acs.chemrev.0c00928.
(412) Ueda, T.; Tohda, H.; Chikazumi, N.; Eckstein, F.; Watanabe, K. Phosphorothioate-Containing RNAs Show MRNA Activity in the Prokaryotic

Translation Systems in Vitro. *Nucleic Acids Res.* **1991**, *19* (3), 547–552. https://doi.org/10.1093/nar/19.3.547.

(413) Stump, W. T.; Hall, K. B. SP6 RNA Polymerase Efficiently Synthesizes RNA from Short Double-Stranded DNA Templates. *Nucleic Acids Res.* **1993**, *21* (23), 5480–5484. https://doi.org/10.1093/nar/21.23.5480.

(414) Meiklejohn, A. L.; Gralla, J. D. Activation of the Lac Promoter and Its Variants: Synergistic Effects of Catabolite Activator Protein and Supercoiling in Vitro. *J. Mol. Biol.* **1989**, *207* (4), 661–673. https://doi.org/10.1016/0022-2836(89)90236-2.

(415) Bass, S. H.; Yansura, D. G. Application of the E. Coli Trp Promoter. *Mol. Biotechnol.* **2000**, *16* (3), 253–260. https://doi.org/10.1385/MB:16:3:253.

(416) de Boer, H. A.; Comstock, L. J.; Vasser, M. The Tac Promoter: A Functional Hybrid Derived from the Trp and Lac Promoters. *Proc. Natl. Acad. Sci.* **1983**, *80* (1), 21–25. https://doi.org/10.1073/pnas.80.1.21.

(417) Wang, X.; Xu, Z.; Tian, Z.; Zhang, X.; Xu, D.; Li, Q.; Zhang, J.; Wang, T. The EF-1α Promoter Maintains High-Level Transgene Expression from Episomal Vectors in Transfected CHO-K1 Cells. *J. Cell. Mol. Med.* **2017**, *21* (11), 3044–3054. https://doi.org/10.1111/jcmm.13216.

(418) Norris, M. D.; Seidel, K.; Kirschning, A. Externally Induced Drug Release Systems with Magnetic Nanoparticle Carriers: An Emerging Field in Nanomedicine. *Adv. Ther.* **2019**, *2* (1), 1800092. https://doi.org/10.1002/adtp.201800092.

(419) N'Guyen, T. T. T.; Duong, H. T. T.; Basuki, J.; Montembault, V.; Pascual, S.; Guibert, C.; Fresnais, J.; Boyer, C.; Whittaker, M. R.; Davis, T. P.; Fontaine, L. Functional Iron Oxide Magnetic Nanoparticles with Hyperthermia-Induced Drug Release Ability by Using a Combination of Orthogonal Click Reactions. *Angew. Chem. Int. Ed.* **2013**, *52* (52), 14152–14156. https://doi.org/10.1002/anie.201306724.

(420) Hammad, M.; Nica, V.; Hempelmann, R. On-Command Controlled Drug Release by Diels-Alder Reaction Using Bi-Magnetic Core/Shell Nano-Carriers. *Colloids Surf. B Biointerfaces* **2017**, *150*, 15–22. https://doi.org/10.1016/j.colsurfb.2016.11.005.

(421) Seidel, K.; Balakrishnan, A.; Alexiou, C.; Janko, C.; Komoll, R.-M.; Wang, L.-L.; Kirschning, A.; Ott, M. Synthesis of Magnetic-Nanoparticle/Ansamitocin Conjugates—Inductive Heating Leads to Decreased Cell Proliferation In Vitro and Attenuation Of Tumour Growth In Vivo. *Chem. – Eur. J.* **2017**, *23* (50), 12326–12337. https://doi.org/10.1002/chem.201701491.

(422) Derfus, A. M.; von Maltzahn, G.; Harris, T. J.; Duza, T.; Vecchio, K. S.; Ruoslahti, E.; Bhatia, S. N. Remotely Triggered Release from Magnetic Nanoparticles. *Adv. Mater.* **2007**, *19* (22), 3932–3936. https://doi.org/10.1002/adma.200700091.

(423) Chen, P.-S.; Chiu, W.-T.; Hsu, P.-L.; Lin, S.-C.; Peng, I.-C.; Wang, C.-Y.; Tsai, S.-J. Pathophysiological Implications of Hypoxia in Human Diseases. *J. Biomed. Sci.* **2020**, *27* (1), 63. https://doi.org/10.1186/s12929-020-00658-7.

(424) Wallabregue, A. L. D.; Bolland, H.; Faulkner, S.; Hammond, E. M.; Conway, S. J. Two Color Imaging of Different Hypoxia Levels in Cancer Cells. *J. Am. Chem. Soc.* **2023**, *145* (4), 2572–2583. https://doi.org/10.1021/jacs.2c12493.

(425) Hernick, M.; Borch, R. F. Studies on the Mechanisms of Activation of Indolequinone Phosphoramidate Prodrugs. *J. Med. Chem.* **2003**, *46* (1), 148–154. https://doi.org/10.1021/jm0203229.

(426) Tanabe, K.; Makimura, Y.; Tachi, Y.; Imagawa-Sato, A.; Nishimoto, S. Hypoxia-Selective Activation of 5-Fluorodeoxyuridine Prodrug Possessing Indolequinone

Structure: Radiolytic Reduction and Cytotoxicity Characteristics. *Bioorg. Med. Chem. Lett.* **2005**, *15* (9), 2321–2324. https://doi.org/10.1016/j.bmcl.2005.03.013.

(427) Crooke, S. T.; Geary, R. S. Clinical Pharmacological Properties of Mipomersen (Kynamro), a Second Generation Antisense Inhibitor of Apolipoprotein B. *Br. J. Clin. Pharmacol.* **2013**, *76* (2), 269–276. https://doi.org/10.1111/j.1365-2125.2012.04469.x.

(428) Iwamoto, N.; Butler, D. C. D. D.; Svrzikapa, N.; Mohapatra, S.; Zlatev, I.; Sah, Di. W. Y. Y.; Meena; Standley, S. M.; Lu, G.; Apponi, L. H.; Frank-Kamenetsky, M.; Zhang, J. J.; Vargeese, C.; Verdine, G. L. Control of Phosphorothioate Stereochemistry Substantially Increases the Efficacy of Antisense Oligonucleotides. *Nat. Biotechnol.* **2017**, *35* (9), 845–851. https://doi.org/10.1038/nbt.3948.

(429) Østergaard, M. E.; De Hoyos, C. L.; Wan, W. B.; Shen, W.; Low, A.; Berdeja, A.; Vasquez, G.; Murray, S.; Migawa, M. T.; Liang, X. H.; Swayze, E. E.; Crooke, S. T.; Seth, P. P. Understanding the Effect of Controlling Phosphorothioate Chirality in the DNA Gap on the Potency and Safety of Gapmer Antisense Oligonucleotides. *Nucleic Acids Res.* **2020**, *48* (4), 1691–1700. https://doi.org/10.1093/nar/gkaa031.

(430) Knouse, K. W.; deGruyter, J. N.; Schmidt, M. A.; Zheng, B.; Vantourout, J. C.; Kingston, C.; Mercer, S. E.; Mcdonald, I. M.; Olson, R. E.; Zhu, Y.; Hang, C.; Zhu, J.; Yuan, C.; Wang, Q.; Park, P.; Eastgate, M. D.; Baran, P. S. Unlocking P(V): Reagents for Chiral Phosphorothioate Synthesis. *Science* **2018**, *361* (6408), 1234–1238. https://doi.org/10.1126/SCIENCE.AAU3369.

(431) Huang, Y.; Knouse, K. W.; Qiu, S.; Hao, W.; Padial, N. M.; Vantourout, J. C.; Zheng, B.; Mercer, S. E.; Lopez-Ogalla, J.; Narayan, R.; Olson, R. E.; Blackmond, D. G.; Eastgate, M. D.; Schmidt, M. A.; McDonald, I. M.; Baran, P. S. A P(V) Platform for Oligonucleotide Synthesis. *Science* **2021**, *373* (6560), 1265–1270. https://doi.org/10.1126/science.abi9727.

(432) Favre, A.; Grugier, J.; Brans, A.; Joris, B.; Marchand-Brynaert, J. 6-Aminopenicillanic Acid (6-APA) Derivatives Equipped with Anchoring Arms. *Tetrahedron* **2012**, *68* (52), 10818–10826. https://doi.org/10.1016/j.tet.2011.10.100.

(433) Susumu, K.; Uyeda, H. T.; Medintz, I. L.; Pons, T.; Delehanty, J. B.; Mattoussi, H. Enhancing the Stability and Biological Functionalities of Quantum Dots via Compact Multifunctional Ligands. *J. Am. Chem. Soc.* **2007**, *129* (45), 13987–13996. https://doi.org/10.1021/ja0749744.

(434) Trester-Zedlitz, M.; Kamada, K.; Burley, S. K.; Fenyö, D.; Chait, B. T.; Muir, T. W. A Modular Cross-Linking Approach for Exploring Protein Interactions. *J. Am. Chem. Soc.* **2003**, *125* (9), 2416–2425. https://doi.org/10.1021/ja026917a.

9 APPENDICES

A - DNA SEQUENCES OF GENES 236
B - NMR SPECTRA 243
C - OLIGONUCLEOTIDE MASS SPECTRA 259
D - REACTION SCREENING FOR PS MODIFICATION 274
E - PHOTOCLEAVAGE MASS SPECTROMETRY DATA 280
F - MELTING TEMPERATURE DATA 283
G - HPLC PURIFICATIONS OF MODIFIED OLIGONUCLEOTIDES 287

A - DNA SEQUENCES OF GENES

	Gene	Sequence (5' – 3')
1	*mVenus*	GAAATTAATACGACTCACTATAGGGTCTAGAAATAATTTTGTTTA ACTTTAAGAAGGAGGTATACAT**ATG**GTGAGCAAGGGCGAGGAG CTGTTCACCGGGGTGGTGCCCATCCTGGTCGAGCTGGACGGC GACGTAAACGGCCACAAGTTCAGCGTGTCCGGCGAGGGCGAG GGCGATGCCACCTACGGCAAGCTGACCCTGAAGCTCATCTGCA CCACCGGCAAGCTGCCCGTGCCCTGGCCCACCCTCGTGACCA CCCTCGGCTACGGCCTGCAGTGCTTCGCCCGCTACCCCGACC ACATGAAGCAGCACGACTTCTTCAAGTCCGCCATGCCCGAAGG CTACGTCCAGGAGCGCACCATCTTCTTCAAGGACGACGGCAAC TACAAGACCCGCGCCGAGGTGAAGTTCGAGGGCGACACCCTG GTGAACCGCATCGAGCTGAAGGGCATCGACTTCAAGGAGGAC GGCAACATCCTGGGGCACAAGCTGGAGTACAACTACAACAGCC ACAACGTCTATATCACCGCCGACAAGCAGAAGAACGGCATCAA GGCCAACTTCAAGATCCGCCACAACATCGAGGACGGCGGCGT GCAGCTCGCCGACCACTACCAGCAGAACACCCCCATCGGCGA CGGCCCCGTGCTGCTGCCCGACAACCACTACCTGAGCTACCA GTCCAAGCTGAGCAAAGACCCCAACGAGAAGCGCGATCACAT GGTCCTGCTGGAGTTCGTGACCGCCGCCGGGATCACTCTCGG CATGGACGAGCTGTACAAG**TAA**TGAGGATCCCGGGAATTCTCG AGTAAGGTTAACCTGCAGGAGGCCTTTAATTAAGGTGGTGCGG CCGCGCTAGCGGTCCCGGGGGATCGATCCGGCTGCTAACAAA GCCCGAAAGGAAGCTGAGTTGGCTGCTGCCACCGCTGAGCAA TAACTAGCATAACCCCTTGGGGCCTCTAAACGGGTCTTGAGGG GTTTTTTGCTGAAAGGAGGAACTATATC
2	*lacZ*	GAAATTAATACGACTCACTATAGGGTCTAGAAATAATTTTGTTTA ACTTTAAGAAGGAGGTATACAT**ATG**ACCATGATTACGGATTCAC TGGCCGTCGTTTTACAACGTCGTGACTGGGAAAACCCTGGCGT TACCCAACTTAATCGCCTTGCAGCACATCCCCCTTTCGCCAGCT GGCGTAATAGCGAAGAGGCCCGCACCGATCGCCCTTCCCAAC AGTTGCGCAGCCTGAATGGCGAATGGCGCTTTGCCTGGTTTCC GGCACCAGAAGCGGTGCCGGAAAGCTGGCTGGAGTGCGATCT

		TCCTGAGGCCGATACTGTCGTCGTCCCCTCAAACTGGCAGATG CACGGTTACGATGCGCCCATCTACACCAACGTGACCTATCCCA TTACGGTCAATCCGCCGTTTGTTCCCACGGAGAATCCGACGGG TTGTTACTCGCTCACATTTAATGTTGATGAAAGCTGGCTACAGG AAGGCCAGACGCGAATTATTTTTGATGGCGTTAACTCGGCGTTT CATCTGTGGTGCAACGGGCGCTGGGTCGGTTACGGCCAGGAC AGTCGTTTGCCGTCTGAATTTGACCTGAGCGCATTTTTACGCGC CGGAGAAAACCGCCTCGCGGTGATGGTGCTGCGCTGGAGTGA CGGCAGTTATCTGGAAGATCAGGATATGTGGCGGATGAGCGG CATTTTCCGTGACGTCTCGTTGCTGCATAAACCGACTACACAAA TCAGCGATTTCCATGTTGCCACTCGCTTTAATGATGATTTCAGC CGCGCTGTACTGGAGGCTGAAGTTCAGATGTGCGGCGAGTTG CGTGACTACCTACGGGTAACAGTTTCTTTATGGCAGGGTGAAA CGCAGGTCGCCAGCGGCACCGCGCCTTTCGGCGGTGAAATTA TCGATGAGCGTGGTGGTTATGCCGATCGCGTCACACTACGTCT GAACGTCGAAAACCCGAAACTGTGGAGCGCCGAAATCCCGAAT CTCTATCGTGCGGTGGTTGAACTGCACACCGCCGACGGCACG CTGATTGAAGCAGAAGCCTGCGATGTCGGTTTCCGCGAGGTGC GGATTGAAAATGGTCTGCTGCTGCTGAACGGCAAGCCGTTGCT GATTCGAGGCGTTAACCGTCACGAGCATCATCCTCTGCATGGT CAGGTCATGGATGAGCAGACGATGGTGCAGGATATCCTGCTGA TGAAGCAGAACAACTTTAACGCCGTGCGCTGTTCGCATTATCC GAACCATCCGCTGTGGTACACGCTGTGCGACCGCTACGGCCT GTATGTGGTGGATGAAGCCAATATTGAAACCCACGGCATGGTG CCAATGAATCGTCTGACCGATGATCCGCGCTGGCTACCGGCGA TGAGCGAACGCGTAACGCGAATGGTGCAGCGCGATCGTAATC ACCCGAGTGTGATCATCTGGTCGCTGGGGAATGAATCAGGCCA CGGCGCTAATCACGACGCGCTGTATCGCTGGATCAAATCTGTC GATCCTTCCCGCCCGGTGCAGTATGAAGGCGGCGGAGCCGAC ACCACGGCCACCGATATTATTTGCCCGATGTACGCGCGCGTGG ATGAAGACCAGCCCTTCCCGGCTGTGCCGAAATGGTCCATCAA AAAATGGCTTTCGCTACCTGGAGAGACGCGCCCGCTGATCCTT TGCGAATACGCCCACGCGATGGGTAACAGTCTTGGCGGTTTCG CTAAATACTGGCAGGCGTTTCGTCAGTATCCCCGTTTACAGGG CGGCTTCGTCTGGGACTGGGTGGATCAGTCGCTGATTAAATAT GATGAAAACGGCAACCCGTGGTCGGCTTACGGCGGTGATTTTG

		GCGATACGCCGAACGATCGCCAGTTCTGTATGAACGGTCTGGT CTTTGCCGACCGCACGCCGCATCCAGCGCTGACGGAAGCAAA ACACCAGCAGCAGTTTTTCCAGTTCCGTTTATCCGGGCAAACC ATCGAAGTGACCAGCGAATACCTGTTCCGTCATAGCGATAACG AGCTCCTGCACTGGATGGTGGCGCTGGATGGTAAGCCGCTGG CAAGCGGTGAAGTGCCTCTGGATGTCGCTCCACAAGGTAAACA GTTGATTGAACTGCCTGAACTACCGCAGCCGGAGAGCGCCGG GCAACTCTGGCTCACAGTACGCGTAGTGCAACCGAACGCGAC CGCATGGTCAGAAGCCGGACACATCAGCGCCTGGCAGCAGTG GCGTCTGGCTGAAAACCTCAGCGTGACACTCCCCGCCGCGTC CCACGCCATCCCGCATCTGACCACCAGCGAAATGGATTTTTGC ATCGAGCTGGGTAATAAGCGTTGGCAATTTAACCGCCAGTCAG GCTTTCTTTCACAGATGTGGATTGGCGATAAAAAACAACTGCTG ACGCCGCTGCGCGATCAGTTCACCCGTGCACCGCTGGATAAC GACATTGGCGTAAGTGAAGCGACCCGCATTGACCCTAACGCCT GGGTCGAACGCTGGAAGGCGGCGGGCCATTACCAGGCCGAA GCAGCGTTGTTGCAGTGCACGGCAGATACACTTGCTGATGCGG TGCTGATTACGACCGCTCACGCGTGGCAGCATCAGGGGAAAA CCTTATTTATCAGCCGGAAAACCTACCGGATTGATGGTAGTGGT CAAATGGCGATTACCGTTGATGTTGAAGTGGCGAGCGATACAC CGCATCCGGCGCGGATTGGCCTGAACTGCCAGCTGGCGCAGG TAGCAGAGCGGGTAAACTGGCTCGGATTAGGGCCGCAAGAAA ACTATCCCGACCGCCTTACTGCCGCCTGTTTTGACCGCTGGGA TCTGCCATTGTCAGACATGTATACCCCGTACGTCTTCCCGAGC GAAAACGGTCTGCGCTGCGGGACGCGCGAATTGAATTATGGC CCACACCAGTGGCGCGGCGACTTCCAGTTCAACATCAGCCGCT ACAGTCAACAGCAACTGATGGAAACCAGCCATCGCCATCTGCT GCACGCGGAAGAAGGCACATGGCTGAATATCGACGGTTTCCAT ATGGGGATTGGTGGCGACGACTCCTGGAGCCCGTCAGTATCG GCGGAATTCCAGCTGAGCGCCGGTCGCTACCATTACCAGTTGG TCTGGTGTCAAAAA**TAA**TGAGGATCCCGGGAATTCTCGAGTAA GGTTAACCTGCAGGAGGCCTTTAATTAAGGTGGTGCGGCCGC GCTAGCGGTCCCGGGGGATCGATCCGGCTGCTAACAAAGCCC GAAAGGAAGCTGAGTTGGCTGCTGCCACCGCTGAGCAATAACT AGCATAACCCCTTGGGGCCTCTAAACGGGTCTTGAGGGGTTTT TTGCTGAAAGGAGGAACTATATC

3	*α*	GAAATTAATACGACTCACTATAGGGTCTAGAAATAATTTTGTTTA ACTTTAAGAAGGAGGTATACAT**ATG**ACCATGATTACGGATTCAC TGGCCGTCGTTTTACAACGTCGTGACTGGGAAAACCCTGGCGT TACCCAACTTAATCGCCTTGCAGCACATCCCCCTTTCGCCAGCT GGCGTAATAGCGAAGAGGCCCGCACCGATCGCCCTTCCCAAC AGTTGCGCAGCCTGAATGGCGAATGGCGCTTTGCCTGGTTTCC GGCACCAGAAGCGGTGCCGGAAAGCTGGCTGGAGTGCGATCT TCCTGAGGCCGATACTGTCGTCGTCCCCTCAAACTGGCAGATG CACGGTTACGATGCGCCCATCTACACCAACGTGACCTATCCCA TTACGGTCAATCCGCCGTTTGTTCCCACGGAGAATCCGACGGG TTGTTACTCGCTCACATTTAATGTTGATGAAAGCTGGCTACAGG AAGGCCAGACGCGAATTATTTTTGATGGCGTTAACTCGGCGTTT CATCTGTGGTGCAACGGGCGCTGGGTCGGTTACGGCCAGGAC AGTCGTTTGCCGTCTGAATTTGACCTGAGCGCATTTTTACGCGC CGGAGAAAACCGCCTCGCGGTGATGGTGCTGCGCTGGAGTGA CGGCAGTTATCTGGAAGATCAGGATATGTGGCGGATGAGCGG CATTTTCCGTGACGTCTCGTTGCTGCATAAACCGACTACACAAA TCAGCGATTTCCATGTTGCCACTCGCTTTAATGATGATTTCAGC CGCGCTGTACTGGAGGCTGAAGTTCAGATGTGCGGCGAGTTG CGTGACTACCTACGGGTAACAGTTTCTTTATGGCAGGGTGAAA CGCAGGTCGCCAGCGGCACCGCGCCTTTCGGCGGTGAAATTA TCGATGAGCGTGGTGGTTATGCCGATCGCGTCACACTACGTCT GAACGTCGAAAACCCGAAACTGTGGAGCGCCGAAATCCCGAAT CTCTATCGTGCGGTGGTTGAACTGCACACCGCCGACGGCACG CTGATTGAAGCAGAAGCCTGCGATGTCGGTTTCCGCGAGGTGC GGATTGAAAATGGTCTGCTGCTGCTGAACGGCAAGCCGTTGCT GATTCGAGGCGTTAACCGTCACGAGCATCATCCTCTGCATGGT CAGGTCATGGATGAGCAGACGATGGTGCAGGATATCCTGCTGA TGAAGCAGAACAACTTTAACGCCGTGCGCTGTTCGCATTATCC GAACCATCCGCTGTGGTACACGCTGTGCGACCGCTACGGCCT GTATGTGGTGGATGAAGCCAATATTGAAACCCACGGCATGGTG CCAATGAATCGTCTGACCGATGATCCGCGCTGGCTACCGGCGA TGAGCGAACGCGTAACGCGAATGGTGCAGCGCGATCGTAATC ACCCGAGTGTGATCATCTGGTCGCTGGGGAATGAATCAGGCCA CGGCGCTAATCACGACGCGCTGTATCGCTGGATCAAATCTGTC GATCCTTCCCGCCCGGTGCAGTATGAAGGCGGCGGAGCCGAC

		ACCACGGCCACCGATATTATTTGCCCGATGTACGCGCGCGTGG ATGAAGACCAGCCCTTCCCGGCTGTGCCGAAATGGTCCATCAA AAAATGGCTTTCGCTACCTGGAGAGACGCGCCCGCTGATCCTT TGCGAATACGCCCACGCGATGGGTAACAGTCTTGGCGGTTTCG CTAAATACTGGCAGGCGTTTCGTCAGTATCCCCGTTTACAGGG CGGCTTCGTCTGGGACTGGGTGGATCAGTCGCTGATTAAATAT GATGAAAACGGCAACCCGTGGTCGGCTTACGGCGGTGATTTTG GCGATACGCCGAACGATCGCCAGTTCTGTATGAACGGTCTGGT CTTTGCCGACCGCACGCCGCATCCAGCGCTGACGGAAGCAAA ACACCAGCAGCAGTTTTTCCAGTTCCGTTTATCCGGGCAAACC ATCGAAGTGACCAGCGAATACCTGTTCCGTCATAGCGATAACG AGCTCCTGCACTGGATGGTGGCGCTGGATGGTAAGCCGCTGG CAAGCGGTGAAGTGCCTCTGGATGTCGCTCCACAAGGTAAACA GTTGATTGAACTGCCTGAACTACCGCAGCCGGAGAGCGCCGG GCAACTCTGGCTCACAGTACGCGTAGTGCAACCGAACGCGAC CGCATGGTCAGAAGCCGGACACATCAGCGCCTGGCAGCAGTG GCGTCTGGCTGAAAACCTCAGCGTGACACTCCCCGCCGCGTC CCACGCC**TAA**TAATGAGGATCCCGGGAATTCTCGAGTAAGGTT AACCTGCAGGAGGCCTTTAATTAAGGTGGTGCGGCCGCGCTA GCGGTCCCGGGGGATCGATCCGGCTGCTAACAAAGCCCGAAA GGAAGCTGAGTTGGCTGCTGCCACCGCTGAGCAATAACTAGCA TAACCCCTTGGGGCCTCTAAACGGGTCTTGAGGGGTTTTTTGC TGAAAGGAGGAACTATATCCGGAA
4	*ω*	GAAATTAATACGACTCACTATAGGGTCTAGAAATAATTTTGTTTA ACTTTAAGAAGGAGGTATACAT**ATG**ATCCCGCATCTGACCACCA GCGAAATGGATTTTTGCATCGAGCTGGGTAATAAGCGTTGGCA ATTTAACCGCCAGTCAGGCTTTCTTTCACAGATGTGGATTGGCG ATAAAAAACAACTGCTGACGCCGCTGCGCGATCAGTTCACCCG TGCACCGCTGGATAACGACATTGGCGTAAGTGAAGCGACCCG CATTGACCCTAACGCCTGGGTCGAACGCTGGAAGGCGGCGGG CCATTACCAGGCCGAAGCAGCGTTGTTGCAGTGCACGGCAGAT ACACTTGCTGATGCGGTGCTGATTACGACCGCTCACGCGTGGC AGCATCAGGGGAAAACCTTATTTATCAGCCGGAAAACCTACCG GATTGATGGTAGTGGTCAAATGGCGATTACCGTTGATGTTGAA GTGGCGAGCGATACACCGCATCCGGCGCGGATTGGCCTGAAC TGCCAGCTGGCGCAGGTAGCAGAGCGGGTAAACTGGCTCGGA

		TTAGGGCCGCAAGAAAACTATCCCGACCGCCTTACTGCCGCCT GTTTTGACCGCTGGGATCTGCCATTGTCAGACATGTATACCCC GTACGTCTTCCCGAGCGAAAACGGTCTGCGCTGCGGGACGCG CGAATTGAATTATGGCCCACACCAGTGGCGCGGCGACTTCCAG TTCAACATCAGCCGCTACAGTCAACAGCAACTGATGGAAACCA GCCATCGCCATCTGCTGCACGCGGAAGAAGGCACATGGCTGA ATATCGACGGTTTCCATATGGGGATTGGTGGCGACGACTCCTG GAGCCCGTCAGTATCGGCGGAATTCCAGCTGAGCGCCGGTCG CTACCATTACCAGTTGGTCTGGTGTCAAAAA**TAA**TGAGGATCCC GGGAATTCTCGAGTAAGGTTAACCTGCAGGAGGCCTTTAATTA AGGTGGTGCGGCCGCGCTAGCGGTCCCGGGGGATCGATCCG GCTGCTAACAAAGCCCGAAAGGAAGCTGAGTTGGCTGCTGCCA CCGCTGAGCAATAACTAGCATAACCCCTTGGGGCCTCTAAACG GGTCTTGAGGGGTTTTTTGCTGAAAGGAGGAACTATATC
5	*mNeonGreen*	GAAATTAATACGACTCACTATAGGGTCTAGAAATAATTTTGTTTA ACTTTAAGAAGGAGGTATACATATGGTGAGCAAAGGCGAAGAG GATAATATGGCAAGCCTGCCTGCAACAC**ATG**AACTGCATATTTT TGGTAGCATTAACGGCGTGGATTTTGATATGGTTGGTCAAGGC ACCGGTAATCCGAATGATGGTTATGAAGAACTGAATCTGAAAAG CACCAAAGGCGATCTGCAGTTTAGCCCGTGGATTCTGGTTCCG CATATTGGTTATGGTTTTCATCAGTATCTGCCGTATCCGGATGG TATGAGCCCGTTTCAGGCAGCAATGGTTGATGGTAGCGGTTAT CAGGTTCATCGTACCATGCAGTTTGAAGATGGTGCAAGCCTGA CCGTTAATTATCGTTATACCTATGAAGGCAGCCACATTAAAGGT GAAGCACAGGTTAAAGGTACAGGTTTTCCGGCAGATGGTCCGG TTATGACCAATAGTCTGACCGCAGCAGATTGGTGTCGTAGCAA AAAAACCTATCCGAACGATAAAACCATCATCAGCACCTTCAAAT GGTCATATACCACCGGCAATGGTAAACGTTATCGTAGCACCGC ACGTACCACCTATACCTTTGCAAAACCGATGGCAGCAAACTATC TGAAAAATCAGCCGATGTATGTGTTTCGCAAAACGGAACTGAAA CATTCCAAAACCGAGCTGAACTTTAAAGAATGGCAGAAAGCATT TACCGATGTGATGGGTATGGATGAGCTGTACAAA**TAA**TGAGGA TCCCGGGAATTCTCGAGTAAGGTTAACCTGCAGGAGGCCTTTA ATTAAGGTGGTGCGGCCGCGCTAGCGGTCCCGGGGGATCGAT CCGGCTGCTAACAAAGCCCGAAAGGAAGCTGAGTTGGCTGCT

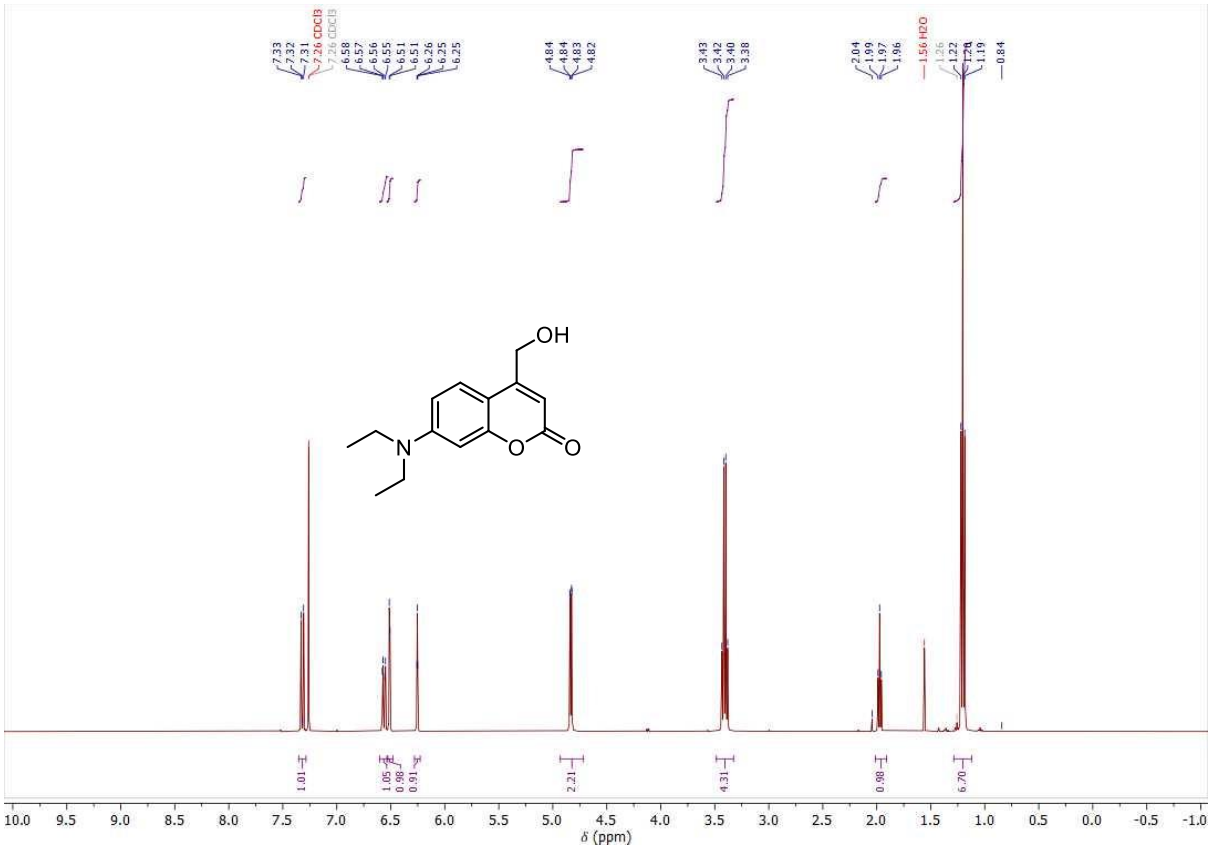
		GCCACCGCTGAGCAATAACTAGCATAACCCCTTGGGGCCTCTA AACGGGTCTTGAGGGGTTTTTTGCTGAAAGGAGGAACTATATC
6	*mCherry*	GAAATTAATACGACTCACTATAGGGTCTAGAAATAATTTTGTTTA ACTTTAAGAAGGAGGTATACAT**ATG**GTGAGCAAGGGCGAGGAG GATAACATGGCCATCATCAAGGAGTTCATGCGCTTCAAGGTGC ACATGGAGGGCTCCGTGAACGGCCACGAGTTCGAGATCGAGG GCGAGGGCGAGGGCCGCCCCTACGAGGGCACCCAGACCGCC AAGCTGAAGGTGACCAAGGGTGGCCCCCTGCCCTTCGCCTGG GACATCCTGTCCCCTCAGTTCATGTACGGCTCCAAGGCCTACG TGAAGCACCCCGCCGACATCCCCGACTACTTGAAGCTGTCCTT CCCCGAGGGCTTCAAGTGGGAGCGCGTGATGAACTTCGAGGA CGGCGGCGTGGTGACCGTGACCCAGGACTCCTCCCTGCAGGA CGGCGAGTTCATCTACAAGGTGAAGCTGCGCGGCACCAACTTC CCCTCCGACGGCCCCGTAATGCAGAAGAAGACCATGGGCTGG GAGGCCTCCTCCGAGCGGATGTACCCCGAGGACGGCGCCCTG AAGGGCGAGATCAAGCAGAGGCTGAAGCTGAAGGACGGCGGC CACTACGACGCTGAGGTCAAGACCACCTACAAGGCCAAGAAGC CCGTGCAGCTGCCCGGCGCCTACAACGTCAACATCAAGTTGGA CATCACCTCCCACAACGAGGACTACACCATCGTGGAACAGTAC GAACGCGCCGAGGGCCGCCACTCCACCGGCGGCATGGACGA GCTGTACAAG**TAA**TGAGGATCCCGGGAATTCTCGAGTAAGGTT AACCTGCAGGAGGCCTTTAATTAAGGTGGTGCGGCCGCGCTA GCGGTCCCGGGGGATCGATCCGGCTGCTAACAAAGCCCGAAA GGAAGCTGAGTTGGCTGCTGCCACCGCTGAGCAATAACTAGCA TAACCCCTTGGGGCCTCTAAACGGGTCTTGAGGGGTTTTTTGC TGAAAGGAGGAACTATATC

Table 9-1: Sequences of linear DNA templates used for cell-free expression, produced by PCR.
T7-Promoter and -Terminator Regions are underlined, protein start- and stop-codons are in bold.

B - NMR SPECTRA

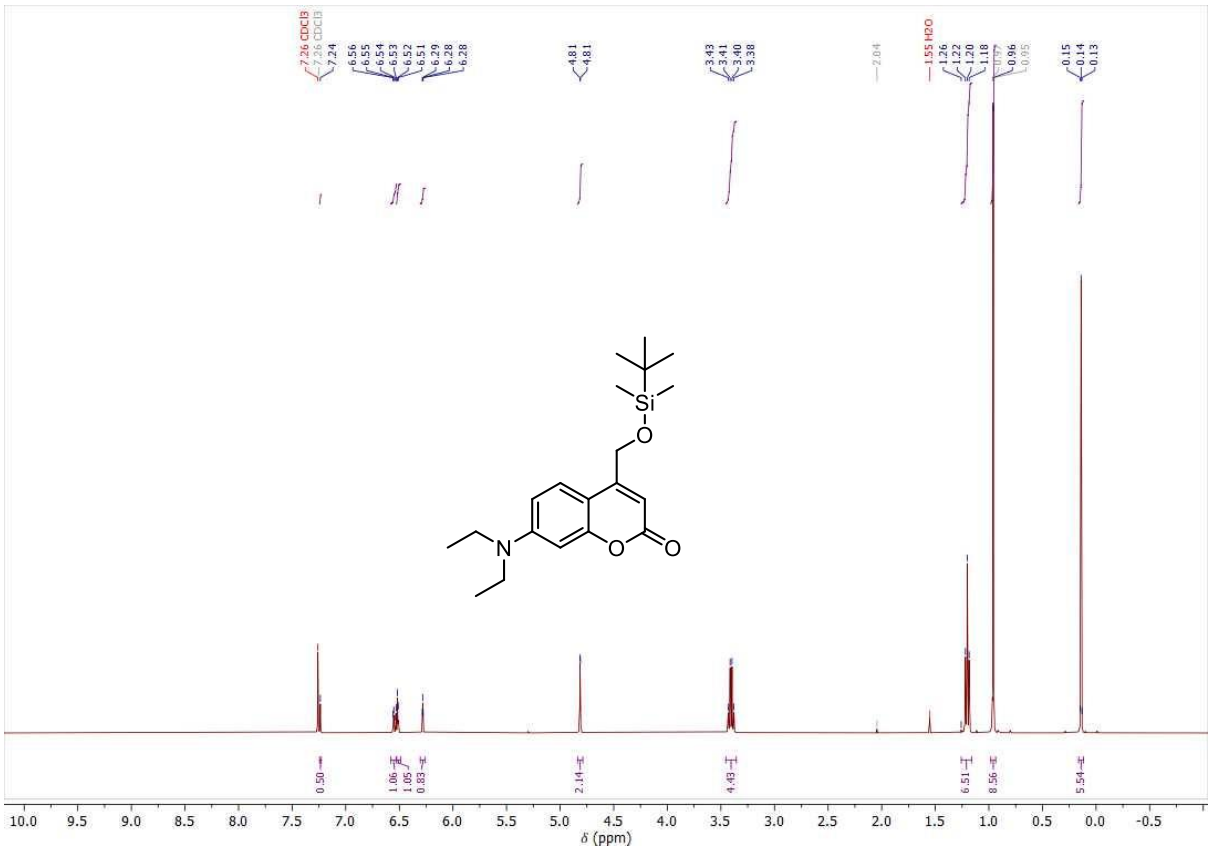
7-(Diethylamino)-4-(hydroxymethyl)-2H-chromen-2-one 1

^{1}H-NMR (400 MHz, $CDCl_3$)



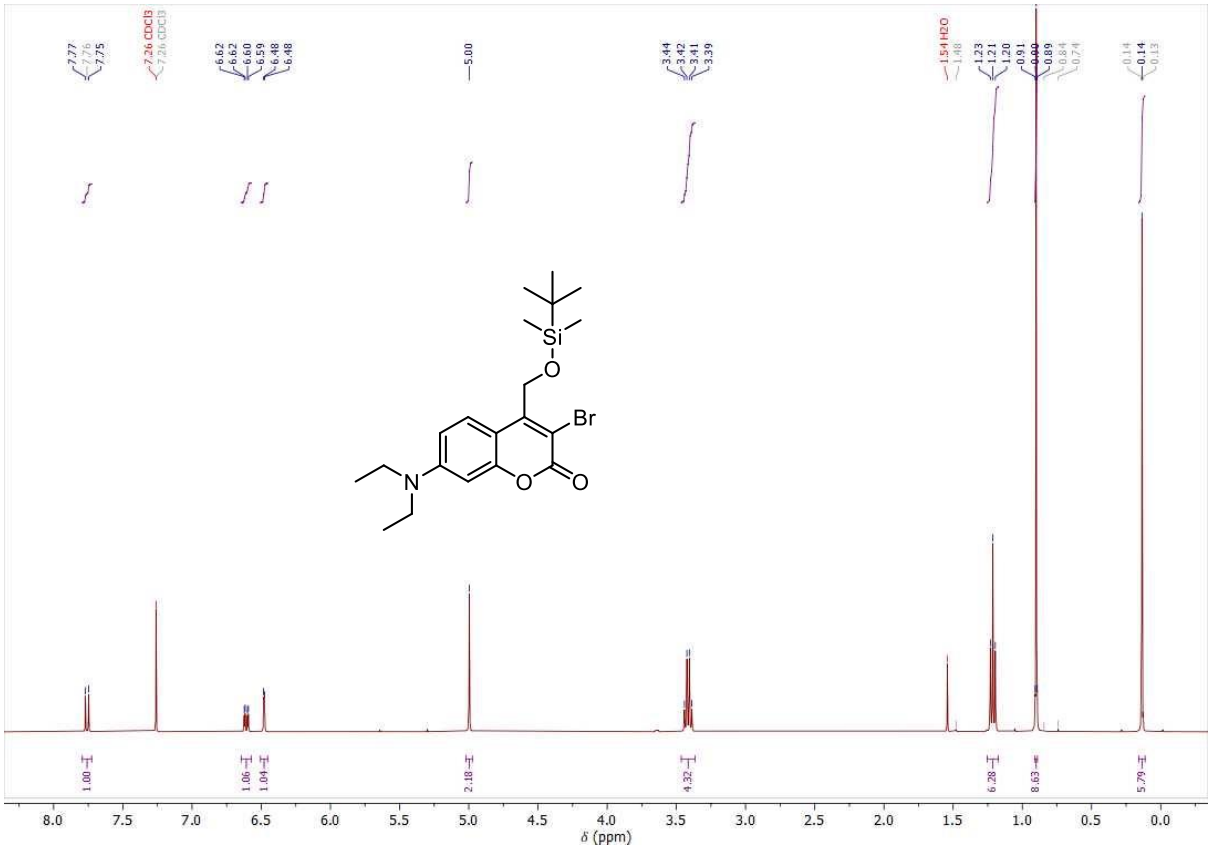
4-(((*tert*-Butyldimethylsilyl)oxy)methyl)-7-(diethylamino)-2H-chromen-2-one 2

^{1}H-NMR (400 MHz, $CDCl_3$)



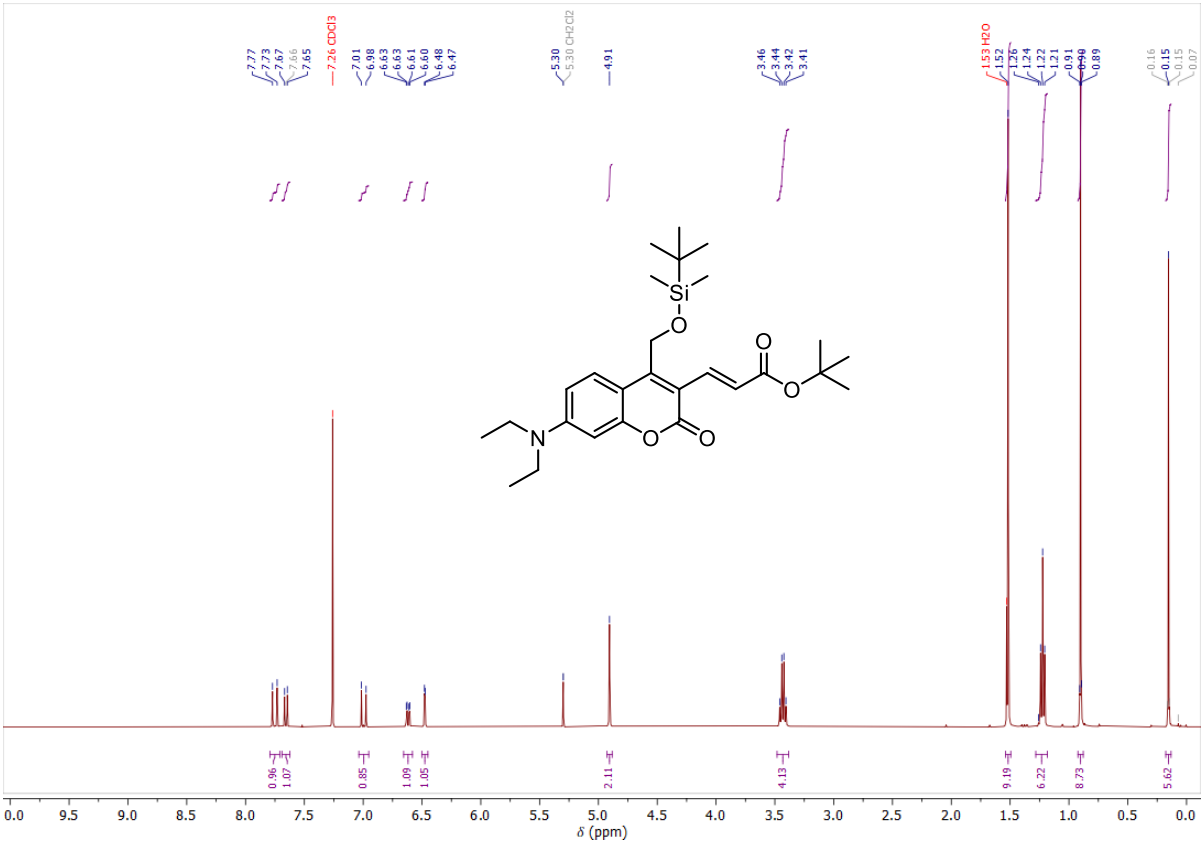
3-Bromo-4-(((*tert*-butyldimethylsilyl)oxy)methyl)-7-(diethylamino)-2H-chromen-2-one 3

^{1}H-NMR (400 MHz, $CDCl_3$)



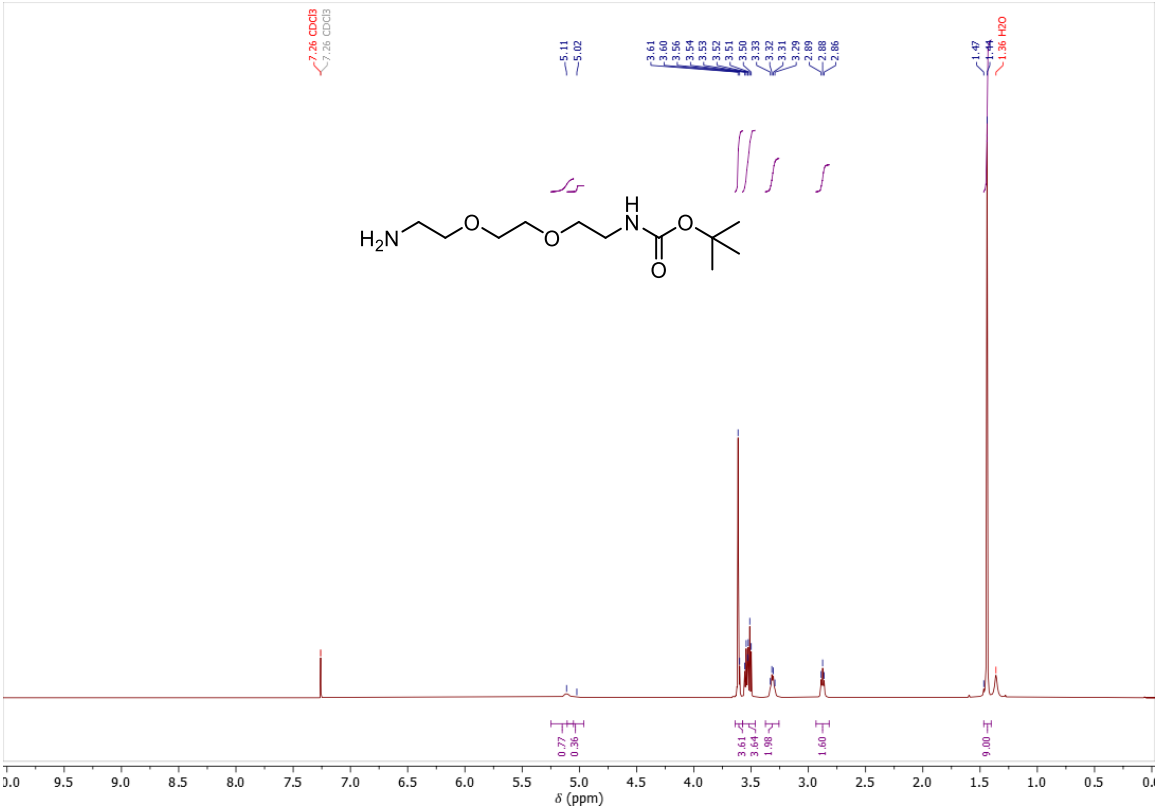
tert-Butyl (*E*)-3-(4-(((*tert*-butyldimethylsilyl)oxy)methyl)-7-(diethylamino)-2-oxo-2H-chromen-3-yl)acrylate 4

^{1}H-NMR (400 MHz, $CDCl_3$)



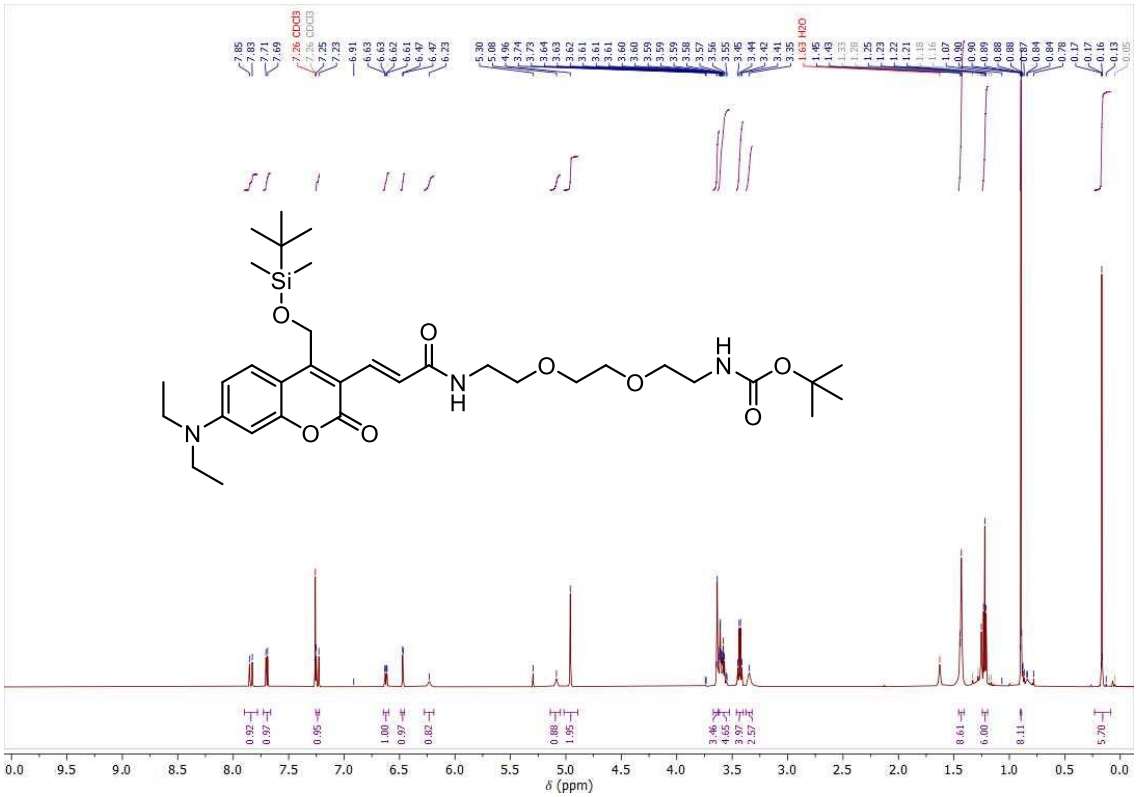
tert-Butyl (2-(2-(2-aminoethoxy)ethoxy)ethyl)carbamate 5

^{1}H-NMR (400 MHz, $CDCl_3$)

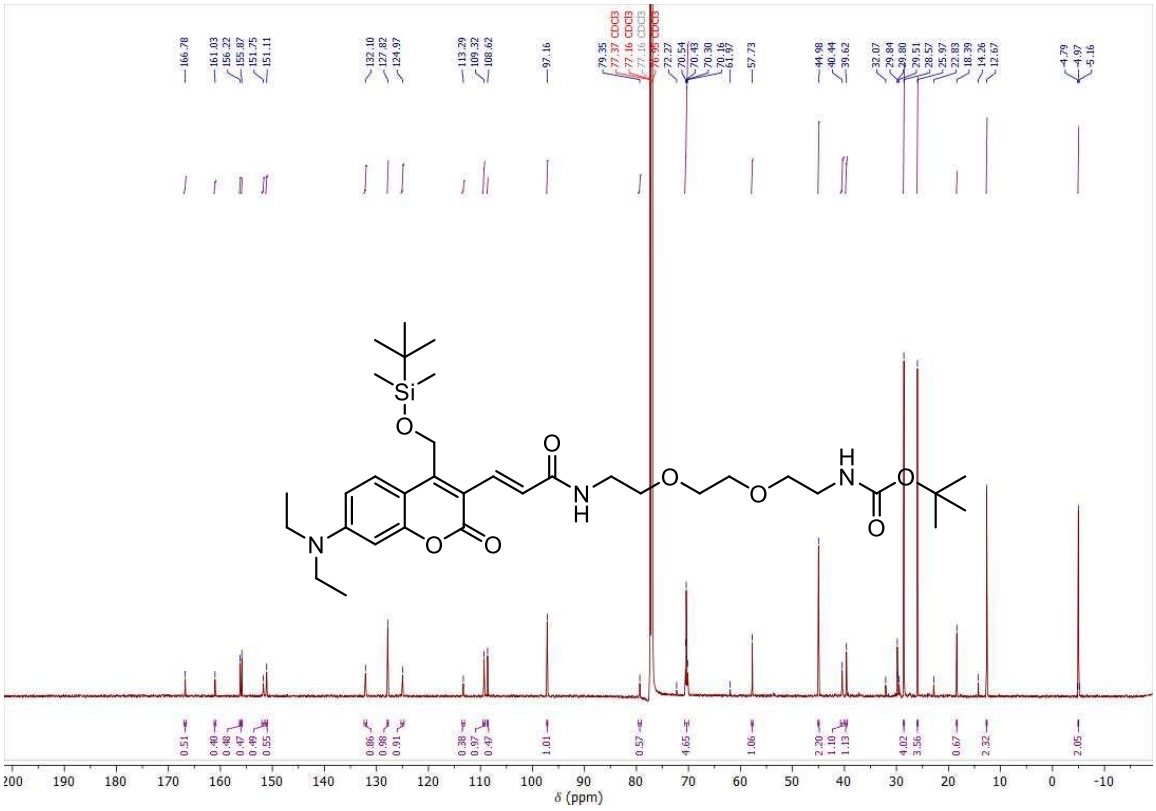


tert-Butyl-(*E*)-(2-(2-(2-(3-(4-(((*tert*-butyldimethylsilyl)oxy)methyl)-7-(diethylamino)-2-oxo-2H-chromen-3-yl)acrylamido)ethoxy)ethoxy)ethyl)carbamate 6a

^{1}H-NMR (600 MHz, $CDCl_3$)

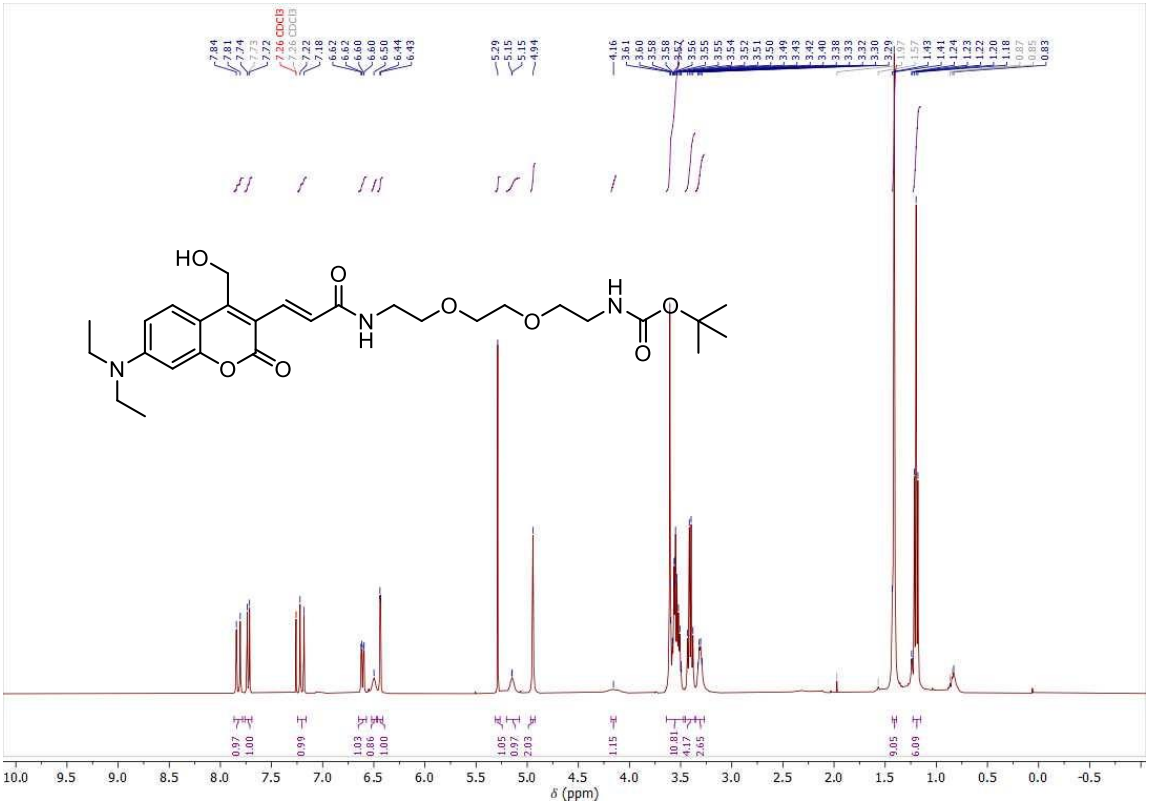


^{13}C-NMR (126 MHz, $CDCl_3$)

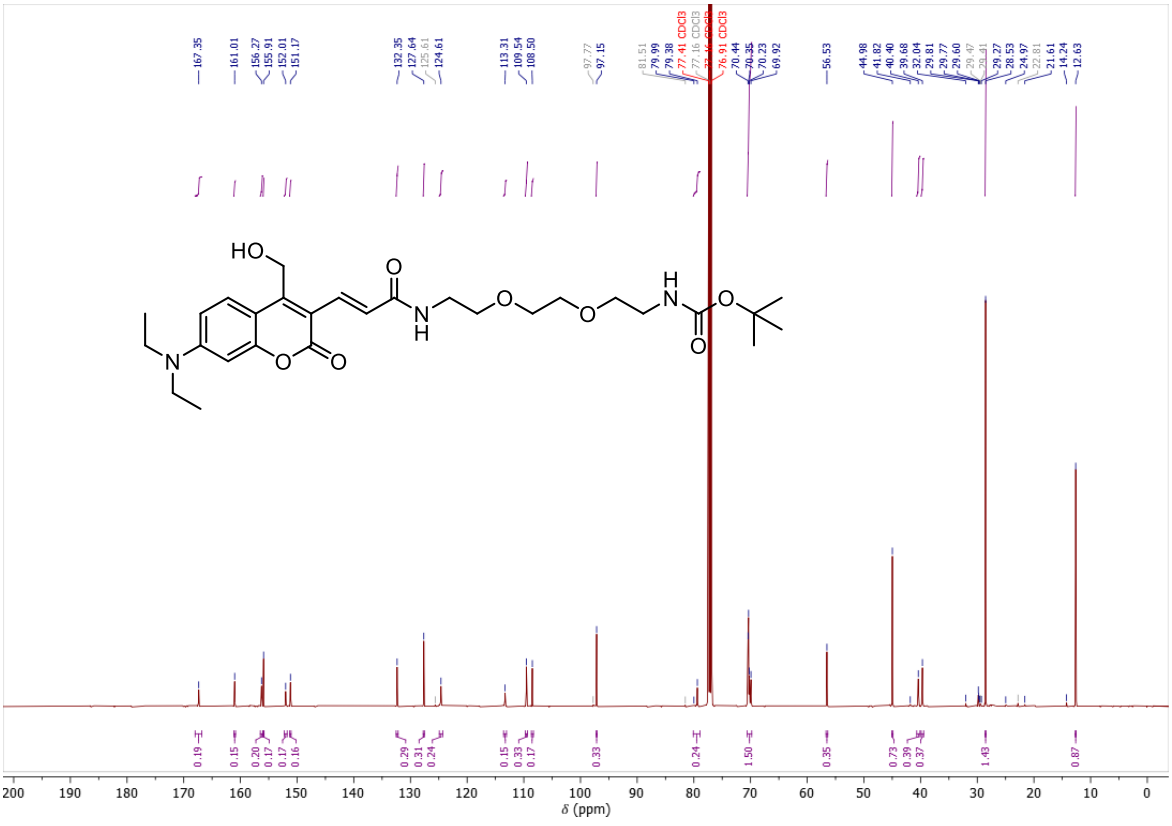


tert-Butyl (*E*)-(2-(2-(2-(3-(7-(diethylamino)-4-(hydroxymethyl)-2-oxo-2H-chromen-3-yl)acrylamido)ethoxy)ethoxy)ethyl)carbamate 6b

^{1}H-NMR (500 MHz, $CDCl_3$)

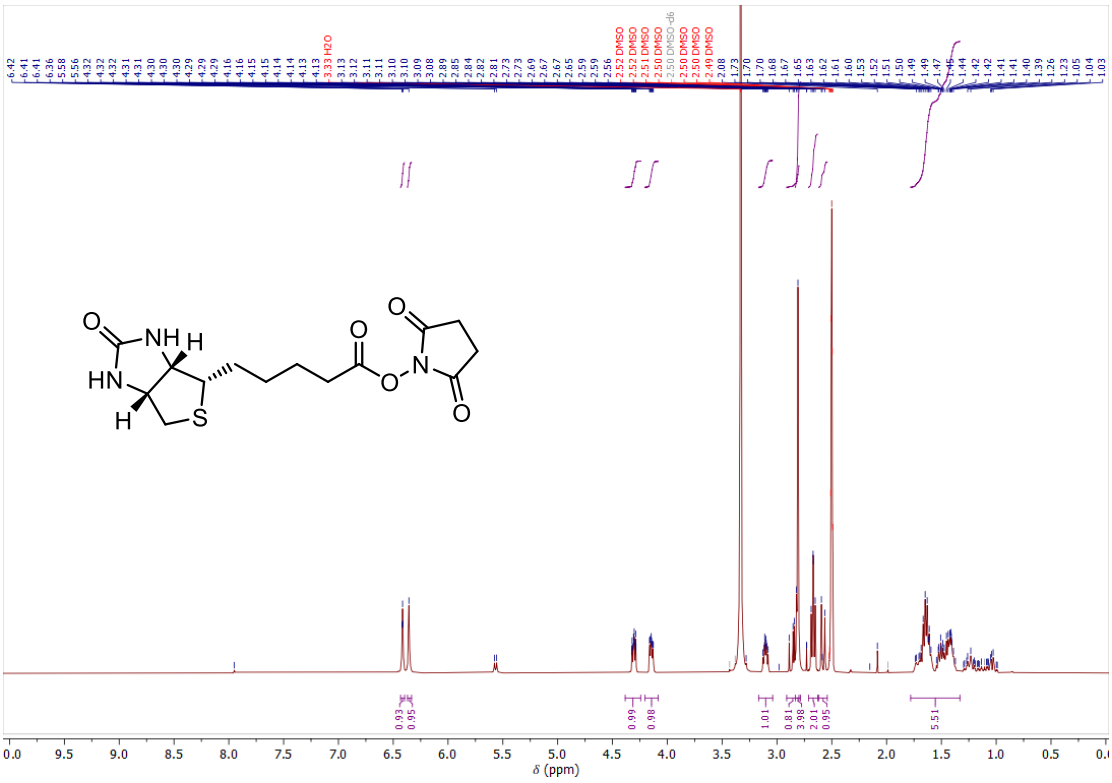


^{13}C-NMR (126 MHz, $CDCl_3$)



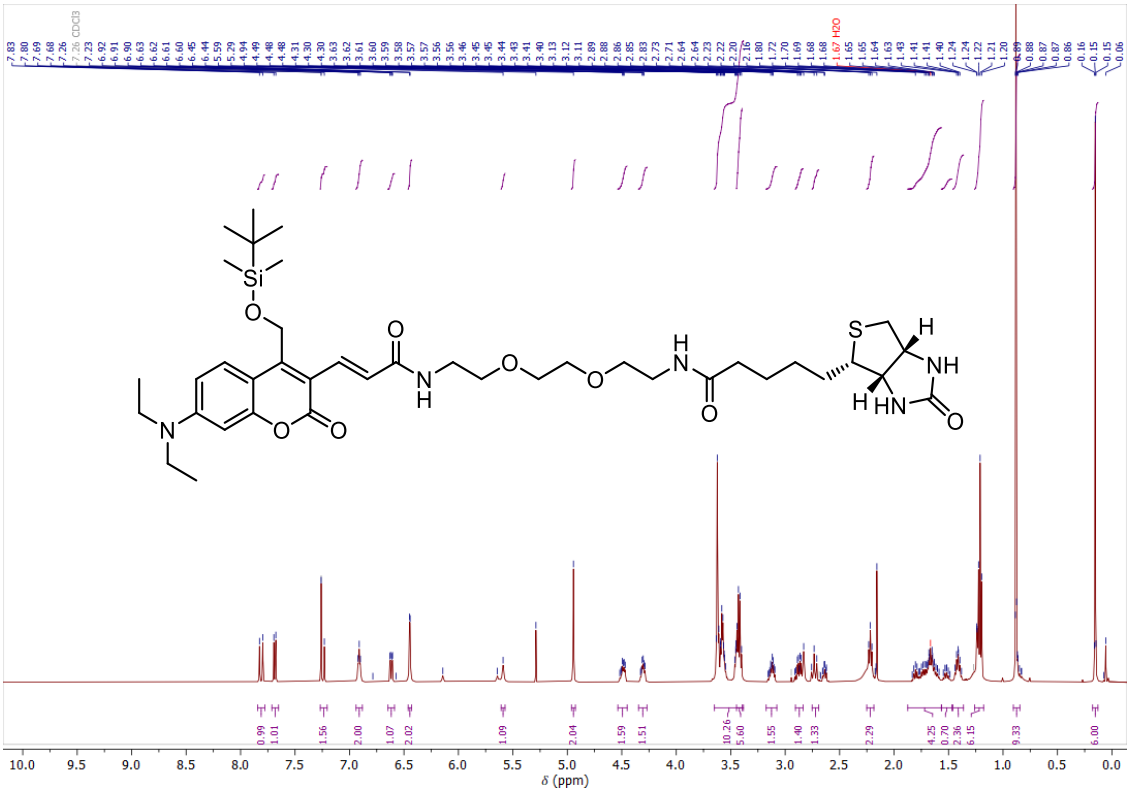
Biotin-*N*-hydroxysuccinimide ester 7

^{1}H-NMR (400 MHz, DMSO)

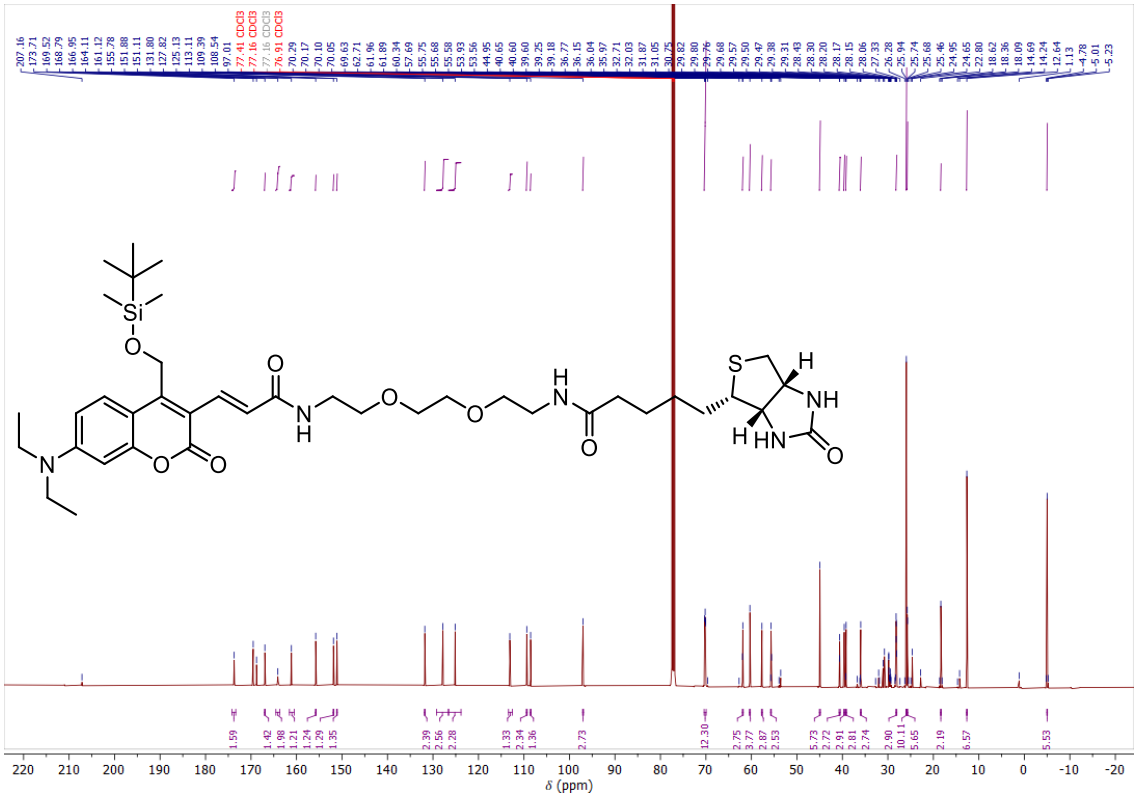


N-(2-(2-(2-(((*E*)-3-(4-(((*tert*-Butyldimethylsilyl)oxy)methyl)-7-(diethylamino)-2-oxo-2H-chromen-3-yl)acrylamido)ethoxy)ethoxy)ethyl)-5-((3aS,4S,6aR)-2-oxohexahydro-1H-thieno[3,4-d]imidazol-4-yl)pentanamide 8

^{1}H-NMR (500 MHz, $CDCl_3$)

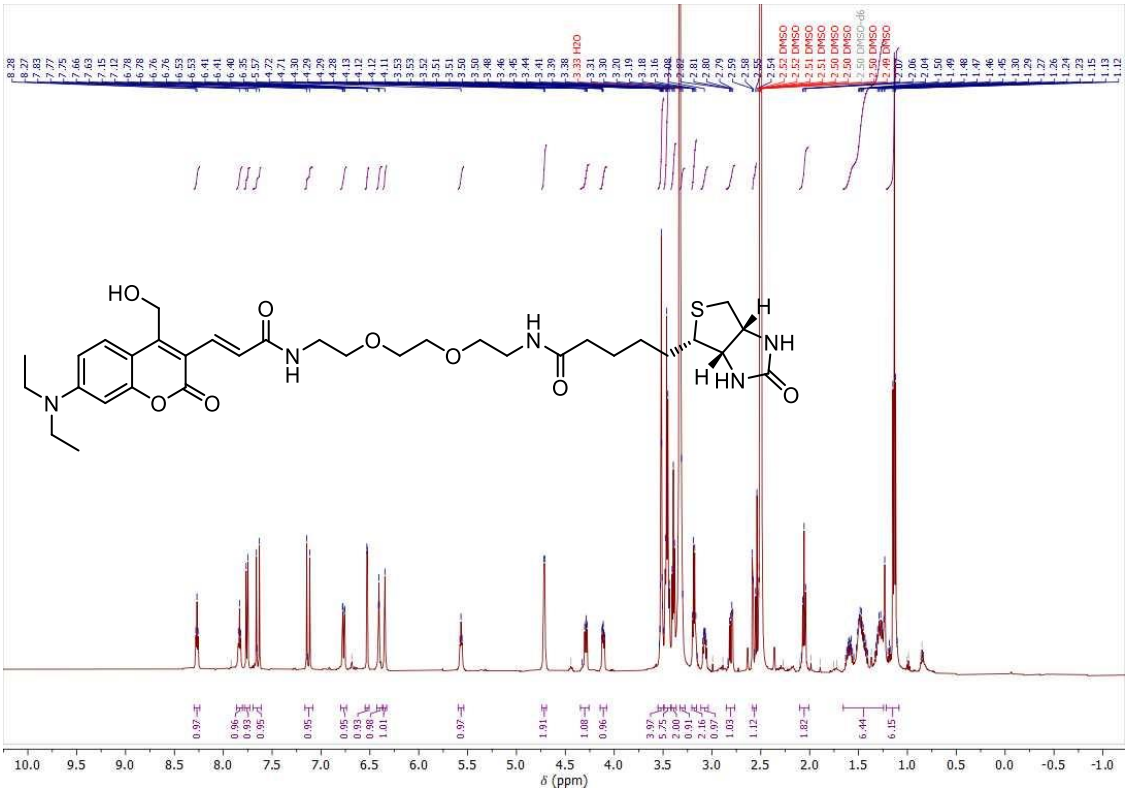


^{13}C-NMR (126 MHz, $CDCl_3$)

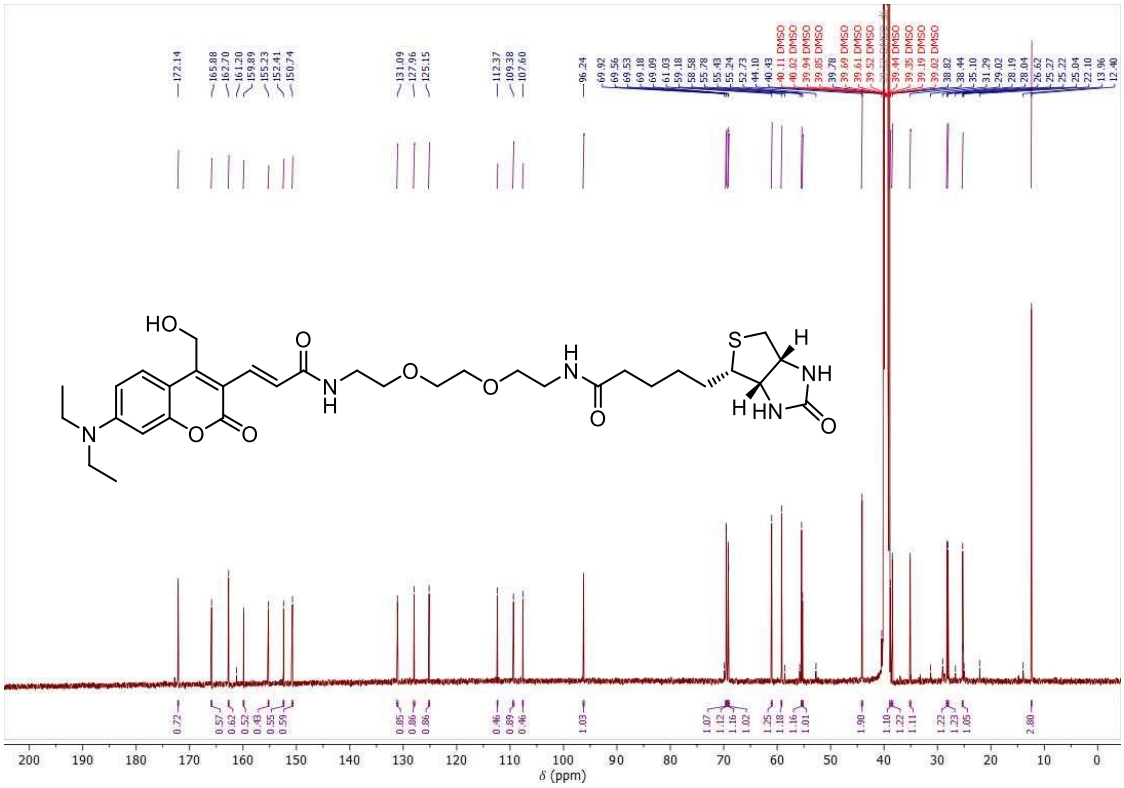


N-(2-(2-(2-((*E*)-3-(7-(Diethylamino)-4-(hydroxymethyl)-2-oxo-2H-chromen-3-yl)acrylamido)ethoxy)ethoxy)ethyl-5-((3aS,4S,6aR)-2-oxohexahydro-1H-thieno[3,4-d]imidazol-4-yl)pentanamide 9

^{1}H-NMR (500 MHz, DMSO)

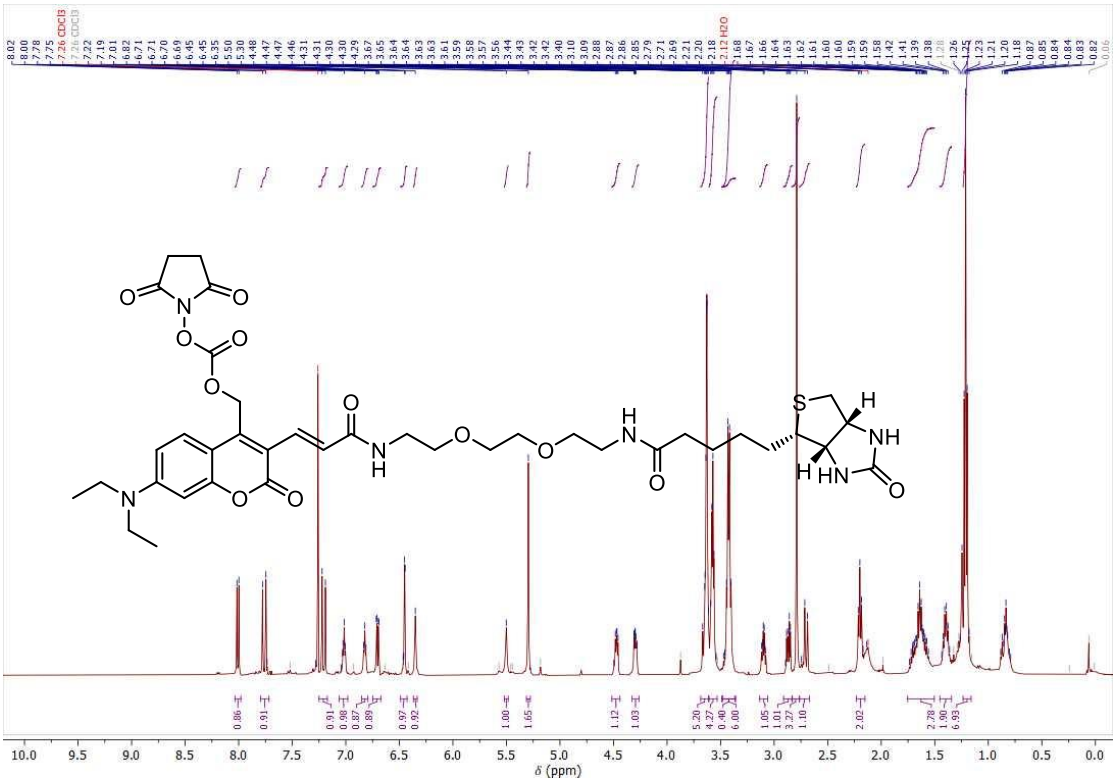


^{13}C-NMR (126 MHz, DMSO)

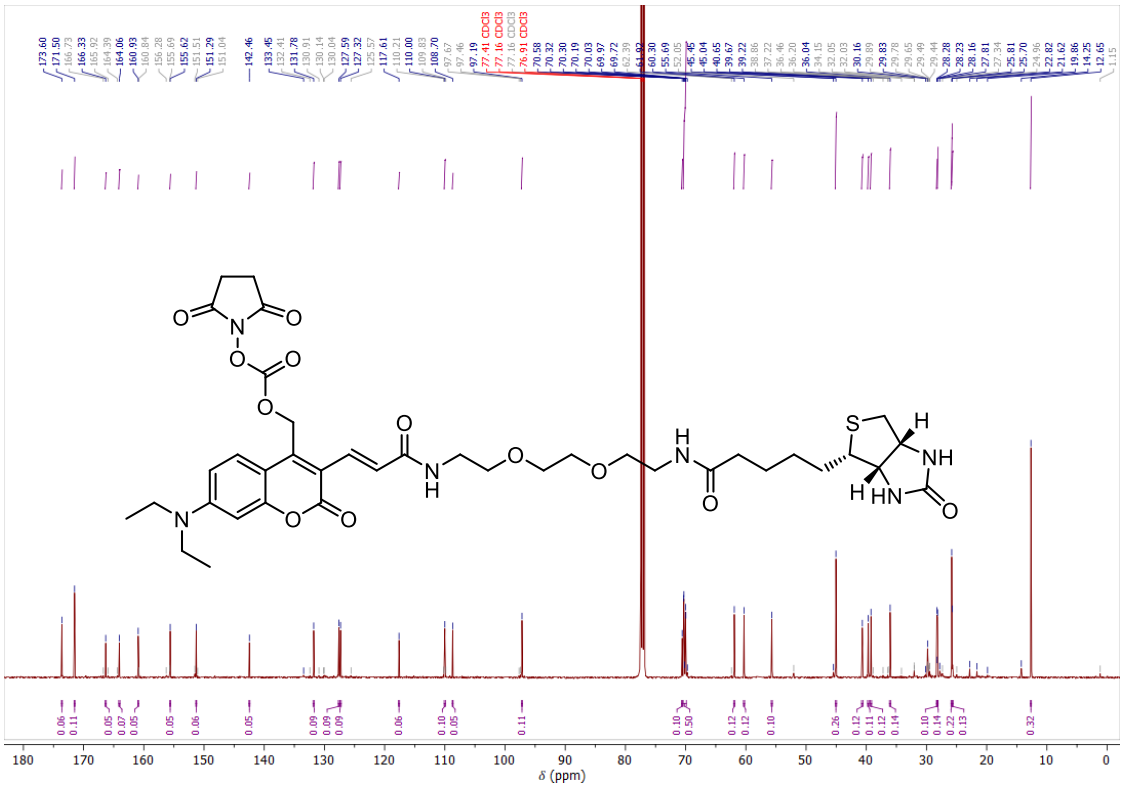


(7-(Diethylamino)-3-((*E*)-3,14-dioxo-18-((3aS,4S,6aR)-2-oxohexahydro-1H-thieno[3,4-d]imidazol-4-yl)-7,10-dioxa-4,13-diazaoctadec-1-en-1-yl)-2-oxo-2H-chromen-4-yl)methyl (2,5-dioxopyrrolidin-1-yl) carbonate 10a

^{1}H-NMR (500 MHz, $CDCl_3$)

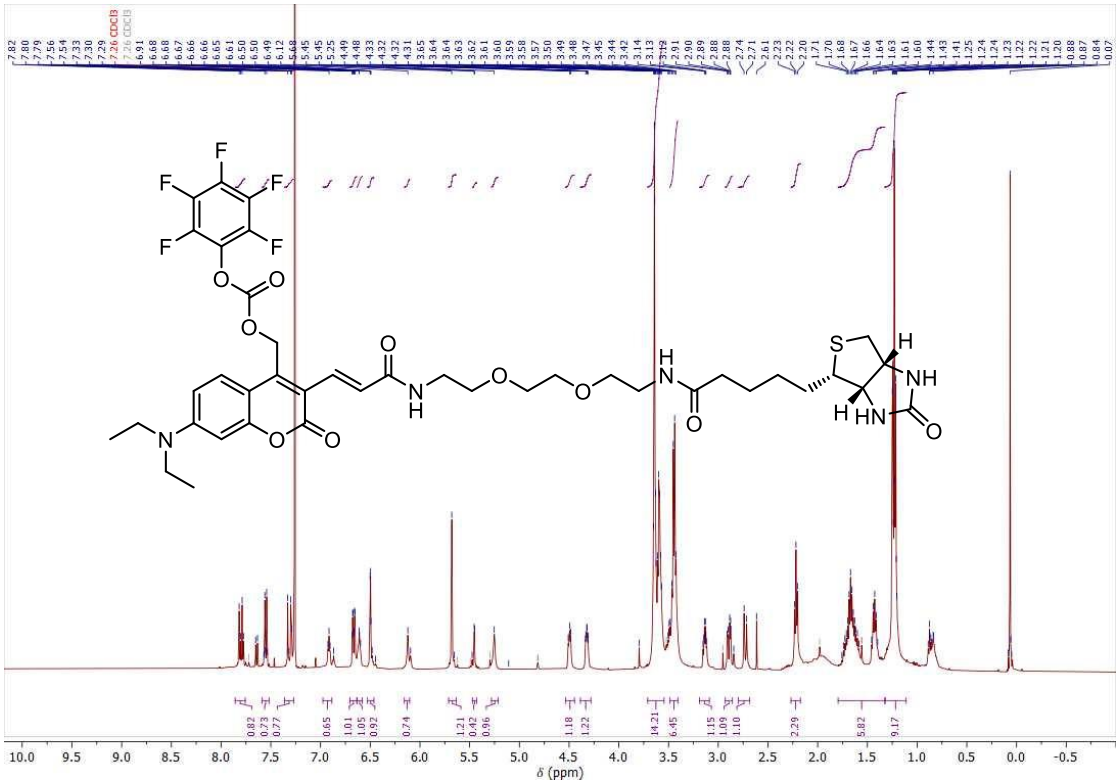


^{13}C-NMR (126 MHz, $CDCl_3$)

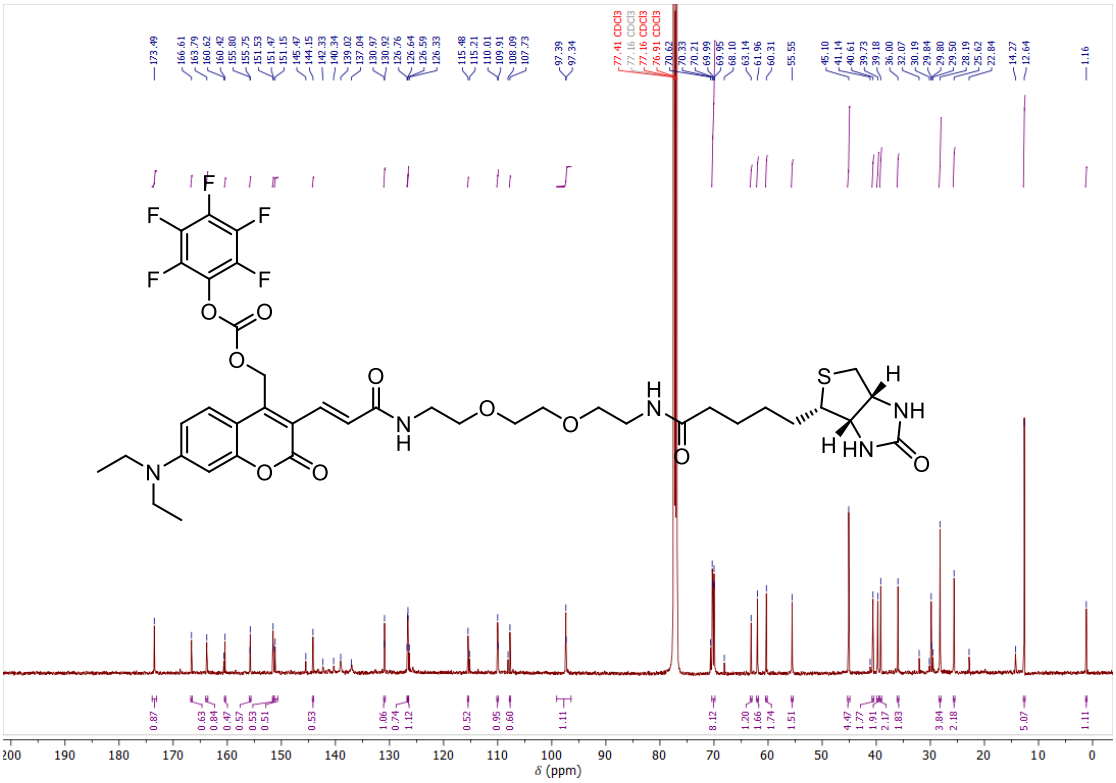


(7-(Diethylamino)-3-((*E*)-3,14-dioxo-18-((3aS,4S,6aR)-2-oxohexahydro-1H-thieno[3,4-d]imidazol-4-yl)-7,10-dioxa-4,13-diazaoctadec-1-en-1-yl)-2-oxo-2H-chromen-4-yl)methyl (perfluorophenyl) carbonate 10b

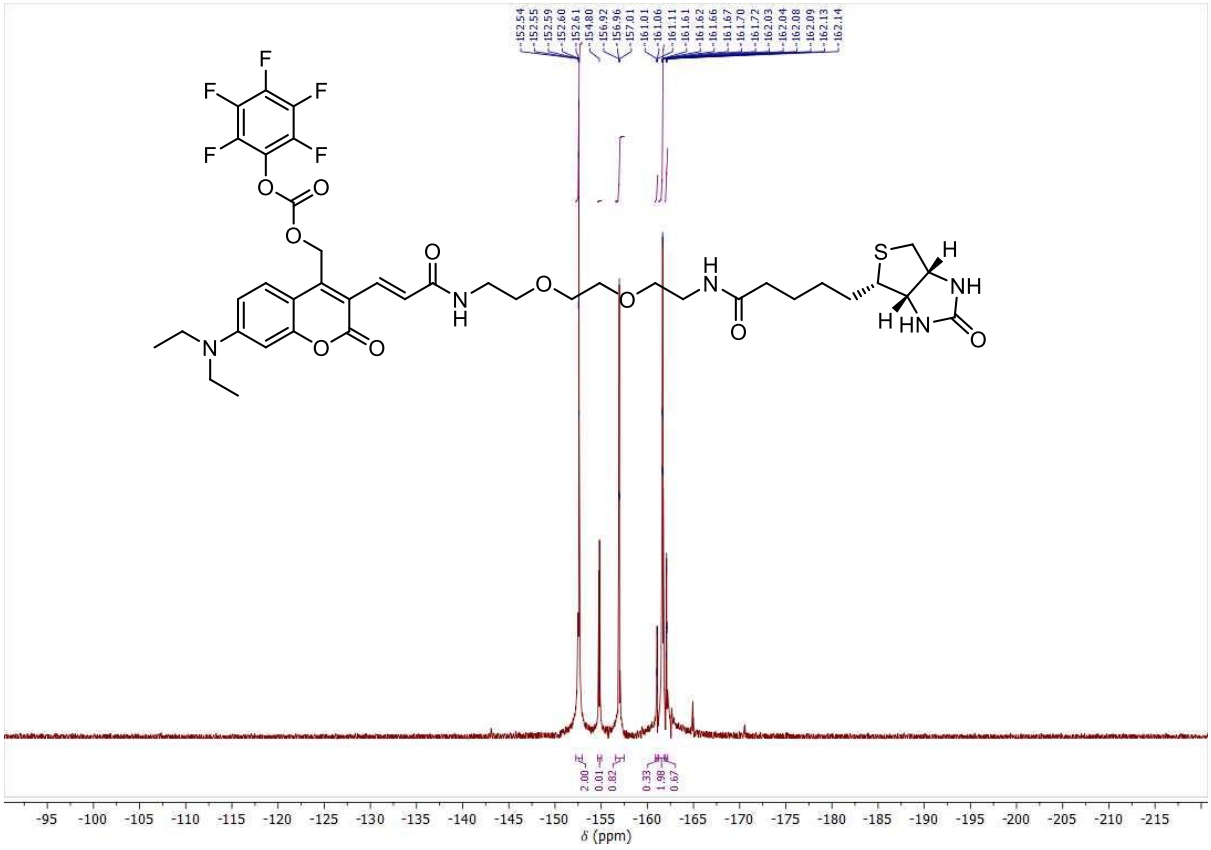
^{1}H-NMR (500 MHz, $CDCl_3$)



^{13}C-NMR (126 MHz, $CDCl_3$)

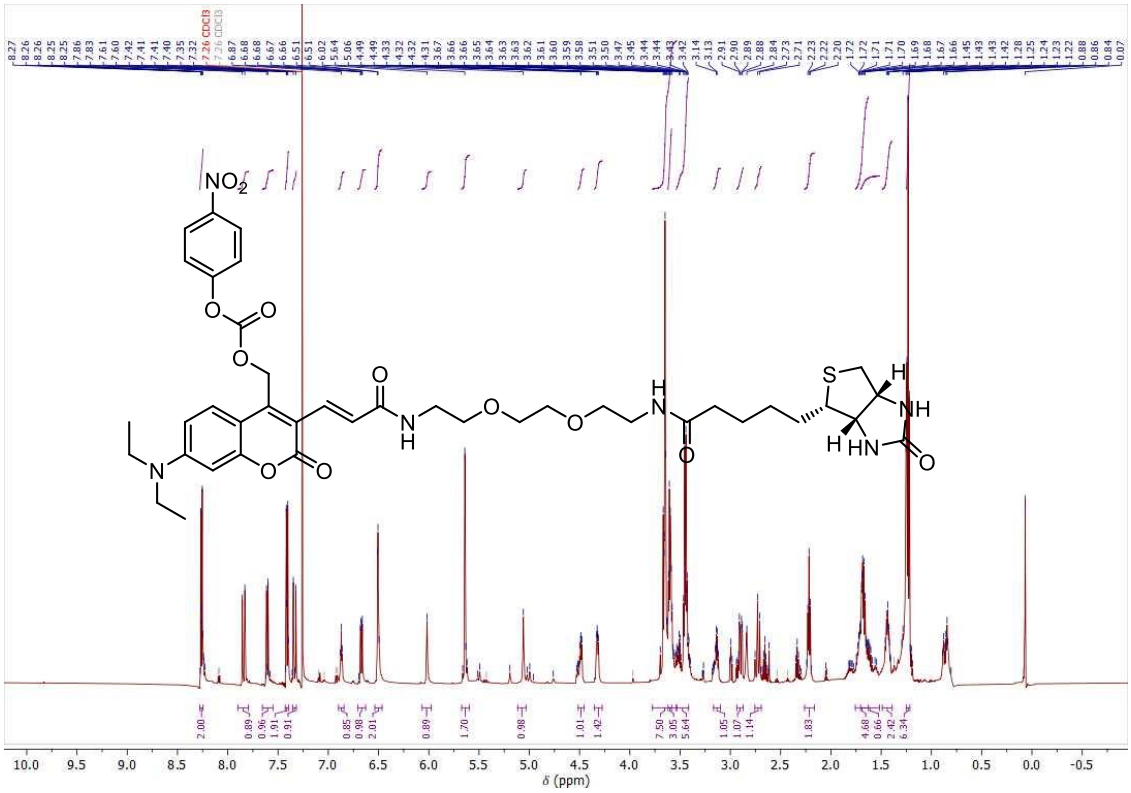


^{19}F-NMR (471 MHz, $CDCl_3$)

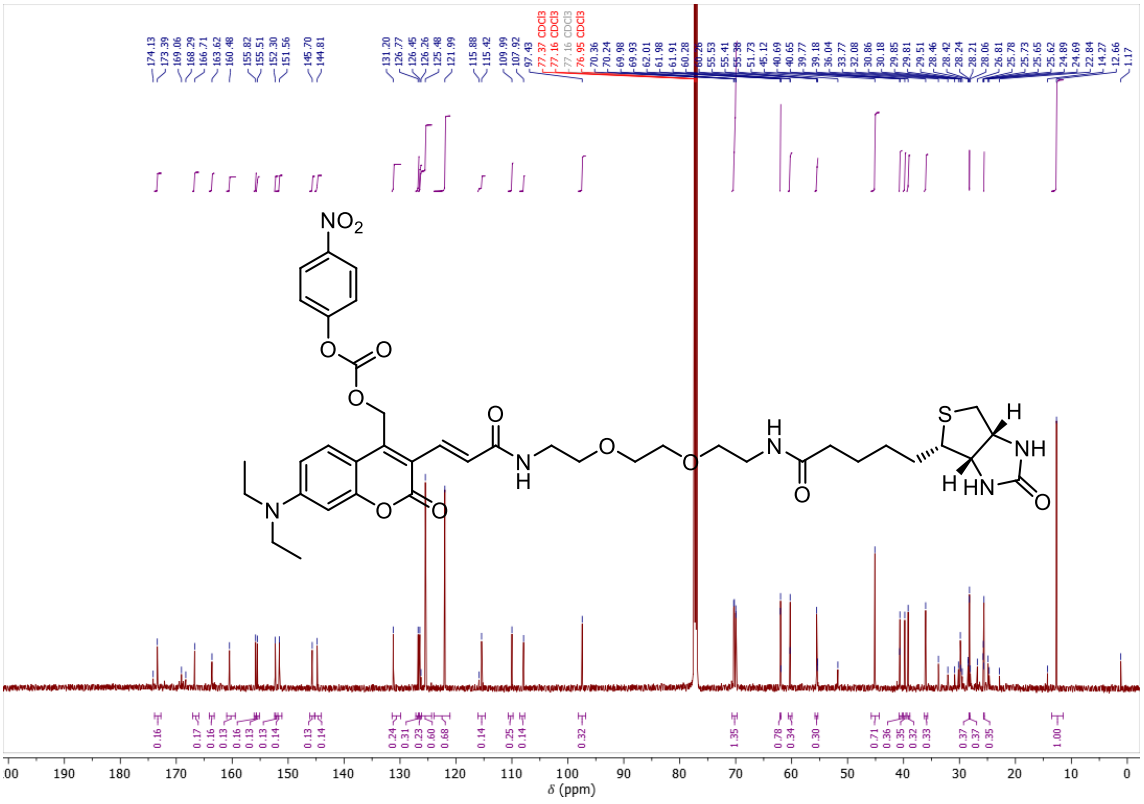


(7-(Diethylamino)-3-((*E*)-3,14-dioxo-18-((3aS,4S,6aR)-2-oxohexahydro-1H-thieno[3,4-d]imidazol-4-yl)-7,10-dioxa-4,13-diazaoctadec-1-en-1-yl)-2-oxo-2H-chromen-4-yl)methyl (4-nitrophenyl) carbonate 10c

^{1}H-NMR (600 MHz, $CDCl_3$)

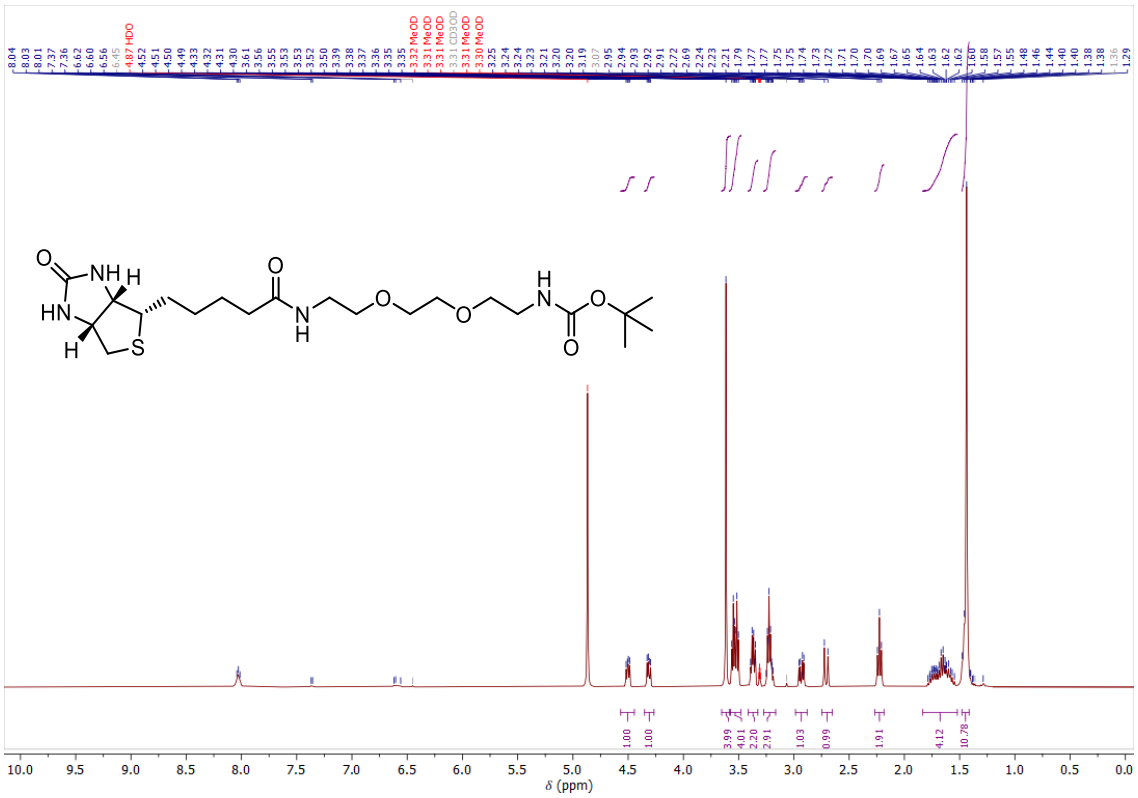


^{13}C-NMR (151 MHz, $CDCl_3$)



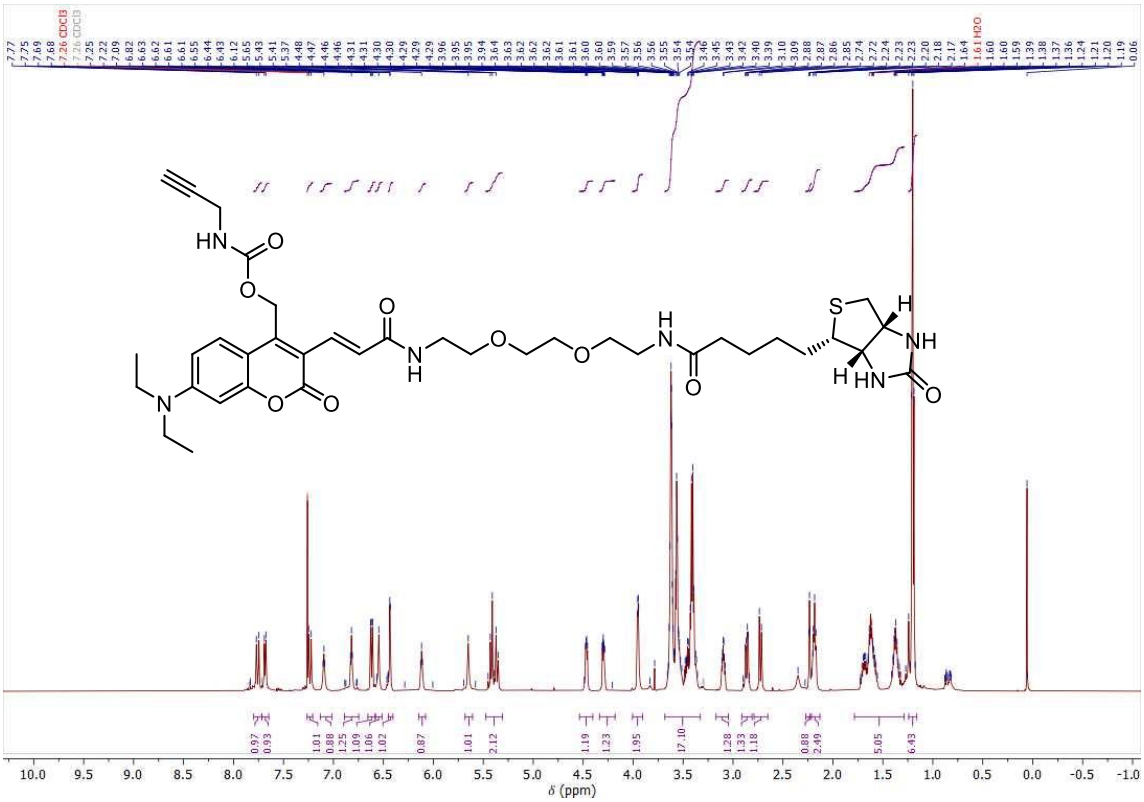
N-Boc-*N'*-biotinyl-3,6-dioxaoctane-1,8-diamine 11

^{1}H-NMR (400 MHz, CD_3OD)

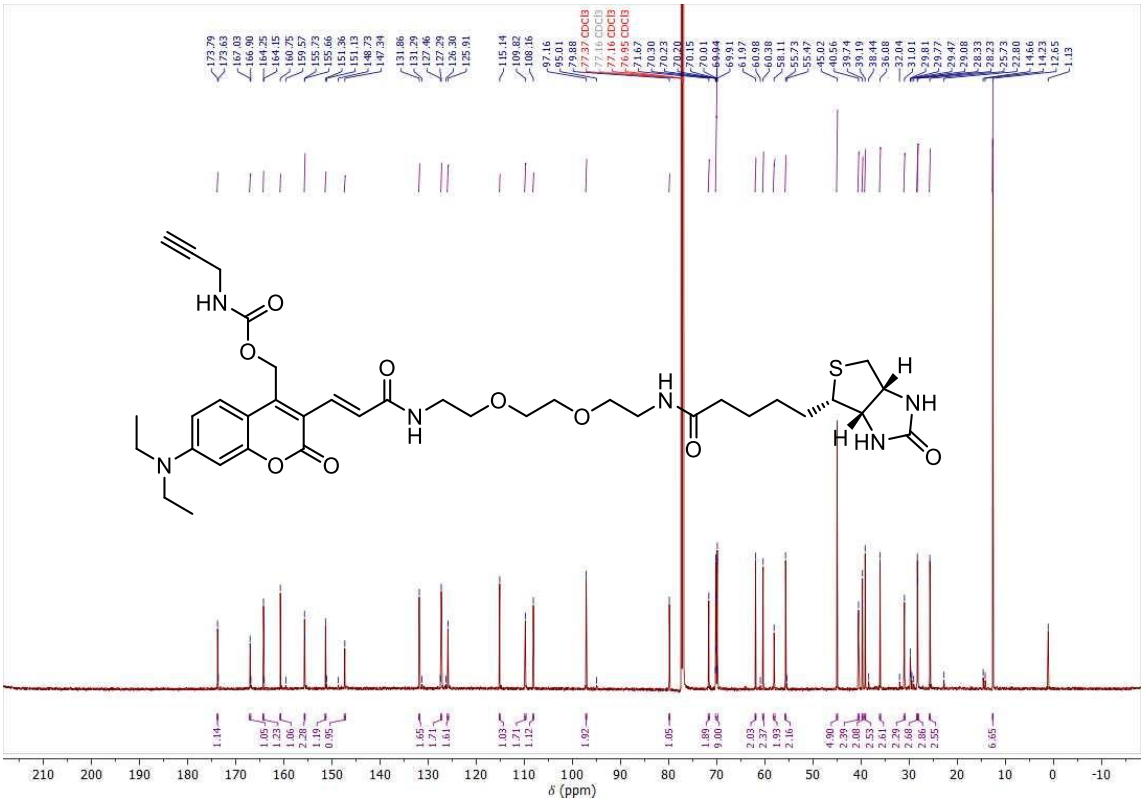


(7-(Diethylamino)-3-((*E*)-3,14-dioxo-18-((3aS,4S,6aR)-2-oxohexahydro-1H-thieno[3,4-d]imidazol-4-yl)-7,10-dioxa-4,13-diazaoctadec-1-en-1-yl)-2-oxo-2H-chromen-4-yl)methyl prop-2-yn-1-ylcarbamate 12

^{1}H-NMR (600 MHz, $CDCl_3$)



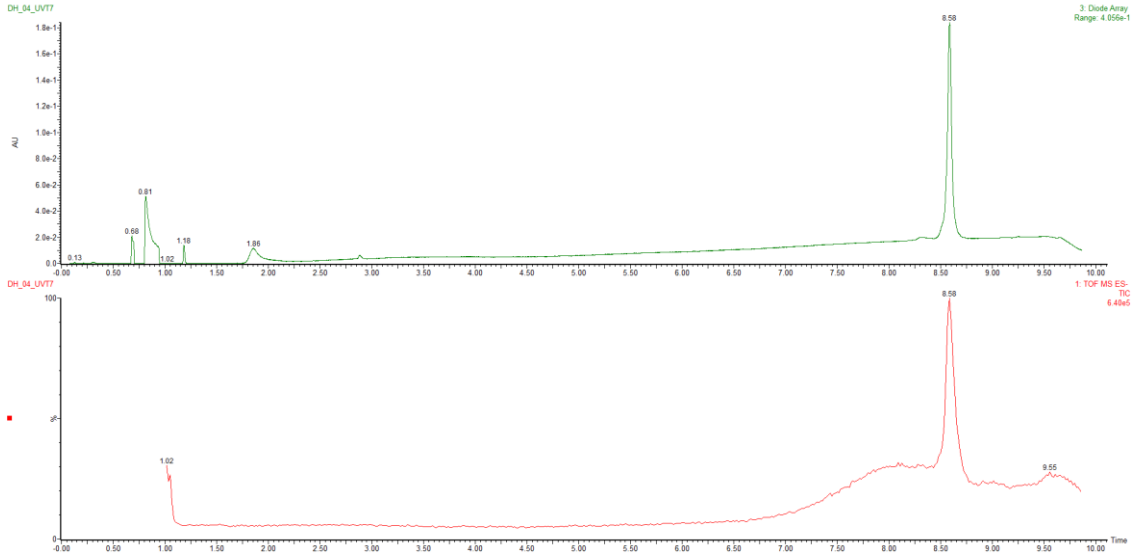
^{13}C-NMR (151 MHz, $CDCl_3$)



C - OLIGONUCLEOTIDE MASS SPECTRA

uvLA-T7 (click-chemistry-tools)

LC-UV and TIC

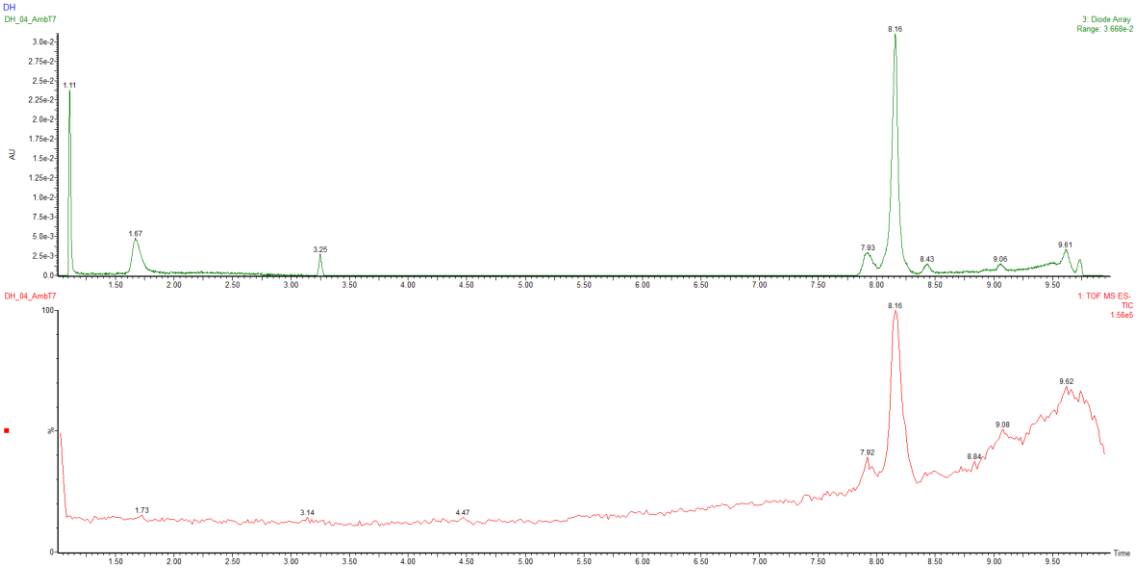


Mass After Deconvolution:

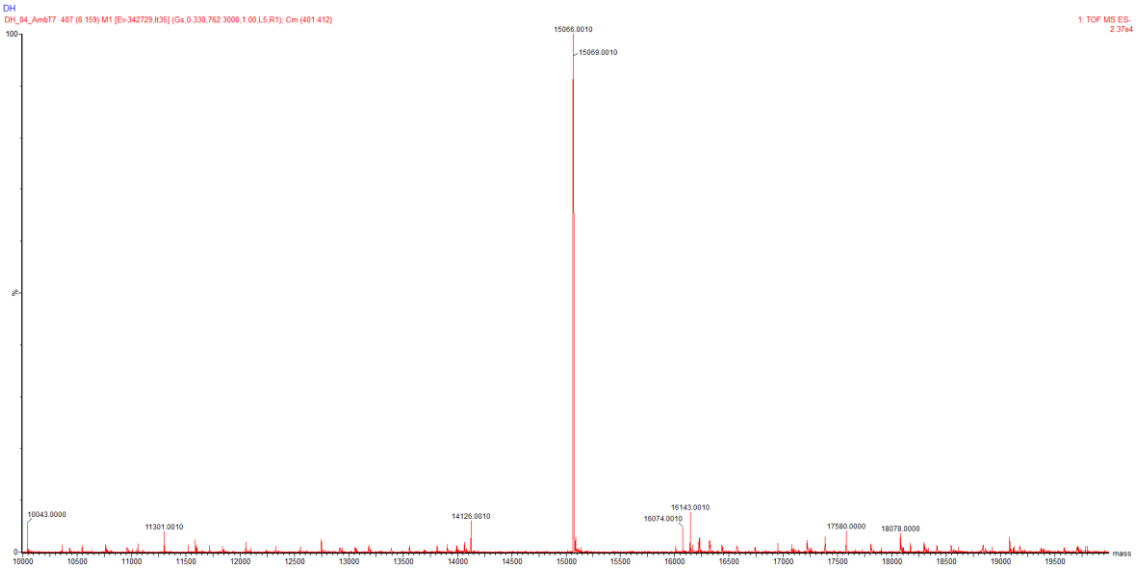


uvLA-T7 (Ambergen)

LC-UV and TIC

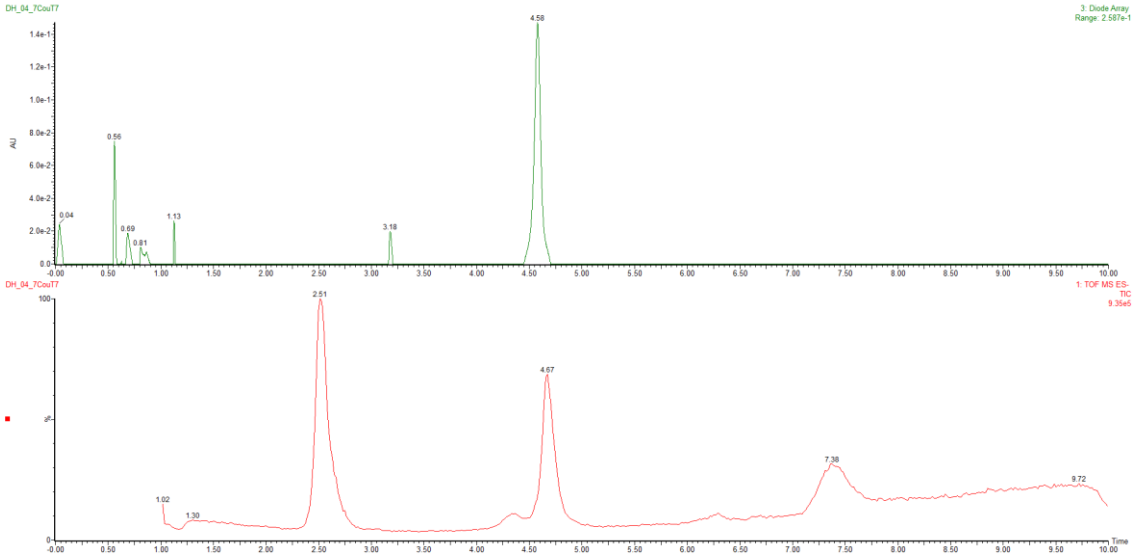


Mass After Deconvolution:



bLA-T7

LC-UV and TIC

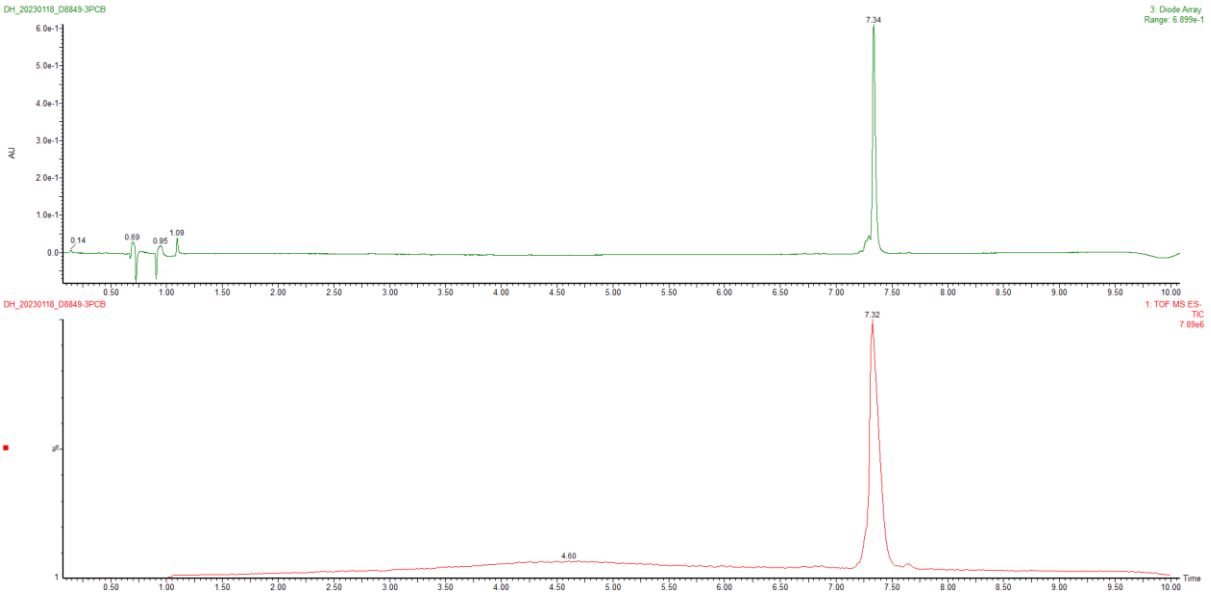


Mass After Deconvolution:



uvLA-V1 biotin

LC-UV and TIC

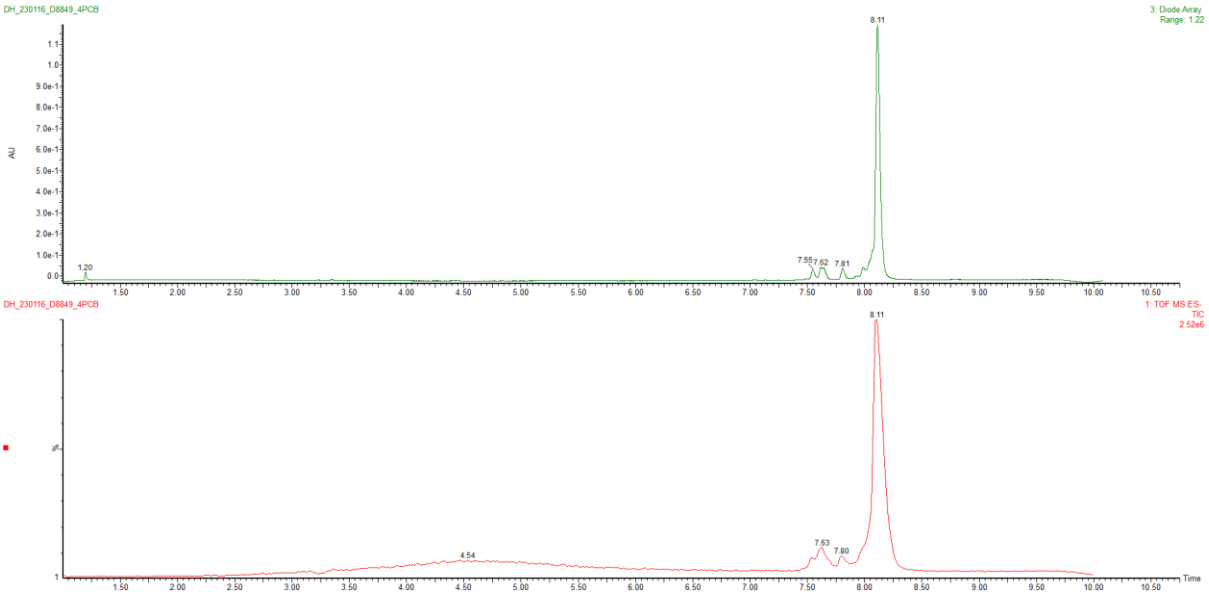


Mass after Deconvolution



uvLA-V2 biotin

LC-UV and TIC

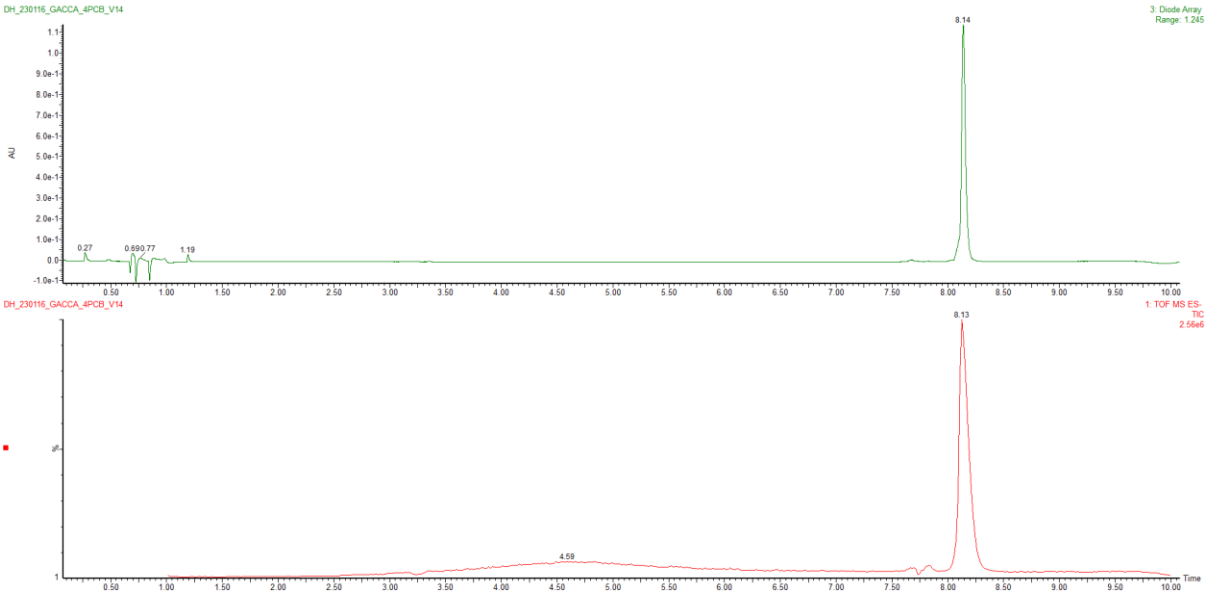


Mass after deconvolution



uvLA-V3 biotin

LC-UV and TIC

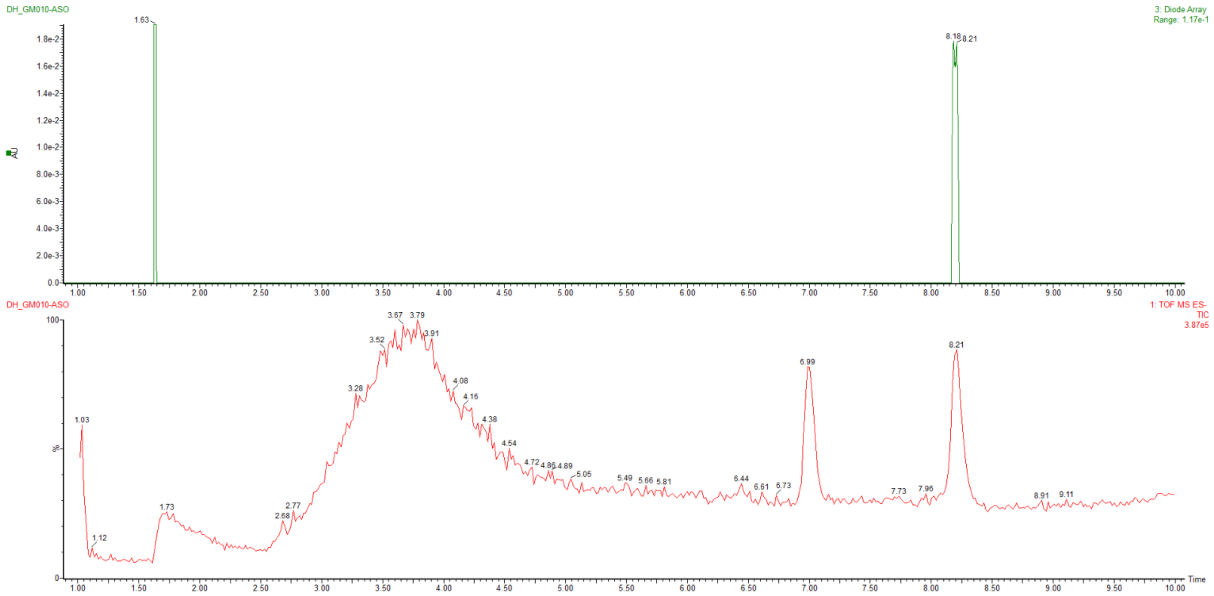


Mass after Deconvolution

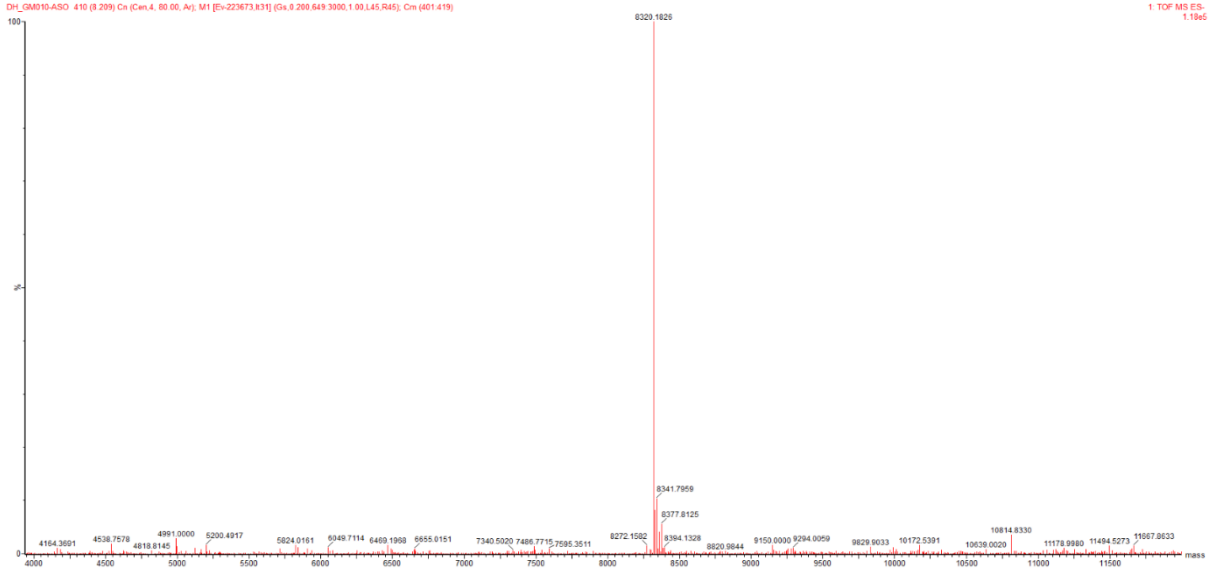


bLA-C1 biotin

LC-UV and TIC

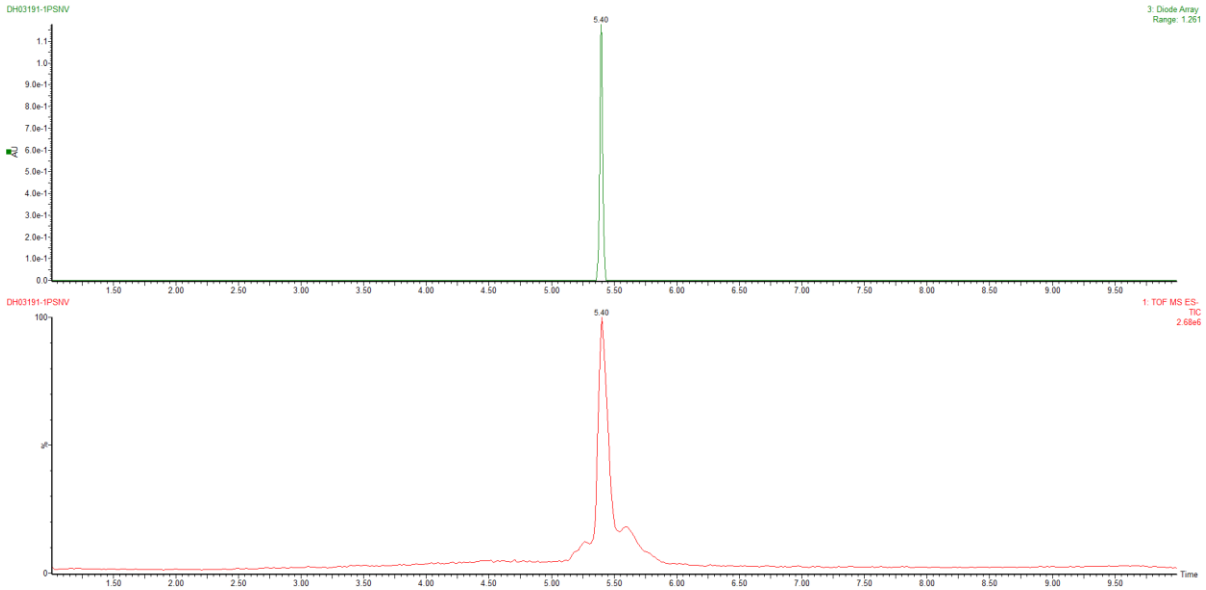


Mass after Deconvolution

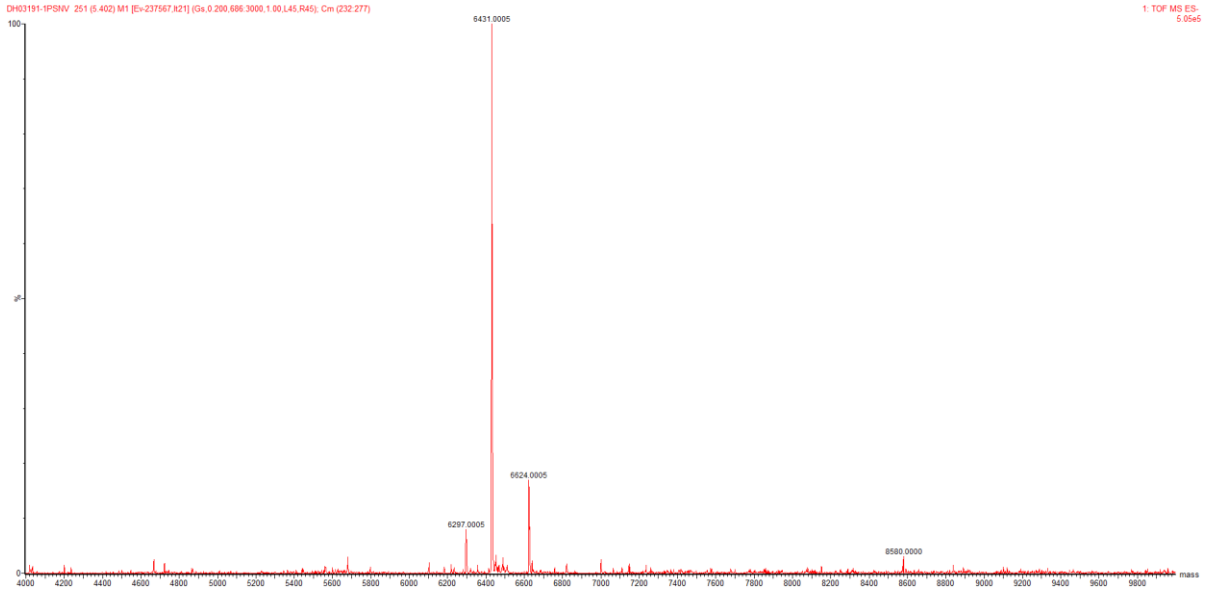


1PSNV

LC-UV and TIC

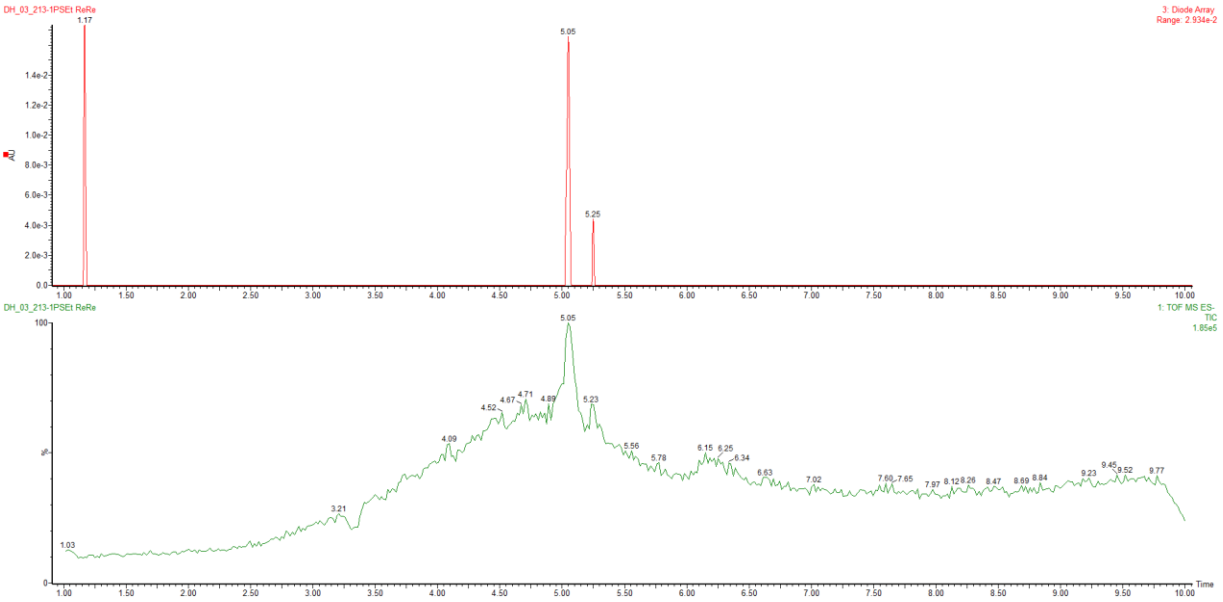


Mass after Deconvolution



20nt-1PSEt

LC-UV and TIC

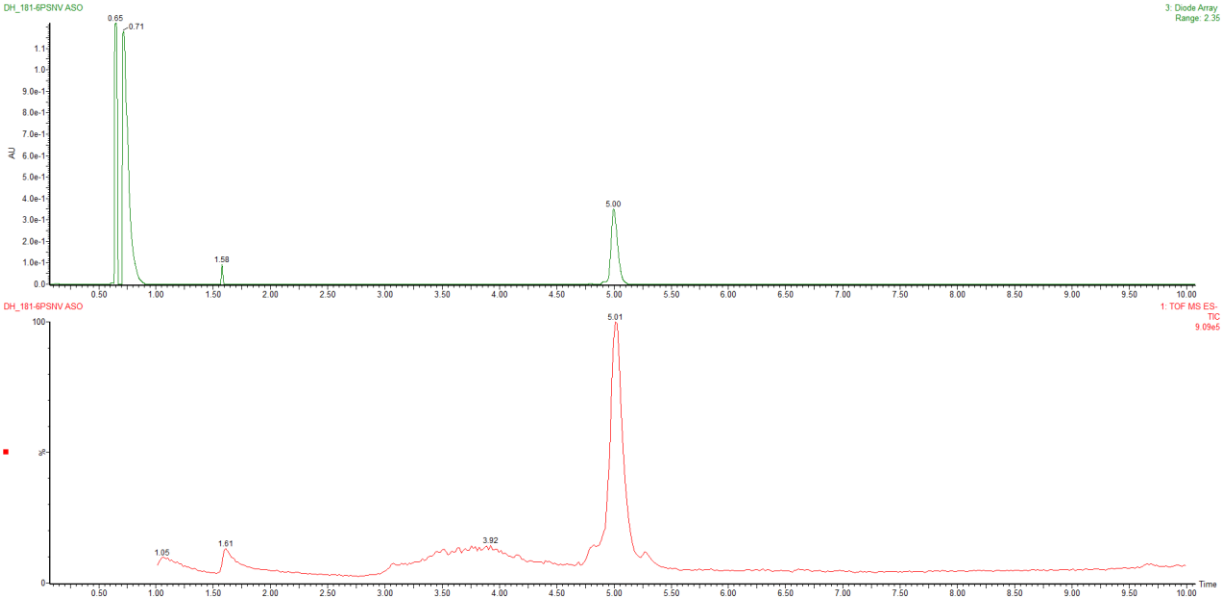


Mass After Deconvolution:



20nt-6PSNV

LC-UV and TIC

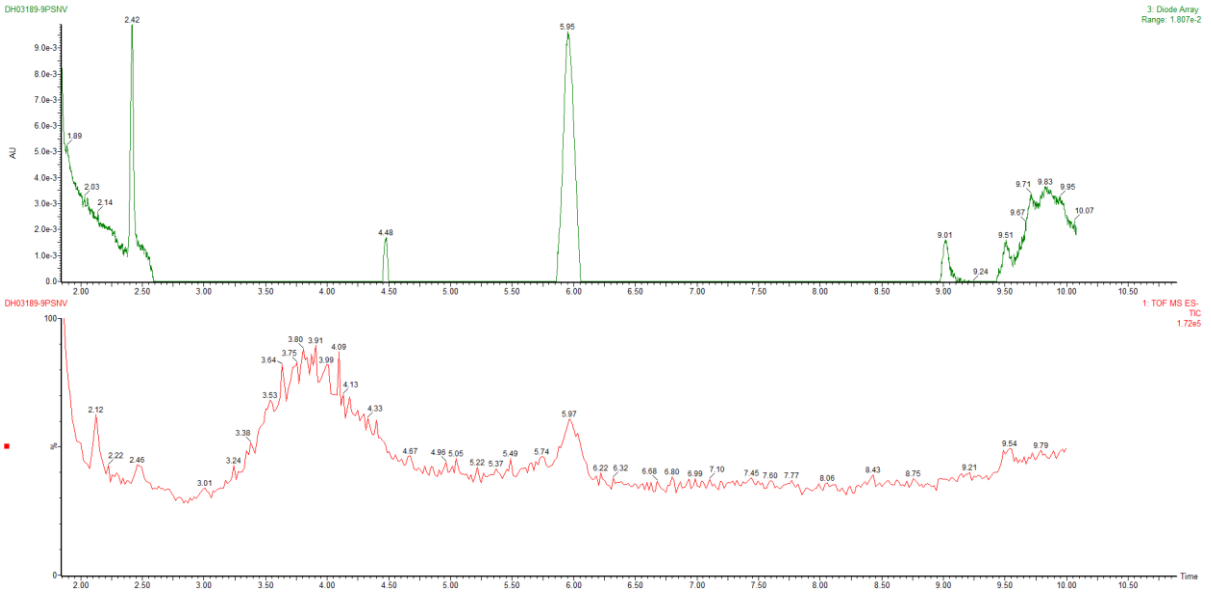


Mass After Deconvolution:

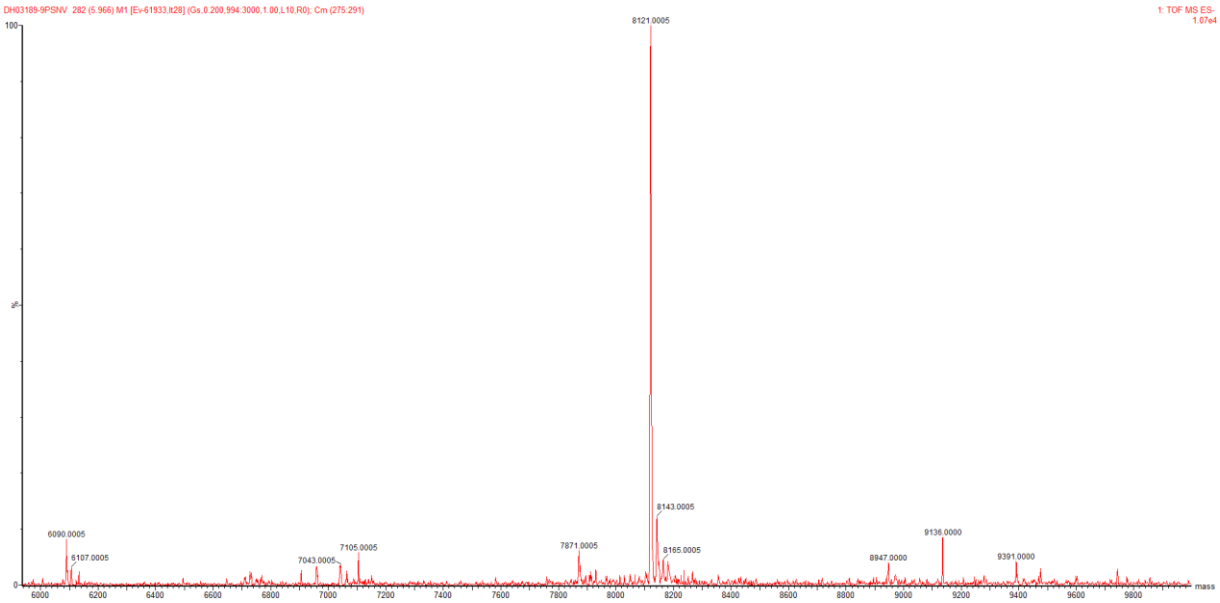


20nt-9PSNV

LC-UV and TIC

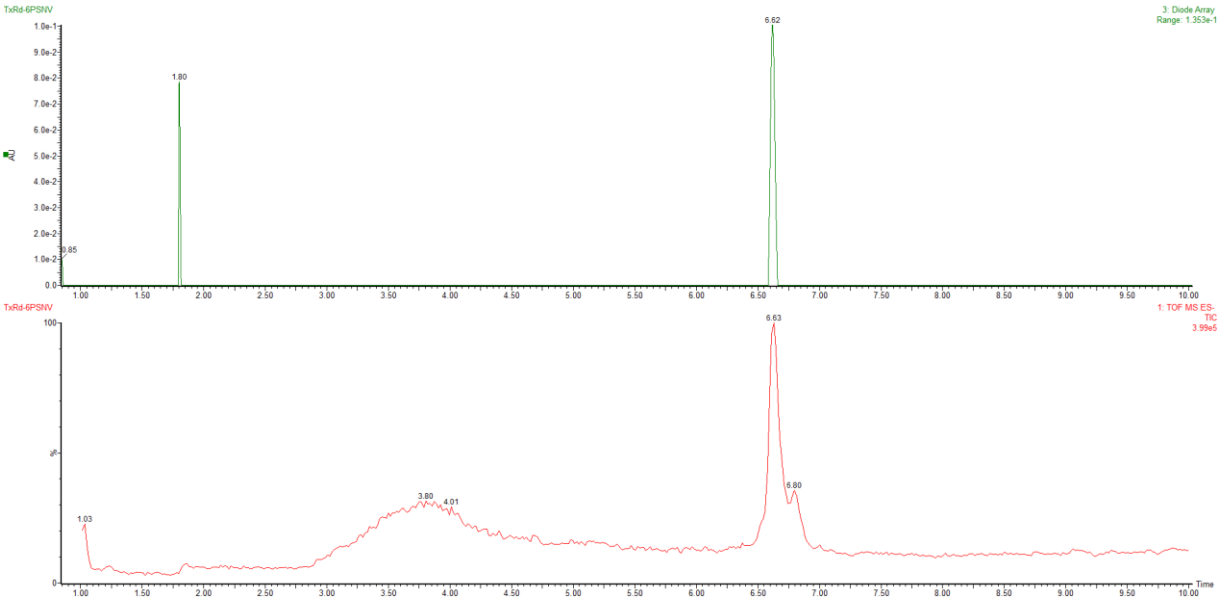


Mass After Deconvolution:



TxRd-20nt-6PSNV

LC-UV and TIC

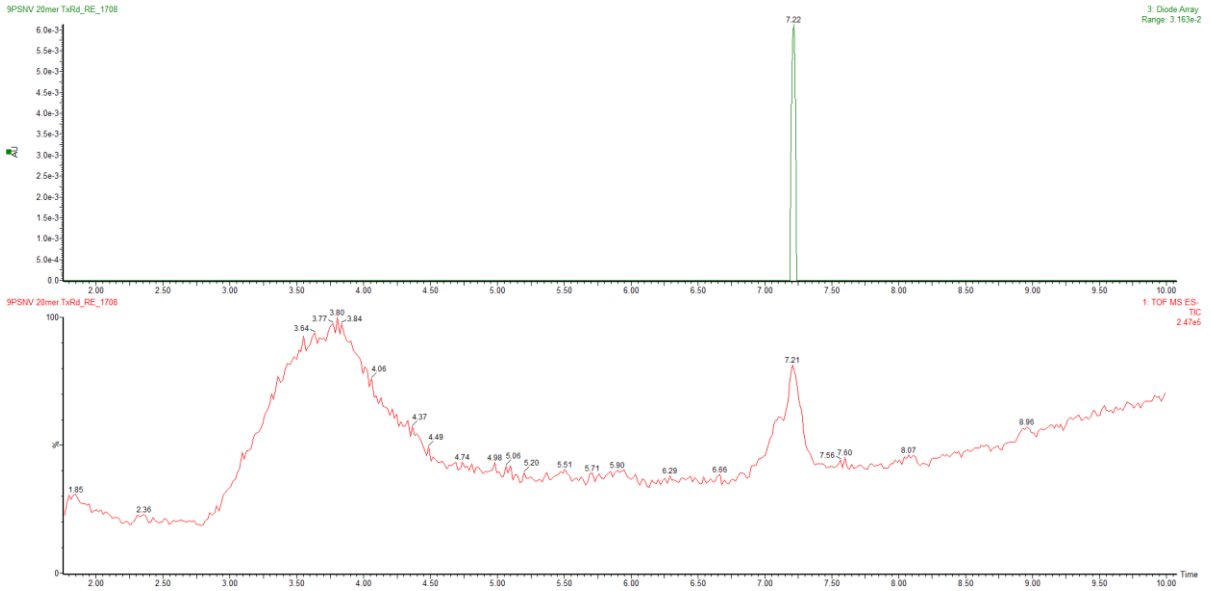


Mass After Deconvolution:

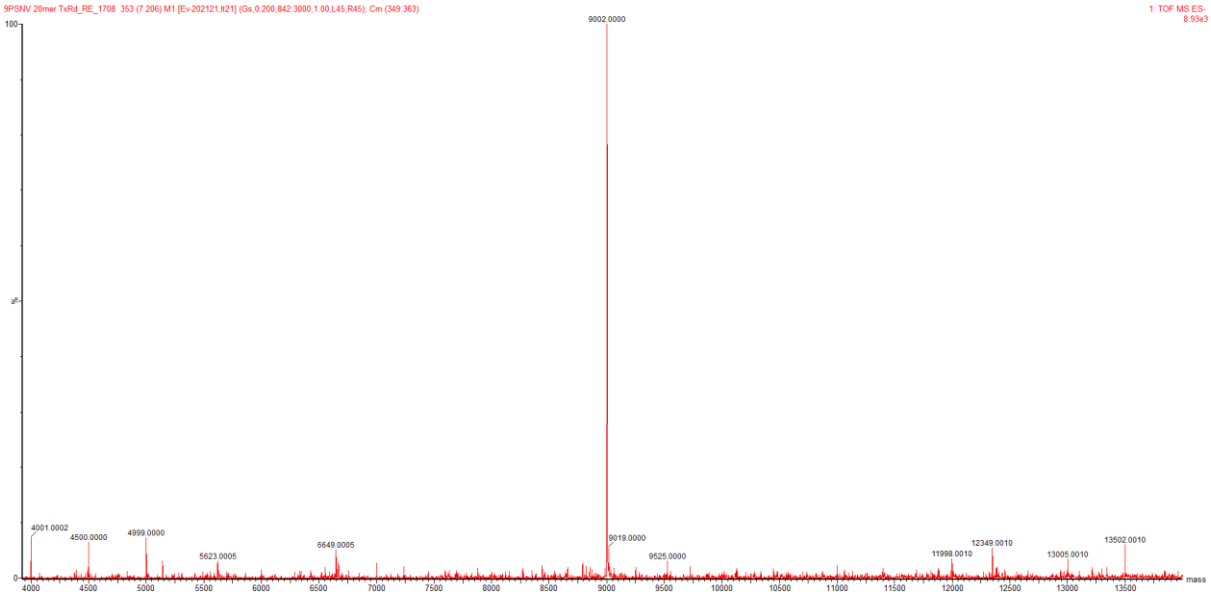


TxRd-20nt-9PSNV

LC-UV and TIC

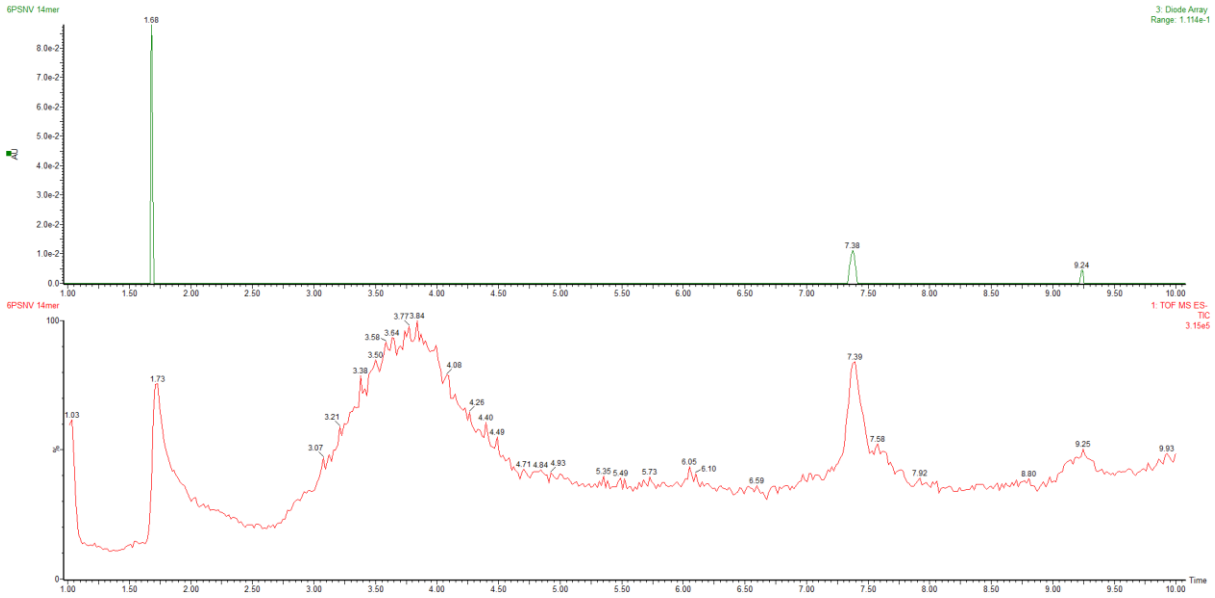


Mass After Deconvolution:

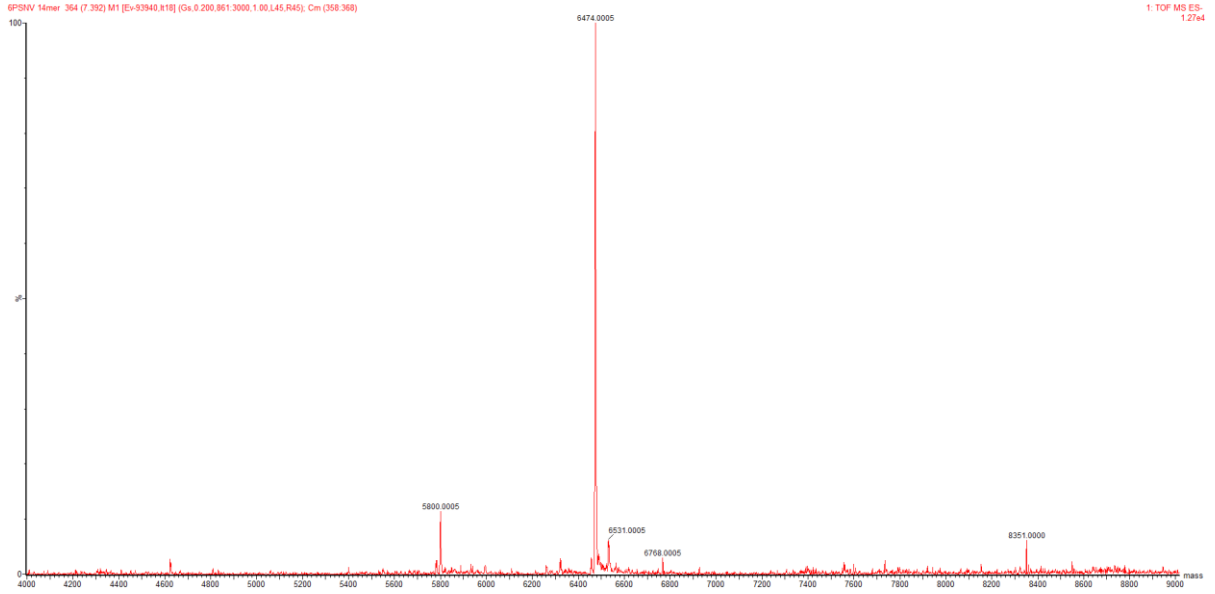


TxRd-14nt-6PSNV

LC-UV and TIC

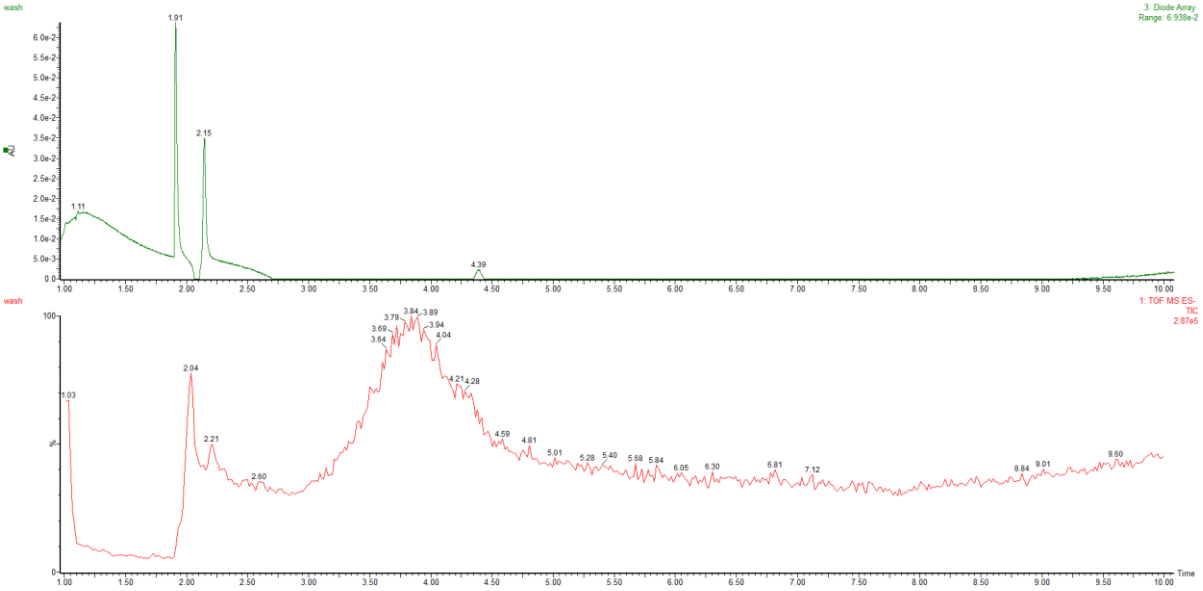


Mass After Deconvolution:



Blank

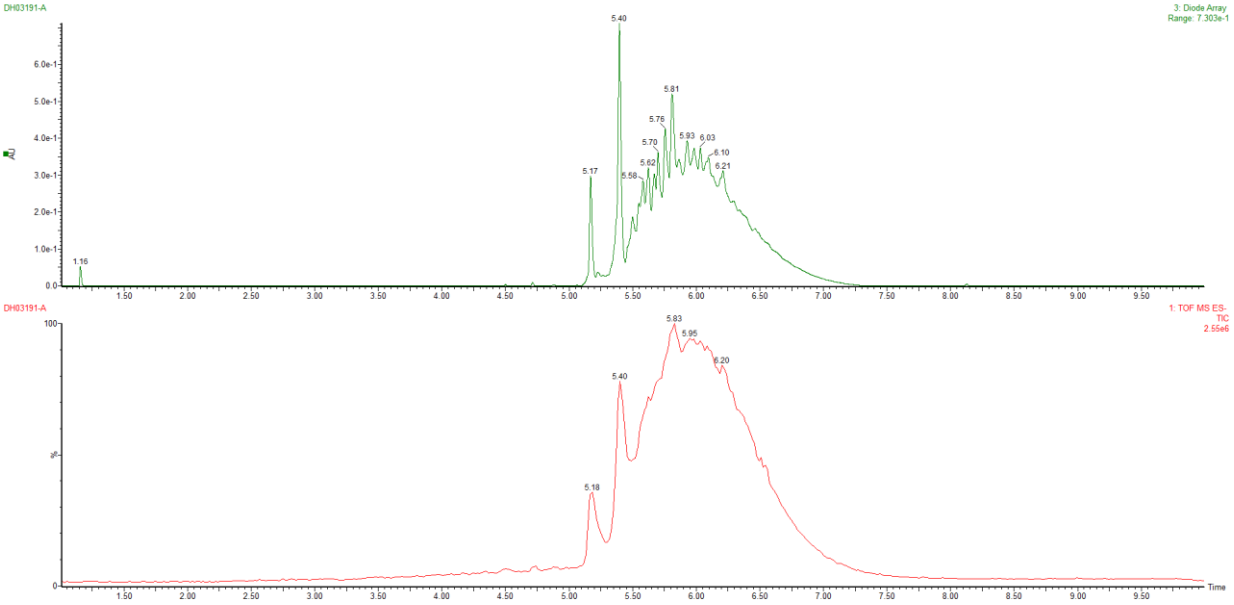
LC-UV and TIC



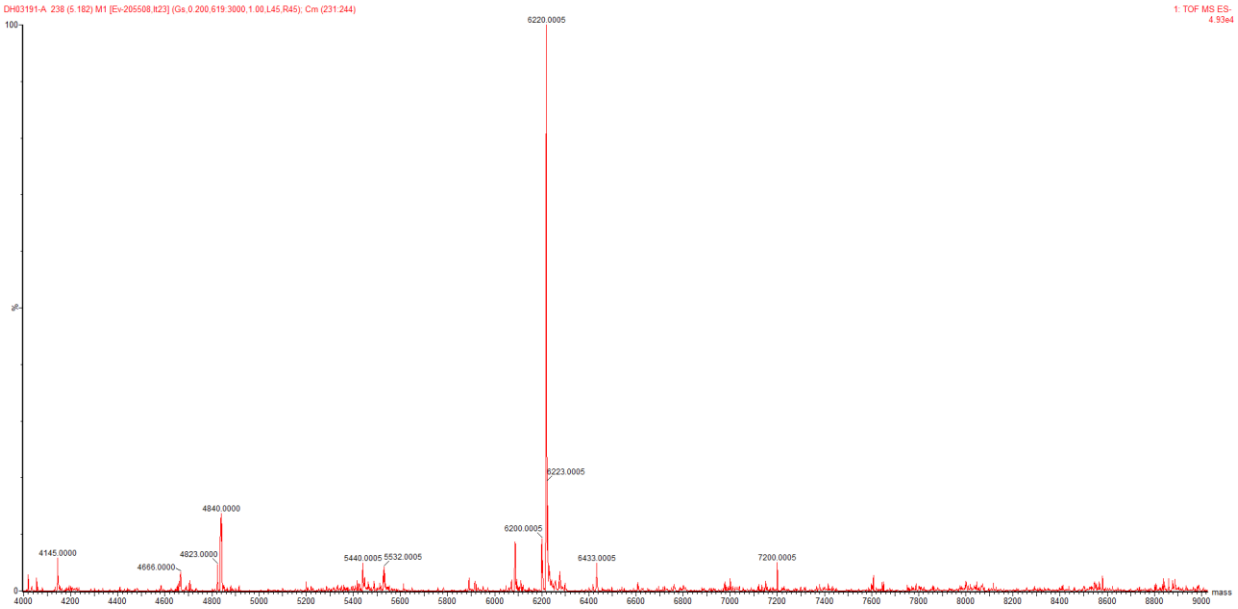
D - Reaction Screening for PS Modification

Condition 1: $NaHCO_3$ buffer

LC-UV



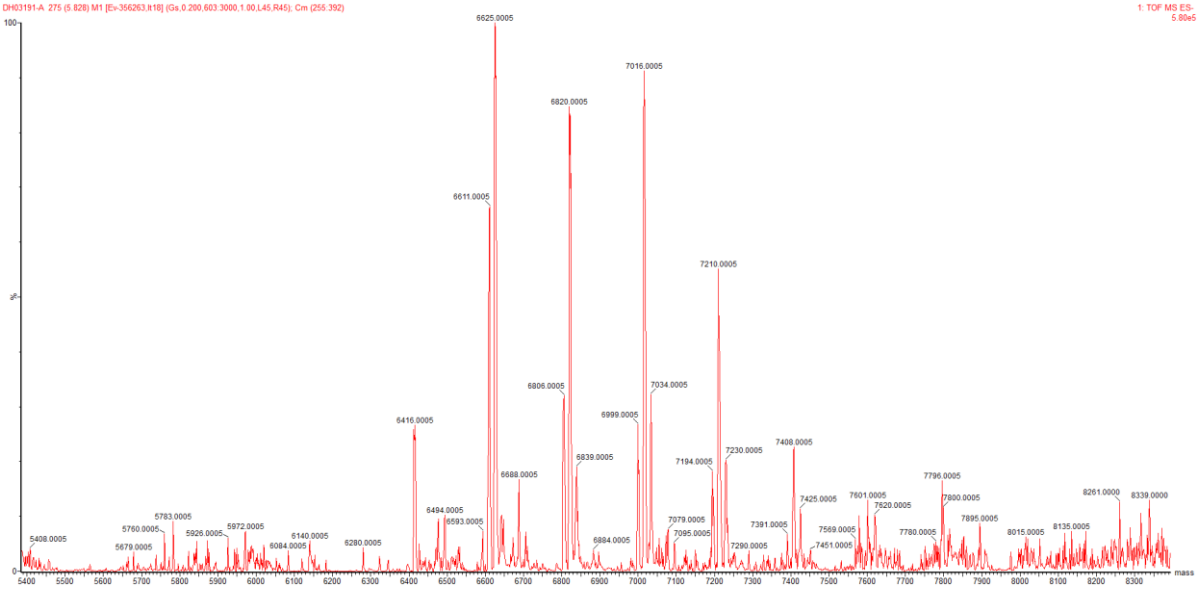
Deconvoluted peak at 5.18 minutes



Deconvoluted peak at 5.40 minutes

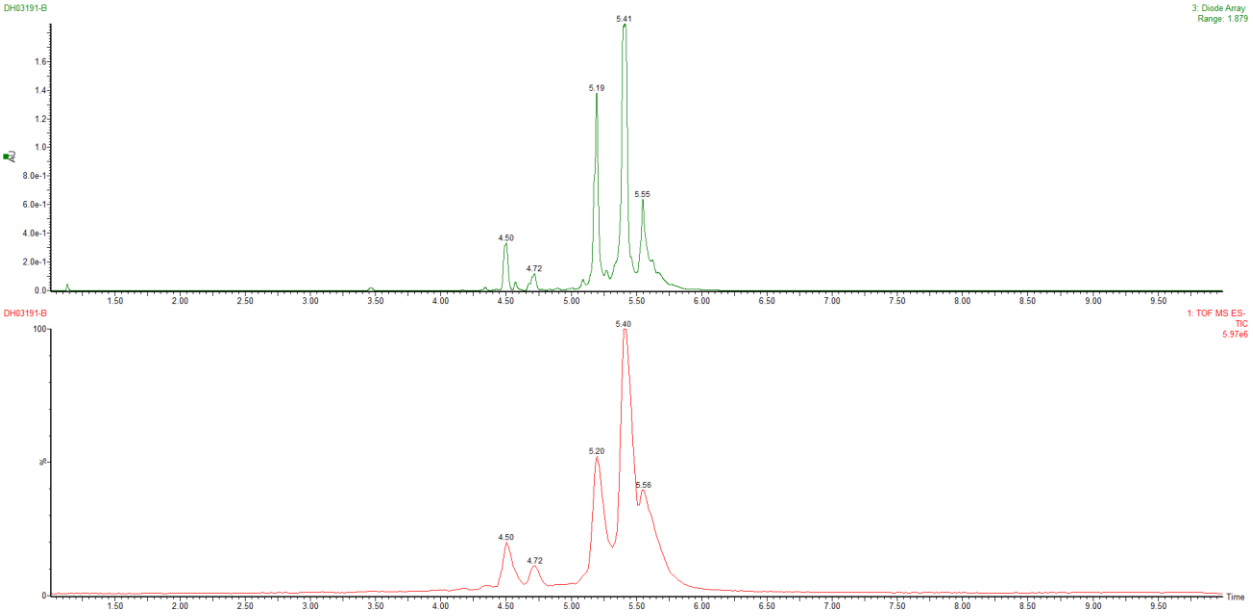


Deconvoluted peaks at 5.5-6.5 minutes

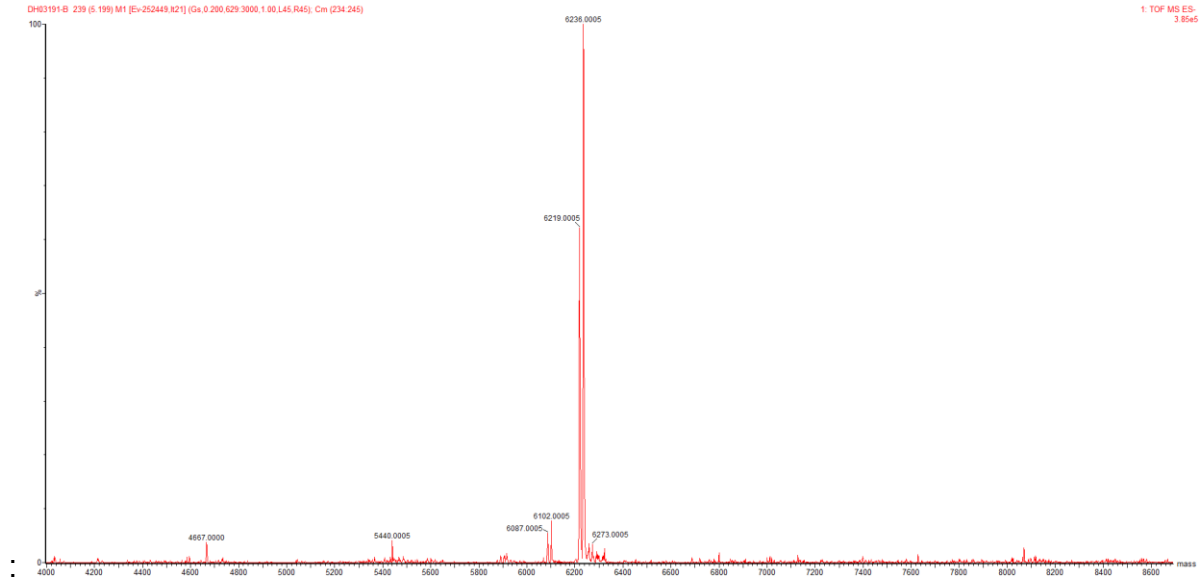


Condition 2: Tris buffer

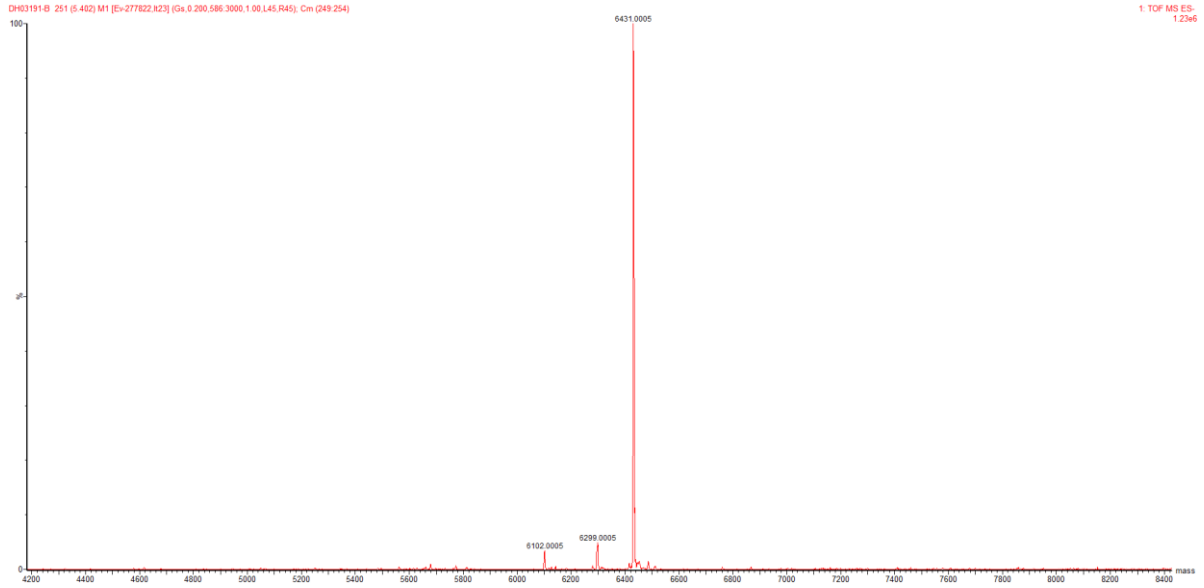
Chromatogram



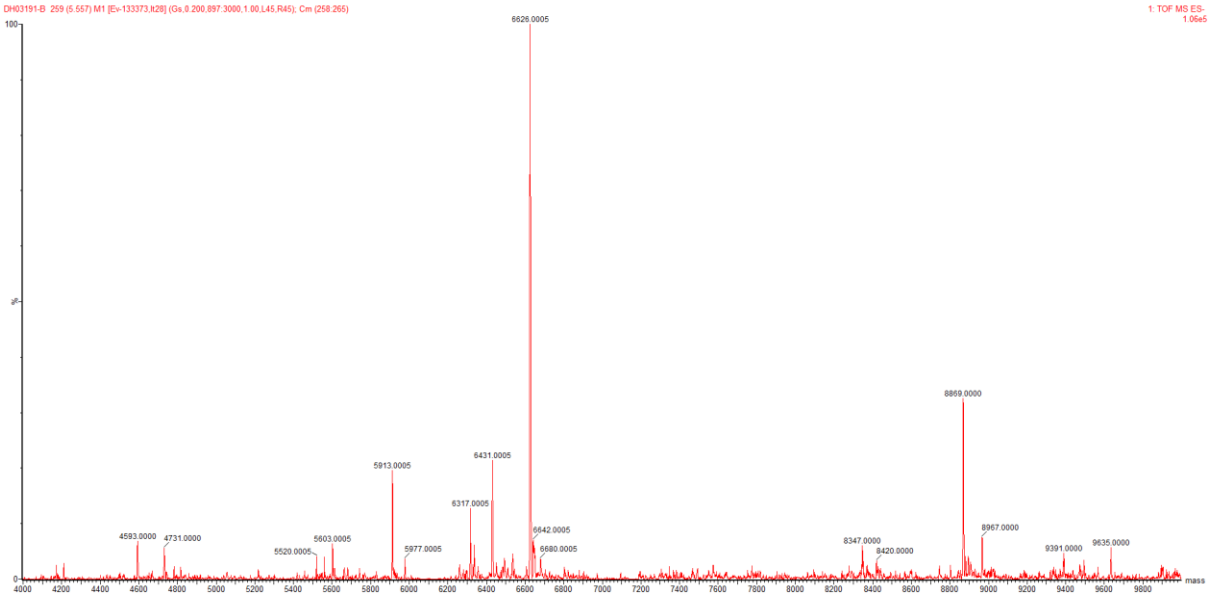
Deconvoluted peak at 5.20 minutes



Deconvoluted peak at 5.40 minutes

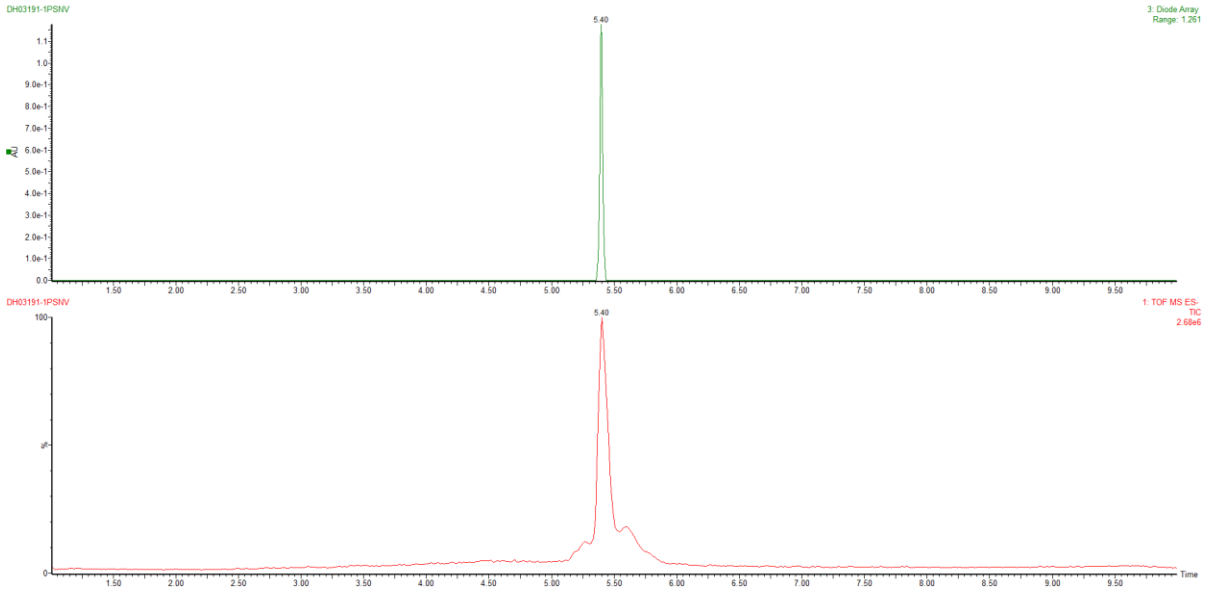


Deconvoluted peak at 5.56 minutes

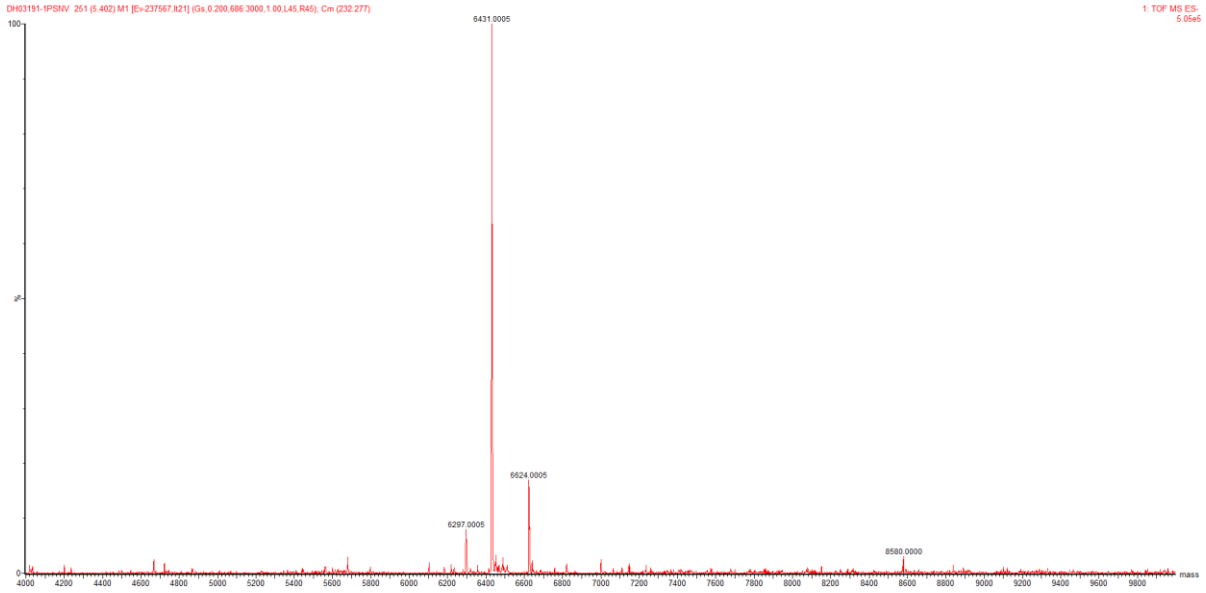


Condition 3: HEPES buffer

Chromatogram

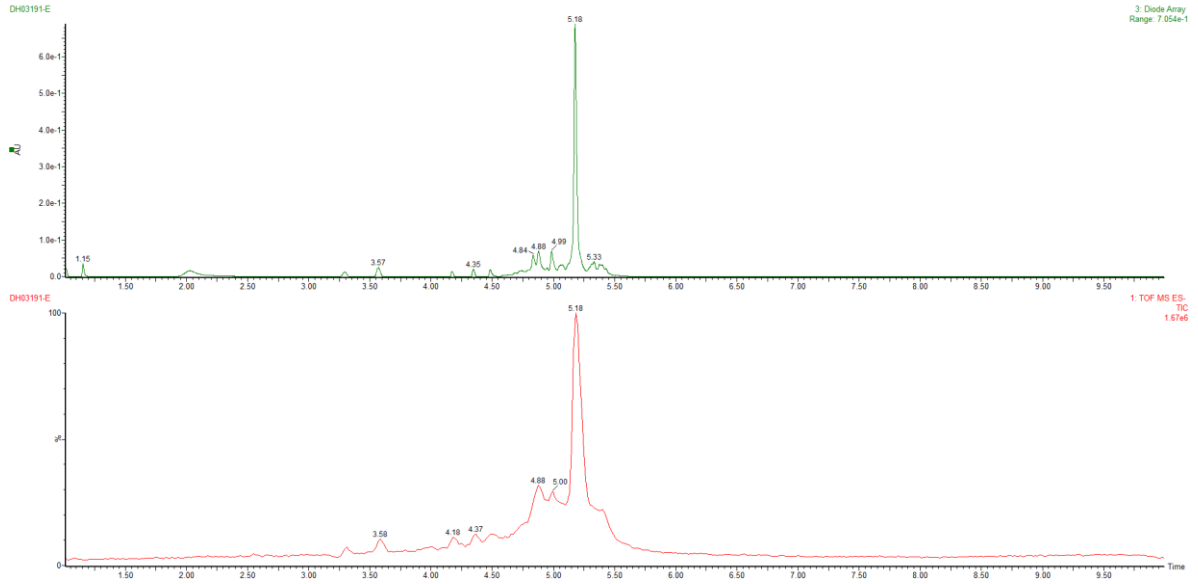


Deconvoluted peak at 5.40 minutes

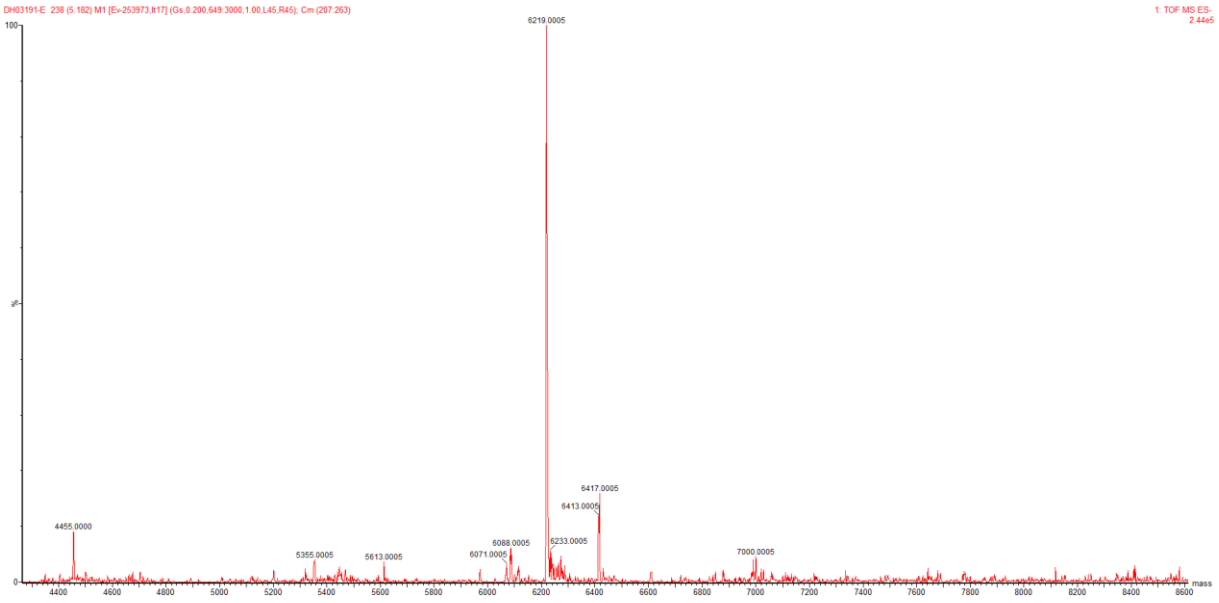


PO-only control with HEPES buffer

Chromatogram



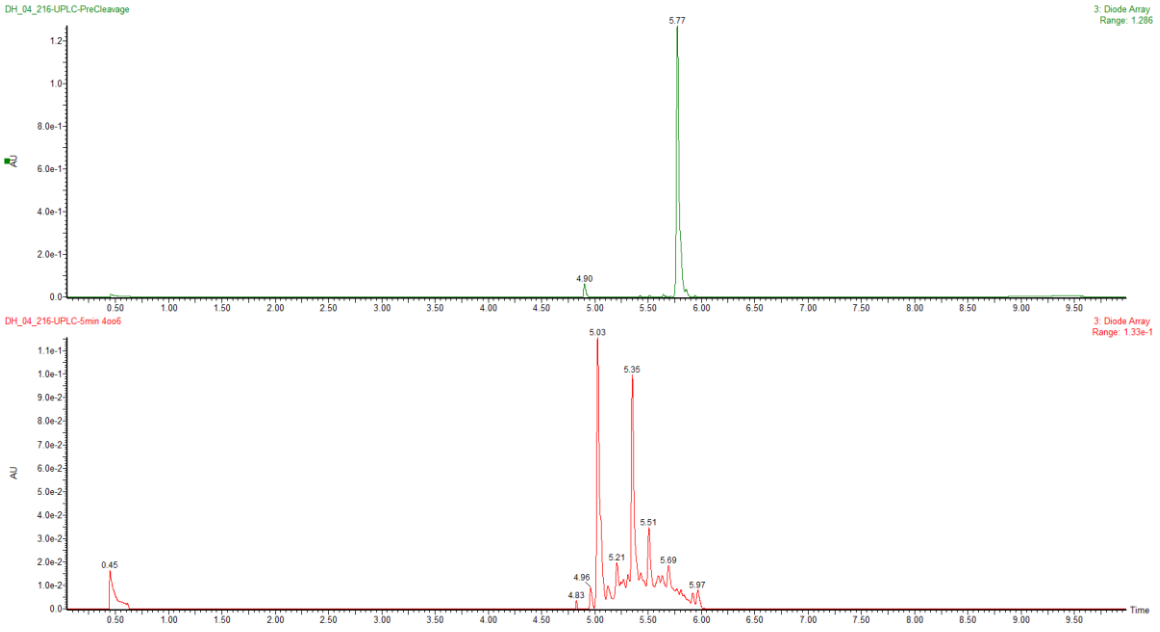
Deconvoluted peak at 5.18 minutes



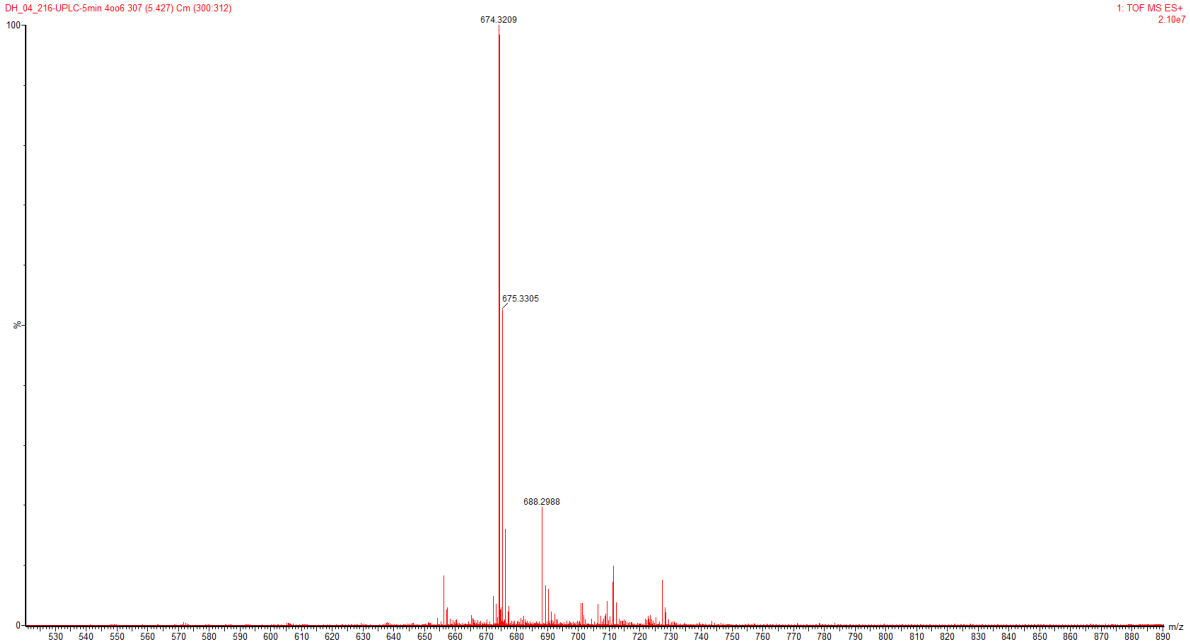
E - PHOTOCLEAVAGE MASS SPECTROMETRY DATA

Photocleavage of Coumarin 11

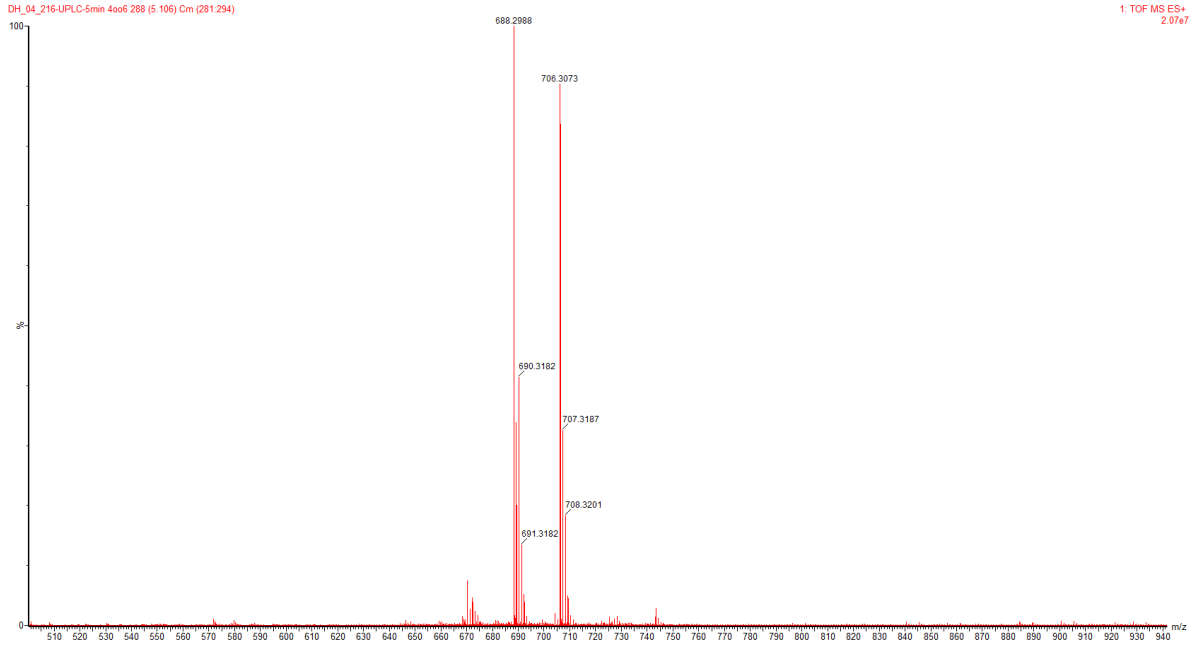
LC-UV Traces Pre- and Post- Photolysis



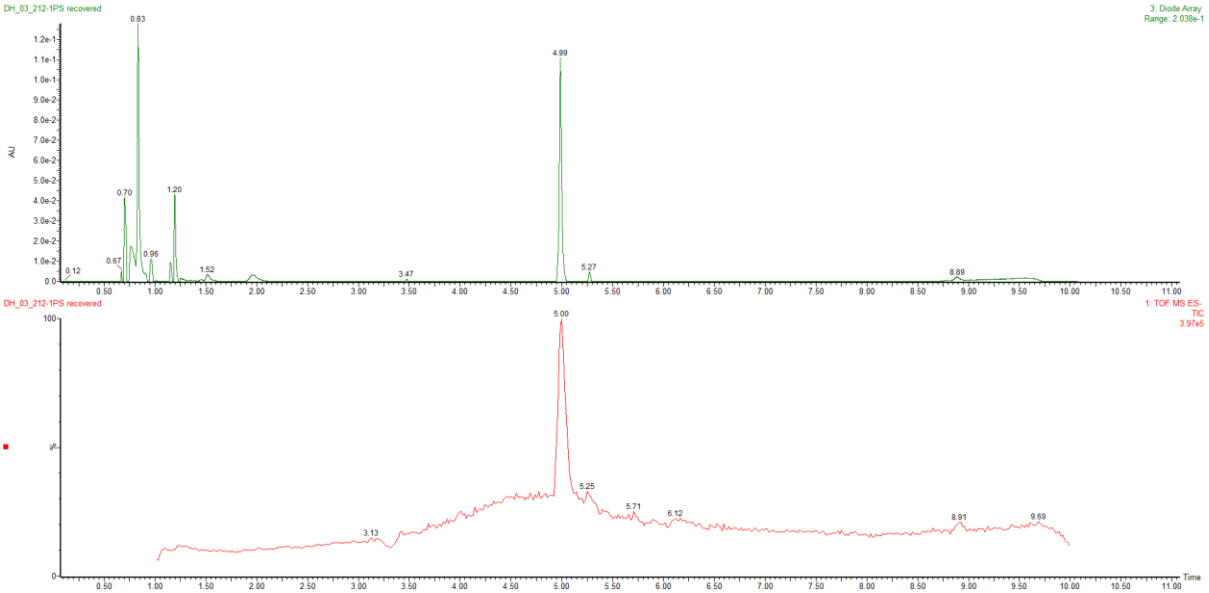
Mass-Spectrum of Peak at 5.35



Mass Spectrum of Peak at 5.03



Photocleavage of 1PSNV oligonucleotide



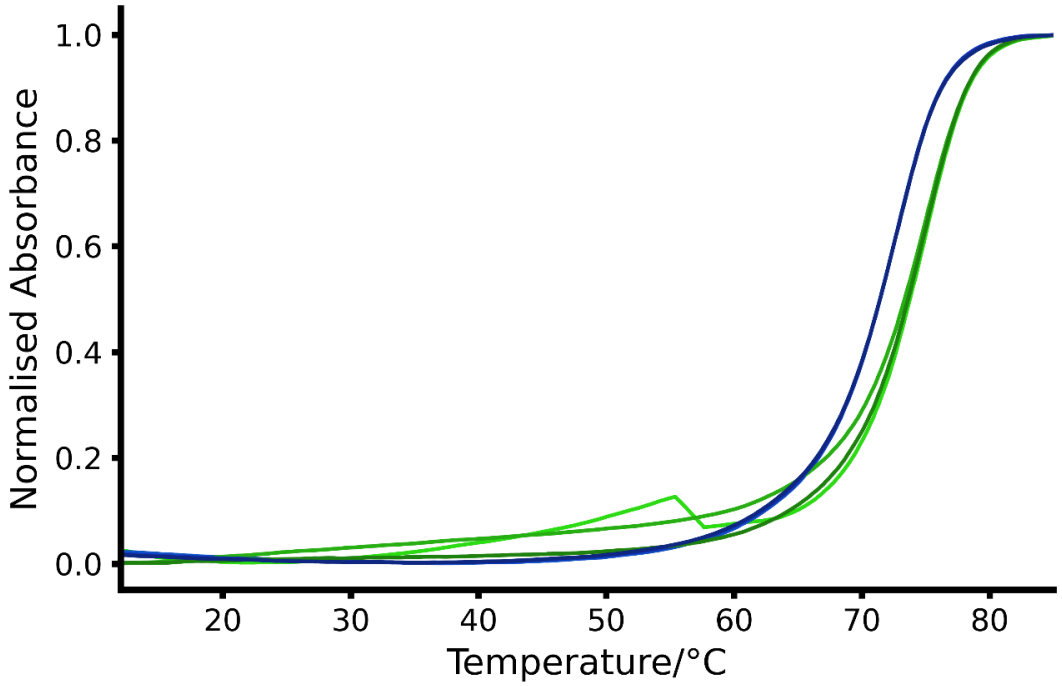
LCMS chromatogram of photocleavage product from 1PSNV ON**.**



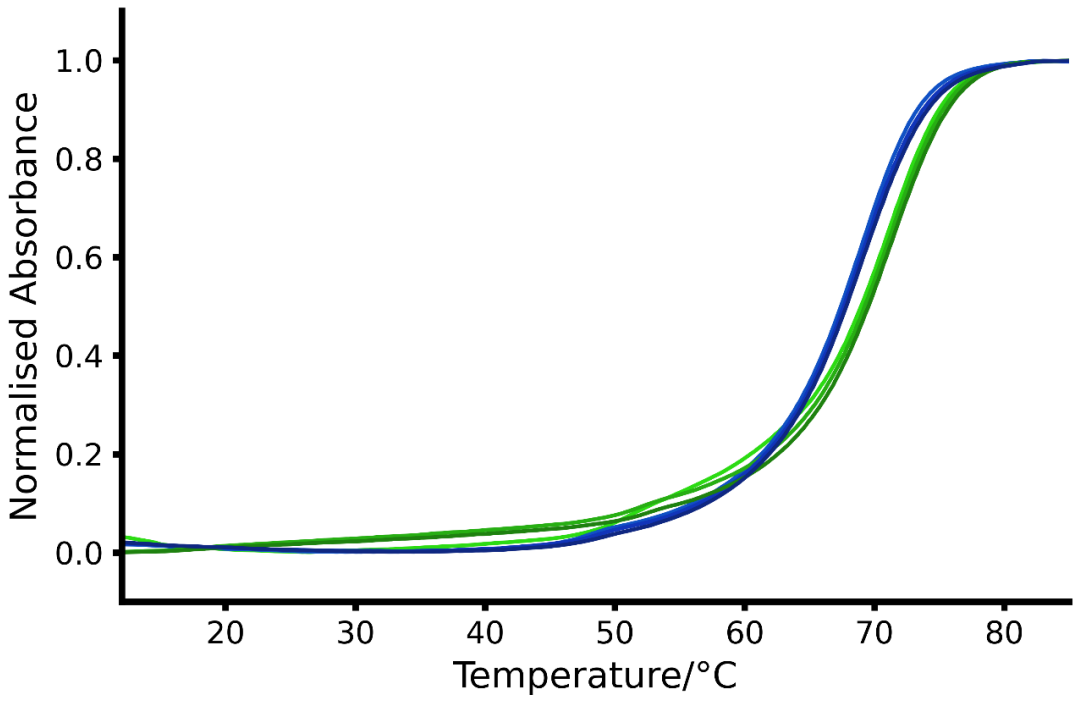
Mass of photocleavage product. The observed mass of 6236 corresponds to the original PS-containing oligonucleotide (Expected Mass 6236).

F - Melting Temperature Data

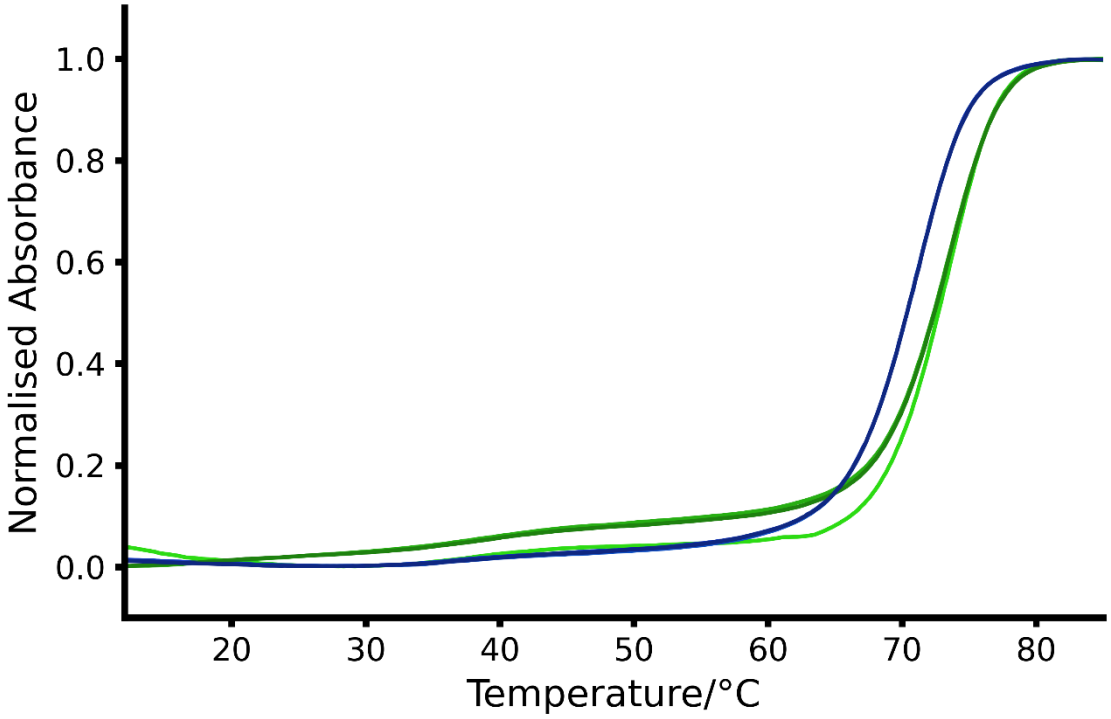
1PS ASO



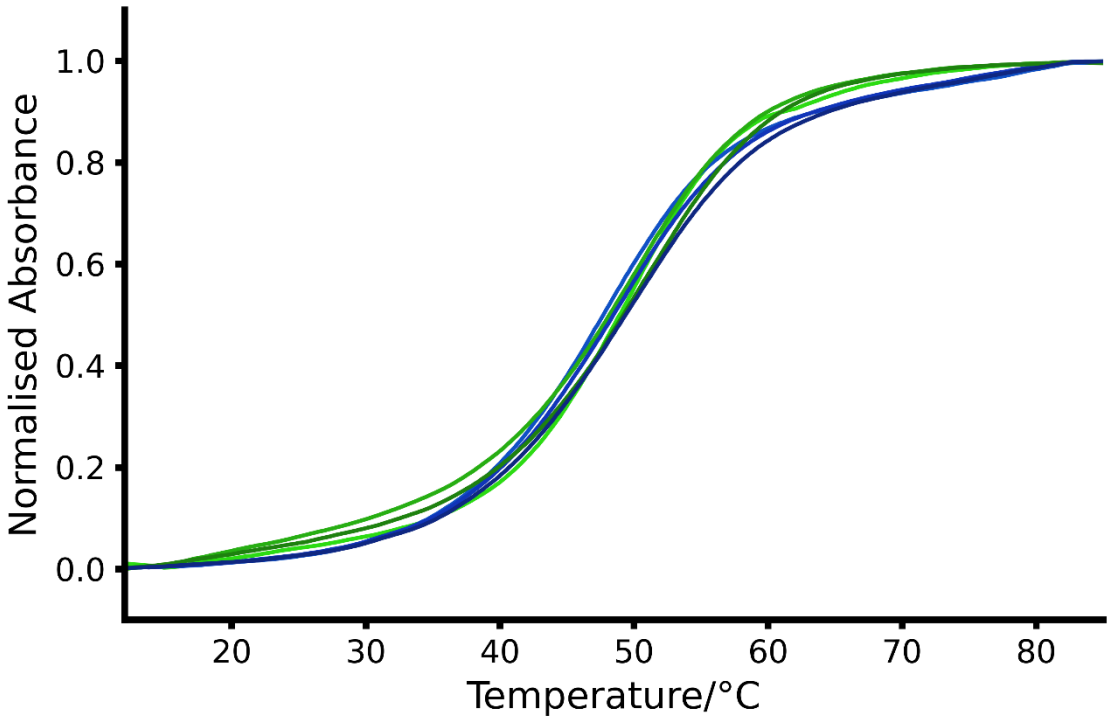
1PSNV ASO



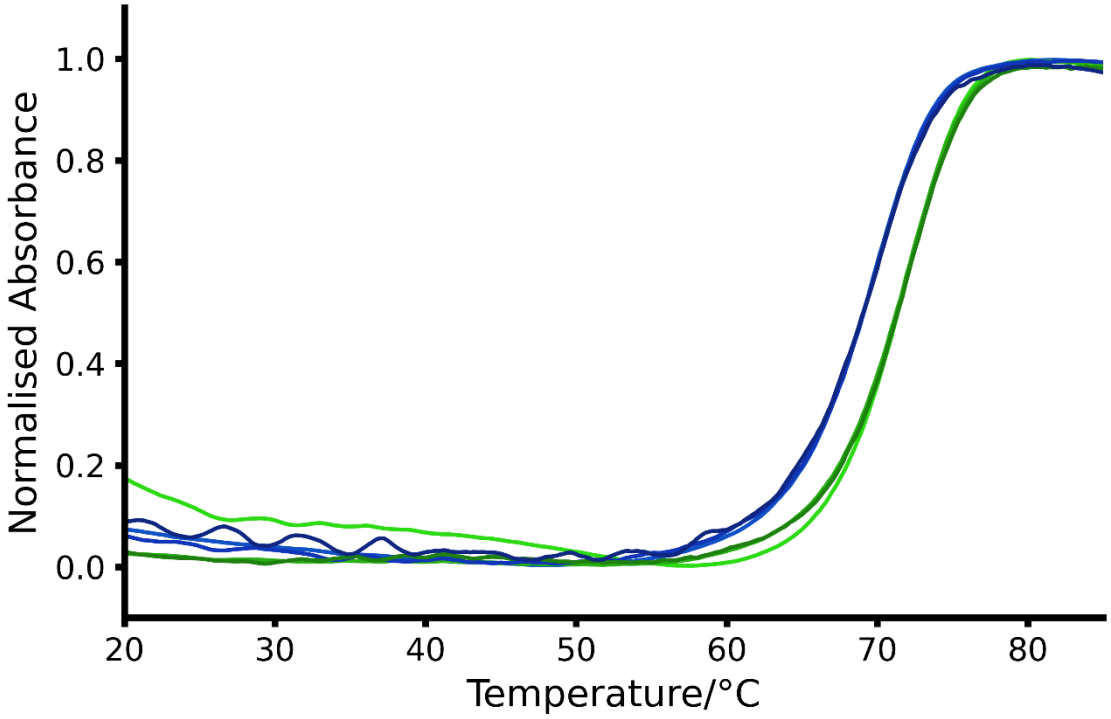
6PS ASO



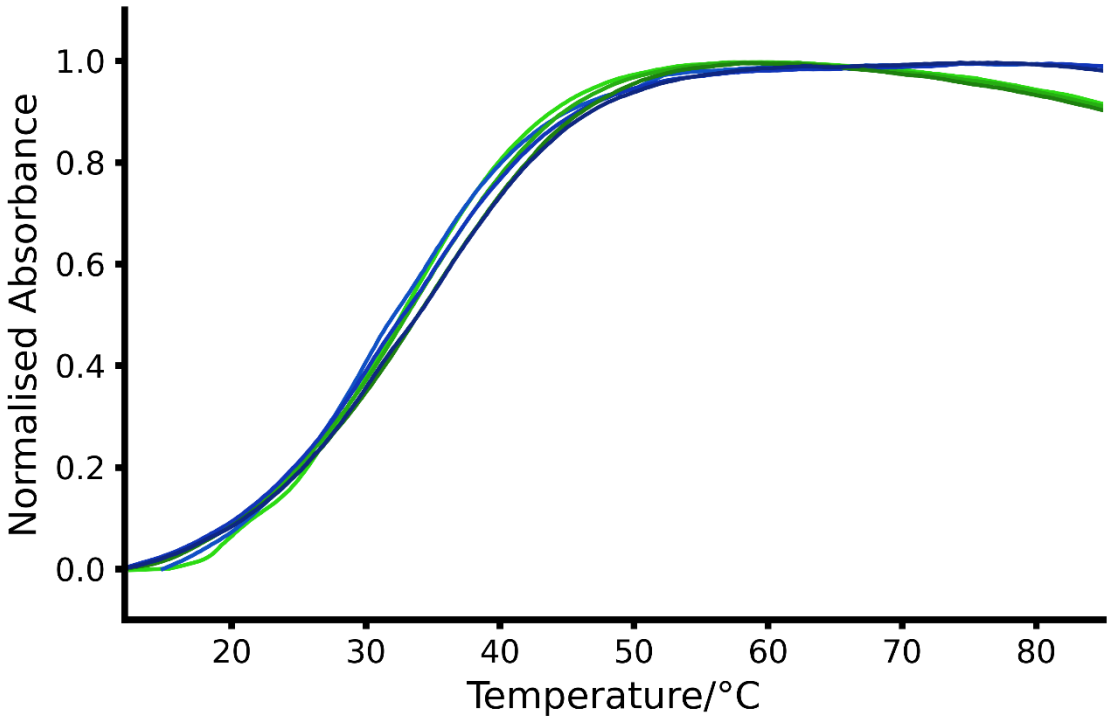
6PSNV ASO



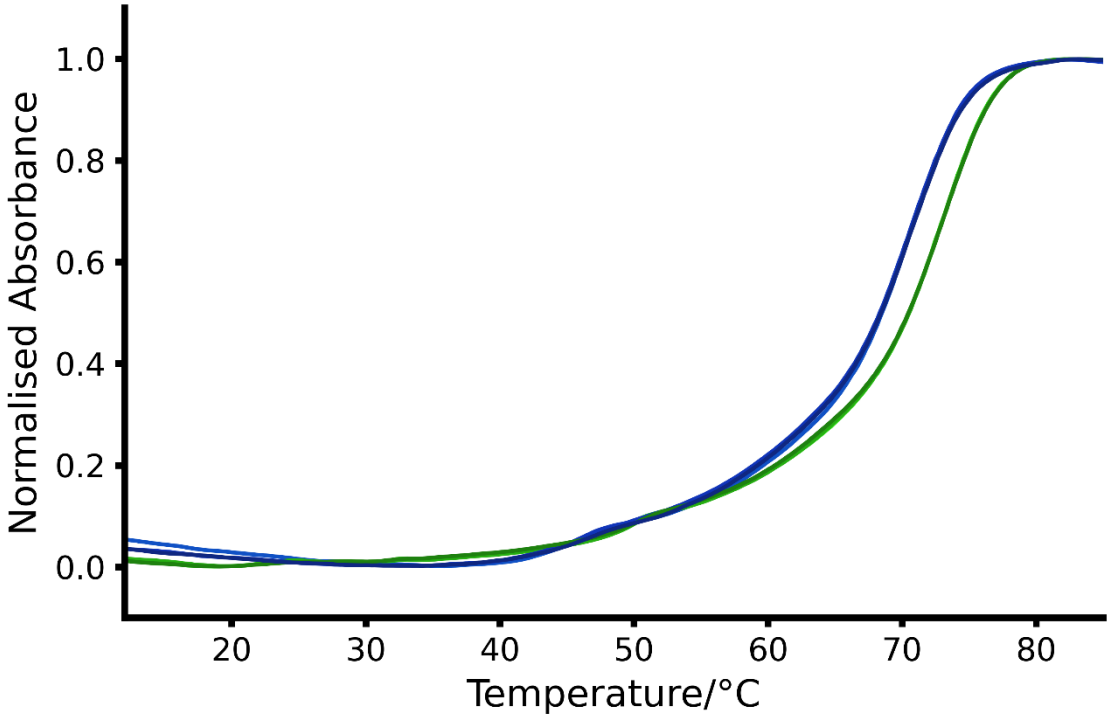
9PS ASO



9PSNV ASO

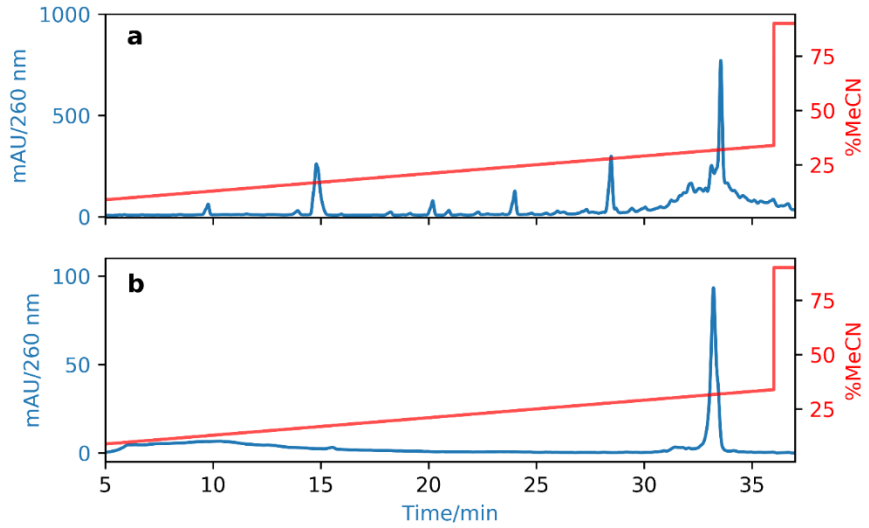


1PSEt ASO


Normalised Absorbance
1.0
0.8
0.6
0.4
0.2
0.0
20
30
40
50
60
70
80
Temperature/°C

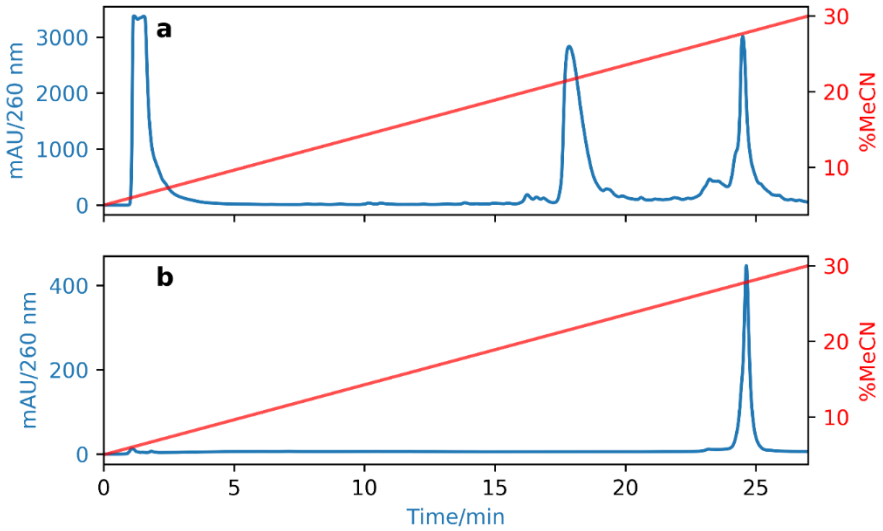
G - HPLC Purifications of modified Oligonucleotides

HPLC Trace of bLA-T7



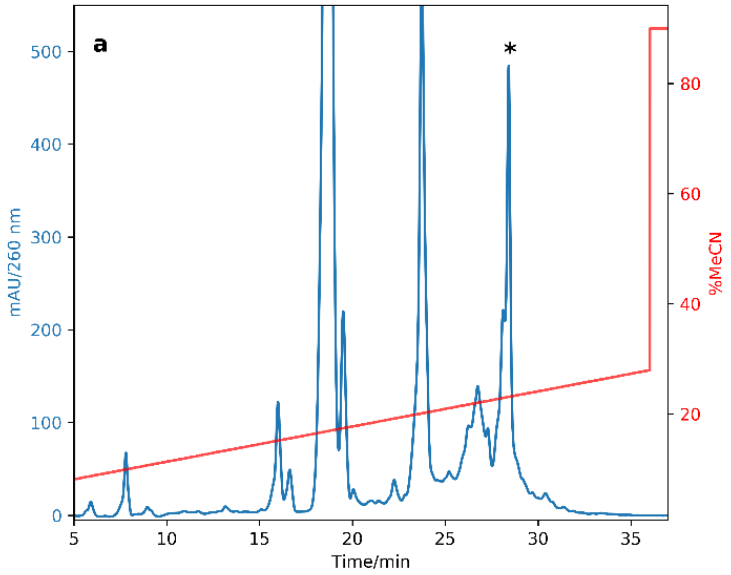
a) Crude HPLC trace of reaction of PFP-Carbonate **10b** with 7-amine containing oligonucleotide (**Table 7-1,** Entry 1). **b)** HPLC trace of purified bLA-T7.

HPLC Trace of uvLA-T7 (click-chemistry-tools)



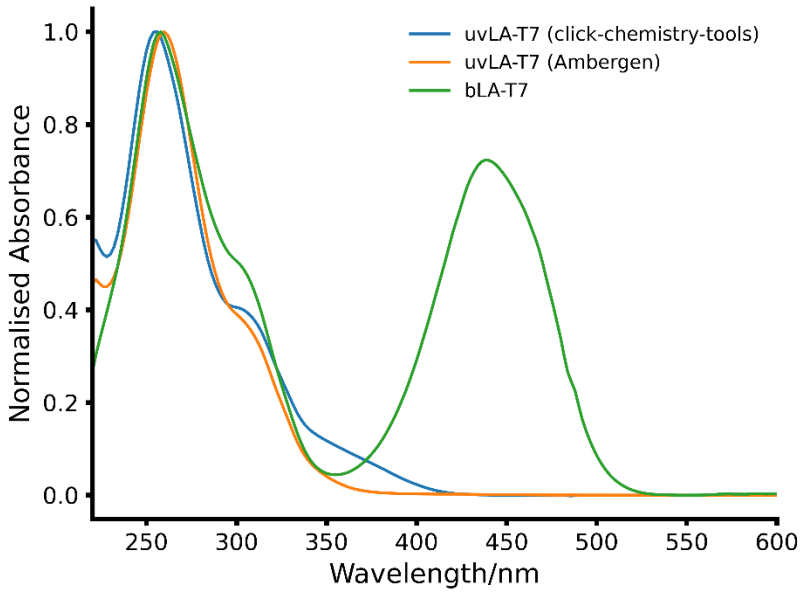
a) Crude HPLC trace of reaction of UV photocleavable biotin NHS ester (click-chemistry-tools) with 7-amine containing oligonucleotide (**Table 7-1**, Entry 1). **b)** HPLC trace of purified uvLA-T7.

HPLC Trace of uvLA-T7 (Ambergen)



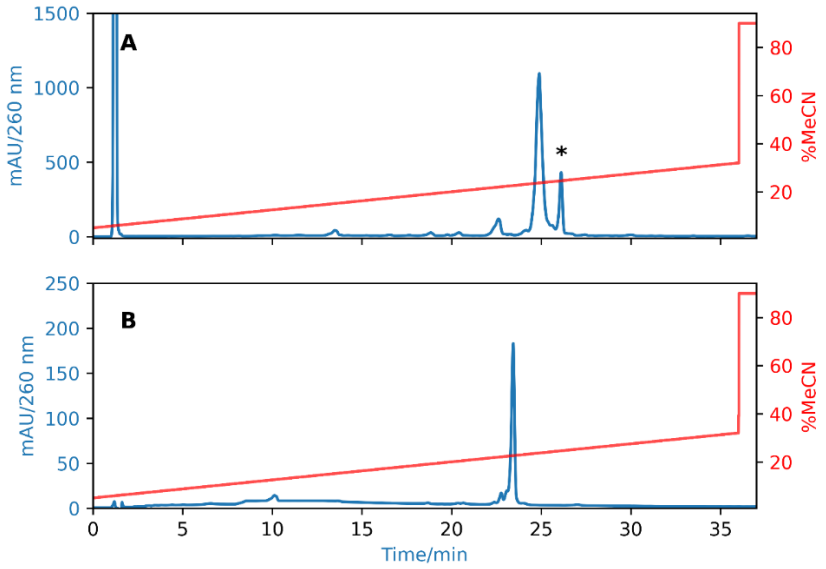
a) Crude HPLC trace of reaction of UV photocleavable biotin NHS ester (Ambergen) with 7 amine containing oligonucleotide (**Table 7-1**, Entry 1). Note: Purified uvLA-T7 was not reinjected onto HPLC due to limited amount obtained in reaction and was only analysed by LCMS.

UV-Vis Traces of LA-T7 ssDNA



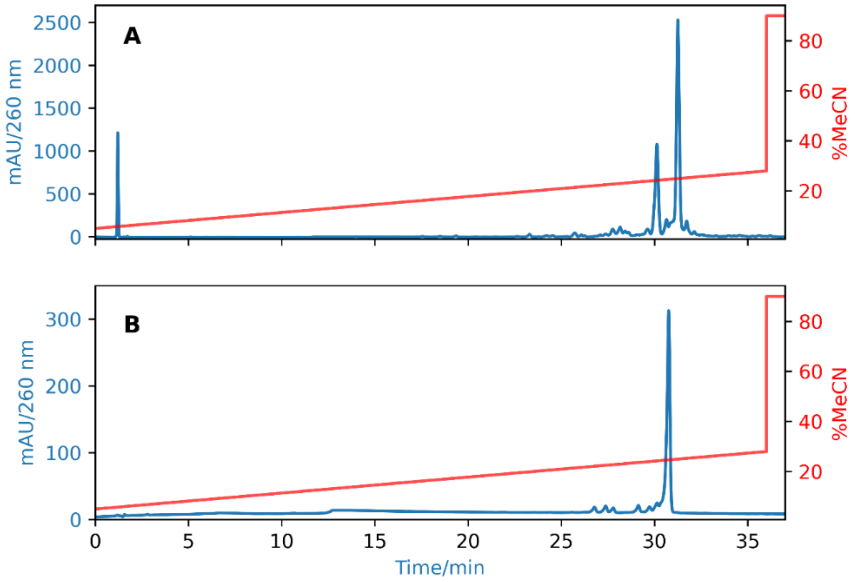
UV-Vis traces of LA-biotin-modified T7 promoter sequence containing ssDNA

HPLC Trace of uvLA-V1



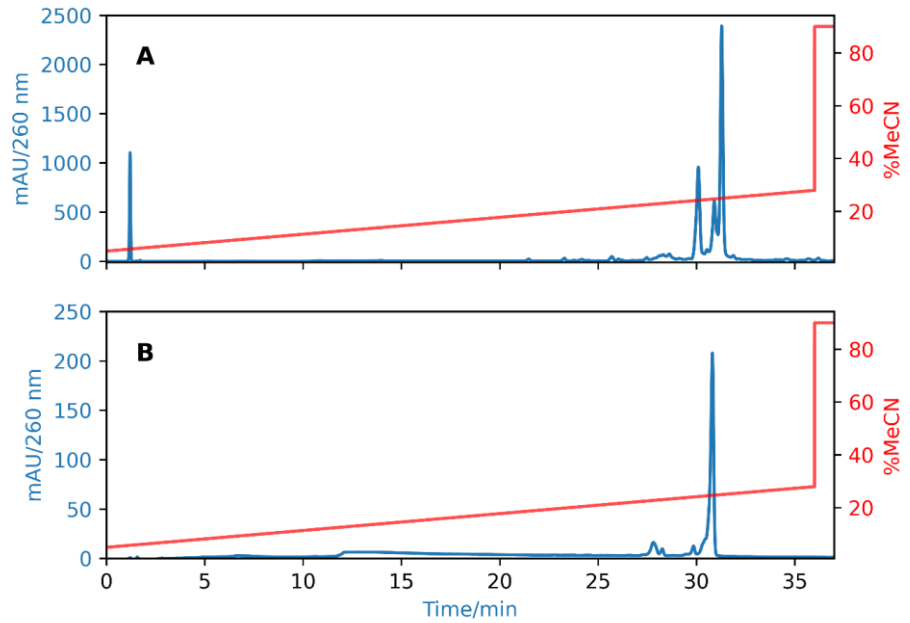
A) Crude HPLC trace of **V1** (**Table 7-3**) after reaction with uvLA-biotin. The desired oligonucleotide is highlighted by " * ". **B**) HPLC trace after HPLC purification.

HPLC Trace of uvLA-V2 biotin



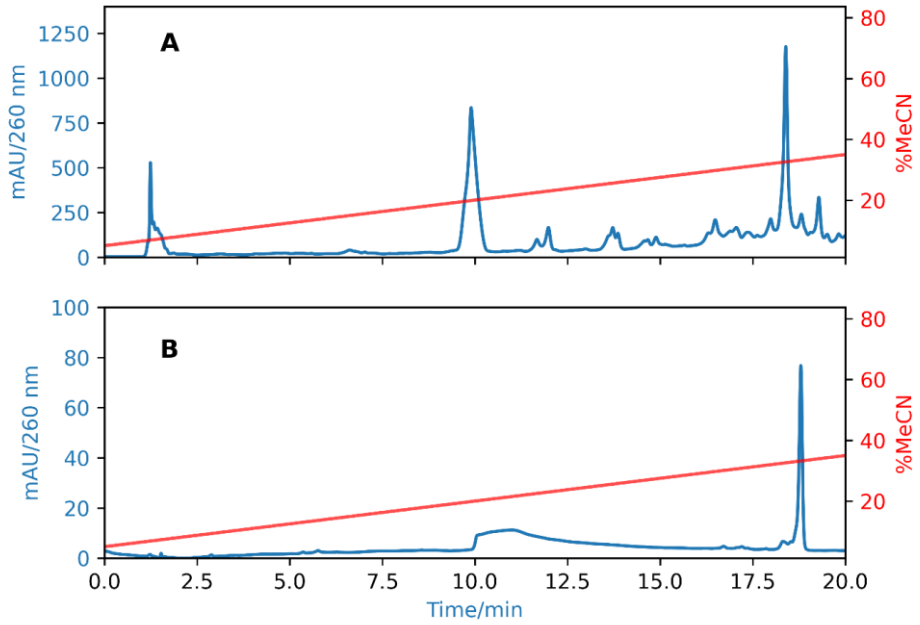
A) Crude HPLC trace of **V2** (**Table 7-3**) after reaction with uvLA-biotin. **B**) HPLC trace after HPLC purification.

HPLC Trace of uvLA-V3 biotin



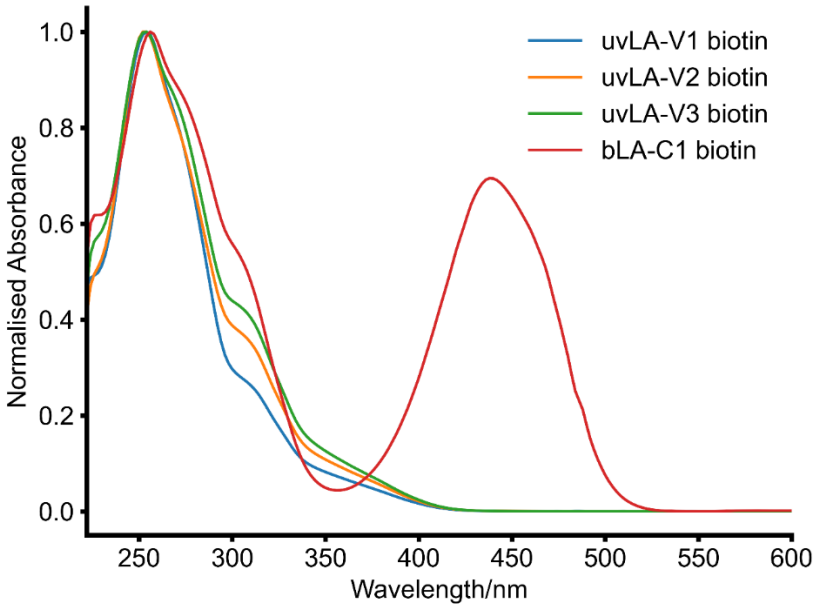
A) Crude HPLC trace of **V3** after reaction with uvLA-biotin. **B**) HPLC trace after HPLC purification.

HPLC Trace of bLA-C1 biotin



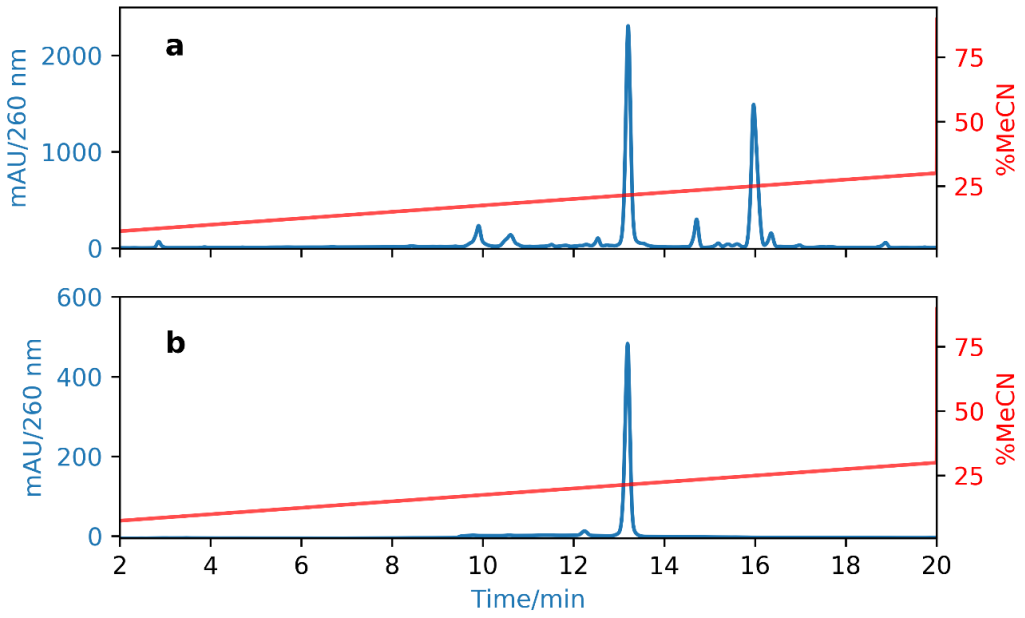
A) Crude HPLC trace of **C1** after reaction with bLA-biotin. **B**) HPLC trace after HPLC purification.

UV-Vis Traces of LA-ASOs V1-V3 and C1



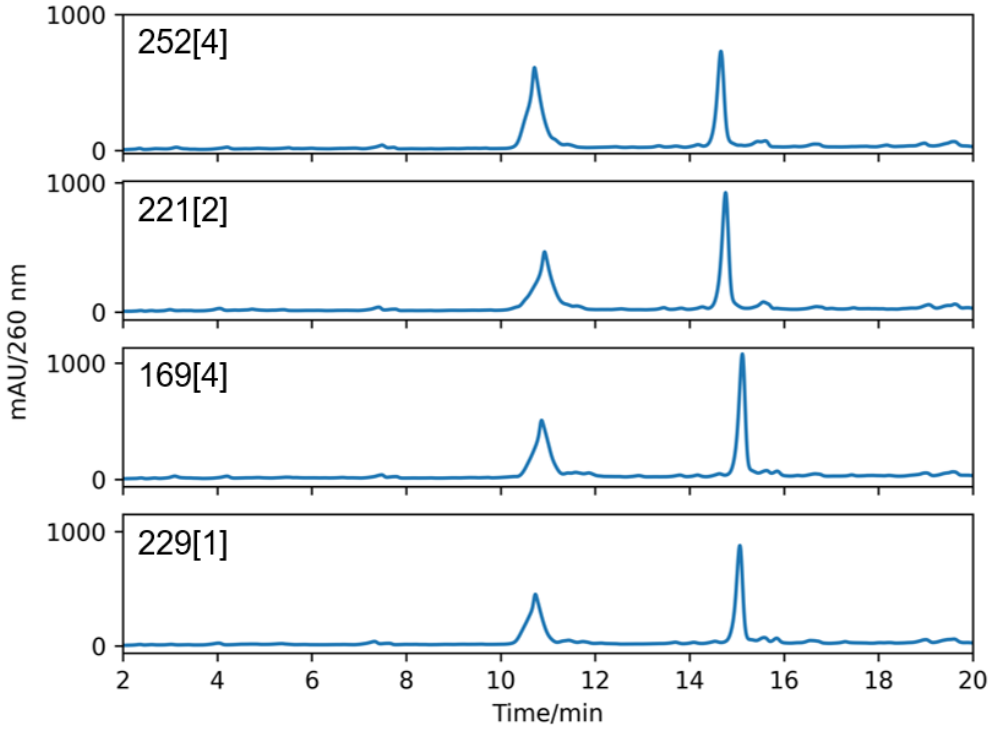
UV-Visible traces of PC-Biotin-modified oligonucleotides used in Chapter 3 as recorded by HPLC.

HPLC Trace of uvLA-Biotin-modified 252[4]



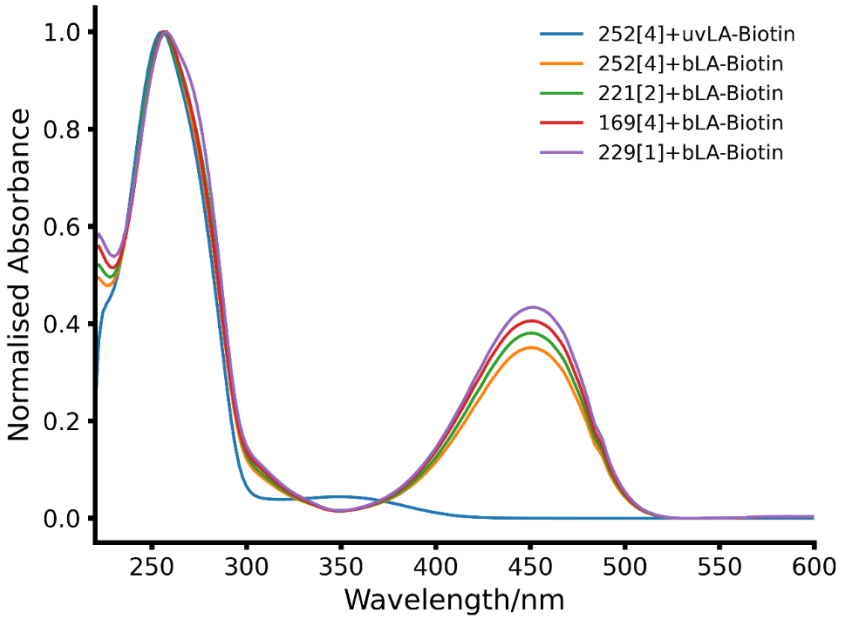
Purification of uvLA-Biotin modified 252[4] oligonucleotide. **a**) Crude reaction trace. **b**) Purified oligonucleotide trace.

Crude HPLC Traces of terminally bLA-Biotin-modified oligonucleotides



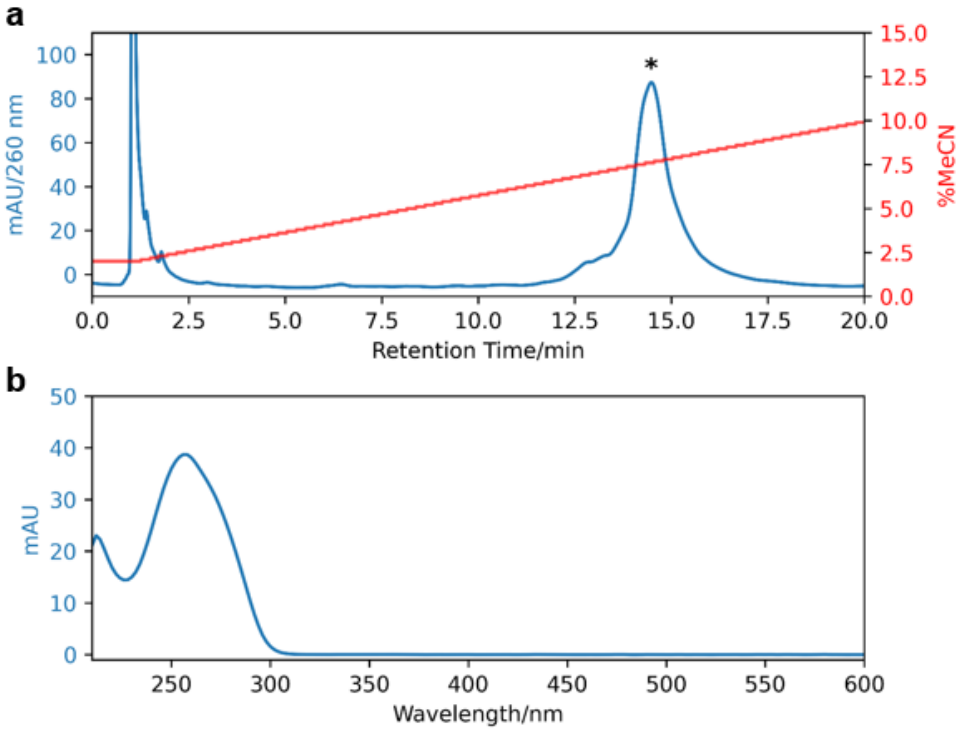
Crude Chromatograms of terminally bLA-Biotin-modified oligonucleotides.

UV-Visible Absorbance Traces of terminally LA-Biotin-modified Oligonucleotides



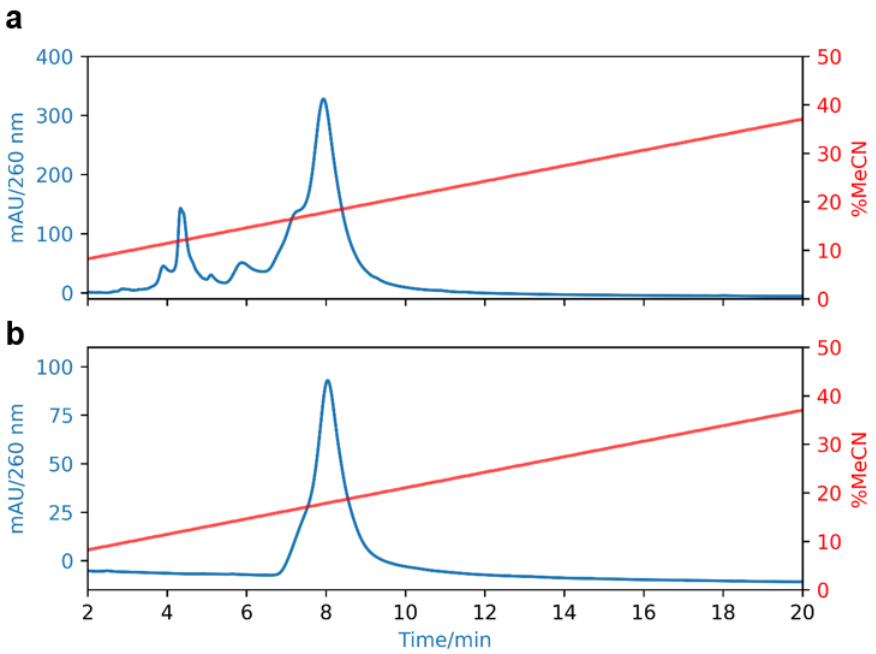
UV-Visible traces of PC-Biotin-modified oligonucleotides used in Chapter 4 as recorded by HPLC.

1PSEt



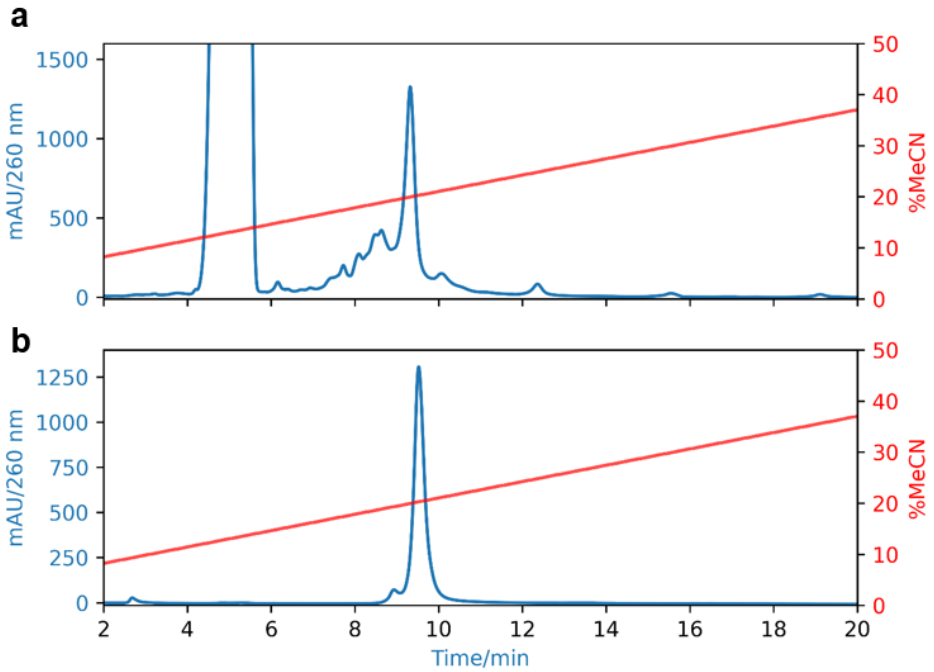
HPLC Purification of ethyl-modified 1PS-oligonucleotide. Crude reaction mixture and the absorbance spectrum of the *-labelled peak.

1PSNV



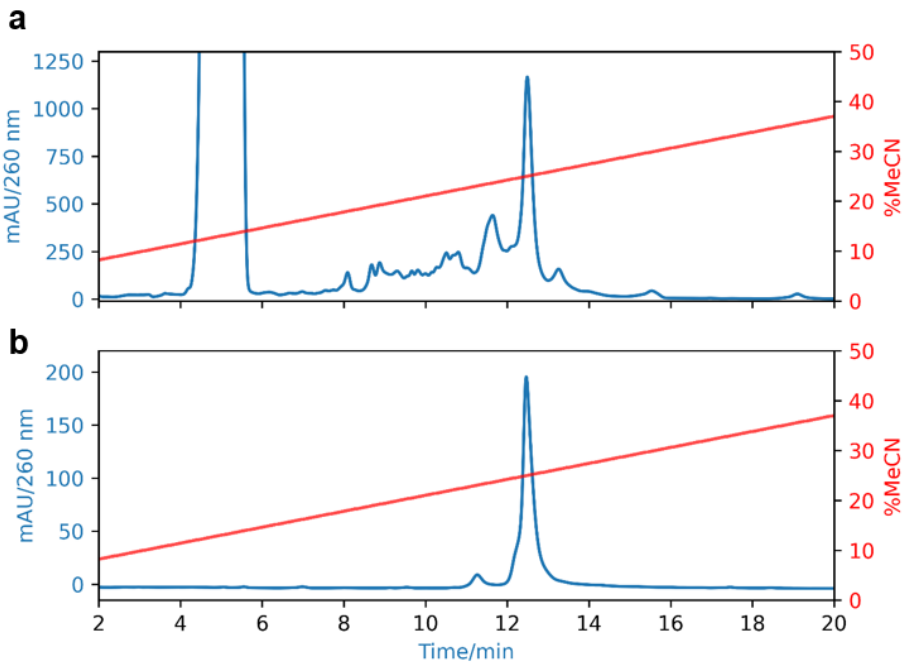
HPLC Purification of nitroveratryl-modified 1PS-oligonucleotide. **a)** Crude reaction mixture. **b)** Purified oligonucleotide.

6PSNV



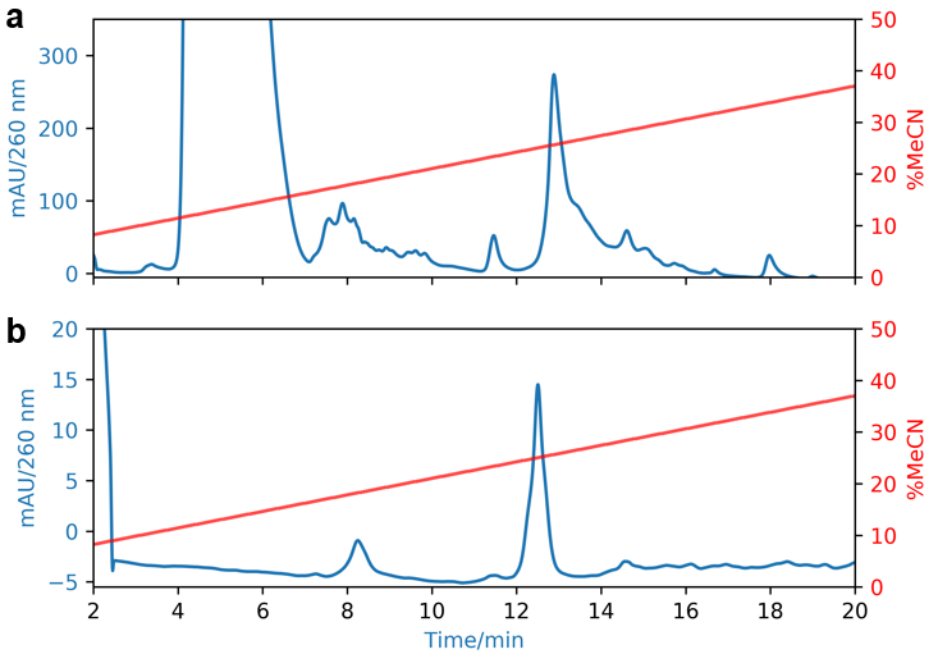
HPLC Purification of nitroveratryl-modified 6PS-oligonucleotide. **a)** Crude reaction mixture. **b)** Purified oligonucleotide.

9PSNV



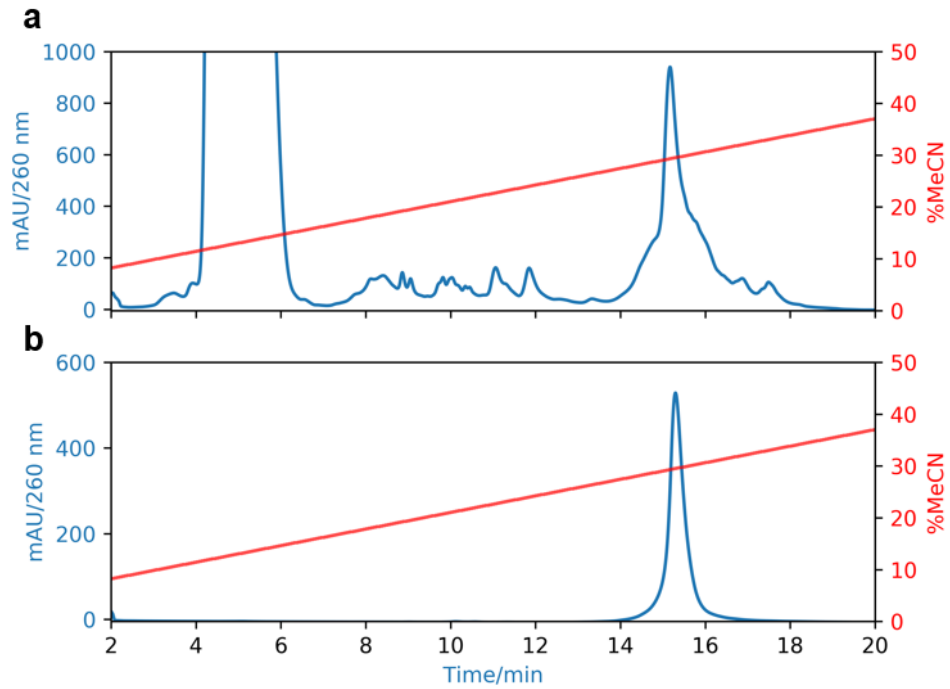
HPLC Purification of nitroveratryl-modified 9PS-oligonucleotide. **a)** Crude reaction mixture. **b)** Purified oligonucleotide.

TxRd-20nt-6PSNV



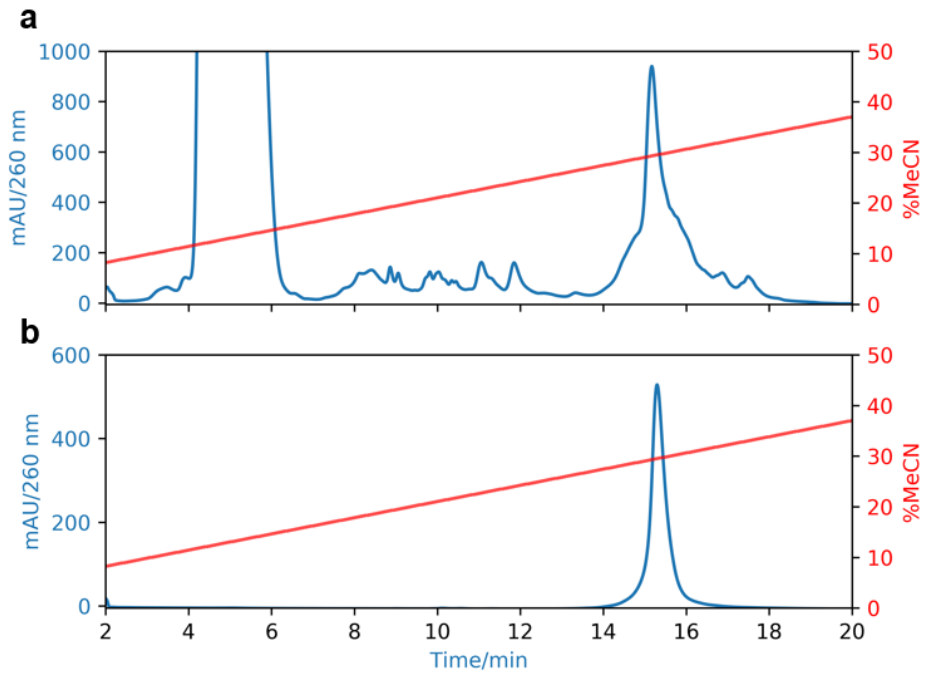
HPLC Purification of TxRd-tagged nitroveratryl-modified 20nt-6PS-oligonucleotide a) Crude reaction mixture. b) Purified oligonucleotide.

TxRd-20nt-9PSNV



HPLC Purification of TxRd-tagged nitroveratryl-modified 9PS-oligonucleotide. **a**) Crude reaction mixture. **b**) Purified oligonucleotide.

TxRd-14nt-6PSNV



HPLC Purification of TxRd-tagged nitroveratryl-modified 14nt-ON. **a**) Crude reaction mixture. **b**) Purified oligonucleotide.